
Exploring Higher Dimensional Quantum Field Theories Through Fixed Points

by Miss Rebecca M. Simms

Thesis submitted in accordance with the requirements of the
University of Liverpool for the degree of Doctor of Philosophy



Theoretical Physics Division
Department of Mathematical Sciences
University of Liverpool
United Kingdom

August 2018

Exploring Higher Dimensional Quantum Field Theories Through Fixed Points

by Miss Rebecca M. Simms

Abstract

Renormalization was popularised in the 1940s following the appearance of non-sensical infinities in the calculation of the self-energy of the electron. Notably this led to Quantum Electrodynamics becoming a fully renormalizable quantum field theory. One useful tool that emerges from the technical aspects of renormalization is the Renormalization Group. In particular, the β -function defines the variation of the coupling constants with energy. The vanishing of the β -function at a particular value of the coupling is known as a fixed point, the location of which can be found using perturbation theory. Properties of quantum field theories such as ultraviolet behaviour can be studied using these fixed points. The calculation of two different types of fixed points forms the spine of this thesis.

In Part I the d -dimensional Wilson-Fisher fixed point is used to connect scalar quantum field theories in different space-time dimensions. Specifically we look at dimensions greater than four and explore the property of universality through the Vasil'ev large N expansion. Different universality classes are examined, the first contains ϕ^4 theory with $O(N)$ symmetry while another incorporates $O(N) \times O(m)$ Landau-Ginzburg-Wilson theory. In the latter we perform a full fixed point stability analysis and conformal window search which determines where conformal symmetry is present. Part I develops techniques that may later be applicable to calculations involving beyond the Standard Model physics including asymptotic safety, quantum gravity and emergent symmetries.

Part II focuses on the non-trivial Banks-Zaks fixed point of four dimensional Quantum Chromodynamics. Using a variety of colour groups and representations we calculate the location of the fixed point and corresponding critical exponents to pinpoint exactly where the true value of the conformal window lies. Additionally a number of different renormalization schemes are used, including the momentum subtraction (MOM) and interpolating momentum subtraction (iMOM) schemes. This allows us to study where in the conformal window scheme dependence is most apparent. Both the Landau gauge and maximal abelian gauge are utilized to extend the analysis. Throughout this thesis we compare and contrast perturbative results with non-perturbative calculations such as those performed in lattice.

Declaration

I hereby declare that all work described in this thesis is the result of my own research activities unless reference to others is given. None of this material has been previously submitted to this or any other university. All work was carried out in the Theoretical Physics Division of the Department of Mathematical Sciences during the period of October 2014 to September 2018.

Publication List

Contributions from this work have been published in the following:

- [1] J.A. Gracey & R.M. Simms, *Banks-Zaks Fixed Point Analysis in Momentum Subtraction Schemes*, Phys. Rev. **D91** (2015) no.8, 085037.
- [2] J.A. Gracey & R.M. Simms, *Six Dimensional Landau-Ginzburg-Wilson Theory*, Phys. Rev. **D95** (2017) no.2, 025029.
- [3] J.A. Gracey & R.M. Simms, *Higher Dimensional Higher Derivative ϕ^4 Theory*, Phys. Rev. **D96** (2017) no.2, 025022.
- [4] J.A. Gracey & R.M. Simms, *Renormalization of QCD in the Interpolating Momentum Subtraction Scheme at Three Loops*, Phys. Rev. **D97** (2018) no.8, 085016.

Acknowledgements

The first person I wish to thank is my supervisor Prof. J.A. Gracey, without whom the work presented here would have been inconceivable. Thank you for the many useful discussions on books, travel, cricket and sometimes physics. I would certainly not have enjoyed the past four years as much without your encouragement and enthusiasm. I am also grateful for the support provided by my secondary supervisor Prof. I. Jack. I would like to thank STFC and the University of Liverpool for the financial assistance throughout my PhD. During these four years I have been lucky enough to travel to many academic institutions around Europe. I thank the Galileo Galilei Institute for Theoretical Physics (GGI) in Florence, Italy for providing a productive and engaging workspace. I would like to thank the Abdus Salam International Centre for Theoretical Physics (ICTP) in Trieste, Italy for providing a fantastic conference program and for the financial support which allowed me to attend. I would also like to thank Humboldt University in Berlin and Prof. Dr. D. Kreimer for the invitation to present my work and for the warm hospitality provided. My knowledge and love for physics has only grown on my travels and I thank everyone along the way who has supported my work. In particular I thank Henry for helping me find my way around Berlin. My thanks also go to Colin and Glyn for being brilliant office mates and to Matt and Alex for their support and friendship.

I would like to acknowledge and thank the following people who have supported me, not only during my PhD, but throughout my life. To my Mum and Dad, whose love and guidance are with me in whatever I pursue. To Holly, a pretty great little sister for all my complaining, thank you for your support and friendship. My heartfelt thanks go to my Nan and Auntie Julie for their support and unconditional love. Thanks also go to my Granddad, who I know would be proud of everything I have achieved. I would particularly like to thank Jack and Florence whose interest in my work and heart-warming kindness has been much appreciated. I am very grateful that you both have been part of my life these past couple of years. Finally, I am profoundly grateful to Paul for always having

confidence in me even when I did not. Thank you for always believing in me and for your love, encouragement and patience. Above all else, thank you for being my best friend. The memories we make together I will treasure always. I love you all dearly.

Contents

Abstract	iii
Declaration	iv
Acknowledgements	vi
1 Introduction	1
I Fixed Points of Scalar Quantum Field Theories	10
2 Background	11
2.1 Renormalizing Quantum Field Theory	11
2.1.1 Dimensional Regularisation	12
2.1.2 Renormalizing ϕ^4 Theory in Four Dimensions	13
2.1.3 Renormalization Schemes	18
2.1.4 Weinberg's Theorem	20
2.2 The Renormalization Group	23
2.2.1 Critical Exponents and Universality	28
2.2.2 Relation Between RG Functions and Renormalization Constants	30
2.3 Computational Methods	32
2.3.1 Conformal Integration	33
2.3.2 The Large N Expansion	38
2.3.3 Summary	53
3 Ten Dimensional $O(N)$ Scalar Field Theory	55
3.1 Introduction	55
3.2 $O(N)$ Symmetric Scalar Field Theories	57
3.3 Ten Dimensions	66
3.4 Calculation Techniques	67

3.4.1	Integral Reduction	70
3.4.2	2-point Master Integrals	75
3.4.3	Tarasov Method	79
3.4.4	Master Integrals with Three Propagators	82
3.4.5	Master Integrals with Four Propagators	88
3.4.6	The Vacuum Bubble Expansion	95
3.4.7	Renormalization	100
3.5	Large N Checks and Results	102
3.6	Discussion	106
4	$O(N) \times O(m)$ Landau-Ginzburg-Wilson Theory in Six	
	Dimensions	108
4.1	Introduction	108
4.2	Landau-Ginzburg-Wilson Theory	109
4.3	Six Dimensions	113
4.4	Calculation Techniques	115
4.4.1	Integral Reduction of the 2-point Function	120
4.4.2	2-point Master Integrals	127
4.4.3	3-point Interactions and the Insertion of a Propagator . . .	131
4.4.4	$T^{ab}T^{ac}T^{bc}$ and $\phi^{ia}\phi^{ib}T^{ab}$ Interactions	134
4.4.5	Renormalization	136
4.5	Mass Mixing Matrix	138
4.6	Results	142
4.7	Large N Analysis	155
4.8	Conformal Window Search	160
4.9	Fixed Point Analysis	169
4.10	Discussion	183
5	Higher Derivative Higher Dimensional Quantum Field	
	Theory	186
5.1	Introduction	186
5.2	Critical Exponents of Higher Derivative Higher Dimensional	
	Theories	190
5.2.1	Calculation of NLO Diagrams	194
5.2.2	Calculation of χ_1 and η_2	205
5.3	Perturbative Results for $n = 2$	208
5.4	Fixed Point Analysis	212
5.5	Discussion	216

II	The Banks-Zaks Fixed Point of Quantum Chromodynamics	219
6	Background	220
6.1	Gauge Theories	220
6.2	Quantum Chromodynamics	222
6.2.1	The Banks-Zaks Fixed Point	232
6.3	Renormalization Scheme Dependence	235
7	Banks-Zaks Fixed Point Analysis in Momentum Subtraction Renormalization Schemes	238
7.1	Introduction	238
7.2	Renormalization Group Functions	239
7.3	Mass Operator Anomalous Dimension	242
7.4	Results	246
7.5	Discussion	258
8	Banks-Zaks Fixed Point Analysis in Interpolating Momentum Subtraction Renormalization Schemes	260
8.1	Introduction	260
8.2	Maximal Abelian Gauge	262
8.3	Renormalization Group Functions	265
8.4	Results	273
8.5	Discussion	282
9	Perspective	285
	Appendix	291
A	Master Integrals for Scalar Calculations	291
B	Feynman Diagrams for $O(N) \times O(m)$ Landau-Ginzburg-Wilson Theory in Six Dimensions	299
C	Reduction Relations for the 2-point Function in Landau-Ginzburg-Wilson Theory at Three Loops	304
D	Banks-Zaks Fixed Points and Critical Exponents for $\overline{\text{MS}}$, mMOM and MOMi Renormalization Schemes	307
E	Banks-Zaks Fixed Points and Critical Exponents for iMOMi Renormalization Schemes	329

F Renormalization Group Functions γ_A, γ_ψ and γ_c of QCD in $\overline{\text{MS}}$ Scheme	337
Bibliography	339

Introduction

The Standard Model of particle physics was developed in the latter half of the 20th century with contributions from many of the greatest physicists throughout history. The Standard Model describes all non-gravitational fundamental forces and classifies all observed elementary particles. The first breakthrough in its evolution came in 1961 with Sheldon Glashow's discovery of a way to combine electromagnetic and weak interactions, [5]. Several years later in 1967, Steven Weinberg and Abdus Salam, [6, 7], incorporated the Higgs mechanism into Glashow's electroweak interaction resulting in its modern form. In the Standard Model the Higgs mechanism refers specifically to the generation of masses for the electroweak gauge bosons through electroweak symmetry breaking. The Higgs mechanism was first proposed in 1964 simultaneously by three independent groups: by Robert Brout and François Englert, [8]; by Peter Higgs, [9, 10]; and by Gerald Guralnik, Carl Richard Hagen and Tom Kibble, [11]. Following experimental results produced at CERN, [12–14], electroweak theory became widely accepted with Glashow, Salam and Weinberg sharing the Nobel prize for physics in 1979. In 1964 Murray Gell-Mann and George Zweig came up with the idea that hadrons, sub-atomic particles which take part in the strong interaction, were composed of quarks, [15, 16]. The name 'quark' was an invention credited to Gell-Mann and initially only three were proposed; up, down and strange. The discovery of more particles led to the introduction of three additional quarks; top, bottom and charm. Colour degrees of freedom would later emerge from hadrons in the work of Oscar Wallace Greenberg, Moo-Young Han and Yoichiro Nambu, [17, 18].

In total there are six quarks in the Standard Model, all experimentally verified and found to have fractional charge, [19, 20]. The theory of the strong interaction

acquired its current form in 1973 when asymptotic freedom was proposed, [21,22]. This gave theorists a model to understand why quarks interact weakly at high energies. While at low energies the interactions become strong, leading to the confinement of quarks and gluons within composite hadrons and mesons. The term ‘Standard Model’ was first coined by Abraham Pais and Sam Treiman in 1975, with reference to electroweak theory and only four quarks, [23]. The Standard Model is believed to be theoretically self-consistent and has proven to be hugely successful in providing experimental predictions. However many elements of real world physics remain unexplained. Most significantly, incorporating gravity into the Standard Model remains a mystery. As does the existence of dark matter in the Universe and where it fits into the Standard Model. There are also philosophical questions which remain such as why three generations of quarks exist and not, for example, four. Nevertheless the Standard Model remains to this day the most robust tool available for modelling the world around us. The framework for calculations involving the Standard Model is provided by quantum field theory (QFT) and necessarily involves a Lagrangian to control the dynamics and kinematics of the theory. Quantum field theory is an unavoidable consequence of the reconciliation of quantum mechanics with special relativity, [24]. It emerged through the quantization of the electromagnetic field by Paul Dirac in the 1920s in a QFT known now as Quantum Electrodynamics (QED), [25]. Later Dirac’s procedure became a model for the quantization of other fields, with Werner Heisenberg and Wolfgang Pauli establishing the basic structure of modern QFT, [26,27].

Quantum field theory was previously believed to be fundamental. However because of the failure to quantize general relativity, it is now thought to be a very good low energy approximation; an effective field theory to a more fundamental theory. Additionally despite its early success quantum field theory was found to be plagued with theoretical difficulties. Perturbation techniques used to calculate the self-energy of the electron in the 1930s discovered nonsensical infinities in the answer. From the 1930s to the beginning of the Second World War physicists tried different tricks such as truncation to avoid the problematic infinities. The ‘divergence’ problem was finally solved in the case of QED through a procedure known as renormalization in 1947-1949 by a combination of physicists including Richard Feynman, [28–37]. Renormalization theory suggests that divergences are more than failures of specific calculations. Furthermore infinities may be systematically removed via a redefinition of the parameters of the theory and using a measured finite value instead of infinite ‘bare’ values. A consequence for QED is that the physical charge and mass of the electron must be measured and cannot

be derived from first principles. Nevertheless quantum field theory has been a resounding success story. Perturbation theory in particular yields well-defined predictions in renormalizable QFT's in better agreement with experiment than anything physics has encountered before. In the following decades QFT was extended to describe not only the electromagnetic force but also the weak and strong (nuclear) forces, the latter now recognised as Quantum Chromodynamics (QCD).

Notably quantum field theory has helped develop mathematical tools which can be utilized for a wide array of problems not just in the Standard Model but also for physics outside of it. For example, Feynman's visualisation of space-time diagrams via 'Feynman diagrams' gives a simple graphical set of rules to calculate scattering processes. Another important tool is the Renormalization Group (RG) which comes from a technical aspect in the renormalization procedure and forms the theoretical backbone of this thesis. The Renormalization Group is a mathematical apparatus which allows a systematic investigation of the changes in a physical system as viewed at different scales. The key results that emerge are the Renormalization Group equations introduced by Curtis Callan and Kurt Symanzik in 1970, [38, 39]. One important RG equation is the β -function, calculations of which give a perturbative estimate of the variation of the coupling constant with scale. The vanishing of the β -function at specific values of the coupling constants are known as fixed points and are thought to be associated with conformal symmetry as they are necessarily scale invariant. Fixed points will occur naturally if the coupling is attracted to or running towards a point. In some quantum field theories the running coupling appears to become infinite at a finite momentum scale. Most notably this occurs in the isolated theory of QED not embedded in the Standard Model. This is known as the Landau pole problem and may be considered to be a mathematical inconsistency in a theory purporting to be complete. It may also be a sign that the perturbative approximation of the coupling breaks down at a strong coupling. The Landau problem can be avoided if an ultraviolet (UV) fixed point appears in the theory. A quantum field theory has a UV fixed point if its Renormalization Group flow approaches a fixed point in the ultraviolet limit. It has been suggested that a theory with a UV fixed point may not be an effective field theory at all as it is well-defined at high energy.

Parallel breakthroughs in the understanding of phase transitions in condensed matter physics by Leo Kadanoff, [40], Kenneth G. Wilson and Michael Fisher, [41], led to novel insights based on the Renormalization Group. A deeper understanding of the physical meaning behind the Renormalization Group and scale came in the form of the block spin Renormalization Group, [40]. The blocking idea is

a way to define the components of the theory at large distances as aggregates of components at shorter distances. This led to a reformulation of quantum field theory by Wilson which provided insight into the evolution of effective field theories with scale, [42–44]. A remarkable conclusion was reached, in general most observables are ‘irrelevant’ which means that macroscopic physics is dominated by only a few observables in most systems. This helped to understand universal properties of a wide class of systems with a large number of degrees of freedom. Applications of Wilson’s work led to developments in the theory of second-order phase transitions and critical phenomena, [42–44], for which he was awarded the Nobel prize for physics in 1982. The term universal is used in this context to emphasize the curious property that systems, which may seem physically unrelated, unexpectedly share some non-trivial large scale properties. Universality of the large distance behaviour is related to fixed points of the Renormalization Group flow. Wilson and Fisher in 1972 succeeded in determining a set of fixed points in d -dimensions, known as the Wilson-Fisher fixed points, relevant for a large class of phase transitions. Quantum field theories in the same universality class will, among other things, share a d -dimensional Wilson-Fisher fixed point.

The application of the Renormalization Group to particle physics exploded in the 1970s with the establishment of the Standard Model. The Renormalization Group was initially devised in particle physics, but nowadays its applications extend to solid-state physics, fluid mechanics, physical cosmology and even nanotechnology. It is also the modern key idea underlying critical phenomena in condensed matter physics, [45]. The flexibility of the Renormalization Group to different problems has led to this thesis being split into two parts. Part I will focus on the application of universality to connect theories in different dimensions. Specifically we focus on scalar quantum field theories in dimensions greater than four. The motivation behind this lies in the apparent connection of ultraviolet stable fixed points in higher dimensional theories with lower dimensional infrared (IR) fixed points, [46]. Although this statement was initially applied to QCD, with knowledge of the non-trivial IR fixed point in four dimensions thought to be obtainable through a higher dimensions, the same idea can also be applied to other quantum field theories. Part I will contain scalar theories only with the reason for this being twofold. First we wish to use scalar theories as a testing ground, or as toy models, to develop ideas about universality before applying them to more Standard Model-like theories. It is in these future calculations that beyond the Standard Model (BSM) physics may be discovered. In particular we develop the large N technique introduced by A.N. Vasil’ev et al., [47–50], to compute d -dimensional critical exponents at criticality. Additionally scalar theories

will still provide an interesting fixed point structure which can be analysed for any potential conformal windows and for ultraviolet stability behaviour.

In Chapter 3 we introduce a set of connected scalar theories possessing the $O(N)$ symmetry group. These theories have received significant interest in recent years with the Renormalization Group functions calculated in six and eight space-time dimensions, [51–54]. As well as acting as a laboratory for universality ideas, the main motivation for looking at this class of $O(N)$ theories stems from the potential relation to beyond the Standard Model physics in the form of the AdS/CFT correspondence of AdS critical $O(N)$ vector models, [55, 56]. The six dimensional theory has also been of particular interest for comparison with recent five dimensional bootstrap results, [57–62]. Other non-perturbative techniques have been applied to $O(N)$ scalar theories, notably the Functional Renormalization Group (FRG) has been used to study the theory in five dimensions, [63–65]. In Chapter 3 we build the ten dimensional Lagrangian with $O(N)$ symmetry which shares some universal properties with these scalar theories. The methodology of calculating in a dimension greater than four is discussed and the Renormalization Group functions are constructed in ten dimensions. Critical exponents which describe the behaviour of physical quantities at criticality are also found and hence universality through the large N expansion is established. The analysis into higher dimensional scalar field theories is continued in Chapter 4. A Lagrangian for the six dimensional $O(N) \times O(m)$ Landau-Ginzburg-Wilson theory is created, connected at the d -dimensional Wilson-Fisher fixed point to the four dimensional model of the same name. This theory has applications relevant to physics in frustrated magnets. As an $O(N) \times O(m)$ symmetry group is present we obtain a more exotic fixed point structure including complex fixed points. Therefore, although a key motivation is to establish a tangible connection between the four and six dimensional theories, our analysis will mainly focus on the qualitative meaning of this richer fixed point structure. It is hoped that data obtained will be comparable with non-perturbative bootstrap results in five dimensions similar to those performed in three dimensions, [66, 67].

Chapters 3 and 4 focus on the universality of theories in differing dimensions at a single d -dimensional fixed point. However we speculate that, in fact, these theories may be part of a single d -dimensional universal theory. In d -dimensions the universal theory contains all possible interactions between fields with only a finite number becoming relevant in fixed dimensions. Consequently operators in a higher dimension may stay relevant for lower dimensions and influence the physics. In Chapter 5 we look at the connection of fixed points in a slightly

different way. Using the perturbative large N expansion we build a new tower of connected scalar theories across dimensions containing higher derivative kinetic terms. The main motivation here is to establish new results for the Vasil'ev et al. large N expansion. It is hoped that these original results will prove invaluable for future calculations involving higher derivative models which have connections with physics via elasticity, [68]. Research has already begun into higher dimensional fermionic theories, with six and eight dimensional extensions of QED and QCD considered, [54,69,70]. Another possible extension of the research presented here is to the idea of asymptotically safe quantum field theories. A well known property of QCD is asymptotic freedom, where the coupling flows to the trivial fixed point in the ultraviolet regime. Quarks therefore act as ‘quasi-free’ particles at high energy. Asymptotic safety is similar, however in the ultraviolet the theory instead flows to a stable non-trivial fixed point, [71]. Therefore at high energy the theory is well-defined at that fixed point. Six dimensional $O(2)$ and $O(3)$ scalar models have been studied in the context of asymptotically safe quantum field theories, [72]. Moreover the Functional Renormalization Group has been utilized to establish a line of asymptotically safe UV couplings for scalar theories in [73]. Gauge and gauge-Yukawa theories have also been analysed in the context of asymptotic safety, [74–77].

One important question that arises is if asymptotic safety can be applied to the theory of quantum gravity. The Functional Renormalization Group has provided evidence for the possible existence of asymptotic safety in quantum gravity models, [78–80]. One significant result is that it has been shown that an asymptotically safe quantum gravity model can predict the quark mass, [81,82], and give an upper bound on the abelian gauge coupling, [83]. Furthermore an asymptotically safe Standard Model via vector like fermions has also been analysed, [84]. For beyond the Standard Model physics, dark matter, [85], and supersymmetric (SUSY) models, [86], have also been investigated for possible asymptotically safe fixed points. There has also been research into asymptotic safety on the lattice in the form of the $O(N)$ non-linear σ model, [87]. The bulk of current research in this area has been performed using non-perturbative methods, particularly for quantum gravity models. One hopes in future research the techniques developed in this thesis for scalar theories may be transferable to perturbative quantum gravity models in four and higher dimensions.

Part II will focus on the computation of another non-trivial fixed point, the Banks-Zaks fixed point of QCD, along with its associated critical exponents. The Banks-Zaks fixed point is the first non-trivial fixed point of the QCD β -function.

It is an infrared stable fixed point as is expected from confinement. QCD is a high energy field theory, however if the value of the coupling at the fixed point is very small, more specifically if it is less than one, perturbation theory can be performed in the weak coupling. The existence of the fixed point was first discovered by William E. Caswell in 1974, and later used by Thomas Banks and Alexander Zaks in their analysis of the phase structure of vector-like gauge theories with massless fermions, [88]. The conformal window of QCD is the range of quark flavours for which the Banks-Zaks fixed point exists and is of significant interest as it can be an indication of whether conformal symmetry is present. The location of the fixed point along with the conformal window can be perturbatively calculated. However as perturbation theory is a truncated series one can only obtain estimates which are improved by calculating to a high loop order. Moreover as the Renormalization Group functions of QCD are in general only renormalization scheme independent at leading order, different schemes may be employed to obtain better convergence. Critical exponents of QCD are computed by evaluating the Renormalization Group functions at the non-trivial fixed point. In particular the quark mass anomalous dimension exponent is of interest due to its relation to chiral symmetry breaking. As critical exponents are physical quantities, their value should be independent of the renormalization scheme used. In other words critical exponents are RG invariants. In practice however this does not work out as perturbation theory is being used.

In Part II the Banks-Zaks fixed point and critical exponents are calculated in various schemes to discover where scheme dependence is most apparent in the conformal window and which scheme, if any, has the best convergence. This analysis was inspired by and extends the work of Thomas Rytov and Robert Shrock, [89–97], which looked at the modified minimal subtraction ($\overline{\text{MS}}$), minimal momentum subtraction (mMOM) and modified regularisation invariant (RI') renormalization schemes, among other issues. In Chapter 7 the momentum subtraction schemes (MOM) are used to calculate the location of the Banks-Zaks fixed point and value of the associated critical exponents. The MOM renormalization schemes are kinematic and were introduced by William Celmaster and Richard J. Gonsalves in 1979, [98, 99]. The renormalization in these schemes takes place at the symmetric subtraction point and for QCD it leads to three separate renormalization schemes based on the 3-point QCD vertices: quark-gluon, triple gluon and ghost-gluon. As the MOM schemes are a different class to the previous schemes investigated, [89–97], one hopes to obtain a more non-trivial insight into scheme dependence. In Chapter 8 the analysis is repeated for the interpolating momentum subtraction schemes (iMOM), [100–103]. Originally

introduced for the specific case of the quark mass operator renormalization only, they are a more general set of kinematic renormalization schemes. The iMOM schemes will depend on a parameter which tags the external momentum of one of the legs in the 3-point vertex functions. This parameter ω is the origin of the interpolation and setting its value to unity one retains the MOM schemes. Once again three separate iMOM schemes are available based on the different 3-point vertices.

The analysis of Chapters 7 and 8 will be in the Landau gauge for comparison with [97]. Although the β -function is gauge independent in a mass independent renormalization scheme like $\overline{\text{MS}}$, in general it will be gauge dependent, [98,99,104]. Therefore it is beneficial to extend the analysis to a second gauge fixing other than the standard linear covariant gauge. The main motivation for repeating the analysis in the maximal abelian gauge (MAG) is the availability of the three loop Renormalization Group functions in different schemes. Therefore our analysis can be extended to compare data in two different gauges without performing any new renormalization. For comparison with the results of [97] the location of the Banks-Zaks fixed point and corresponding critical exponents are analysed in the conformal window of three different colour groups; $SU(2)$, $SU(3)$ and $SU(4)$. The investigation also extends to representations besides the fundamental to include the adjoint representation along with the two-index symmetric and anti-symmetric representations. This is in part to understand where the conformal window lies and the true range for which it exists in perturbation theory. Alternative representations may also be applied to problems beyond the Standard Model and be relevant to several problems such as those underlying technicolor theories. Data obtained in Chapters 7 and 8 can also be compared with recent lattice research.

Since publication of our original results, [1,4], scheme dependence of the quark mass anomalous dimension has been further analysed to five loops in [105], extending the four loop results of [97]. Furthermore in recent years strong evidence for scheme independence of this exponent along with others has been provided using a finite order perturbative expansion, [106–111]. This approach, introduced by [88], uses a scheme independent expansion parameter dependent only on the number of quark flavours. For example, a scheme independent expansion for the quark mass anomalous dimension has been computed in QCD and supersymmetric QCD (SQCD) to four loops, [106,107]. Additionally scheme independent expansions for the quark mass anomalous dimension to four loops and the exponent associated with the first derivative of the β -function to five loops were found for

general asymptotically free gauge theories with general gauge groups, [108, 110], with $SU(N_c)$, [109], and with $SO(N_c)$ and $Sp(N_c)$, [111]. Similar expansions have also been found for several asymptotically free chiral gauge theories, [112], and $\mathcal{N} = 1$ SQCD, [113]. Most recently a scheme independent calculation of the anomalous dimension of several baryon operators in an $SU(3)$ asymptotically free gauge theory was computed in [114]. Furthermore, to support earlier work in [94, 97, 106–111], scheme independent expansions for exponents were calculated using $\overline{\text{RI}}'$ and different MOM schemes which yielded identical results, [114].

Part I

Fixed Points of Scalar Quantum Field Theories

Background

In advance of presenting original research some essential background knowledge and computational methods are discussed. For this I am indebted to the following literature; [115–120].

2.1 Renormalizing Quantum Field Theory

The development of the Standard Model is driven by theoretical and experimental physics. For theorists, the Standard Model is a paradigm of a quantum field theory (QFT) and can be studied using both perturbative and non-perturbative methods. To improve the reliability of perturbative results calculating to a high loop order is required. However calculations involving loops are generically infinite. Consider an integral commonly encountered in one loop computations with loop momenta k . When mass m is small and negligible, then

$$\int \frac{d^4k}{(k^2 - m^2)^2} \longrightarrow \int_{\varepsilon}^{\Lambda} \frac{d^4k}{(k^2)^2} = \ln \Lambda - \ln \varepsilon \quad (2.1)$$

where ε and Λ are cut-offs and which tends to infinity when $\varepsilon \rightarrow 0$ or $\Lambda \rightarrow \infty$, where the integral is considered in four dimensional Minkowski space. At large momenta as $\Lambda \rightarrow \infty$ the integral will therefore diverge. This is known as an ultraviolet (UV) divergence as opposed to an infrared (IR) divergence which occurs at low energy when $\varepsilon \rightarrow 0$. Ultraviolet divergences appear in almost every attempt to calculate beyond leading order (LO). This presents a problem as it is impossible to obtain meaningful physical results if infinities appear within a computation. Remarkably in the late 1930s Dirac, Bohr and others were ready to give up on Quantum Electrodynamics (QED) altogether because of divergence issues. The

problem was solved in the case of Quantum Electrodynamics through a procedure known as renormalization in 1947-49 by Hans Kramers, Hans Bethe [28], Julian Schwinger [29–32], Richard Feynman [33–35] and Shin’ichiro Tomonaga [36]; the procedure was then systematised by Freeman Dyson in 1949, [37]. Renormalization theory is based on UV divergences as these can be handled systematically. We shall ignore IR divergences for now as they are absent in massive theories. The theory of renormalization states that divergences arise from the assumption that the variables of the classical theory are valid and equivalent to the variables which describe the quantum theory. Renormalization is a systematic and mathematically consistent method of redefining the variables in a way that removes the infinities. Therefore the integrals will be finite but will also depend on some regulating parameter. It turns out that values for observables will be independent of the regulator which can then be removed. There are two key components to renormalization, the regularisation used to identify potential divergences and the way in which we choose to remove these divergences from the theory.

2.1.1 Dimensional Regularisation

In four dimensional Minkowski space many Feynman integrals are divergent and moreover the nature of the divergences are not quantified. To avoid integrals diverging we choose a regulator to transform an ill-defined integral into a mathematically well-defined one. There are three main regularisations used in quantum field theory. The first is a cut-off procedure, such as Pauli-Villars which introduces a parameter Λ to restrict the large momenta. However one problem which arises is the loss of gauge symmetry. The second method is lattice regularisation which replaces the continuum space-time by a lattice. This technique is very good for probing non-perturbative dynamics and low energy Quantum Chromodynamics (QCD). It is particularly useful for studying infrared physics numerically where perturbation theory is not applicable. This technique however requires supercomputers which can be costly to implement. It also breaks Lorentz symmetry. The most popular regularisation used in perturbation theory is dimensional regularisation, first introduced by Carlos Guido Bollini and Juan José Giambiagi in 1972, [121], and developed extensively in gauge theories by Gerard ’t Hooft and Martinus Veltman, [122]. This regularisation analytically continues the space-time to d -dimensions where d is a complex variable and can be written as $d = 4 - 2\epsilon$. The regularising parameter is given by ϵ and is assumed to be very small, $|\epsilon| \ll 1$.

In practice dimensional regularisation involves replacing the integration mea-

sure in the integral as follows,

$$\int \frac{d^4 k}{(2\pi)^4} \longrightarrow \int \frac{d^d k}{(2\pi)^d} .$$

The Feynman integrals will therefore be evaluated as functions of d and singularities will appear as poles in ϵ . Dimensional regularisation does not break gauge or Lorentz symmetry, although it does break supersymmetry (SUSY). Dimensional reduction is a variant of the regularisation which does preserve supersymmetry, [123–125]. Notably ultraviolet and infrared divergences are indistinguishable using this type of dimensional regulator which one must take into account during calculations. Every regularisation will introduce an arbitrary mass scale. In cut-off this scale is Λ , while for lattice it is the length of the lattice square a . For dimensional regularisation the arbitrary mass scale arises from the change in the dimensionality of the integral measure. As we still require the action to be dimensionless, the coupling constant must be rescaled in such a way that it is dimensionless in d -dimensions. Hence

$$g \longrightarrow g\mu^{+\epsilon} \tag{2.2}$$

where μ is the arbitrary scale associated with the regulator. Note that these scales are arbitrary and cannot appear in observables leading to the Renormalization Group (RG) formalism, more on which later.

2.1.2 Renormalizing ϕ^4 Theory in Four Dimensions

Once divergences have been quantified one must find a way to remove them. To illustrate how renormalization works we take ϕ^4 theory as an example to develop the procedure which will be applicable to every renormalizable quantum field theory. The Lagrangian for ϕ^4 theory in four dimensions is given by

$$L = \frac{1}{2}(\partial_\mu\phi)^2 - \frac{1}{2}m^2\phi^2 - \frac{1}{4!}g\phi^4 \tag{2.3}$$

where g is the coupling constant and m is the mass. The Feynman rules can be found from the Lagrangian and are illustrated in figure 2.1.

$$\begin{array}{c} \text{---} \\ p \longrightarrow \end{array} = \frac{i}{p^2 - m^2 + i\epsilon} \quad \begin{array}{c} \diagup \\ \diagdown \end{array} = ig$$

Figure 2.1: The Feynman rules for ϕ^4 theory in four dimensions.

It is important to note at this point that JAXODRAW, [188, 189], has been used to visually present all Feynman diagrams in this thesis. Divergences emerge at the one loop level which can be seen in the Feynman diagram of figure 2.2. The incoming momenta is given by p_i , while the internal loop momenta is denoted by k .

$$= \frac{i^2 (ig)^2}{2} \int \frac{d^4 k}{(2\pi)^4} \frac{1}{(k^2 - m^2)((k-p)^2 - m^2)}$$

Figure 2.2: A one loop Feynman diagram of ϕ^4 theory, \mathfrak{I}_a , which will contain UV divergences.

An important point to note is that a subtraction point must be chosen for the renormalization, this is an external momentum set-up where the renormalization takes place. Here we choose the completely symmetric momentum configuration which has the conditions

$$\begin{aligned} p_i^2 &= -\mu^2 & \text{where } i &= 1, \dots, 4 \quad \text{and} \\ p_i p_j &= +\frac{\mu^2}{3} & \text{where } i &\neq j. \end{aligned} \quad (2.4)$$

Momentum is also conserved, $p_1 + p_2 + p_3 + p_4 = 0$. There is a huge amount of arbitrariness in the momentum configuration. However one should ultimately obtain the same physical predictions irrespective of which set-up is chosen.

We require the Feynman integral to be evaluated to the finite part in order to obtain a function of p^2 and m^2 , which contains the physics. To identify the divergences one uses dimensional regularisation which necessarily involves rescaling the coupling,

$$\mathfrak{I}_a = \frac{-ig^2(\mu^2)^\epsilon}{2} \int \frac{d^d k}{(2\pi)^d} \frac{1}{(k^2 + m^2)((k-p)^2 + m^2)}. \quad (2.5)$$

A Wick rotation has been applied to the integral which moves the calculation from Minkowski into Euclidean space. The integral can then be evaluated using Feynman (or Schwinger) parameters,

$$\mathfrak{I}_a = \frac{-ig^2(\mu^2)^\epsilon}{2} \int_0^1 dx \int \frac{d^d k}{(2\pi)^d} \frac{1}{[k^2 + x(1-x)p^2 + m^2]^2}.$$

To evaluate the integral over the loop momentum k one can use the following

identity which is derived using the Euler β -function,

$$\mathbf{I}_E(\alpha, \beta) = \int \frac{d^d k}{(2\pi)^d} \frac{(k^2)^\alpha}{(k^2 + m^2)^\beta} = \frac{(m^2)^{d/2+\alpha-\beta}}{(4\pi)^{d/2}} \frac{\Gamma(\alpha + \frac{d}{2})\Gamma(\beta - \alpha - \frac{d}{2})}{\Gamma(\frac{d}{2})\Gamma(\beta)}. \quad (2.6)$$

This simplifies the one loop integral to the following form

$$\mathcal{J}_a = \frac{-ig^2\mu^{2\epsilon}}{2} \frac{\Gamma(2-d/2)}{(4\pi)^{d/2}} \int_0^1 (x(1-x)p^2 + m^2)^{d/2-2} dx,$$

which is a one dimensional parameter integral and can be written exactly as a function of p^2 and m^2 . However for practical purposes we expand in powers of ϵ where $d = 4 - 2\epsilon$,

$$\mathcal{J}_a = \frac{-ig^2}{32\pi^2} \left[\frac{1}{\epsilon} + \ln(4\pi e^{-\gamma}) - \int_0^1 dx \ln \left(\frac{x(1-x)p^2 + m^2}{\mu^2} \right) + O(\epsilon) \right]. \quad (2.7)$$

The Euler-Mascheroni constant is given by γ and utilizing the Mandelstam variables, [116], $s = (p_1 + p_2)^2$, $t = (p_1 + p_3)^2$ and $u = (p_1 + p_4)^2$, one finds

$$\mathcal{J}_a = \frac{-ig^2}{32\pi^2} \left[\frac{1}{\epsilon} + \ln(4\pi e^{-\gamma}) - F(s) + O(\epsilon^2) \right] \quad (2.8)$$

where the finite integral in (2.7) has been denoted by the function $F(s)$. As long as $\epsilon \rightarrow 0$ the integral is well defined. However as we ultimately want to lift the regularisation by setting ϵ to zero, divergences will be produced. We therefore need to find a way to systematically remove these divergences. To begin the renormalization start at the one loop level and look at the 4-point scattering amplitude, $\Gamma_4(p_i)$. The 4-point scattering amplitude is illustrated in figure 2.3 with only the tree and one loop diagrams included thus far.

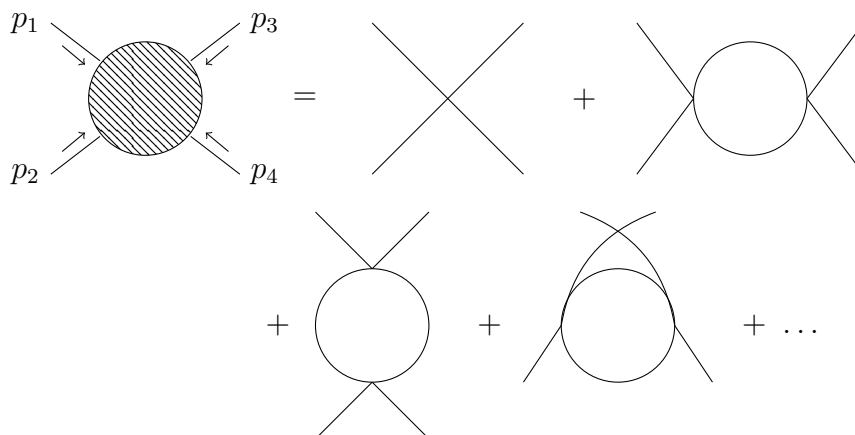


Figure 2.3: The 4-point scattering amplitude for ϕ^4 theory, $\Gamma_4(p_i)$, expanded out to one loop level.

This is calculated to be

$$\Gamma_4(p_i) = ig - \frac{ig^2}{32\pi^2} \left[\frac{3}{\epsilon} + 3\ln(4\pi e^{-\gamma}) - F(s) - F(t) - F(u) + O(\epsilon) \right] + O(g^4).$$

The reason divergences emerge in this theory originates from the initial assumption that the variables of the classical theory are equivalent to the variables which describe the quantum theory. We therefore start the computation again, but this time begin with a Lagrangian which is structurally the same as Lagrangian (3.2) but is written in terms of the ‘bare’ variables ϕ_0 , m_0 and g_0 ,

$$L = \frac{1}{2}(\partial_\mu\phi_0)^2 - \frac{1}{2}m_0^2\phi_0^2 - \frac{g_0}{4!}(\phi_0)^4. \quad (2.9)$$

Renormalized variables ϕ , m and g can then be introduced which are related to the bare variables via a rescaling,

$$\phi_0 = \sqrt{Z_\phi}\phi, \quad m_0 = Z_m m, \quad g_0 = \mu^\epsilon g Z_g. \quad (2.10)$$

The renormalization constants for the field, mass and coupling are given by Z_ϕ , Z_m and Z_g respectively. After inserting the rescaled variables the Lagrangian becomes

$$L = \frac{1}{2}Z_\phi(\partial_\mu\phi)^2 - \frac{1}{2}m^2Z_\phi Z_m\phi^2 - \frac{g}{4!}\mu^\epsilon Z_g Z_\phi^2\phi^4. \quad (2.11)$$

New Feynman rules illustrated in figure 2.4 can be read from Lagrangian (2.11) which involve the renormalization constants.

$$\begin{array}{c} \text{---} \\ p \rightarrow \end{array} = \frac{1}{Z_\phi p^2 - Z_\phi Z_m m^2} \begin{array}{c} \diagup \\ \diagdown \end{array} = ig Z_g \mu^\epsilon Z_\phi^2$$

Figure 2.4: The Feynman rules for ϕ^4 theory including renormalization constants.

This is one way to develop a renormalized quantum field theory. However in perturbation theory the free and interacting parts of the Lagrangian can be defined differently by introducing counterterms,

$$\begin{aligned} Z_\phi &= 1 + A, \\ Z_m Z_\phi &= 1 + B, \\ Z_g Z_\phi^2 &= 1 + C. \end{aligned} \quad (2.12)$$

The counterterms A , B and C are expansions in the power of the coupling,

$$A = \sum_{n=1}^{\infty} a_n g^n \quad , \quad B = \sum_{n=1}^{\infty} b_n g^n \quad , \quad C = \sum_{n=1}^{\infty} c_n g^n .$$

Inserting the counterterms into the Lagrangian we find

$$L = \frac{1}{2}(\partial_\mu \phi)^2 - \frac{1}{2}m^2 \phi^2 + \frac{1}{2}A(\partial_\mu \phi)^2 - \frac{1}{2}m^2 B \phi^2 - \frac{g}{4!} \mu^\epsilon \phi^4 - \frac{g}{4!} C \mu^\epsilon \phi^4 .$$

The Lagrangian can then be separated into free and interacting parts as follows

$$\begin{aligned} L_F &= \frac{1}{2}(\partial_\mu \phi)^2 - \frac{1}{2}m^2 \phi^2 + \frac{1}{2}A(\partial_\mu \phi)^2 - \frac{1}{2}m^2 B \phi^2 , \\ L_I &= -\frac{g}{4!} \mu^\epsilon \phi^4 - \frac{g}{4!} C \mu^\epsilon \phi^4 \end{aligned}$$

where $L = L_F + L_I$. If we try to read the Feynman rules from this Lagrangian one finds two additional rules which are the counterterms. They are denoted by a square inserted onto the propagator and are illustrated in figure 2.5.

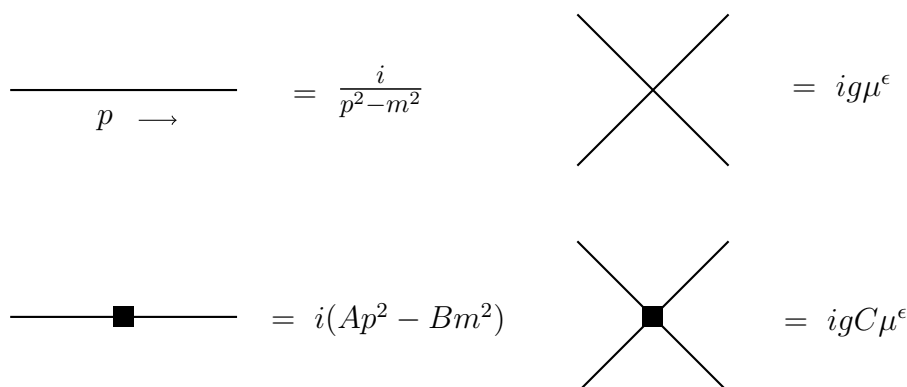


Figure 2.5: The Feynman rules for ϕ^4 theory including the counterterms.

The value for the 4-point Green's function $\Gamma_4(p_i)$ to one loop including counterterms becomes

$$\begin{aligned} \Gamma_4(p_i) \Big|_{s,t,u=-\frac{4}{3}\mu^2} &= ig - \frac{3ig^2}{32\pi^2} \left[\frac{1}{\epsilon} + \ln(4\pi e^{-\gamma}) - F\left(-\frac{4}{3}\mu^2\right) + O(\epsilon) \right] \\ &+ ig^2 c_1 + O(g^4) \end{aligned} \quad (2.13)$$

where the counterterm C has been expanded out to c_1 which is sufficient to absorb the divergence present at one loop. For now the counterterms A , B and C are completely arbitrary. Note that as we intend to set $\epsilon \rightarrow 0$ one can ignore the μ^ϵ piece of the counterterm. To lift the regularisation one uses the freedom of the choice of variable c_1 to ensure that $\Gamma_4(p_i)$ is finite as $\epsilon \rightarrow 0$. Therefore we set

$c_1 = 3/(32\pi^2\epsilon)$ and the Green's function becomes

$$\Gamma_4(p_i) \Big|_{s,t,u=-\frac{4}{3}\mu^2} = ig + \frac{3ig^2}{32\pi^2} \left[\ln(4\pi e^{-\gamma}) + F\left(-\frac{4}{3}\mu^2\right) + O(\epsilon) \right] + O(g^4) \quad (2.14)$$

as $\epsilon \rightarrow 0$. The choice of c_1 is called the renormalization scheme. If only the divergent part of the function is included in the counterterm this is the minimal subtraction (MS) scheme, [104, 122]. Equally one could select a different scheme and obtain the same result for observables. Any choice for the value of the counterterm should render the 4-point Green's function finite.

2.1.3 Renormalization Schemes

The way in which the renormalization constants are determined can be broken down into two stages. First, one has to specify the point where the renormalization constants are to be defined. By this we mean the momentum configuration of the external legs of the divergent n -point functions. In other words the values of the square of each external momentum have to be specified. As previously stated, for ϕ^4 theory the momentum configuration chosen was at the completely symmetric point

$$\Gamma_4(p_1^2, p_2^2, p_3^2, p_4^2) = \Gamma_4(-\mu^2, -\mu^2, -\mu^2, -\mu^2) .$$

Clearly there are infinitely many possibilities for such momenta values but there are a subset which have to be avoided. These are where the sum of a strict subset of the external momenta is zero. Termed an exceptional momentum configuration such momenta values can lead to infrared problems in the evaluation of the final value of the Green's function. The second general feature of renormalization is the prescription for defining the renormalization constants associated with each Green's function. This is known as the renormalization scheme. There are again infinitely many ways of doing this and all schemes should ultimately give the same physical results. For ϕ^4 theory above we implemented the minimal subtraction scheme of [104, 122], which is the simplest scheme to work with. In the MS scheme the renormalization constants are determined by removing only the divergence with respect to the regulator.

The most commonly used scheme is the modified minimal subtraction ($\overline{\text{MS}}$) scheme, [126]. It is a variation on the MS scheme where not only is the pole removed but also a specific finite part which is $\ln(4\pi e^{-\gamma})$. It is speculated that the removal of this extra piece improves the convergence of the series for the

Green's function, [126]. Renormalization schemes can be either kinematic or non-kinematic, with the latter meaning that it carries no information within the renormalization constants with respect to the location of the subtraction point. By contrast renormalization constants of a kinematic scheme contain data corresponding to that point. Additionally schemes can also be physical or non-physical, with $\overline{\text{MS}}$ being an example of a non-physical scheme. A physical scheme, an example being the on-shell scheme, is one where the external legs are on their mass shell at the subtraction point which makes it harder to calculate to a high loop order in. In contrast the $\overline{\text{MS}}$ does not require the finite pieces of the integral which simplifies the calculation. The schemes can also have renormalization constants which are mass independent or mass dependent. Mass independent schemes are easier to calculate in as there are nice simplifying features within the Renormalization Group formalism.

To complete the one loop renormalization of ϕ^4 theory we also have to compute the 2-point Green's function which is the mass renormalization. The 2-point Green's function, $\Gamma_2(p)$, at one loop including the relevant counterterm is illustrated in figure 2.6.



Figure 2.6: The 2-point scattering amplitude for ϕ^4 theory $\Gamma_2(p)$, with counterterms expanded out to one loop.

The 2-point function evaluated at one loop is

$$\Gamma_2(p) = \frac{i}{p^2 - m^2} - \frac{im^2g}{32\pi^2\epsilon} + ig(a_1p^2 - b_1m^2) + O(g^2). \quad (2.15)$$

In the $\overline{\text{MS}}$ renormalization scheme the counterterms are chosen to be $a_1 = 0$ and $b_1 = -1/(32\pi^2\epsilon)$ which renders the 2-point Green's function finite. This completes the one loop renormalization. Therefore to one loop the renormalization constants for ϕ^4 theory in the $\overline{\text{MS}}$ renormalization scheme are

$$\begin{aligned} Z_\phi &= 1 + O(g^2), \\ Z_m &= 1 - \frac{g}{32\pi^2\epsilon} + O(g^2), \\ Z_g &= 1 + \frac{3g}{32\pi^2\epsilon} + O(g^2). \end{aligned} \quad (2.16)$$

Note that along with the coupling and mass renormalization computed by calculating the 2 and 4-point Green's functions, there is also the wave-function renormalization. However in ϕ^4 theory the one loop Green's function to calculate the wave-function renormalization is not present as it is a 3-point function. Therefore the wave-function renormalization begins at two loops, as is clear from the above renormalization constant Z_ϕ which does not have a one loop term. In a standard renormalization procedure for any quantum field theory we first set the counterterms of the 2-point Green's function to one loop before then finding the counterterms for the higher point functions at one loop. The renormalization process then iterates to higher loops. For example for $\Gamma_2(p)$ the two loop Green's function will also include the diagrams presented in figure 2.7.

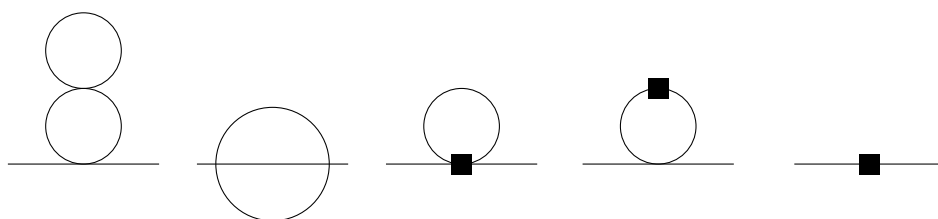


Figure 2.7: The 2-point Feynman diagrams included in the Green's function at two loops including counterterms.

The first two diagrams of figure 2.7 will contain the two loop divergences associated with the mass and wave-function renormalization. The third diagram involves the term c_1 which has already been fixed by the one loop coupling renormalization. Moreover the fourth diagram contains a_1 and b_1 which have also been fixed in the previous one loop mass renormalization. Finally the last diagram was included in the one loop renormalization, it has now been expanded to two loops to introduce the terms a_2 and b_2 which are used to absorb the two loop divergences which are present after summing all contributions.

2.1.4 Weinberg's Theorem

It is useful to establish where divergences may occur in a theory before any calculation is performed. From the renormalization of ϕ^4 theory we know that the two graphs displayed in figure 2.8 are divergent. Written in integral form diagram (b) of figure 2.8 is

$$\mathfrak{J}_b = g\mu^\epsilon \int \frac{d^d k}{(2\pi)^d} \frac{1}{k^2 + m^2}. \quad (2.17)$$

There are four powers of the loop momentum k in the numerator and two in the denominator, the integral would therefore diverge quadratically at large k if a

cut-off was used. Likewise for diagram (a) of figure 2.8, there are four powers of the loop momentum k in both the numerator and denominator which leads to divergence in the form of a pole. It is useful to find a way of obtaining the degree of divergence of any graph for an arbitrary theory without performing any computation.

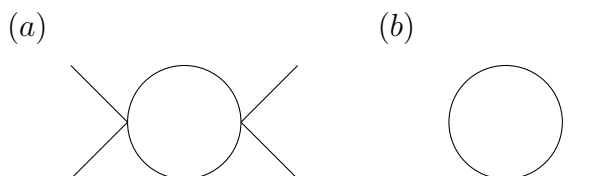


Figure 2.8: Two of the one loop divergent diagrams contained in ϕ^4 theory in four dimensions.

Consider a diagram containing n vertices, E external lines, I internal lines and L loops in d space-time dimensions. The superficial degree of divergence \mathcal{D} of this diagram is given by, [116],

$$\mathcal{D} = dL - 2I. \quad (2.18)$$

The diagrams in figure 2.8 have superficial degree of divergence $\mathcal{D} = 2$ and $\mathcal{D} = 0$ respectively, reflecting quadratic and logarithmic divergences. We can write \mathcal{D} in a different way by noting that there are I internal momenta and the momentum is conserved at each vertex n . Also as we have overall momentum conservation there are $n - 1$ relations between the momenta. Hence the number of independent momenta is $I - n + 1$ which is equal to the number of loops in the diagram. In ϕ^4 theory each vertex has four legs, so there are $4n$ legs overall. However the internal ones are counted twice because they are connected to two vertices, therefore $4n = E + 2I$. Putting all of this together one can rewrite the degree of divergences as, [116],

$$\mathcal{D} = d - \left(\frac{d}{2} - 1\right)E + n(d - 4). \quad (2.19)$$

In four dimensions one has $D = 4 - E$ which shows that the degree of divergence depends on the number of external lines only not on the order in perturbation theory. Therefore a diagram with a greater number of external legs will be more likely to converge. The analogous formula for ϕ^r theory is given by, [116],

$$\mathcal{D} = d - \left(\frac{d}{2} - 1\right)E + n\left[\frac{r}{2}(d - 2) - d\right], \quad (2.20)$$

and in four dimensions we have $\mathcal{D} = 4 - E + n(r - 4)$. According to Weinberg's theorem, [127], a Feynman diagram converges if its degree of divergence \mathcal{D} , to-

gether with the degree of divergence of all its sub-graphs, is negative. We shall not prove this here, however a full proof is given in [116].

The degree of divergence can also be looked at from the point of view of the dimensionality of the fields. For the action of a theory to remain dimensionless we require the dimension of the Lagrangian to be equal to the dimension the theory exists in. More specifically, $[L] = +d$, which means each term in the Lagrangian must have mass dimension d . Examining the dimensionality of a general kinetic term, $\partial^\mu \phi \partial_\mu \phi$, determines the dimension of the field,

$$[\phi] = \frac{d}{2} - 1 .$$

Similarly if we have an interaction term $g\phi^r$, then the dimension of the coupling must be

$$[g] = d + r - \frac{rd}{2} .$$

These are the canonical, engineering or classical dimensions. In ϕ^4 theory for example the coupling will have the canonical dimension $[g] = 4 - d$. In quantum field theory the dimensions of the field and other parameters will not be the canonical values, they will also develop anomalous dimensions through quantum corrections. We will return to this in depth later. Inserting the dimensions of the field and coupling into equation (2.20) we can eliminate r ,

$$\mathcal{D} = d - \left(\frac{d}{2} - 1 \right) E - n\delta \quad (2.21)$$

where $\delta = [g]$. Consequently a renormalizable theory must be one whose coupling constant g has a mass dimension greater than or equal to zero. More specifically if

$$\begin{aligned} [g] = 0 &\Rightarrow \text{The theory is renormalizable,} \\ [g] < 0 &\Rightarrow \text{The theory is non-renormalizable,} \\ [g] > 0 &\Rightarrow \text{The theory is super-renormalizable.} \end{aligned}$$

If a theory is super-renormalizable that means not all available counterterms are required to ensure the theory is finite and within these there may only be a finite number of terms in the perturbative expansion. However IR issues may still emerge. Note that in gauge and supersymmetric theories these internal symmetries may reduce the overall degree of divergence. For ϕ^4 theory one can look at the nature of the divergences more explicitly. That is, if we define $\Delta =$

$d - 4$, then

$$\begin{aligned}\Delta = 0 &\Rightarrow \text{Logarithmic divergences in the theory,} \\ \Delta > 0 &\Rightarrow \text{Quadratic divergences in the theory,} \\ \Delta < 0 &\Rightarrow \text{Finite theory.}\end{aligned}$$

2.2 The Renormalization Group

A regularised and renormalized quantum field theory will be finite provided the theory is renormalizable. Notably an arbitrary fictitious scale μ has been introduced as a consequence of the need to regularise divergences. Ultimately physical predictions cannot depend on this scale. The theory of the Renormalization Group postulates that one can change the arbitrary scale μ of the theory in such a way that the physics on energy scales below μ remains unchanged. In other words a theory must be RG invariant. In order for that to be possible the coupling must change with μ . The action at a particular energy scale is known as the Wilsonian effective action $S[\phi; \mu, g_i]$, and a key Renormalization Group equation which illustrates this point is given by, [117],

$$S[Z(\mu)^{1/2}\phi; \mu, g_i(\mu)] = S[Z(\mu')^{1/2}\phi; \mu', g_i(\mu')]. \quad (2.22)$$

If one assumes the n -point Green's function has been renormalized, that is,

$$\Gamma_{(n)}(p_i) = \langle \phi(p_1) \dots \phi(p_n) \rangle.$$

Then the bare Green's function is denoted by

$$\Gamma_{0(n)}(p_i) = \langle \phi_0(p_1) \dots \phi_0(p_n) \rangle.$$

As the bare Green's function is independent of the arbitrary energy scale μ it must be the case that

$$\mu \frac{d}{d\mu} \Gamma_{0(n)}(p_i) = 0. \quad (2.23)$$

The renormalized and bare Green's functions are not unconnected as the bare parameters can be rescaled to the renormalized versions via the renormalization constants. Specifically for the n -point Green's function we have $\Gamma_{0(n)}(p_i) = Z_\phi^{n/2} \Gamma_{(n)}(p_i)$, which after differentiating with respect to μ becomes

$$0 = \mu \frac{d}{d\mu} \left(Z_\phi^{n/2} \Gamma_{(n)} \right). \quad (2.24)$$

The renormalization constant Z_ϕ and the renormalized Green's function $\Gamma_{(n)}(p_i)$ both depend on μ implicitly and explicitly. The reason being that the coupling constant depends on μ as it is rescaled from the bare coupling. The renormalized or running coupling $g(\mu)$ is not the physical coupling but can be related to it. Additionally the renormalized mass becomes a running mass, $m(\mu)$ which is also not a physical mass. Therefore as $\Gamma_{(n)} = \Gamma_{(n)}(p_i, \mu, g(\mu), m(\mu))$ the chain rule can be applied to equation (2.24),

$$0 = \left[\mu \frac{\partial}{\partial \mu} + \mu \frac{\partial g}{\partial \mu} \frac{\partial}{\partial g} + \frac{n}{2} Z_\phi^{-1} \mu \frac{\partial Z_\phi}{\partial \mu} + \mu \frac{\partial m}{\partial \mu} \frac{\partial}{\partial m} \right] \Gamma_{(n)}(p_i). \quad (2.25)$$

This is known as the Callan-Symanzik equation which can be used to define the Renormalization Group functions.

More specifically one can define the β -function, mass anomalous dimension and wave-function anomalous dimension,

$$\begin{aligned} \beta(g) &= \mu \frac{\partial g}{\partial \mu}, \\ \gamma_m(g) &= \frac{\mu}{m} \frac{\partial m}{\partial \mu}, \\ \gamma_\phi(g) &= \mu \frac{\partial(\ln Z_\phi)}{\partial \mu}. \end{aligned} \quad (2.26)$$

The β -function is a fundamental object that is well defined but is derived from the renormalization constant Z_g which is divergent. The anomalous dimensions are a measure of the quantum corrections to the dimension of an object. Usually they are small numerically but in certain instances they can be large enough to shift the overall dimension to an integer different from the canonical one. Hence a new theory is obtained. Equally an operator can gain a large anomalous dimension and become relevant in a different dimension. This is related to effective field theories where, for example, a six dimensional operator is relevant in four dimensions. Inserting these RG functions into equation (2.25) one finds

$$0 = \left[\mu \frac{\partial}{\partial \mu} + \beta(g) \frac{\partial}{\partial g} + \gamma_m(g) m \frac{\partial}{\partial m} + \frac{n}{2} \gamma_\phi(g) \right] \Gamma_{(n)}(p_i). \quad (2.27)$$

The Renormalization Group functions are scheme dependent as they are derived from the renormalization constants which undoubtedly depend on the scheme. Note that in a gauge theory the RG functions will also be gauge dependent in the sense that they depend on a gauge parameter. The explicit form of the running

coupling $g(\mu)$ can be found using the one loop β -function

$$\beta(g) = \mu \frac{\partial g(\mu)}{\partial \mu} = (d-4)g + Ag^2 \quad (2.28)$$

where A is some constant. In four dimensions the first term vanishes and the differential equation can be solved,

$$g(\mu) = - \frac{1}{A \ln(\frac{\mu}{\Lambda})} . \quad (2.29)$$

This is the explicit form of the running coupling at one loop where Λ is the constant of integration known as the Λ -parameter. This presents a problem at $\mu = \Lambda$ which is known as the Landau pole. Important properties can be deduced from the one loop value of the running coupling. For example, if $A < 0$ then at high energy ($\mu \rightarrow \infty$) the coupling will tend to zero. This is known as asymptotic freedom and implies that at sufficiently high energy the theory is effectively free. Asymptotic freedom is an important characteristic of Quantum Chromodynamics. Alternatively if $A > 0$ then at low energy ($\mu \rightarrow 0$) the coupling will decrease. This property is present in Quantum Chromodynamics and is known as confinement.

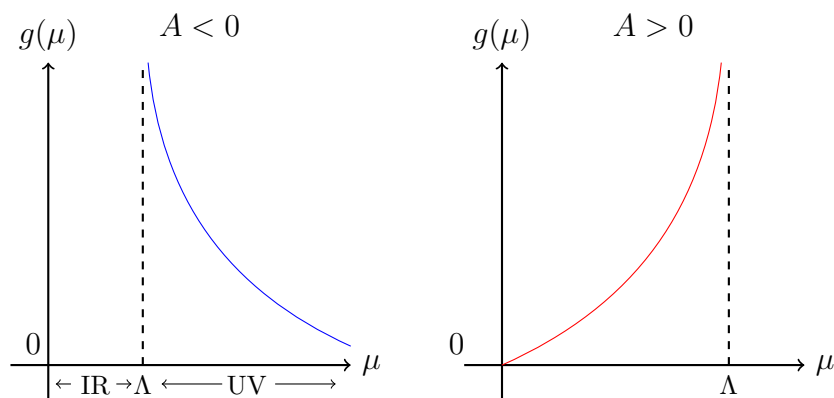


Figure 2.9: Renormalization flow for the one loop running coupling $g(\mu)$ for $A < 0$ (left) and $A > 0$ (right).

For the graph of $A < 0$ in figure 2.9 it is clear to see that for large energy perturbation theory is valid but as μ decreases the coupling increases to a value before $\mu = \Lambda$ where perturbation theory is no longer credible. The scale Λ is a fundamental scale and in QCD is denoted by Λ_{QCD} . The value of Λ_{QCD} quantifies where perturbation theory breaks down and is dependent on quark and colour numbers. It also distinguishes between IR and UV parts of the theory and is a non-perturbative quantity. As the running coupling is scheme dependent this means that Λ is also scheme dependent, however the values of Λ in different schemes are related exactly by a one loop calculation. If we take a higher order

of the β -function there will be corrections to the value of the running coupling. Consider now the scheme dependence of the β -function. Assume we have two β -functions defined in different renormalization schemes and given by

$$\beta(g) = \mu \frac{\partial g}{\partial \mu} \quad , \quad \bar{\beta}(\bar{g}) = \mu \frac{\partial \bar{g}}{\partial \mu}$$

where $\beta(g) = Ag^2 + Bg^3$ and $\bar{\beta}(\bar{g}) = \bar{A}\bar{g}^2 + \bar{B}\bar{g}^3$, to two loops. Assume that the couplings are related by constants, $\bar{g}(g) = g + Xg^2$. Using some simple algebra one can obtain $\bar{\beta}(\bar{g})$ as a function of A and B ,

$$\begin{aligned} \bar{\beta}(\bar{g}) &= \mu \frac{\partial \bar{g}}{\partial \mu} = \beta(g) \frac{\partial \bar{g}}{\partial g} \\ &= (Ag^2 + Bg^3)(1 + 2Xg) = Ag^2 + g^3(B + 2XA) . \end{aligned}$$

As we know that $g = \bar{g} - X\bar{g}^2$, then

$$\begin{aligned} \bar{\beta}(\bar{g}) &= A(\bar{g}^2 - 2X\bar{g}^3) + (B + 2XA)\bar{g}^3 + O(\bar{g}^4) \\ &= A\bar{g}^2 + B\bar{g}^3 + O(\bar{g}^4) , \end{aligned}$$

therefore $A = \bar{A}$ and $B = \bar{B}$. This proves to two loops the coefficients of the β -function are scheme independent in a single coupling theory. In multi-coupling theories the β -function will only be scheme independent at leading order. In general the leading order term of any RG function will be scheme independent. Note that this does not always mean the one loop term. For example, the wavefunction anomalous dimension γ_ϕ of ϕ^4 theory has a leading order term at two loops. Additionally in gauge theories the β -function is independent of the gauge in a mass independent renormalization scheme such as $\overline{\text{MS}}$. However in general the β -function is gauge dependent and hence the running coupling is gauge dependent in principle.

An important property of the β -function is the existence of fixed points. That is, values of the coupling g^* for which the β -function vanishes

$$\beta(g^*) = 0 . \tag{2.30}$$

Fixed points underlie phase transitions. The trivial fixed point $g^* = 0$ is known as the Gaussian fixed point and describes the free field theory. Non-trivial fixed point may also exist. The d -dimensional non-trivial fixed point closest to the origin is known as the Wilson-Fisher fixed point, [41], the location of which is refined by calculating to a higher loop order. In practice adding more loops will

move $g^* \neq 0$ closer and closer to the origin. Theories at fixed points are special because as well as only having massless state particles they have no dimensionful parameters at all. In other words they are scale invariant. The existence of a non-trivial fixed point requires conditions on the perturbative β -function. If the β -function has the form $\beta(g) = Ag^2 + Bg^3$, then the constants A and B must have opposite signs for the non-trivial fixed point to exist. Moreover the fixed point must have a positive value, $g^* = -A/B > 0$. In QCD the values of A and B have opposite signs for $9 \leq N_f \leq 16$. This range is known as the two loop conformal window and is defined as the number of quark flavours N_f where the non-trivial fixed point exists. The non-trivial fixed point of QCD is known as the Banks-Zaks fixed point, [88]. The range of the conformal window can be studied perturbatively with a high loop order used to pinpoint the exact location of the boundaries.

The Renormalization Group flow is a significant aspect of any renormalizable theory, the value of the coupling in the UV and IR limits are of great interest as theorists strive to understand how theories behave at very high and low energies. A toy model containing a non-trivial fixed point is illustrated in figure 2.10. Arrows indicate the UV Renormalization Group flow as $\mu \rightarrow \infty$ which is known as the UV flow. Reversing the direction of the arrows produces an IR Renormalization Group flow. From the diagram one can conclude that for $g < g^* \neq 0$ the flow is away from the non-trivial fixed point towards the Gaussian fixed point. Hence the trivial fixed point is UV stable. Consequently the non-trivial fixed point is UV unstable and hence IR stable. The stability of a fixed point can also be established by examining the eigenvalues of the associated stability matrix \mathcal{S} evaluated at the fixed point

$$\mathcal{S} = \left. \frac{\partial \beta_i(g_j)}{\partial g_j} \right|_{g=g^*}. \quad (2.31)$$

Here $\beta_i(g_j)$ are a set of β -functions where $1 \leq i, j \leq N_{cc}$ where N_{cc} is the number of coupling constants present in the theory. Positive eigenvalues signify an unstable fixed point while stability is indicated by negative values of the stability matrix. A mixed signal suggests that we have a saddle point.

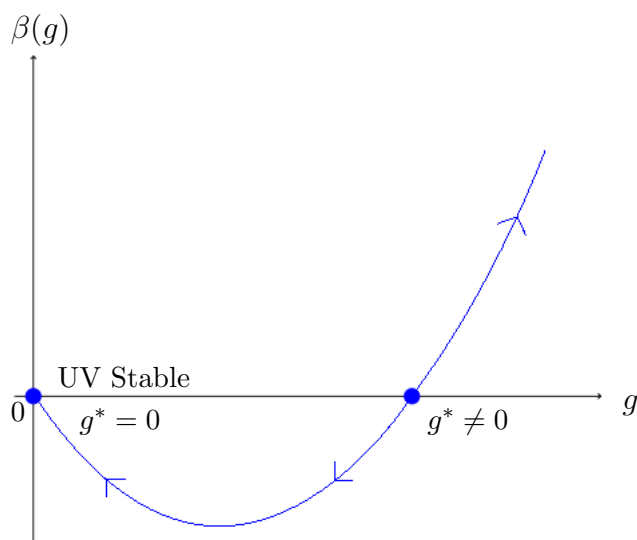


Figure 2.10: The ultraviolet Renormalization Group flow for a toy β -function with a non-trivial fixed point.

2.2.1 Critical Exponents and Universality

To understand what critical exponents mean for quantum field theory, we first look at how they are derived in statistical physics. Critical exponents describe the behaviour of physical quantities near continuous phase transitions. A continuous, or second order, phase transition is a change of phase in a macroscopic system in equilibrium not accompanied by latent heat. By latent heat we mean the heat required to convert a solid into a liquid or vapour, or a liquid into a vapour, without a change of temperature. Phase transitions that do involve latent heat, like the freezing of water, will be called first order or discontinuous. An example of a second-order phase transition is the ferromagnetic transition known as the ‘Ising model’, [119]. Analogous to fixed points in QFT, a critical point is a position in the phase diagram where a continuous phase transition takes place. Two immediate questions arise. Why study continuous phase transitions when most changes in Nature are discontinuous? Moreover, if the critical point is a continuous phase transition, why is this a point of interest?

The answer to both of these questions lies in the phenomenon of universality which states that properties of a system near the critical point appear to be the same for completely different physical systems. This implies, for example, that the specific heat near the liquid-gas critical point may behave the same way as the specific heat near the paramagnet-ferromagnet phase transition in an otherwise entirely different magnetic system. In other words macroscopic properties of a system near a continuous phase transition thus appear to be rather inde-

pendent of the microscopic interactions between particles. They depend only on some broad characteristics of the system, like its dimensionality, symmetry and presence or absence of sufficiently long-ranged interactions. The universality hypothesis is not only intuitive, it has been confirmed in the context of statistical physics by experiment. Moreover this phenomenon of different systems exhibiting the same critical behaviour can be successfully explained by the Renormalization Group, [118, 119].

As an example we consider a ferromagnet which has two external parameters of interest, the temperature T and the applied magnetic field H , [118]. In a ferromagnet there are domains in which the magnetic fields of the individual atoms align, but the orientation of the magnetic fields of the domains is random. When an external magnetic field is applied to a ferromagnet, the magnetic fields of the individual domains tend to line up in the direction of the external field. Local magnetisation is constrained to lie parallel or anti-parallel to a particular axis. Below the Curie temperature T_c , neighbouring magnetic spins align in a ferromagnet in the absence of an applied magnetic field. Above the Curie temperature the magnetic spins are randomly aligned in a paramagnet unless a magnetic field is applied. The values $H = 0$ and $T = T_c$ together give a critical point at which the first order transition becomes continuous, [119]. Quantities of interest exhibit power law behaviour sufficiently close to the critical point from which critical exponents can be found. Power laws near the critical point can be derived from the assumption of scaling. If we define the reduced temperature $t = (T - T_c)/T_c$, and the reduced external magnetic field $h = H/(k_B T_c)$ where k_B is the Boltzmann constant, the critical exponents can be defined as follows. The critical exponent α is derived from the power law involving specific heat C in a zero field, [118],

$$C \sim A|t|^{-\alpha}$$

where A is the amplitude. Additionally more exponents can be derived from power laws involving the zero field susceptibility χ , magnetisation M and the correlation length ξ , respectively. They are, [118],

$$\begin{aligned} \chi &\equiv \left. \frac{\partial M}{\partial H} \right|_{H=0} \propto |t|^{-\gamma}, \\ M &\propto |h|^{1/\delta}, \\ \xi &\propto |t|^{-\nu}. \end{aligned}$$

There are of course more exponents and some can be related via hyper-scaling relations. The values of α , γ , δ and ν are non-trivial and are not completely

independent numbers, they are however universal. Known as the ‘Ising’ exponents, they are the same for a whole class of various phase transitions not just the ferromagnet transition.

In quantum field theory the critical exponents have the same universal properties but are instead calculated using the RG functions. For example, the exponent η is found by evaluating the anomalous dimension of the field at the non-trivial fixed point

$$\gamma_\phi(g^*) = \eta . \quad (2.32)$$

At different non-trivial fixed points the anomalous dimension takes different values. Additionally the first derivative of the β -function evaluated at the non-trivial fixed point gives a measure of corrections to scaling via the exponent ω ,

$$\beta'(g^*) = \omega . \quad (2.33)$$

Critical exponents can also be obtained using hyper-scaling relations. In gauge theories critical exponents can be used to understand properties of the theory. For example, the quark mass anomalous dimension in QCD evaluated at the non-trivial fixed point is a measure of chiral symmetry breaking. Note that the underlying phase transition propagator in coordinate space behaves as

$$\langle \phi(x)\phi(y) \rangle \sim \frac{1}{((x-y)^2)^{d/2-1+\eta}} \quad (2.34)$$

with the exponent clearly present. Critical exponents are Renormalization Group invariants as they are physical quantities. In other words the value of critical exponent will be scheme independent. Two quantum field theories are said to be in the same universality class if they share a common non-trivial fixed point, which gives identical values when used to evaluate the critical exponents of each theory.

2.2.2 Relation Between RG Functions and Renormalization Constants

Once all Green’s functions have been computed and renormalized we want to find a way of perturbatively calculating the Renormalization Group functions. The β -function can then be used, for example, to analyse the fixed point properties and UV or IR behaviour of a theory. As it turns out, the RG functions can be deduced using relations that involve the renormalization constants. We detail the derivation of these relations here. To begin we take a massless single coupling theory with coupling constant g and field ϕ . Once all Feynman diagrams

have been computed the n -point Green's functions are summed together. IR divergences that may arise are only a problem if one considers diagrams on an individual level. By summing together graphs the IR singularities naturally cancel. We can therefore focus on potential UV divergences which can be renormalized. In essence each Feynman diagram has been computed as a function of the bare parameters. The Green's functions can be rescaled using the renormalization constants for the field and coupling given in (2.10). Associated counterterms absorb the UV divergences at a particular loop order. By summing together graphs before introducing counterterms we bypass the need to carry out subtractions on each individual diagram which can be tedious.

Once the values of the counterterms are known they can be inserted into relations involving the RG functions. The relation for the β -function can be derived by taking the equation of the bare coupling constant in (2.10) and differentiating with respect to μ . The left-hand side will be zero as g_0 is a bare parameter. The right-hand side is slightly more complicated as each parameter must be differentiated in turn,

$$0 = \frac{\epsilon}{2}g(\mu) + \beta(g) + \beta(g)\frac{\partial}{\partial g} \ln Z_g(g) . \quad (2.35)$$

As the renormalization constants have been defined in the renormalization process their values can be inserted order by order into the above equation to establish the β -function. Deriving the relation for the γ -function is as straightforward, with the definition of the γ -function in equation (2.26) differentiated with respect to μ ,

$$\gamma_\phi(g) = \beta(g)\frac{\partial}{\partial g} \ln Z_\phi . \quad (2.36)$$

Again this can be solved order by order for the anomalous dimension of the field by substituting in values for the renormalization constant of the field ϕ . Note that this relation has been derived with the assumption that no gauge or mass parameter is present.

Multi-coupling theories are more complicated and we derive the relations for a two coupling theory here as it will be needed later. Assume we have a theory with two couplings, g_1 and g_2 , and two scalar fields, ϕ_1 and ϕ_2 . Once again the theory will be massless and will not contain a gauge parameter. The bare parameters are rescaled as follows,

$$\begin{aligned} \phi_{10} &= \sqrt{Z_{\phi_1}}\phi_1 , \\ \phi_{20} &= \sqrt{Z_{\phi_2}}\phi_2 , \end{aligned}$$

$$g_{i0} = Z_{g_i}(g_1, g_2)g_i(\mu)\mu^\epsilon . \quad (2.37)$$

It is easy to see where the main difficulty in working with a multi-coupling theory arises. As the renormalization constant Z_g can depend on both couplings, the relations for the β -functions will be more involved. To make things simpler the renormalization constant for the coupling can be redefined,

$$Z_{g_i\text{def}} = Z_{g_i}(g_1, g_2)g_i(\mu) \quad (2.38)$$

where $i = 1, 2$ so that the third definition in (2.37) becomes

$$g_{i0} = Z_{g_i\text{def}}(g_1, g_2)\mu^\epsilon . \quad (2.39)$$

We take the same path as in the single coupling theory and differentiate both sides of equation (2.39) with respect to μ . Initially we take $i = 1$,

$$0 = \frac{\epsilon}{2}Z_{g_1\text{def}} + \beta_j(g_j)\frac{\partial}{\partial g_j}Z_{g_1\text{def}}(g_1, g_2) \quad (2.40)$$

where there is a summation over $j = 1, 2$. Differentiating (2.39) again this time with $i = 2$ produces a similar second relation. Therefore we are left with two equations that can be solved simultaneously order by order to find the β -functions $\beta_1(g_1, g_2)$ and $\beta_2(g_1, g_2)$,

$$\begin{aligned} 0 &= \frac{\epsilon}{2}Z_{g_1\text{def}} + \beta_1\frac{\partial}{\partial g_1}Z_{g_1\text{def}} + \beta_2\frac{\partial}{\partial g_2}Z_{g_1\text{def}} , \\ 0 &= \frac{\epsilon}{2}Z_{g_2\text{def}} + \beta_1\frac{\partial}{\partial g_1}Z_{g_2\text{def}} + \beta_2\frac{\partial}{\partial g_2}Z_{g_2\text{def}} . \end{aligned} \quad (2.41)$$

The derivation for the anomalous dimensions of the fields follows a similar method producing a pair of equations which can be solved order by order using known renormalization constants to find $\gamma_{\phi_1}(g_1, g_2)$ and $\gamma_{\phi_2}(g_1, g_2)$,

$$\begin{aligned} \gamma_{\phi_1}(g_1, g_2) &= \beta_1\frac{\partial}{\partial g_1}\ln Z_{\phi_1} + \beta_2\frac{\partial}{\partial g_2}\ln Z_{\phi_1} , \\ \gamma_{\phi_2}(g_1, g_2) &= \beta_1\frac{\partial}{\partial g_1}\ln Z_{\phi_2} + \beta_2\frac{\partial}{\partial g_2}\ln Z_{\phi_2} . \end{aligned} \quad (2.42)$$

2.3 Computational Methods

The calculation of Feynman diagrams is an intrinsic element of quantum field theory and a process that has been refined and improved over many years. Through-

out this thesis we calculate Feynman graphs and related Renormalization Group functions using many perturbative and other methods. Before discussing original calculations some important computational techniques are introduced. First we discuss conformal integration which can be used in the computation of Feynman diagrams at many loop orders. Importantly the large N expansion is then introduced which is an alternative perturbative expansion to the traditional coupling constant or ϵ -expansion. The large N expansion is one of the most prominent tools used in our calculation of critical exponents.

2.3.1 Conformal Integration

In renormalizing ϕ^4 theory we considered massless Feynman diagrams to be in momentum space with integration variables corresponding to the momentum circulating around a loop. However it is also possible to describe diagrams in a coordinate space representation. This means that when a Feynman integral is drawn the integration variables are represented as the vertices. Propagators are denoted by lines between two coordinates in coordinate space and the power on the propagator is given by a number or symbol beside the line as is illustrated in figure 2.11.

$$\begin{array}{ccc} \bullet & \xrightarrow{\alpha} & \bullet \\ 0 & & x \end{array} \equiv \frac{1}{((x)^2)^\alpha}$$

$$\begin{array}{ccc} \bullet & \xrightarrow{\alpha} & \bullet \\ x & & y \end{array} \equiv \frac{1}{((x - y)^2)^\alpha}$$

Figure 2.11: Coordinate space propagators.

One can map between coordinate and momentum space representations using a Fourier transformation. Notation and conventions used here were first introduced by Vasil'ev et al. in [47–50] and we follow a similar approach to that summarised in [128]. In Vasil'ev et al. notation the Fourier transform is given by

$$\frac{1}{(x^2)^\alpha} = \frac{a(\alpha)}{2^{2\alpha}\pi^\mu} \int d^d k \frac{e^{ikx}}{(k^2)^{\mu-\alpha}}, \quad (2.43)$$

where x is in coordinate space and k is the conjugate momenta. We use the notation $d = 2\mu$ for presentation purposes, this symbol should not be confused with the mass scale appearing in dimensional regularisation. Additionally we introduce the function

$$a(\alpha) = \frac{\Gamma(\mu - \alpha)}{\Gamma(\alpha)} \quad (2.44)$$

which is singular when $\alpha = \mu + n$ and n is zero or any positive integer. Properties of the function $a(\alpha)$ can be derived such as

$$\begin{aligned} a(\alpha)a(\mu - \alpha) &= 1, \\ a(\alpha) &= \frac{a(\alpha - 1)}{(\alpha - 1)(\mu - \alpha)}, \\ a(\alpha) &= \alpha(\mu - \alpha - 1)a(\alpha + 1), \end{aligned} \quad (2.45)$$

which will prove invaluable when conformally integrating. The proof of the third identity is established by first multiplying the numerator and denominator of the function $a(\alpha)$ by α and $\mu - \alpha - 1$,

$$a(\alpha) = \frac{\Gamma(\mu - \alpha)}{\Gamma(\alpha)} = \frac{\alpha\Gamma(\mu - \alpha)(\mu - \alpha - 1)}{\alpha\Gamma(\alpha)(\mu - \alpha - 1)}.$$

The Γ -function identity $\Gamma(z + 1) = z\Gamma(z)$ can then be used to complete the proof,

$$a(\alpha) = \frac{\alpha\Gamma(\mu - \alpha - 1)(\mu - \alpha - 1)}{\Gamma(\alpha + 1)} = \alpha(\mu - \alpha - 1)a(\alpha + 1).$$

Using Vasil'ev et al. conformal notation the elementary one loop self-energy diagram in momentum space can be replaced by a graph in coordinate space. See figure 2.12.

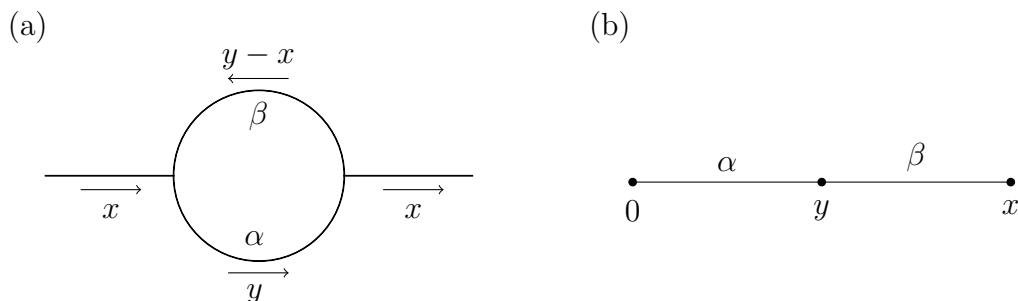


Figure 2.12: One loop self-energy diagram in (a) momentum space representation and (b) coordinate space representation.

The power on each propagator has also been labelled in the momentum space diagram as they are assumed to be arbitrary. This diagram can be evaluated in coordinate space using the relation in figure 2.13.

$$\begin{array}{c} \bullet \\ 0 \end{array} \xrightarrow{\alpha} \begin{array}{c} \bullet \\ y \end{array} \xrightarrow{\beta} \begin{array}{c} \bullet \\ x \end{array} = \nu(\alpha, \beta, 2\mu - \alpha - \beta) \begin{array}{c} \bullet \\ 0 \end{array} \xrightarrow{\alpha + \beta - \mu} \begin{array}{c} \bullet \\ x \end{array}$$

Figure 2.13: Conformal integration applied to the one loop self-energy Feynman diagram.

The large boldfaced dot indicates the point at which one performs the conformal integration. In this case we are integrating over the y variable. The notation $\nu(\alpha, \beta, \gamma) = \pi^\mu a(\alpha)a(\beta)a(\gamma)$ has also been implemented. For the proof of figure 2.13 one first notes that the Feynman diagram can be written as the following integral,

$$\mathfrak{J}_c = \int \frac{d^d y}{(2\pi)^d} \frac{1}{(y^2)^\alpha ((x-y)^2)^\beta}, \quad (2.46)$$

which can be rewritten using Feynman parameters

$$\mathfrak{J}_c = \int_0^1 \int_y \frac{u^{\beta-1} (1-u)^{\alpha-1} du}{[u(y-x)^2 + (1-u)y^2]^{\alpha+\beta}} \frac{\Gamma(\alpha+\beta)}{\Gamma(\alpha)\Gamma(\beta)}.$$

The expression has been simplified using the notation

$$\int_y = \int \frac{d^d y}{(2\pi)^d}.$$

The integral can be rearranged by expanding out the denominator and completing the square,

$$\mathfrak{J}_c = \int_0^1 \int_y \frac{u^{\beta-1} (1-u)^{\alpha-1} du}{[(y-ux)^2 + u(1-u)x^2]^{\alpha+\beta}} \frac{\Gamma(\alpha+\beta)}{\Gamma(\alpha)\Gamma(\beta)}.$$

The Lorentz transformation, $y \rightarrow y - ux$, can then be taken as $d^d y$ is Lorentz invariant,

$$\mathfrak{J}_c = \frac{\Gamma(\alpha+\beta)}{\Gamma(\alpha)\Gamma(\beta)} \int_0^1 \int_y \frac{u^{\beta-1} (1-u)^{\alpha-1} du}{[y^2 + u(1-u)x^2]^{\alpha+\beta}}.$$

Applying identity (2.6) the integration over the y variable can be completed

$$\mathfrak{J}_c = \frac{\Gamma(\alpha+\beta)\Gamma(\alpha+\beta-\frac{d}{2})}{\Gamma(\alpha)\Gamma(\beta)\Gamma(\alpha+\beta)(4\pi)^{d/2}} \int_0^1 (u(1-u)x^2)^{\frac{d}{2}-\alpha-\beta} u^{\beta-1} (1-u)^{\alpha-1} du.$$

The integral can then be simplified by collecting terms and integrating with respect to u using the Euler β -function. We obtain

$$\begin{aligned} \mathfrak{J}_c &= \frac{\Gamma(\alpha+\beta-\mu)}{\Gamma(\alpha)\Gamma(\beta)} \frac{\Gamma(\mu-\alpha)\Gamma(\mu-\beta)}{\Gamma(2\mu-\alpha-\beta)} \frac{1}{(x^2)^{\alpha+\beta-\mu}} \\ &= \nu(\alpha, \beta, 2\mu-\alpha-\beta) \frac{1}{(x^2)^{\alpha+\beta-\mu}}, \end{aligned}$$

as represented in figure 2.13. In practice Feynman diagrams have more complicated integration points as the coordinate space representation will have more than two lines intersecting at a point. Therefore more involved integration techniques are needed to evaluate these Feynman graphs.

A useful tool in conformal integration is the property of uniqueness. This approach was first introduced in three dimensions, [129], and later developed for d -dimensions, [134]. Uniqueness allows conformal integration at an integration point with three intersecting lines, see figure 2.14. Note that the point of integration has again been indicated by a boldfaced dot. For clarity, the one loop Feynman diagram is illustrated in coordinate space on the left-hand side of figure 2.14 and has been represented in momentum space in figure 2.15.

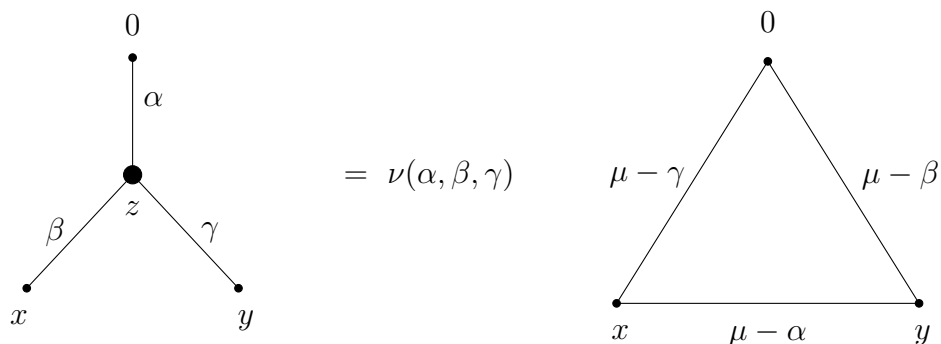


Figure 2.14: Coordinate representation of conformal integration using the uniqueness condition where z is the integration variable.

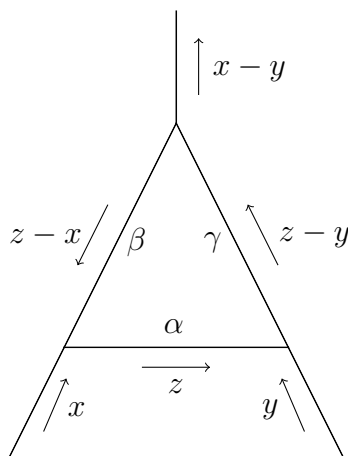


Figure 2.15: Momentum representation of the one loop Feynman diagram, \mathfrak{J}_d , that is conformally integrated in coordinate space in figure 2.14.

The derivation of figure 2.14 is given by [48–50] and we briefly cover the main points here. The Feynman diagram on the left-hand side of figure 2.14 can be written as a one loop Feynman integral

$$\mathfrak{J}_d = \int \frac{d^d z}{(z^2)^\alpha ((z-x)^2)^\beta ((z-y)^2)^\gamma}. \quad (2.47)$$

The first step is to apply conformal transformations which change the integration

coordinates as well as the external points through

$$x_\mu \rightarrow \frac{x_\mu}{x^2} \quad , \quad y_\mu \rightarrow \frac{y_\mu}{y^2} \quad , \quad z_\mu \rightarrow \frac{z_\mu}{z^2} . \quad (2.48)$$

The integration measure via the Jacobian also produces contributions to the lines joining the origin since

$$d^d z \rightarrow \frac{d^d z}{(z^2)^d} .$$

From the conformal transformations we also note the following relations

$$\begin{aligned} (z-x)^2 &\rightarrow \frac{(z-x)^2}{x^2 z^2} , \\ (z-y)^2 &\rightarrow \frac{(z-y)^2}{y^2 z^2} . \end{aligned}$$

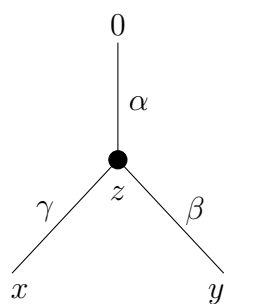
Applying the conformal transformation to the one loop Feynman integral one finds

$$\mathfrak{J}_d = \int \frac{(x^2 z^2)^\beta (y^2 z^2)^\gamma}{(z-x)^{2\beta} (z-y)^{2\gamma}} z^{2\alpha} \frac{d^d z}{(z^2)^d} .$$

The integral can be rearranged by grouping terms together

$$\mathfrak{J}_d = (x^2)^\beta (y^2)^\gamma \int \frac{(z^2)^{\alpha+\beta+\gamma-d}}{((z-x)^2)^\beta ((z-y)^2)^\gamma} d^d z . \quad (2.49)$$

If $\alpha + \beta + \gamma = d$ or $d + n$ where n is some positive integer, then the integral can be computed. For $n = 0$ this condition is called uniqueness and so many steps from uniqueness if $n > 0$.



The diagram shows a central black dot representing a vertex. Four lines extend from this vertex: a vertical line upwards to a point labeled '0', a line downwards and to the left to a point labeled 'x', a line downwards and to the right to a point labeled 'y', and a line extending downwards to a point labeled 'z'. The line to '0' is labeled with the Greek letter alpha (α). The line to 'x' is labeled with the Greek letter gamma (γ). The line to 'y' is labeled with the Greek letter beta (β). The line to 'z' is labeled with the expression alpha + beta + gamma = d. To the right of the diagram, the integral expression from equation (2.49) is shown:
$$= (x^2)^\beta (y^2)^\gamma \int \frac{d^d z}{((z-x)^2)^\beta ((z-y)^2)^\gamma}$$

Figure 2.16: The uniqueness condition, $\alpha + \beta + \gamma = d$, applied to the Feynman integral (2.49).

The simplified integral on the right-hand side of figure 2.16 can be conformally integrated using the identity given in figure 2.13 with z as the integration variable,

$$\mathfrak{J}_d = \frac{(x^2)^\beta (y^2)^\gamma \nu(\beta, \gamma, 2\mu - \beta - \gamma)}{((x-y)^2)^{\beta+\gamma-\mu}} .$$

Using the uniqueness rule we have $\beta + \gamma - \mu = \mu - \alpha$. Hence

$$\mathfrak{J}_d = \frac{(x^2)^\beta (y^2)^\gamma \nu(\beta, \gamma, \alpha)}{((x - y)^2)^{\mu - \alpha}}. \quad (2.50)$$

The original conformal transformation can be undone and the variables rearranged into the same form as figure 2.14,

$$\mathfrak{J}_d = \frac{\nu(\alpha, \beta, \gamma)}{(x^2)^{\mu - \gamma} (y^2)^{\mu - \beta} (z^2)^{\mu - \alpha}}. \quad (2.51)$$

Here we have rearranged $\nu(\alpha, \beta, \gamma)$ as it is completely symmetric. The natural extension to this rule with $\alpha + \beta + \gamma = d + 1$ has been proven in [130–134].

2.3.2 The Large N Expansion

The large N expansion is a perturbative expansion in $1/N$ analogous to the traditional coupling or ϵ -expansion. In a scalar theory the parameter N is given by the number of scalar fields and is always assumed to be large. Although its roots can be traced back earlier, we introduce here the fixed point large N expansion developed in the 1980s by Vasil'ev et al. in a series of papers, [47–50]. The large N expansion was first used to calculate critical exponents of the nonlinear sigma model (NL σ M) to several orders. In later years it was applied to the Gross-Neveu model, [135–142] and has become an important tool for perturbative quantum field theory ever since. The main difference between the large N and ϵ -expansion is that critical exponents expanded in $1/N$ will be calculated at criticality in an arbitrary dimension of space. Whereas in the ϵ -expansion the exponents will necessarily depend on the dimension via ϵ , as $2\epsilon = D_c - d$ where D_c is the critical dimension in which the theory exists.

An important application of the large N expansion is its ability to verify if theories lie in a universality class or not. As early as 1976 theorists began studying universality classes that spanned several dimensions. That is, looking at several theories that lie in the same universality class but individually exist in different dimensions. The theories will share a d -dimensional Wilson-Fisher fixed point and their critical exponents will be identical at this fixed point. The critical exponents of a theory that may or may not lie in the universality class can be computed using the ϵ -expansion. Knowledge of the exponents in d -dimensions via the large N expansion enables us to compare values of the ϵ -expansion exponents with these d -dimensional exponents set in that specific critical dimension order by order. Complete agreement of the two expansions confirms that the

theory does exist in the universality class. The explanation behind this lies in the fact that critical exponents corresponding to RG functions are calculated at non-trivial fixed points where there is scale invariance. Therefore information on RG functions is encoded in the critical exponents.

To illustrate how the large N expansion works in practice we calculate the critical exponents η and χ of the $O(N)$ universality class at leading order. The $O(N)$ universality class is well studied and contains not only the NL σ M which is renormalizable in two dimensions but also four dimensional ϕ^4 theory with an $O(N)$ symmetry. This calculation was first published in work by Vasil'ev et al., [47–50], which we follow here closely. More detail and background information is provided for the benefit of the reader and to clarify certain techniques used. The NL σ M is important as it gives a 2-dimensional expansion with which one can study the Wilson-Fisher fixed point of the $O(N)$ universality class. The Lagrangian for the NL σ M is

$$L^{\text{NL}\sigma\text{M}} = \frac{1}{2}g_{ab}(\phi)\partial_\mu\phi^a\partial^\mu\phi^b, \quad (2.52)$$

where $1 \leq a \leq (N-1)$ and $g_{ab}(\phi)$ is a metric of the sphere in the chosen coordinate system. The Lagrangian is invariant under the $O(N)$ symmetry group and can be rewritten by introducing a Lagrange multiplier

$$L^{\text{NL}\sigma\text{M}} = \frac{1}{2}(\partial\phi^i)^2 + \frac{\sigma}{2}\phi^i\phi^i - \frac{\sigma}{2\lambda} \quad (2.53)$$

where $1 \leq i \leq N$. The Lagrangian is perturbatively renormalizable in two dimensions and the Lagrange multiplier gives the constraint $\phi^i\phi^i = 1/\lambda$. The parameter λ can be rescaled as follows

$$L^{\text{NL}\sigma\text{M}} = \frac{1}{2}\partial_\mu\phi^i\partial^\mu\phi^i + \frac{1}{2}g\sigma\phi^i\phi^i - \frac{1}{2}\sigma. \quad (2.54)$$

The Lagrange multiplier is necessary in order to restrict the $O(N)$ scalar fields to lie on the N -sphere. Choosing a coordinate system for the constraint that the length of ϕ^i is fixed to be the coupling constant would produce the non-linear version of (2.54) which is (2.52). The canonical or classical dimensions of fields in the NL σ M can be deduced from (2.54) using the dimensionless action which implies $[L] = +d$. Hence

$$[\phi^i] = \frac{d}{2} - 1, \quad [\sigma] = 2. \quad (2.55)$$

The final term of equation (2.54) is unusual as ordinarily one would not have a

linear term in the Lagrangian. Linear terms do not couple to any other field and therefore play no part in the drawing of Feynman diagrams for the theory, this creates a problem as we do want the σ field to propagate. Within large N it will be possible to see this. The diagrammatic technique of the $1/N$ expansion can be readily obtained by inserting kinetic terms for the σ field and rewriting equation (2.54) in the form, [143, 144],

$$L^{\text{NL}\sigma\text{M}} = \frac{1}{2}\partial_\mu\phi^i\partial^\mu\phi^i + \frac{1}{2}\sigma\phi^i\phi^i + \frac{1}{2}\sigma K\sigma - \frac{1}{2}\sigma K\sigma, \quad (2.56)$$

where K^{-1} is the bare propagator of the field σ . The addition of $(1/2)\sigma K\sigma$ is included in the free part of the Lagrangian while the subtraction of the same term is included as an interaction. Therefore the Lagrangian (2.56) can be broken in to two parts,

$$\begin{aligned} L_F^{\text{NL}\sigma\text{M}} &= \frac{1}{2}\partial_\mu\phi^i\partial^\mu\phi^i + \frac{1}{2}\sigma K\sigma, \\ L_I^{\text{NL}\sigma\text{M}} &= \frac{1}{2}\sigma\phi^i\phi^i - \frac{1}{2}\sigma K\sigma \end{aligned}$$

where $L^{\text{NL}\sigma\text{M}} = L_F^{\text{NL}\sigma\text{M}} + L_I^{\text{NL}\sigma\text{M}}$. Note that the Lagrangian has not been changed in any meaningful way as the last two terms of (2.56) will always cancel. The Lagrangian has simply been manipulated to generate a propagating σ field which is produced because the potential of the σ field experiences dynamical symmetry breaking. Hence a dynamical mass for σ is generated through a nonzero vacuum expectation value (VeV) for σ . This mass does not show up in traditional perturbation theory because the new dynamically produced minimum of the effective potential σ_c is non-perturbative. However it can be accessed via the large N expansion. The mass will not impact calculations as it becomes zero at criticality. Dynamical symmetry breaking in the $\text{NL}\sigma\text{M}$ is explained in greater detail in [135, 143].

The large N technique works at the Wilson-Fisher fixed point where there exists a universal theory whose critical properties are defined by the interaction $\sigma\phi^i\phi^i$. At a fixed point the theory is scale invariant and if a QFT is scale invariant then the scaling dimension of the operators are fixed numbers, otherwise they are functions depending on the distance scale. Therefore at criticality all Green's functions have scaling behaviour in the asymptotic limit. This means one can write down critical point propagators of the two fields σ and ϕ^i for the $\text{NL}\sigma\text{M}$ in coordinate space as follows

$$\phi(x-y) \sim \frac{A}{((x-y)^2)^\alpha}, \quad \sigma(x-y) \sim \frac{B}{((x-y)^2)^\beta}. \quad (2.57)$$

The ϕ^i propagator is isotopic in the $O(N)$ indices, the unit matrix has been omitted above for simplicity. The propagating σ field is now consistent and accommodated with the non-perturbative dynamical σ field observed in the traditional large N approach. In other words in the true vacuum of the NL σ M quantum theory there is a bound state of two ϕ^i fields which cannot be observed in perturbative calculations. That bound state has a non-fundamental propagator and can be accessed through the large N expansion. The values A and B are x and y independent amplitudes. There are corrections to scaling which we will ignore for now, instead focusing on the leading order terms. The values of α and β represent the full dimension of the fields and including both the canonical and anomalous part they are

$$\begin{aligned} [\phi^i] &= \alpha = \frac{d}{2} - 1 + \frac{\eta}{2}, \\ [\sigma] &= \beta = 2 - \eta - \chi. \end{aligned} \quad (2.58)$$

The term η gives the anomalous dimension of the ϕ^i field while χ represents the anomalous dimensions of the vertex $\sigma\phi^i\phi^i$. When evaluated at a fixed point they are known as critical exponents,

$$\eta = \gamma_{\phi^i}(g^*) \quad , \quad \chi = \gamma_{\sigma\phi^i\phi^i}(g^*) . \quad (2.59)$$

As the critical exponents are functions of two variables, $\eta = \eta(\epsilon, N)$ and $\chi = \chi(\epsilon, N)$, they can be expanded in powers of ϵ as in traditional perturbation theory, or in the parameter $1/N$ where N is assumed to be large. When calculating critical exponents in the large N expansion one performs the second type of expansion. Hence

$$\eta = \sum_{n=1}^{\infty} \frac{\eta_n(\epsilon)}{N^n} = \frac{\eta_1}{N} + \frac{\eta_2}{N^2} + \frac{\eta_3}{N^3} + \frac{\eta_4}{N^4} + \dots \quad (2.60)$$

where the values $\eta_n(\epsilon)$ are computed in an arbitrary space-time dimension d . Similarly,

$$\chi = \sum_{n=1}^{\infty} \frac{\chi_n(\epsilon)}{N^n} = \frac{\chi_1}{N} + \frac{\chi_2}{N^2} + \frac{\chi_3}{N^3} + \frac{\chi_4}{N^4} + \dots . \quad (2.61)$$

While canonical dimensions can be determined using dimensionality arguments, coefficients η_n and χ_n of the expansions (2.60) and (2.61) are deduced by solving the skeleton Dyson-Schwinger equations at criticality. This exploits the critical RG equations and scaling behaviour of the propagators.

For clarity we summarise the essence of the large N expansion as follows. We

want to calculate the critical exponents of the NL σ M. Instead of perturbatively expanding the RG functions in ϵ where $d = 2 - 2\epsilon$, we can expand in the parameter $1/N$ at criticality. The large N computation of the critical exponents will give values in an arbitrary space-time dimension d . The large N expansion is in effect a way of reordering the Feynman diagrams so that the graphs contributing to the RG functions are treated in an order different from conventional perturbation theory. Before calculating η and χ in the NL σ M we briefly discuss the reordering of a simple toy model. This illustrates more clearly how the large N expansion works in practice.

Assume we have a toy model which has the following β -function

$$\begin{aligned} \beta(g) = & -\epsilon g + [A + N]g^2 + [BN + C]g^3 \\ & + [DN^2 + EN + F]g^4 + O(g^5) \end{aligned} \quad (2.62)$$

where A, B, C, D, E and F are some constants. The β -function is an expansion in the coupling g , however it can be rewritten in a different order. Requiring the theory to be at criticality, $\beta(g^*) = 0$, then at leading order one can solve for the critical coupling

$$g^* = \frac{\epsilon}{N + A}.$$

This fixed point is of order $O(1/N)$ and inserting this into equation (2.62) one can reorder the expansion of the β -function in terms of $1/N, 1/N^2, 1/N^3$ and so on. This reordering is illustrated in figure 2.17.

$$\begin{aligned} \beta(g) = & -\epsilon g + \boxed{N + A}g^2 \\ & + \boxed{BN + C}g^3 \\ & + \boxed{DN^2 + EN + F}g^4 \end{aligned}$$

Figure 2.17: The β -function of a toy model which can be reordered by inserting $g^* = O(1/N)$. The red highlighted text indicates the new leading order ($O(1/N)$) term and the yellow signifies the new NLO ($O(1/N^2)$) terms. The blue and green highlighted text indicates the new NNLO ($O(1/N^3)$) and NNNLO ($O(1/N^4)$) terms, respectively.

Reordering the β -function in the $1/N$ expansion gives

$$\begin{aligned} \beta(g) = & -\epsilon g + Ng^2 + \left(Ag^2 + BNg^3 + DN^2g^4 \right) \\ & + \left(Cg^3 + ENg^4 \right) + O(1/N^4). \end{aligned} \quad (2.63)$$

Note that the first term $-\epsilon g$ is also technically a leading order term in $1/N$, however as it is only used to define the leading order critical coupling it can be ignored. Importantly the large N method relies on the two-loop term of equation (2.62) being linear in N in order to solve the leading order term for the coupling. This presents a problem in certain theories such as QCD with symmetry group $SU(N_c)$, for example, which has an infinite number of graphs at leading order in $1/N_c$. Instead QCD is accessible via the large N_f expansion where N_f is the number of massless quarks.

Having illustrated the rearranging of the β -function we return to the computation of the leading order exponents for the NL σ M. The skeleton Dyson-Schwinger equations for the NL σ M in the large N expansion are given in figure 2.18. At criticality they can be used to find η and χ . Taking only skeleton Dyson-Schwinger equations means no self-energy corrections are included.

$$\begin{aligned}
 0 &= \phi^{-1}(x) + \text{[Diagram 1]} + \text{[Diagram 2]} + \text{[Diagram 3]} \\
 0 &= \sigma^{-1}(x) + \frac{1}{2} \text{[Diagram 4]} + \text{[Diagram 5]} + \text{[Diagram 6]}
 \end{aligned}$$

Figure 2.18: Skeleton Dyson-Schwinger equations of the NL σ M in the large N expansion. Solid lines indicate ϕ^i field propagators while dotted lines are σ field propagators.

Note that all terms in figure 2.18 are in coordinate space. The first two terms in each equation are leading order in $1/N$ and can be used to calculate η_1 . The terms $\phi^{-1}(x)$ and $\sigma^{-1}(x)$ are simply the 2-point functions of each field. The final two graphs in each equation are next to leading order (NLO) diagrams in $1/N$. The ordering of each diagram is simplified by noting the following; each closed ϕ^i loop has a factor of N and every σ propagator counts $1/N$. The factor $1/2$ included in the second equation is a symmetry factor. Computing leading order diagrams uses Fourier transforms. It is therefore essential to introduce some new notation. Recall that the general Fourier transformation used to map between momentum and coordinate space is

$$f(x) = \int \frac{d^d k}{(2\pi)^d} \tilde{f}(k) e^{ikx}, \quad (2.64)$$

with inverse

$$\tilde{f}(k) = \int d^d x f(x) e^{-ikx} . \quad (2.65)$$

The Vasil'ev et al. Fourier transformations were first described in [47], and were stated in equation (2.43). For the computation of $\sigma^{-1}(x)$, the critical point propagator is given in equation (2.57) in coordinate space and can be rewritten as

$$\sigma(x) = \frac{B}{(x^2)^\beta} . \quad (2.66)$$

The general Fourier transformation is used to map this propagator into momentum space

$$\tilde{\sigma}(k) = \int \frac{B}{(x^2)^\beta} e^{-ikx} d^d k .$$

Applying the transformation of (2.43) and setting $\tilde{B} = 2^{2(\mu-\beta)} B/a(\mu-\beta)$ the integral can be completed. As a reminder, we use the notation $d = 2\mu$. Taking the inverse we find

$$\tilde{\sigma}^{-1}(k) = \frac{1}{\tilde{B}(k^2)^{\beta-\mu}} .$$

The integral however is in momentum space. Applying the inverse of the general Fourier transformation given by equation (2.65) maps it back into coordinate space,

$$\sigma^{-1}(x) = \frac{1}{\tilde{B}} \int \frac{d^d k}{(2\pi)^d} \frac{e^{ikx}}{(k^2)^{\beta-\mu}} .$$

Finally to solve the integral the inverse transformation of (2.43) can be applied, which leaves

$$\sigma^{-1}(x) = \frac{1}{\tilde{B}} \frac{2^{2(2\mu-\beta)}}{a(2\mu-\beta)} \frac{1}{(x^2)^{2\mu-\beta}} \frac{1}{(2\pi)^d} .$$

This expression can be simplified by first inserting the value for \tilde{B} and noting that $a(\mu-\beta)/a(2\mu-\beta) = a(\beta-\mu)/a(\beta)$,

$$\sigma^{-1}(x) = \frac{a(\beta-\mu)}{Ba(\beta)} \frac{1}{(x^2)^{2\mu-\beta}} = \frac{p(\beta)}{B(x^2)^{2\mu-\beta}} \quad (2.67)$$

where the notation $p(\beta) = a(\beta-\mu)/a(\beta)$ has been introduced, [47–50]. For the leading order $\phi^{-1}(x)$ term a similar derivation is used to find

$$\phi^{-1}(x) = \frac{p(\alpha)}{A(x^2)^{2\mu-\alpha}} . \quad (2.68)$$

The final two leading order diagrams present in the skeleton Dyson-Schwinger equations can be obtained by counting internal propagators and are given in figure 2.19. Note that the factor of N appears in the second diagram due to the

The exponent on the x^2 term can be simplified, $2\alpha + \beta - 2\mu = -\chi$, by inserting the values of α and β . The equations then become

$$\begin{aligned} p(\alpha) + z(x^2)^\chi &= 0, \\ \frac{2}{N}p(\beta) + z(x^2)^\chi &= 0. \end{aligned}$$

This can be further simplified as χ can be neglected at leading order. Note that by leading order here we mean of the order $O(1)$. Therefore we have

$$p(\alpha) + z + O(1/N) = 0, \quad (2.70a)$$

$$\frac{2}{N}p(\beta) + z + O(1/N) = 0. \quad (2.70b)$$

This set of equations can be solved simultaneously to find

$$p(\alpha) = \frac{2p(\beta)}{N}, \quad (2.71)$$

which can be used to obtain the leading order term of the critical exponent η . To do this we substitute in the values for α and β and begin by solving the left-hand side of equation (2.71),

$$\begin{aligned} p(\alpha) = p\left(\mu - 1 + \frac{\eta}{2}\right) &= \frac{a(\mu - 1 + \frac{\eta}{2} - \mu)}{a(\mu - 1 + \frac{\eta}{2})} \\ &= \frac{\Gamma(\mu - \frac{\eta}{2} + 1) \Gamma(\mu - 1 + \frac{\eta}{2})}{\Gamma(\frac{\eta}{2} - 1) \Gamma(1 - \frac{\eta}{2})}. \end{aligned}$$

We neglect all terms of order $O(1/N)$, however one term in the denominator cannot be simplified as a pole would be produced by $\Gamma(-1)$. Hence we are left with

$$p(\alpha) = p\left(\mu - 1 + \frac{\eta}{2}\right) = \frac{\Gamma(\mu + 1)\Gamma(\mu - 1)}{\Gamma(\frac{\eta}{2} - 1)\Gamma(1)} + \dots$$

There is however a way around this problem. Implementing identity $z\Gamma(z) = \Gamma(z + 1)$ twice to the term $\Gamma(\eta/2 - 1)$ removes the pole,

$$p(\alpha) = p\left(\mu - 1 + \frac{\eta}{2}\right) = \Gamma(\mu + 1)\Gamma(\mu - 1)\left(\frac{\eta}{2} - 1\right)\left(\frac{\eta}{2}\right) + \dots$$

Expanding η in terms of $1/N$ and limiting to only leading order we obtain

$$p(\alpha) = p\left(\mu - 1 + \frac{\eta}{2}\right) = \Gamma(\mu + 1)\Gamma(\mu - 1)\left(-\frac{\eta_1}{2N}\right) + O\left(\frac{1}{N^2}\right).$$

The right-hand side of equation (2.71) is much simpler to solve as no poles appear,

$$\frac{2p(\beta)}{N} = \frac{2}{N} \frac{\Gamma(2\mu - 2)}{\Gamma(2 - \mu)\Gamma(\mu - 2)} .$$

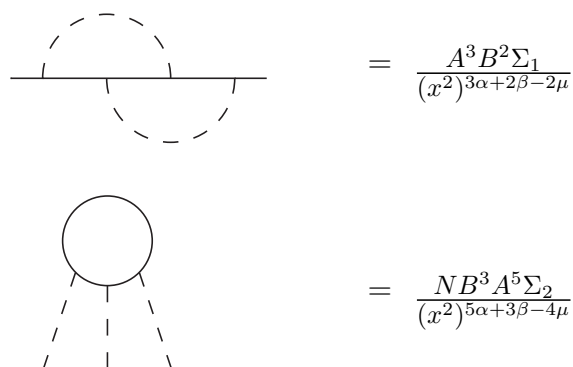
We have neglected to include η and χ in the β term as we only included terms at leading order. Putting both sides of the equation together and solving for the leading order term of η gives

$$\eta_1 = - \frac{4\Gamma(2\mu - 2)}{\Gamma(2 - \mu)\Gamma(\mu - 2)\Gamma(\mu + 1)\Gamma(\mu - 1)} . \quad (2.72)$$

Note that factors of $1/N$ have cancelled in the above expression. As z is also an expansion of $1/N$, that is $z = z_1/N + z_2/N^2 + \dots$, equation (2.70a) can be used to find its leading order term,

$$z_1 = \frac{\eta_1\Gamma(\mu + 1)\Gamma(\mu - 1)}{2} . \quad (2.73)$$

We also want to find the leading order term of χ . To do this consider only the first skeleton Dyson-Schwinger equation. However now the next to leading order Feynman diagrams have to be included. Expressions for the next to leading order diagrams are given in figure 2.21.



$$= \frac{A^3 B^2 \Sigma_1}{(x^2)^{3\alpha+2\beta-2\mu}}$$

$$= \frac{NB^3 A^5 \Sigma_2}{(x^2)^{5\alpha+3\beta-4\mu}}$$

Figure 2.21: The next to leading order diagrams in the first skeleton Dyson-Schwinger equation for the ϕ^i field.

Here Σ_1 and Σ_2 are the values of the dimensionless integrals for each next to leading order diagram, respectively. The first diagram of figure 2.21 can be written as an integral in coordinate space over two integration parameters, see figure 2.22.

$$= \int_{y,z} (y^2)^{-\alpha} ((y-x)^2)^{-\beta} (z^2)^{-\beta} ((y-z)^2)^{-\alpha} ((x-z)^2)^{-\alpha}$$

Figure 2.22: Coordinate space representation of the first NLO Feynman diagram in figure 2.21.

From the conformal representation of figure 2.22 it is clear to see that the power $3\alpha + 2\beta$ in the first diagram of figure 2.21 comes from the power on the propagators. The factor 2μ meanwhile is due to the two integration variables y and z . The factors of A and B in figure 2.21 count the number of internal ϕ^i and σ propagators. This leaves the value of Σ_1 dimensionless. Similarly the second diagram of figure 2.21 can be written as an integral over four integration parameters. As with the first diagram, $5\alpha + 3\beta$ gives the powers on the propagators while the term 4μ is due to the four integration variables. The N factor is due to the ϕ^i loop present in the diagram. Removing these factors from the integral leaves the value of Σ_2 dimensionless. The second diagram of figure 2.21 is illustrated in coordinate space in figure 2.23 where

$$f(x, y, z, v, w) = (w^2)^\alpha ((w-x)^2)^\alpha ((z-x)^2)^\beta ((v-z)^2)^\alpha (v^2)^\beta ((y-z)^2)^\alpha ((v-y)^2)^\alpha .$$

$$= \int_{w,y,z,v} f(x, y, z, v, w)^{-1}$$

Figure 2.23: Conformal representation of the second NLO Feynman diagram in figure 2.21.

Both NLO diagrams will be calculated explicitly in Chapter 5. Inserting the NLO diagrams, along with LO terms already computed, into the first skeleton Dyson-Schwinger equation we find

$$0 = p(\alpha) + \frac{A^2 B}{(x^2)^{\alpha+\beta}} (x^2)^{2\mu-\alpha} + \frac{A^4 B^2 \Sigma_1}{(x^2)^{3\alpha+2\beta-2\mu}} (x^2)^{2\mu-\alpha} + \frac{N A^6 B^3 \Sigma_2}{(x^2)^{5\alpha+3\beta-4\mu}} (x^2)^{2\mu-\alpha} .$$

Each term is multiplied by A and $(x^2)^{2\mu-\alpha}$. As before we also set $z = A^2 B$,

$$0 = p(\alpha) + \frac{z}{(x^2)^{2\alpha+\beta-2\mu}} + \frac{z^2 \Sigma_1}{(x^2)^{4\alpha+2\beta-4\mu}} + \frac{N z^3 \Sigma_2}{(x^2)^{6\alpha+3\beta-6\mu}}. \quad (2.74)$$

Naively if one tries to explicitly compute the next to leading order diagrams using conformal integration one would encounter divergence in the form of poles from terms such as $\nu(\mu, \mu, 0)$, as well as logarithmic divergences. Therefore the theory needs to be regularised before renormalizing. For $2 < d < 4$ the NL σ M is renormalizable in accordance with Bogolyubov's classification, [145], since there are only a finite number of types of divergent diagrams. In contrast to ordinary perturbation theory with a $d = D_c - 2\epsilon$ expansion, the transition to non-integer dimensions in our case does not in itself regularise the theory. The vertex $\sigma\phi^i\phi^i$ will remain logarithmic for any $d = 2\mu$ when the fields have the dimension $\alpha = \mu - 1$ and $\beta = 2$.

The analogue of dimensional regularisation for the large N expansion is analytic regularisation, which violates the dimensionless nature of the vertex by a small shift in the dimension of the field σ . We can introduce the regularisation by the shift $\beta = \beta - \Delta$ in the dimension of the field σ without changing the dimension of the field ϕ^i . Equivalently we could also use $\chi \rightarrow \chi + \Delta$. As a result of the shift the vertex $\sigma\phi^i\phi^i$ acquires the dimension $-\Delta$ and therefore we must place in front of it some coefficient g_c of dimension Δ , the 'bare coupling constant', to keep the vertex dimensionless. The letter Δ plays the part of ϵ in dimensional regularisation and divergences will appear in the form of poles with respect to Δ . The next to leading order diagrams can therefore be separated into divergent and convergent, or finite, pieces.

$$\begin{aligned}
 & \text{Diagram 1 (Dashed Loop)} = \frac{K_1}{\Delta} + \Sigma'_1 \\
 & \text{Diagram 2 (Solid Loop)} = \frac{K_2}{\Delta} + \Sigma'_2
 \end{aligned}$$

Figure 2.24: The next to leading order diagrams in the skeleton Dyson-Schwinger equation for the ϕ field split into divergent and finite parts.

In figure 2.24, K_1 and K_2 are the coefficients of the divergent parts of both diagrams, while Σ'_1 and Σ'_2 are the finite pieces. Note that Δ will be taken to zero

after renormalization as ϵ is during dimensional regularisation. By introducing a regularisation equation (2.74) is modified,

$$\begin{aligned}
0 = p(\alpha) &+ \left[\left(\frac{z_1}{N} + \frac{z_2}{N^2} \right) \frac{1}{(x^2)^{2\alpha+\beta-\Delta-2\mu}} \right] \\
&+ \left[\frac{z_1^2}{N^2} \frac{1}{(x^2)^{4\alpha+2\beta-2\Delta-4\mu}} \left(\frac{K_1}{\Delta} + \Sigma'_1 \right) \right] \\
&+ \left[\frac{z_1^3}{N^2} \frac{1}{(x^2)^{6\alpha+3\beta-3\Delta-6\mu}} \left(\frac{K_2}{\Delta} + \Sigma'_2 \right) \right] + O\left(\frac{1}{N^3}\right). \quad (2.75)
\end{aligned}$$

Note that the term z has been expanded out to include terms up to order $O(1/N^2)$. It is clear to see that logarithmic divergences will appear when Taylor expanding the x^2 terms. This is in addition to the poles associated with the divergent next to leading order diagrams.

Having identified where the divergences occur in the theory we must now renormalize. To do this recall the Lagrangian of the NL σ M,

$$L^{\text{NL}\sigma\text{M}} = \frac{1}{2}(\partial\phi_0^i)^2 + \frac{1}{2}\sigma_0\phi_0^i\phi_0^i - \frac{1}{2\lambda}\sigma_0. \quad (2.76)$$

As in conventional renormalization we have assumed the parameters of the theory are bare. Note that the bare coupling constant g_0 introduced in front of the interaction term to ensure the vertex is dimensionless has been rescaled into the parameter λ . Every operator will have an associated renormalization constant, i.e. $\mathcal{O}_0 = Z_{\mathcal{O}}\mathcal{O}$, where \mathcal{O} is some operator. We can therefore introduce the following renormalization constants, [47–50],

$$\phi_0 = \sqrt{Z_\phi}\phi \quad , \quad \sigma_0 = \sqrt{Z_\sigma}\sigma \quad , \quad \sigma_0\phi_0\phi_0 = Z_v\sigma\phi\phi. \quad (2.77)$$

The vertex renormalization constant is given by Z_v . The Lagrangian becomes, [47–50],

$$L^{\text{NL}\sigma\text{M}} = \frac{1}{2}Z_\phi(\partial\phi^i)^2 + \frac{1}{2}Z_v\sigma\phi^i\phi^i + \dots. \quad (2.78)$$

The final term of Lagrangian (2.76) is linear and does not couple to any other field. It does not affect the renormalization and therefore we have neglected to include it here. It is important to clarify at this point that leading order diagrams are not divergent, as is obvious from their computation; next to leading order diagrams are divergent and along with divergences in the form of poles we will also have logarithmic divergences. In other words introducing Δ will produce $\ln(x^2)$ terms which could spoil the scaling behaviour. When the 2-point counterterm is fixed explicitly to remove the simple poles in Δ , the $\ln(x^2)$ terms should also cancel.

Therefore as 2-point counterterms remove simple and logarithmic poles, we do not need to introduce 1-point counterterms. Thus the renormalization constants can be set as

$$\begin{aligned} Z_\phi &= Z_\sigma = 1, \\ Z_v &= 1 + m, \end{aligned} \quad (2.79)$$

where m gives the counterterms in an expansion of N and Δ given by

$$m = \frac{m_1}{N\Delta} + \frac{m_{22}}{N^2\Delta^2} + \frac{m_{21}}{N\Delta^2} + \dots \quad (2.80)$$

Note that the next to leading order counterterms will also not be required as they are of the order $O(1/N^3)$ and we are only including terms up to order $O(1/N^2)$.

Inserting the counterterms in the Lagrangian we find

$$\begin{aligned} L^{\text{NL}\sigma\text{M}} &= \frac{1}{2}(\partial\phi^i)^2 - (1+m)\frac{1}{2}\sigma\phi^i\phi^i \\ &= \frac{1}{2}(\partial\phi^i)^2 - \frac{1}{2}\sigma\phi^i\phi^i - \frac{m_1}{N\Delta}\sigma\phi^i\phi^i + \dots \end{aligned}$$

Diagrammatically the first skeleton Dyson-Schwinger equation with counterterms is illustrated in figure 2.25.

Figure 2.25: The skeleton Dyson-Schwinger equation for the ϕ field with 2-point renormalization counterterms included. NLO counterterms are not included as they are not necessary to remove all divergences at order $O(1/N^2)$.

Substituting Renormalization Group constants and subsequent counterterms into the first skeleton Dyson-Schwinger equation one finds,

$$\begin{aligned} 0 &= p(\alpha) + \left[\left(\frac{z_1}{N} + \frac{z_2}{N^2} \right) \frac{1}{(x^2)^{2\alpha+\beta-\Delta-2\mu}} \left(1 + \frac{2m_1}{N\Delta} \right) \right] \\ &+ \left[\frac{z_1^2}{N^2} \frac{1}{(x^2)^{4\alpha+2\beta-2\Delta-4\mu}} \left(\frac{K_1}{\Delta} + \Sigma'_1 \right) \right] \\ &+ \left[\frac{z_1^3}{N^2} \frac{1}{(x^2)^{6\alpha+3\beta-3\Delta-6\mu}} \left(\frac{K_2}{\Delta} + \Sigma'_2 \right) \right] + O\left(\frac{1}{N^3} \right). \end{aligned}$$

The factor of two in front of the counterterm m_1 is included as two counterterms are present. Note that the above equation has two expansions, one in the parameter z with respect to $1/N$ and the other in m which is an expansion in both $1/N$ and $1/\Delta$. Only terms of order $O(1/N^2)$ have been incorporated. Inserting $\alpha = \mu - 1 + \eta/2$ and $\beta = 2 - \eta - \chi$ the equation becomes,

$$\begin{aligned} 0 &= p\left(\mu - 1 + \frac{\eta}{2}\right) + \left[\left(\frac{z_1}{N} + \frac{z_2}{N^2} + \frac{2m_1 z_1}{N^2 \Delta}\right) \frac{1}{(x^2)^{-\chi - \Delta}}\right] \\ &\quad + \left[\frac{z_1^2}{N^2} \frac{1}{(x^2)^{-2\chi - 2\Delta}} \left(\frac{K_1}{\Delta} + \Sigma'_1\right)\right] \\ &\quad + \left[\frac{z_1^3}{N^2} \frac{1}{(x^2)^{-3\chi - 3\Delta}} \left(\frac{K_2}{\Delta} + \Sigma'_2\right)\right] + O\left(\frac{1}{N^3}\right). \end{aligned}$$

Recall that η and χ can also be expanded in $1/N$, see equations (2.60) and (2.61). Therefore we can Taylor expand the x^2 term in both χ and Δ ,

$$\begin{aligned} 0 &= p\left(\mu - 1 + \frac{\eta_1}{2N}\right) \\ &\quad + \left[\left(\frac{z_1}{N} + \frac{z_2}{N^2} + \frac{2m_1 z_1}{N^2 \Delta}\right) \left(1 + \frac{\chi_1}{N} \ln(x^2)\right) \left(1 + \Delta \ln(x^2)\right)\right] \\ &\quad + \left[\frac{z_1^2}{N^2} \left(\frac{K_1}{\Delta} + \Sigma'_1\right) \left(1 + 2\Delta \ln(x^2)\right) \left(1 + 2\frac{\chi_1}{N} \ln(x^2)\right)\right] \\ &\quad + \left[\frac{z_1^3}{N^2} \left(\frac{K_2}{\Delta} + \Sigma'_2\right) \left(1 + 3\Delta \ln(x^2)\right) \left(1 + 3\frac{\chi_1}{N} \ln(x^2)\right)\right] \\ &\quad + O\left(\frac{1}{N^3}\right). \end{aligned}$$

We must fix the counterterm to remove simple poles in Δ . Additionally we still have to take $x^2 \rightarrow 0$ limit to approach the critical point asymptotically. Hence the $\ln(x^2)$ terms have to be absent after renormalization. This defines χ_1 . In other words two constraints are obtained to establish a value for the χ_1 term. Matching terms with factors $(1/N^2) \ln(x^2)$ gives the first constraint, while matching terms with factor $1/(N^2 \Delta)$ gives the second

$$z_1 \chi_1 + 2m_1 z_1 + 2z_1^2 K_1 + 3z_1^3 K_2 = 0, \quad (2.81a)$$

$$2m_1 z_1 + z_1^2 K_1 + z_1^3 K_2 = 0. \quad (2.81b)$$

Rearranging the second constraint and substituting into the first gives an equation for χ_1 ,

$$\chi_1 = -z_1 K_1 - 2z_1^2 K_2. \quad (2.82)$$

The value of z_1 has already been calculated in equation (2.73). Expressions for K_1 and K_2 have been determined in [49]. The computation of K_1 and K_2 relies

on conformal integration and in particular the uniqueness condition which allows 3-point vertices to be integrated over in coordinate space.

We perform this calculation in Chapter 5 for a slightly different theory, explaining the details of this method is therefore left until then. However a particular quirk should be noted here regarding the computation of the next to leading order diagrams. As we shall see in Chapter 5, the uniqueness condition is not exactly satisfied as $2\alpha + \beta = d - \chi$ at each 3-point vertex. However the χ term can be neglected at leading order. The uniqueness condition is therefore satisfied and the diagrams can be calculated. This point will be revisited in Chapter 5, for the moment we simply state the values for K_1 and K_2 which were found to be, [49],

$$\begin{aligned} K_1 &= \frac{2\pi^{2\mu} a^2(\alpha) a(\beta)}{\Gamma(\mu)}, \\ K_2 &= \frac{\pi^{4\mu} a^3(\alpha) a^3(\beta) a(\mu + \alpha - \beta)}{\Gamma(\mu)}. \end{aligned} \quad (2.83)$$

Finally, using leading order values of α and β , the value of the critical exponent χ_1 can be found

$$\chi_1 = \eta_1 \left(\frac{\mu(-5 + 4\mu)}{2 - \mu} \right). \quad (2.84)$$

We have calculated the leading order terms of the critical exponents η and χ . Higher order corrections to these results have been calculated, [48–50]. These are the d -dimensional values of the critical exponents for the entire $O(N)$ universality class.

Therefore to confirm whether a theory lies in this $O(N)$ universality class or not, the exponents of the theory can be computed in an ϵ -expansion around its critical dimension and compared with large N results order by order. For example, if one were to compute the critical exponents of ϕ^4 theory with an $O(N)$ symmetry using a coupling or ϵ -expansion, they would perfectly match the large N results with $d = 2\mu = 4 - 2\epsilon$ to every available order. Hence confirming that ϕ^4 theory is in the $O(N)$ universality class.

2.3.3 Summary

In this Chapter we have introduced and discussed background techniques that will be used throughout this thesis. Renormalization ideas, in particular the Renormalization Group, will be referenced throughout our original work. Using

the β -functions we will analyse the fixed point properties and stability of many theories that have not until now been fully investigated. Universality has also been discussed here which will be a central thread through each Chapter of Part I. The computational method of conformal integration has been explored here for the benefit of the reader as it will be used extensively throughout. Much of the background has focused on the large N expansion for two main reasons. Firstly, the large N expansion will be used in every Chapter of Part I for different universality classes. The second reason is that the critical point large N formalism is a non-standard QFT technique, which is rarely fully derived or explained in modern literature. It is therefore important to explain the set-up before discussing any original work.

Ten Dimensional $O(N)$ Scalar Field Theory

3.1 Introduction

Conformal invariance is a fundamental concept in statistical mechanics, condensed matter and high energy physics. A conformal field theory (CFT) is one which is invariant under the conformal group. In two dimensions the conformal group is infinite dimensional and hence conformal symmetry becomes a very powerful constraint on a quantum field theory (QFT). For this reason two dimensional CFT's have been studied extensively. It is in two dimensions that conformal field theories can sometimes be exactly solved. It is therefore more interesting to look at conformal field theories beyond two dimensions where the conformal group is finite. One question that arises is whether theories above two dimensions keep conformal invariance. The relationship between scale and conformal invariance has been a topic of interest for many years. One question in particular is whether scale invariant field theories enjoy the full conformal symmetry under the assumption of locality and unitarity. Can a quantum field theory above two dimensions flow to a nearby scale invariant theory without conformal invariance? While it is possible for a QFT to be scale invariant but not conformally invariant, examples are rare. For this reason the terms are often used interchangeably in the context of QFT, even though the scale symmetry group is smaller.

The equivalence of scale and conformal invariance in two dimensions was proved in the 1980s, [146, 147], the second of which uses the strict assumption of unitarity. However as neither generalised their proof to higher dimensions, it

is not known in dimensions above two if this statement is still correct. In four dimensions perturbative checks were performed, [146, 148], and general perturbative arguments given, [149, 150], all of which provided no conclusive proof for the equivalence but equally found no counterexamples. Beyond perturbation theory the conditions for the equivalence have been analysed in four dimensions, [151]. There have also been attempts to prove this equivalence in higher dimensions, particular in six dimensions with important results obtained in [152–154]. A strict proof is not given in any of the above literature without restrictive assumptions; moreover there is no known reason why the equivalence should be true for $d \geq 2$. However, no evidence has been found to contradict the possibility of scale and conformal invariance being equivalent. Furthermore, if scale invariant but not conformal unitary theories exist this would have not only theoretical but also phenomenological consequences.

Supposing that the equivalence between scale and conformal invariance is not correct, scale invariant theories in higher dimensions are still interesting to study for a number of reasons. Predominantly this is due to the apparent connection of ultraviolet (UV) stable fixed points in a higher dimensional theory with infrared (IR) stable fixed points in a lower dimensional theory, [46]. This is known as UV/IR duality and for this reason a universality class is sometimes referred to as UV completion. The connectivity of QTF's in differing dimensions containing the same underlying symmetry is of particular interest. This connectivity derives from the critical point Renormalization Group (RG) equation and Wilson-Fisher fixed point, [41, 43, 44, 155, 156], which is a core property in d -dimensions. The most widely known example is the use of the Wilson-Fisher fixed point underlying the Ising model as well as the super-fluid phase transition, dilute polymer solutions and Heisenberg ferromagnet. Information about the properties of their phase transitions can be accessed by the continuum scalar quantum field theory with a ϕ^4 interaction. When endowed with an $O(N)$ symmetry the $N = 1$ case corresponds to the Ising model whereas the ferromagnet is described by the value of $N = 3$. Equally dilute polymer solutions and super-fluidity correspond to the cases of $N = 0$, known as the replica limit, and $N = 2$ respectively. We briefly discussed the connection of scalar ϕ^4 theory containing $O(N)$ symmetry with the two dimensional non-linear sigma model (NL σ M) in the previous Chapter. This group of theories is termed the ' $O(N)$ universality class'.

Remarkably information on phase transition of the Heisenberg magnet in three dimensions can be obtained by renormalizing the $O(N)$ scalar ϕ^4 theory in four dimensions. In other words, in the approach to three dimensions through the

ϵ -expansion, where the spacetime dimension is $d = 4 - 2\epsilon$, only the quartic operator present in the $O(N)$ scalar theory is relevant. In practical terms to obtain accurate information on the phase transition properties, one would have to know the Renormalization Group functions of $O(N)$ ϕ^4 theory to a large loop order. This has been achieved in recent years to five, [157–161], six, [162–165], and seven loops, [165], in the modified minimal subtraction ($\overline{\text{MS}}$) scheme. From a bigger perspective our understanding of the universality of this particular Wilson-Fisher fixed point has been extended above and beyond four dimensions in recent years. This will be the focus of the current Chapter. We will begin by first recapping the work of [51–54] in four, six and eight dimensions on the $O(N)$ universality class. We then construct a ten dimensional Lagrangian in section 3.3 with all the conditions necessary to extend the universality class to a higher dimension. The RG functions of the ten dimensional theory will be perturbatively calculated and the resulting ϵ -expanded critical exponents compared order by order with known large N results. Hence providing conclusive evidence of ten dimensional Lagrangian existing in this universality class along with the NL σ M, ϕ^4 theory and the six and eight dimensional theories discussed. Finally in section 3.5 we attempt to examine the fixed point behaviour of the ten dimensional theory. Note that this calculation in ten dimensions is original with results published in [3].

3.2 $O(N)$ Symmetric Scalar Field Theories

The Euclidean field theory of N real massless scalar fields with an $O(N)$ invariant quartic interaction is given by the Lagrangian

$$L^{(4)} = \frac{1}{2} \partial_\mu \phi^i \partial^\mu \phi^i + \frac{1}{8} g_1^2 (\phi^i \phi^i)^2, \quad (3.1)$$

where $1 \leq i \leq N$. This Lagrangian is perturbatively renormalizable in four space-time dimensions. It is super-renormalizable in three space-time dimensions. While this version of the Lagrangian is the one widely used to construct the Renormalization Group functions, the interaction can be rewritten in terms of a Hubbard-Stratonovich auxiliary field σ to produce an equivalent Lagrangian which will be renormalizable in the $1/N$ expansion,

$$L^{(4)} = \frac{1}{2} \partial_\mu \phi^i \partial^\mu \phi^i + \frac{g_1}{2} \sigma \phi^i \phi^i - \frac{1}{2} \sigma^2. \quad (3.2)$$

One can integrate out σ via its equation of motion, $\sigma = g_1 \phi^i \phi^i$, to obtain the original Lagrangian. In $2 < d < 4$ dimensions the quartic interaction of La-

grangian (3.1) generates a flow from a free UV fixed point to an interacting IR fixed point near four dimensions, [51]. This can be seen from dimensional analysis where the interaction term becomes relevant for $d < 4$ dimensions. In $d = 4 - 2\epsilon$ dimensions this fixed point can be studied perturbatively in the framework of the Wilson-Fisher ϵ -expansion, [41, 166]. The behaviour of the fixed point has been analysed and subsequent critical exponents computed in [51–53]. To develop a picture of the fixed point structure we state the one-loop results with the β -function calculated to be, [51],

$$\beta(g_1) = -\epsilon g_1 + (N+8)\frac{g_1^2}{6} \quad (3.3)$$

and the weakly coupled IR fixed point at leading order located at

$$g_1^* = \frac{6\epsilon}{N+8} + O(\epsilon^2). \quad (3.4)$$

Higher order corrections in ϵ will change the value of g_1^* but not its existence, [52, 53]. The IR stability of the fixed point can be verified by computing the value of $\partial\beta(g_1)/\partial g_1$ at the fixed point g_1^* . There also exists a trivial Gaussian fixed point at $g_1^* = 0$ which is IR unstable and hence UV stable. The anomalous dimensions of the fundamental field ϕ^i and its composite at the fixed point have been calculated to leading order (LO), [51],

$$\begin{aligned} \gamma_\phi(g_1^*) &= \frac{N+2}{4(N+8)^2}\epsilon^2 + O(\epsilon^3), \\ \gamma_{\phi^2}(g_1^*) &= \frac{N+2}{N+8}\epsilon + O(\epsilon^2). \end{aligned} \quad (3.5)$$

Along with the corresponding scaling dimensions,

$$\begin{aligned} \Delta_\phi &= \frac{d}{2} - 1 + \gamma_\phi(g_1^*) \\ &= 1 - \frac{\epsilon}{2} + \frac{N+2}{4(N+8)^2}\epsilon^2 + O(\epsilon^3), \\ \Delta_{\phi^2} &= d - 2 + \gamma_{\phi^2}(g_1^*) \\ &= 2 - \frac{6}{N+8}\epsilon + O(\epsilon^2). \end{aligned}$$

Above four dimensions the interaction term becomes irrelevant and the free theory, $g_1^* = 0$, becomes IR stable. The non-trivial fixed point still exists above four dimensions in the form of a UV stable fixed point in $d = 4 + 2\epsilon$, [51],

$$g_1^* = -\frac{6\epsilon}{N+8} + O(\epsilon^2). \quad (3.6)$$

Anomalous dimensions at this fixed point are given by equations (3.5) with $\epsilon \rightarrow -\epsilon$. As the anomalous dimension $\gamma_\phi(g_1^*)$ begins with an ϵ^2 term, the dimension of ϕ^i is still positive and therefore stays above the unitary bound, $\Delta \geq d/2 - 1$, for sufficiently small ϵ . However as the fixed point (3.6) is negative, questions can be raised about its stability with [51] suggesting it should be referred to as ‘metastable’. It is well known from the literature that this four dimensional theory lies in the same universality class as the two dimensional NL σ M. This connectivity of Lagrangian (3.2) with the underlying two dimensional CFT was outlined in [52]. The Lagrangian for the NL σ M was given in equation (2.52) and rewritten in the large N formalism in equation (2.54) by introducing a Lagrange multiplier. The NL σ M shares the same $O(N)$ symmetry as the four dimensional ϕ^4 theory.

There are early indications in the form of the Lagrangian’s that both the NL σ M and ϕ^4 theory lie in the same universality class. Firstly they both contain the interaction term, $\sigma\phi^i\phi^i$, and the dimensionality of the two fields ϕ^i and σ in both theories are given by equation (2.55). Note that the dimension of the ϕ^i field will be the same in d -dimensions for both theories but will be different in the individual dimensions. As the interaction term alone defines the dynamics and the quadratic term defines the dimensionalities for the propagators, the two theories can be thought of as being equivalent at the Wilson-Fisher fixed point in the dimension range $2 < d < 4$. A more concrete proof of this universality is available through the large N expansion of the critical exponents, [47–50]. The leading order terms for the exponents η and χ were calculated in the previous Chapter, see equations (2.72) and (2.84). For the benefit of the reader we recall how these exponents are connected to the Renormalization Group functions,

$$\gamma_\phi(g_i^*) = \eta \quad , \quad \gamma_\sigma(g_i^*) = -\eta + \chi \quad (3.7)$$

where $1 \leq i \leq N_{cc}$ and N_{cc} is the number of coupling constants in the theory. As well as providing evidence of the universality between the NL σ M and ϕ^4 theory the combination of the large N and ϵ -expansions provides a good approximation for the critical behaviour in $2 < d < 4$ dimensions.

As there is no apparent physical reason for the $O(N)$ universality class to end at four dimensions, we can look at extending the connectivity to higher dimensions. One possible candidate is six dimensional ϕ^3 theory. This theory contains a non-trivial interacting fixed point and has recently been considered in [51–53, 168, 169, 182]. The Lagrangian which is perturbatively renormalizable

in six space-time dimensions is given by

$$L^{(4,6)} = \frac{1}{2} (\partial_\mu \phi^i)^2 + \frac{1}{2} (\partial_\mu \sigma)^2 + \frac{g_1}{2} \sigma \phi^i \phi^i + \frac{g_2}{6} \sigma^3. \quad (3.8)$$

Our notation of $L^{(d_1, d_2)}$ is to indicate the dimension of the base quartic four-dimensional theory, which is d_1 , and the particular critical dimension, d_2 , where the theory is renormalizable. This is an $O(N)$ symmetric theory of $N + 1$ scalar fields where there exists an $O(N)$ multiplet of fields ϕ^i and a single scalar field σ . As with the Lagrangian's in two and four dimensions we have $i = 1, \dots, N$ and the σ field has been introduced. One difference that Lagrangian (3.8) has with lower dimensional theories is that σ cannot be eliminated either as a Lagrange multiplier or as an auxiliary field. The additional interaction present in (3.8) ensures renormalizability in six space-time dimensions. The idea of studying a cubic theory in $d = 6 - 2\epsilon$ dimensions is not a new one. Michael Fisher has explored such an ϵ -expansion in the theory of a single scalar field as a possible description of the Lee-Yang singularity in the Ising model, [170]. This case corresponds to the $N = 0$ version of (3.8). Renormalization Group functions for similar cubic theories have been calculated in $d = 6 - 2\epsilon$ for the $O(N)$ and $O(1)$ cases in [171–173]. The fixed point structure of Lagrangian (3.8) has been thoroughly studied using an ϵ and large N expansion, [51–53]. We note some of the key results here. The one loop β -functions are, [51, 53],

$$\beta_1(g_1, g_2) = -\frac{\epsilon}{2} g_1 + \frac{(8 - N)g_1^3 + 12g_1^2 g_2 - g_1 g_2^2}{24}, \quad (3.9a)$$

$$\beta_2(g_1, g_2) = -\frac{\epsilon}{2} g_2 + \frac{4N g_1^3 - N g_1^2 g_2 + 3g_2^3}{8}. \quad (3.9b)$$

The anomalous dimensions to one loop are given by, [53],

$$\begin{aligned} \gamma_\phi(g_1, g_2) &= -\frac{g_1^2}{6}, \\ \gamma_\sigma(g_1, g_2) &= \frac{-[N g_1^2 + g_2^2]}{12}. \end{aligned}$$

The β -functions and anomalous dimensions have been extended to three and four loops in [52, 53]. It was noted that for large N the β -functions can be simplified, [51],

$$\beta_1(g_1, g_2) = -\frac{\epsilon}{2} g_1 + \frac{N g_1^3}{12(4\pi)^3}, \quad (3.10a)$$

$$\beta_2(g_1, g_2) = -\frac{\epsilon}{2} g_2 + \frac{-4N g_1^3 + N g_1^2 g_2}{4(4\pi)^3}. \quad (3.10b)$$

An IR stable interacting fixed point emerges from this large N approximation, [51], at leading order which is located at

$$g_1^* = i\sqrt{\frac{12\epsilon}{N}} \quad , \quad g_2^* = 6g_1^* . \quad (3.11)$$

It is straightforward to compute corrections at large N by solving (3.9a) and (3.9b) in powers of $1/N$, [51–53]. It was noted in [51] that the coefficients in this expansion appear to increase quite rapidly. This suggests that the large N expansion may break down at some finite N . This proves to be the case when examining finite N solutions as the IR interacting fixed point disappears below a critical value of N . Note that along with the leading order solution (3.11) there are three additional solutions that are symmetric to this fixed point with respect to the origin. At large N the IR stability of the fixed point can be seen from the fact that the matrix $\partial\beta_i(g_j)/\partial g_j$ evaluated at the interacting fixed point has two positive eigenvalues. This suggests UV instability and hence IR stability. The critical exponents η and χ calculated for the cubic theory at this fixed point are in precise agreement with the large N solutions, (2.72) and (2.84), analytically continued to $d = 6 - 2\epsilon$ dimensions, [52, 53]. The equivalence of the coefficients for the two expansions provides conclusive evidence that ϕ^3 theory exists in the $O(N)$ universality class. Hence the $O(N)$ symmetric universality class exists not only for $2 < d < 4$ dimensions but also extends to $4 < d < 6$. Moreover it shows that the IR stable fixed point of the cubic theory describes the same physics as the UV fixed point found in the $4 + 2\epsilon$ expansion of ϕ^4 theory.

An analysis of fixed points for the six dimensional theory at finite N was also carried out, [51–53, 174], which enabled an approximation of the conformal window to be calculated. In [51] it was noted that there are various critical values of N for which the fixed point structure has different properties. Treating N as a continuous parameter the critical value of N where the interacting IR fixed point becomes stable was found to be $N_{\text{crit}} \approx 1038$ at leading order, [174]. Using resummation methods the value $N_{\text{crit}} \approx 400$ was found on a four loop level, [53]. At $N < N_{\text{crit}}$ the non-trivial fixed point disappears into the complex plane. As discussed in [175] this is a rather generic behaviour at the lower end of the conformal window; the conformality is lost through the annihilation of a UV fixed point and an IR fixed point. This was also argued to happen at the lower (strongly coupled) edge of the conformal window for a four dimensional $SU(N_c)$ gauge theory with N_f flavours of quarks, [175]. It is interesting to observe that the same type of behaviour occurs at the lower edge of the conformal window of ϕ^3 theory in $d = 6 - 2\epsilon$ dimensions which exists from N_{crit} to infinity. For all

N the β -functions (3.9a) and (3.9b) have nine solutions, the trivial fixed point located at $(g_1^*, g_2^*) = (0, 0)$, two pure imaginary solutions and two saddle points located at $N = 500$ and $N = 2000$ at leading order, [52]. These saddle points are not IR stable but are always real. The remaining four solutions change behaviour depending on the value of N . For $N \leq 1038$ all four fixed point are complex, while for $N > 1038$ they are all real.

It is of interest to look at simpler cubic models where there is no or different symmetries present due to the connection of these models to condensed matter and statistical physics problems. For example, the $N = 0$ case of one scalar field relates to the Lee-Yang edge singularity problem, [170], where the coupling is imaginary. The single scalar cubic field theory has no fixed points at real couplings due to the negative sign of the β -function for the second coupling, which can be seen by setting $N = 0$ in equations (3.9a) and (3.9b). However it does have a fixed point at imaginary couplings. The main critical exponent of interest for this problem is ς which is related to the anomalous dimension of ϕ^i through a hyper-scaling law

$$\varsigma = \frac{[d - 2 + \eta]}{[d + 2 - \eta]}.$$

Note that as the Lee-Yang problem stretches across dimensions to $d = 1$ one has to be careful using perturbation theory. To gain estimates Padé and Padé-Borel resummation methods for η can be used before evaluating ς , [53]. Results can then be compared with figures obtained using other methods such as the strong coupling expansion, [176], Monte Carlo methods and conformal bootstrap analysis, [177].

Utilizing non-perturbative methods along with traditional perturbative techniques is important for the integrity of results. Therefore it is highly desirable to provide further analysis from the non-perturbative point of view. We summarise current non-perturbative work done on the $O(N)$ universality class as well as issues surrounding this as it will be relevant for later Chapters where new work is presented. There have been attempts to obtain a more rigorous approach to $O(N)$ symmetric CFTs using conformal bootstrap ideas. The Conformal bootstrap has been applied to the dimension range $2 < d < 4$ for ϕ^4 theory, [61, 178], and for the cubic $O(N)$ theory in $4 < d < 6$ dimensions, [51, 52, 58, 59, 62, 168, 169]. The second case was seen as a potential route to accessing the five dimensional quantum field theory with a conformal symmetry. Theories in five dimensions are of particular physics interest due to the AdS₆/CFT₅ correspondence where dual

theories in the AdS₆ bulk include higher spin fields in the large N limit, [56]. As higher order corrections for the critical value of N were found to have large negative coefficients, [52, 53], the critical value of N must be lower in five dimensions. To three loops the five dimensional critical value of N was calculated as, [52],

$$N_{\text{crit}} \Big|_{d=5} = 64.253 ,$$

by simply setting $\epsilon = 1/2$ in the expansion. The reduction from $N_{\text{crit}} \approx 1038$ in six dimensions to $N_{\text{crit}} \approx 64$ is not unexpected. An analogous phenomenon occurs in the Abelian Higgs models containing N_f complex scalars which has a fixed point in $d = 4 - 2\epsilon$ dimensions for $N_f \geq 183$, [179, 180], while non-perturbative studies show in three dimensions that N_f is much lower.

Conformal bootstrap results for the fixed point structure and critical value of N in five dimensions have given a wide array of results. The existence of an $O(N)$ invariant CFT in five dimensions was proven by the discovery of a non-trivial fixed point that exists for lower values of N all the way down to $N = 1$, [58]. This suggests that an interacting unitary CFT exists in five dimensions for all non-zero N . Similarly using conformal bootstrap in $d = 5$ and $d = 5.95$ dimensions evidence was provided by [62] for the interacting fixed point found perturbatively and it was conjectured that in five dimensions there is no interacting $O(N)$ CFT for $N < 15$. This value is close to the estimate $N_{\text{crit}} \approx 14$ obtained from extrapolating the $4 + 2\epsilon$ expansion to $\epsilon = 1/2$, [52]. However a similar conformal bootstrap calculation did not find any evidence of this five dimensional conformal window, [59]. Contradicting conformal bootstrap results are not unusual as varying conditions are used for different bootstrap programs. In the case of [59] it is possible that the lower bound of the current central charge may not have captured the conformal window. However another possibility for these conflicting results is the poor asymptotic behaviour of the large N expansion. It was observed that the asymptotic behaviour of the $1/N$ expansion in five dimensions is significantly worse than in three dimensions, [51].

Other non-perturbative techniques besides conformal bootstrap have been applied to the $O(N)$ cubic theory in the dimension range $2 < d < 6$. The Functional Renormalization Group (FRG) was used as an approach to the critical $O(N)$ model above four dimensions by [181] and later in [63, 65]. The first worked with a local potential approximation of the original pure $O(N)$ model with quartic self interaction and found no physically admissible fixed point solution with a stable potential in the dimension range $4 < d < 6$. However this formalism may have

missed important non-perturbative information that is encoded in the Hubbard-Stratonovich parametrization. The later publications compared FRG results with the ϵ -expansion, favourably for $d \rightarrow 6$ although for $d \rightarrow 5$ the differences between the two approaches became sizeable. Additionally [65] produced proof of the existence of the universality class up to six dimensions. As a further application, the symmetry group of the cubic theory can be modified from $O(N)$ to the symplectic group, $Sp(N)$. The $1/N$ expansion for the $Sp(N)$ case was computed and found to be related to the corresponding $O(N)$ symmetric theory by a change of sign, $N \rightarrow -N$, [182]. Therefore the results point to the existence of an interacting non-unitary five dimensional CFT with $Sp(N)$ symmetry, [182]. This theory of anti-commuting scalar fields may be of interest in statistical mechanics and in the higher spin dS/CFT correspondence.

The $O(N)$ universality class was extended to eight dimensions in [54], and later reviewed in [156]. The Lagrangian is given by

$$L^{(4,8)} = \frac{1}{2} \partial_\mu \phi^i \partial^\mu \phi^i + \frac{1}{2} (\square \sigma)^2 + \frac{1}{2} g_1 \sigma \phi^i \phi^i + \frac{1}{6} g_2 \sigma^2 \square \sigma + \frac{1}{24} g_3^2 \sigma^4, \quad (3.12)$$

which is perturbatively renormalizable in eight dimensions. All possible relevant interactions are included to ensure renormalizability which is the reason for an interaction with a derivative coupling. On dimensional grounds there are more possible interactions with derivatives but only one is independent. They are all related by integration by parts (IBP) where the total derivative operators can be dropped from the Lagrangian as they can be integrated out of the action. Additionally (3.12) has a double pole σ propagator which is due to the fact that the canonical dimension of σ at the Wilson-Fisher fixed point is always two. This is also the reason why σ has a momentum dependent propagator in (3.8) but not in lower dimensions. The ϵ -expansion was used to calculate η and χ for the eight dimensional theory and then compared with the large N exponents where $d = 8 - 2\epsilon$, [54]. This ensured (3.12) exists in the same $O(N)$ universality class as the NL σ M, four dimensional ϕ^4 theory and the six dimensional cubic theory. An attempt to analyse the fixed point structure and conformal window of (3.12) found an interesting property. In eight dimensions several values of N_{crit} at leading order were found, [54],

$$N_{\text{crit}}^A = 0.006773, \\ N_{\text{crit}}^B = 0.043641,$$

$$N_{\text{crit}}^C = 0.109780 .$$

This suggests in effect that there is no conformal window, unlike the six dimensional case, as stable fixed points emerge for all $N \geq 1$. To illustrate this point the fixed point structure at leading order was computed for $N = 500$. Several fixed points emerged with one being stable. The fixed point structure of the eight dimensional theory is not as rich as the six dimensional case. However there is a related theory which does share similarities with Lagrangian (3.8), namely the eight dimensional theory (3.12) with an $Sp(N)$ symmetry. Varying scalar theories by altering the symmetry group was first considered for the six dimensional case, [182,183]. The first of which provided evidence that the $Sp(N)$ model contained a non-unitary UV fixed point in $d = 6 + 2\epsilon$ dimensions and suggested that the fixed points survive in seven dimensions. The absence of unitarity is due to the presence of anti-commuting scalars incorporated by the $Sp(N)$ symmetry. The RG functions for the $Sp(N)$ model can be derived from those of the $O(N)$ model by mapping $N \rightarrow -N$. The critical values of N for the eight dimensional $Sp(N)$ model which form the bounds of the conformal window were calculated to leading order, [54],

$$\begin{aligned} N_{\text{crit}}^A &= 13563.468614 + O(\epsilon) , \\ N_{\text{crit}}^B &= 6720.118606 + O(\epsilon) , \\ N_{\text{crit}}^C &= 6145.191926 + O(\epsilon) , \\ N_{\text{crit}}^D &= 2.894045 + O(\epsilon) . \end{aligned}$$

Above N_{crit}^A all fixed points were found to be real while for $N_{\text{crit}}^B < N < N_{\text{crit}}^A$ the fixed points are complex. In the interval between N_{crit}^B and N_{crit}^C all fixed points become real again while for $N_{\text{crit}}^D < N < N_{\text{crit}}^C$ only complex fixed point were found.

We have briefly reviewed the relevant published literature on the $O(N)$ universality class in the dimension range $2 < d < 8$ for motivation as to why this universality class is so important. Perturbative and non-perturbative work endowed with $O(N)$ and related symmetries has been examined. Although much of the literature has focused on calculations performed in even dimensions, physics in the fixed dimensions $d = 3, 5$ and 7 can be accessed through non-perturbative methods or by the perturbative ϵ and large N expansions. Most importantly we discussed calculations of the critical exponents in four, six and eight dimensions which matched with large N results, providing strong evidence for this universality class. An illustration of how these theories are linked is provided in figure 3.1. This diagram shows, for example, that the Wilson-Fisher fixed point obtained

using the $2 + 2\epsilon$ expansion in the NL σ M is equivalent to the fixed point of the $4 - 2\epsilon$ expansion in ϕ^4 theory. The former non-trivial fixed point will be UV stable while the latter is IR stable.

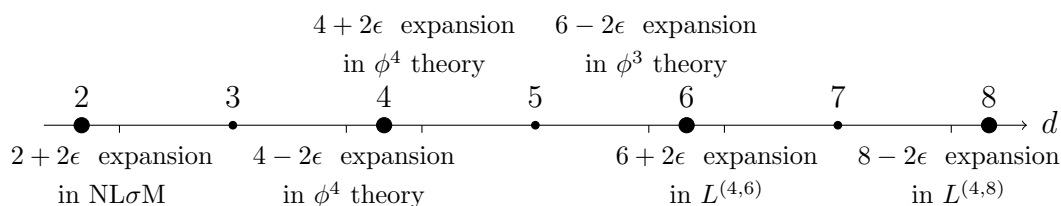


Figure 3.1: Summary of the $O(N)$ universality class of interacting symmetric scalar theories thus far. The interacting theory may be described in $2 + 2\epsilon$ and $4 + 2\epsilon$ dimensions by a UV stable Wilson-Fisher fixed point of the NL σ M and ϕ^4 theory respectively. In $4 - 2\epsilon$ and $6 - 2\epsilon$ dimensions it may be described as an IR stable fixed point of ϕ^4 and the cubic theory respectively. While for $6 + 2\epsilon$ and $8 - 2\epsilon$ dimensions the interacting theory may be described by a UV stable fixed point of the cubic and 8-dimensional theories respectively.

3.3 Ten Dimensions

There also exists a ten dimensional extension of the $O(N)$ symmetric universality class of scalar theories. The calculation of the RG functions in ten dimensions has been published in [3] and adds original results to the development of the tower of theories. As well as extending the universality class to a higher dimension, the main motivation for looking at the ten dimensional case is to analyse the fixed point structure for comparison with lower dimensions. The first step in the calculation is to construct the ten dimensional Lagrangian. The key here is the use of the canonical dimensions of the two basic fields given by (2.55). Recall that at the Wilson-Fisher fixed point the universal interaction alone defines the dynamics; quadratic terms define the dimensionality of the fields.

Using the canonical dimensions of the basic fields we ensure all relevant interactions at ten dimensions are included in the Lagrangian which ensures renormalizability. Note that the auxiliary field σ will have the same canonical dimension throughout the universality class, while ϕ^i has a canonical dimension of 1, 2, 3 and 4 in four, six, eight and ten dimensions, respectively. One consequence is that in each of these dimensions the $\sigma\phi^i\phi^i$ operator is preserved and moreover no new $\phi^i - \sigma$ interactions can be included. In order to ensure renormalizability in ten dimensions, extra pure σ (spectator) interactions have to be added which can include derivative interactions. The ten dimensional scalar Lagrangian is

therefore given by

$$\begin{aligned}
L^{(4,10)} = & \frac{1}{2} \partial_\mu \phi^i \partial^\mu \phi^i + \frac{1}{2} (\square \partial^\mu \sigma) (\square \partial_\mu \sigma) + \frac{1}{2} g_1 \sigma \phi^i \phi^i + \frac{1}{6} g_2 \sigma^2 \square^2 \sigma \\
& + \frac{1}{2} g_3 \sigma (\square \sigma)^2 + \frac{1}{24} g_4^2 \sigma^3 \square \sigma + \frac{1}{120} g_5^3 \sigma^5 .
\end{aligned} \tag{3.13}$$

This Lagrangian will contain an $O(N)$ symmetry and to provide conclusive evidence it lies in the same universality class as the previous $O(N)$ theories, we compute the critical exponents perturbatively using the ϵ -expansion. These exponents can then be compared order by order with known large N results. The Feynman rules for the ten dimensional theory can be found from Lagrangian (3.13). In essence the free Lagrangian determines the propagator while the interaction terms define the vertex rules. Note that solid lines indicate ϕ^i fields while the σ fields are illustrated using dotted lines.

Figure 3.2: Feynman rules for the Green's functions of $O(N)$ symmetric scalar theory with Lagrangian $L^{(4,10)}$. Note all momenta are directed inwards in the vertices.

3.4 Calculation Techniques

The computational methods and techniques used for this calculation are discussed here. A similar set-up will be implemented for computations in the following Chapters with subtle differences noted when appropriate. Given the vast number of Feynman diagrams considered throughout this thesis we utilize several computer programs which simplify the calculation process, [184–187]. To begin all

Feynman diagrams corresponding to each of the Green's functions are electronically generated using the QGRAF package, [184]. Specifying the incoming particles and allowed interactions, the loop momenta and the number of loops, QGRAF will define the graphical structure of all possible diagrams. In our set-up we choose to have all particles incoming, as is consistent with our momentum routing in the Feynman rules. The QGRAF input model file used for the ten dimensional calculation is shown in figure 3.3.

```
[phi, phi, +]
[sigma, sigma, +]
[sigma, phi, phi]
[sigma, sigma, sigma]
[sigma, sigma, sigma, sigma]
[sigma, sigma, sigma, sigma, sigma]
```

Figure 3.3: QGRAF input model file for the ten dimensional calculation.

We forbid all tadpole and snail diagrams from the output and include only one-particle irreducible (1PI) graphs. A diagram is irreducible if it cannot be split into two disconnected graphs by cutting only one internal line. Tadpole diagrams cannot be considered irreducible as they contain one external leg and are therefore excluded. Since we are in a massless regime we also have no need to consider snail diagrams due to them vanishing when using dimensional regularisation. Both tadpole and snail graphs are illustrated in figure 3.4.

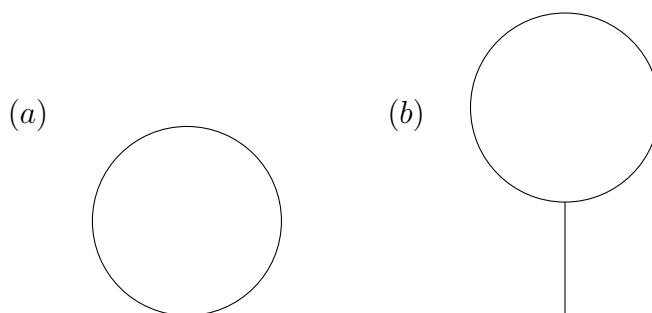


Figure 3.4: (a) Snail Feynman diagram, (b) Tadpole Feynman diagram.

The total number of Feynman diagrams generated for the ten dimensional theory is given in table 3.1. Two-point functions will be calculated to two loops while all higher point interactions will be calculated to one loop only. Therefore the β -function for each coupling and the anomalous dimensions will be computed

to one and two loops respectively. Although computational limitations would eventually hinder our progress, we could in theory calculate the β -functions to a higher loop order. However for the purpose of a qualitative fixed point analysis calculating to one loop is sufficient.

	$\phi\phi$	$\sigma\sigma$	$\sigma\phi\phi$	$\sigma^2\Box^2\sigma$ and $\sigma(\Box\sigma)^2$	$\sigma^3\Box\sigma$	σ^5
Tree Level	-	-	1	1	1	1
One Loop	1	2	2	5	19	89
Two Loop	5	11	-	-	-	-

Table 3.1: Number of Feynman Diagrams computed for each 2, 3, 4 and 5- point function. Total number of Feynman diagrams is 138.

As an example we have displayed the QGRAF output data for a 3-point Feynman diagram in figure 3.5 along with its graphical representation in figure 3.6. The 3-point diagram contains both ϕ^i and σ fields, the ordering of each vertex and internal line structure which connects them is encoded in the QGRAF output. Once all Feynman diagrams have been generated we identify and order the graphs into their basic topologies and apply $O(N)$ indices automatically using FORM, [185]. The computer package FORM and its threaded version TFORM, [186], have been used extensively throughout this calculation. The Feynman rules for the propagators and vertices are then substituted in. This ensures the graphs are picked up at the appropriate place in the subsequent program.

Finally REDUZE [187, 190], is used to simplify the Feynman diagrams into a final set of master integrals which can be computed by hand. Throughout this thesis the first version of REDUZE is implemented, [187], which is written in GINAC [191], and works by using a C++ implementation of the Laporta algorithm. The Laporta algorithm systematically reduces scalar integrals to a set of basic master integrals using a technique known as integration by parts, [192, 193].

```
*vx(sigma(2),phi(-1),phi(1))
*vxi(sigma(3),phi(-3),phi(1))
*vxi(sigma(-5),sigma(2),sigma(3))
```

Figure 3.5: QGRAF output file for a 3-point Feynman diagram.

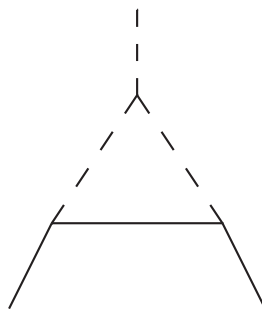


Figure 3.6: 3-point Feynman diagram at one loop with σ and ϕ^i fields.

In the REDUZE implementation of the Laporta algorithm the package starts with an auxiliary topology and uses integration by parts (IBP) and Lorentz invariant (LI) relations to generate connections involving this topology and lower topologies which can be obtained by removing an internal propagator. Any integrals that cannot be ultimately simplified this way are called master integrals. Consider a diagram with l loops and m independent external momenta. An auxiliary topology (or integral family) is an ordered set of all propagators $A_n = \{P_1, \dots, P_n\}$ where all scalar products containing at least one loop momenta k_i can be expressed as a linear combination of propagators from this set A_n . An auxiliary topology for any diagram must contain exactly $l[\frac{1}{2}(l+1) + m]$ propagators or a reduction cannot happen. A database containing relations between integrals is constructed which can be used to simplify Feynman integrals. The Laporta algorithm creates all possible relations between the scalar integrals thus resulting in a large degree of redundancy in reducing graphs. With the Laporta algorithm it is possible to compute any l -loop and n -point function provided one has a big enough computer and disk capacity. It is important to understand what REDUZE is doing internally when performing integral reduction before any master integrals are calculated. We will illustrate the procedure by applying the Laporta algorithm to the scalar 3-point function at one loop.

3.4.1 Integral Reduction

A 3-point Feynman diagram at one loop that can be reduced is displayed in figure 3.7. There are two independent external momenta p and q , while k describes the internal loop momenta.

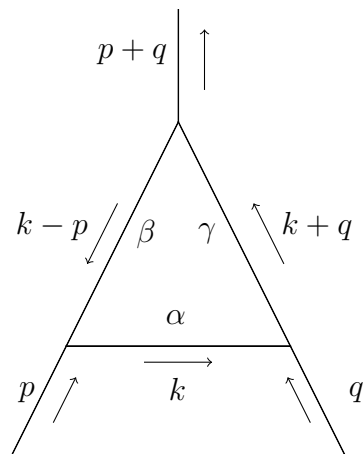


Figure 3.7: A one loop 3-point Feynman diagram.

The general definition of the one loop diagram containing three propagators is

$$\mathcal{I}_{31}(\alpha, \beta, \gamma) = \int \frac{d^d k}{(2\pi)^d} \frac{1}{(k^2)^\alpha ((k-p)^2)^\beta ((k+q)^2)^\gamma}. \quad (3.14)$$

The notation is explained here as it will be used throughout this Chapter. For \mathcal{I}_{ij} the first index i of the subscript will denote the number of external propagators while j signifies the loop order. The integral will be assumed to be at the completely symmetric point unless a superscript O label is present. This integrand is of the form $1/(abc)$ where a , b and c are products of the propagators. We will reduce this integral at the fully symmetric point where each external leg has the same value of squared momenta and the following conditions are satisfied

$$\begin{aligned} p^2 &= q^2 = (p+q)^2 = -\mu^2, \\ pq &= pr = qr = \frac{\mu^2}{2}. \end{aligned} \quad (3.15)$$

This gives a symmetric identity on the 3-point integral

$$\mathcal{I}_{31}(\alpha, \beta, \gamma) = \mathcal{I}_{31}(\alpha, \gamma, \beta) = \mathcal{I}_{31}(\beta, \gamma, \alpha) = \dots \quad (3.16)$$

As an example, if we take the integral $\mathcal{I}_{31}(2, 1, 1)$ given by

$$\mathcal{I}_{31}(2, 1, 1) = \int \frac{d^d k}{(2\pi)^d} \frac{1}{(k^2)^2 (k-p)^2 (k+q)^2} \quad (3.17)$$

one can derive the relation $\mathcal{I}_{31}(2, 1, 1) = \mathcal{I}_{31}(1, 2, 1) = \mathcal{I}_{31}(1, 1, 2)$. Written out completely in integral form this is

$$\mathcal{I}_{31}(2, 1, 1) = \int \frac{d^d k}{(2\pi)^d} \frac{1}{(k^2)^2 (k-p)^2 (k+q)^2} \quad (3.18a)$$

$$= \int \frac{d^d k}{(2\pi)^d} \frac{1}{k^2((k-p)^2)(k+q)^2} \quad (3.18b)$$

$$= \int \frac{d^d k}{(2\pi)^d} \frac{1}{k^2(k-p)^2((k+q)^2)} . \quad (3.18c)$$

To prove this relation more explicitly, one can take integral (3.17) and perform a change of variable $k \rightarrow k+p$. Using the symmetric point conditions of (3.16) this retrieves the third relation (3.18c). Similarly by using the change of variable $k \rightarrow k-q$ one can find the second relation (3.18b).

Using the method of integration by parts we want to reduce the integral given by equation (3.14) down to a set of master integrals which can be solved by hand, or by other methods. Using dimensional regularisation properties we know that an integral over a total derivative is zero

$$\int d^d k \frac{\partial}{\partial k^\mu} f(k^2) = 0 . \quad (3.19)$$

This is also zero on Lorentz grounds if $f(k^2)$ is a scalar. Applying (3.19) to equation (3.14) the following relation can be found

$$\int \frac{d^d k}{(2\pi)^d} \frac{\partial}{\partial k^\mu} [k^\mu I_{31}(\alpha, \beta, \gamma)] = \int \frac{d^d k}{(2\pi)^d} \left[dI_{31}(\alpha, \beta, \gamma) + k^\mu \frac{\partial}{\partial k^\mu} I_{31}(\alpha, \beta, \gamma) \right] = 0$$

where we have used the notation $\mathcal{I}_{31}(\alpha, \beta, \gamma) = \int_k I_{31}(\alpha, \beta, \gamma)$ to simplify the equation. The second term can be moved to the right-hand side to obtain

$$d \int \frac{d^d k}{(2\pi)^d} I_{31}(\alpha, \beta, \gamma) = - \int \frac{d^d k}{(2\pi)^d} k^\mu \frac{\partial}{\partial k^\mu} I_{31}(\alpha, \beta, \gamma) . \quad (3.20)$$

Explicitly differentiating each term in the denominator of $I_{31}(\alpha, \beta, \gamma)$ in turn one finds

$$\begin{aligned} \int_k \frac{d}{(k^2)^\alpha ((k-p)^2)^\beta ((k+q)^2)^\gamma} &= 2\alpha \int_k \frac{k^2}{(k^2)^{\alpha+1} ((k-p)^2)^\beta ((k+q)^2)^\gamma} \\ &+ 2\beta \int_k \frac{k(k-p)}{(k^2)^\alpha ((k-p)^2)^{\beta+1} ((k+q)^2)^\gamma} \\ &+ 2\gamma \int_k \frac{k(k+q)}{(k^2)^\alpha ((k-p)^2)^\beta ((k+q)^2)^{\gamma+1}} . \end{aligned}$$

The numerator of each individual integral can be rearranged using basic algebra

$$\int_k \frac{d}{(k^2)^\alpha ((k-p)^2)^\beta ((k+q)^2)^\gamma} = 2\alpha \int_k \frac{1}{(k^2)^\alpha ((k-p)^2)^\beta ((k+q)^2)^\gamma}$$

$$\begin{aligned}
& + \beta \int_k \frac{k^2 + (k-p)^2 - p^2}{(k^2)^\alpha ((k-p)^2)^{\beta+1} ((k+q)^2)^\gamma} \\
& + \gamma \int_k \frac{k^2 + (k+q)^2 - q^2}{(k^2)^\alpha ((k-p)^2)^\beta ((k+q)^2)^{\gamma+1}} .
\end{aligned}$$

These integrals can then be rewritten using the notation $\mathcal{I}_{31}(\alpha, \beta, \gamma)$. Implementing this convention and factorising terms on both sides of the equation the following relation is obtained

$$\begin{aligned}
(d - 2\alpha - \beta - \gamma)\mathcal{I}_{31}(\alpha, \beta, \gamma) & = \beta[\mathcal{I}_{31}(\alpha - 1, \beta + 1, \gamma) - p^2\mathcal{I}_{31}(\alpha, \beta + 1, \gamma)] \\
& + \gamma[\mathcal{I}_{31}(\alpha - 1, \beta, \gamma + 1) - q^2\mathcal{I}_{31}(\alpha, \beta, \gamma + 1)] . \quad (3.21)
\end{aligned}$$

Taking the most general case by setting $\alpha = \beta = \gamma = 1$,

$$\mathcal{I}_{31}(1, 2, 1) = \frac{1}{\mu^2} \left[\frac{1}{2}(d-4)\mathcal{I}_{31}(1, 1, 1) - \mathcal{I}_{31}(0, 2, 1) \right] . \quad (3.22)$$

The identity given by equation (3.16) has been used to simplify the above relation which is illustrated in figure 3.8. Integrals $\mathcal{I}_{31}(0, 2, 1)$ and $\mathcal{I}_{31}(1, 1, 1)$ are master integrals which can be calculated by hand. Additionally the integral $\mathcal{I}_{31}(0, 2, 1)$ is proportional to $\mathcal{I}_{31}(0, 1, 1)$ as

$$\mathcal{I}_{31}(0, 2, 1) = \nu(2, 1, d-3) = \frac{\pi^{d/2}\Gamma(\frac{d}{2}-2)\Gamma(\frac{d}{2}-1)\Gamma(3-\frac{d}{2})}{\Gamma(d-3)} ,$$

then, due to the property $\Gamma(z+1) = z\Gamma(z)$,

$$\mathcal{I}_{31}(0, 2, 1) = \frac{\pi^{d/2}\Gamma(\frac{d}{2}-1)^2\Gamma(2-\frac{d}{2})(d-3)}{\Gamma(d-2)} = (3-d)\nu(1, 1, d-2) .$$

Therefore

$$\mathcal{I}_{31}(0, 2, 1) = (3-d)\mathcal{I}_{31}(0, 1, 1) .$$

A comprehensive derivation of the solution to the 3-point integral $\mathcal{I}_{31}(1, 1, 1)$ in $d = 4 - 2\epsilon$ dimensions is given by [194, 197] with the latter notation used here,

$$\begin{aligned}
\mathcal{I}_{31}(1, 1, 1) & = \frac{1}{\mu^2} \left(\frac{2\pi^2}{9} - \frac{2}{3}\psi' \left(\frac{1}{3} \right) + \left[12s_3 \left(\frac{\pi}{6} \right) - \frac{35}{108} \frac{\pi^3}{\sqrt{3}} - \frac{\log^2(3)\pi}{4\sqrt{3}} \right] \epsilon \right. \\
& \left. + O(\epsilon^2) \right) \quad (3.23)
\end{aligned}$$

where

$$s_n(z) = \frac{1}{\sqrt{3}} \Im \left[\text{Li}_n \left(\frac{e^{iz}}{\sqrt{3}} \right) \right] \quad (3.24)$$

and $\text{Li}_n(z)$ is the polylogarithm function for $n \geq 2$. The digamma function is

given by $\psi(z) = \Gamma'(z)/\Gamma(z)$ where the prime denotes the derivative of the Γ -function. We have used the notation of [194] but it is worth noting that they are related to cyclotomic polynomials, [198]. To assist the evaluation of the integral numerically we note

$$\begin{aligned}\zeta_3 &= 1.20205690, \quad \psi'(\tfrac{1}{3}) = 10.09559713, \quad \psi'''(\tfrac{1}{3}) = 488.1838167 \\ s_2(\tfrac{\pi}{2}) &= 0.32225882, \quad s_2(\tfrac{\pi}{6}) = 0.22459602, \quad s_3(\tfrac{\pi}{2}) = 0.32948320 \\ s_3(\tfrac{\pi}{6}) &= 0.19259341.\end{aligned}$$

In this thesis the Laporta algorithm will always reduce Feynman diagrams down to a set of master integrals containing simple propagators of the form $1/k^2$. This means that even graphs containing tensor structure in the numerator are reduced down to simple scalar diagrams. Note that in general master integrals can contain double propagators of the form $1/(k^2)^2$, however we do not encounter these in any of our calculations.

Figure 3.8: Reduction of a 3-point integral at one loop with higher power propagators to a set of master integrals.

Inserting the value of the master integral $\mathcal{I}_{31}(0, 2, 1)$ for completeness,

$$\mathcal{I}_{31}(1, 2, 1) = \frac{1}{2\mu^2} \left[(d-4)\mathcal{I}_1(1, 1, 1) - \frac{2\Gamma(3 - \frac{d}{2})\Gamma(\frac{d}{2} - 2)\Gamma(\frac{d}{2} - 1)(-\mu^2)^{\frac{d}{2}-3}}{(4\pi)^{\frac{d}{2}}\Gamma(d-3)} \right]. \quad (3.25)$$

This gives a basic understanding of how the Laporta algorithm works using integration by parts. The Laporta algorithm can be applied to diagrams with more complex structures and a higher numbers of loops in principle. In subsequent calculations we will derive the reduction of the 3-point function at the completely off-shell point which is more involved and requires a different external momentum set-up. The 2-point and 4-point functions at the fully symmetric point will also be reduced. For now we have enough understanding of how REDUZE works internally to move on and begin calculating the master integrals themselves.

3.4.2 2-point Master Integrals

At one and two loops QGRAF produces nineteen 2-point Feynman diagrams containing ϕ^i and σ fields. The three one loop graphs are illustrated in figure 3.9, while the two loop diagrams are given in figures 3.10 and 3.11. At two loops we have five diagrams with incoming ϕ^i fields and eleven graphs containing incoming σ fields.

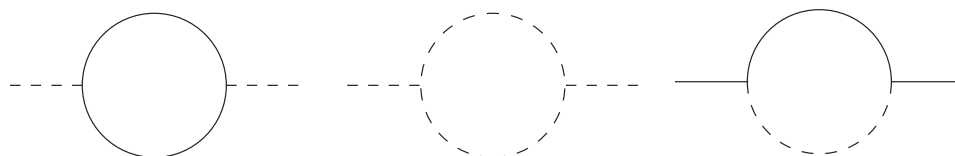


Figure 3.9: One loop 2-point Feynman diagrams.

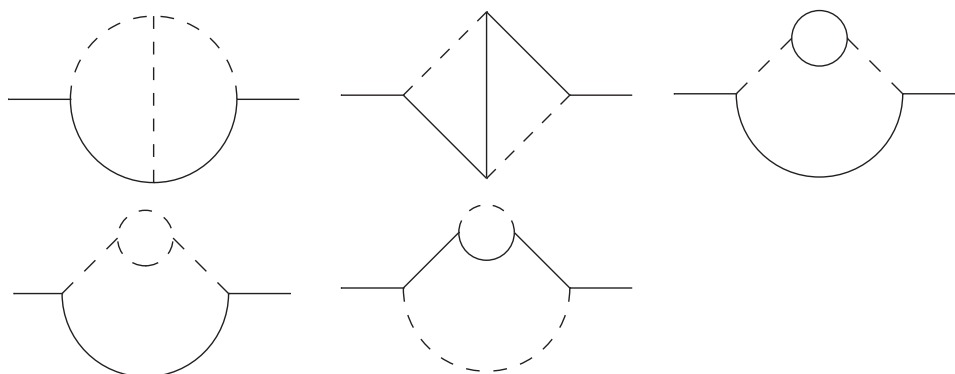


Figure 3.10: Two loop 2-point Feynman diagrams with incoming ϕ^i fields.

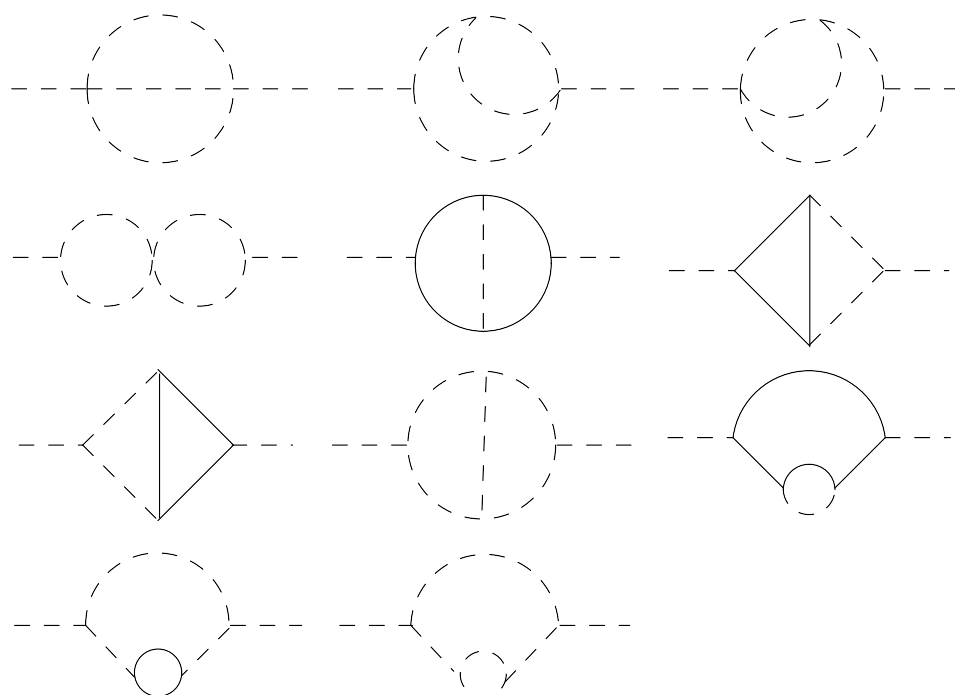


Figure 3.11: Two loop 2-point Feynman diagrams with incoming σ fields.

All nineteen Feynman diagrams can be reduced using the Laporta algorithm to a set of master integrals. The one loop master integral is illustrated in figure 3.12 and is labelled $\mathcal{I}_{21}(1, 1)$ where the second subscript indicates one loop. The two loop master integrals are given in figure 3.13 and are labelled $(\mathcal{I}_{21}(1, 1))^2$ and $\mathcal{I}_{22}(1, 1, 0, 0, 1)$. The notation for the second two loop master integral becomes more clear when looking at the 2-point auxiliary topology or integral family at two loops which is illustrated in figure 3.14. The values $\alpha, \beta, \gamma, \rho$ and δ signify the power on each of the five propagators and by contracting two of these propagators we obtain the second 2-point master integral. The internal loop momenta are denoted as k and q and all master integrals are constructed using propagators of the form $1/k^2$, irrespective of what fields the original diagrams which have been reduced contain.

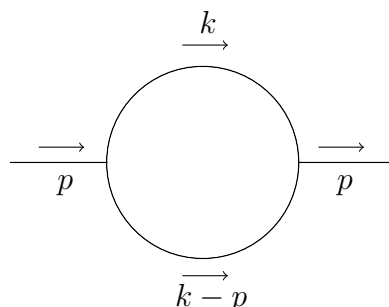


Figure 3.12: The 2-point master Feynman diagram at one loop, $\mathcal{I}_{21}(1, 1)$.

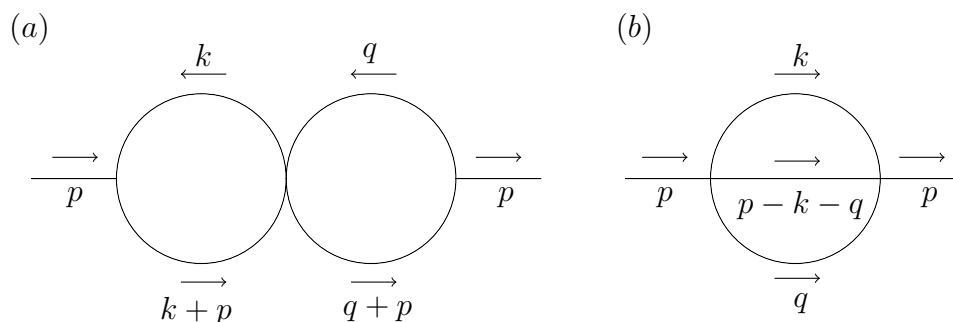


Figure 3.13: The 2-point master Feynman diagrams at two loops (a) $(\mathcal{I}_{21}(1, 1))^2$, (b) $\mathcal{I}_{22}(1, 1, 0, 0, 1)$.

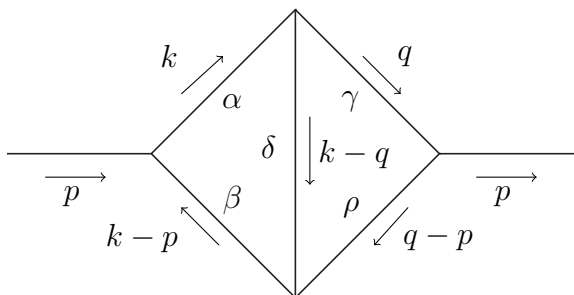


Figure 3.14: The integral family $\mathcal{I}_{22}(\alpha, \beta, \gamma, \rho, \delta)$ for 2-point Feynman diagram at two loops.

The 2-point master Feynman diagram at one loop can be defined as an integral of the form

$$\mathcal{I}_{21}(1, 1) = \int \frac{d^d k}{(2\pi)^d} \frac{1}{k^2(k-p)^2}. \quad (3.26)$$

Using identity (2.6) from the previous Chapter this integral can be easily solved

$$\mathcal{I}_{21}(1, 1) = \frac{\Gamma(2 - \frac{d}{2})\Gamma(\frac{d}{2} - 1)^2(p^2)^{\frac{d}{2}-2}}{(4\pi)^{\frac{d}{2}}\Gamma(d-2)}. \quad (3.27)$$

For the theory of interest the value of the master integral in $d = 10 - 2\epsilon$ dimensions is

$$\begin{aligned} \mathcal{I}_{21}^{(d=10-2\epsilon)}(1, 1) &= \left[-\frac{1}{840\epsilon} - \frac{44}{11025} + \left(\frac{\pi^2}{10080} - \frac{10973}{10080} \right) \epsilon \right. \\ &\quad + \left(\frac{11\pi^2}{33075} - \frac{2449616}{121550625} + \frac{\zeta_3}{360} \right) \epsilon^2 \\ &\quad \left. + O(\epsilon^3) \right] \frac{(p^2)^3}{(4\pi)^5}. \end{aligned} \quad (3.28)$$

Note that the factor of 2ϵ in the dimension is purely a convention choice on behalf of the author to enable a more convenient matching with large N results later. The symbol ζ_n is the Riemann zeta function. The full set of master integrals for this diagram and other relevant master integrals in four, six, eight and ten dimensions are listed in Appendix A. The first 2-point diagram at two loops given in figure 3.13 (a) can be calculated using the same identity (2.6) used for the one loop graph. The general d -dimensional result is

$$\begin{aligned} (\mathcal{I}_{21}(1, 1))^2 &= \int \frac{d^d k}{(2\pi)^d} \frac{1}{(k^2)^2((k+p)^2)^2} \\ &= \frac{\Gamma(2 - \frac{d}{2})^2\Gamma(\frac{d}{2} - 1)^4(p^2)^{d-4}}{(4\pi)^d\Gamma(d-2)^2}, \end{aligned} \quad (3.29)$$

and in $d = 10 - 2\epsilon$ dimensions this becomes

$$\begin{aligned}
(\mathcal{I}_{21}^{(d=10-2\epsilon)}(1, 1))^2 &= \left[\frac{1}{705600\epsilon^2} + \frac{11}{1157625\epsilon} - \frac{\pi^2}{4233600} + \frac{6239}{162067500} \right. \\
&\quad + \left(\frac{1578028}{12762815625} - \frac{\zeta_3}{151200} - \frac{11\pi^2}{6945750} \right) \epsilon \\
&\quad + \left(-\frac{22\zeta_3}{496125} + \frac{186958937}{536038256250} - \frac{6239\pi^2}{972405000} \right. \\
&\quad \left. \left. - \frac{\pi^4}{12096000} \right) \epsilon^2 + O(\epsilon^3) \right] \frac{(p^2)^6}{(4\pi)^{10}}. \tag{3.30}
\end{aligned}$$

Finally one can evaluate the diagram illustrated in figure 3.13 (b) by computing the following integral

$$\mathcal{I}_{22}(1, 1, 0, 0, 1) = \int \frac{d^d k}{(2\pi)^d} \frac{d^d q}{(2\pi)^d} \frac{1}{k^2 q^2 (p - k - q)^2}. \tag{3.31}$$

The conformal or chain integration technique introduced in the previous Chapter is used to evaluate the integral. The solution is illustrated in figure 3.15.

$$\begin{aligned}
&= \nu(1, 1, d-2) \nu(1, 2 - \frac{d}{2}, \frac{3}{2}d - 3) \nu(1, 1, d-2) \\
&= \nu(1, 1, d-2) \nu(1, 2 - \frac{d}{2}, \frac{3}{2}d - 3) (p^2)^{d-3}
\end{aligned}$$

Figure 3.15: Integration of the 2-point Feynman diagram $\mathcal{I}_{22}(1, 1, 0, 0, 1)$ at two loops.

Coordinate space integration has been implemented twice as is apparent from the inclusion of two $\nu(\alpha, \beta, \gamma)$ terms. This leaves us with a single propagator which can be rewritten in terms of p^2 . The general solution in d -dimensions can then be written as

$$\mathcal{I}_{22}(1, 1, 0, 0, 1) = \frac{\Gamma(\frac{d}{2} - 1)^3 \Gamma(3 - d) \pi^d}{\Gamma(\frac{3}{2}d - 3) (p^2)^{3-d}}. \tag{3.32}$$

For completeness we note the result in $d = 10 - 2\epsilon$ dimensions,

$$\mathcal{I}_{22}^{(d=10-2\epsilon)}(1, 1, 0, 0, 1) = \left[-\frac{1}{1862784000\epsilon} - \frac{11129}{4917749760000} \right]$$

$$\begin{aligned}
& + \left(-\frac{19\pi^2}{89413632000} - \frac{3968371859}{636160108953600000} \right) \epsilon \\
& + \left(-\frac{2742996689341}{186606965293056000000} + \frac{67\zeta_3}{44706816000} \right. \\
& \left. - \frac{211451\pi^2}{236051988480000} \right) \epsilon^2 + O(\epsilon^3) \Big] (p^2)^7. \quad (3.33)
\end{aligned}$$

The computed master Feynman integrals at one and two loops can then be substituted into the relations derived by REDUZE to solve for all nineteen 2-point functions.

3.4.3 Tarasov Method

The 3 and 4-point master integrals require a new technique as unlike the 2-point diagrams, they cannot be computed as easily in ten dimensions. Tarasov's method of relating d and $(d+2)$ -dimensional integrals was first developed in [195, 196] and will be introduced here. Tarasov observed that the Schwinger parameter representation of a d -dimensional topology could be simply rewritten as a sum of $(d+2)$ -dimensional integrals with the same topologies but higher power propagators. The latter can then be integrated to master integrals using an integration by parts routine. The unknown master integrals can then be solved for. Therefore, known results for the master integrals in four dimensions can be used to solve for the same integrals or a parallel topology in six dimensions. Following that we can use the obtained six dimensional results to find eight dimensional integrals and so on until we derive results in ten dimensions. To understand the Tarasov methodology it is sufficient work through an example using the 3-point function, the 4-point function will follow a very similar derivation. Techniques introduced in [47–50] will be followed closely here.

We begin by looking at the 3-point one loop graph illustrated in figure 3.7. As a reminder this diagram is represented by the following integral

$$\mathcal{I}_{31}(\alpha, \beta, \gamma) = \int \frac{d^d k}{(2\pi)^d} \frac{1}{(k^2)^\alpha ((k-p)^2)^\beta ((k+q)^2)^\gamma}. \quad (3.34)$$

All propagators can be put into parametric form using the identity

$$\frac{1}{(k^2)^\alpha} = \frac{i^{-\alpha}}{\Gamma(\alpha)} \int_0^\infty d\lambda_i \lambda_i^{\alpha-1} \exp(i\lambda_i k^2). \quad (3.35)$$

The integral then becomes

$$\begin{aligned} \mathcal{I}_{31}(\alpha, \beta, \gamma) &= \int \frac{d^d k}{(2\pi)^d} \left(\frac{i^{-\alpha}}{\Gamma(\alpha)} \int_0^\infty d\lambda_1 \lambda_1^{\alpha-1} \exp(i\lambda_1 k^2) \right) \\ &\quad \times \left(\frac{i^{-\beta}}{\Gamma(\beta)} \int_0^\infty d\lambda_2 \lambda_2^{\beta-1} \exp(i\lambda_2 (k-p)^2) \right) \\ &\quad \times \left(\frac{i^{-\gamma}}{\Gamma(\gamma)} \int_0^\infty d\lambda_3 \lambda_3^{\gamma-1} \exp(i\lambda_3 (k+q)^2) \right). \end{aligned}$$

This equation can be simplified by expanding out the brackets and introducing the notation $A = \lambda_1 + \lambda_2 + \lambda_3$ and $B = \lambda_3 q - \lambda_2 p$,

$$\begin{aligned} \mathcal{I}_{31}(\alpha, \beta, \gamma) &= \int \frac{d^d k}{(2\pi)^d} \int_0^\infty \int_0^\infty \int_0^\infty d\lambda_1 d\lambda_2 d\lambda_3 \frac{i^{-\alpha} i^{-\beta} i^{-\gamma}}{\Gamma(\alpha)\Gamma(\beta)\Gamma(\gamma)} \lambda_1^{\alpha-1} \lambda_2^{\beta-1} \lambda_3^{\gamma-1} \\ &\quad \times \exp[ik^2 A + 2kB + \lambda_3 q^2 - \lambda_2 p^2]. \end{aligned}$$

The following d -dimensional Gaussian integral formula, [196],

$$\int d^d k \exp[i(xk^2 + 2pk)] = i \left(\frac{\pi}{ix} \right)^{d/2} \exp \left(i \frac{ip^2}{x} \right),$$

can then be used to simplify the result further. The 3-point integral can now be written as

$$\begin{aligned} \mathcal{I}_{31}(\alpha, \beta, \gamma) &= \frac{i^{-(\alpha+\beta+\gamma)}}{(2\pi)^d} \int_0^\infty \int_0^\infty \int_0^\infty d\lambda_1 d\lambda_2 d\lambda_3 \frac{\lambda_1^{\alpha-1} \lambda_2^{\beta-1} \lambda_3^{\gamma-1}}{\Gamma(\alpha)\Gamma(\beta)\Gamma(\gamma)} i \left(\frac{\pi}{i} \right)^{d/2} \\ &\quad \times \exp \left(\frac{-iB^2}{A} \right) \exp(\lambda_3 q^2 - \lambda_2 p^2) \frac{1}{A^{d/2}}. \end{aligned}$$

The paramount step in this derivation is contained in the following algebraic rearrangement. A factor of A is inserted into the numerator by reducing the power of the same variable in the denominator. This has the effect of raising the power on the propagator in the original Feynman integral by one, as will become clear when looking at the graphical representation of this equation,

$$\begin{aligned} \mathcal{I}_{31}(\alpha, \beta, \gamma) &= \frac{i^{-(\alpha+\beta+\gamma)}}{(2\pi)^d} \int_0^\infty \int_0^\infty \int_0^\infty d\lambda_1 d\lambda_2 d\lambda_3 \frac{\lambda_1^{\alpha-1} \lambda_2^{\beta-1} \lambda_3^{\gamma-1}}{\Gamma(\alpha)\Gamma(\beta)\Gamma(\gamma)} \left(\frac{\pi}{i} \right)^{d/2} \\ &\quad \times \exp \left(\frac{-iB^2}{A} \right) \exp(\lambda_3 q^2 - \lambda_2 p^2) \frac{A}{A^{\frac{d+2}{2}}}. \end{aligned}$$

Taking the most general case by setting $\alpha = \beta = \gamma = 1$ and translating into the original integral form,

$$\mathcal{I}_{31}^{(d)}(1, 1, 1) = \int \frac{d^{d+2} k}{(2\pi)^{d+2} (k^2)^2 (k-p)^2 (k+q)^2}$$

$$\begin{aligned}
& + \int \frac{d^{d+2}k}{(2\pi)^{d+2}k^2((k-p)^2)^2(k+q)^2} \\
& + \int \frac{d^{d+2}k}{(2\pi)^{d+2}k^2(k-p)^2((k+q)^2)^2} . \quad (3.36)
\end{aligned}$$

The integral $\mathcal{I}_{31}^{(d)}(1, 1, 1)$ is d -dimensional while the three integrals on the right-hand side of the equation are $(d+2)$ -dimensional. This relation is illustrated in figure 3.16 with the d -dimensional integrals moved to the right-hand side. The power on each of the propagators is displayed rather than momentum flow and the dimension of each diagram is explicitly labelled.

$$\left[\begin{array}{c} \text{Triangle 1} \\ \text{Triangle 2} \\ \text{Triangle 3} \end{array} \right]_{(d+2)} - \text{Triangle 4}_d = 0$$

Figure 3.16: Tarasov method of relating d and $(d+2)$ -dimensional Feynman integrals.

The integration by parts routine introduced in figure 3.8 can be used to reduce the $(d+2)$ -dimensional diagrams,

$$\frac{1}{\mu^2} \left[\frac{3}{2}(d-4)\mathcal{I}_{31}^{(d+2)}(1, 1, 1) - 3\mathcal{I}_{31}^{(d+2)}(0, 2, 1) \right] - \mathcal{I}_{31}^{(d)}(1, 1, 1) = 0 . \quad (3.37)$$

This is illustrated in figure 3.17 for clarity.

$$\frac{3}{2\mu^2}(d-4) \text{Triangle}_d = \text{Triangle}_d + \frac{3}{\mu^2} \text{Circle}_{(d+2)}$$

Figure 3.17: The 3-point graph at one loop with both the Tarasov method and an IBP routine applied at the fully symmetric point.

Figure 3.17 relates d and $(d+2)$ -dimensional one loop 3-point integrals at the fully symmetric point. To summarise, if the d -dimensional 3-point graph at one loop is known then only the simpler $(d+2)$ -dimensional diagrams containing

two propagators need to be calculated before one can solve for the 3-point ($d + 2$)-dimensional result. Therefore the known four dimensional result for the 3-point graph at one loop can be related to the diagram in ten dimensions by iteration. Note that computing the simpler diagram with two propagators is a trivial task in any dimension. Any higher loop 2-point integrals in $(d + 2)$ -dimensions that arise in can be simplified using REDUZE. The wide ranging usability of the Tarasov method over a number of theories has made it a tool of great importance throughout quantum field theory.

3.4.4 Master Integrals with Three Propagators

We now return to calculating the ten dimensional master integrals for the $O(N)$ scalar theory. When looking at the 3-point function in this theory one considers the Green's function at either the completely symmetric point or a completely off-shell point. The former is appropriate to use when there is either non-derivative 3-point interactions or a single 3-point vertex, such as the $\sigma\phi^i\phi^i$ interaction. The off-shell configuration is used when there is more than one 3-point interaction and they involve derivative couplings. This is applicable for the two independent σ self-interactions.

The tree and one loop diagrams for the $\sigma\phi^i\phi^i$ interaction are illustrated in figure 3.18. For the interactions $\sigma^2\Box^2\sigma$ and $\sigma(\Box\sigma)^2$ the tree and one loop diagrams are displayed in figure 3.19. Note that the two σ 3-point self-interactions will produce the same diagrams.

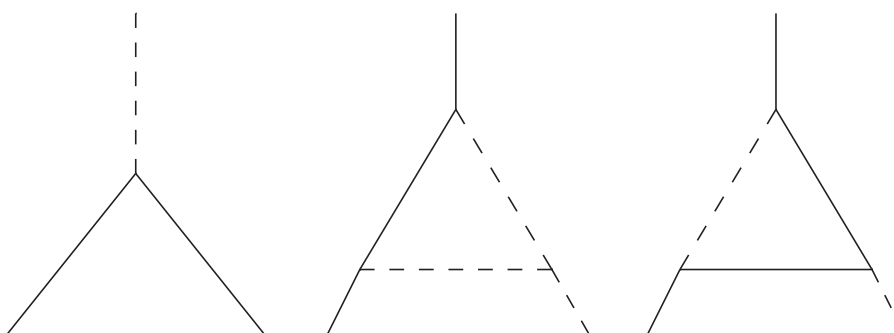


Figure 3.18: Tree and one loop Feynman diagrams for the 3-point interaction $\sigma\phi^i\phi^i$.

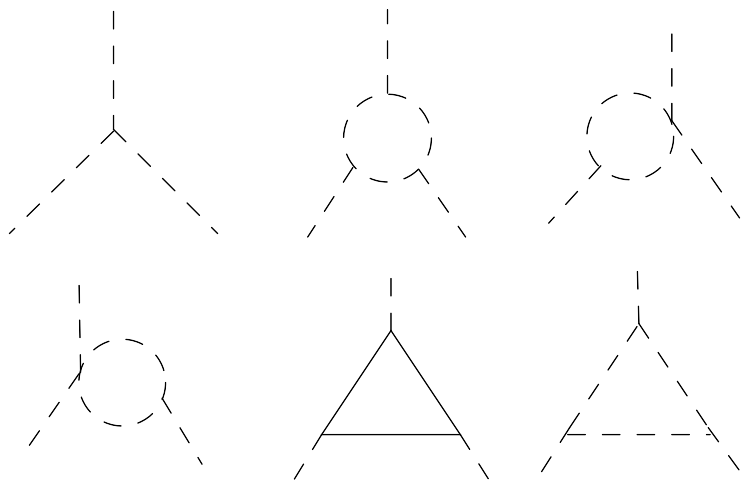


Figure 3.19: Tree and one loop Feynman diagrams for the 3-point self-interactions $\sigma^2 \square^2 \sigma$ and $\sigma(\square\sigma)^2$.

Tree diagrams are trivial to calculate while all one loop Feynman graphs can be reduced to a combination of 2-point integrals and the 3-point master integral $\mathcal{I}_{31}(1, 1, 1)$, illustrated in figure 3.7, using REDUZE. First we wish to evaluate the master integral at the completely symmetric point in ten dimensions. The four dimensional result has been calculated in [194] and is given by equation (3.23). Using the Tarsov method iteratively the 3-point master integral in $d = 10 - 2\epsilon$ dimensions can be found to be

$$\begin{aligned} \mathcal{I}_{31}^{(d=10-2\epsilon)}(1, 1, 1) = & \left[-\frac{1}{56\epsilon} + \left(-\frac{2995}{42336} - \frac{\pi^2}{243} + \frac{1}{162}\psi'\left(\frac{1}{3}\right) \right) \right. \\ & + \left(-\frac{23539}{125000} - \frac{367\pi^2}{54432} - \frac{1}{9}s_3(\pi/6) + \frac{1}{81}\psi'\left(\frac{1}{3}\right) \right) \\ & \left. + \frac{35\sqrt{3}\pi^3}{34992} + \frac{\sqrt{3}\ln(3)^2\pi}{1296} \right] \epsilon + O(\epsilon^2) (\mu^2)^4. \quad (3.38) \end{aligned}$$

This ten dimensional master integral can be inserted into relations derived from the Laporta algorithm to find all 3-point one loop diagrams at the completely symmetric point.

Finding integration by parts relations for 3-point diagrams at the completely off-shell point is more complicated. As previously stated the off-shell computation is needed as more than one 3-point interaction involving derivative couplings is present. These interactions will become a problem when renormalizing the theory as the two independent operators, $\sigma^2 \square^2 \sigma$ and $\sigma(\square\sigma)^2$, have different Feynman rules and therefore their associated coupling constants have separate renormalization constants. Evaluating the master integral at the completely off-shell point allows us to distinguish between the renormalization constants. The one loop

3-point Feynman diagram at the completely off-shell point is illustrated in figure 3.20 where all external momenta are different.

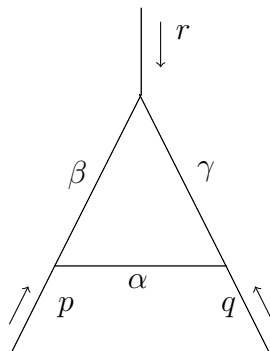


Figure 3.20: 3-point master Feynman diagram at one loop $\mathcal{I}_1^O(\alpha, \beta, \gamma)$.

The completely off-shell momentum configuration is given by

$$\begin{aligned} r^2 &= -\mu^2, \\ p^2 &= -\mu^2 x, \\ q^2 &= -\mu^2 y \end{aligned} \tag{3.39}$$

where x and y are some parameters and $p + q = -r$. The completely off-shell result for the 3-point diagram at one loop in four dimensions has been calculated in [197]. We can therefore implement the Tarasov method to find the off-shell master integral in higher dimensions. However when deriving the Tarasov relation of equation (3.37) we assumed all Feynman diagrams were fully symmetric. As we are now looking at the completely off-shell case the symmetric integration by parts routine used is no longer applicable.

Therefore we need to apply the Laporta algorithm again to the one loop 3-point function, this time at the completely off-shell point. To do this we pick up the reduction at the point of equation (3.21), restated here for the benefit of the reader,

$$\begin{aligned} (d - 2\alpha - \beta - \gamma)\mathcal{I}_{31}^O(\alpha, \beta, \gamma) &= \beta(\mathcal{I}_{31}^O(\alpha - 1, \beta + 1, \gamma) - p^2\mathcal{I}_{31}^O(\alpha, \beta + 1, \gamma)) \\ &+ \gamma(\mathcal{I}_{31}^O(\alpha - 1, \beta, \gamma + 1) - q^2\mathcal{I}_{31}^O(\alpha, \beta, \gamma + 1)). \end{aligned}$$

The O denoted the fact that we are now considering the integrals in the completely off-shell momentum configuration. Once again we take the general case

$$\alpha = \beta = \gamma = 1,$$

$$(d-4)\mathcal{I}_{31}^O(1,1,1) = \mathcal{I}_{31}^O(0,2,1) - p^2\mathcal{I}_{31}^O(1,2,1) + \mathcal{I}_{31}^O(0,1,2) - q^2\mathcal{I}_{31}^O(1,1,2). \quad (3.40)$$

The main difference in the off-shell case is that instead of relating diagrams via symmetry relations we instead make the replacement

$$p \rightarrow q \quad , \quad q \rightarrow r \quad , \quad r \rightarrow p. \quad (3.41)$$

This alters equation (3.40) to become

$$(d-4)\mathcal{I}_{31}^O(1,1,1) = \mathcal{I}_{31}^O(2,1,0) - q^2\mathcal{I}_{31}^O(2,1,1) + \mathcal{I}_{31}^O(1,2,0) - r^2\mathcal{I}_{31}^O(1,2,1). \quad (3.42)$$

Repeating the same replacement by applying (3.41) to (3.42) a third equation is obtained,

$$(d-4)\mathcal{I}_{31}^O(1,1,1) = \mathcal{I}_{31}^O(1,0,2) - r^2\mathcal{I}_{31}^O(1,1,2) + \mathcal{I}_{31}^O(2,0,1) - p^2\mathcal{I}_{31}^O(2,1,1). \quad (3.43)$$

We are left with a system of three equations; (3.40), (3.42) and (3.43), which can be rearranged into a more useful form by moving diagrams with higher power propagators to the left hand-side.

$$\begin{aligned} p^2\mathcal{I}_{31}^O(1,2,1) + q^2\mathcal{I}_{31}^O(1,1,2) &= (4-d)\mathcal{I}_{31}^O(1,1,1) + \mathcal{I}_{31}^O(1,0,2) + \mathcal{I}_{31}^O(2,0,1) , \\ q^2\mathcal{I}_{31}^O(1,1,2) + r^2\mathcal{I}_{31}^O(1,2,1) &= (4-d)\mathcal{I}_{31}^O(1,1,1) + \mathcal{I}_{31}^O(1,2,0) + \mathcal{I}_{31}^O(2,1,0) , \\ r^2\mathcal{I}_{31}^O(1,1,2) + p^2\mathcal{I}_{31}^O(2,1,1) &= (4-d)\mathcal{I}_{31}^O(1,1,1) + \mathcal{I}_{31}^O(1,0,2) + \mathcal{I}_{31}^O(2,0,1) . \end{aligned}$$

The system of equations can be solved using matrix form,

$$\underbrace{\begin{pmatrix} p^2 & q^2 & 0 \\ r^2 & 0 & q^2 \\ 0 & r^2 & p^2 \end{pmatrix}}_A \begin{pmatrix} \mathcal{I}_{31}^O(1,2,1) \\ \mathcal{I}_{31}^O(1,1,2) \\ \mathcal{I}_{31}^O(2,1,1) \end{pmatrix} = \begin{pmatrix} (4-d)\mathcal{I}_{31}^O(1,1,1) + \mathcal{I}_{31}^O(0,2,1) + \mathcal{I}_{31}^O(0,1,2) \\ (4-d)\mathcal{I}_{31}^O(1,1,1) + \mathcal{I}_{31}^O(2,1,0) + \mathcal{I}_{31}^O(1,2,0) \\ (4-d)\mathcal{I}_{31}^O(1,1,1) + \mathcal{I}_{31}^O(1,0,2) + \mathcal{I}_{31}^O(2,0,1) \end{pmatrix} .$$

Multiplying both sides by the matrix A^{-1} , the integration by parts relations for the 3-point function at the completely off-shell point can be obtained

$$\begin{pmatrix} \mathcal{I}_{31}^O(1,2,1) \\ \mathcal{I}_{31}^O(1,1,2) \\ \mathcal{I}_{31}^O(2,1,1) \end{pmatrix} = + \frac{1}{2p^2q^2r^2} \begin{pmatrix} r^2q^2 & q^2p^2 & -q^4 \\ r^2p^2 & -p^4 & p^2q^2 \\ -r^4 & p^2r^2 & r^2q^2 \end{pmatrix}$$

$$\times \begin{pmatrix} (4-d)\mathcal{I}_{31}^O(1,1,1) + \mathcal{I}_{31}^O(0,2,1) + \mathcal{I}_{31}^O(0,1,2) \\ (4-d)\mathcal{I}_{31}^O(1,1,1) + \mathcal{I}_{31}^O(2,1,0) + \mathcal{I}_{31}^O(1,2,0) \\ (4-d)\mathcal{I}_{31}^O(1,1,1) + \mathcal{I}_{31}^O(1,0,2) + \mathcal{I}_{31}^O(2,0,1) \end{pmatrix} .$$

As an example,

$$\begin{aligned} \mathcal{I}_{31}^O(1,2,1) &= \frac{1}{2p^2q^2r^2} \left[(d-4)\mathcal{I}_{31}^O(1,1,1)(q^4 - q^2p^2 - r^2q^2) \right. \\ &\quad + r^2q^2 \left(\mathcal{I}_{31}^O(0,2,1) + \mathcal{I}_{31}^O(0,1,2) \right) \\ &\quad \left. + q^2p^2 \left(\mathcal{I}_{31}^O(2,1,0) + \mathcal{I}_{31}^O(1,2,0) \right) - q^4 \left(\mathcal{I}_{31}^O(1,0,2) + \mathcal{I}_{31}^O(2,0,1) \right) \right] . \end{aligned}$$

From the off-shell configuration we know $\mathcal{I}_{31}^O(1,2,1) \neq \mathcal{I}_{31}^O(1,1,2) \neq \mathcal{I}_{31}^O(2,1,1)$, unlike the symmetric case. The relations for $\mathcal{I}_{31}^O(1,1,2)$ and $\mathcal{I}_{31}^O(2,1,1)$ need to be obtained separately using the same method as for $\mathcal{I}_{31}^O(1,2,1)$. These IBP relations can then be substituted into figure 3.16 to give the Tarasov relation for the 3-point function in an off-shell momentum configuration,

$$\begin{aligned} 0 &= \frac{1}{2p^2q^2r^2} \left[(r^4 - 2r^2p^2 - 2r^2q^2)\mathcal{I}_{31}^{O(d+2)}(0,1,2) \right. \\ &\quad + (p^4 - 2p^2q^2 - 2p^2r^2)\mathcal{I}_{31}^{O(d+2)}(1,2,0) \\ &\quad + (q^2 - 2p^2q^2 - 2r^2q^2)\mathcal{I}_{31}^{O(d+2)}(2,0,1) \\ &\quad \left. + (d-4)(2r^2q^2 + 2q^2p^2 + 2r^2p^2 - p^4 - q^4 - r^4)\mathcal{I}_{31}^{O(d+2)}(1,1,1) \right] \\ &\quad - \mathcal{I}_{31}^{O(d)}(1,1,1) . \end{aligned} \tag{3.44}$$

Note that the symmetric point case can be used as a check for equation (3.44). The $(d+2)$ -dimensional 3-point master integral in the off-shell configuration can be found from the relation (3.44). As the four dimensional off-shell result is known, [197], one can iteratively derive the ten dimensional result with only the 2-point integrals needing to be directly calculated.

These 2-point diagrams were computed previously in subsection 3.4.2 at the completely symmetric point. The only difference in the off-shell configuration is the incoming momenta. Note that as integrals $\mathcal{I}_{31}^O(0,1,2)$, $\mathcal{I}_{31}^O(1,2,0)$ and $\mathcal{I}_{31}^O(2,0,1)$ are proportional to $\mathcal{I}_{31}^O(0,1,1)$, $\mathcal{I}_{31}^O(1,1,0)$ and $\mathcal{I}_{31}^O(1,0,1)$ respectively, they can be calculated instead. The first 2-point integral in d -dimensions is given by

$$\mathcal{I}_{31}^O(0,1,1) = \int \frac{d^d k}{(2\pi)^d k^2 (k-r)^2}$$

$$= \frac{\Gamma(2 - \frac{d}{2})\Gamma(\frac{d}{2} - 1)^2(-\mu^2)^{\frac{d}{2}-2}}{\Gamma(d-2)(4\pi)^{\frac{d}{2}}}. \quad (3.45a)$$

In $d = 10 - 2\epsilon$ dimensions as $r^2 = -\mu^2$ we have

$$\begin{aligned} \mathcal{I}_{31}^{O(d=10-2\epsilon)}(0, 1, 1) &= \left[-\frac{1}{840\epsilon} - \frac{44}{11025} + \left(\frac{\pi^2}{10080} - \frac{10973}{1157625} \right) \epsilon \right. \\ &\quad \left. + \left(\frac{1}{360}\zeta_3 + \frac{11}{33075}\pi^2 - \frac{2449616}{121550625} \right) \epsilon^2 + O(\epsilon^3) \right] \\ &\quad \times \left[-1 + \epsilon - \frac{1}{2}\epsilon^2 + O(\epsilon^3) \right] \mu^6. \end{aligned}$$

The second integral computed in d -dimensions is

$$\begin{aligned} \mathcal{I}_{31}^O(1, 1, 0) &= \int \frac{d^d k}{(2\pi)^d k^2 (k-p)^2} \\ &= \frac{\Gamma(2 - \frac{d}{2})\Gamma(\frac{d}{2} - 1)^2(-\mu^2 x)^{\frac{d}{2}-2}}{\Gamma(d-2)(4\pi)^{\frac{d}{2}}}. \end{aligned} \quad (3.45b)$$

In $d = 10 - 2\epsilon$ dimensions as $p^2 = -\mu^2 x$ this is

$$\begin{aligned} \mathcal{I}_{31}^{O(d=10-2\epsilon)}(1, 1, 0) &= \left[-\frac{1}{840\epsilon} - \frac{44}{11025} + \left(\frac{\pi^2}{10080} - \frac{10973}{1157625} \right) \epsilon \right. \\ &\quad \left. + \left(\frac{1}{360}\zeta_3 + \frac{11}{33075}\pi^2 - \frac{2449616}{121550625} \right) \epsilon^2 + O(\epsilon^3) \right] \\ &\quad \times \left[-1 + \ln(x)\epsilon - \frac{1}{2}\ln(x)^2\epsilon^2 + O(\epsilon^3) \right] (\mu^6 x^3). \end{aligned}$$

The final 2-point integral is calculated to be

$$\begin{aligned} \mathcal{I}_{31}^O(1, 0, 1) &= \int \frac{d^d k}{(2\pi)^d k^2 (k-q)^2} \\ &= \frac{\Gamma(2 - \frac{d}{2})\Gamma(\frac{d}{2} - 1)^2(-\mu^2 y)^{\frac{d}{2}-2}}{\Gamma(d-2)(4\pi)^{\frac{d}{2}}} \end{aligned} \quad (3.45c)$$

in d -dimensions and in $d = 10 - 2\epsilon$ dimensions as $q^2 = -\mu^2 y$ we have

$$\begin{aligned} \mathcal{I}_{31}^{O(d=10-2\epsilon)}(1, 0, 1) &= \left[-\frac{1}{840\epsilon} - \frac{44}{11025} + \left(\frac{\pi^2}{10080} - \frac{10973}{1157625} \right) \epsilon \right. \\ &\quad \left. + \left(\frac{1}{360}\zeta_3 + \frac{11}{33075}\pi^2 - \frac{2449616}{121550625} \right) \epsilon^2 + O(\epsilon^3) \right] \\ &\quad \times \left[-1 + \ln(y)\epsilon - \frac{1}{2}\ln(y)^2\epsilon^2 + O(\epsilon^3) \right] (\mu^6 y^3). \end{aligned}$$

Note that all three integrals agree at $x = y = 1$, in other words at the completely

symmetric point. Finally the $d = 10 - 2\epsilon$ dimensional 3-point master integral at the completely off-shell point can be derived

$$\begin{aligned}
\mathcal{I}_{31}^{O(d=10-2\epsilon)}(1, 1, 1) &= \frac{[(y+1+x)x + y^2 + y + 1]\mu^4}{360\epsilon} \\
&\quad \frac{[(51x^2 - 25y - 51(y+1)x)x^2 + 51(y^4 - y^3 - y + 1) \\
&\quad - (51y^2 - 26y + 51)(y+1)x - 15(y-1-x)\ln(y)y^3 \\
&\quad + 15(y+1-x)\ln(x)x^3 + 15(y-1+x)]\mu^4}{5400((y-1)^2 + x^2 - 2(y+1)x)} \\
&+ O(\epsilon) .
\end{aligned} \tag{3.46}$$

The full list of master integrals for the off-shell point in four, six, eight and ten dimensions can be found in Appendix A. The ten dimensional master integral is inserted along with calculated 2-point integrals into integration by parts relations to acquire all 3-point diagrams at one loop for the $\sigma^2 \square^2 \sigma$ and $\sigma(\square\sigma)^2$ interactions at the completely off-shell point.

3.4.5 Master Integrals with Four Propagators

The auxiliary topology for the 4-point function at one loop $\mathcal{I}_{41}(\alpha, \beta, \gamma, \delta)$ where α , β , γ and δ denote the power on each associated propagator is illustrated in figure 3.21. As the 4-point function contains only σ fields, $\sigma^3 \square \sigma$, the figure contains all σ fields.

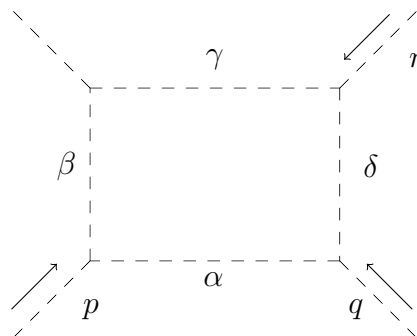


Figure 3.21: The auxiliary topology or integral family for the 4-point function $\mathcal{I}_{41}(\alpha, \beta, \gamma, \delta)$ at one loop with all σ fields.

The three independent incoming momenta are given by p , q and r . We consider the 4-point function at the completely symmetric point with momentum configuration

$$\begin{aligned}
p^2 &= q^2 = r^2 = (p+q+r)^2 = -\mu^2 \\
pq &= pr = qp = \frac{\mu^2}{3}
\end{aligned} \tag{3.47}$$

The 4-point function contains nineteen one loop Feynman diagrams along with one tree level diagram. The four one loop master integrals are illustrated in figure 3.22. The tree level diagram is trivial to compute and the nineteen one loop diagrams will reduce down to one or a combination of the master integrals.

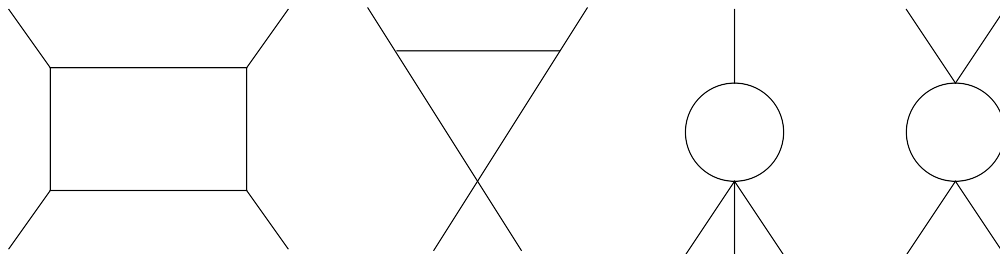


Figure 3.22: The four master integrals for the 4-point function at one loop, from left to right; $\mathcal{I}_{41}(1, 1, 1, 1)$, $\mathcal{I}_{41}(1, 1, 1, 0)$, $\mathcal{I}_{41}(1, 1, 0, 0)$ and $\mathcal{I}_{41}(1, 0, 1, 0)$.

All propagators in the masters integrals will be of the form $1/(k^2)$. Note that only four master integrals are present as we are calculating at the completely symmetric point, therefore

$$\mathcal{I}_{41}(1, 1, 0, 0) = \mathcal{I}_{41}(0, 0, 1, 1) = \mathcal{I}_{41}(0, 1, 1, 0) = \mathcal{I}_{41}(1, 0, 0, 1) \quad (3.48)$$

and

$$\mathcal{I}_{41}(0, 1, 0, 1) = \mathcal{I}_{41}(1, 0, 1, 0) . \quad (3.49)$$

This is clear to see from the incoming momentum set-up. To begin we calculate the master integral $\mathcal{I}_{41}(1, 1, 1, 1)$ given in figure 3.23. This master integral is illustrated with all external momentum and internal loop momentum k labelled. The result of $\mathcal{I}_{41}(1, 1, 1, 1)$ can be obtained using the Tarasov method.

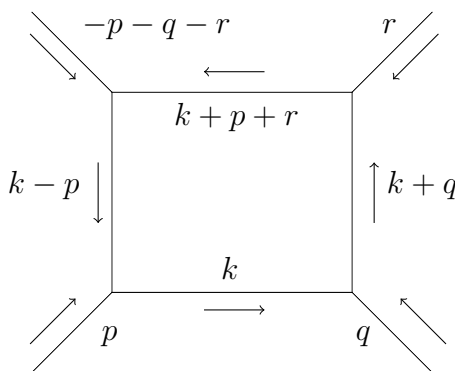


Figure 3.23: One loop 4-point master Feynman diagram $\mathcal{I}_{41}(1, 1, 1, 1)$.

The derivation of the Tarasov relation for the 4-point function follows the same steps as the 3-point case, we therefore simply state the relation,

$$\mathcal{I}_{41}^{(d)}(1, 1, 1, 1) = \mathcal{I}_{41}^{(d+2)}(2, 1, 1, 1) + \mathcal{I}_{41}^{(d+2)}(1, 2, 1, 1)$$

$$+ \mathcal{I}_{41}^{(d+2)}(1, 1, 2, 1) + \mathcal{I}_{41}^{(d+2)}(1, 1, 1, 2). \quad (3.50)$$

This is illustrated in figure 3.24, similarities with the 3-point result are clear to see.

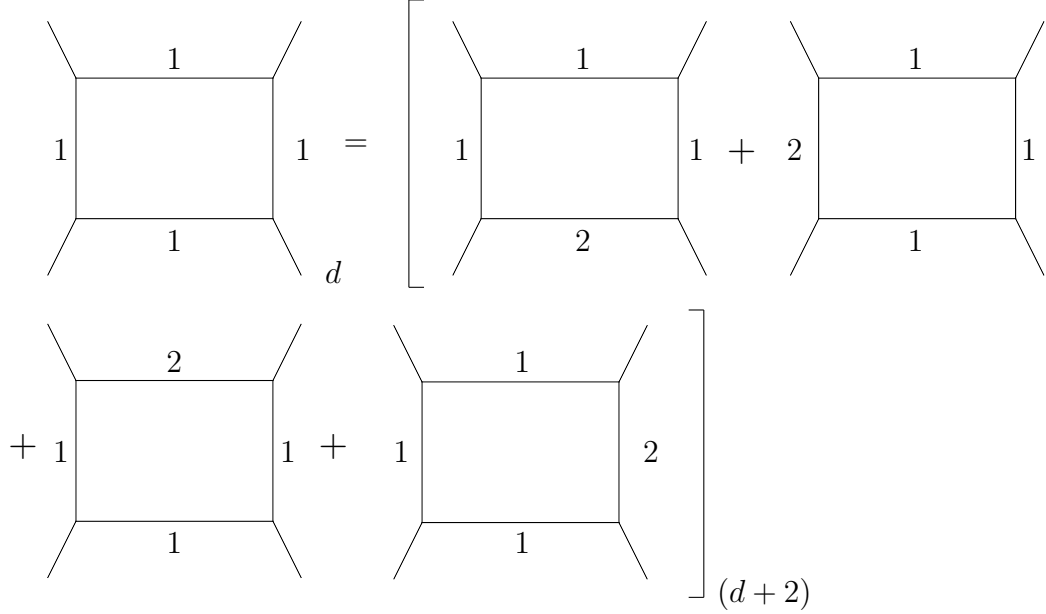


Figure 3.24: Tarasov method applied to the 4-point Feynman diagram $\mathcal{I}_{41}(1, 1, 1, 1)$ at one loop.

The four dimensional 4-point function at one loop has been calculated at the completely symmetric point in [199, 200]. Additionally the $(d+2)$ -dimensional diagrams in figure 3.24 can be reduced using the integration by parts routine of the Laporta algorithm. To begin the reduction first note that the general definition of a one loop diagram containing four propagators is

$$\mathcal{I}_{41}(\alpha, \beta, \gamma, \delta) = \int \frac{d^d k}{(2\pi)^d} \frac{1}{(k^2)^\alpha ((k+q)^2)^\beta ((k+q+r)^2)^\gamma ((k-p)^2)^\delta}. \quad (3.51)$$

As we are reducing this integral at the fully symmetric point the following symmetry relations will apply

$$\mathcal{I}_{41}(2, 1, 1, 1) = \mathcal{I}_{41}(1, 2, 1, 1) = \mathcal{I}_{41}(1, 1, 2, 1) = \mathcal{I}_{41}(1, 1, 1, 2). \quad (3.52)$$

As with the 3-point example we apply identity (3.19) to the 4-point function and differentiate each term of the propagator in turn to obtain

$$\begin{aligned} & \int_k \frac{d}{(k^2)^\alpha ((k+q)^2)^\beta ((k+q+r)^2)^\gamma ((k-p)^2)^\delta} \\ &= 2\alpha \int_k \frac{k^2}{((k^2)^{\alpha+1} ((k+q)^2)^\beta ((k+q+r)^2)^\gamma ((k-p)^2)^\delta} \end{aligned}$$

$$\begin{aligned}
& + 2\beta \int_k \frac{k(k+q)}{((k^2)^\alpha((k+q)^2)^{\beta+1}((k+q+r)^2)^\gamma((k-p)^2)^\delta)} \\
& + 2\gamma \int_k \frac{k(k+q+r)}{((k^2)^\alpha((k+q)^2)^\beta((k+q+r)^2)^{\gamma+1}((k-p)^2)^\delta)} \\
& + 2\delta \int_k \frac{k(k-p)}{((k^2)^\alpha((k+q)^2)^\beta((k+q+r)^2)^\gamma((k-p)^2)^{\delta+1}} .
\end{aligned}$$

Algebraically rearranging terms in the numerator of each integral and factorising terms on both sides of the equation the following relation is obtained, given in $\mathcal{I}_{41}(\alpha, \beta, \gamma, \delta)$ notation,

$$\begin{aligned}
\mathcal{I}_{41}(\alpha, \beta, \gamma, \delta) = & \frac{1}{d-2\alpha-\beta-\gamma-\delta} \left(\beta[\mathcal{I}_{41}(\alpha-1, \beta+1, \gamma, \delta) \right. \\
& - q^2\mathcal{I}_{41}(\alpha, \beta+1, \gamma, \delta)] + \gamma[\mathcal{I}_{41}(\alpha-1, \beta, \gamma+1, \delta) \\
& - (q+r)^2\mathcal{I}_{41}(\alpha, \beta, \gamma+1, \delta)] + \delta[\mathcal{I}_{41}(\alpha-1, \beta, \gamma, \delta+1) \\
& \left. - p^2\mathcal{I}_{41}(\alpha, \beta, \gamma, \delta+1)] \right) .
\end{aligned}$$

Taking the most general case by setting $\alpha = \beta = \gamma = \delta = 1$,

$$\begin{aligned}
(d-5)\mathcal{I}_{41}(1, 1, 1, 1) = & \mathcal{I}_{41}(0, 2, 1, 1) - q^2\mathcal{I}_{41}(1, 2, 1, 1) + \mathcal{I}_{41}(0, 1, 2, 1) \\
& - (q+r)^2\mathcal{I}_{41}(1, 1, 2, 1) + \mathcal{I}_{41}(0, 1, 1, 2) \\
& - p^2\mathcal{I}_{41}(1, 1, 1, 2) .
\end{aligned}$$

A reduction relation for the 4-point integral at the symmetric point can then be found with $\mathcal{I}_{41}(1, 1, 1, 1)$ as the master integral,

$$\begin{aligned}
\mathcal{I}_{41}(1, 2, 1, 1) = & \frac{1}{10\mu^2} \left[(d-5)\mathcal{I}_{41}(1, 1, 1, 1) - \mathcal{I}_{41}(0, 2, 1, 1) - \mathcal{I}_{41}(0, 1, 2, 1) \right. \\
& \left. - \mathcal{I}_{41}(0, 1, 1, 2) \right] .
\end{aligned}$$

Substituting this reduction into the 4-point Tarasov relation we find an equation from which the ten dimensional master integral can be deduced. Symmetry relations given by equation (3.52) have been applied to simplify the result,

$$\begin{aligned}
\mathcal{I}_{41}^{(d)}(1, 1, 1, 1) = & \frac{4}{10\mu^2} \left[(d-5)\mathcal{I}_{41}^{(d+2)}(1, 1, 1, 1) - \mathcal{I}_{41}^{(d+2)}(0, 2, 1, 1) \right. \\
& \left. - \mathcal{I}_{41}^{(d+2)}(0, 1, 2, 1) - \mathcal{I}_{41}^{(d+2)}(0, 1, 1, 2) \right] . \quad (3.53)
\end{aligned}$$

Diagrammatically this relation is illustrated in figure 3.25. The three $(d+2)$ -dimensional diagrams with a zero power on one of the propagators are not sym-

obtain a system of three independent equations which have been put into matrix form

$$\begin{pmatrix} \mathcal{I}_{41}(0, 1, 1, 2) \\ \mathcal{I}_{41}(0, 2, 1, 1) \\ \mathcal{I}_{41}(0, 1, 2, 1) \end{pmatrix} = \frac{1}{2p^2q^2r^2} \begin{pmatrix} r^2q^2 & q^2p^2 & -q^4 \\ r^2p^2 & -p^2 & p^2q^2 \\ -r^4 & p^2r^2 & r^2q^2 \end{pmatrix} \\ \times \begin{pmatrix} (4-d)\mathcal{I}_{41}(0, 1, 1, 1) + \mathcal{I}_{41}(0, 1, 0, 2) + \mathcal{I}_{41}(0, 2, 0, 1) \\ (4-d)\mathcal{I}_{41}(0, 1, 1, 1) + \mathcal{I}_{41}(0, 0, 2, 1) + \mathcal{I}_{41}(0, 0, 1, 2) \\ (4-d)\mathcal{I}_{41}(0, 1, 1, 1) + \mathcal{I}_{41}(0, 2, 1, 0) + \mathcal{I}_{41}(0, 1, 2, 0) \end{pmatrix} .$$

This system of equations can be substituted into the Tarasov relation of equation (3.53) with the following result then derived,

$$\begin{aligned} \mathcal{I}_{41}^{(d)}(1, 1, 1, 1) &= \frac{4}{10\mu^2} \left[(d-5)\mathcal{I}_{41}^{(d+2)}(1, 1, 1, 1) \right. \\ &\quad - \frac{1}{2p^2q^2r^2} \left((d-4)(r^4 + p^4 + q^4 - 2p^2q^2 - 2r^2p^2 \right. \\ &\quad \quad - 2r^2q^2)\mathcal{I}_{41}(0, 1, 1, 1) + r^2q^2[\mathcal{I}_{41}^{(d+2)}(0, 1, 0, 2) \\ &\quad \quad + \mathcal{I}_{41}^{(d+2)}(0, 2, 0, 1) + \mathcal{I}_{41}^{(d+2)}(0, 2, 1, 0) \\ &\quad \quad + \mathcal{I}_{41}^{(d+2)}(0, 1, 2, 0)] + q^2p^2[\mathcal{I}_{41}^{(d+2)}(0, 0, 2, 1) \\ &\quad \quad + \mathcal{I}_{41}^{(d+2)}(0, 0, 1, 2) + \mathcal{I}_{41}^{(d+2)}(0, 2, 1, 0) \\ &\quad \quad + \mathcal{I}_{41}^{(d+2)}(0, 1, 2, 0)] + \mathcal{I}_{41}^{(d+2)}(0, 2, 1, 0) \\ &\quad \quad + p^2r^2[\mathcal{I}_{41}^{(d+2)}(0, 0, 2, 1) + \mathcal{I}_{41}^{(d+2)}(0, 0, 1, 2) \\ &\quad \quad + \mathcal{I}_{41}^{(d+2)}(0, 1, 0, 2) + \mathcal{I}_{41}^{(d+2)}(0, 2, 0, 1)] \\ &\quad \quad - q^4[\mathcal{I}_{41}^{(d+2)}(0, 2, 1, 0) + \mathcal{I}_{41}^{(d+2)}(0, 1, 2, 0)] \\ &\quad \quad - p^4[\mathcal{I}_{41}^{(d+2)}(0, 0, 2, 1) + \mathcal{I}_{41}^{(d+2)}(0, 0, 1, 2)] \\ &\quad \quad \left. \left. - r^4[\mathcal{I}_{41}^{(d+2)}(0, 1, 0, 2) + \mathcal{I}_{41}^{(d+2)}(0, 2, 0, 1)] \right) \right] . \end{aligned}$$

Although this looks complicated, it turns out that only two integrals need to be computed by hand. The first of these, the 3-point integral $\mathcal{I}_{41}(0, 1, 1, 1)$ at the completely off-shell point was computed in section 3.4.4 in ten dimensions albeit with only three external legs.

The modification to four external legs is not difficult and involves only a change in the momentum configuration at one of the vertices. Furthermore of the six graphs containing only two non-zero values of α , β , γ and δ only two are independent as

$$\mathcal{I}_{41}(0, 1, 0, 2) = \mathcal{I}_{41}(0, 2, 0, 1) = \mathcal{I}_{41}(0, 2, 1, 0) = \mathcal{I}_{41}(0, 1, 2, 0)$$

and

$$\mathcal{I}_{41}(0, 0, 2, 1) = \mathcal{I}_{41}(0, 0, 1, 2) ,$$

which are obvious from the symmetry relations (3.48) and (3.49). The two independent Feynman diagrams with only two non-zero powers of propagators are illustrated in figure 3.27 where for figure (a) we have $(p + q)^2 - \frac{4}{3}\mu^2$ and for (b) we have $p^2 = -\mu^2$.

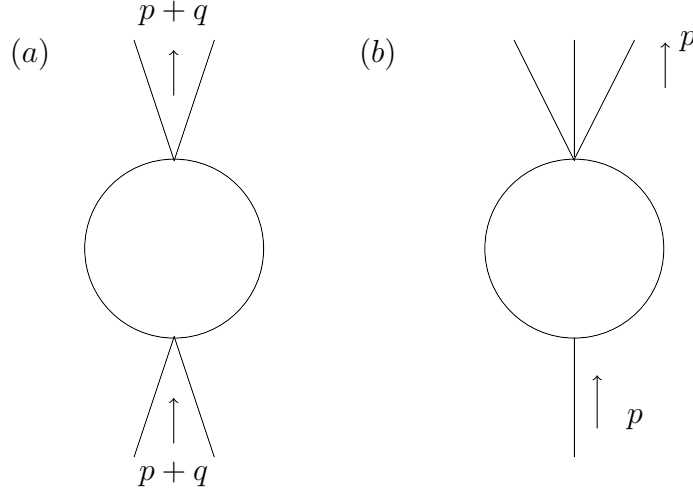


Figure 3.27: The two independent 2-point Feynman diagrams with four external legs. Integral representation as follows; (a) $\mathcal{I}_{41}(0, 1, 0, 2)$, (b) $\mathcal{I}_{41}(0, 0, 2, 1)$

These integrals can be computed by hand and give the following results in d -dimensions

$$\begin{aligned} \mathcal{I}_{41}(0, 1, 0, 2) &= \left(-\frac{4}{3}\mu^2 \right)^{\frac{d}{2}-2} \frac{\Gamma(2 - \frac{d}{2})\Gamma(\frac{d}{2} - 1)^2}{(4\pi)^{\frac{d}{2}}\Gamma(d - 2)} , \\ \mathcal{I}_{41}(0, 0, 2, 1) &= (-\mu^2)^{\frac{d}{2}-2} \frac{\Gamma(2 - \frac{d}{2})\Gamma(\frac{d}{2} - 1)^2}{(4\pi)^{\frac{d}{2}}\Gamma(d - 2)} . \end{aligned}$$

In $d = 10 - 2\epsilon$ dimensions these integrals are

$$\begin{aligned} \mathcal{I}_{41}^{(d=10-2\epsilon)}(0, 1, 0, 2) &= \left[-\frac{1}{840\epsilon} - \frac{44}{11025} + \left(\frac{\pi^2}{10080} - \frac{10973}{1157625} \right) \epsilon \right. \\ &\quad \left. + O(\epsilon^2) \right] \times \left[-\left(\frac{4}{3} \right)^3 \mu^6 - \left(\frac{4}{3} \right)^3 \mu^6 \epsilon + O(\epsilon^2) \right] , \\ \mathcal{I}_{41}^{(d=10-2\epsilon)}(0, 0, 2, 1) &= \left[-\frac{1}{840\epsilon} - \frac{44}{11025} + \left(\frac{\pi^2}{10080} - \frac{10973}{1157625} \right) \epsilon \right. \\ &\quad \left. + O(\epsilon^2) \right] \times \left[-\mu^6 - \mu^6 \epsilon + O(\epsilon^2) \right] . \end{aligned}$$

Putting all of these results together and using the Tarasov relation, the 4-point master integral in first six, then eight and finally ten dimensions can be iteratively

calculated. The result in $d = 10 - 2\epsilon$ dimensions is

$$\begin{aligned}
 \mathcal{I}_{41}^{(d=10-2\epsilon)}(1, 1, 1, 1) &= \frac{1}{18\epsilon} \mu^2 \\
 &+ \frac{\mu^2}{69120} \left[-4209\phi_1\left(\frac{3}{4}, \frac{3}{4}\right) + 1500\phi_1\left(\frac{9}{16}, \frac{9}{16}\right) \right. \\
 &\quad \left. + 15088 - 1992 \ln(2) + 996 \ln(3) - 3840 \right] \\
 &+ O(\epsilon) .
 \end{aligned} \tag{3.54}$$

3.4.6 The Vacuum Bubble Expansion

Along with one tree level diagram displayed in figure 3.28, the 5-point function produces 89 one loop Feynman diagrams with five different topologies which are illustrated in figure 3.29. Each of the 89 one loop diagrams will have the same form as one of the five topologies but may contain a different internal propagator structure.

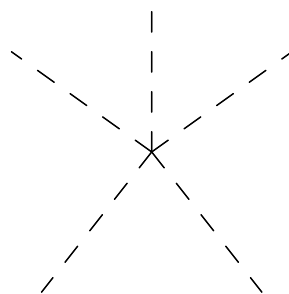


Figure 3.28: Tree level Feynman diagram for the 5-point function σ^5 .

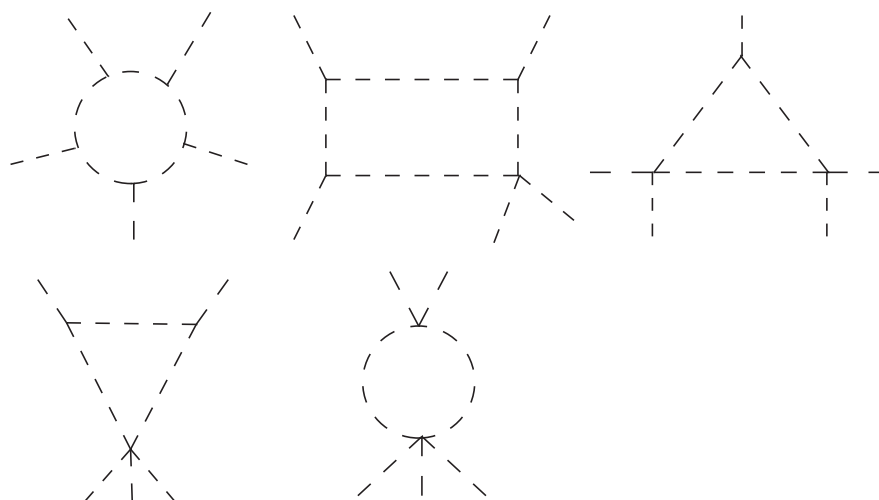


Figure 3.29: The five topologies for the one loop 5-point function $\mathcal{I}_{51}(\alpha, \beta, \gamma, \rho, \delta)$.

Integration by parts via the Laporta algorithm has been a useful tool in reducing the 3 and 4-point functions. However it is less efficient when looking at the

5-point function for the theory of interest. The first diagram displayed in figure 3.29 has several 3-point σ self-interactions which gives the integral a complicated numerator that is laborious to reduce for the $O(N)$ scalar theory. When taking into account all 89 one loop diagrams, implementing an integration by parts routine becomes time consuming. At this point it is important to note that in calculating the Renormalization Group functions one only requires the divergent piece of each diagram. Therefore we can introduce a new technique called the vacuum bubble expansion, [201–203]. The vacuum bubble expansion is an approximation that can be applied to each 5-point diagram in turn to find only the divergent piece of the graph. Consequently we will not require any master integrals. One advantage of using the vacuum bubble expansion is that we work directly in ten dimensions, bypassing the need for the Tarasov relation.

Before applying the vacuum bubble expansion to a specific one loop diagram, we briefly look at what the process entails. A feature of every mass independent renormalization scheme such as $\overline{\text{MS}}$, is that the pole part of a dimensionally regularised Feynman diagram is a polynomial in both mass and external momenta. This can be shown on the basis of given Feynman rules alone without any theoretical arguments. Consequently an expansion in external momenta and masses can be performed before integrating over loop momenta which simplifies the integral, [201]. For our massless theory we will expand in the external momenta. The main difficulty in doing this is the appearance of spurious IR divergences. Within the framework of dimensional regularisation these IR divergences can appear indistinguishable from UV divergences and would not cancel when summing together all of the Feynman diagrams. To combat these spurious divergences we can use a form of IR rearrangement by adding an artificial mass to each Feynman diagram before expansion. This auxiliary mass which will be the same in all Feynman diagrams prevents the production of any IR divergence. Introducing an artificial mass and expanding in the external momenta will not alter the values for the divergent pieces of the one loop diagrams. The integrals produced after expanding in the external momenta will be simple completely massive tadpoles. Therefore the problem of evaluating a one loop UV counterterm reduces to the computation of the divergent part of a one loop completely massive tadpole, which by definition will be independent of external momenta. The expansion of each scalar propagator is given by the identity, [201],

$$\frac{1}{(k+p)^2} = \frac{1}{k^2+m^2} + \frac{-p^2-2kp+m^2}{k^2+m^2} \frac{1}{(k+p)^2} \quad (3.55)$$

where p is a linear combination of external momenta, k is a linear combination

of loop momenta and m is the introduced artificial mass. The second term on the right-hand side of the expansion has the same form as the propagator, so can be decomposed in the same way. Repeating this step several times, we expand the original propagator into a sum of term with very simple denominators and a more complicated term whose contribution to the overall degree of divergence decreases with each iteration,

$$\begin{aligned} \frac{1}{(q+p)^2} &= \frac{1}{q^2+m^2} + \frac{-p^2+2qp}{(q^2+m^2)^2} + \frac{(-p^2-2qp)^2}{(q^2+m^2)^3} - \frac{m^2}{(q^2+m^2)^2} \\ &+ \frac{m^4+2m^2(-p^2-2qp)}{(q^2+m^2)^3} + \frac{(-p^2-2qp+m^2)^3}{(q^2+m^2)^3(q+p)^2} . \end{aligned}$$

The expansion in external momenta can be viewed as an exact splitting of propagators into parts that are polynomial in external momenta and parts that contribute to integrands with a lower degree of divergence. Performing such an operation appropriately many times one can split the integral into a convergent piece and a part that is a polynomial in external momenta.

Using Weinberg's theorem, [127], only the first term on the right-hand side of the expansion (3.55) is divergent, so only this integral is required to find the pole for this specific theory in ten dimensions. All other terms are convergent so can be ignored when only considering divergent parts. As we are only considering one-loop diagrams here there is no need to consider sub-divergences of graphs. When looking at higher loop orders one must ensure all sub-graphs have a negative degree of divergence as well as the diagram in its entirety to ensure it is finite. Furthermore, when looking at higher loop diagrams terms in the expansion that have an m^2 in the numerator can be replaced by local counterterms proportional to m^2 which cancel the corresponding sub-divergences in integrals with no m^2 in the numerator. These counterterms may not preserve symmetry conditions, fortunately the number of counterterms will be small.

As there are no sub-divergences in the one loop 5-point diagrams we can implement Weinberg's theorem to simplify our calculation. Using the degree-of-divergence arguments we drop all but the first term in the expansion, this single Feynman integral will depend only on loop momenta and the introduced mass. More formally they are referred to as tadpole diagrams. As a simple example to illustrate the method, we take a single 5-point diagram at one loop with all external ϕ^i fields and apply the vacuum bubble expansion. The Feynman diagram is illustrated in figure 3.30 where the loop momenta is denoted k and the integral

is defined by

$$\mathcal{I}_{51a} = \int \frac{d^d k}{(2\pi)^d} \frac{1}{k^2(k+p)^2(k+p+q)^2(k+p+q+r)^2(k+p+q+r+s)^2}. \quad (3.56)$$

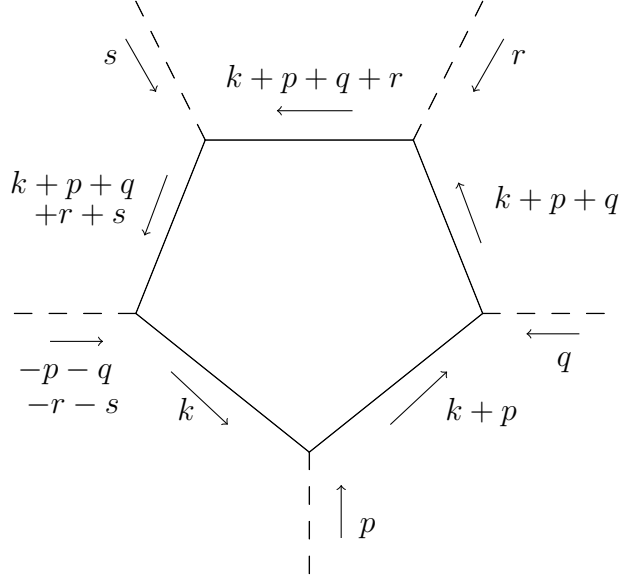


Figure 3.30: 5-point Feynman diagram at one loop $\mathcal{I}_{51a}(1, 1, 1, 1, 1)$.

Each propagator in this integral is expanded using equation (3.55). Note that the artificial mass introduced will remain the same for each expansion. The five propagator integral becomes

$$\mathcal{I}_{51a}(1, 1, 1, 1, 1) = \int \frac{d^d k}{(2\pi)^d} \left[\frac{1}{(k^2 + m^2)^5} + \frac{m^2}{(k^2 + m^2)^5 k^2} + \dots \right].$$

Inserting the expansion again into the second term of this integral

$$\mathcal{I}_{51a}(1, 1, 1, 1, 1) = \int \frac{d^d k}{(2\pi)^d} \left[\frac{1}{(k^2 + m^2)^5} + \frac{m^2}{(k^2 + m^2)^6} + \frac{m^4}{(k^2 + m^2)^6 k^2} + \dots \right].$$

The final two terms along with all subsequent terms that have not been written are finite in ten dimensions by degree-of-divergence arguments. Therefore only the first term is required to find the divergent part of the Feynman diagram. Note that p , q , r and s momenta are included only in the finite parts of the diagram. This term is simply the massive tadpole Feynman diagram illustrated in figure 3.31, where the number five signifies the power on the propagator. This tadpole graph can be easily calculated using basic field theory arguments,

$$\mathcal{I}_{51a}(1, 1, 1, 1, 1) = \int \frac{d^d k}{(2\pi)^d} \frac{1}{(k^2 + m^2)^5} = \frac{m^{d-10} \Gamma(5 - \frac{d}{2})}{(4\pi)^{d/2} \Gamma(5)}. \quad (3.57)$$

For completeness the ϵ -expansion in $d = 10 - 2\epsilon$ dimensions is

$$\mathcal{I}_{51a}(1, 1, 1, 1, 1) = \frac{m^{-2\epsilon}}{(4\pi)^5} \left(\frac{1}{24\epsilon} + \frac{\pi^2}{288}\epsilon - \frac{\zeta_3}{72}\epsilon^2 + O(\epsilon^3) \right). \quad (3.58)$$

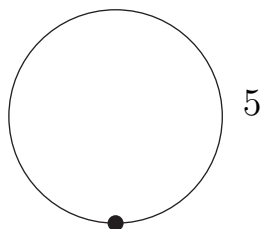


Figure 3.31: Massive tadpole Feynman diagram.

The divergent piece of all 89 one loop Feynman diagrams can be computed using this method. A more involved example is illustrated by the 5-point graph in figure 3.32 which has a more complicated numerator structure than the previous diagram due to the presence of 3-point σ self-interactions.

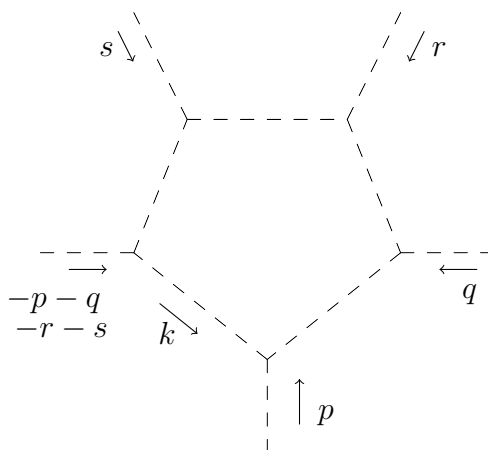


Figure 3.32: A σ 5-point Feynman diagram at one loop, containing internal 3-point σ self-interactions.

This is more complicated than the previous 5-point example as internal propagators will be of the form $1/(k^2)^5$ instead of $1/k^2$. Moreover at each 3-point vertex in figure 3.32 there are \square^2 interactions present due to the coupling $\sigma^2 \square^2 \sigma$ in Lagrangian (3.13). However as the integral will overall be dimensionless like figure 3.31, the vacuum bubble expansion can be used. We will just encounter a far more complicated numerator structure, the tedious reduction of which can be handled using FORM.

To briefly summarise what has been achieved thus far; all 138 Feynman diagrams have been computed, or have at least had the divergent pieces extracted.

For the 2, 3 and 4-point functions this involved using an integration by parts routine encompassed in the Laporta algorithm to reduce all diagrams to master integrals. These master integrals were either calculated by hand or found using existing four dimensional results and the Tarasov method. The 5-point functions were dealt with using the vacuum bubble expansion technique. Finally now that the divergent part of all diagrams is known the Green's functions can be renormalized.

3.4.7 Renormalization

Once all Green's functions have been computed we can sum all n -point graphs together. Potential IR singularities that arise are only a problem if one considers diagrams on an individual level. By summing diagrams the IR singularities naturally cancel and so do not pose a problem. In essence we have computed each diagram as a function of the bare parameters. To determine the associated counterterms we use FORM as a tool to rescale the Green's functions via

$$\begin{aligned}\phi_0^i &= \phi^i \sqrt{Z_\phi} , \\ \sigma_0 &= \sigma \sqrt{Z_\sigma} , \\ g_{0j} &= Z_{g_j}(g_j)g_j(\mu)\mu^{\epsilon/2}\end{aligned}\tag{3.59}$$

where $j = 1, \dots, 5$. In multi-coupling theories one defines the bare coupling constant in a slightly different way which makes the renormalization easier,

$$g_{0j} = Z_{g_j\text{def}}(g_j)\mu^{\epsilon/2}\tag{3.60}$$

where the notation $Z_{g_j\text{def}}(g_j) = Z_{g_j}(g_j)g_j(\mu)$ has been introduced. Once counterterms have been implemented the divergences at a particular loop order are absorbed into the renormalization constants of the associated Green's function. At one loop the 2-point renormalization constants are defined first, followed by the 3-point renormalization constant and so on. The two loop 2-point function counterterms are defined last of all. The renormalization constants are constructed as

$$\begin{aligned}Z_\phi &= 1 + \frac{z_{\phi 11}}{\epsilon} + \left(\frac{z_{\phi 22}}{\epsilon^2} + \frac{z_{\phi 21}}{\epsilon} \right) + \dots , \\ Z_\sigma &= 1 + \frac{z_{\sigma 11}}{\epsilon} + \left(\frac{z_{\sigma 22}}{\epsilon^2} + \frac{z_{\sigma 21}}{\epsilon} \right) + \dots , \\ Z_{g_1\text{def}} &= g_1 + \frac{z_{g_1 11}}{\epsilon} + \left(\frac{z_{g_1 122}}{\epsilon^2} + \frac{z_{g_1 121}}{\epsilon} \right) + \dots ,\end{aligned}$$

$$\begin{aligned}
Z_{g_2\text{def}} &= g_2 + \frac{z_{g211}}{\epsilon} + \left(\frac{z_{g222}}{\epsilon^2} + \frac{z_{g221}}{\epsilon} \right) + \dots, \\
Z_{g_3\text{def}} &= g_3 + \frac{z_{g311}}{\epsilon} + \left(\frac{z_{g322}}{\epsilon^2} + \frac{z_{g321}}{\epsilon} \right) + \dots, \\
Z_{g_4\text{def}} &= g_4 + \frac{z_{g411}}{\epsilon} + \left(\frac{z_{g422}}{\epsilon^2} + \frac{z_{g421}}{\epsilon} \right) + \dots, \\
Z_{g_5\text{def}} &= g_5 + \frac{z_{g511}}{\epsilon} + \left(\frac{z_{g522}}{\epsilon^2} + \frac{z_{g521}}{\epsilon} \right) + \dots. \tag{3.61}
\end{aligned}$$

The notation here needs some explanation. The index i in both $z_{\phi ij}$ and $z_{\sigma ij}$ signifies the loop order, while the j denotes the power of the pole associated with the counterterm. For the counterterms associated with the coupling renormalization constant, $z_{g jlk}$ we have $j = 1, \dots, 5$ and i denotes the number of the coupling. Furthermore, l is the loop order and k signifies the power of the pole in ϵ .

By summing together graphs before introducing counterterms we bypass the need to carry out subtractions on each individual Feynman diagram which can be tedious. Finally REDUZE can be used, alongside FORM to manipulate the results into the desired output. The counterterms can then be inserted into the definitions of the β and γ -functions,

$$\begin{aligned}
0 &= \frac{1}{4}(d-10)Z_{g_1\text{def}} - \beta_1 \frac{\partial Z_{g_1\text{def}}}{\partial g_1} - \beta_2 \frac{\partial Z_{g_1\text{def}}}{\partial g_2} - \beta_3 \frac{\partial Z_{g_1\text{def}}}{\partial g_3} \\
&\quad - \beta_4 \frac{\partial Z_{g_1\text{def}}}{\partial g_4} - \beta_5 \frac{\partial Z_{g_1\text{def}}}{\partial g_5}, \\
0 &= \frac{1}{4}(d-10)Z_{g_2\text{def}} - \beta_1 \frac{\partial Z_{g_2\text{def}}}{\partial g_1} - \beta_2 \frac{\partial Z_{g_2\text{def}}}{\partial g_2} - \beta_3 \frac{\partial Z_{g_2\text{def}}}{\partial g_3} \\
&\quad - \beta_4 \frac{\partial Z_{g_2\text{def}}}{\partial g_4} - \beta_5 \frac{\partial Z_{g_2\text{def}}}{\partial g_5}, \\
0 &= \frac{1}{4}(d-10)Z_{g_3\text{def}} - \beta_1 \frac{\partial Z_{g_3\text{def}}}{\partial g_1} - \beta_2 \frac{\partial Z_{g_3\text{def}}}{\partial g_2} - \beta_3 \frac{\partial Z_{g_3\text{def}}}{\partial g_3} \\
&\quad - \beta_4 \frac{\partial Z_{g_3\text{def}}}{\partial g_4} - \beta_5 \frac{\partial Z_{g_3\text{def}}}{\partial g_5}, \\
0 &= \frac{1}{4}(d-10)Z_{g_4\text{def}} - \beta_1 \frac{\partial Z_{g_4\text{def}}}{\partial g_1} - \beta_2 \frac{\partial Z_{g_4\text{def}}}{\partial g_2} - \beta_3 \frac{\partial Z_{g_4\text{def}}}{\partial g_3} \\
&\quad - \beta_4 \frac{\partial Z_{g_4\text{def}}}{\partial g_4} - \beta_5 \frac{\partial Z_{g_4\text{def}}}{\partial g_5}, \\
0 &= \frac{1}{4}(d-10)Z_{g_5\text{def}} - \beta_1 \frac{\partial Z_{g_5\text{def}}}{\partial g_1} - \beta_2 \frac{\partial Z_{g_5\text{def}}}{\partial g_2} - \beta_3 \frac{\partial Z_{g_5\text{def}}}{\partial g_3} \\
&\quad - \beta_4 \frac{\partial Z_{g_5\text{def}}}{\partial g_4} - \beta_5 \frac{\partial Z_{g_5\text{def}}}{\partial g_5}, \\
\gamma_\phi &= \frac{\beta_1}{Z_\phi} \frac{\partial Z_\phi}{\partial g_1} + \frac{\beta_2}{Z_\phi} \frac{\partial Z_\phi}{\partial g_2} + \frac{\beta_3}{Z_\phi} \frac{\partial Z_\phi}{\partial g_3} + \frac{\beta_4}{Z_\phi} \frac{\partial Z_\phi}{\partial g_4} + \frac{\beta_5}{Z_\phi} \frac{\partial Z_\phi}{\partial g_5},
\end{aligned}$$

$$\gamma_\sigma = \frac{\beta_1}{Z_\sigma} \frac{\partial Z_\sigma}{\partial g_1} + \frac{\beta_2}{Z_\sigma} \frac{\partial Z_\sigma}{\partial g_2} + \frac{\beta_3}{Z_\sigma} \frac{\partial Z_\sigma}{\partial g_3} + \frac{\beta_4}{Z_\sigma} \frac{\partial Z_\sigma}{\partial g_4} + \frac{\beta_5}{Z_\sigma} \frac{\partial Z_\sigma}{\partial g_5} \quad (3.62)$$

where the first five equations can be solved to find $\beta_i(g_j)$ and the final two can be used to determine the anomalous dimensions of the fields. All Renormalization Group functions have been determined using dimensional regularisation with the renormalization constants defined with respect to the $\overline{\text{MS}}$ scheme. Note that in the critical dimension ten of the Lagrangian we assume the coupling constants are dimensionless in that space-time dimension but the standard arbitrary scale is introduced to preserve dimensionlessness of the coupling in the regularised theory.

3.5 Large N Checks and Results

The Renormalization Group functions for $L^{(4,10)}$ which extend the $O(N)$ universality class are given below to as high a loop order as is computationally viable. Practical limitations appear in the construction of the databases we use to apply the Laporta and Tarasov algorithms when attempting to extend these results to higher loop order. In particular the three loop 2-point master integrals in ten dimensions require a significant amount of integration by parts due to the high propagator power which is time consuming. However, we take the point of view that it will be evident even with RG functions at one and two loops that the connection between all theories is established. To be consistent with other work on the $O(N)$ universality class we will use the same convention and notation as that of [54]. We have

$$\begin{aligned} \gamma_\phi^{(d=10)}(g_i) &= -\frac{g_1^2}{40} \\ &\quad + [-5301Ng_1^2 + 16758g_1^2 + 120540g_1g_2 + 302820g_1g_3 \\ &\quad - 14114g_2^2 - 18032g_2g_3 - 15779g_3^2] \frac{g_1^2}{254016000} + O(g_i^4), \\ \gamma_\sigma^{(d=10)}(g_i) &= [-9Ng_1^2 - 86g_2^2 + 112g_2g_3 - 71g_3^2] \frac{1}{15120} \\ &\quad + [664524Ng_1^4 + 6713280Ng_1^3g_2 + 1451520Ng_1^3g_3 \\ &\quad - 1128852Ng_1^2g_2^2 + 1202544Ng_1^2g_2g_3 - 797022Ng_1^2g_3^2 \\ &\quad + 4415512g_2^4 + 6451480g_2^3g_3 - 14360000g_2^2g_3^2 \\ &\quad - 3621996g_2^2g_4^2 - 10763088g_2g_3^3 + 10666782g_2g_3g_4^2 \\ &\quad + 8993886g_3^4 - 1885086g_3^2g_4^2 - 496125g_4^4] \frac{1}{96018048000} \\ &\quad + O(g_i^4), \\ \beta_1^{(d=10)}(g_i) &= [-9Ng_1^2 + 504g_1^2 + 840g_1g_2 + 420g_1g_3 - 86g_2^2 + 112g_2g_3 \end{aligned}$$

$$\begin{aligned}
& -71g_3^2] \frac{g_1}{30240} + O(g_i^5) , \\
\beta_2^{(d=10)}(g_i) &= [756Ng_1^3 - 81Ng_1^2g_2 + 1298g_2^3 + 1764g_2^2g_3 - 1395g_2g_3^2 - 1134g_2g_4^2 \\
& \quad - 308g_3^3 + 1134g_3g_4^2] \frac{1}{90720} + O(g_i^5) , \\
\beta_3^{(d=10)}(g_i) &= [756Ng_1^3 - 81Ng_1^2g_3 - 448g_2^3 - 1782g_2^2g_3 + 3024g_2g_3^2 + 1134g_2g_4^2 \\
& \quad + 565g_3^3 - 1134g_3g_4^2] \frac{1}{90720} + O(g_i^6) , \\
\beta_4^{(d=10)}(g_i) &= [11340Ng_1^4 - 81Ng_1^2g_4^2 + 896g_2^4 - 4256g_2^3g_3 - 7728g_2^2g_3^2 + 234g_2^2g_4^2 \\
& \quad - 4088g_2g_3^3 + 8820g_2g_3g_4^2 + 2268g_2g_5^3 - 700g_3^4 + 3015g_3^2g_4^2 \\
& \quad - 2268g_3g_5^3 - 1134g_4^4] \frac{1}{6804} + O(g_i^6) , \\
\beta_5^{(d=10)}(g_i) &= [-27216Ng_1^5 - 81Ng_1^2g_5^3 - 3584g_2^5 - 8960g_2^4g_3 - 8960g_2^3g_3^2 \\
& \quad + 10080g_2^3g_4^2 - 4480g_2^2g_3^3 + 15120g_2^2g_3g_4^2 - 10854g_2^2g_5^3 - 1120g_2g_3^4 \\
& \quad + 7560g_2g_3^2g_4^2 - 9072g_2g_3g_5^3 - 5670g_2g_4^4 - 112g_3^5 + 1260g_3^3g_4^2 \\
& \quad - 3159g_3^2g_5^3 - 2835g_3g_4^4 + 5670g_4^2g_5^3] \frac{1}{54432} + O(g_i^7) . \quad (3.63)
\end{aligned}$$

The main reason for constructing the Renormalization Group functions is to verify that the critical exponents at the Wilson-Fisher fixed point are consistent with large N critical exponents for the underlying theory. In order to carry out the comparison we follow the process introduced in [51, 52] and first define

$$\begin{aligned}
g_1 &= f \times x , \\
g_2 &= f \times y , \\
g_3 &= f \times z , \\
g_4^2 &= f^2 \times t , \\
g_5^3 &= f^3 \times w
\end{aligned}$$

where f is given by

$$f = \frac{i\sqrt{1680\epsilon N}}{N} . \quad (3.64)$$

The values of the critical coupling constants g_i^* can be found by solving

$$\beta_i^{(d=10)}(g_j^*) = 0 \quad (3.65)$$

where g_j^* is a power series in $1/N$,

$$\begin{aligned}
x &= x_0 + \frac{x_1}{N} + \frac{x_2}{N^2} + \frac{x_3}{N^3} + O\left(\frac{1}{N^4}\right) , \\
y &= y_0 + \frac{y_1}{N} + \frac{y_2}{N^2} + \frac{y_3}{N^3} + O\left(\frac{1}{N^4}\right) ,
\end{aligned}$$

$$\begin{aligned}
z &= z_0 + \frac{z_1}{N} + \frac{z_2}{N^2} + \frac{z_3}{N^3} + O\left(\frac{1}{N^4}\right), \\
t &= t_0 + \frac{t_1}{N} + \frac{t_2}{N^2} + \frac{t_3}{N^3} + O\left(\frac{1}{N^4}\right), \\
w &= w_0 + \frac{w_1}{N} + \frac{w_2}{N^2} + \frac{w_3}{N^3} + O\left(\frac{1}{N^4}\right).
\end{aligned}$$

Each coefficient is itself a power series in ϵ aside from the leading order $1/N$ term which only involves ϵ due to the structure of the N dependence at two and higher loops,

$$\begin{aligned}
x_0 &= x_{00} + x_{01}\epsilon + x_{02}\epsilon^2 + x_{03}\epsilon^3 + O(\epsilon^4), \\
x_1 &= x_{10} + x_{11}\epsilon + x_{12}\epsilon^2 + x_{13}\epsilon^3 + O(\epsilon^4), \\
x_2 &= x_{20} + x_{21}\epsilon + x_{22}\epsilon^2 + x_{23}\epsilon^3 + O(\epsilon^4), \\
x_3 &= x_{30} + x_{31}\epsilon + x_{32}\epsilon^2 + x_{33}\epsilon^3 + O(\epsilon^4), \\
y_0 &= y_{00} + y_{01}\epsilon + y_{02}\epsilon^2 + y_{03}\epsilon^3 + O(\epsilon^4), \\
&\vdots \\
w_3 &= w_{30} + w_{31}\epsilon + w_{32}\epsilon^2 + w_{33}\epsilon^3 + O(\epsilon^4).
\end{aligned}$$

Each of the five critical couplings are stated below for completeness. It is clear to see that all terms of the ϵ expansion except at leading order are zero,

$$\begin{aligned}
g_1^* &= f \left[1 + \frac{518}{N} + \frac{402486}{N^2} - \frac{82820416420}{9N^3} + O\left(\frac{1}{N^4}\right) \right], \\
g_2^* &= f \left[14 + \frac{207172}{3N} + \frac{2760690380}{3N^2} + \frac{154150156688920}{9N^3} + O\left(\frac{1}{N^4}\right) \right], \\
g_3^* &= f \left[14 + \frac{207172}{3N} + \frac{2760690380}{3N^2} + \frac{154150156688920}{9N^3} + O\left(\frac{1}{N^4}\right) \right], \\
g_4^* &= f \left[280 - \frac{900032}{N} - \frac{172076679040}{N^2} - \frac{100301616147074048}{9N^3} \right. \\
&\quad \left. + O\left(\frac{1}{N^4}\right) \right], \\
g_5^* &= f \left[-840 + \frac{142989840}{N} - \frac{13410729934000}{N^2} + \frac{2522538684967218400}{3N^3} \right. \\
&\quad \left. + O\left(\frac{1}{N^4}\right) \right].
\end{aligned}$$

Once these critical couplings are determined the field anomalous dimensions $\gamma_\phi^{(d=10)}(g_i^*)$ and $\gamma_\sigma^{(d=10)}(g_i^*)$ are evaluated at criticality as a series in $1/N$. The coefficient of each term in ϵ of each successive power of $1/N$ should be in total agreement with the critical exponents η and $\eta + \chi$ respectively, the leading order

terms of which are given in equations (2.72) and (2.84). The large N critical exponents are also given in [47–49]. The field anomalous dimensions evaluated at the critical coupling are

$$\begin{aligned}
\gamma_\phi^{(d=10)}(g_i) &= \left[42\epsilon - \frac{589\epsilon^2}{10} - \frac{5741\epsilon^3}{200} + \left(-\frac{89689}{4000} + 84\zeta_3 \right) \epsilon^4 \right] \frac{1}{N} \\
&\quad + \left[43512\epsilon - \frac{1288917\epsilon^2}{5} + \frac{28725321\epsilon^3}{100} \right] \frac{1}{N^2} + O\left(\frac{1}{N^3}\right), \\
\gamma_\sigma^{(d=10)}(g_i) &= \left[2016\epsilon - \frac{15536\epsilon^2}{5} - \frac{72488\epsilon^3}{75} + \left(-\frac{1017964}{1135} + 4032\zeta_3 \right) \epsilon^4 \right] \frac{1}{N} \\
&\quad + \left[\frac{32223968\epsilon}{3} - \frac{5296010132\epsilon^2}{135} + \left(\frac{35923867327}{2025} \right. \right. \\
&\quad \left. \left. - 13641600\zeta_3 \right) \epsilon^3 \right] \frac{1}{N^2} + O\left(\frac{1}{N^3}\right). \tag{3.66}
\end{aligned}$$

We have checked the correspondence holds for the anomalous field dimensions and the large N exponents. More precisely the $1/N$ term of $\gamma_\phi^{(d=10)}(g_i)$ is in exact agreement with the exponent $(1/2)\eta_1$, while the $1/N^2$ term is in exact agreement with exponent $(1/2)\eta_2$. The factor of $1/2$ is due to conventional differences used in past papers on the large N expansion. Furthermore the $1/N$ term of $\gamma_\sigma^{(d=10)}(g_i)$ matches the exponent $-\eta_1 - \chi_1$ and the $1/N^2$ term is in exact agreement with exponent $-\eta_2 - \chi_2$. Such agreement should be regarded as evidence for the underlying universality of the core interaction across the dimensions and the well-established universality of the Wilson-Fisher fixed point of $O(N)$ ϕ^4 theory.

Equally the agreement is a reassuring check that we have correctly performed the renormalization to one and two loops which relied on the evaluation of various master integrals to higher dimensions. Having established the connection with the underlying universal theory the next step would be analysing aspects of the non-trivial fixed point structure and in particular the location, if it exists of the conformal window. To access the conformal window one has to solve a set of equations, [51, 52], which for five couplings is

$$\begin{aligned}
\beta_1(g_i^*) &= \beta_2(g_i^*) = \beta_3(g_i^*) = \beta_4(g_i^*) = \beta_5(g_i^*) = 0, \\
\det \left(\frac{\partial \beta_i}{\partial g_j} \right) &= 0 \tag{3.67}
\end{aligned}$$

where $i, j = 1, \dots, 5$. The first five equations determine the critical couplings and the final equation, which is the vanishing of the Hessian, provides the condition where there is a change in the stability of a fixed point. Unfortunately as the β -functions are dependent on three variables, $\beta_i(g_j, \epsilon, N)$, and five couplings are

present, attempting to solve (3.67) is difficult and time consuming. As our main goal was to verify the universality class up to ten dimensions, we therefore leave this analysis for future work until computational limitations are overcome. We will however analyse the fixed point structure for other theories in later Chapters.

3.6 Discussion

As part of an investigation into the $O(N)$ scalar universality class we reviewed the established connection between the $NL\sigma M$ in two dimensions and four dimensional ϕ^4 theory. This particular universality class has been extended in recent years to include six dimensional ϕ^3 theory and an eight dimensional scalar theory with the $O(N)$ symmetry group, [51–54]. The main motivation for studying universality is due to the potential of extracting properties of one theory by examining another. More specifically it has been suggested that it may be possible to access non-perturbative fixed points through perturbative fixed points in a higher dimension. For example, the non-perturbative fixed point in four dimensional Quantum Chromodynamics (QCD), the Banks-Zaks fixed point, [88], may be studied by considering the six dimensional extension to QCD which contains a non-trivial perturbative fixed point. The connectivity of these two theories enables the Banks-Zaks fixed point to be accessed using a perturbative expansion in six dimensions. It was hoped that the $O(N)$ universality class discussed here would not only contain similar features but would give a simple testing ground to examine universal properties. Indeed the Heisenberg magnet in three space-time dimensions can be examined by perturbatively renormalizing $O(N)$ ϕ^4 theory in four dimensions. The resulting perturbative RG functions will be in $d = 4 - 2\epsilon$ dimensions and the three dimensional results can be obtained by setting $\epsilon = 1/2$. Furthermore, the conformal field theory with $O(N)$ symmetry existing in five dimensions is of great physical interest due to the AdS_6/CFT_5 correspondence and can be accessed via six dimensional ϕ^3 theory, [56].

In this Chapter we focused on extending the $O(N)$ universality class to ten dimensions. The main motivation being to add confidence to the overall universality class and provide results which may be compared with conformal bootstrap and other non-perturbative research. Moreover the ten dimensional theory can act as a laboratory where one could test ideas on not only universality, but also introduce tools used for calculating in higher dimensions. In this Chapter we built a new Lagrangian which is perturbatively renormalizable in ten dimensions using dimensionality arguments before computing associated Renor-

malization Group functions to as high a loop order as was viable. The Tarasov method, [195, 196], was utilized which relates d and $(d + 2)$ -dimensional Feynman master integrals. We also exploited the integration by parts reduction encoded in REDUZE, [187, 190, 192, 194], which was imperative to the computation. Note that Tarasov method raised one question regarding whether there is a deeper connection in the Tarasov construction of relating d and $(d + 2)$ -dimensional Feynman integrals with the underlying field theories. In other words is there a way of proceeding more fundamentally via a path integral construction without having to make the connection at the Renormalization Group function level? This is a topic of great interest and one which requires fundamental study.

After Renormalization Group functions were computed in ten dimensions the associated critical exponents could be calculated and matched with known large N results. Hence establishing the ten dimensional theory as an extension of the $O(N)$ universality class. An important observation is that there is more than one way to look at this tower of theories. Instead of having separate theories in different dimensions that are connected at the Wilson-Fisher d -dimensional fixed point, one instead has a single d -dimensional universal theory. This universal theory contains the Wilson-Fisher fixed point and the core universal interaction $\sigma\phi^i\phi^i$, as well as all possible interactions between the two fields, σ and ϕ^i . When we try to write down a specific Lagrangian in a fixed dimension such as ten, for example, the universal interaction will be relevant in that specific dimension. Moreover a finite number of additional ‘spectator’ interactions will also be relevant in the specified dimension. Therefore a Lagrangian can be formulated containing a finite number of terms with the physics being driven by the core universal interaction. This gives an alternative way of thinking about how and why the theories discussed in this Chapter may influence each other.

It also opens up a whole new landscape for model building and applications to beyond the Standard Model (BSM) physics. If universality plays a role in how the physics in scalar theories is driven then surely the same can be said for gauge theories. In principle the construction of a similar tower of gauge theories should be feasible based on what has been found in the scalar theory case. Moreover, it should be relevant to possible directions beyond the Standard Model. For instance, for certain gauge groups, such as $SU(3) \times SU(2) \times U(1)$, there may be a flow to a non-trivial fixed point which connects with a unified theory. Before discussing model building in regards to gauge theories we first look at another scalar universality class. This time the tower of theories will contain a more complex symmetry group and hence an enriched fixed point structure to study.

$$O(N) \times O(m)$$

Landau-Ginzburg-Wilson Theory in Six Dimensions

4.1 Introduction

We have looked at the universality class of a scalar theory endowed with $O(N)$ symmetry to ten space-time dimensions. Scalar field theories with more complex symmetries have been the subject of interest in recent years in the context of trying to develop our understanding of conformal field theories (CFTs) in dimensions greater than two using established concepts, [204–210], in a modern application, [61, 211–213]. The main aim being to find conformal windows of theories where non-trivial fixed points of the β -function exist. In this window one in principle has a theory where ideas for extending Zamolodchikov’s c -theorem, [214], to higher dimensions can be explored as well as other properties of strictly two dimensional CFTs. Considerable work has been done in recent years to extend the perturbative results of higher dimensional scalar theories. There has also been significant interest utilizing non-perturbative methods to study scalar field theories in higher dimensions. In particular, the non-perturbative conformal bootstrap technique is used because of the potential application to non-scalar theories and scalar theories with symmetry other than $O(N)$, [61, 211–213].

The aim of this Chapter is to continue investigating higher dimensional scalar field theories, but now look toward more complex symmetry groups. Specifically we now want to renormalize the six dimensional extension of the Landau-

Ginzburg-Wilson (LGW) theory and provide three loop perturbative results to complement recent [66] and future bootstrap studies. In effect this is a ϕ^3 type theory with an $O(N) \times O(m)$ symmetry. The Landau-Ginzburg-Wilson model has applications to condensed matter problems such as randomly dilute spin models, [215, 216]. The enhanced symmetry group also allows us to analyse a more enriched fixed point structure and potential conformal window. Recent conformal bootstrap analysis provided on the Landau-Ginzburg-Wilson model in three dimensions, [66], gave a theoretical prediction of the phase diagram in frustrated spin models with non-collinear order. Furthermore the work of [67] provided a detailed conformal bootstrap analysis for $O(N) \times O(2)$, particularly looking at the model $O(4) \times O(2)$ which describes the chiral phase transition in two flavour Quantum Chromodynamics (QCD) in four dimensions. Along with providing complementary results to bootstrap studies, a second motivation for looking at the Landau-Ginzburg-Wilson model is to continue the exploration of the tower of theories across dimensions which are in the same universality class as the Wilson-Fisher fixed point, [41]. This is sometimes known as the ultraviolet (UV) completion of a theory and was first recognised in [46, 217], but its power has been exploited in recent years.

We will first review results in the four-dimensional Landau-Ginzburg-Wilson theory including the known large N values for the critical exponents. We then introduce the six dimensional Lagrangian in the same universality class. Renormalizing the Landau-Ginzburg-Wilson model perturbatively in six dimensions we obtain new results for the Renormalization Group (RG) functions to three loops. A notable difference in this Chapter compared to the last is that we will also perform a mass renormalization in section 4.5. We will also provide a fresh fixed point analysis and conformal window search for the model in six dimensions to be compared with the four dimensional results, [218].

4.2 Landau-Ginzburg-Wilson Theory

The model we wish to consider is a six dimensional scalar theory with $O(N) \times O(m)$ symmetry which lies in the same universality class as the four dimensional Landau-Ginzburg-Wilson theory with the same symmetry. We begin by recalling the relevant aspects of the latter theory before constructing the six dimensional Lagrangian. The four dimensional Lagrangian involves a quartic interaction for

a scalar field ϕ^{ia} where $1 \leq i \leq N$ and $1 \leq a \leq m$, [218],

$$L^{(\text{LGW4})} = \frac{1}{2} \partial^\mu \phi^{ia} \partial_\mu \phi^{ia} + \frac{\bar{g}_1}{4!} (\phi^{ia} \phi^{ia})^2 + \frac{\bar{g}_2}{4!} [(\phi^{ia} \phi^{ib})^2 - (\phi^{ia} \phi^{ia})^2].$$

The couplings of the respective interactions are given by \bar{g}_i . This version of the Landau-Ginzburg-Wilson theory is not the most useful for developing the large N expansion or indeed for seeing the connection with higher dimensional theories. Instead it is better to reformulate $L^{(\text{LGW4})}$ in terms of cubic interactions by introducing a set of auxiliary fields $\tilde{\sigma}$ and \tilde{T}^{ab} . The latter is symmetric and traceless in its $O(m)$ indices. Then the Lagrangian becomes, [218],

$$L^{(\text{LGW4})} = \frac{1}{2} \partial^\mu \phi^{ia} \partial_\mu \phi^{ia} + \frac{1}{2} \tilde{\sigma} \phi^{ia} \phi^{ia} + \frac{1}{2} \tilde{T}^{ab} \phi^{ia} \phi^{ib} - \frac{3\tilde{\sigma}^2}{2\tilde{g}_1} - \frac{3\tilde{T}^{ab}\tilde{T}^{ab}}{2\tilde{g}_2}$$

where we have rescaled the couplings, $\tilde{g}_1 = \bar{g}_1 + (m-1)\tilde{g}_2/m$ and $\bar{g}_2 = \tilde{g}_2$, [215,216]. In this new formulation the coupling constants appear within the quadratic part of the Lagrangian which is the first step in constructing the critical exponents using the large N methods of [48,49]. However, for perturbative calculations it is more appropriate for the couplings to appear with the actual interactions. Using a simple rescaling,

$$L^{(\text{LGW4})} = \frac{1}{2} \partial^\mu \phi^{ia} \partial_\mu \phi^{ia} + \frac{1}{2} \sigma^2 + \frac{1}{2} T^{ab} T^{ab} + \frac{1}{2} g_1 \sigma \phi^{ia} \phi^{ia} + \frac{1}{2} g_2 T^{ab} \phi^{ia} \phi^{ib}. \quad (4.1)$$

This is this formulation that one uses to build the six dimensional theory. The Renormalization Group functions of (4.1) have been computed to several loop orders, [218,219]. The two loop results of the β -functions are stated below so that one may examine some of the fixed point properties of the $O(N) \times O(m)$ four dimensional theory. They are

$$\begin{aligned} \beta_1(\bar{g}_1, \bar{g}_2) &= \frac{1}{2}(d-4)\bar{g}_1 + \frac{(mN+8)}{6}\bar{g}_1^2 - \frac{1}{6}(3mN+14)\bar{g}_1^3 \\ &+ (m-1)(N-1) \left(\frac{11}{9}\bar{g}_1^2 - \frac{13}{12}\bar{g}_1\bar{g}_2 + \frac{5}{18}\bar{g}_2^2 \right) \bar{g}_2 \\ &- \frac{1}{3}(m-1)(N-1)\bar{g}_2 \left(\bar{g}_1 - \frac{\bar{g}_2}{2} \right) + O(\bar{g}_i^4) \end{aligned} \quad (4.2)$$

and

$$\begin{aligned} \beta_2(\bar{g}_1, \bar{g}_2) &= \frac{1}{2}(d-4)\bar{g}_2 + 2\bar{g}_1\bar{g}_2 + \frac{1}{6}(m+N-8)\bar{g}_2^2 - \frac{1}{18}(5mN+82)\bar{g}_1^2\bar{g}_2 \\ &+ \frac{1}{9}[5mN-11(m+N)+53]\bar{g}_1\bar{g}_2^2 - \frac{1}{36}[13mN-35(m+N)] \end{aligned}$$

$$+ 99]\bar{g}_2^3 + O(\bar{g}_i^4) \quad (4.3)$$

where the order symbol is understood to mean any combination of the two coupling constants. There are several fixed points which can be derived from these β -functions. These are known as the free field Gaussian fixed point $(\bar{g}_1^*, \bar{g}_2^*) = (0, 0)$, the fixed point corresponding to the Heisenberg model $(\bar{g}_1^*, \bar{g}_2^*) = (\bar{g}_1, 0)$ and two fixed points where both critical couplings are non-zero. In the fixed point corresponding to the Heisenberg case we have $\bar{g}_1 \neq 0$ and $\bar{g}_2 = 0$, irrespective of whether m is set to unity or not. In the case where $m \neq 1$ the parameter m always appears as a multiplier of N . In the context of the (\bar{g}_1, \bar{g}_2) -plane the Heisenberg fixed point is actually a saddle-point and so is unstable to perturbations in the \bar{g}_2 direction. Note that for the single coupling $O(N)$ scalar theory discussed in Chapter 3, the Heisenberg fixed point will be stable. For the two fixed points where both critical couplings are non-zero, one is known as the chiral stable (CS) fixed point and the other as the anti-chiral unstable (AU) fixed point. To differentiate between these we look at the eigenvalues of the stability matrix, $\partial\beta_i(g_j)/\partial g_j$, with the former having two negative eigenvalues. In contrast the stability matrix evaluated at the AU fixed point will give two positive eigenvalues.

To connect the different Landau-Ginzburg-Wilson theories in four and six dimensions we will compare results of the critical exponents in each of these dimensions. Alternatively it is more convenient to compare exponents with the large N results for this universality class which are given in [218, 220]. It is therefore worthwhile recalling these large N results and giving a perspective on the fixed point structure of the four dimensional theory. Recall in the large N method of [48, 49] the critical exponents are computed by analysing the skeleton Dyson-Schwinger equations at criticality. At that point the propagators obey scaling law type forms where the powers are in effect the critical exponents. The critical exponents can be expanded as a power series in $1/N$, where N is large. Each coefficient of this power series can be deduced by evaluating the relevant Feynman diagrams at each order of the $1/N$ expansion. The divergent diagrams are analytically regularised which means they are determined as functions of the space-time dimension d . Therefore the large N exponents correspond to the universal quantum field theory (QFT) which underlies the Wilson-Fisher fixed point in d -dimensions. Thus when the ϵ -expanded Renormalization Group functions are computed perturbatively in $d = D_c - 2\epsilon$ where D_c is the critical dimension of a specific theory, they will agree with large N results set in that critical dimension at the same fixed point. The four dimensional Landau-Ginzburg-Wilson theory has exponents which match the large N critical exponents computed in [218, 220]

at the three non-trivial fixed points.

The different solutions for the Heisenberg (H), CS and AU fixed points emerge from simple conditions which are best seen in the Lagrangian formulation involving the fields σ and T^{ab} . These conditions can be summarised by the vector (σ, T^{ab}) so that the Heisenberg fixed point is $(\sigma, 0)$, AU is $(0, T^{ab})$ and the CS fixed point is given by (σ, T^{ab}) , where a zero entry in the vector means the corresponding field is absent at that fixed point. In other words in the large N construction the critical exponents for a particular fixed point are determined by including only those non-zero fields in the vector in the skeleton Dyson-Schwinger expansion. If we define the scaling dimensions of the fields ϕ^{ia} , σ and T^{ab} by α , β and γ respectively then we can define the anomalous dimensions as follows

$$\alpha = \mu - 1 + \frac{1}{2}\eta \quad , \quad \beta = 2 - \eta - \chi \quad , \quad \gamma = 2 - \eta - \chi_T$$

where $d = 2\mu$. Here η corresponds to the anomalous dimension of ϕ^{ia} . The exponents χ and χ_T correspond to the respective vertex anomalous dimensions of σ and T^{ab} with the ϕ^{ia} field. For completeness we will state the leading order (LO) large N critical exponents for the universal theory, originally computed in [48, 49, 218],

$$\begin{aligned} \eta_1^{\text{H}} &= - \frac{4\Gamma(2\mu - 2)}{\Gamma(2 - \mu)\Gamma(\mu - 1)\Gamma(\mu - 2)\Gamma(\mu + 1)m} \quad , \\ \eta_1^{\text{CS}} &= - \frac{2(m + 1)\Gamma(2\mu - 2)}{\Gamma(\mu + 1)\Gamma(\mu - 1)\Gamma(\mu - 2)\Gamma(2 - \mu)} \quad , \\ \eta_1^{\text{AU}} &= - \frac{2(m - 1)(m + 2)\Gamma(2\mu - 2)}{m\Gamma(\mu + 1)\Gamma(\mu - 1)\Gamma(\mu - 2)\Gamma(2 - \mu)} \quad , \\ \chi_1^{\text{H}} &= - \frac{\mu(4\mu - 5)\eta_1^{\text{H}}}{(\mu - 2)} \quad , \quad \chi_1^{\text{CS}} = - \frac{\mu(4\mu - 5)\eta_1^{\text{CS}}}{(\mu - 2)} \quad , \\ \chi_{T,1}^{\text{CS}} &= - \frac{\mu[(2\mu - 3)m + (4\mu - 5)]\eta_1^{\text{CS}}}{(\mu - 2)(m + 1)} \quad , \\ \chi_{T,1}^{\text{AU}} &= - \frac{\mu(m - 2)[(m + 4)(2\mu - 3) + 1]\eta_1^{\text{AU}}}{(m - 1)(m + 2)(\mu - 2)} \quad . \end{aligned} \quad (4.4)$$

Note that χ_1^{H} is the same as in the $O(N)$ case given by (2.84) as is expected. Higher order corrections are available in [48, 49, 218, 220]. For the four dimensional Landau-Ginzburg-Wilson theory the exponents corresponding to the critical slope of the β -function has also been determined, [220]. Using

$$\omega = (\mu - 2) + \sum_{i=1}^{\infty} \frac{\omega_i}{N^i} \quad (4.5)$$

then, [220],

$$\begin{aligned}
\omega_{+1}^{\text{H}} &= - \frac{4(2\mu - 1)^2 \Gamma(2\mu - 2)}{\Gamma(2 - \mu) \Gamma(\mu - 1) \Gamma(\mu - 2) \Gamma(\mu + 1) m N} , \\
\omega_{+1}^{\text{AU}} &= - \left[2\mu^2 - 3\mu - 1 + \frac{\mu(m - 2)[2\mu - 5 - 2(m + 4)(2\mu - 3)]}{(m - 1)(m + 2)} \right] \frac{\eta_1^{\text{AU}}}{N} , \\
\omega_{\pm 1}^{\text{CS}} &= \frac{(2\mu - 1)\eta_1^{\text{CS}}}{2(m + 1)(\mu - 2)N} \left[m(\mu - 1)(\mu - 4) + (2\mu^2 - 7\mu + 4) \right. \\
&\quad \left. \pm \mu[(m^2 - 1)(\mu - 1)^2 + 2(m - 1)(2\mu - 3)(\mu - 1) \right. \\
&\quad \left. + (5\mu - 8)^2]^{\frac{1}{2}} \right] . \tag{4.6}
\end{aligned}$$

Where \pm corresponds to two solutions in the CS case due to the presence of two fields σ and T^{ab} . For the other fixed points only one solution is present since there is in effect only one coupling constant relevant at these respectively points. The additional critical exponent ω gives an insight into the stability of each fixed point. The large N exponents provide a fundamental insight into the critical point structure of the underlying universal theory in the large N expansion. Note that although the large N results provided by (4.4) and (4.6) will be useful for checking the explicit perturbative expressions, it will be the fixed point structure of the $O(N) \times O(m)$ theory in six dimensions which is our main focus.

4.3 Six Dimensions

One can build a six dimensional Landau-Ginzburg-Wilson Lagrangian following the same formulation of (4.1). This extension of the universality class is based on the dimensionality of the fields and ensuring that the Lagrangian is renormalizable in six dimensions. As the action must be dimensionless the dimension of the ϕ^{ia} field is restricted to $[\phi^{ia}] = d/2 - 1$ while the σ and T^{ab} fields both have dimension $[\sigma] = [T^{ab}] = 2$. Clearly the Lagrangian (4.1) is renormalizable in four space-time dimensions as all relevant interactions are present. The key to constructing the six dimensional extension is the retention of the two basic interactions of ϕ^{ia} with the auxiliary fields, which are $\sigma\phi^{ia}\phi^{ia}$ and $T^{ab}\phi^{ia}\phi^{ib}$. This ensures that the dimensionality of all three fields are preserved at the connecting Wilson-Fisher fixed point in d -dimensions. To ensure the six dimensional Lagrangian is perturbatively renormalizable all additional relevant interactions involving the auxiliary fields are included. This leads to

$$L^{(\text{LGW6})} = \frac{1}{2} \partial^\mu \phi^{ia} \partial_\mu \phi^{ia} + \frac{1}{2} \partial_\mu \sigma \partial^\mu \sigma + \frac{1}{2} \partial^\mu T^{ab} \partial_\mu T^{ab} + \frac{1}{2} g_1 \sigma \phi^{ia} \phi^{ia}$$

$$\begin{aligned}
& + \frac{1}{6}g_2\sigma^3 + \frac{1}{2}g_3T^{ab}\phi^{ia}\phi^{ia} + \frac{1}{2}g_4\sigma T^{ab}T^{ab} \\
& + \frac{1}{6}g_5T^{ab}T^{ac}T^{bc}
\end{aligned} \tag{4.7}$$

as the ultraviolet completion which should be equivalent to (4.1) at the Wilson-Fisher fixed point. Note that the six dimensional Lagrangian includes more interactions than the four dimensional case, as was the case for the ten dimensional $O(N)$ scalar theory. The additional interactions which depend solely on σ and T^{ab} are referred to as spectator interactions since they are only present in the critical dimension of six. Additionally the σ and T^{ab} fields now cease being auxiliary fields and become propagating with fundamental propagators. The interactions associated with couplings g_1 and g_3 are core interactions and are present at the Wilson-Fisher fixed point throughout all dimensions. They seed the universal theory in the sense that they determine the canonical dimensions of the fields. Thereby they induce the structure of the spectator interactions in each critical dimension by requiring renormalizability.

We focus much of our attention on the critical theory, however we can also include masses in the Lagrangian for the three basic fields,

$$L_m^{(\text{LGW6})} = L^{(\text{LGW6})} - \frac{1}{2}m_1^2\phi^{ia}\phi^{ia} - \frac{1}{2}m_2^2\sigma^2 - \frac{1}{2}m_3^2T^{ab}T^{ab} \tag{4.8}$$

where m_i are masses. Similar terms can be added to $L^{(\text{LGW4})}$. Having established the six dimensional Lagrangian for Landau-Ginzburg-Wilson theory, we wish to determine the Renormalization Group functions for Lagrangian (4.7) to three loops and analyse the fixed point structure and value of any possible conformal window present. As in Chapter 3, we will also perform a large N analysis for the critical exponents to ensure the six dimensional Lagrangian (4.7) lies in the same universality class as (4.1). In addition to the wave function and coupling constant renormalization we will consider the renormalization of the three masses present in Lagrangian (4.8) and determine the mass mixing matrix of anomalous dimensions to three loops. As this is the first calculation where we have considered a massive Lagrangian we include relevant background on the different techniques to deal with the inclusion of mass. All results for this calculation have been published in [2].

4.4 Calculation Techniques

We want to derive the Renormalization Group functions of the six dimensional Landau-Ginzburg-Wilson model given by Lagrangian (4.7). In particular we wish to compute the β -functions for each of the five couplings along with the three γ -functions, all to three loops. The methodology to acquire these results builds on the same techniques used in [53] and described in Chapter 3. The same procedure is used of obtaining all Feynman diagrams using QGRAF, [184], and inserting the relevant group theory before reducing these graphs to a combination of master integrals which can be solved by hand, [187]. The Feynman diagrams for each interaction will then be combined and renormalized to obtain counterterms from the Renormalization Group functions can be found. As in the ten dimensional case discussed in the previous Chapter, we use the Tarasov method to lift four dimensional master integrals to six dimensions. The main difference between the $O(N)$ calculation and the present theory is that the latter has a more complicated symmetry group. This can be seen from the additional indices in Lagrangian (4.7). The Feynman rules for six dimensional Landau-Ginzburg-Wilson theory are illustrated in figure 4.1 where the group theory term are defined in equations (4.9) to (4.13). Note that solid lines indicate ϕ^{ia} fields and dotted lines signify σ fields as before. The new T^{ab} fields are denoted as wiggly lines.

$$\begin{array}{l}
 \frac{\overline{\phi^{ia}}}{\phi^{jb}} = \frac{\delta_{ij}\delta_{ab}}{p^2} \quad \sigma \text{ --- } \sigma = \frac{1}{p^2} \quad \overset{\sim}{T^{ab}} \overset{\sim}{T^{cd}} = \frac{P^{abcd}}{p^2} \\
 \begin{array}{c} \sigma \\ | \\ \phi^{ia} \text{ --- } \phi^{jb} \end{array} = g_1 \delta_{ij} \delta_{ab} \quad \begin{array}{c} \sigma \\ | \\ \sigma \text{ --- } \sigma \end{array} = g_2 \\
 \begin{array}{c} T^{ab} \\ | \\ \phi^{ia} \text{ --- } \phi^{jb} \end{array} = g_3 \delta_{ij} P^{abcd} \quad \begin{array}{c} \sigma \\ | \\ \overset{\sim}{T^{ab}} \overset{\sim}{T^{cd}} \end{array} = g_4 P^{abcd} \\
 \begin{array}{c} T^{ab} \\ | \\ T^{cd} \text{ --- } T^{ef} \end{array} = g_5 P_3^{abcdef}
 \end{array}$$

Figure 4.1: Feynman rules for the Green's functions of $O(N) \times O(m)$ Landau-Ginzburg-Wilson theory in six dimensions.

To begin our computation we generate all Feynman diagrams electronically us-

ing the QGRAF package, [184]. The input model file is given by figure 4.2, where the notation AAA corresponds to the $T^{ab}T^{ac}T^{bc}$ vertex, for instance. Once again we forbid all tadpole and snail diagrams from the output and include only one-particle irreducible (1PI) graphs. The number of diagrams generated for the 2 and 3-point graphs to three loops are listed in table 4.1. Note that we do not actually have to generate the Feynman diagrams for the 3-point interactions σ^3 , $\sigma\phi^{ia}\phi^{jb}$, and $\sigma T^{ab}T^{cd}$ to any loop order. These will be discarded at the appropriate point later. To avoid calculating these diagrams directly we can instead employ a trick that involves nullifying a vertex to obtain the divergent piece of the diagrams corresponding to these interactions. This will be explained in much greater detail in section 4.4.3. For now briefly recall that to compute the Renormalization Group functions only the divergent parts of Feynman diagrams is required. Unfortunately this short-cut can not be applied to all 3-point interactions. We do therefore need to generate graphs for the interactions $T^{ab}\phi^{ia}\phi^{jb}$ and $T^{ab}T^{cd}T^{ef}$ to three loops.

```
[phi, phi, +]
[sigma, sigma, +]
[AA, AA, +]
[sigma, phi, phi]
[sigma, sigma, sigma]
[AA, phi, phi]
[sigma, AA, AA]
[AA, AA, AA]
```

Figure 4.2: The QGRAF input model file for the six dimensional Landau-Ginzburg-Wilson calculation.

Green's function	Tree Level	One Loop	Two Loops	Three Loops
$\phi^{ia}\phi^{jb}$	-	2	23	514
$\sigma\sigma$	-	3	19	343
$T^{ab}T^{cd}$	-	3	27	589
$T^{ab}\phi^{ia}\phi^{jb}$	1	5	137	4984
$T^{ab}T^{ac}T^{bc}$	1	5	155	5857

Table 4.1: Number of Feynman diagrams computed to three loops for each of the 2 and 3-point Green's functions. Total number of diagrams is 12666. The interactions $\sigma\phi^{ia}\phi^{jb}$, σ^3 and $\sigma T^{ab}T^{cd}$ are not needed as they can be generated from 2-point graphs.

All one loop diagrams are illustrated in figures 4.3 to 4.8. For completeness the diagrams for all 3-point interactions, including the interactions which we do not generate, are illustrated. Additionally to display the types of interactions that are possible all 2-point graphs to two loops are given in Appendix B.

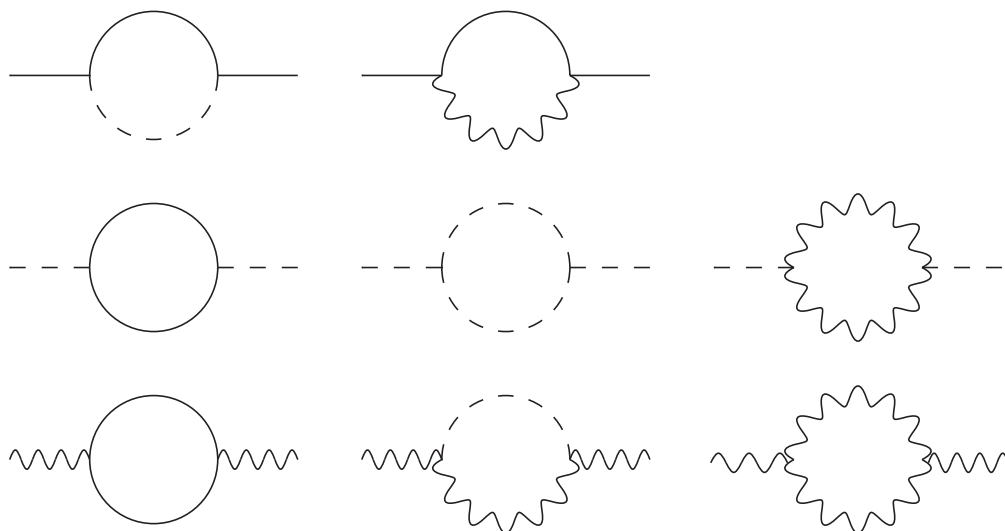


Figure 4.3: All Feynman diagrams for the ϕ^{ia} , σ and T^{ab} 2-point functions to one loop.

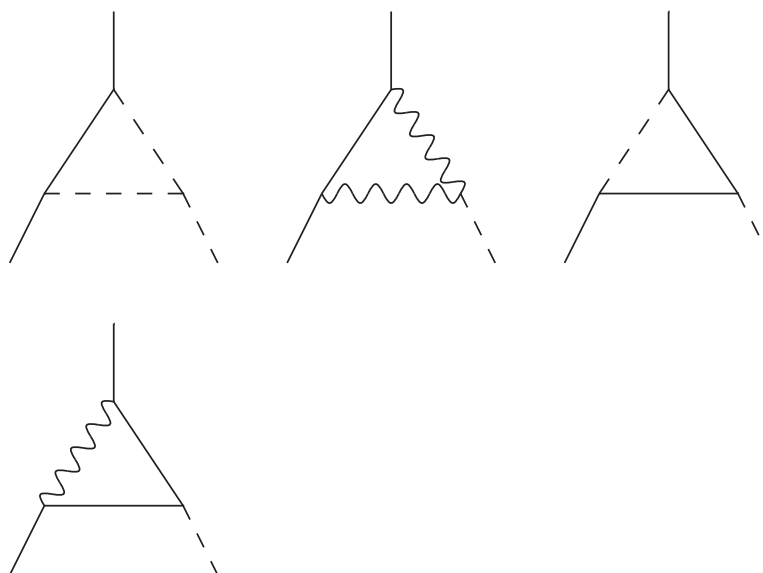


Figure 4.4: All Feynman diagrams for the 3-point $\sigma\phi^{ia}\phi^{jb}$ interaction to one loop.

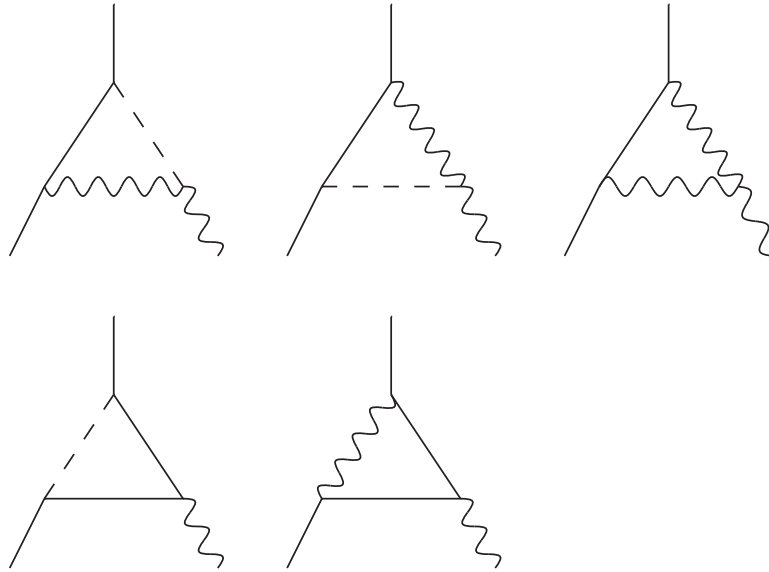


Figure 4.5: All Feynman diagrams for the 3-point $\phi^{ia}\phi^{jb}T^{ab}$ interaction to one loop.

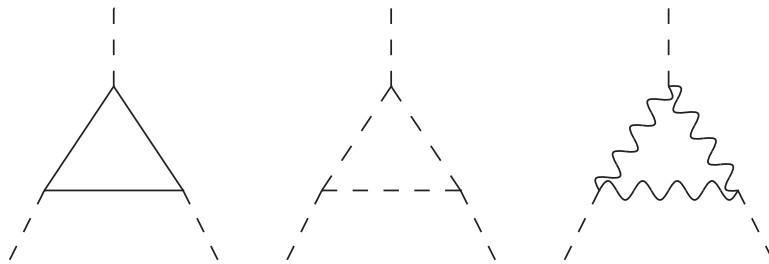


Figure 4.6: All Feynman diagrams for the 3-point $\sigma\sigma\sigma$ interaction to one loop.

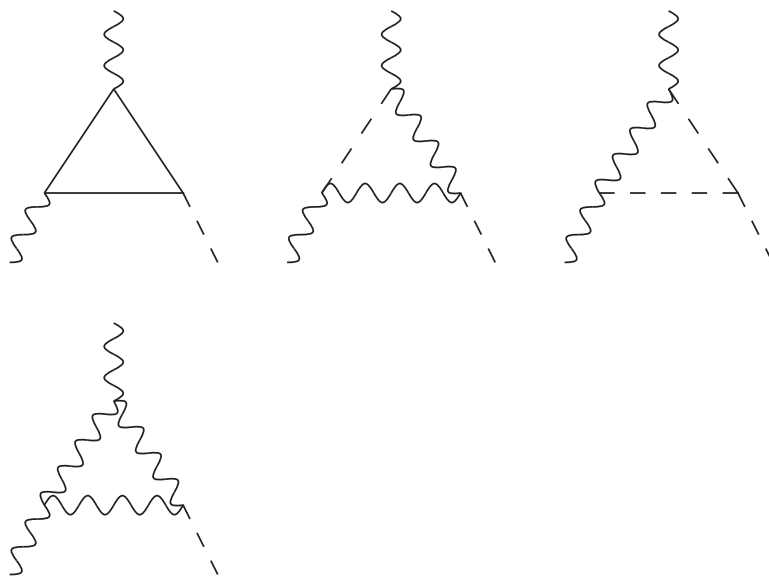


Figure 4.7: All Feynman diagrams for the 3-point $\sigma T^{ab}T^{cd}$ interaction to one loop.

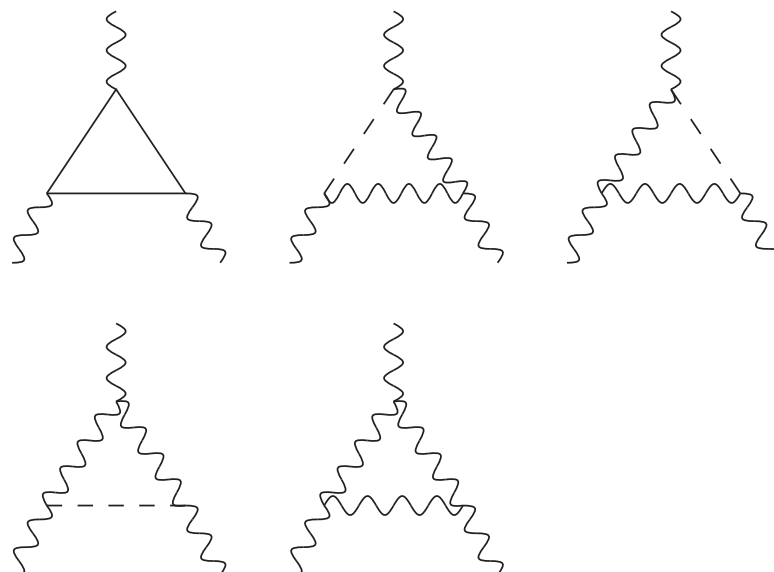


Figure 4.8: All Feynman diagrams for the 3-point $T^{ab}T^{ac}T^{bc}$ interaction to one loop.

To show the form of QGRAF one example of the output data for a 2-point Feynman diagram at three loops is displayed along with a graphical representation in figure 4.9. The diagram contains two external T^{ab} fields and a combination of ϕ^{ia} and σ internal fields. The ordering of each vertex and the internal line structure which connects them is encoded in the QGRAF output. The factor 1/2 is a symmetry factor for the Feynman diagram.

```

1/2
*vxA(AA(-1),phi(1),phi(2))
*vxA(AA(-3),phi(3),phi(4))
*vxA(sigma(6),phi(1),phi(5))
*vxA(sigma(7),phi(2),phi(8))
*vxA(sigma(7),phi(3),phi(5))
*vxA(sigma(6),phi(4),phi(8))

```

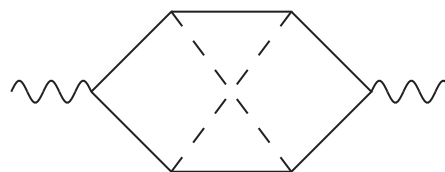


Figure 4.9: QGRAF output and the graphical representation of a 2-point Feynman diagram with external T^{ab} fields.

After every Feynman diagram has been generated we identify and order the graphs into their basic topologies and apply the indices corresponding to the symmetry group $O(N) \times O(m)$ automatically using FORM, [185]. The $O(N) \times O(m)$ symmetry gives the Feynman rules for the propagators and vertices involving T^{ab} an associated colour tensor. In other words the T^{ab} propagator will involve the

tensor, [218],

$$P^{abcd} = \frac{1}{2}[\delta^{ac}\delta^{bd} + \delta^{ad}\delta^{bc} - \frac{2}{m}\delta^{ab}\delta^{cd}] \quad (4.9)$$

which satisfies the trace properties

$$P^{abcc} = P^{aacd} = 0, \quad P^{abcb} = \frac{(m-1)(m+2)}{2m}\delta^{ac}. \quad (4.10)$$

It also satisfies the projection relations

$$P^{abpq}P^{pqcd} = P^{abcd}, \quad P^{abpq}P^{cpdq} = \frac{(m-2)}{2m}P^{abcd}. \quad (4.11)$$

Equipped with this Feynman rule the triple T^{ab} vertex involves the rank 6 colour tensor

$$P_3^{abcdef} = P^{abpq}P^{cdpr}P^{efqr}. \quad (4.12)$$

Consequently,

$$\begin{aligned} P_3^{abcdpq}P^{efpq} &= P_3^{abcdef}, & P_3^{abcded} &= \frac{(m-2)(m+4)}{4m}P^{abce} \\ P_3^{abpqrs}P_3^{cdpqrs} &= \frac{(m-2)(m+4)}{4m}P^{abcd} \end{aligned} \quad (4.13)$$

for instance. Encoding these within the FORM module allows the group theory evolution of the higher loop graphs to process more efficiently. The Feynman rules for the propagators are then substituted in, which ensures the graphs are picked up at the appropriate place in the subsequent program. Next the Feynman diagrams are reduced to a combination of master integrals. It turns out that only the 2-point master integrals to three loops are required, owing to the shortcut which can be used in computing the $\sigma\phi^{ia}\phi^{jb}$, σ^3 and $\sigma T^{ab}T^{cd}$ interactions. Similarly other 3-point interactions, $\phi^{ia}\phi^{jb}T^{cd}$ and $T^{ab}T^{cd}T^{ef}$, can be reduced to a combination of 2-point master integrals by setting one external momenta to zero. A more detailed explanation on these subtleties will follow in sections 4.4.3 and 4.4.4.

4.4.1 Integral Reduction of the 2-point Function

All diagrams for the 2-point function to three loops have been generated with the relevant Feynman rules substituted in. Now REDUZE, [187, 190], can be used to simplify the Feynman diagrams into a set of integrals which can be computed by hand. REDUZE works using a C++ implementation of the Laporta algorithm which uses integration by parts to systematically reduce scalar integrals to a set of basic master integrals, [192]. The one loop reduction of the 2-point function is

trivial to show. All one loop 2-point functions reduce down to one basic master integral illustrated in 3.12. The two loop reduction is more complicated and was used in Chapter 3 without derivation which we present here. The auxiliary topology, or integral family, of the 2-point two loop function is displayed in figure 3.14. As a Feynman integral the auxiliary topology is

$$\mathcal{I}_{22}(\alpha, \beta, \gamma, \rho, \delta) = \int \frac{d^d k d^d q}{(2\pi)^{2d}} \frac{1}{(k^2)^\alpha ((k-p)^2)^\beta (q^2)^\gamma ((q-p)^2)^\rho ((k-q)^2)^\delta} \quad (4.14)$$

where the notation $\mathcal{I}_{22}(\alpha, \beta, \gamma, \rho, \delta) = \int_{k,q} I_{22}(\alpha, \beta, \gamma, \rho, \delta)$ can be implemented. The integral is of the form $1/(abcde)$ where a, b, c, d and e are products of the propagators and the loop momenta is denoted by k and q . The external legs satisfy the condition $p^2 = -\mu^2$. The reduction of the 2-point function at two loop was discussed in [221] and briefly mentioned in [222]. The same initial steps as the reduction of the 3-point one loop function in Chapter 3 are followed.

Using the dimensional regularisation property of equation (3.19) we obtain the following identity,

$$d \int \frac{d^d k d^d q}{(2\pi)^{2d}} I_{22}(\alpha, \beta, \gamma, \rho, \delta) = - \int \frac{d^d k d^d q}{(2\pi)^{2d}} k^\mu \frac{\partial}{\partial k^\mu} I_{22}(\alpha, \beta, \gamma, \rho, \delta). \quad (4.15)$$

This is the same result as equation (3.20) except that we now have a two loop integral. To obtain a reduction relation only one of the loops needs to be differentiated, in this case the loop on the right-hand side of figure 4.10 which is just the 3-point one loop diagram. We could as easily differentiate over the left-hand loop, in which case we replace k^μ with q^μ in equation (4.15).

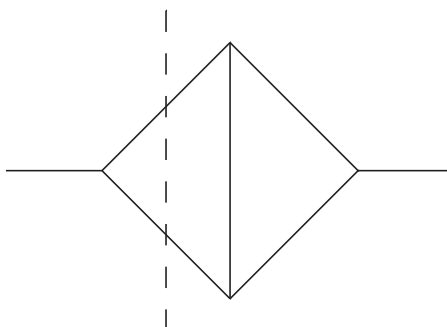


Figure 4.10: To obtain a reduction relation only one of the two loops needs to be differentiated, in this case we choose the loop on the right-hand side of the dashed line.

To begin the reduction each term in the denominator of $\mathcal{I}_{22}(\alpha, \beta, \gamma, \rho, \delta)$ is ex-

plicitly differentiated in turn with respect to k

$$\begin{aligned}
d\mathcal{I}_{22}(\alpha, \beta, \gamma, \rho, \delta) &= 2\alpha \int_{k,q} \frac{k^2}{(k^2)^{\alpha+1}((k-p)^2)^\beta(q^2)^\gamma((q-p)^2)^\rho((k-q)^2)^\delta} \\
&+ 2\beta \int_{k,q} \frac{k(k-p)}{(k^2)^\alpha((k-p)^2)^{\beta+1}(q^2)^\gamma((q-p)^2)^\rho((k-q)^2)^\delta} \\
&+ 2\delta \int_{k,q} \frac{k(k-q)}{(k^2)^\alpha((k-p)^2)^\beta(q^2)^\gamma((q-p)^2)^\rho((k-q)^2)^{\delta+1}} .
\end{aligned}$$

The numerator in each of these integrals can be rearranged,

$$\begin{aligned}
d\mathcal{I}_{22}(\alpha, \beta, \gamma, \rho, \delta) &= 2\alpha \int_{k,q} \frac{k^2}{(k^2)^{\alpha+1}((k-p)^2)^\beta(q^2)^\gamma((q-p)^2)^\rho((k-q)^2)^\delta} \\
&+ \beta \int_{k,q} \frac{(k-p)^2 + k^2 - p^2}{(k^2)^\alpha((k-p)^2)^{\beta+1}(q^2)^\gamma((q-p)^2)^\rho((k-q)^2)^\delta} \\
&+ \delta \int_{k,q} \frac{(k-q)^2 + k^2 - q^2}{(k^2)^\alpha((k-p)^2)^\beta(q^2)^\gamma((q-p)^2)^\rho((k-q)^2)^{\delta+1}} .
\end{aligned}$$

The integrals on the right-hand side can then be rewritten into the notation $\mathcal{I}_{22}(\alpha, \beta, \gamma, \rho, \delta)$. Additionally the equation can be simplified by factorising terms on both sides of the equation. We remind the reader at this point that the notation $\mathcal{I}_{22}(\alpha + 1, \beta, \gamma, \rho, \delta)$ indicates that the power on the k^2 propagator has been increased by one,

$$\begin{aligned}
(d - 2\alpha - \beta - \delta)\mathcal{I}_{22}(\alpha, \beta, \gamma, \rho, \delta) &= \beta\mathcal{I}_{22}(\alpha - 1, \beta + 1, \gamma, \rho, \delta) \\
&- p^2\beta\mathcal{I}_{22}(\alpha, \beta + 1, \gamma, \rho, \delta) \\
&+ \delta\mathcal{I}_{22}(\alpha - 1, \beta, \gamma, \rho, \delta + 1) \\
&- \delta\mathcal{I}_{22}(\alpha, \beta, \gamma - 1, \rho, \delta + 1) . \quad (4.16)
\end{aligned}$$

This equation is illustrated in figure 4.11 where the + indicates the power on that particular propagator has been increased by one.

$$\begin{aligned}
(d - 2\alpha - \beta - \delta) \text{---} \text{diamond} &= \beta \text{---} \text{circle}^+ - \beta p^2 \text{---} \text{diamond}^+ \\
&+ \delta \text{---} \text{circle}^+ - \delta \text{---} \text{circle}^+
\end{aligned}$$

Figure 4.11: The first relation derived from the reduction of the 2-point two loop function, $\mathcal{I}_{22}(\alpha, \beta, \gamma, \rho, \delta)$.

Figure 4.11 illustrates how the basic topology of the 2-point two loop function can be reduced into a combination of lower topology 2-point diagrams where an internal propagator has been removed and the same topology with a higher power propagator. Three additional reduction relations similar to equation (4.16) can be obtained by utilizing two symmetries that are present in the 2-point function. Namely,

$$k - p \rightarrow q - p \quad , \quad k \rightarrow q$$

and

$$k - p \rightarrow k \quad , \quad q - p \rightarrow q .$$

The first symmetry changes which way around the loops are positioned, while the second reflects the Feynman diagram in the horizontal axis. Applying both of these symmetries individually, as well as once together, three additional reduction relations can be found

$$\begin{aligned} (d - 2\beta - \alpha - \delta)\mathcal{I}_{22}(\alpha, \beta, \gamma, \rho, \delta) &= \alpha\mathcal{I}_2(\alpha + 1, \beta - 1, \gamma, \rho, \delta) \\ &\quad - p^2\alpha\mathcal{I}_{22}(\alpha + 1, \beta, \gamma, \rho, \delta) \\ &\quad + \delta\mathcal{I}_{22}(\alpha, \beta - 1, \gamma, \rho, \delta + 1) \\ &\quad - \delta\mathcal{I}_{22}(\alpha, \beta, \gamma, \rho - 1, \delta + 1) , \end{aligned} \quad (4.17a)$$

$$\begin{aligned} (d - 2\gamma - \rho - \delta)\mathcal{I}_{22}(\alpha, \beta, \gamma, \rho, \delta) &= \rho\mathcal{I}_{22}(\alpha, \beta, \gamma - 1, \rho + 1, \delta) \\ &\quad - p^2\rho\mathcal{I}_{22}(\alpha, \beta, \gamma, \rho + 1, \delta) \\ &\quad + \delta\mathcal{I}_{22}(\alpha, \beta, \gamma - 1, \rho, \delta + 1) \\ &\quad - \delta\mathcal{I}_{22}(\alpha - 1, \beta, \gamma, \rho, \delta + 1) , \end{aligned} \quad (4.17b)$$

$$\begin{aligned} (d - 2\rho - \gamma - \delta)\mathcal{I}_{22}(\alpha, \beta, \gamma, \rho, \delta) &= \gamma\mathcal{I}_{22}(\alpha, \beta, \gamma + 1, \rho - 1, \delta) \\ &\quad - p^2\gamma\mathcal{I}_{22}(\alpha, \beta, \gamma + 1, \rho, \delta) \\ &\quad + \delta\mathcal{I}_{22}(\alpha, \beta, \gamma, \rho - 1, \delta + 1) \\ &\quad - \delta\mathcal{I}_{22}(\alpha, \beta - 1, \gamma, \rho, \delta + 1) . \end{aligned} \quad (4.17c)$$

A fifth relation can be obtained by modifying identity (4.15). Instead of differentiating over the loop momenta k we instead choose to differentiate with respect to the incoming/outgoing momenta p . More precisely, we will now use the following identity

$$d \int \frac{d^d k d^d q}{(2\pi)^{2d}} \mathcal{I}_{22}(\alpha, \beta, \gamma, \rho, \delta) = - \int \frac{d^d k d^d q}{(2\pi)^{2d}} p^\mu \frac{\partial}{\partial p^\mu} \mathcal{I}_{22}(\alpha, \beta, \gamma, \rho, \delta) . \quad (4.18)$$

Differentiating each term in the denominator of $\mathcal{I}_{22}(\alpha, \beta, \gamma, \rho, \delta)$ in turn with

respect to p we find,

$$d\mathcal{I}_{22}(\alpha, \beta, \gamma, \rho, \delta) = 2\beta \int_{k,q} \frac{p(p-k)}{(k^2)^\alpha ((k-p)^2)^{\beta+1} (q^2)^\gamma ((q-p)^2)^\rho ((k-q)^2)^\delta} + 2\rho \int_{k,q} \frac{p(p-q)}{(k^2)^\alpha ((k-p)^2)^\beta (q^2)^\gamma ((q-p)^2)^{\rho+1} ((k-q)^2)^\delta} .$$

Once again the numerator in each integral can be rearranged,

$$d\mathcal{I}_{22}(\alpha, \beta, \gamma, \rho, \delta) = \beta \int_{k,q} \frac{(p-k)^2 + p^2 - k^2}{(k^2)^\alpha ((k-p)^2)^{\beta+1} (q^2)^\gamma ((q-p)^2)^\rho ((k-q)^2)^\delta} + \rho \int_{k,q} \frac{(p-q)^2 + p^2 - q^2}{(k^2)^\alpha ((k-p)^2)^\beta (q^2)^\gamma ((q-p)^2)^{\rho+1} ((k-q)^2)^\delta} .$$

Rewriting all integrals in the notation $\mathcal{I}_{22}(\alpha, \beta, \gamma, \rho, \delta)$ and simplifying, a fifth reduction relation can be obtained

$$(d - \beta - \rho)\mathcal{I}_{22}(\alpha, \beta, \gamma, \rho, \delta) = p^2\beta\mathcal{I}_{22}(\alpha, \beta + 1, \gamma, \rho, \delta) - \beta\mathcal{I}_{22}(\alpha - 1, \beta + 1, \gamma, \rho, \delta) + p^2\rho\mathcal{I}_{22}(\alpha, \beta, \gamma, \rho + 1, \delta) - \rho\mathcal{I}_{22}(\alpha, \beta, \gamma - 1, \rho + 1, \delta) . \quad (4.19)$$

The final relation can be derived by adjusting the identity (4.15) to differentiate over the momenta p and multiply by a vector $(p - q)$,

$$d \int \frac{d^d k d^d q}{(2\pi)^{2d}} \mathcal{I}_{22}(\alpha, \beta, \gamma, \rho, \delta) = - \int \frac{d^d k d^d q}{(2\pi)^{2d}} \frac{\partial}{\partial p^\mu} (p - q)^\mu \mathcal{I}_{22}(\alpha, \beta, \gamma, \rho, \delta) . \quad (4.20)$$

Differentiating each term in the denominator of the two loop Feynman diagram with respect to p and multiplying by a $(p - q)$ vector we find

$$d\mathcal{I}_{22}(\alpha, \beta, \gamma, \rho, \delta) = 2\beta \int_{k,q} \frac{(p-q)^\mu (p-k)^\mu}{(k^2)^\alpha ((k-p)^2)^{\beta+1} (q^2)^\gamma ((q-p)^2)^\rho ((k-q)^2)^\delta} + 2\rho \int_{k,q} \frac{(q-p)^2}{(k^2)^\alpha ((k-p)^2)^\beta (q^2)^\gamma ((q-p)^2)^{\rho+1} ((k-q)^2)^\delta} .$$

Making use of identities such as, [221],

$$2(p-q)^\mu (p-k)^\mu = (p-q)^2 + (p-k)^2 - (q-k)^2 , \quad (4.21)$$

the relation becomes

$$d\mathcal{I}_{22}(\alpha, \beta, \gamma, \rho, \delta) = \beta \int_{k,q} \frac{(p-q)^2 + (p-k)^2 + (q-k)^2}{(k^2)^\alpha ((k-p)^2)^{\beta+1} (q^2)^\gamma ((q-p)^2)^\rho ((k-q)^2)^\delta}$$

$$+ 2\rho \int_{k,q} \frac{(q-p)^2}{(k^2)^\alpha ((k-p)^2)^\beta (q^2)^\gamma ((q-p)^2)^{\rho+1} ((k-q)^2)^\delta} .$$

Using the familiar $\mathcal{I}_{22}(\alpha, \beta, \gamma, \rho, \delta)$ notation for the right-hand side of the equation and simplifying, the sixth and final reduction relation is found

$$(d - \beta - 2\rho)\mathcal{I}_{22}(\alpha, \beta, \gamma, \rho, \delta) = \beta[\mathcal{I}_{22}(\alpha, \beta + 1, \gamma, \rho - 1, \delta) - \mathcal{I}_{22}(\alpha, \beta + 1, \gamma, \rho, \delta - 1)] . \quad (4.22)$$

This sixth relation has been illustrated in figure 4.12 as it is the only relation which includes the second master integral, known as the ‘spectacle’ graph. All other relations contain only the first master integral.

Figure 4.12: The sixth reduction relation of the 2-point two loop Feynman integral $\mathcal{I}_{22}(\alpha, \beta, \gamma, \rho, \delta)$. The loop momenta has been illustrated.

Taking the most general case by setting $\alpha = \beta = \gamma = \rho = \delta = 1$ and rearranging the six integration by parts relations so that the higher order topologies sit on the left-hand side, the final result given by the REDUZE program for the 2-point two loop graph can be found,

$$p^2\mathcal{I}_{22}(1, 2, 1, 1, 1) = (4 - d)\mathcal{I}_{22}(1, 1, 1, 1, 1) + \mathcal{I}_{22}(0, 2, 1, 1, 1) + \mathcal{I}_{22}(0, 1, 1, 1, 2) - \mathcal{I}_{22}(1, 1, 0, 1, 2) , \quad (4.23a)$$

$$p^2\mathcal{I}_{22}(2, 1, 1, 1, 1) = (4 - d)\mathcal{I}_{22}(1, 1, 1, 1, 1) + \mathcal{I}_{22}(2, 0, 1, 1, 1) + \mathcal{I}_{22}(1, 0, 1, 1, 2) - \mathcal{I}_{22}(1, 1, 1, 0, 2) , \quad (4.23b)$$

$$p^2\mathcal{I}_{22}(1, 1, 1, 2, 1) = (4 - d)\mathcal{I}_{22}(1, 1, 1, 1, 1) + \mathcal{I}_{22}(1, 1, 0, 2, 1) + \mathcal{I}_{22}(1, 1, 0, 1, 2) - \mathcal{I}_{22}(0, 1, 1, 1, 2) , \quad (4.23c)$$

$$p^2\mathcal{I}_{22}(1, 1, 2, 1, 1) = (4 - d)\mathcal{I}_{22}(1, 1, 1, 1, 1) + \mathcal{I}_{22}(1, 1, 2, 0, 1) + \mathcal{I}_{22}(1, 1, 1, 0, 2) - \mathcal{I}_{22}(1, 0, 1, 1, 2) , \quad (4.23d)$$

$$p^2\mathcal{I}_{22}(1, 2, 1, 1, 1) + p^2\mathcal{I}_{22}(1, 1, 1, 2, 1) = (d - 2)\mathcal{I}_{22}(1, 1, 1, 1, 1) + \mathcal{I}_{22}(0, 2, 1, 1, 1) + \mathcal{I}_{22}(1, 1, 0, 2, 1) , \quad (4.23e)$$

$$(d - 3)\mathcal{I}_{22}(1, 1, 1, 1, 1) = \mathcal{I}_{22}(1, 2, 1, 0, 1) - \mathcal{I}_{22}(1, 2, 1, 1, 0) . \quad (4.23f)$$

These six IBP relations can be used within REDUZE to reduce any 2-point two loop integral to a combination of master integrals. As an example, the relation (4.23f)

is displayed in figure 4.13. This can be substituted into relations (4.23a)-(4.23e) to solve for two loop 2-point diagrams with higher power propagators.

Figure 4.13: Reduction of the 2-point two loop Feynman diagram $\mathcal{I}_{22}(1, 1, 1, 1, 1)$ down to a combination of the two different master integrals.

It is important to note that while the second diagram on the right-hand side of figure 4.13 is a master integral, the ‘spectacle’ graph. The first diagram is not, however it is related to the other 2-point master integral known as the ‘sunset’ diagram.

Figure 4.14: The first diagram of the right-hand side of figure 4.13 is related to the ‘sunset’ 2-point master integral.

This can be shown via integration in coordinate space as the ‘sunset’ master integral can be integrated down to the integral $\mathcal{I}_{22}(0, 1, 2, 1, 1)$.

Figure 4.15: The ‘sunset’ master Feynman diagram integrates down to the integral $\mathcal{I}_{22}(0, 1, 2, 1, 1)$.

We have derived the reduction relation for the 2-point Green’s function at two loops to illustrate what REDUZE does internally. The reduction of the 2-point three loop function is a much more involved process and hence the full derivation is not included here. We do however discuss how the REDUZE program deals with such an integral family in the following subsection. All that remains is to compute the master integrals in six dimensions.

4.4.2 2-point Master Integrals

The 2-point one loop master integral has been illustrated in figure 3.12 while the two masters integrals derived for the two loop function were given in figure 3.13. Note that for this theory all propagators in the master integrals are of the form $1/k^2$. The one and two loop master integrals were calculated in Chapter 3 using conformal integration. The results in $d = 6 - 2\epsilon$ dimensions are

$$\begin{aligned} \mathcal{I}_{21}^{(d=6-2\epsilon)}(1, 1) &= \left[-\frac{1}{6\epsilon} - \frac{4}{9} + \left(\frac{\pi^2}{72} - \frac{26}{27}\right)\epsilon + \left(-\frac{160}{81} + \frac{\pi^2}{27} + \frac{7\zeta_3}{18}\right)\epsilon^2 \right. \\ &\quad + \left(\frac{28\zeta_3}{27} + \frac{13\pi^2}{162} + \frac{47\pi^4}{8640} - \frac{968}{243}\right)\epsilon^3 \\ &\quad \left. + O(\epsilon^4) \right] \frac{p^2}{(4\pi)^3}, \end{aligned} \quad (4.24)$$

$$\begin{aligned} \mathcal{I}_{22}^{(d=6-2\epsilon)}(1, 1, 1, 1, 0) &= \left[\frac{1}{36\epsilon^2} + \frac{4}{27\epsilon} - \frac{\pi^2}{216} + \frac{14}{27} + \left(\frac{368}{243} - \frac{2\pi^2}{81} - \frac{7\zeta_3}{54}\right)\epsilon \right. \\ &\quad + \left(-\frac{56\zeta_3}{81} + \frac{2924}{729} - \frac{7\pi^2}{81} - \frac{7\pi^4}{4320}\right)\epsilon^2 \\ &\quad \left. + O(\epsilon^3) \right] \frac{(p^2)^2}{(4\pi)^6}, \end{aligned} \quad (4.25)$$

$$\begin{aligned} \mathcal{I}_{22}^{(d=6-2\epsilon)}(1, 1, 0, 0, 1) &= \left[-\frac{1}{1440\epsilon} - \frac{451}{86400} + \left(\frac{\pi^2}{8640} - \frac{129811}{5184000}\right)\epsilon \right. \\ &\quad + \left(-\frac{30725071}{311040000} + \frac{451\pi^2}{518400} + \frac{\zeta_3}{135}\right)\epsilon^2 \\ &\quad + \left(\frac{451\zeta_3}{8100} + \frac{129811\pi^2}{31104000} + \frac{19\pi^4}{172800} - \frac{6551286931}{18662400000}\right)\epsilon^3 \\ &\quad \left. + O(\epsilon^4) \right] (p^2)^3 \pi^6. \end{aligned} \quad (4.26)$$

The symbol ζ_n is the Riemann zeta function where $\zeta_2 = \pi^2/6$ and $\zeta_4 = \pi^4/90$. The reduction of the 2-point Feynman diagrams at three loops also uses REDUZE, [187, 190]. However the reduction at three loops is more complicated due to the number of propagators present and the fact that three auxiliary topologies exist. Previously for the one and two loop Green's functions only one auxiliary topology was present. The three auxiliary topologies of the 2-point function at three loops are illustrated in figure 4.16. The first topology is non-planar, while the second and third topologies are known as the 'Benz' and 'Ladder' diagrams respectively. In our set-up the second and third topologies will each reduce down to a combination of the other plus the non-planar topology. Therefore we only need to perform a reduction on one of these auxiliary topologies as well as on the non-planar diagram. The choice of base family in REDUZE is down to the user. We have chosen to reduce the 'Ladder' topology here, however we could

have easily chosen to reduce the ‘Benz’ diagram.

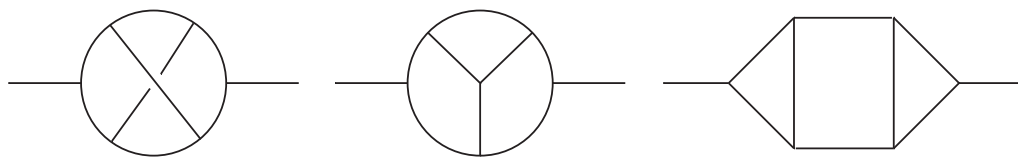


Figure 4.16: The three integral families, or auxiliary topologies, for the 2-point function at three loops. From left to right; the ‘Non-planar’, the ‘Benz’ and the ‘Ladder’ diagram.

The reduction of the three loop topologies involves REDUZE and follows the same process as the two loop case. We will discuss the main challenges involved at three loops without going into detail on the internal integration by parts algorithm. The biggest difference in the set up is that we need to perform two separate reductions one for each integral family, each requiring a different specified internal propagator structure. After both reductions have been performed we are left with two databases containing relations between these topologies and master integrals which can be used to simplify three loop Feynman diagrams.

It turns out that only six master integrals exist for the 2-point function at three loops. These are the non-planar diagram itself containing only $1/k^2$ propagators and five additional master integrals which are illustrated in figure 4.18. These five master integrals are all derived from the reduction of the ‘Ladder’ topology. The labelling of the power on the propagators which is used to differentiate between master integrals is displayed in figure 4.17.

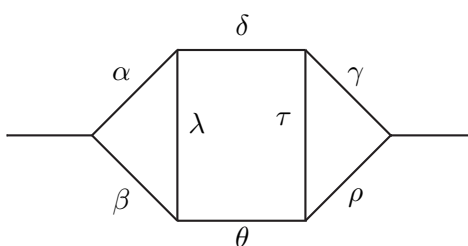


Figure 4.17: The ‘Ladder’ auxiliary topology for the 2-point function at three loops with the power on each of the propagators labelled and $\mathcal{I}_{23l}(\alpha, \beta, \gamma, \rho, \delta, \theta, \lambda, \tau)$.

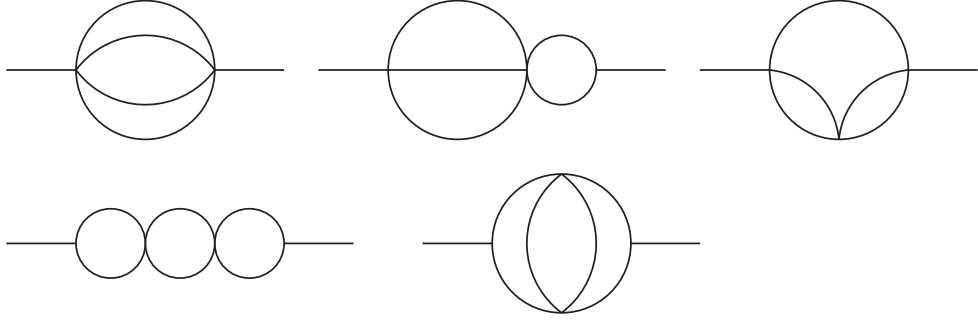


Figure 4.18: The five master integrals associated with the reduction of the ‘Ladder’ topology of the 2-point function at three loop. Labelling from left to right on top line; $\mathcal{I}_{23l}(0, 1, 1, 0, 0, 0, 1, 1)$, $\mathcal{I}_{23l}(0, 1, 1, 1, 1, 0, 1, 0)$ and $\mathcal{I}_{23l}(0, 1, 0, 1, 1, 0, 1, 1)$. Labelling from left to right on bottom line; $\mathcal{I}_{23l}(1, 1, 1, 1, 1, 1, 0, 0)$ and $\mathcal{I}_{23l}(1, 1, 1, 1, 0, 0, 1, 1)$.

To illustrate what a REDUZE IBP output looks like a relation between a 2-point diagram at three loops and its master integrals is given in Appendix C. Of the six master integrals all but two can be directly computed in $d = 6 - 2\epsilon$ dimensions using conformal integration techniques. The results are

$$\begin{aligned}
\mathcal{I}_{23l}^{(d=6-2\epsilon)}(0, 1, 1, 0, 0, 0, 1, 1) &= \left[-\frac{1}{1814400\epsilon} - \frac{617}{84672000} \right. \\
&+ \left(\frac{\pi^2}{7257600} - \frac{18360367}{320060160000} \right) \epsilon \\
&+ \left(-\frac{3163717187}{8961684480000} + \frac{617\pi^2}{338688000} \right. \\
&\quad \left. \left. + \frac{29\zeta_3}{1814400} \right) \epsilon^2 + O(\epsilon^3) \right] \frac{1}{(p^2)^5}, \\
\mathcal{I}_{23l}^{(d=6-2\epsilon)}(0, 1, 1, 1, 1, 0, 1, 0) &= \left[\frac{1}{8640\epsilon^2} + \frac{611}{518400\epsilon} + \frac{74257}{10368000} - 34560\pi^2 \right. \\
&+ \left(\frac{63435631}{1866240000} - \frac{611\pi^2}{2073600} - \frac{13\zeta_3}{8640} \right) \epsilon \\
&+ \left(\frac{15631687091}{111974400000} - \frac{74257\pi^2}{41472000} - \frac{17\pi^4}{829440} \right. \\
&\quad \left. - \frac{7943\zeta_3}{518400} \right) \epsilon^2 + O(\epsilon^3) \right] (p^2)^4, \\
\mathcal{I}_{23l}^{(d=6-2\epsilon)}(0, 1, 0, 1, 1, 0, 1, 1) &= \left[+\frac{1}{19440\epsilon^2} + \frac{167}{291600\epsilon} - \frac{\pi^2}{77760} + \frac{8477}{2187000} \right. \\
&+ \left(-\frac{167\pi^2}{1166400} - \frac{23\zeta_3}{19440} + \frac{114329}{5467500} \right) \epsilon \\
&+ \left(\frac{1363033}{13668750} - \frac{8477\pi^2}{8748000} - \frac{11\pi^4}{622080} - \frac{3841\zeta_3}{291600} \right) \epsilon^2 \\
&\quad \left. + O(\epsilon^3) \right] (p^2)^4,
\end{aligned}$$

$$\begin{aligned}
\mathcal{I}_{23l}^{(6-2\epsilon)}(1, 1, 1, 1, 1, 1, 0, 0) = & \left[-\frac{1}{216\epsilon^3} - \frac{1}{27\epsilon^2} + \left(+\frac{\pi^2}{864} - \frac{29}{162} \right) \frac{1}{\epsilon} + \frac{\pi^2}{108} \right. \\
& + \frac{7\zeta_3}{216} - \frac{496}{729} + \left(+\frac{37\pi^4}{103680} + \frac{29\pi^2}{648} + \frac{7\zeta_3}{27} \right. \\
& \left. \left. - \frac{1636}{729} \right) \epsilon + \left(-\frac{7\pi^2\zeta_3}{864} + \frac{203\zeta_3}{162} + \frac{31\zeta_5}{360} \right. \right. \\
& \left. \left. + \frac{124\pi^2}{729} + \frac{37\pi^4}{12960} - \frac{14752}{2187} \right) \epsilon^2 + O(\epsilon^3) \right] (p^2)^3 .
\end{aligned}$$

The other two graphs, $\mathcal{I}_{23l}(1, 1, 1, 1, 0, 1, 1)$ and the non-planar diagram which is labelled $\mathcal{I}_{23n}(1, 1, 1, 1, 1, 1, 1, 1)$, can be calculated in six dimensions by using known four dimensional results, [223]. The Tarasov method which relates d and $(d+2)$ -dimensional integrals, [195, 196], is used to lift the four dimensional results to six dimensions. The Tarasov method for the 3-point one loop function was derived in Chapter 3, the 2-point relation is extremely similar. Therefore the results of the remaining two master integrals in six dimensions can be calculated as

$$\begin{aligned}
\mathcal{I}_{23l}^{(d=6-2\epsilon)}(1, 1, 1, 1, 0, 0, 1, 1) = & \left[\frac{1}{1296\epsilon^3} + \frac{103}{15552\epsilon^2} + \left(-\frac{\pi^2}{5184} + \frac{30161}{933120} \right) \frac{1}{\epsilon} \right. \\
& + \frac{7\zeta_3}{1296} - \frac{103\pi^2}{62208} + \frac{6057823}{55987200} \\
& + \left(\frac{680542229}{3359232000} - \frac{30161\pi^2}{3732480} + \frac{721\zeta_3}{15552} + \frac{25\zeta_4}{2304} \right) \epsilon \\
& + \left(-\frac{94706404133}{201553920000} - \frac{7\zeta_3\pi^2}{5184} - \frac{6057823\pi^2}{223948800} \right. \\
& \left. + \frac{296591\zeta_3}{933120} + \frac{2575\zeta_4}{27648} + \frac{599\zeta_5}{2160} \right) \epsilon^2 \\
& \left. + O(\epsilon^3) \right] (p^2)^3 , \\
\mathcal{I}_{23n}^{(d=6-2\epsilon)}(1, 1, 1, 1, 1, 1, 1, 1) = & \left[-\frac{1}{36\epsilon^2} + \left(-\frac{23}{72} + \frac{\zeta_3}{18} \right) \frac{1}{\epsilon} - \frac{2683}{1296} + \frac{\zeta_4}{12} + \frac{\zeta_3}{2} \right. \\
& + \frac{\pi^2}{144} + \left(-\frac{2803}{288} - \frac{4\zeta_5}{9} + \frac{3\zeta_4}{4} + \frac{875\zeta_3}{324} + \frac{23\pi^2}{288} \right. \\
& \left. - \frac{\pi^2\zeta_3}{72} \right) \epsilon + \left(-\frac{1652863}{46656} - \frac{47\zeta_6}{32} - \frac{101\zeta_5}{9} \right. \\
& \left. + \frac{6829\zeta_4}{1728} + \frac{7163\zeta_3}{648} + \frac{7\zeta_3^2}{18} + \frac{2683\pi^2}{5184} - \frac{\pi^2\zeta_3}{8} \right) \epsilon^2 \\
& \left. + O(\epsilon^3) \right] (p^2) . \tag{4.27}
\end{aligned}$$

As the values of all six dimensional master integrals are known they can be inserted into the database of reduction relations to solve for every 2-point Feynman

diagram at three loops.

4.4.3 3-point Interactions and the Insertion of a Propagator

Having calculated all of the 2-point integrals we now turn our attention to the 3-point Green's functions which are required for the computation of the five β -functions. Fortunately there is a short-cut which can be used in the computation of the 3-point graphs. They can be calculated purely from 2-point diagrams by exploiting certain properties of the specific field theory. Consider the six dimensional LGW Lagrangian and recall that the 2-point scalar propagators can be formally expanded. To demonstrate how this works the ϕ^{ia} propagator is used as an example,

$$\frac{\delta_{ij}\delta_{ab}}{k^2} \longrightarrow \frac{\delta_{ij}\delta_{ab}}{k^2} + \frac{\delta_{ij}\delta_{ab}g_1}{(k^2)^2}. \quad (4.28)$$

This expansion is illustrated in figure 4.19.

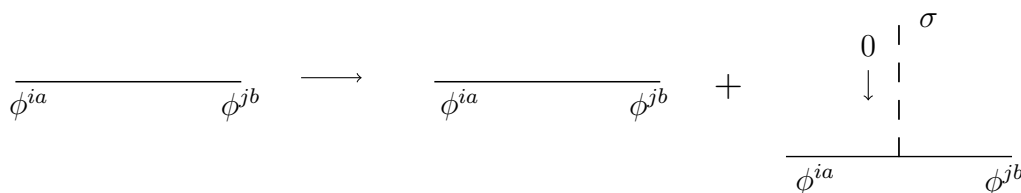


Figure 4.19: Expansion of the ϕ^{ia} propagator to include an insertion of a σ field.

The first term on the right-hand side of equation (4.28) corresponds to the massless theory. The second term represents the zero momentum insertion of an additional σ propagator, it is in effect a 3-point vertex insertion at zero momentum. Diagrammatically for the self energy renormalization this corresponds to a 2-point function with a zero momentum insertion, but more importantly this term would correspond to a 3-point graph where one of the external legs has a nullified momentum. In other words it is equivalent to a diagram contributing to the coupling constant renormalization. As all calculations are performed using dimensional regularisation in the modified minimal subtraction ($\overline{\text{MS}}$) renormalization scheme, the β -function renormalization constant can be correctly extracted from this nullified external momentum configuration. Indeed in four dimensional gauge theories this is the standard procedure for three loop renormalization, [224, 225]. This technique is explained in great detail in [53].

In performing this expansion one truncates at the linear term in g_1 to retain only one insertion per propagator as this reproduces all the relevant graphs for the respective vertex renormalization. This method can be applied to generate nearly

all of the 3-point diagrams required to three loops. To see how this insertion works in practice at a higher loop order we have illustrated the insertion on a one loop diagram in figure 4.28.

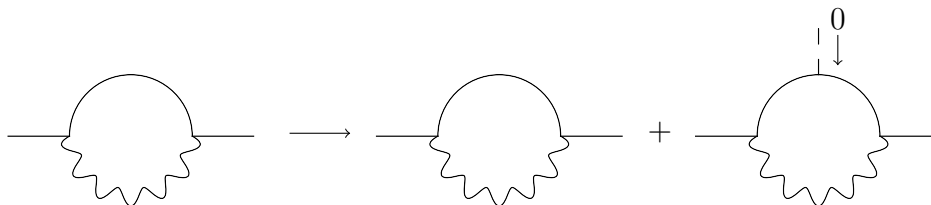


Figure 4.20: Insertion of a σ propagator on a one loop 2-point graph.

It is clear to see from figure 4.20 that a 3-point graph has been generated. The nullified vertex in the diagram means that 2-point master integrals can be used to evaluate it after a reduction. In summary, to calculate the 3-point Feynman diagrams we generate all 2-point graphs using QGRAF. Modified Feynman rules can then be inserted using expansions such as (4.28) which insert a third nullified propagator. Nearly all 3-point diagrams can be generated in this way. The three modified propagators used, excluding the one already given, are

$$\begin{aligned} \frac{1}{k^2} &\rightarrow \frac{1}{k^2} + \frac{g_2}{(k^2)^2}, \\ \frac{P^{abcd}}{k^2} &\rightarrow \frac{P^{abcd}}{k^2} + \frac{g_4 P^{abcd}}{(k^2)^2}. \end{aligned} \quad (4.29)$$

The first expansion in (4.29) describes a σ field insertion onto a σ 2-point propagator which recreates the 3-point interaction σ^3 . The final expansion gives a σ insertion to produce the $\sigma T^{ab}T^{cd}$ interaction. Note that the first expansion given by equation (4.28) describes the interaction $\sigma\phi^{ia}\phi^{jb}$. Therefore all graphs for the $\sigma\phi^{ia}\phi^{jb}$, σ^3 , and $\sigma T^{ab}T^{cd}$ 3-point functions to three loops can be generated using this technique.

One concern is that nullifying an external momenta could introduce unwanted infrared (IR) divergences which would be indistinguishable from UV divergences in dimensional regularisation. Indeed in four dimensions if a nullified leg was present in a massless graph then it would be IR singular. Fortunately it is not an issue here as in a six dimensional scalar theory such a propagator is by contrast IR safe. To explain this further, if we have a scalar 3-point function at one loop this can be shown to be finite using power counting in four dimensions. However if we nullify one external leg, IR divergences will appear and will be indistinguishable from any potential UV divergences. This becomes a problem when renormalizing. Importantly, in six dimensions the 3-point graph at one loop

is UV divergent. Additionally if we nullify one external leg, no IR divergences appear as $1/(k^2)^2$ is not divergent in six dimensions unlike in four. Hence all divergences that appear in the 3-point diagram with one nullified external leg will be ultraviolet. Therefore in a six dimensional theory the UV divergences can be safely extracted using this method. Further explanations on this concern are given in [3, 226]. Alternatively if we look at equation (2.6) of Chapter 2 and set $\alpha = 0$ then we can see that a zero mass, or this this case propagator, insertion ($m^2 \rightarrow 0$) is possible if and only if $d - 2\beta > 0$. For $\beta < 3$ this occurs for $d > 4$, therefore the insertion is IR safe in six dimensions but not in four.

Another concern that arises in using this technique is the possible miscalculation of symmetry factors. In particular whether the 3-point graph we wish to evaluate will have the same symmetry factor as the 2-point function with an insertion. This will prove not to be a problem, as we shall illustrate using an example at one loop. If we take the 3-point function with three external σ fields and internal ϕ^{ia} fields we calculate the symmetry factor to be 1. However, the 2-point graph with an insertion has a symmetry factor of $1/2$. This could prove to be a stumbling block in the graph generation, if not for the fact that the insertion of the σ propagator can be placed in two different ways. This is illustrated in figure 4.21. As there are two graphs with symmetry factor $1/2$, this gives an overall symmetry factor of 1 which is needed to keep consistency in the calculation. This will be the case for all diagrams up to the three loops.

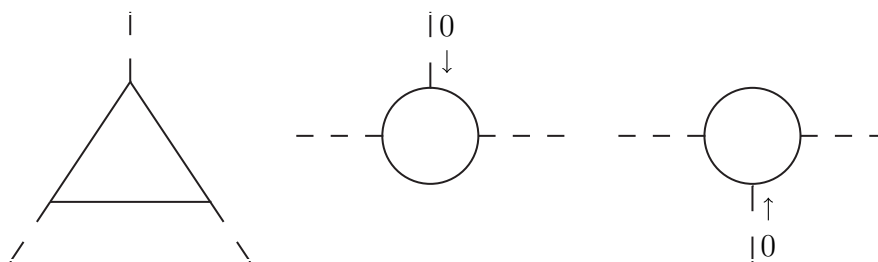


Figure 4.21: The 3-point one loop Feynman diagram and the two 2-point graphs with a nullified σ field insertion. The symmetry factor of the first diagram is 1, while each of the original 2-point graphs before appearing in figure 4.20 have symmetry factor $1/2$.

We have exploited this procedure as it can be used to minimize the amount of computations required. There are limitations however as it misses out certain graphs which involve the $\phi^{ia}\phi^{ib}T^{ab}$ and $T^{ab}T^{ac}T^{bc}$ vertices. While we have used this short-cut for the coupling constant renormalization to find β_1 , β_2 and β_4 the expansions do not generate all the graphs needed for β_3 and β_5 . This is clear from the lack of g_3 and g_5 terms in equation (4.29). A solution to the problem of

generating these rogue diagrams involves a different technique.

4.4.4 $T^{ab}T^{ac}T^{bc}$ and $\phi^{ia}\phi^{ib}T^{ab}$ Interactions

The 3-point Feynman diagrams associated with the $\sigma\phi^{ia}\phi^{jb}$, $\sigma\sigma T^{ab}$ and σ^3 interactions can be computed by inserting a nullified propagator on 2-point graphs. Hence the 2-point master integrals can be used for the calculation of the 3-point diagrams. As no 3-point master integrals are needed a considerable amount of time is saved. Unfortunately not all 3-point interactions can be generated in this way. The $\phi^{ia}\phi^{jb}T^{ab}$ and $T^{ab}T^{cd}T^{ef}$ functions can not be computed using this method. If they could be then the propagators (4.28) and (4.29) would instead read

$$\begin{aligned} \frac{\delta_{ij}\delta_{ab}}{k^2} &\rightarrow \frac{\delta_{ij}\delta_{ab}}{k^2} + \frac{\delta_{ij}\delta_{ab}g_1}{(k^2)^2} + \frac{\delta_{ij}P^{abcd}g_3}{(k^2)^2} \\ \frac{1}{k^2} &\rightarrow \frac{1}{k^2} + \frac{g_2}{(k^2)^2}, \\ \frac{P^{abcd}}{k^2} &\rightarrow \frac{P^{abcd}}{k^2} + \frac{P^{abcd}g_4}{(k^2)^2} + \frac{P_3^{abcdef}g_5}{(k^2)^2}. \end{aligned} \quad (4.30)$$

However these replacements will not generate all 3-point graphs for $\phi^{ia}\phi^{jb}T^{ab}$ and $T^{ab}T^{ab}T^{ab}$ simply from the 2-point diagrams. The problem here lies principally with four graphs, displayed in figure 4.22, and the way in which QGRAF sets up their generation.

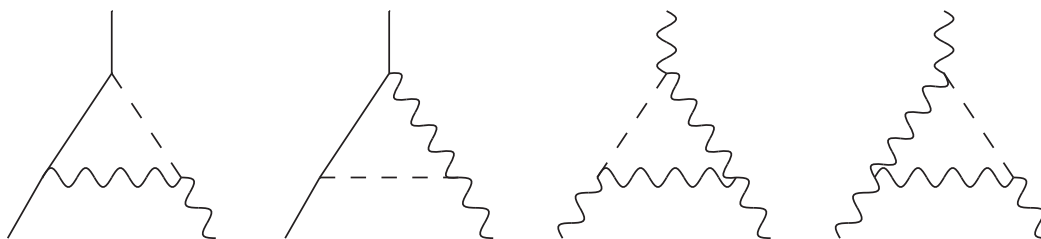


Figure 4.22: The four ‘problem’ diagrams that are not generated using the insertion of a propagator on a 2-point function at one loop.

It is obvious why the first two graphs will not be generated as the three internal fields are different. There is no possible 2-point function to which a propagator can be added to that will generate these 3-point diagrams. The problem with the final two diagrams of figure 4.22 is more subtle and involves the QGRAF internal set-up. When a 2-point one loop diagram is generated by QGRAF, the two external fields are given fixed labels, see figure 4.23 for an example. It would therefore only be possible to generate one of the 3-point diagrams. If we were to rearrange the labels to produce the second graph one would run into over-counting problems.

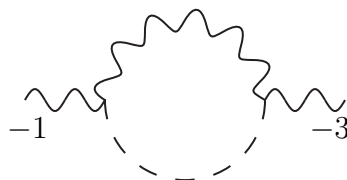


Figure 4.23: QGRAF generation of a 2-point Feynman diagram at one loop. The external σ fields are given fixed labels, rearranging these labels manually may result in over counting problems.

Therefore the coupling constant renormalization associated with the $\phi^{ia}\phi^{jb}T^{ab}$ and $T^{ab}T^{ac}T^{bc}$ interactions can not be calculated simply by using the expansions (4.30). There is however another trick that can be employed which also eliminates the need to calculate 3-point master integrals. To begin all 3-point diagrams for $\phi^{ia}\phi^{jb}T^{ab}$ and $T^{ab}T^{ac}T^{bc}$ are generated up to three loops using QGRAF. It can be seen from table (4.1) that this is a considerable number of diagrams. Fortunately the calculation is hugely simplified as the momentum of one external propagator can be set to zero on each of the 3-point diagrams. By nullifying a single leg a 2-point function has essentially been created. This is illustrate below in figure 4.24.

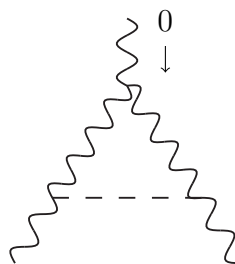


Figure 4.24: Nullifying an external propagator on a 3-point diagram produces a 2-point function at one loop.

Although this proved tedious for the number of diagrams there were no major difficulties. With one nullified external leg the 3-point diagrams can now be treated as 2-point and hence the 2-point master integrals can be used in their evaluation. To clarify any divergence issues, the 3-point graph with a nullified propagator will have the same divergence structure in six dimensions as the 2-point diagram. The 3-point graph with one nullified external momenta will produce UV divergence in six dimensions but no IR divergences. Therefore the UV divergences of the 3-point diagram will match those produced by the 2-point graph. Furthermore only the divergent parts of each diagram are required to solve for the Renormalization Group functions in the $\overline{\text{MS}}$ scheme. Once all 2 and 3-point Green's functions have been computed, or at the very least have had their divergent piece extracted, the theory can be renormalized.

4.4.5 Renormalization

The renormalization of the six dimensional Landau-Ginzburg-Wilson theory follows the same methodology as the renormalization in the previous Chapter. Once all Green's functions to three loops have been calculated FORM is used to sum all 2 and 3-point diagrams together. Potential IR singularities that may arise are only a problem if one considers diagrams on an individual level. By summing graphs these IR singularities naturally cancel and so do not pose a problem. We can therefore focus on UV divergences which emerge. In essence we have up to now computed each graph as a function of the bare parameters. To determine the counterterms which will be used to absorb UV divergences, FORM is implemented to rescale all Green's functions,

$$\begin{aligned}
\phi_0^{ia} &= \sqrt{Z_\phi} \phi^{ia} , \\
\sigma_0 &= \sqrt{Z_\sigma} \sigma , \\
T_0^{ab} &= \sqrt{Z_T} T^{ab} , \\
g_{0j} &= Z_{g_j}(g_j) g_j(\mu) \mu^{\epsilon/2}
\end{aligned} \tag{4.31}$$

where $j = 1, \dots, 5$. As this is a multi-coupling renormalization the redefinition $Z_{g_j \text{def}} = Z_{g_j}(g_j) g_j(\mu)$ is introduced. The fourth rescaling of (4.31) then becomes

$$g_{0j} = Z_{g_j \text{def}}(g_j) \mu^{\epsilon/2} . \tag{4.32}$$

The renormalization constants are defined the same as in equation (3.61). In addition to these definitions we now also have a renormalization constant for the T^{ab} field

$$Z_T = 1 + \frac{z_{T11}}{\epsilon} + \left(\frac{z_{T22}}{\epsilon^2} + \frac{z_{T21}}{\epsilon} \right) + \dots ,$$

which has the same conventions as (3.61). The UV divergences are absorbed into these counterterms order by order. To manipulate the results into a suitable output REDUZE alongside FORM are used. The counterterms are inserted into the definitions of the Renormalization Group functions to solve for the β -functions and anomalous dimension of the fields. The idea behind this for a two coupling theory was discussed in Chapter 2. The relations used to find the Renormalization Group functions for a five coupling theory in six dimensions are

$$\begin{aligned}
0 &= \frac{1}{4}(d-6)Z_{g_1 \text{def}} - \beta_1 \frac{\partial Z_{g_1 \text{def}}}{\partial g_1} - \beta_2 \frac{\partial Z_{g_1 \text{def}}}{\partial g_2} \\
&\quad - \beta_3 \frac{\partial Z_{g_1 \text{def}}}{\partial g_3} - \beta_4 \frac{\partial Z_{g_1 \text{def}}}{\partial g_4} - \beta_5 \frac{\partial Z_{g_1 \text{def}}}{\partial g_5} ,
\end{aligned}$$

$$\begin{aligned}
0 &= \frac{1}{4}(d-6)Z_{g_2\text{def}} - \beta_1 \frac{\partial Z_{g_2\text{def}}}{\partial g_1} - \beta_2 \frac{\partial Z_{g_2\text{def}}}{\partial g_2} \\
&\quad - \beta_3 \frac{\partial Z_{g_2\text{def}}}{\partial g_3} - \beta_4 \frac{\partial Z_{g_2\text{def}}}{\partial g_4} - \beta_5 \frac{\partial Z_{g_2\text{def}}}{\partial g_5}, \\
0 &= \frac{1}{4}(d-6)Z_{g_3\text{def}} - \beta_1 \frac{\partial Z_{g_3\text{def}}}{\partial g_1} - \beta_2 \frac{\partial Z_{g_3\text{def}}}{\partial g_2} \\
&\quad - \beta_3 \frac{\partial Z_{g_3\text{def}}}{\partial g_3} - \beta_4 \frac{\partial Z_{g_3\text{def}}}{\partial g_4} - \beta_5 \frac{\partial Z_{g_3\text{def}}}{\partial g_5}, \\
0 &= \frac{1}{4}(d-6)Z_{g_4\text{def}} - \beta_1 \frac{\partial Z_{g_4\text{def}}}{\partial g_1} - \beta_2 \frac{\partial Z_{g_4\text{def}}}{\partial g_2} \\
&\quad - \beta_3 \frac{\partial Z_{g_4\text{def}}}{\partial g_3} - \beta_4 \frac{\partial Z_{g_4\text{def}}}{\partial g_4} - \beta_5 \frac{\partial Z_{g_4\text{def}}}{\partial g_5}, \\
0 &= \frac{1}{4}(d-6)Z_{g_5\text{def}} - \beta_1 \frac{\partial Z_{g_5\text{def}}}{\partial g_1} - \beta_2 \frac{\partial Z_{g_5\text{def}}}{\partial g_2} \\
&\quad - \beta_3 \frac{\partial Z_{g_5\text{def}}}{\partial g_3} - \beta_4 \frac{\partial Z_{g_5\text{def}}}{\partial g_4} - \beta_5 \frac{\partial Z_{g_5\text{def}}}{\partial g_5}
\end{aligned} \tag{4.33}$$

for the β -functions and for the three anomalous dimensions of the fields the following relations are used

$$\begin{aligned}
\gamma_\phi &= \frac{\beta_1}{Z_\phi} \frac{\partial Z_\phi}{\partial g_1} + \frac{\beta_2}{Z_\phi} \frac{\partial Z_\phi}{\partial g_2} + \frac{\beta_3}{Z_\phi} \frac{\partial Z_\phi}{\partial g_3} \\
&\quad + \frac{\beta_4}{Z_\phi} \frac{\partial Z_\phi}{\partial g_4} + \frac{\beta_5}{Z_\phi} \frac{\partial Z_\phi}{\partial g_5}, \\
\gamma_\sigma &= \frac{\beta_1}{Z_\sigma} \frac{\partial Z_\sigma}{\partial g_1} + \frac{\beta_2}{Z_\sigma} \frac{\partial Z_\sigma}{\partial g_2} + \frac{\beta_3}{Z_\sigma} \frac{\partial Z_\sigma}{\partial g_3} \\
&\quad + \frac{\beta_4}{Z_\sigma} \frac{\partial Z_\sigma}{\partial g_4} + \frac{\beta_5}{Z_\sigma} \frac{\partial Z_\sigma}{\partial g_5}, \\
\gamma_T &= \frac{\beta_1}{Z_T} \frac{\partial Z_T}{\partial g_1} + \frac{\beta_2}{Z_T} \frac{\partial Z_T}{\partial g_2} + \frac{\beta_3}{Z_T} \frac{\partial Z_T}{\partial g_3} \\
&\quad + \frac{\beta_4}{Z_T} \frac{\partial Z_T}{\partial g_4} + \frac{\beta_5}{Z_T} \frac{\partial Z_T}{\partial g_5}.
\end{aligned} \tag{4.34}$$

These relations can be solved order by order by substituting in counterterms to find the three loop results for the RG functions. All Renormalization Group functions have been determined using dimensional regularisation with the renormalization constants defined with respect to the $\overline{\text{MS}}$ scheme. Note that in the critical dimension of six of the Landau-Ginzburg-Wilson Lagrangian we assume the coupling constants are dimensionless in that dimension. The standard arbitrary scale μ is introduced to preserved dimensionlessness of the coupling in the regularised theory.

4.5 Mass Mixing Matrix

Although the main focus so far has been on critical theories, the six dimensional Landau-Ginzburg-Wilson Lagrangian can be modified to include mass for the three basic fields. This was shown in Lagrangian (4.8) and is repeated here for the benefit of the reader,

$$L_m^{(\text{LGW6})} = L^{(\text{LGW6})} - \frac{1}{2}m_1^2\phi^{ia}\phi^{ia} - \frac{1}{2}m_2^2\sigma^2 - \frac{1}{2}m_3^2T^{ab}T^{ab} \quad (4.35)$$

where m_i are the three masses. Using dimensionality arguments we can show that in six dimensions the three fields have identical canonical dimensions, $[\phi^{ia}] = [\sigma] = [T^{ab}] = 2$. It therefore follows that the mass terms for the three fields will also have the same canonical dimension, $[m_1^2] = [m_2^2] = [m_3^2] = 2$. We want to consider the renormalization of the massive theory to three loops. The way in which we approach the renormalization of the mass operators does not follow traditional methods. Instead we use a technique similar to that used in obtaining the 3-point functions for the coupling constant renormalization. Exploiting certain properties of the specific field theory we can formally expand all 2-point scalar propagators. This has the effect of inserting a zero momentum propagator to all 2-point functions. However it will now necessarily be a mass insertion. The 2-point master integrals can then be utilized to compute all diagrams required for the mass renormalization. The propagators for the three fields ϕ^{ia} , σ and T^{ab} can be expanded respectively, as

$$\begin{aligned} \frac{\delta_{ab}\delta_{ij}}{k^2} &\rightarrow \frac{\delta_{ab}\delta_{ij}}{k^2} + \frac{\delta_{ab}\delta_{ij}m_1^2}{(k^2)^2}, \\ \frac{1}{k^2} &\rightarrow \frac{1}{k^2} + \frac{m_2^2}{(k^2)^2}, \\ \frac{P^{abcd}}{k^2} &\rightarrow \frac{P^{abcd}}{k^2} + \frac{P^{abcd}m_3^2}{(k^2)^2}. \end{aligned} \quad (4.36)$$

The first term on the right-hand side corresponds to the massless theory. The second term represents the zero momentum insertion of the mass operator on the propagator. A mass will be inserted in turn on to every propagator of each graph up to three loops. The expansions are truncated at this point to reproduce all relevant graphs and diagrams of order $O(m_i^4)$ are dropped. Note that no IR problems will arise in six dimensions as the mass insertion is IR safe in six dimensions, unlike in four.

As the three mass operators have the same canonical dimension in six dimensions they will mix. The mass mixing is also apparent when looking at certain

Feynman diagrams, for example the two loop graph illustrated in figure 4.25.

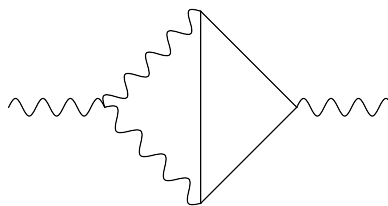


Figure 4.25: A two loop Feynman diagram with external T^{ab} fields that will produce mass mixing.

As there are two different types of internal propagators present both of the masses m_1 and m_3 can be inserted into this diagram producing mass mixing. We want to determine the mass mixing matrix of anomalous dimensions to three loops. Following that the results for the mass mixing matrix can be compared with large N results. This is not as straightforward as for the wave-function and coupling constant renormalization. To establish where the large N results come from we look back to the four dimensional Landau-Ginzburg-Wilson Lagrangian which is used in perturbation theory,

$$L^{(\text{LGW4})} = \frac{1}{2} \partial^\mu \phi^{ia} \partial_\mu \phi^{ia} + \frac{1}{2} \sigma^2 + \frac{1}{2} T^{ab} T^{ab} + \frac{1}{2} g_1 \sigma \phi^{ia} \phi^{ia} + \frac{1}{2} g_2 T^{ab} \phi^{ia} \phi^{ia} .$$

Quadratic terms are present to implement the auxiliary field formulation of the quartic interaction and the fields σ and T^{ab} are massless. In contrast, for six dimensional perturbation theory the fields σ and T^{ab} are no longer auxiliary fields and have associated mass operators. More precisely in six dimensions the fields σ and T^{ab} have no auxiliary interpretation and so the quadratic parts have to appear with a mass in order to have consistent dimensionality. If the fields σ and T^{ab} are massless in four dimensions, where do large N results come from? The answer is found by looking at the large N formalism of four dimensional LGW theory,

$$L^{(\text{LGW4})} = \frac{1}{2} \partial^\mu \phi^{ia} \partial_\mu \phi^{ia} + \frac{1}{2} \tilde{\sigma} \phi^{ia} \phi^{ia} + \frac{1}{2} \tilde{T}^{ab} \phi^{ia} \phi^{ib} - \frac{3\tilde{\sigma}^2}{2\tilde{g}_1} - \frac{3\tilde{T}^{ab}\tilde{T}^{ab}}{2\tilde{g}_2} .$$

This version of the Lagrangian is most useful for developing the large N expansion and seeing the connection with higher dimensional theories. The coupling constants appear within the quadratic part of the Lagrangian which is the first step in constructing the critical exponents using the large N methods of [47–50]. Using dimensionality arguments we find the canonical dimensions of the three fields in this large N formalism to be $[\phi^{ia}] = 1$ and $[\sigma] = [T^{ab}] = 2$ in four dimen-

sions. Moreover in four dimensions the coupling constants are dimensionless as expected, $[\tilde{g}_1] = [\tilde{g}_2] = 0$. However away from four dimensions \tilde{g}_1 and \tilde{g}_2 do not remain dimensionless. For example in six dimensions $[\tilde{g}_1] = [\tilde{g}_2] = 4 - d = -2$. Therefore in higher dimensions they can be interpreted as mass scales. In other words at criticality the critical exponent of the coupling, that is ω , evaluated at each of the three fixed points will be related to the field mass anomalous dimensions of σ and T^{ab} computed in six dimensional perturbation theory and then evaluated at criticality. Recall that the exponent ω is given by $\omega = \beta'(g^*)$. In reality this is not a direct relation since we have a mass mixing matrix. Instead we compare the appropriate exponent ω with the eigen-anomalous dimension of the mass mixing matrix at criticality.

The situation for ϕ^{ia} is different. In six dimensional perturbation theory, the three masses have the same canonical dimension and hence we obtain a 3×3 mass mixing matrix. However in the four dimensional large N formalism of the Lagrangian the canonical dimension of the field ϕ^{ia} differs from the other two as $[\phi^{ia}] = 1$ and $[\sigma] = [T^{ab}] = 2$. Hence the field mass anomalous dimension associated with the mass operator $\frac{1}{2}\phi^{ia}\phi^{ia}$ is not related to an ω exponent. Instead the ϕ^{ia} mass anomalous dimension is given by the anomalous dimension of the σ field. In other words it is proportional to the sum of η and χ ,

$$\gamma_m^\phi(g_i^*) \propto \eta + \chi .$$

To summarise, we can perturbatively calculate the 3×3 mass mixing matrix in six dimensions by introducing a mass insertion on each propagator of the 2-point graphs using expansions (4.36). The eigenvalues of the mass mixing matrix evaluated at criticality are compared with the exponent ω evaluated at the three different fixed points. Additionally the mass anomalous dimension of ϕ^{ia} at criticality in six dimensions can be compared with an exponent proportional to the sum of η and χ which completes the large N checks.

To calculate the mass mixing matrix in six dimensions we not only have to compute all 2-point graphs with a mass insertion but also renormalize the theory. All Green's functions are summed together and we note that the parameters such as the mass operators used thus far are bare quantities. To determine the renormalization constants and associated counterterms FORM is used as a tool to rescale the mass operators

$$m_{i0}^2 = Z_{ijm} m_j^2 \tag{4.37}$$

where $i, j = 1, 2, 3$ and

$$Z_{ijm} = \begin{pmatrix} Z_{11m} & Z_{12m} & Z_{13m} \\ Z_{21m} & Z_{22m} & Z_{23m} \\ Z_{31m} & Z_{32m} & Z_{33m} \end{pmatrix}.$$

More specifically the following renormalization constants are introduced

$$\begin{aligned} m_{10}^2 &= Z_{11m}m_1^2 + Z_{12m}m_2^2 + Z_{13m}m_3^2, \\ m_{20}^2 &= Z_{21m}m_1^2 + Z_{22m}m_2^2 + Z_{23m}m_3^2, \\ m_{30}^2 &= Z_{31m}m_1^2 + Z_{32m}m_2^2 + Z_{33m}m_3^2 \end{aligned}$$

which are defined as

$$\begin{aligned} Z_{11m} &= 1 + \frac{z_{11m11}}{\epsilon} + \left(\frac{z_{11m22}}{\epsilon^2} + \frac{z_{11m21}}{\epsilon} \right) + \left(\frac{z_{11m33}}{\epsilon^3} + \frac{z_{11m32}}{\epsilon^2} + \frac{z_{11m31}}{\epsilon} \right) \\ &\quad + \dots, \\ Z_{12m} &= \frac{z_{12m11}}{\epsilon} + \left(\frac{z_{12m22}}{\epsilon^2} + \frac{z_{12m21}}{\epsilon} \right) + \left(\frac{z_{12m33}}{\epsilon^3} + \frac{z_{12m32}}{\epsilon^2} + \frac{z_{12m31}}{\epsilon} \right) \\ &\quad + \dots, \\ Z_{13m} &= \frac{z_{13m11}}{\epsilon} + \left(\frac{z_{13m22}}{\epsilon^2} + \frac{z_{13m21}}{\epsilon} \right) + \left(\frac{z_{13m33}}{\epsilon^3} + \frac{z_{13m32}}{\epsilon^2} + \frac{z_{13m31}}{\epsilon} \right) \\ &\quad + \dots, \\ Z_{21m} &= \frac{z_{21m11}}{\epsilon} + \left(\frac{z_{21m22}}{\epsilon^2} + \frac{z_{21m21}}{\epsilon} \right) + \left(\frac{z_{21m33}}{\epsilon^3} + \frac{z_{21m32}}{\epsilon^2} + \frac{z_{21m31}}{\epsilon} \right) \\ &\quad + \dots, \\ &\quad \vdots \end{aligned}$$

and so on. Note that the diagonal elements of Z_{ijm} start at one as the mass mixing matrix begins with the unit matrix, that is $Z_{ijm} = \mathbb{I}_{ij}$ when $g_i \equiv 0$. To explain the notation, for the counterterms z_{ijmkl} the values of i and j are numbers associated with the renormalization constant. Additionally k denotes the loop order of the counterterm and l gives the power of the associated pole. Once counterterms have been implemented the divergences at particular loop orders are absorbed into the renormalization constant of the mass operators. By summing together all graphs before introducing counterterms we bypass the need to carry out subtractions on each individual Feynman diagram which can be tedious. Note that the mass renormalization here was performed in the $\overline{\text{MS}}$ scheme. Finally REDUZE and FORM are used to manipulate results into a desired output. The renormalization constants can then be inserted into

$$0 = \beta_k \frac{\partial Z_{ijm}}{\partial g_k} + Z_{ijm} \gamma_{ij} \quad (4.38)$$

to calculate the mass mixing matrix $\gamma_{ij}(g_k)$. To derive equation (4.38) we recall the definition of the bare mass operator in equation (4.37), differentiate with respect to μ and then multiply by μ ,

$$\mu \frac{\partial}{\partial \mu} m_{i0}^2 = \mu \frac{\partial}{\partial \mu} (Z_{ijm} m_j^2). \quad (4.39)$$

The left-hand side of this definition will simply be zero. While the right-hand side will produce two separate terms

$$0 = \mu \frac{\partial Z_{ijm}}{\partial \mu} m_j^2 + Z_{ijm} \mu \frac{\partial m_j^2}{\partial \mu}.$$

Note that $\mu(\partial m_j^2/\partial \mu) = \gamma_{ij} m_j^2$ which transforms the equation to become

$$0 = \mu \frac{\partial g_k}{\partial \mu} \frac{\partial Z_{ijm}}{\partial g_k} m_j^2 + Z_{ijm} \gamma_{ij} m_j^2$$

which can be simplified using the definition of the β -function to obtain (4.38). The β -functions for the theory have already been computed and the renormalization constants have been obtained. Therefore the mass mixing matrix $\gamma_{ij}(g_k)$ can be found by solving the relation (4.38) order by order. The results for the entries of the mass mixing matrix as well as other Renormalization Group functions are stated in the following subsection.

4.6 Results

The results of our computations are the Renormalization Group functions. All results listed here have been published in [2]. As we will mainly focus our analysis on the $O(N) \times O(2)$ theory we record these, partly because of that but also due to space consideration, but note that the full $O(N) \times O(m)$ expressions are provided in the data file of [2]. First, the anomalous dimensions for the three fields are

$$\begin{aligned} \gamma_\phi(g_i)|_{m=2} = & -\frac{1}{6} [g_1^2 + g_3^2] \\ & + \frac{1}{432} [-22N g_1^4 + 26g_1^4 + 48g_3^3 g_2 - 11g_1^2 g_2^2 + 52g_1^2 g_3^2 - 22g_1^2 g_4^2 \\ & \quad + 144g_1 g_3^2 g_4 - 11N g_3^4 - 22g_3^4 - 22g_3^2 g_4^2] \\ & + \frac{1}{31104} [52N^2 g_1^6 - 464N g_1^6 + 5184\zeta_3 g_1^6 - 9064g_1^6 + 5292N g_1^5 g_2 \\ & \quad - 3264g_1^5 g_2 - 772N g_1^4 g_2^2 + 5184\zeta_3 g_1^4 g_2^2 - 11762g_1^4 g_2^2 \\ & \quad + 40N g_1^4 g_3^2 + 15552\zeta_3 g_1^4 g_3^2 - 27192g_1^4 g_3^2 + 104N g_1^4 g_4^2 \\ & \quad + 236g_1^4 g_4^2 + 942g_1^3 g_2^3 - 3264g_1^3 g_2 g_3^2 + 2388g_1^3 g_2 g_4^2] \end{aligned}$$

$$\begin{aligned}
& + 5292Ng_1^3g_3^2g_4 - 9792g_1^3g_3^2g_4 - 504g_1^3g_4^3 + 327g_1^2g_4^4 \\
& + 118g_1^2g_2^2g_3^2 - 772g_1^2g_2^2g_4^2 + 10368\zeta_3g_1^2g_2g_3^2g_4 \\
& - 23760g_1^2g_2g_3^2g_4 + 2904g_1^2g_2g_4^3 - 736Ng_1^2g_3^4 + 2304g_1^2g_3^4 \\
& - 1648Ng_1^2g_3^2g_4^2 + 20736\zeta_3g_1^2g_3^2g_4^2 - 47048g_1^2g_3^2g_4^2 \\
& - 144g_1^2g_4^4 + 1194g_1g_2^2g_3^2g_4 - 756g_1g_2g_3^2g_4^2 \\
& + 5292Ng_1g_3^4g_4 + 1944g_1g_3^4g_4 + 6408g_1g_3^2g_4^3 \\
& - 412g_2^2g_3^2g_4^2 + 1452g_2g_3^2g_4^3 + 13N^2g_3^6 - 1282Ng_3^6 \\
& + 5184\zeta_3g_3^6 - 9844g_3^6 - 360Ng_3^4g_4^2 - 3724g_3^4g_4^2 \\
& - 144g_3^2g_4^4] + O(g_i^8) , \\
\gamma_\sigma(g_i)|_{m=2} &= \frac{1}{12} [-2Ng_1^2 - g_2^2 - 2g_4^2] \\
& + \frac{1}{432} [4Ng_1^4 + 96Ng_1^3g_2 - 22Ng_1^2g_2^2 + 4Ng_1^2g_3^2 + 96Ng_1g_3^2g_4 \\
& \quad + 13g_2^4 - 22g_2^2g_4^2 + 96g_2g_4^3 - 22Ng_3^2g_4^2 + 4g_4^4] \\
& + \frac{1}{62208} [-11048N^2g_1^6 + 10368\zeta_3Ng_1^6 - 17120Ng_1^6 \\
& \quad + 4608N^2g_1^5g_2 + 2112Ng_1^5g_2 + 12N^2g_1^4g_2^2 \\
& \quad + 25920\zeta_3Ng_1^4g_2^2 - 53292Ng_1^4g_2^2 + 20736\zeta_3Ng_1^4g_3^2 \\
& \quad - 34240Ng_1^4g_3^2 - 824Ng_1^4g_4^2 - 3120Ng_1^3g_2^3 \\
& \quad - 2688Ng_1^3g_2g_3^2 + 4608Ng_1^3g_2g_4^2 + 11712Ng_1^3g_3^2g_4 \\
& \quad - 20448Ng_1^3g_4^3 + 1904Ng_1^2g_2^4 - 392Ng_1^2g_2^2g_3^2 \\
& \quad + 24Ng_1^2g_2^2g_4^2 + 31104\zeta_3Ng_1^2g_2g_3^2g_4 - 66672Ng_1^2g_2g_3^2g_4 \\
& \quad + 4608Ng_1^2g_2g_4^3 - 5524N^2g_1^2g_3^4 - 3776Ng_1^2g_3^4 \\
& \quad + 41472\zeta_3Ng_1^2g_3^2g_4^2 - 77824Ng_1^2g_3^2g_4^2 - 824Ng_1^2g_4^4 \\
& \quad + 5808Ng_1g_2^2g_3^2g_4 - 12240Ng_1g_2g_3^2g_4^2 + 2304N^2g_1g_3^4g_4 \\
& \quad - 672Ng_1g_3^4g_4 + 4992Ng_1g_3^2g_4^3 + 2592\zeta_3g_2^6 - 5195g_2^6 \\
& \quad + 1904g_2^4g_4^2 - 3120g_2^3g_4^3 - 1648Ng_2^2g_3^2g_4^2 + 25920\zeta_3g_2^2g_4^4 \\
& \quad - 53280g_2^2g_4^4 + 4776Ng_2g_3^2g_4^3 + 6720g_2g_4^5 + 6N^2g_3^4g_4^2 \\
& \quad - 8408Ng_3^4g_4^2 + 680Ng_3^2g_4^4 + 10368\zeta_3g_4^6 - 28168g_4^6] \\
& + O(g_i^8) , \\
\gamma_T(g_i)|_{m=2} &= \frac{1}{12} [-Ng_3^2 - 2g_4^2] \\
& + \frac{1}{432} [2Ng_1^2g_3^2 - 22Ng_1^2g_4^2 + 96Ng_1g_3^2g_4 - 11g_2^2g_4^2 + 48g_2g_4^3 \\
& \quad - 22Ng_3^4 - 11Ng_3^2g_4^2 + 4g_4^4] \\
& + \frac{1}{31104} [-206N^2g_1^4g_3^2 + 2592\zeta_3Ng_1^4g_3^2 - 4280Ng_1^4g_3^2 \\
& \quad + 52N^2g_1^4g_4^2 - 196Ng_1^4g_4^2 + 1200Ng_1^3g_2g_3^2]
\end{aligned}$$

$$\begin{aligned}
& + 2904N g_1^3 g_2 g_4^2 + 1152N^2 g_1^3 g_3^2 g_4 - 1344N g_1^3 g_3^2 g_4 \\
& - 504N g_1^3 g_4^3 - 103N g_1^2 g_2^2 g_3^2 - 772N g_1^2 g_2^2 g_4^2 \\
& + 5184\zeta_3 N g_1^2 g_2 g_3^2 g_4 - 9576N g_1^2 g_2 g_3^2 g_4 + 2388N g_1^2 g_2 g_4^3 \\
& - 2556N^2 g_1^2 g_3^4 + 2168N g_1^2 g_3^4 - 46N^2 g_1^2 g_3^2 g_4^2 \\
& + 15552\zeta_3 N g_1^2 g_3^2 g_4^2 - 33836N g_1^2 g_3^2 g_4^2 + 340N g_1^2 g_4^4 \\
& + 576N g_1 g_2^2 g_3^2 g_4 - 5364N g_1 g_2 g_3^2 g_4^2 + 576N^2 g_1 g_3^4 g_4 \\
& + 8376N g_1 g_3^4 g_4 + 2496N g_1 g_3^2 g_4^3 + 327g_2^4 g_4^2 + 942g_2^3 g_4^3 \\
& - 23N g_2^2 g_3^2 g_4^2 + 5184\zeta_3 g_2^2 g_4^4 - 12534g_2^2 g_4^4 + 576N g_2 g_3^2 g_4^3 \\
& + 2028g_2 g_4^5 - 412N^2 g_3^6 + 2592\zeta_3 N g_3^6 - 5354N g_3^6 \\
& + 13N^2 g_3^4 g_4^2 - 2152N g_3^4 g_4^2 + 5184\zeta_3 g_4^6 - 36N g_3^2 g_4^4 \\
& - 9476g_4^6] + O(g_i^8) \tag{4.40}
\end{aligned}$$

where the argument of the functions represents all five coupling constants. The five β -functions are

$$\begin{aligned}
\beta_1(g_i)|_{m=2} &= \frac{1}{24} [-2N g_1^3 + 8g_1^3 + 12g_1^2 g_2 - g_1 g_2^2 + 8g_1 g_3^2 - 2g_1 g_4^2 + 12g_3^2 g_4] \\
&+ \frac{1}{864} [-172N g_1^5 - 536g_1^5 + 264N g_1^4 g_2 - 360g_1^4 g_2 - 22N g_1^3 g_2^2 \\
&\quad - 628g_1^3 g_2^2 + 4N g_1^3 g_3^2 - 1072g_1^3 g_3^2 + 40g_1^3 g_4^2 - 24g_1^2 g_3^3 \\
&\quad - 240g_1^2 g_2 g_3^2 + 168g_1^2 g_2 g_4^2 + 96N g_1^2 g_3^2 g_4 - 600g_1^2 g_3^2 g_4 \\
&\quad - 216g_1^2 g_4^3 + 13g_1 g_2^4 - 22g_1 g_2^2 g_4^2 - 648g_1 g_2 g_3^2 g_4 + 96g_1 g_2 g_4^3 \\
&\quad - 88N g_1 g_3^4 + 16g_1 g_3^4 - 22N g_1 g_3^2 g_4^2 - 1256g_1 g_3^2 g_4^2 \\
&\quad + 4g_1 g_4^4 - 108g_2 g_3^2 g_4^2 + 84N g_3^4 g_4 - 24g_3^4 g_4 + 60g_3^2 g_4^3] \\
&+ \frac{1}{124416} [14648N^2 g_1^7 + 259200\zeta_3 N g_1^7 - 81376N g_1^7 + 20736\zeta_3 g_1^7 \\
&\quad + 251360g_1^7 - 144N^2 g_1^6 g_2 - 311040\zeta_3 N g_1^6 g_2 \\
&\quad + 249408N g_1^6 g_2 + 186624\zeta_3 g_1^6 g_2 + 18000g_1^6 g_2 \\
&\quad + 12N^2 g_1^5 g_2^2 + 25920\zeta_3 N g_1^5 g_2^2 - 107980N g_1^5 g_2^2 \\
&\quad - 41472\zeta_3 g_1^5 g_2^2 + 358480g_1^5 g_2^2 + 20736\zeta_3 N g_1^5 g_3^2 \\
&\quad - 106848N g_1^5 g_3^2 + 62208\zeta_3 g_1^5 g_3^2 + 754080g_1^5 g_3^2 \\
&\quad + 23496N g_1^5 g_4^2 - 15712g_1^5 g_4^2 - 9120N g_1^4 g_2^3 \\
&\quad + 124416\zeta_3 g_1^4 g_2^3 + 97776g_1^4 g_2^3 + 7488N g_1^4 g_2 g_3^2 \\
&\quad + 248832\zeta_3 g_1^4 g_2 g_3^2 + 59712g_1^4 g_2 g_3^2 - 4896N g_1^4 g_2 g_4^2 \\
&\quad - 20736g_1^4 g_2 g_4^2 - 186624\zeta_3 N g_1^4 g_3^2 g_4 + 160704N g_1^4 g_3^2 g_4 \\
&\quad + 435456\zeta_3 g_1^4 g_3^2 g_4 - 29424g_1^4 g_3^2 g_4 + 6624N g_1^4 g_4^3 \\
&\quad - 50688g_1^4 g_4^3 + 1904N g_1^3 g_2^4 + 62208\zeta_3 g_1^3 g_2^4 + 9960g_1^3 g_2^4
\end{aligned}$$

$$\begin{aligned}
& - 392Ng_1^3g_2^2g_3^2 + 158032g_1^3g_2^2g_3^2 + 24Ng_1^3g_2^2g_4^2 \\
& - 44032g_1^3g_2^2g_4^2 + 31104\zeta_3Ng_1^3g_2g_3^2g_4 + 142128g_1^2g_2^2g_3^2g_4 \\
& - 98352Ng_1^3g_2g_3^2g_4 - 82944\zeta_3g_1^3g_2g_3^2g_4 - 31104\zeta_3g_1^2g_2^5 \\
& + 4608Ng_1^3g_2g_4^3 - 124416\zeta_3g_1^3g_2g_4^3 + 17664g_1^3g_2g_4^3 \\
& - 5524N^2g_1^3g_3^4 + 373248\zeta_3Ng_1^3g_3^4 - 27552Ng_1^3g_3^4 \\
& - 124416\zeta_3g_1^3g_3^4 + 218016g_1^3g_3^4 + 41472\zeta_3Ng_1^3g_3^2g_4^2 \\
& - 62336Ng_1^3g_3^2g_4^2 - 165888\zeta_3g_1^3g_3^2g_4^2 + 924160g_1^3g_3^2g_4^2 \\
& - 824Ng_1^3g_4^4 + 248832\zeta_3g_1^3g_4^4 + 43968g_1^3g_4^4 \\
& + 33612g_1^2g_2^5 - 8352g_1^2g_2^3g_3^2 - 6000g_1^2g_2^3g_4^2 \\
& + 5808Ng_1^2g_2^2g_3^2g_4 + 124416\zeta_3g_1^2g_2^2g_3^2g_4 \\
& - 10656g_1^2g_2^2g_4^3 - 93312\zeta_3Ng_1^2g_2g_3^4 + 100488Ng_1^2g_2g_3^4 \\
& - 36480g_1^2g_2g_3^4 - 20688Ng_1^2g_2g_3^2g_4^2 + 373248\zeta_3g_1^2g_2g_3^2g_4^2 \\
& + 275568g_1^2g_2g_3^2g_4^2 - 186624\zeta_3g_1^2g_2g_4^4 + 245616g_1^2g_2g_4^4 \\
& + 2304N^2g_1^2g_3^4g_4 - 248832\zeta_3Ng_1^2g_3^4g_4 \\
& + 655776g_1^3g_2g_3^2g_4 + 128688Ng_1^2g_3^4g_4 + 248832\zeta_3g_1^2g_3^4g_4 \\
& - 201120g_1^2g_3^4g_4 - 16128Ng_1^2g_3^2g_4^3 + 248832\zeta_3g_1^2g_3^2g_4^3 \\
& + 183840g_1^2g_3^2g_4^3 + 2592\zeta_3g_1g_2^6 - 3120g_1g_2^3g_4^3 \\
& + 1904g_1g_2^4g_4^2 - 27072g_1g_2^3g_3^2g_4 - 1648Ng_1g_2^2g_3^2g_4^2 \\
& + 186624\zeta_3g_1g_2^2g_3^2g_4^2 + 60176g_1g_2^2g_3^2g_4^2 + 25920\zeta_3g_1g_2^2g_4^4 \\
& - 53280g_1g_2^2g_4^4 - 42912Ng_1g_2g_3^4g_4 - 124416\zeta_3g_1g_2g_3^4g_4 \\
& + 36288g_1g_2g_3^4g_4 + 4776Ng_1g_2g_3^2g_4^3 + 62208\zeta_3g_1g_2g_3^2g_4^3 \\
& + 60672g_1g_2g_3^2g_4^3 + 6720g_1g_2g_4^5 + 6424N^2g_1g_3^6 \\
& + 32144Ng_1g_3^6 + 82944\zeta_3g_1g_3^6 + 72416g_1g_3^6 - 5195g_1g_2^6 \\
& - 45512Ng_1g_3^4g_2^2 + 209504g_1g_3^4g_2^2 + 680Ng_1g_3^2g_4^4 \\
& + 124416\zeta_3g_1g_3^2g_4^4 - 85632g_1g_3^2g_4^4 + 10368\zeta_3g_1g_4^6 \\
& - 28168g_1g_4^6 + 11808g_2^3g_3^2g_4^2 - 62208\zeta_3g_2^2g_3^2g_4^3 \\
& + 63744g_2^2g_3^2g_4^3 + 3600Ng_2g_3^4g_4^2 - 62208\zeta_3g_2g_3^4g_4^2 \\
& + 70272g_2g_3^4g_4^2 - 43488g_2g_3^2g_4^4 - 1188N^2g_3^6g_4 \\
& + 31848Ng_3^6g_4 - 62208\zeta_3g_3^6g_4 + 165840g_3^6g_4 \\
& + 124416\zeta_3g_3^4g_4^3 - 2208Ng_3^4g_4^3 - 16128g_1^2g_4^5 \\
& + 6N^2g_1g_3^4g_2^2 + 23136g_3^4g_4^3 - 62208\zeta_3g_3^2g_4^5 \\
& + 118320g_3^2g_4^5] + O(g_i^9) ,
\end{aligned}$$

$$\beta_2(g_i)|_{m=2} = \frac{1}{8} [8Ng_1^3 - 2Ng_1^2g_2 + 3g_2^3 - 2g_2g_4^2 + 8g_4^3]$$

$$\begin{aligned}
& + \frac{1}{288} [-48Ng_1^5 - 644Ng_1^4g_2 - 120Ng_1^3g_2^2 - 48Ng_1^3g_3^2 + 62Ng_1^2g_3^3 \\
& \quad + 4Ng_1^2g_2g_3^2 - 648Ng_1^2g_3^2g_4 + 96Ng_1g_2g_3^2g_4 - 216Ng_1g_3^2g_4^2 \\
& \quad - 125g_2^5 + 62g_2^3g_4^2 - 120g_2^2g_4^3 - 22Ng_2g_3^2g_4^2 - 644g_2g_4^4 \\
& \quad + 84Ng_3^2g_4^3 - 48g_4^5] \\
& + \frac{1}{41472} [110784N^2g_1^7 + 68448Ng_1^7 - 153896N^2g_1^6g_2 \\
& \quad + 10368\zeta_3Ng_1^6g_2 + 118816Ng_1^6g_2 + 45216N^2g_1^5g_2^2 \\
& \quad + 124416\zeta_3Ng_1^5g_2^2 + 50592Ng_1^5g_2^2 + 136896Ng_1^5g_2^2 \\
& \quad + 1920Ng_1^5g_4^2 - 3156N^2g_1^4g_2^3 + 88128\zeta_3Ng_1^4g_2^3 \\
& \quad + 255780Ng_1^4g_2^3 + 20736\zeta_3Ng_1^4g_2g_3^2 + 111200Ng_1^4g_2g_3^2 \\
& \quad - 65912Ng_1^4g_2g_4^2 + 116928Ng_1^4g_3^2g_4 + 108864Ng_1^4g_4^3 \\
& \quad - 41472\zeta_3Ng_1^3g_2^4 - 17376Ng_1^3g_2^4 - 45888Ng_1^3g_2^2g_3^2 \\
& \quad + 45216Ng_1^3g_2^2g_4^2 + 248832\zeta_3Ng_1^3g_2g_3^2g_4 \\
& \quad + 37632Ng_1^3g_2g_3^2g_4 - 175968Ng_1^3g_2g_3^3 + 55392N^2g_1^3g_3^4 \\
& \quad + 10560Ng_1^3g_3^4 + 269760Ng_1^3g_3^2g_4^2 + 108864Ng_1^3g_4^4 \\
& \quad - 12544Ng_1^2g_2^5 + 4264Ng_1^2g_2^3g_3^2 - 6312Ng_1^2g_2^3g_4^2 \\
& \quad - 155520\zeta_3Ng_1^2g_2^2g_3^2g_4 + 174384Ng_1^2g_2^2g_3^2g_4 \\
& \quad + 45216Ng_1^2g_2^2g_4^3 - 5524N^2g_1^2g_2g_3^4 - 3776Ng_1^2g_2g_3^4 \\
& \quad + 476928\zeta_3Ng_1^2g_2g_3^2g_4^2 + 181376Ng_1^2g_2g_3^2g_4^2 \\
& \quad - 65912Ng_1^2g_2g_4^4 - 71424N^2g_1^2g_3^4g_4 - 25632Ng_1^2g_3^4g_4 \\
& \quad + 273936Ng_1^2g_3^2g_4^3 + 1920Ng_1^2g_4^5 - 14064Ng_1g_2^3g_3^2g_4 \\
& \quad + 3312Ng_1g_2^2g_3^2g_4^2 + 2304N^2g_1g_2g_3^4g_4 - 672Ng_1g_2g_3^4g_4 \\
& \quad - 124416\zeta_3Ng_1g_2g_3^2g_4^3 + 30912Ng_1g_2g_3^2g_4^3 \\
& \quad + 20304N^2g_1g_3^4g_4^2 - 35424Ng_1g_3^4g_4^2 - 61344Ng_1g_3^2g_4^4 \\
& \quad + 12960\zeta_3g_2^7 + 33085g_2^7 - 12544g_2^5g_4^2 - 41472\zeta_3g_2^4g_4^3 \\
& \quad - 17376g_2^4g_4^3 + 5648Ng_2^3g_3^2g_4^2 + 88128\zeta_3g_2^3g_4^4 \\
& \quad + 252624g_2^3g_4^4 - 24600Ng_2^2g_3^2g_4^3 + 124416\zeta_3g_2^2g_4^5 \\
& \quad + 95808g_2^2g_4^5 + 6N^2g_2g_3^4g_4^2 - 8408Ng_2g_3^4g_4^2 \\
& \quad - 4360Ng_2g_3^2g_4^4 + 10368\zeta_3g_2g_4^6 - 35080g_2g_4^6 \\
& \quad - 1584N^2g_3^4g_4^3 + 61248Ng_3^4g_4^3 - 1776Ng_3^2g_4^5 \\
& \quad + 179232g_4^7] + O(g_i^9), \\
\beta_3(g_i)|_{m=2} & = \frac{g_3}{24} [8g_1^2 + 24g_1g_4 - Ng_3^2 - 4g_3^2 - 2g_4^2] \\
& + \frac{g_3}{864} [40Ng_1^4 - 536g_1^4 - 120g_1^3g_2 + 168Ng_1^3g_4 - 480g_1^3g_4 \\
& \quad + 20g_1^2g_2^2 - 648g_1^2g_2g_4 - 214Ng_1^2g_3^2 + 56g_1^2g_3^2 - 22Ng_1^2g_4^2
\end{aligned}$$

$$\begin{aligned}
& -1256g_1^2g_4^2 + 84g_1g_2^2g_4 - 216g_1g_2g_4^2 + 180Ng_1g_3^2g_4 \\
& + 24g_1g_3^2g_4 + 120g_1g_4^3 - 11g_2^2g_4^2 + 48g_2g_4^3 - 44Ng_3^4 \\
& - 476g_3^4 - 11Ng_3^2g_4^2 - 260g_3^2g_4^2 + 4g_4^4] \\
& + \frac{g_3}{62208} [-688N^2g_1^6 - 22480Ng_1^6 + 10368\zeta_3g_1^6 + 125680g_1^6 \\
& - 10440Ng_1^5g_2 + 62208\zeta_3g_1^5g_2 - 11856g_1^5g_2 \\
& - 62208\zeta_3Ng_1^5g_4 + 40176Ng_1^5g_4 + 62208\zeta_3g_1^5g_4 \\
& + 41712g_1^5g_4 + 1312Ng_1^4g_2^2 - 20736\zeta_3g_1^4g_2^2 + 74048g_1^4g_2^2 \\
& - 45216Ng_1^4g_2g_4 + 127440g_1^4g_2g_4 + 6562N^2g_1^4g_3^2 \\
& + 189216\zeta_3Ng_1^4g_3^2 + 4032Ng_1^4g_3^2 - 93312\zeta_3g_1^4g_3^2 \\
& + 131280g_1^4g_3^2 + 52N^2g_1^4g_4^2 - 40452Ng_1^4g_4^2 + 158032g_1^4g_4^2 \\
& - 11436g_1^3g_2^3 + 5712Ng_1^3g_2^2g_4 + 62208\zeta_3g_1^3g_2^2g_4 \\
& + 52752g_1^3g_2^2g_4 - 31104\zeta_3Ng_1^3g_2g_3^2 + 15456Ng_1^3g_2g_3^2 \\
& - 16176g_1^3g_2g_3^2 - 8184Ng_1^3g_2g_4^2 + 62208g_1^3\zeta_3g_2g_4^2 \\
& + 80808g_1^3g_2g_4^2 + 360N^2g_1^3g_3^2g_4 - 186624\zeta_3Ng_1^3g_3^2g_4 \\
& + 212856Ng_1^3g_3^2g_4 + 62208\zeta_3g_1^3g_3^2g_4 + 25680g_1^3g_3^2g_4 \\
& - 2712Ng_1^3g_4^3 + 124416\zeta_3g_1^3g_4^3 + 80592g_1^3g_4^3 - 204g_1^2g_2^4 \\
& - 31104\zeta_3g_1^2g_2^3g_4 + 9360g_1^2g_2^3g_4 + 3281Ng_1^2g_2^2g_3^2 \\
& + 2828g_1^2g_2^2g_3^2 - 772Ng_1^2g_2^2g_4^2 + 124416\zeta_3g_1^2g_2^2g_4^2 \\
& - 5168g_1^2g_2^2g_4^2 + 5184\zeta_3Ng_1^2g_2g_3^2g_4 + 6984Ng_1^2g_2g_3^2g_4 \\
& - 41472\zeta_3g_1^2g_2g_3^2g_4 + 25056g_1^2g_2g_3^2g_4 + 2388Ng_1^2g_2g_3^4 \\
& + 62208\zeta_3g_1^2g_2g_4^3 - 9312g_1^2g_2g_4^3 + 828N^2g_1^2g_3^4 \\
& - 59016Ng_1^2g_3^4 + 186624\zeta_3g_1^2g_3^4 - 15744g_1^2g_3^4 \\
& - 46N^2g_1^2g_3^2g_4^2 + 15552\zeta_3Ng_1^2g_3^2g_4^2 - 56812Ng_1^2g_3^2g_4^2 \\
& - 20736\zeta_3g_1^2g_3^2g_4^2 + 280544g_1^2g_3^2g_4^2 + 340Ng_1^2g_4^4 \\
& + 32352g_1^2g_4^4 - 1716g_1g_2^4g_4 - 13320g_1g_2^3g_4^2 \\
& - 1584N^2g_1^5g_4 + 180Ng_1g_2^2g_3^2g_4 + 8364g_1g_2^2g_3^2g_4 \\
& - 62208\zeta_3g_1g_2^2g_4^3 + 96912g_1g_2^2g_4^3 - 7740Ng_1g_2g_3^2g_4^2 \\
& - 62208\zeta_3g_1g_2g_3^2g_4^2 + 76536g_1g_2g_3^2g_4^2 - 22320g_1g_2g_4^4 \\
& + 180N^2g_1g_3^4g_4 - 17184Ng_1g_3^4g_4 + 121056g_1g_3^4g_4 \\
& + 5520Ng_1g_3^2g_4^3 + 62208\zeta_3g_1g_3^2g_4^3 + 129984g_1g_3^2g_4^3 \\
& - 62208\zeta_3g_1g_4^5 + 56112g_1g_4^5 + 327g_2^4g_4^2 + 942g_2^3g_4^3 \\
& - 23Ng_2^2g_3^2g_4^2 + 2560g_2^2g_3^2g_4^2 + 5184\zeta_3g_2^2g_4^4 - 12534g_2^2g_4^4 \\
& + 576Ng_2g_3^2g_4^3 - 24312g_2g_3^2g_4^3 + 2028g_2g_4^5 - 386N^2g_3^6
\end{aligned}$$

$$\begin{aligned}
& + 2592\zeta_3 N g_3^6 + 18434 N g_3^6 + 10368\zeta_3 g_3^6 + 23512 g_3^6 \\
& + 13 N^2 g_3^4 g_4^2 - 8416 N g_3^4 g_4^2 + 93312\zeta_3 g_3^4 g_4^2 - 70304 g_3^4 g_4^2 \\
& - 36 N g_3^2 g_4^4 + 62208\zeta_3 g_3^2 g_4^4 + 9648 g_3^2 g_4^4 - 9476 g_4^6 \\
& + 5184\zeta_3 g_4^6] + O(g_i^9), \\
\beta_4(g_i)|_{m=2} = & \frac{1}{24} [-2 N g_1^2 g_4 + 12 N g_1 g_3^2 - g_2^2 g_4 + 12 g_2 g_4^2 - 2 N g_3^2 g_4 + 6 g_4^3] \\
& + \frac{1}{864} [4 N g_1^4 g_4 + 96 N g_1^3 g_2 g_4 - 72 N g_1^3 g_3^2 - 216 N g_1^3 g_4^2 \\
& - 22 N g_1^2 g_2^2 g_4 - 324 N g_1^2 g_2 g_3^2 + 168 N g_1^2 g_2 g_4^2 \\
& - 1288 N g_1^2 g_3^2 g_4 + 40 N g_1^2 g_4^3 - 216 N g_1 g_2 g_3^2 g_4 + 144 N g_1 g_3^4 \\
& - 36 N g_1 g_3^2 g_4^2 + 13 g_2^4 g_4 - 24 g_2^3 g_4^2 - 650 g_2^2 g_4^3 + 42 N g_2 g_3^2 g_4^2 \\
& - 96 g_2 g_4^4 - 152 N g_3^4 g_4 + 40 N g_3^2 g_4^3 - 708 g_4^5] \\
& + \frac{1}{124416} [-11048 N^2 g_1^6 g_4 + 10368\zeta_3 N g_1^6 g_4 - 17120 N g_1^6 g_4 \\
& + 4608 N^2 g_1^5 g_2 g_4 + 2112 N g_1^5 g_2 g_4 + 57312 N^2 g_1^5 g_3^2 \\
& + 102672 N g_1^5 g_3^2 + 27072 N^2 g_1^5 g_4^2 - 43200 N g_1^5 g_4^2 \\
& + 12 N^2 g_1^4 g_2^2 g_4 + 25920\zeta_3 N g_1^4 g_2^2 g_4 - 53292 N g_1^4 g_2^2 g_4 \\
& - 32544 N^2 g_1^4 g_2 g_3^2 + 58464 N g_1^4 g_2 g_3^2 - 4752 N^2 g_1^4 g_2 g_4^2 \\
& - 186624\zeta_3 N g_1^4 g_2 g_4^2 + 250368 N g_1^4 g_2 g_4^2 \\
& - 143672 N^2 g_1^4 g_3^2 g_4 + 31104\zeta_3 N g_1^4 g_3^2 g_4 \\
& + 239520 N g_1^4 g_3^2 g_4 - 1376 N^2 g_1^4 g_4^3 + 248832\zeta_3 N g_1^4 g_4^3 \\
& + 44520 N g_1^4 g_4^3 - 3120 N g_1^3 g_2^3 g_4 + 79200 N g_1^3 g_2^2 g_3^2 \\
& - 10656 N g_1^3 g_2^2 g_4^2 + 27072 N^2 g_1^3 g_2 g_3^2 g_4 \\
& + 248832\zeta_3 N g_1^3 g_2 g_3^2 g_4 - 15168 N g_1^3 g_2 g_3^2 g_4 \\
& - 124416\zeta_3 N g_1^3 g_2 g_4^3 + 22272 N g_1^3 g_2 g_4^3 \\
& + 108864 N^2 g_1^3 g_3^4 + 8640 N g_1^3 g_3^4 + 31680 N^2 g_1^3 g_3^2 g_4^2 \\
& + 248832\zeta_3 N g_1^3 g_3^2 g_4^2 + 82656 N g_1^3 g_3^2 g_4^2 - 44064 N g_1^3 g_4^4 \\
& + 1904 N g_1^2 g_2^4 g_4 + 10944 N g_1^2 g_2^3 g_3^2 - 6000 N g_1^2 g_2^3 g_4^2 \\
& + 186624\zeta_3 N g_1^2 g_2^2 g_3^2 g_4 + 67740 N g_1^2 g_2^2 g_3^2 g_4 \\
& - 44008 N g_1^2 g_2^2 g_3^3 - 19440 N^2 g_1^2 g_2 g_3^4 \\
& - 62208\zeta_3 N g_1^2 g_2 g_3^4 + 62352 N g_1^2 g_2 g_3^4 \\
& - 1584 N^2 g_1^2 g_2 g_3^2 g_4^2 + 82944\zeta_3 N g_1^2 g_2 g_3^2 g_4^2 \\
& + 528600 N g_1^2 g_2 g_3^2 g_4^2 - 25632 N g_1^2 g_2 g_4^4 \\
& - 106612 N^2 g_1^2 g_3^4 g_4 + 33696 N g_1^2 g_3^4 g_4 - 1768 N^2 g_1^2 g_3^2 g_4^3 \\
& + 41472\zeta_3 N g_1^2 g_3^2 g_4^3 + 635376 N g_1^2 g_3^2 g_4^3 + 7784 N g_1^2 g_4^5 \\
& - 25344 N g_1 g_2^3 g_3^2 g_4 - 62208\zeta_3 N g_1 g_2^2 g_3^2 g_4^2
\end{aligned}$$

$$\begin{aligned}
& + 85656N g_1 g_2^2 g_3^2 g_4^2 + 6768N^2 g_1 g_2 g_3^4 g_4 \\
& - 124416\zeta_3 N g_1 g_2 g_3^4 g_4 + 44928N g_1 g_2 g_3^4 g_4 \\
& - 177120N g_1 g_2 g_3^2 g_4^3 + 11864g_2^4 g_4^3 \\
& + 31104N^2 g_1 g_3^6 - 62208\zeta_3 N g_1 g_3^6 + 162576N g_1 g_3^6 \\
& + 24912N^2 g_1 g_3^4 g_4^2 + 124416\zeta_3 N g_1 g_3^4 g_4^2 \\
& - 11232N g_1 g_3^4 g_4^2 - 124416\zeta_3 N g_1 g_3^2 g_4^4 \\
& + 3312N g_1 g_3^2 g_4^4 + 2592\zeta_3 g_2^6 g_4 - 5195g_2^6 g_4 \\
& - 31104\zeta_3 g_2^5 g_4^2 + 33612g_2^5 g_4^2 + 62208\zeta_3 g_2^4 g_4^3 \\
& + 2592N g_2^3 g_3^2 g_4^2 + 124416\zeta_3 g_2^3 g_4^4 + 88656g_2^3 g_4^4 \\
& - 16788N g_2^2 g_3^2 g_4^3 - 15552\zeta_3 g_2^2 g_4^5 + 250512g_2^2 g_4^5 \\
& - 396N^2 g_2 g_3^4 g_4^2 + 15072N g_2 g_3^4 g_4^2 + 16680N g_2 g_3^2 g_4^4 \\
& - 124416\zeta_3 g_2 g_4^6 + 267264g_2 g_4^6 - 13168N^2 g_3^6 g_4 \\
& + 72576\zeta_3 N g_3^6 g_4 - 4856N g_3^6 g_4 - 1130N^2 g_3^4 g_4^3 \\
& + 124416\zeta_3 N g_3^4 g_4^3 + 88584N g_3^4 g_4^3 - 41896N g_3^2 g_4^5 \\
& + 279936\zeta_3 g_4^7 + 184632g_4^7] + O(g_i^9), \\
\beta_5(g_i)|_{m=2} &= \frac{1}{8} [4N g_3^3 - N g_3^2 g_5 + 10g_4^2 g_5 - 3g_5^3] \\
& + \frac{1}{1152} [-96N g_1^2 g_3^3 + 8N g_1^2 g_3^2 g_5 + 248N g_1^2 g_4^2 g_5 - 2592N g_1 g_3^3 g_4 \\
& - 480N g_1 g_3^2 g_4 g_5 + 124g_2^2 g_4^2 g_5 - 1248g_2 g_4^3 g_5 + 336N g_3^5 \\
& + 344N g_3^4 g_5 - 432N g_3^3 g_4^2 + 324N g_3^3 g_5^2 + 292N g_3^2 g_4^2 g_5 \\
& - 126N g_3^2 g_5^3 - 2864g_4^4 g_5 + 2340g_4^2 g_5^3 - 513g_5^5] \\
& + \frac{1}{165888} [3840N^2 g_1^4 g_3^3 + 136896N g_1^4 g_3^3 - 1648N^2 g_1^4 g_3^2 g_5 \\
& + 20736\zeta_3 N g_1^4 g_3^2 g_5 - 34240N g_1^4 g_3^2 g_5 - 5920N^2 g_1^4 g_4^2 g_5 \\
& + 17056N g_1^4 g_4^2 g_5 - 19008N g_1^3 g_2 g_3^3 + 9600N g_1^3 g_2 g_3^2 g_5 \\
& - 56256N g_1^3 g_2 g_4^2 g_5 - 130176N^2 g_1^3 g_3^3 g_4 \\
& + 581760N g_1^3 g_3^3 g_4 + 63360N^2 g_1^3 g_3^2 g_4 g_5 \\
& + 30528N g_1^3 g_4^3 g_5 - 72576N g_1 g_3^2 g_4 g_5^3 \\
& - 183552N g_1^3 g_3^2 g_4 g_5 - 165888\zeta_3 N g_1^3 g_4^3 g_5 \\
& + 1920N g_1^2 g_2^2 g_3^3 - 824N g_1^2 g_2^2 g_3^2 g_5 + 16672N g_1^2 g_2^2 g_4^2 g_5 \\
& + 311040N g_1^2 g_2 g_3^3 g_4 - 207360\zeta_3 N g_1^2 g_2 g_3^2 g_4 g_5 \\
& + 161856N g_1^2 g_2 g_3^2 g_4 g_5 - 107616N g_1^2 g_2 g_4^3 g_5 \\
& - 119616N g_1^2 g_3^5 - 98208N^2 g_1^2 g_3^4 g_5 - 37952N g_1^2 g_3^4 g_5 \\
& + 27072N^2 g_1^2 g_3^3 g_4^2 + 995328\zeta_3 N g_1^2 g_3^3 g_4^2 - 6984N g_1^2 g_3^2 g_5^3 \\
& + 64800N g_1^2 g_3^3 g_5^2 - 6704N^2 g_1^2 g_3^2 g_4^2 g_5 + 217728N^2 g_1^2 g_3^5
\end{aligned}$$

$$\begin{aligned}
& + 622080\zeta_3 N g_1^2 g_3^2 g_4^2 g_5 + 1466912 N g_1^2 g_3^2 g_4^2 g_5 \\
& - 114592 N g_1^2 g_4^4 g_5 + 74448 N g_1^2 g_4^2 g_5^3 + 21120 N g_1^2 g_3^3 g_4^2 \\
& - 65088 N g_1 g_2^2 g_3^3 g_4 + 31680 N g_1 g_2^2 g_3^2 g_4 g_5 \\
& + 497664 \zeta_3 N g_1 g_2 g_3^3 g_4^2 + 300672 N g_1 g_2 g_3^3 g_4^2 \\
& - 42912 N g_1 g_2 g_3^2 g_4^2 g_5 - 220608 N^2 g_1 g_3^5 g_4 \\
& - 248832 \zeta_3 N g_1 g_3^5 g_4 - 45504 N g_1 g_3^5 g_4 \\
& + 58752 N^2 g_1 g_3^4 g_4 g_5 - 497664 \zeta_3 N g_1 g_3^4 g_4 g_5 \\
& - 250944 N g_1 g_3^4 g_4 g_5 + 248832 \zeta_3 N g_1 g_3^3 g_4^3 \\
& + 1087488 N g_1 g_3^3 g_4^3 - 559872 \zeta_3 N g_1 g_3^3 g_4 g_5^2 \\
& - 909792 N g_1 g_3^3 g_4 g_5^2 - 497664 \zeta_3 N g_1 g_3^2 g_4^3 g_5 \\
& - 14592 N g_1 g_3^2 g_4^3 g_5 + 186624 \zeta_3 N g_1 g_3^2 g_4 g_5^3 \\
& - 4248 g_2^4 g_4^2 g_5 - 82944 \zeta_3 g_2^3 g_4^3 g_5 - 38544 g_2^3 g_4^3 g_5 \\
& + 13536 N g_2^2 g_3^3 g_4^2 - 3352 N g_2^2 g_3^2 g_4^2 g_5 + 290304 \zeta_3 g_2^2 g_4^4 g_5 \\
& + 549360 g_2^2 g_4^4 g_5 + 37224 g_2^2 g_4^2 g_5^3 - 82944 \zeta_3 N g_2 g_3^3 g_4^3 \\
& - 76032 N g_2 g_3^3 g_4^3 - 6336 N g_2 g_3^2 g_4^3 g_5 + 497664 \zeta_3 g_2 g_4^5 g_5 \\
& + 444768 g_2 g_4^5 g_5 - 311040 \zeta_3 g_2 g_4^3 g_5^3 - 387504 g_2 g_4^3 g_5^3 \\
& + 6816 N^2 g_3^7 - 124416 \zeta_3 N g_3^7 + 275712 N g_3^7 \\
& + 64528 N^2 g_3^6 g_5 + 207360 \zeta_3 N g_3^6 g_5 + 15920 N g_3^6 g_5 \\
& + 27072 N^2 g_3^5 g_4^2 - 248832 \zeta_3 N g_3^5 g_4^2 + 87936 N g_3^5 g_4^2 \\
& - 30456 N^2 g_3^5 g_5^2 + 279936 \zeta_3 N g_3^5 g_5^2 - 5184 N g_3^5 g_5^2 \\
& - 4648 N^2 g_3^4 g_4^2 g_5 - 62208 \zeta_3 N g_3^4 g_4^2 g_5 - 167936 N g_3^4 g_4^2 g_5 \\
& + 2376 N^2 g_3^4 g_5^3 + 139968 \zeta_3 N g_3^4 g_5^3 + 199728 N g_3^4 g_5^3 \\
& - 12096 N g_3^3 g_4^4 + 186624 \zeta_3 N g_3^3 g_4^2 g_5^2 + 16848 N g_3^3 g_4^2 g_5^2 \\
& - 77760 \zeta_3 N g_3^3 g_4^4 + 19116 N g_3^3 g_4^4 - 96864 N g_3^2 g_4^4 g_5 \\
& + 90360 N g_3^2 g_4^2 g_5^3 - 28026 N g_3^2 g_5^5 + 373248 \zeta_3 g_4^6 g_5 \\
& + 1293344 g_4^6 g_5 - 933120 \zeta_3 g_4^4 g_5^3 - 1361376 g_4^4 g_5^3 \\
& + 629856 \zeta_3 g_4^2 g_5^5 + 760428 g_4^2 g_5^5 - 104976 \zeta_3 g_5^7 \\
& - 137295 g_5^7] + O(g_i^9) . \tag{4.41}
\end{aligned}$$

One test of the expressions we have computed is that the double and triple poles of all the underlying renormalization constants correctly emerge as predicted by the Renormalization Group formalism. Equally we have checked the limit back to the pure $O(N)$ theory where the $O(m)$ indices are completely passive and found agreement with [52]. The final checks which we derive from the comparison with the large N exponents we will leave to the following subsection. Note that the

elements of the mass mixing matrix, again for $O(N) \times O(2)$, are

$$\begin{aligned}
\gamma_{11}(g_i)|_{m=2} &= \frac{1}{3}[g_1^2 + g_3^2] \\
&+ \frac{1}{216} [-44Ng_1^4 - 134g_1^4 - 30g_1^3g_2 + 5g_1^2g_2^2 - 268g_1^2g_3^2 + 10g_1^2g_4^2 \\
&\quad - 90g_1g_3^2g_4 - 22Ng_3^4 + 4g_3^4 + 10g_3^2g_4^2] \\
&+ \frac{1}{15552} [3212N^2g_1^6 + 31104\zeta_3Ng_1^6 - 8032Ng_1^6 + 2592\zeta_3g_1^6 \\
&\quad + 31420g_1^6 - 15552\zeta_3Ng_1^5g_2 + 4518Ng_1^5g_2 + 15552\zeta_3g_1^5g_2 \\
&\quad - 2964g_1^5g_2 + 7852Ng_1^4g_2^2 - 5184\zeta_3g_1^4g_2^2 + 18512g_1^4g_2^2 \\
&\quad - 9076Ng_1^4g_3^2 + 7776\zeta_3g_1^4g_3^2 + 94260g_1^4g_3^2 + 3040Ng_1^4g_4^2 \\
&\quad - 1964g_1^4g_4^2 - 2859g_1^3g_2^3 + 15552\zeta_3g_1^3g_2g_3^2 - 2964g_1^3g_2g_3^2 \\
&\quad - 1578g_1^3g_2g_4^2 - 15552\zeta_3Ng_1^3g_3^2g_4 + 4518Ng_1^3g_3^2g_4 \\
&\quad + 46656\zeta_3g_1^3g_3^2g_4 - 8892g_1^3g_3^2g_4 - 4140g_1^3g_4^3 - 51g_1^2g_2^4 \\
&\quad - 982g_1^2g_2^2g_3^2 + 328g_1^2g_2^2g_4^2 - 10368\zeta_3g_1^2g_2g_3^2g_4 \\
&\quad + 38988g_1^2g_2g_3^2g_4 - 1032g_1^2g_2g_4^3 + 46656\zeta_3Ng_1^2g_3^4 \\
&\quad - 2972Ng_1^2g_3^4 - 15552\zeta_3g_1^2g_3^4 + 27252g_1^2g_3^4 \\
&\quad + 12664Ng_1^2g_3^2g_4^2 - 20736\zeta_3g_1^2g_3^2g_4^2 + 74048g_1^2g_3^2g_4^2 \\
&\quad + 312g_1^2g_4^4 - 789g_1g_2^2g_3^2g_4 - 6210g_1g_2g_3^2g_4^2 \\
&\quad - 15552\zeta_3Ng_1g_3^4g_4 + 4518Ng_1g_3^4g_4 + 15552\zeta_3g_1g_3^4g_4 \\
&\quad - 17928g_1g_3^4g_4 - 10944g_1g_3^2g_4^3 + 250g_2^2g_3^2g_4^2 - 516g_2g_3^2g_4^3 \\
&\quad + 803N^2g_3^6 + 4018Ng_3^6 + 10368\zeta_3g_3^6 + 9052g_3^6 \\
&\quad + 4686Ng_3^4g_4^2 + 8854g_3^4g_4^2 + 312g_3^2g_4^4] + O(g_i^8), \\
\gamma_{12}(g_i)|_{m=2} &= Ng_1^2 + \frac{N}{12} [-2g_1^4 - 18g_1^3g_2 - 3g_1^2g_2^2 - 2g_1^2g_3^2 - 18g_1g_3^2g_4 - 3g_3^2g_4^2] \\
&+ \frac{N}{864} [2308Ng_1^6 + 1426g_1^6 - 1984Ng_1^5g_2 + 1822g_1^5g_2 + 282Ng_1^4g_2^2 \\
&\quad + 864\zeta_3g_1^4g_2^2 + 1430g_1^4g_2^2 + 2852g_1^4g_3^2 + 40g_1^4g_4^2 \\
&\quad + 864\zeta_3g_1^3g_2^3 + 1420g_1^3g_2^3 + 2020g_1^3g_2g_3^2 - 904g_1^3g_2g_4^2 \\
&\quad + 1426g_1^3g_3^2g_4 + 1512g_1^3g_4^3 - 21g_1^2g_2^4 - 300g_1^2g_2^2g_3^2 \\
&\quad + 282g_1^2g_2^2g_4^2 + 1728\zeta_3g_1^2g_2g_3^2g_4 + 1260g_1^2g_2g_3^2g_4 \\
&\quad - 1080g_1^2g_2g_4^3 + 1154Ng_1^2g_3^4 + 220g_1^2g_3^4 + 4060g_1^2g_3^2g_4^2 \\
&\quad + 756g_1^2g_4^4 - 864\zeta_3g_1g_2^2g_3^2g_4 + 828g_1g_2^2g_3^2g_4 \\
&\quad + 3456\zeta_3g_1g_2g_3^2g_4^2 + 1332g_1g_2g_3^2g_4^2 - 992Ng_1g_3^4g_4 \\
&\quad - 356g_1g_3^4g_4 + 1796g_1g_3^2g_4^3 + 324g_2^2g_3^2g_4^2 - 432g_2g_3^2g_4^3 \\
&\quad + 141Ng_3^4g_4^2 - 246g_3^4g_4^2 + 66g_3^2g_4^4] + O(g_i^8),
\end{aligned}$$

$$\begin{aligned}
\gamma_{13}(g_i)|_{m=2} &= \frac{1}{2}Ng_3^2 + \frac{N}{24} [-2g_1^2g_3^2 - 6g_1^2g_4^2 - 36g_1g_3^2g_4 + 4g_3^4 - 3g_3^2g_4^2] \\
&+ \frac{N}{1728} [796Ng_1^4g_3^2 + 1426g_1^4g_3^2 + 376Ng_1^4g_4^2 - 600g_1^4g_4^2 \\
&\quad - 198g_1^3g_2g_3^2 - 1728\zeta_3g_1^3g_2g_4^2 + 1656g_1^3g_2g_4^2 \\
&\quad - 1984Ng_1^3g_3^2g_4 + 4040g_1^3g_3^2g_4 + 3456\zeta_3g_1^3g_4^3 + 576g_1^3g_4^3 \\
&\quad + 20g_1^2g_2^2g_3^2 + 836g_1^2g_2^2g_4^2 + 2160g_1^2g_2g_3^2g_4 - 864g_1^2g_2g_4^3 \\
&\quad + 1512Ng_1^2g_3^4 + 120g_1^2g_3^4 + 188Ng_1^2g_3^2g_4^2 + 3456\zeta_3g_1^2g_3^2g_4^2 \\
&\quad + 1660g_1^2g_3^2g_4^2 + 132g_1^2g_4^4 - 452g_1g_2^2g_3^2g_4 + 1728\zeta_3g_1g_2g_3^2g_4^2 \\
&\quad + 1800g_1g_2g_3^2g_4^2 - 992Ng_1g_3^4g_4 - 226g_1g_3^4g_4 + 3592g_1g_3^2g_4^3 \\
&\quad + 47g_2^2g_3^2g_4^2 - 540g_2g_3^2g_4^3 + 432Ng_3^6 - 864\zeta_3g_3^6 + 2258g_3^6 \\
&\quad + 94Ng_3^4g_4^2 + 780g_3^4g_4^2 + 822g_3^2g_4^4] + O(g_i^8),
\end{aligned}$$

$$\begin{aligned}
\gamma_{21}(g_i)|_{m=2} &= \frac{g_1^2}{2} \\
&+ \frac{1}{72} [14Ng_1^4 - 20g_1^4 - 54g_1^3g_2 - 2g_1^2g_2^2 - 20g_1^2g_3^2 + 14g_1^2g_4^2 \\
&\quad - 54g_1g_3^2g_4 - 9g_3^2g_4^2] \\
&+ \frac{1}{10368} [-396N^2g_1^6 - 15552\zeta_3Ng_1^6 + 17596Ng_1^6 + 5184\zeta_3g_1^6 \\
&\quad + 3476g_1^6 - 9792Ng_1^5g_2 + 17532g_1^5g_2 - 500Ng_1^4g_2^2 \\
&\quad + 10368\zeta_3g_1^4g_2^2 + 10054g_1^4g_2^2 + 848Ng_1^4g_3^2 + 10368\zeta_3g_1^4g_3^2 \\
&\quad + 6952g_1^4g_3^2 - 792Ng_1^4g_4^2 - 676g_1^4g_4^2 + 5184\zeta_3g_1^3g_2^3 \\
&\quad + 864g_1^3g_2^3 + 13824g_1^3g_2g_3^2 - 3888g_1^3g_2g_4^2 - 2640Ng_1^3g_3^2g_4 \\
&\quad + 24948g_1^3g_3^2g_4 - 10368\zeta_3g_1^3g_4^3 + 7344g_1^3g_4^3 - 2592\zeta_3g_1^2g_2^4 \\
&\quad + 2801g_1^2g_2^4 - 696g_1^2g_2^2g_3^2 - 500g_1^2g_2^2g_4^2 \\
&\quad + 12744g_1^2g_2g_3^2g_4 - 5904g_1^2g_2g_4^3 - 7776\zeta_3Ng_1^2g_3^4 \\
&\quad + 8374Ng_1^2g_3^4 - 3040g_1^2g_3^4 - 704Ng_1^2g_3^2g_4^2 \\
&\quad + 20736\zeta_3g_1^2g_3^2g_4^2 + 17600g_1^2g_3^2g_4^2 - 5184\zeta_3g_1^2g_4^4 \\
&\quad + 10532g_1^2g_4^4 - 2256g_1g_2^2g_3^2g_4 + 15552\zeta_3g_1g_2g_3^2g_4^2 \\
&\quad + 7128g_1g_2g_3^2g_4^2 - 3576Ng_1g_3^4g_4 - 10368\zeta_3g_1g_3^4g_4 \\
&\quad + 3024g_1g_3^4g_4 + 5184\zeta_3g_1g_3^2g_4^3 - 3672g_1g_3^2g_4^3 \\
&\quad + 984g_2^2g_3^2g_4^2 - 5184\zeta_3g_2g_3^2g_4^3 + 4968g_2g_3^2g_4^3 + 300Ng_3^4g_4^2 \\
&\quad - 5184\zeta_3g_3^4g_4^2 + 5856g_3^4g_4^2 + 10368\zeta_3g_1^2g_2g_3^2g_4 \\
&\quad - 672g_3^2g_4^4] + O(g_i^8),
\end{aligned}$$

$$\begin{aligned}
\gamma_{22}(g_i)|_{m=2} &= \frac{1}{12} [-2Ng_1^2 + 5g_2^2 - 2g_4^2] \\
&+ \frac{1}{216} [-160Ng_1^4 - 60Ng_1^3g_2 + 52Ng_1^2g_2^2 + 2Ng_1^2g_3^2 + 48Ng_1g_3^2g_4
\end{aligned}$$

$$\begin{aligned}
& -97g_2^4 + 52g_2^2g_4^2 - 60g_2g_4^3 - 11g_3^2g_4^2N - 160g_4^4] \\
& + \frac{1}{62208} [-82472N^2g_1^6 + 10368\zeta_3Ng_1^6 + 55600Ng_1^6 \\
& \quad + 45216N^2g_1^5g_2 + 124416\zeta_3Ng_1^5g_2 - 28128Ng_1^5g_2 \\
& \quad - 4740N^2g_1^4g_2^2 + 57024\zeta_3Ng_1^4g_2^2 + 308076Ng_1^4g_2^2 \\
& \quad + 20736\zeta_3Ng_1^4g_3^2 + 38480Ng_1^4g_3^2 - 33368Ng_1^4g_4^2 \\
& \quad - 62208\zeta_3Ng_1^3g_2^3 - 22992Ng_1^3g_2^3 - 45888Ng_1^3g_2g_3^2 \\
& \quad + 45216Ng_1^3g_2g_4^2 + 124416\zeta_3Ng_1^3g_3^2g_4 + 24672Ng_1^3g_3^2g_4 \\
& \quad - 98208Ng_1^3g_4^3 - 19768Ng_1^2g_2^4 + 6592Ng_1^2g_2^2g_3^2 \\
& \quad - 9480Ng_1^2g_2^2g_4^2 - 155520\zeta_3Ng_1^2g_2g_3^2g_4 \\
& \quad + 174384Ng_1^2g_2g_3^2g_4 + 45216Ng_1^2g_2g_4^3 - 5524N^2g_1^2g_3^4 \\
& \quad - 3776Ng_1^2g_3^4 + 259200\zeta_3Ng_1^2g_3^2g_4^2 + 51776Ng_1^2g_3^2g_4^2 \\
& \quad - 33368Ng_1^2g_4^4 - 24000Ng_1g_2^2g_3^2g_4 + 3312Ng_1g_2g_3^2g_4^2 \\
& \quad + 2304N^2g_1g_3^4g_4 - 672Ng_1g_3^4g_4 - 62208\zeta_3Ng_1g_3^2g_4^3 \\
& \quad + 17952Ng_1g_2^2g_3^3 + 18144\zeta_3g_2^6 + 52225g_2^6 - 19768g_2^4g_4^2 \\
& \quad - 62208\zeta_3g_2^3g_4^3 - 22992g_2^3g_4^3 + 9296Ng_2^2g_3^2g_4^2 \\
& \quad + 57024\zeta_3g_2^2g_4^4 + 303336g_2^2g_4^4 - 24600Ng_2g_3^2g_4^3 \\
& \quad + 124416\zeta_3g_2g_4^5 + 17088g_2g_4^5 + 6N^2g_3^4g_4^2 - 8408Ng_3^4g_4^2 \\
& \quad - 1840Ng_3^2g_4^4 + 10368\zeta_3g_4^6 - 26872g_4^6] + O(g_i^8), \\
\gamma_{23}(g_i)|_{m=2} &= \frac{g_4^2}{2} \\
& + \frac{1}{144} [-54Ng_1^2g_3^2 + 28Ng_1^2g_4^2 - 36Ng_1g_3^2g_4 - 4g_2^2g_4^2 - 108g_2g_3^3 \\
& \quad + 7Ng_3^2g_4^2 - 12g_4^4] \\
& + \frac{1}{10368} [-2712N^2g_1^4g_3^2 + 6060Ng_1^4g_3^2 - 396N^2g_1^4g_4^2 \\
& \quad - 5184\zeta_3Ng_1^4g_4^2 + 10928Ng_1^4g_4^2 + 6480Ng_1^3g_2g_3^2 \\
& \quad - 5904Ng_1^3g_2g_4^2 + 2256N^2g_1^3g_3^2g_4 + 20736\zeta_3Ng_1^3g_3^2g_4 \\
& \quad - 14400Ng_1^3g_3^2g_4 - 10368\zeta_3Ng_1^3g_4^3 + 7344Ng_1^3g_4^3 \\
& \quad + 912Ng_1^2g_2^2g_3^2 - 500Ng_1^2g_2^2g_4^2 + 15552\zeta_3Ng_1^2g_2g_3^2g_4 \\
& \quad + 8424Ng_1^2g_2g_3^2g_4 - 3888Ng_1^2g_2g_4^3 - 1620N^2g_1^2g_3^4 \\
& \quad - 5184\zeta_3Ng_1^2g_3^4 + 5196Ng_1^2g_3^4 - 132N^2g_1^2g_3^2g_4^2 \\
& \quad - 2592\zeta_3Ng_1^2g_3^2g_4^2 + 37030Ng_1^2g_3^2g_4^2 - 1468Ng_1^2g_4^4 \\
& \quad - 2112Ng_1g_2^2g_3^2g_4 - 5184\zeta_3Ng_1g_2g_3^2g_4^2 + 5616Ng_1g_2g_3^2g_4^2 \\
& \quad + 564N^2g_1g_3^4g_4 - 10368\zeta_3Ng_1g_3^4g_4 - 8064Ng_1g_3^2g_4^3 \\
& \quad + 3744Ng_1g_3^4g_4 - 2592\zeta_3g_2^4g_4^2 + 2801g_2^4g_4^2 + 5184\zeta_3g_2^3g_4^3]
\end{aligned}$$

$$\begin{aligned}
& + 864g_2^3g_4^3 + 216Ng_2^2g_3^2g_4^2 + 10368\zeta_3g_2^2g_4^4 + 9554g_2^2g_4^4 \\
& - 1188Ng_2g_3^2g_4^3 + 7740g_2g_4^5 - 33N^2g_3^4g_4^2 + 1256Ng_3^4g_4^2 \\
& + 632Ng_3^2g_4^4 - 10368\zeta_3g_4^6 + 20676g_4^6] + O(g_i^8), \\
\gamma_{31}(g_i)|_{m=2} &= \frac{g_3^2}{2} + \frac{1}{72} [-20g_1^2g_3^2 - 18g_1^2g_4^2 - 108g_1g_3^2g_4 + 7Ng_3^4 - 2g_3^4 + 5g_3^2g_4^2] \\
& + \frac{1}{10368} [-5184\zeta_3Ng_1^4g_3^2 + 9404Ng_1^4g_3^2 + 5184\zeta_3g_1^4g_3^2 + 3476g_1^4g_3^2 \\
& + 2256Ng_1^4g_4^2 - 1464g_1^4g_4^2 + 3708g_1^3g_2g_3^2 - 5184g_1^3g_2g_4^2 \\
& - 7152Ng_1^3g_3^2g_4 + 27648g_1^3g_3^2g_4 + 20736\zeta_3g_1^3g_4^3 \\
& + 3456g_1^3g_4^3 - 374g_1^2g_2^2g_3^2 + 5016g_1^2g_2^2g_4^2 \\
& + 10368\zeta_3g_1^2g_2g_3^2g_4 + 9504g_1^2g_2g_3^2g_4 - 10368\zeta_3g_1^2g_2g_4^3 \\
& + 9936g_1^2g_2g_4^3 - 10368\zeta_3Ng_1^2g_3^4 + 7768Ng_1^2g_3^4 \\
& + 10368\zeta_3g_1^2g_3^4 - 4808g_1^2g_3^4 - 1760Ng_1^2g_3^2g_4^2 \\
& + 20736\zeta_3g_1^2g_3^2g_4^2 + 22616g_1^2g_3^2g_4^2 - 1344g_1^2g_4^4 \\
& - 2280g_1g_2^2g_3^2g_4 + 9072g_1g_2g_3^2g_4^2 - 6216Ng_1g_3^4g_4 \\
& + 11556g_1g_3^4g_4 + 10368\zeta_3g_1g_3^2g_4^3 - 7344g_1g_3^2g_4^3 \\
& + 344g_2^2g_3^2g_4^2 - 2952g_2g_3^2g_4^3 - 99N^2g_3^6 + 2654Ng_3^6 \\
& - 5184\zeta_3g_3^6 + 13820g_3^6 - 184Ng_3^4g_4^2 + 10368\zeta_3g_3^4g_4^2 \\
& + 1928g_3^4g_4^2 - 5184\zeta_3g_3^2g_4^4 + 9860g_3^2g_4^4] + O(g_i^8), \\
\gamma_{32}(g_i)|_{m=2} &= g_4^2 + \frac{1}{24} [-18Ng_1^2g_3^2 - 12Ng_1g_3^2g_4 - 6g_2^2g_4^2 - 36g_2g_4^3 + 7Ng_3^2g_4^2 \\
& - 4g_4^4] \\
& + \frac{1}{864} [1010Ng_1^4g_3^2 + 756Ng_1^4g_4^2 + 1728\zeta_3Ng_1^3g_2g_3^2 - 900Ng_1^3g_2g_3^2 \\
& - 1080Ng_1^3g_2g_4^2 + 1560Ng_1^3g_3^2g_4 + 1512Ng_1^3g_4^3 \\
& - 432\zeta_3Ng_1^2g_2^2g_3^2 + 846Ng_1^2g_2^2g_3^2 + 282Ng_1^2g_2^2g_4^2 \\
& + 2592\zeta_3Ng_1^2g_2g_3^2g_4 + 2268Ng_1^2g_2g_3^2g_4 - 904Ng_1^2g_2g_4^3 \\
& - 496N^2g_1^2g_3^4 - 178Ng_1^2g_3^4 + 3911Ng_1^2g_3^2g_4^2 + 40Ng_1^2g_4^4 \\
& - 216Ng_1g_2^2g_3^2g_4 - 1728\zeta_3Ng_1g_2g_3^2g_4^2 + 792Ng_1g_2g_3^2g_4^2 \\
& + 282N^2g_1g_3^4g_4 - 492Ng_1g_3^4g_4 - 1344Ng_1g_3^2g_4^3 \\
& - 21g_2^4g_4^2 + 864\zeta_3g_2^3g_4^3 + 1420g_2^3g_4^3 - 204Ng_2^2g_3^2g_4^2 \\
& + 864\zeta_3g_2^2g_4^4 + 1712g_2^2g_4^4 - 70Ng_2g_3^2g_4^3 - 162g_2g_4^5 \\
& - 33N^2g_3^4g_4^2 + 1276Ng_3^4g_4^2 - 37Ng_3^2g_4^4 + 3734g_4^6] \\
& + O(g_i^8), \\
\gamma_{33}(g_i)|_{m=2} &= \frac{1}{12} [-Ng_3^2 + 4g_4^2] \\
& + \frac{1}{432} [2Ng_1^2g_3^2 + 20Ng_1^2g_4^2 - 12Ng_1g_3^2g_4 + 10g_2^2g_4^2 - 60g_2g_4^3]
\end{aligned}$$

$$\begin{aligned}
& -76Ng_3^4 + 31Ng_3^2g_4^2 - 356g_4^4] \\
& + \frac{1}{31104} [-206N^2g_1^4g_3^2 + 2592\zeta_3Ng_1^4g_3^2 - 4280Ng_1^4g_3^2 \\
& \quad - 344N^2g_1^4g_4^2 + 968Ng_1^4g_4^2 + 1200Ng_1^3g_2g_3^2 \\
& \quad - 2064Ng_1^3g_2g_4^2 + 4536N^2g_1^3g_3^2g_4 - 12144Ng_1^3g_3^2g_4 \\
& \quad - 8280Ng_1^3g_4^3 - 103Ng_1^2g_2^2g_3^2 + 656Ng_1^2g_2^2g_4^2 \\
& \quad - 10368\zeta_3Ng_1^2g_2g_3^2g_4 + 5328Ng_1^2g_2g_3^2g_4 - 3156Ng_1^2g_2g_4^3 \\
& \quad - 7416N^2g_1^2g_3^4 + 13436Ng_1^2g_3^4 - 442N^2g_1^2g_3^2g_4^2 \\
& \quad + 113644Ng_1^2g_3^2g_4^2 + 2152Ng_1^2g_4^4 + 2268Ng_1g_2^2g_3^2g_4 \\
& \quad - 7308Ng_1g_2g_3^2g_4^2 + 3960N^2g_1g_3^4g_4 + 31104\zeta_3Ng_1g_3^4g_4 \\
& \quad - 16680Ng_1g_3^4g_4 - 31104\zeta_3Ng_1g_3^2g_4^3 - 15216Ng_1g_3^2g_4^3 \\
& \quad - 102g_2^4g_4^2 - 5718g_2^3g_4^3 - 221Ng_2^2g_3^2g_4^2 - 10368\zeta_3g_2^2g_4^4 \\
& \quad + 52728g_2^2g_4^4 + 1080Ng_2g_3^2g_4^3 + 3108g_2g_4^5 - 3292N^2g_3^6 \\
& \quad + 18144\zeta_3Ng_3^6 - 1214Ng_3^6 - 284N^2g_3^4g_4^2 \\
& \quad + 31104\zeta_3Ng_3^4g_4^2 + 24248Ng_3^4g_4^2 - 10644Ng_3^2g_4^4 \\
& \quad + 67392\zeta_3g_4^6 + 53200g_4^6] + O(g_i^8) . \tag{4.42}
\end{aligned}$$

4.7 Large N Analysis

Equipped with the explicit forms of the Renormalization Group functions we are in a position to check against the large N critical exponents for each of the three fixed points. In order to do this we follow the method introduced in [52] and described in the previous Chapter. To begin the scaled coupling constants are defined as

$$\begin{aligned}
g_1 &= ix\sqrt{\frac{12\epsilon}{mN}} \quad , \quad g_2 = iy\sqrt{\frac{12\epsilon}{mN}} \quad , \quad g_3 = iz\sqrt{\frac{12\epsilon}{N}} \quad , \\
g_4 &= it\sqrt{\frac{12\epsilon}{mN}} \quad , \quad g_5 = iw\sqrt{\frac{12\epsilon}{N}} . \tag{4.43}
\end{aligned}$$

This redefinition is to keep consistency with the results and analysis of [52]. The location of each of the three fixed points in the large N expansion can be deduced by solving

$$\beta_i(g_j^*) = 0 \tag{4.44}$$

where each g_j has been rescaled according to (4.43) and each coefficient of the fixed point of the power $1/N$ is a function of ϵ having set $d = 6 - 2\epsilon$. More

precisely fixed points will have the form

$$\begin{aligned}
x &= x_0 + \frac{x_1}{N} + \frac{x_2}{N^2} + \frac{x_3}{N^3} + O\left(\frac{1}{N^4}\right), \\
y &= y_0 + \frac{y_1}{N} + \frac{y_2}{N^2} + \frac{y_3}{N^3} + O\left(\frac{1}{N^4}\right), \\
z &= x_0 + \frac{z_1}{N} + \frac{z_2}{N^2} + \frac{z_3}{N^3} + O\left(\frac{1}{N^4}\right), \\
t &= t_0 + \frac{t_1}{N} + \frac{t_2}{N^2} + \frac{t_3}{N^3} + O\left(\frac{1}{N^4}\right), \\
w &= w_0 + \frac{w_1}{N} + \frac{w_2}{N^2} + \frac{w_3}{N^3} + O\left(\frac{1}{N^4}\right)
\end{aligned}$$

with each coefficient being a function of ϵ

$$\begin{aligned}
x_0 &= x_{00} + x_{01}\epsilon + x_{02}\epsilon^2 + x_{03}\epsilon^3 + O(\epsilon^4), \\
x_1 &= x_{10} + x_{11}\epsilon + x_{12}\epsilon^2 + x_{13}\epsilon^3 + O(\epsilon^4), \\
x_2 &= x_{20} + x_{21}\epsilon + x_{22}\epsilon^2 + x_{23}\epsilon^3 + O(\epsilon^4), \\
x_3 &= x_{30} + x_{31}\epsilon + x_{32}\epsilon^2 + x_{33}\epsilon^3 + O(\epsilon^4), \\
y_0 &= y_{00} + y_{01}\epsilon + y_{02}\epsilon^2 + y_{03}\epsilon^3 + O(\epsilon^4), \\
&\vdots \\
w_3 &= w_{30} + w_{31}\epsilon + w_{32}\epsilon^2 + w_{33}\epsilon^3 + O(\epsilon^4).
\end{aligned}$$

The three fixed points that emerge are labelled Heisenberg, anti-chiral unstable and chiral stable fixed points. Each of these fixed points are defined by a different field content and therefore for the Heisenberg and AU fixed points several of the coupling constant are zero. Starting with the Heisenberg fixed point, from the respective β -functions, we find

$$\begin{aligned}
x &= 1 + \left(\frac{22}{m} - \frac{155\epsilon}{3m} + \frac{1777\epsilon^2}{36m}\right)\frac{1}{N} \\
&\quad + \left(\frac{726}{m^2} - \frac{3410\epsilon}{m^2} + \left[\frac{29093}{9m^2} - \frac{4680\zeta_3}{m^2}\right]\epsilon^2\right)\frac{1}{N^2} + O\left(\epsilon^3, \frac{1}{N^3}\right), \\
y &= 6 + \left(\frac{972}{m} - \frac{1290\epsilon}{m} + \frac{2781\epsilon^2}{2m}\right)\frac{1}{N} \\
&\quad + \left(\frac{412596}{m^2} - \frac{1036020\epsilon}{m^2} + \left[\frac{1083644}{m^2} - \frac{628560\zeta_3}{m^2}\right]\epsilon^2\right)\frac{1}{N^2} \\
&\quad + O\left(\epsilon^3, \frac{1}{N^3}\right), \\
z &= t = w = 0.
\end{aligned} \tag{4.45}$$

As only the ϕ^{ia} and σ interactions are present in the Heisenberg fixed point all interactions with T^{ab} fields are set to zero, we can therefore check this fixed point against $O(N)$ theory in six dimensions. We find consistency for the Heisenberg fixed point results with that found in [52]. Note that the order symbol represents the truncation point for the two independent expansions. The AU large N fixed point is located at

$$\begin{aligned}
x &= y = t = 0, \\
z &= 1 + \left(-\frac{40}{m} + \frac{7m}{2} + 11 + \left[\frac{299}{3m} - \frac{155}{6} - \frac{25m}{3} \right] \epsilon \right. \\
&\quad \left. + \left[-\frac{3829}{36m} + \frac{1777}{72} + \frac{80m}{9} \right] \epsilon^2 \right) \frac{1}{N} \\
&\quad + \left(\frac{2400}{m^2} - \frac{1320}{m} - \frac{477}{2} + \frac{231m}{2} + \frac{147m^2}{8} + \left[-\frac{14180}{m^2} + \frac{6959}{m} + 1949 \right. \right. \\
&\quad \left. \left. - \frac{2555m}{4} - 150m^2 \right] \epsilon + \left[\frac{38755}{18m^2} - \frac{20664\zeta_3}{m^2} - \frac{136469}{36m} - \frac{19919}{24} \right. \right. \\
&\quad \left. \left. + 1242\zeta_3 + \frac{123919m}{144} - 576m\zeta_3 + \frac{23695m^2}{72} + \frac{102969\zeta_3}{m} \right] \epsilon^2 \right) \frac{1}{N^2} \\
&\quad + O\left(\epsilon^3, \frac{1}{N^3}\right), \\
w &= 6 + \left(-\frac{3240}{m} + 486 + 81m + \left[\frac{5178}{m} - 645 - 150m \right] \epsilon \right. \\
&\quad \left. + \left[-\frac{12105}{2m} + \frac{2781}{4} + 180m \right] \epsilon^2 \right) \frac{1}{N} \\
&\quad + \left(\frac{4874400}{m^2} - \frac{1417320}{m} - 118071 + 32283m + \frac{10161m^2}{4} \right. \\
&\quad \left. + \left[-\frac{14470680}{m^2} + \frac{3945054}{m} + 464454 - \frac{186915m}{2} - 10830m^2 \right] \epsilon \right. \\
&\quad \left. + \left[\frac{16668989}{m^2} - \frac{7556976\zeta_3}{m^2} + \frac{8635273}{2m} + \frac{2238192\zeta_3}{m} - \frac{2355195}{4} \right. \right. \\
&\quad \left. \left. + 236196\zeta_3 + \frac{915527m}{8} - 42120m\zeta_3 + \frac{76709m^2}{4} \right] \epsilon^2 \right) \frac{1}{N^2} \\
&\quad + O\left(\epsilon^3, \frac{1}{N^3}\right). \tag{4.46}
\end{aligned}$$

Finally for the CS type large N fixed point we find

$$\begin{aligned}
x &= 1 + \left(11 + 11m + \left[-\frac{155}{6} - \frac{155m}{6} \right] \epsilon + \left[\frac{1777}{72} + \frac{1777m}{72} \right] \epsilon^2 \right) \frac{1}{N} \\
&\quad + \left(\frac{1563}{2} + 63m - \frac{237m^2}{2} + \left[-\frac{6855}{2} - \frac{835m}{2} + 435m^2 \right] \epsilon \right. \\
&\quad \left. + \left[\frac{35345}{9} - 2646\zeta_3 + \frac{4085m}{72} - 1602m\zeta_3 - \frac{54101m^2}{72} \right] \epsilon^2 \right) \frac{1}{N^2}
\end{aligned}$$

$$\begin{aligned}
& - 432m^2\zeta_3 \Big] \epsilon^2 \Big) \frac{1}{N^2} + O\left(\epsilon^3, \frac{1}{N^3}\right), \\
y = & 6 + \left(486 + 486m + [-645 - 645m]\epsilon + \left[\frac{2781}{4} + \frac{2781m}{4} \right] \epsilon^2 \right) \frac{1}{N} \\
& + \left(248949 + 133398m + 30249m^2 + [-660675 - 317175m + 58170m^2]\epsilon \right. \\
& \quad \left. + \left[\frac{1419565}{2} - 354780\zeta_3 + \frac{1289545m}{4} - 215460m\zeta_3 + \frac{205901m^2}{4} \right. \right. \\
& \quad \left. \left. - 58320m^2\zeta_3 \right] \right) \frac{1}{N^2} + O\left(\epsilon^3, \frac{1}{N^3}\right), \\
z = & 1 + \left(11 + \frac{7m}{2} + \left[-\frac{155}{6} - \frac{25m}{3} \right] \epsilon + \left[\frac{1777}{72} + \frac{80m}{9} \right] \epsilon^2 \right) \frac{1}{N} \\
& + \left(\frac{1563}{2} + \frac{231m}{2} + \frac{147m^2}{8} + \left[-\frac{6855}{2} - \frac{2555m}{4} - 150m^2 \right] \epsilon \right. \\
& \quad \left. + \left[\frac{35345}{9} - 2646\zeta_3 + \frac{123919m}{144} - 576m\zeta_3 + \frac{23695m^2}{72} \right] \epsilon^2 \right) \frac{1}{N^2} \\
& + O\left(\epsilon^3, \frac{1}{N^3}\right), \\
t = & 6 + \left(486 + 216m + [-645 - 315m]\epsilon + \left[\frac{2781}{4} + \frac{1407m}{4} \right] \epsilon^2 \right) \frac{1}{N} \\
& + \left(248949 + 65988m + 7389m^2 + [-660675 - 168030m - 19545m^2]\epsilon \right. \\
& \quad \left. + \left[\frac{1419565}{2} - 354780\zeta_3 + 183756m - 99900m\zeta_3 + 25357m^2 \right. \right. \\
& \quad \left. \left. - 11664m^2\zeta_3 \right] \epsilon^2 \right) \frac{1}{N^2} + O\left(\epsilon^3, \frac{1}{N^3}\right), \\
w = & 6 + \left(-\frac{3240}{m} + 486 + 81m + \left[\frac{5187}{m} - 645 - 150m \right] \epsilon \right. \\
& \quad \left. + \left(-\frac{12105}{2m} + \frac{2781}{4} + 180m \right) \epsilon^2 \right) \frac{1}{N} \\
& + \left(\frac{4874400}{m^2} - \frac{1417320}{m} - 118071 + 32283m + \frac{10161m^2}{4} \right. \\
& \quad \left. + \left(-\frac{14470680}{m^2} + \frac{3945054}{m} + 464454 - \frac{186915m}{2} - 10830m^2 \right) \epsilon \right. \\
& \quad \left. + \left(\frac{16668989}{m^2} - \frac{7556976\zeta_3}{m^2} - \frac{8635273}{2m} + \frac{2238192\zeta_3}{m} - \frac{2355195}{4} \right. \right. \\
& \quad \left. \left. + 236196\zeta_3 + \frac{915527m}{8} - 42120m\zeta_3 + \frac{76709m^2}{4} \right] \epsilon^2 \right) \frac{1}{N^2} \\
& + O\left(\epsilon^3, \frac{1}{N^3}\right), \tag{4.47}
\end{aligned}$$

where all five couplings are non-zero. With these particular fixed points the critical exponents can be determined by evaluating the field anomalous dimensions

at criticality. The critical exponents examined are η , χ and χ_T which correspond to the anomalous dimensions of ϕ^{ia} and the vertex anomalous dimensions of σ and T^{ab} with ϕ^{ia} respectively. The leading order large N terms for the universal theory were stated in equations (4.4) and (4.6). The anomalous dimensions of the three fields evaluated at the CS type fixed point are given below, these can be matched order by order with the leading order large N results and higher order corrections [48, 49, 218, 220],

$$\begin{aligned}
\gamma_\phi^{CS}(g_i^*) &= \left((m+1)\epsilon + \left[-\frac{11m}{6} - \frac{11}{6} \right] \epsilon^2 + \left[-\frac{13m}{36} - \frac{13}{36} \right] \epsilon^3 \right) \frac{1}{N} \\
&\quad + \left([7m^2 + 29m + 52]\epsilon + \left[-\frac{146m^2}{3} - \frac{1127m}{6} - \frac{1921}{6} \right] \epsilon^2 \right. \\
&\quad \quad \left. + \left[\frac{694m^2}{9} + \frac{9641m}{36} + \frac{15043}{36} \right] \epsilon^3 \right) \frac{1}{N^2} + O(\epsilon^4), \\
\gamma_\sigma^{CS}(g_i^*) &= \left([7m^2 + 29m + 52]\epsilon + \left[-\frac{146m^2}{3} - \frac{1127m}{6} - \frac{1921}{6} \right] \epsilon^2 \right. \\
&\quad \left. + \left[\frac{694m^2}{9} + \frac{9641m}{36} + \frac{15043}{36} \right] \epsilon^3 \right) \frac{1}{N} \\
&\quad + \left([1180m^2 - 1360m + 25660]\epsilon + \left[-\frac{966832016}{1000000} m^2 \right. \right. \\
&\quad \quad \left. \left. - \frac{7154681733}{100000} + \frac{8080666662}{1000000} m \right] \epsilon^2 \right) \frac{1}{N^2} + O(\epsilon^4), \\
\gamma_T^{CS}(g_i^*) &= \left([16m + 40]\epsilon + \left[-\frac{208}{3} - \frac{88m}{3} \right] \epsilon^2 + \left[-\frac{88}{9} - \frac{16m}{9} \right] \epsilon^3 \right) \frac{1}{N} \\
&\quad + O(\epsilon^4). \tag{4.48}
\end{aligned}$$

We find agreement out to order $O(\epsilon^3)$ with our results. More specifically, the $1/N$ term of $\gamma_\phi^{CS}(g_i)$ matches the exponent $\frac{1}{2}\eta_1^{CS}$ perfectly, while the $1/N^2$ coefficient agrees with $\frac{1}{2}\eta_2^{CS}$. Note that the factor of $1/2$ is a notational convention used in certain literature. The $1/N$ term of $\gamma_\sigma^{CS}(g_i^*)$ matches the CS critical exponent $-(\eta_1^{CS} + \chi_1^{CS})$ and the $1/N^2$ term is in complete agreement with $-(\eta_2^{CS} + \chi_2^{CS})$. Finally the $1/N$ term of the anomalous dimension $\gamma_T^{CS}(g_i^*)$ evaluated at the CS fixed point matches the critical exponent $-(\eta_1^{CS} + \chi_{T,1}^{CS})$ exactly. Inserting the Heisenberg and AU fixed points into the anomalous dimensions we find that these results will likewise match up with the relevant large N critical exponents.

We also find agreement with the mass mixing matrix. However, the comparison with the mass dimension exponents is not straightforward since one has to compare the anomalous dimensions with the eigenvalues of the mass mixing matrix $\gamma_{ij}(g_k)$ evaluated at each critical point. For instance, at the AU fixed point the exponent ω_{+1}^{AU} is in precise agreement with the critical eigen-anomalous

dimension as there is only one operator there. Equally at the CS fixed point the exponents $\eta + \chi$ and the linear combination $\omega_{+1}^{CS} + \omega_{-1}^{CS}$ are also in exact correspondence with the $O(\epsilon^3)$ terms of the eigen-anomalous dimensions. These non-trivial large N checks at each of the three fixed points on the three loop $\overline{\text{MS}}$ Renormalization Group functions provide confidence that our perturbative computation is correct.

4.8 Conformal Window Search

The main aim of our calculation is to find the conformal window for the six dimensional LGW theory. Recall that the conformal window is the range of N , and in this case m , values for which non-trivial stable fixed points exists. Given the nature of the Renormalization Group equations at three loops, finding the exact location of the conformal window is not straightforward. A similar observation was made in [66] for the four dimensional $O(N) \times O(3)$ Landau-Ginzburg-Wilson theory using the conformal bootstrap method. The conformal window can be found by solving the equations

$$\beta_1(g_i) = \beta_2(g_i) = \beta_3(g_i) = \beta_4(g_i) = \beta_5(g_i) = 0 \quad (4.49)$$

together with the Hessian

$$\det \left(\frac{\partial \beta_i}{\partial g_j} \right) = 0 . \quad (4.50)$$

It turns out that our computer resources were not sufficient to solve the complete system numerically in general. Instead we have resorted to an alternative strategy which is based on an observation made with respect to the $O(N)$ case, [52,53]. It was noticed that the fixed point spectrum was significantly different above and below the conformal window boundary. For $O(N)$ theory in six dimensions the conformal window boundary at leading order was found to be $N_{\text{crit}} \approx 1038$, [174]. Above this value of N_{crit} there are fixed points with real stable couplings, while below this point there are no real stable fixed points. Given this distinguishing property we have solved the equations (4.49) and (4.50) for fixed values of N and then analysed the stability properties of the real solutions to hone in on the boundary. Recall that the stability of a fixed point is determined by finding the eigenvalues of the stability matrix \mathcal{S} at the fixed point where \mathcal{S} is defined by

$$\mathcal{S} = \left(\frac{\partial \beta_i}{\partial g_j} \right) . \quad (4.51)$$

Specifically if all eigenvalues are negative then this signifies ultraviolet stability, while if all eigenvalues are positive then the fixed point would be ultraviolet unstable and consequently infrared stable. Obtaining a mixed signature indicates that the fixed point is a saddle point. In the situation where the eigenvalues are zero, we can only conclude that the fixed point is marginal and beyond the linear approximation. We do not find any such cases for the values of N analysed here. While this may appear to be a tedious process for finding the conformal window it turns out to be relatively quick since one can narrow the search area by a process of sectioning. Here we will search for the conformal boundary of the $O(N) \times O(2)$ case, taking values of N and looking for a change in the number and stability properties of a particular pattern of fixed points. We must however note some important points before doing this.

First, given the fact that there are more couplings here than in the $O(N)$ case the criteria defining the window boundary differs slightly. In the four dimensional Landau-Ginzburg-Wilson model there were three non-trivial fixed points designated Heisenberg, antichiral unstable and chiral stable. With fewer couplings in four dimensions each type of fixed point had a definite stability which led to this notation AU or CS aside from the Heisenberg solution which was necessarily a saddle point. In the six dimensional theory we retain the Heisenberg, antichiral unstable and chiral stable syntax but use it to represent the field content only. These labels will not have any bearing on the stability of a fixed point. More precisely the labels are associated with different combinations of the fields σ and T^{ab} that are active or not at a fixed point. So, for instance, indicating an AU fixed point will mean that only interactions involving the T^{ab} field are present while a CS type of fixed point will correspond to all interactions of $L^{(\text{LGW6})}$ being active. To clarify, for the Heisenberg, AU and CS patterns the fixed point could be stable or unstable and not be related to the U or S of the label type. Illustrating this with the coupling vector $(g_1, g_2, g_3, g_4, g_5)$ their characteristic critical coupling constant patterns respectively are $(x, y, 0, 0, 0)$, $(0, 0, z, 0, w)$ and (x, y, z, t, w) , where we mean that x, y, z, t and w are non-zero in these patterns. Therefore we will refer to Heisenberg, antichiral unstable and chiral stable *types* of solutions. The emergence of these patterns of fixed points within the perturbative context should not be surprising as the fixed N analysis has to at least contain the Heisenberg, AU and CS large N solutions. Finally as in the $O(N)$ case various fixed point solutions are connected to each other via symmetries, [52], and so we focus on a representative fixed point of each such class in the analysis. We also find a large number of fixed points with complex and purely imaginary values which may indicate non-unitary solutions or even the existence of a limit cycle. For the

conformal window search we will focus only on real solutions as they lead to clear stability properties. Complex and imaginary solutions are included in a general fixed point analysis.

We analysed the stability properties of a wide range of fixed points using a sectioning algorithm. Results related to the conformal window will be discussed here. We begin with $m = 2$ and $N = 1106$ for which we have three CS type fixed points. One of these is UV stable which is located at

$$\begin{aligned}
x &= 1.024331 + 0.602917\epsilon - 618.493720\epsilon^2 + O(\epsilon^3), \\
y &= 10.027831 - 224.568795\epsilon + 204744.131100\epsilon^2 + O(\epsilon^3), \\
z &= 1.014679 + 0.242004\epsilon - 259.254500\epsilon^2 + O(\epsilon^3), \\
t &= 8.413935 - 122.062932\epsilon + 110001.339800\epsilon^2 + O(\epsilon^3), \\
w &= 7.750728 - 86.093662\epsilon + 77109.596670\epsilon^2 + O(\epsilon^3). \quad (4.52)
\end{aligned}$$

The 5×5 stability matrix evaluated at this fixed point gives the following five eigenvalues at leading order which are all negative.

$$\begin{aligned}
e_1 &= -1, & e_2 &= -0.809156, \\
e_3 &= -0.021933, & e_4 &= -1.297560, \\
e_5 &= -1.153037.
\end{aligned}$$

The corresponding critical exponents for the UV stable CS fixed point are

$$\begin{aligned}
\gamma_\phi^* &= 0.002810\epsilon - 0.003531\epsilon^2 - 2.095198\epsilon^3 + O(\epsilon^4), \\
\gamma_\sigma^* &= 1.158724\epsilon - 2.828644\epsilon^2 + 2307.673939\epsilon^3 + O(\epsilon^4), \\
\gamma_T^* &= 1.093583\epsilon - 1.472805\epsilon^2 + 1165.028293\epsilon^3 + O(\epsilon^4). \quad (4.53)
\end{aligned}$$

The other two CS style fixed points are saddle points located at

$$\begin{aligned}
x &= 1.023546 - 0.790738\epsilon + 618.557767\epsilon^2 + O(\epsilon^3), \\
y &= 10.288220 + 238.034889\epsilon - 204695.170900\epsilon^2 + O(\epsilon^3), \\
z &= 1.014350 - 0.341297\epsilon + 259.727356\epsilon^2 + O(\epsilon^3), \\
t &= 8.553710 + 126.145941\epsilon - 109987.441000\epsilon^2 + O(\epsilon^3), \\
w &= 7.848666 + 87.779203\epsilon - 77103.604170\epsilon^2 + O(\epsilon^3) \quad (4.54)
\end{aligned}$$

and

$$\begin{aligned}
x &= -0.869900 - 0.200484\epsilon - 0.868576\epsilon^2 + O(\epsilon^3), \\
y &= 20.723963 + 8.470150\epsilon - 14.322290\epsilon^2 + O(\epsilon^3), \\
z &= 1.011451 - 0.019282\epsilon + 0.058843\epsilon^2 + O(\epsilon^3), \\
t &= -4.381299 - 2.162646\epsilon - 6.897939\epsilon^2 + O(\epsilon^3), \\
w &= 5.927808 + 0.692949\epsilon + 3.355853\epsilon^2 + O(\epsilon^3).
\end{aligned} \tag{4.55}$$

In addition there are three Heisenberg type fixed points, one of which is UV stable at

$$\begin{aligned}
x &= 1.010040 - 0.023705\epsilon + 0.020596\epsilon^2 + O(\epsilon^3), \\
y &= 6.557735 - 0.940183\epsilon + 0.810426\epsilon^2 + O(\epsilon^3), \\
z &= 0, \quad t = 0, \quad w = 0.
\end{aligned} \tag{4.56}$$

The stability matrix for the Heisenberg fixed point is a non-zero 2×2 matrix. Evaluated at the Heisenberg fixed point it produces two eigenvalues at leading order which are both negative, confirming UV stability,

$$e_1 = -0.766341, \quad e_2 = -1.$$

The associated critical exponents for the UV stable Heisenberg fixed point are

$$\begin{aligned}
\gamma_\phi^* &= 0.000922\epsilon - 0.001777\epsilon^2 - 0.000152\epsilon^3 + O(\epsilon^4), \\
\gamma_\sigma^* &= 1.039622\epsilon - 0.075355\epsilon^2 - 0.008779\epsilon^3 + O(\epsilon^4), \\
\gamma_T^* &= 0.
\end{aligned} \tag{4.57}$$

The other two Heisenberg like fixed points are saddle points and are located at

$$\begin{aligned}
x &= 0.979414 - 0.003228\epsilon + 0.071572\epsilon^2 + O(\epsilon^3), \\
y &= 17.380571 + 10.947386\epsilon + 21.645075\epsilon^2 + O(\epsilon^3), \\
z &= 0, \quad t = 0, \quad w = 0
\end{aligned} \tag{4.58}$$

and

$$\begin{aligned}
x &= -0.857078 - 0.208350\epsilon - 0.632470\epsilon^2 + O(\epsilon^3), \\
y &= 19.745752 + 9.661778\epsilon - 2.588019\epsilon^2 + O(\epsilon^3), \\
z &= 0, \quad t = 0, \quad w = 0.
\end{aligned} \tag{4.59}$$

There is one AU fixed point which is UV stable situated at

$$\begin{aligned}
x &= 0, & y &= 0, & t &= 0, \\
z &= 0.998197 + 0.006635\epsilon - 0.008935\epsilon^2 + O(\epsilon^3), \\
w &= 5.367450 + 0.851212\epsilon - 1.446454\epsilon^2 + O(\epsilon^3)
\end{aligned} \tag{4.60}$$

with critical exponents

$$\begin{aligned}
\gamma_\phi^* &= 0.001802\epsilon - 0.003273\epsilon^2 - 0.000708\epsilon^3 + O(\epsilon^4), \\
\gamma_\sigma^* &= 0, \\
\gamma_T^* &= 0.996396\epsilon + 0.006664\epsilon^2 + 0.002605\epsilon^3 + O(\epsilon^4).
\end{aligned} \tag{4.61}$$

Keeping $m = 2$ and moving to the lower value of $N = 1105$ a different style of solution emerges. This is first seen in the CS type of fixed points in that there is only one such fixed point which is located at

$$\begin{aligned}
x &= -0.869887 - 0.200513\epsilon - 0.868979\epsilon^2 + O(\epsilon^3), \\
y &= 20.715552 + 8.465518\epsilon - 14.330113\epsilon^2 + O(\epsilon^3), \\
z &= 1.011461 - 0.019297\epsilon + 0.058911\epsilon^2 + O(\epsilon^3), \\
t &= -4.380955 - 2.163247\epsilon - 6.901395\epsilon^2 + O(\epsilon^3), \\
w &= 5.927669 + 0.693620\epsilon + 3.359563\epsilon^2 + O(\epsilon^3).
\end{aligned} \tag{4.62}$$

More crucially, it is a saddle point. In other words there is no CS stable fixed point present at $N = 1105$. Given this change in pattern we regard $N = 1105$ as the boundary for the conformal window in six dimensions. For completeness we state the remaining fixed points at $N = 1105$. There are three Heisenberg fixed points. One is UV stable and is placed at

$$\begin{aligned}
x &= 1.010049 - 0.023726\epsilon + 0.020611\epsilon^2 + O(\epsilon^3), \\
y &= 6.558394 - 0.941587\epsilon + 0.811596\epsilon^2 + O(\epsilon^3), \\
z &= 0, & t &= 0, & w &= 0
\end{aligned} \tag{4.63}$$

with critical exponents

$$\begin{aligned}
\gamma_\phi^* &= 0.000923\epsilon - 0.001779\epsilon^2 - 0.000152\epsilon^3 + O(\epsilon^4), \\
\gamma_\sigma^* &= 1.039662\epsilon - 0.075439\epsilon^2 - 0.008783\epsilon^3 + O(\epsilon^4), \\
\gamma_T^* &= 0.
\end{aligned} \tag{4.64}$$

The other two fixed points are saddle points located at

$$\begin{aligned} x &= -0.857055 - 0.208383\epsilon - 0.632604\epsilon^2 + O(\epsilon^3), \\ y &= 19.736951 + 9.657499\epsilon - 2.589415\epsilon^2 + O(\epsilon^3), \\ z &= 0, \quad t = 0, \quad w = 0 \end{aligned} \quad (4.65)$$

and

$$\begin{aligned} x &= 0.979447 - 0.003297\epsilon + 0.071496\epsilon^2 + O(\epsilon^3), \\ y &= 17.371128 + 10.944494\epsilon + 21.644028\epsilon^2 + O(\epsilon^3), \\ z &= 0, \quad t = 0, \quad w = 0. \end{aligned} \quad (4.66)$$

The one AU fixed point is UV stable and is positioned at

$$\begin{aligned} x &= 0, \quad y = 0, \quad t = 0, \\ z &= 0.998195 + 0.006641\epsilon - 0.008942\epsilon^2 + O(\epsilon^3), \\ w &= 5.367025 + 0.851662\epsilon - 1.447623\epsilon^2 + O(\epsilon^3) \end{aligned} \quad (4.67)$$

with critical exponents

$$\begin{aligned} \gamma_\phi^* &= 0.001803\epsilon - 0.003276\epsilon^2 - 0.000709\epsilon^3 + O(\epsilon^4), \\ \gamma_\sigma^* &= 0, \\ \gamma_T^* &= 0.996393\epsilon + 0.006670\epsilon^2 + 0.002608\epsilon^3 + O(\epsilon^4). \end{aligned} \quad (4.68)$$

For $N > 1106$ and $N < 1105$ the algorithm of section searching was applied for changes in CS fixed point patterns but no further boundaries were found. That is, all values of $N > 1106$ analysed possessed the same fixed point stability structure for CS fixed points as that of $N = 1106$. Similarly all of values of $N < 1105$ analysed contained the same fixed point stability structure for CS fixed points as that of $N = 1105$. One observation of our conformal window analysis is that the boundary at $N = 1105$ is not dissimilar to the leading order value of $N_{\text{crit}} = 1038$, [174], for the $O(N)$ case. In [52, 53] the $O(\epsilon^3)$ corrections to N_{crit} were computed and by using re-summation methods a value of N_{crit} around 400 was found for the five dimensional theory. Unfortunately the section search method cannot be readily extended beyond the leading order which is for the strictly six dimensional theory. Instead solving (4.49) simultaneously with $\det(S) = 0$ would be the way to extract such corrections but was beyond the range of our computational tools. Along with looking at the full conformal window where all interactions are present and all couplings active, we can look

at an alternative version of the conformal window to gain more insight into the properties of fixed points.

So far we have analysed the conformal window of the theory with symmetry group $O(N) \times O(2)$, and found that the change in nature of the fixed points indicates a boundary. Moreover different types of real solutions emerge. We now lift the restriction on the value of m and look at the conformal window of the $O(N) \times O(m)$ Landau-Ginzburg-Wilson theory. However this time we search for the conformal window for the AU pattern of couplings only. In other words we set $x = y = t = 0$ at the outset and for a selection of values of m solve

$$\begin{aligned} \beta_3(g_i) = \beta_5(g_i) &= 0, \\ \det \begin{pmatrix} \partial\beta_3/\partial g_3 & \partial\beta_3/\partial g_5 \\ \partial\beta_5/\partial g_3 & \partial\beta_5/\partial g_5 \end{pmatrix} &= 0. \end{aligned} \quad (4.69)$$

Included in this is the equation for the Hessian which allows the determination of the critical value of N defining the window boundary, which will be denoted $N_{\text{crit}}^{(m)}$ for this AU pattern. The advantage of looking at the AU fixed points only is that we do not have to conduct a section search. To get a perspective on the results the leading order values of $N_{\text{crit}}^{(m)}$ are provided for various m in table 4.2. As $m \rightarrow \infty$ we find that $N_{\text{crit}}^{(m)}$ asymptotes to a straight line, see figure 4.26.

m	1	2	3	4	5	6	10	20	30
$N_{\text{crit}}^{(m)}$	-2946.1	-1087.5	-410.2	0	216.8	421.7	992.3	1999.6	2887.9

m	40	50
$N_{\text{crit}}^{(m)}$	3746.3	4592.9

Table 4.2: Leading order value of $N_{\text{crit}}^{(m)}$ for the AU conformal window for different values of m .

While this is only a partial picture for the situation for $m > 2$ one thing is evident, which is in six dimensions when $m \geq 5$ there should be a change in pattern for AU type fixed points for a fixed N search, akin to that illustrated in our section-based search for $m = 2$. This proves to be true after analysis of the stability matrix. For $m = 3$ the 2×2 stability matrix evaluated at the associated fixed point has eigenvalues $e_1 = 1.118079$ and $e_2 = -1$. It is therefore a saddle point. While for the AU type fixed point found at $m = 5$ the stability matrix produces eigenvalues $e_1 = -1$ and $e_2 = -5.839274$, signifying a UV stable fixed point. Furthermore fixed points at values of $m > 5$ were also found to have negative

stability eigenvalues. This indicates that all AU type fixed points with $m \geq 5$ are UV stable. The solution given in table 4.2 for $m = 4$ reflects the fact that there was no solution rather than an exact value of zero. Although we have recorded zero in the table for the reason that it does appear to be consistent with the monotonic increase in $N_{\text{crit}}^{(m)}$ with m .

Since we are able to solve equations (4.69) the three loop corrections to the leading order values in table 4.2 have been determined for a section of m along with the respective critical couplings,

$$\begin{aligned}
N_{\text{crit}}^{(1)} &= -2946.134605 + 3951.961993\epsilon + 2676.699839\epsilon^2 + O(\epsilon^3), \\
z &= 1.006955 - 0.008027\epsilon + 0.012574\epsilon^2 + O(\epsilon^3), \\
w &= 8.952176 - 0.933006\epsilon + 1.840946\epsilon^2 + O(\epsilon^3), \\
N_{\text{crit}}^{(2)} &= -1087.488959 + 1415.172128\epsilon + 261.248651\epsilon^2 + O(\epsilon^3), \\
z &= 1.001844 - 0.004332\epsilon + 0.005483\epsilon^2 + O(\epsilon^3), \\
w &= 9.000046 - 1.261448\epsilon - 1.365084\epsilon^2 + O(\epsilon^3), \\
N_{\text{crit}}^{(3)} &= -410.145045 + 439.505646\epsilon + 1591.300276\epsilon^2 + O(\epsilon^3), \\
z &= 0.988129 + 0.002686\epsilon + 0.093273\epsilon^2 + O(\epsilon^3), \\
w &= 9.206805 - 2.755615\epsilon + 36.244925\epsilon^2 + O(\epsilon^3), \\
N_{\text{crit}}^{(5)} &= 216.767170 - 419.773422\epsilon + 25581.601520\epsilon^2 + O(\epsilon^3), \\
z &= 1.094548 - 0.073610\epsilon - 9.071267\epsilon^2 + O(\epsilon^3), \\
w &= 8.708936 + 1.332420\epsilon - 267.527508\epsilon^2 + O(\epsilon^3), \\
N_{\text{crit}}^{(6)} &= 421.682453 - 774.149504\epsilon + 8084.140233\epsilon^2 + O(\epsilon^3), \\
z &= 1.053874 - 0.038490\epsilon - 0.487837\epsilon^2 + O(\epsilon^3), \\
w &= 8.724938 + 0.659976\epsilon - 46.386543\epsilon^2 + O(\epsilon^3), \\
N_{\text{crit}}^{(10)} &= 992.309977 - 1796.450905\epsilon + 1605.099447\epsilon^2 + O(\epsilon^3), \\
z &= 1.035563 - 0.025317\epsilon + 0.018625\epsilon^2 + O(\epsilon^3), \\
w &= 8.766117 + 0.281651\epsilon + 0.445942\epsilon^2 + O(\epsilon^3), \\
N_{\text{crit}}^{(20)} &= 1999.619696 - 3823.678958\epsilon - 645.564678\epsilon^2 + O(\epsilon^3), \\
z &= 1.032648 - 0.021711\epsilon + 0.036581\epsilon^2 + O(\epsilon^3), \\
w &= 8.770214 + 0.294322\epsilon + 6.987749\epsilon^2 + O(\epsilon^3), \\
N_{\text{crit}}^{(30)} &= 2887.855771 - 5724.541609\epsilon - 1656.156005\epsilon^2 + O(\epsilon^3), \\
z &= 1.032739 - 0.020634\epsilon + 0.038671\epsilon^2 + O(\epsilon^3), \\
w &= 8.766733 + 0.353761\epsilon + 8.295335\epsilon^2 + O(\epsilon^3), \\
N_{\text{crit}}^{(40)} &= 3746.323521 - 7599.677475\epsilon - 2431.924312\epsilon^2 + O(\epsilon^3),
\end{aligned}$$

$$\begin{aligned}
z &= 1.032998 - 0.020013\epsilon + 0.039622\epsilon^2 + O(\epsilon^3), \\
w &= 8.763914 + 0.398295\epsilon + 8.889004\epsilon^2 + O(\epsilon^3), \\
N_{\text{crit}}^{(50)} &= 4592.876982 - 9466.056881\epsilon - 3115.903624\epsilon^2 + O(\epsilon^3), \\
z &= 1.033232 - 0.019588\epsilon + 0.040210\epsilon^2 + O(\epsilon^3), \\
w &= 8.761832 + 0.430906\epsilon + 9.233526\epsilon^2 + O(\epsilon^3).
\end{aligned} \tag{4.70}$$

An important point to note is that while we have provided values for $N_{\text{crit}}^{(m)}$ and the critical couplings, other solutions related by symmetries were found for each m . This analysis is similar to that of [52, 53] where three solutions are found but the small $N_{\text{crit}}^{(m)}$ solutions discarded as they were negative or had complex critical couplings. We have followed the same reasoning here. Moreover, the negative solutions for $N_{\text{crit}}^{(m)}$ above are in keeping with similar negative solutions for the eight dimensional UV completion of the $O(N)$ sequence of theories, [182]. We have also excluded from this AU analysis values of $N_{\text{crit}}^{(m)}$ which have large critical couplings as such values are clearly outside the perturbative approximation.

Finally we look at the three loop results for the AU conformal window in five dimensions. This is achieved by setting $\epsilon = 1/2$ in the perturbative results (4.70) where $d = 6 - 2\epsilon$. We hope in future they may be useful in comparison with non-perturbative work looking at the Landau-Ginzburg-Wilson model in five dimensions such as conformal bootstrap. Results for this five dimensional analysis are plotted in figure 4.27. As is obvious from the graph, the value of N peaks at $m = 5$ before dropping dramatically into negative values for $m \approx 12.5$.

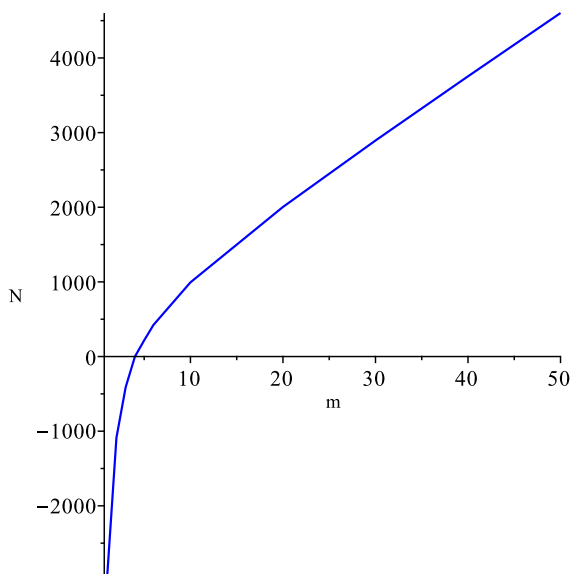


Figure 4.26: Plot of leading order N values in six dimensions against a range of m values for the AU conformal window.

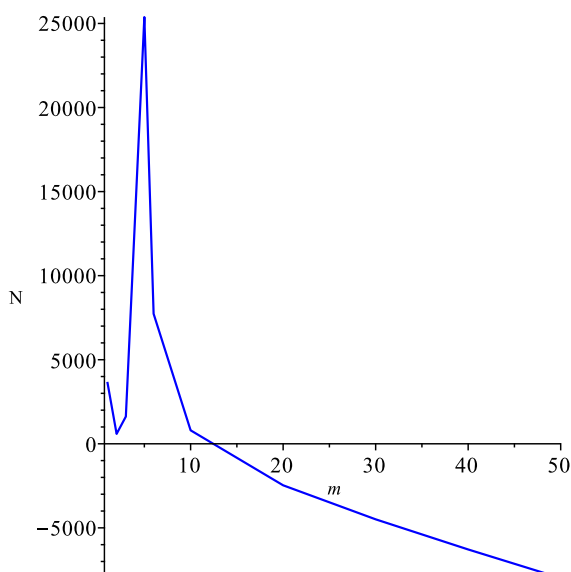


Figure 4.27: Plot of N values to three loops set in five dimensions against a range of m values for the AU conformal window.

4.9 Fixed Point Analysis

In this section we present a fixed point analysis for a variety of specific values of N . The aim is to give a flavour of the fixed point spectrum away from $N = 1105$. In addition we will indicate the potential for another conformal window boundary for non-CS type fixed points. We begin by looking at $N = 1500$, a value above the upper bound of the conformal window, before proceeding to lower values of N . Note that we are looking at the fixed point spectrum for $O(N) \times O(2)$ throughout this analysis. For $N = 1500$ there are three CS style fixed points, one of which is UV stable located at

$$\begin{aligned}
 x &= 1.021605 - 0.048356\epsilon + 0.029508\epsilon^2 + O(\epsilon^3), \\
 y &= 7.526281 - 3.373254\epsilon + 3.656128\epsilon^2 + O(\epsilon^3), \\
 z &= 1.012246 - 0.028825\epsilon + 0.021639\epsilon^2 + O(\epsilon^3), \\
 t &= 6.956845 - 2.194001\epsilon + 2.528779\epsilon^2 + O(\epsilon^3), \\
 w &= 6.695428 - 1.676882\epsilon + 2.013956\epsilon^2 + O(\epsilon^3)
 \end{aligned} \tag{4.71}$$

with the critical exponents

$$\begin{aligned}
 \gamma_\phi^* &= 0.002062\epsilon - 0.004094\epsilon^2 - 0.000048\epsilon^3 + O(\epsilon^4), \\
 \gamma_\sigma^* &= 1.094824\epsilon - 0.199694\epsilon^2 + 0.004627\epsilon^3 + O(\epsilon^4),
 \end{aligned}$$

$$\gamma_T^* = 1.056908\epsilon - 0.124537\epsilon^2 + 0.015105\epsilon^3 + O(\epsilon^4). \quad (4.72)$$

The other two fixed points are saddle points at

$$\begin{aligned} x &= -0.873990 - 0.191329\epsilon - 0.751979\epsilon^2 + O(\epsilon^3), \\ y &= 23.798278 + 10.148911\epsilon - 11.779856\epsilon^2 + O(\epsilon^3), \\ z &= 1.008603 - 0.014934\epsilon + 0.040425\epsilon^2 + O(\epsilon^3), \\ t &= -4.493123 - 1.975523\epsilon - 5.895095\epsilon^2 + O(\epsilon^3), \\ w &= 5.966576 + 0.493814\epsilon + 2.313503\epsilon^2 + O(\epsilon^3) \end{aligned} \quad (4.73)$$

and

$$\begin{aligned} x &= 0.992174 - 0.081030\epsilon - 0.023454\epsilon^2 + O(\epsilon^3), \\ y &= 17.442800 + 28.749545\epsilon + 111.944490\epsilon^2 + O(\epsilon^3), \\ z &= 1.003285 - 0.007810\epsilon + 0.201587\epsilon^2 + O(\epsilon^3), \\ t &= 11.000675 - 0.211700\epsilon - 51.299412\epsilon^2 + O(\epsilon^3), \\ w &= 9.199252 - 3.571347\epsilon - 51.357767\epsilon^2 + O(\epsilon^3). \end{aligned} \quad (4.74)$$

There are three Heisenberg fixed points, one of which is UV stable positioned at

$$\begin{aligned} x &= 1.007396 - 0.017489\epsilon + 0.0157898\epsilon^2 + O(\epsilon^3), \\ y &= 6.381875 - 0.593859\epsilon + 0.531412\epsilon^2 + O(\epsilon^3), \\ z &= 0, \quad t = 0, \quad w = 0 \end{aligned} \quad (4.75)$$

with critical exponents

$$\begin{aligned} \gamma_\phi &= 0.000677\epsilon - 0.001287\epsilon^2 - 0.000149\epsilon^3 + O(\epsilon^4), \\ \gamma_\sigma &= 1.028423\epsilon - 0.052457\epsilon^2 - 0.006877\epsilon^3 + O(\epsilon^4), \\ \gamma_T &= 0. \end{aligned} \quad (4.76)$$

The other two fixed points are saddle points

$$\begin{aligned} x &= 0.969241 + 0.017669\epsilon + 0.098504\epsilon^2 + O(\epsilon^3), \\ y &= 20.750257 + 12.165199\epsilon + 22.046485\epsilon^2 + O(\epsilon^3), \\ z &= 0, \quad t = 0, \quad w = 0 \end{aligned} \quad (4.77)$$

and

$$x = -0.864396 - 0.197825\epsilon - 0.590313\epsilon^2 + O(\epsilon^3),$$

$$\begin{aligned}
y &= 22.944330 + 11.220930\epsilon - 2.024271\epsilon^2 + O(\epsilon^3) , \\
z &= 0 , \quad t = 0 , \quad w = 0 .
\end{aligned} \tag{4.78}$$

We also have one AU fixed point, which is UV stable at

$$\begin{aligned}
x &= 0 , \quad y = 0 , \quad t = 0 , \\
z &= 0.998669 + 0.004891\epsilon - 0.006734\epsilon^2 + O(\epsilon^3) , \\
w &= 5.499130 + 0.705073\epsilon - 1.100501\epsilon^2 + O(\epsilon^3) .
\end{aligned} \tag{4.79}$$

The critical exponents evaluated at this stable fixed point calculated to three loops are

$$\begin{aligned}
\gamma_\phi &= 0.001330\epsilon - 0.002422\epsilon^2 - 0.000512\epsilon^3 + O(\epsilon^4) , \\
\gamma_\sigma &= 0 , \\
\gamma_T &= 0.997340\epsilon + 0.004907\epsilon^2 + 0.001671\epsilon^3 + O(\epsilon^4) .
\end{aligned} \tag{4.80}$$

These fixed points along with their stability properties are what we expect for a value of N above the CS conformal window boundary. Next we move to a value below the conformal boundary. For $N = 1000$ there is one CS style fixed point which is a saddle point at

$$\begin{aligned}
x &= -0.868555 - 0.203744\epsilon - 0.915849\epsilon^2 + O(\epsilon^3) , \\
y &= 19.811433 + 7.966436\epsilon - 15.205442\epsilon^2 + O(\epsilon^3) , \\
z &= 1.012581 - 0.020942\epsilon + 0.066905\epsilon^2 + O(\epsilon^3) , \\
t &= -4.342552 - 2.231269\epsilon - 7.303390\epsilon^2 + O(\epsilon^3) , \\
w &= 5.911324 + 0.770705\epsilon + 3.795188\epsilon^2 + O(\epsilon^3) .
\end{aligned} \tag{4.81}$$

We also have three Heisenberg fixed points, one of which is UV stable located at

$$\begin{aligned}
x &= 1.011102 - 0.026162\epsilon + 0.022238\epsilon^2 + O(\epsilon^3) , \\
y &= 6.637801 - 1.117476\epsilon + 0.962982\epsilon^2 + O(\epsilon^3) , \\
z &= 0 , \quad t = 0 , \quad w = 0
\end{aligned} \tag{4.82}$$

with the critical exponents

$$\begin{aligned}
\gamma_\phi^* &= 0.001022\epsilon - 0.001981\epsilon^2 - 0.000145\epsilon^3 + O(\epsilon^4) , \\
\gamma_\sigma^* &= 1.044358\epsilon - 0.085562\epsilon^2 - 0.009090\epsilon^3 + O(\epsilon^4) , \\
\gamma_T^* &= 0 .
\end{aligned} \tag{4.83}$$

The other two Heisenberg style fixed points are saddle points situated at

$$\begin{aligned} x &= -0.854446 - 0.212078\epsilon - 0.647751\epsilon^2 + O(\epsilon^3), \\ y &= 18.789145 + 9.197094\epsilon - 2.733818\epsilon^2 + O(\epsilon^3), \\ z &= 0, \quad t = 0, \quad w = 0 \end{aligned} \quad (4.84)$$

and

$$\begin{aligned} x &= 0.983210 - 0.011253\epsilon + 0.063259\epsilon^2 + O(\epsilon^3), \\ y &= 16.345805 + 10.658027\epsilon + 21.524495\epsilon^2 + O(\epsilon^3), \\ z &= 0, \quad t = 0, \quad w = 0. \end{aligned} \quad (4.85)$$

There is also one AU fixed point which is UV stable at

$$\begin{aligned} x &= 0, \quad y = 0, \quad t = 0, \\ z &= 0.998006 + 0.007339\epsilon - 0.009793\epsilon^2 + O(\epsilon^3), \\ w &= 5.318846 + 0.901757\epsilon - 1.582315\epsilon^2 + O(\epsilon^3) \end{aligned} \quad (4.86)$$

giving the critical exponents

$$\begin{aligned} \gamma_\phi^* &= 0.001992\epsilon - 0.003615\epsilon^2 - 0.000789\epsilon^3 + O(\epsilon^4), \\ \gamma_\sigma^* &= 0, \\ \gamma_T^* &= 0.996016\epsilon + 0.007374\epsilon^2 + 0.003032\epsilon^3 + O(\epsilon^4). \end{aligned} \quad (4.87)$$

To illustrate the full spectrum of fixed points for one particular value of N we provide the remaining fixed points at $N = 1000$. In addition to other real solutions which do not fit the CS, Heisenberg and AU pattern, we have complex solutions. Note that we have so far excluded solutions related by symmetries and will continue to do so here to reduce the overall number of solutions. Note that by symmetric we mean $g_i \leftrightarrow -g_i$ type reflections. First, we state the complex fixed points of the CS type. There are five sets of these, the first is located at

$$\begin{aligned} x &= (0.030988i - 0.117059) + (0.225504 - 0.026447i)\epsilon \\ &\quad + (0.141512 + 0.0220556i)\epsilon^2 + O(\epsilon^3), \\ y &= (10.616979i + 7.410016) + (-0.306607 + 5.10124i)\epsilon \\ &\quad + (-3.30970 + 5.02141i)\epsilon^2 + O(\epsilon^3), \\ z &= (0.041381i + 0.950398) + (0.073839 - 0.000086i)\epsilon \\ &\quad + (-0.076593 + 0.240769i)\epsilon^2 + O(\epsilon^3), \end{aligned}$$

$$\begin{aligned}
t &= (-3.598246i + 9.770473) + (2.741560 - 4.671500i)\epsilon \\
&\quad + (17.262953 - 21.70028i)\epsilon^2 + O(\epsilon^3), \\
w &\in \{(12.52843i - 8.437892) + (-0.081315 + 6.488068i)\epsilon \\
&\quad + (79.099646 + 19.016683i)\epsilon^2 + O(\epsilon^3), \\
&\quad (-8.157796i + 0.215249) + (10.458651 + 2.563357i)\epsilon \\
&\quad + (-13.448748 + 143.623375i)\epsilon^2 + O(\epsilon^3), \\
&\quad (-4.370634i + 8.222643) + (-1.841641 - 7.930799i)\epsilon \\
&\quad + (5.191836 - 47.804171i)\epsilon^2 + O(\epsilon^3)\} \tag{4.88}
\end{aligned}$$

where we have grouped three solutions together given that the only difference is the location of the w critical couplings. The remaining solutions are

$$\begin{aligned}
x &= (-0.003823i + 1.005167) + (-0.054618 + 0.012486i)\epsilon \\
&\quad + (0.018976 + 0.143820i)\epsilon^2 + O(\epsilon^3) \\
y &= (2.003185i + 18.658117) + (5.392312 + 1.086468i)\epsilon \\
&\quad + (14.851433 - 19.827819i)\epsilon^2 + O(\epsilon^3) \\
z &= (0.008575i + 1.025642) + (-0.085717 - 0.009151i)\epsilon \\
&\quad + (-0.006651 - 0.017253i)\epsilon^2 + O(\epsilon^3) \\
t &= (-4.466842i + 8.052554) + (4.210604 + 3.034436i)\epsilon \\
&\quad + (8.671652 + 12.119131i)\epsilon^2 + O(\epsilon^3) \\
w &\in \{(15.494072i - 6.618774) + (6.586489 - 2.039527i)\epsilon \\
&\quad + (160.338535 - 22.392846i)\epsilon^2 + O(\epsilon^3), \\
&\quad (-2.718385i + 6.100016) + (3.357728 + 1.279947i)\epsilon \\
&\quad + (12.015204 + 7.083669i)\epsilon^2 + O(\epsilon^3), \\
&\quad (-12.775687i + 0.518757) + (0.842674 + 1.030180i)\epsilon \\
&\quad + (56.581857 + 57.905307i)\epsilon^2 + O(\epsilon^3)\}, \tag{4.89}
\end{aligned}$$

$$\begin{aligned}
x &= (0.050822i - 0.763449) + (-0.342230 - 0.090513i)\epsilon \\
&\quad + (-1.048864 - 0.055624i)\epsilon^2 + O(\epsilon^3), \\
y &= (7.435673i + 12.90737) + (11.071087 + 3.990671i)\epsilon \\
&\quad + (10.916564 + 32.815621i)\epsilon^2 + O(\epsilon^3), \\
z &= (0.0450638i + 0.849646) + (0.197056 - 0.055744i)\epsilon \\
&\quad + (0.452791 + 0.136376i)\epsilon^2 + O(\epsilon^3), \\
t &= (-1.982473i + 12.903491) + (6.044935 - 1.720892i)\epsilon
\end{aligned}$$

$$\begin{aligned}
& + (6.597369 - 13.346172i)\epsilon^2 + O(\epsilon^3), \\
w \in & \{(6.421453i - 11.600963) + (-2.494744 + 2.659224i)\epsilon \\
& + (12.554273 + 26.208510i)\epsilon^2 + O(\epsilon^3), \\
& (-3.154923i + 14.29153) + (7.238628 - 2.639826i)\epsilon \\
& + (4.840108 - 21.122141i)\epsilon^2 + O(\epsilon^3), \\
& (-3.266530i - 2.690567) + (1.337926 + 0.955634i)\epsilon \\
& + (33.890419 + 26.868026i)\epsilon^2 + O(\epsilon^3)\} \tag{4.90}
\end{aligned}$$

$$\begin{aligned}
x & = (-0.555294i - 1.513381) + (-23.114452 + 24.950148i)\epsilon \\
& + (3858.041480 + 2762.998578i)\epsilon^2 + O(\epsilon^3), \\
y & = (34.90363i - 21.842603) + (890.252852 + 680.087930i)\epsilon \\
& + (74550.859506 - 131881.754919i)\epsilon^2 + O(\epsilon^3), \\
z & = (0.549418i + 1.214497) + (24.255203 - 14.435870i)\epsilon \\
& + (-2470.779282 - 3096.675176i)\epsilon^2 + O(\epsilon^3), \\
t & = (-29.55207i + 15.18796) + (-850.256009 - 539.584442i)\epsilon \\
& + (-56438.610729 + 124039.167626i)\epsilon^2 + O(\epsilon^3), \\
w \in & \{(42.91263i - 23.15191) + (1127.488695 + 813.413116i)\epsilon \\
& + (82884.915451 - 172830.465074i)\epsilon^2 + O(\epsilon^3), \\
& (0.409667i + 1.270019) + (35.031670 + 22.655513i)\epsilon \\
& + (1486.251233 - 4603.586046i)\epsilon^2 + O(\epsilon^3), \\
& (-43.32229i + 21.88189) + (-1155.605341 - 813.415117i)\epsilon \\
& + (-84174.229119 + 179594.341857i)\epsilon^2 + O(\epsilon^3)\}, \tag{4.91}
\end{aligned}$$

and

$$\begin{aligned}
x & = (-0.006320i - 1.030086) + (0.107095 + 0.043240i)\epsilon \\
& + (-0.036554 + 0.122859i)\epsilon^2 + O(\epsilon^3), \\
y & = (2.138785i - 9.592803) + (-5.961631 - 11.215238i)\epsilon \\
& + (-22.616924 - 62.894519i)\epsilon^2 + O(\epsilon^3), \\
z & = (0.002767i + 1.0176108) + (-0.059037 - 0.021032i)\epsilon \\
& + (0.043635 - 0.043068i)\epsilon^2 + O(\epsilon^3), \\
t & = (1.198860i - 8.255330) + (-2.187227 - 7.108184i)\epsilon \\
& + (-8.358400 - 32.699994i)\epsilon^2 + O(\epsilon^3), \\
w \in & \{(13.36369i - 4.799020) + (10.845688 - 1.270978i)\epsilon
\end{aligned}$$

$$\begin{aligned}
& + (139.104337 - 28.027224i)\epsilon^2 + O(\epsilon^3), \\
& (-12.50645i - 2.865408) + (-1.424629 - 4.030314i)\epsilon \\
& + (67.742495 + 17.073470i)\epsilon^2 + O(\epsilon^3), \\
& (-0.857238i + 7.664428) + (1.116387 + 5.387238i)\epsilon \\
& + (4.573636 + 22.217349i)\epsilon^2 + O(\epsilon^3) \}. \tag{4.92}
\end{aligned}$$

There are also several sets of solutions where some of the fixed points are either real or imaginary in addition to one being fully complex

$$\begin{aligned}
x & = 0.114419i - 0.553587i\epsilon + 6.740110i\epsilon^2 + O(\epsilon^3), \\
y & = 22.486625i - 31.203475i\epsilon + 603.274688i\epsilon^2 + O(\epsilon^3), \\
z & = 1.070456 - 0.504440\epsilon + 9.518801\epsilon^2 + O(\epsilon^3), \\
t & = -11.601013i + 36.808088i\epsilon - 722.589642i\epsilon^2 + O(\epsilon^3), \\
w & \in \{(22.427674i - 1.617314) + (1.687428 - 38.335633i)\epsilon \\
& + (255.539793 + 718.517860i)\epsilon^2 + O(\epsilon^3), \\
& 3.234627 + 8.891244\epsilon - 144.067750\epsilon^2 + O(\epsilon^3)\} \tag{4.93}
\end{aligned}$$

and

$$\begin{aligned}
x & = -0.868555 - 0.203744\epsilon - 0.915849\epsilon^2 + O(\epsilon^3), \\
y & = 19.811433 + 7.966436\epsilon - 15.205442\epsilon^2 + O(\epsilon^3), \\
z & = 1.012581 - 0.020942\epsilon + 0.066905\epsilon^2 + O(\epsilon^3), \\
t & = -4.342552 - 2.231269\epsilon - 7.303390\epsilon^2 + O(\epsilon^3), \\
w & = (15.014668i - 2.955662) + (4.805741 + 1.917129i)\epsilon \\
& + (111.835693 - 52.975405i)\epsilon^2 + O(\epsilon^3). \tag{4.94}
\end{aligned}$$

This completes the set of all CS style solutions. For the remainder of the solutions we found that at least one of the critical couplings were zero. First we group solutions where the couplings were either real or imaginary and found

$$\begin{aligned}
x & = 0, \quad t = 0, \\
y & = 14.907120i + 11.502407i\epsilon - 10.399304i\epsilon^2 + O(\epsilon^3), \\
z & = 0.998006 + 0.007339\epsilon - 0.009793\epsilon^2 + O(\epsilon^3), \\
w & \in \{(15.559942i - 2.659423) + (4.519271 + 2.244641i)\epsilon \\
& + (110.184708 - 62.342815i)\epsilon^2 + O(\epsilon^3), \\
& 5.318846 + 0.901757\epsilon - 1.582315\epsilon^2 + O(\epsilon^3)\} \tag{4.95}
\end{aligned}$$

and

$$\begin{aligned}
x &= 0, & z &= 0, & t &= 0, \\
y &= 14.907120i + 11.502407i\epsilon - 10.399304i\epsilon^2 + O(\epsilon^3), \\
w &\in \{10.540926 + 8.344899\epsilon - 16.563109\epsilon^2 + O(\epsilon^3), 0\}. \quad (4.96)
\end{aligned}$$

Included in the first set is a complex w coupling. However the remaining solutions have an imaginary y coupling and real or no w critical coupling. This is an example which is similar to pure ϕ^3 theory when its coupling is purely imaginary. That particular $O(N)$ model describes the Lee-Yang edge singularity problem, [170]. Additionally the solution (4.96) corresponds to the Lagrangian without a ϕ^{ia} field. In the case of the only non-zero coupling y this is the pure cubic theory involving only the σ field. The remaining solutions with any complex roots all have vanishing critical z couplings and are located at

$$\begin{aligned}
x &= (0.102517i - 1.069257) + (-0.187674 - 0.485282i)\epsilon, \\
&\quad + (6.388101 + 3.227418i)\epsilon^2 + O(\epsilon^3) \\
y &= (8.388316i + 4.182323) + (-31.690792 - 0.719078i)\epsilon, \\
&\quad + (394.496262 - 256.273660i)\epsilon^2 + O(\epsilon^3), \\
z &= 0, \\
t &= (-12.684990i - 5.204227) + (23.207111 + 4.566306i)\epsilon \\
&\quad + (-270.175902 + 154.130691i)\epsilon^2 + O(\epsilon^3), \\
w &\in \{(13.394284i + 8.214396) + (-30.663870 - 17.742257i)\epsilon \\
&\quad + (479.083975 - 270.124833i)\epsilon^2 + O(\epsilon^3), 0\} \quad (4.97)
\end{aligned}$$

and

$$\begin{aligned}
x &= 0, & z &= 0, \\
y &= (12.918644i + 4.311494) + (2.006636 + 9.961474i)\epsilon \\
&\quad + (-0.372460 - 5.181172i)\epsilon^2 + O(\epsilon^3), \\
t &= (9.765251i - 1.446829) + (-0.575941 + 7.513693i)\epsilon \\
&\quad + (-1.501827 - 7.061748i)\epsilon^2 + O(\epsilon^3), \\
w &\in \{(7.382858i - 3.189516) + (-1.150870 + 6.001629i)\epsilon \\
&\quad + (-0.334518 - 6.569977i)\epsilon^2 + O(\epsilon^3), 0\}. \quad (4.98)
\end{aligned}$$

The remainder of the solutions are real but interesting patterns emerge in several cases. First we record the fixed points where there is no pairing with another set.

There were four such cases. Of all the real solutions we find only the first two correspond to UV stable fixed points which are located at

$$\begin{aligned}
x &= 1.011102 - 0.026162\epsilon + 0.022238\epsilon^2 + O(\epsilon^3), \\
y &= 6.637801 - 1.117476\epsilon + 0.962982\epsilon^2 + O(\epsilon^3), \\
z &= 0, \quad t = 0, \\
w &= 10.540926 + 8.344899\epsilon - 16.563109\epsilon^2 + O(\epsilon^3) \quad (4.99)
\end{aligned}$$

and

$$\begin{aligned}
x &= 0, \quad y = 0, \quad z = 0, \quad t = 0, \\
w &= 10.540926 + 8.344899\epsilon - 16.563109\epsilon^2 + O(\epsilon^3). \quad (4.100)
\end{aligned}$$

The second solution of (4.100) corresponds to the pure T^{ab} theory when $m = 2$ but the $(0, 0, 0, 0, w)$ structure could be analysed in isolation for arbitrary m . The stability of these two fixed points appears to be driven by the vanishing of the couplings g_3 and g_4 . In this case there is no interaction whatsoever between the pair of fields $\{\phi^{ia}, \sigma\}$ and T^{ab} which is apparent when looking at $L^{(LGW6)}$. In other words, one is dealing with a partitioned Lagrangian and the coupling constant space is also partitioned. So the stability here is a reflection of the stability of the two separate Lagrangian's. In the second of these two stable solutions the situation is effectively trivial since it reflects that one of the two partitioned Lagrangian's is a free field theory which has a zero β -function. That such solutions representing the sum of independent Lagrangian's emerge ought not to be a surprise and should be regarded as an internal consistency check in our analysis of solutions.

The remaining unpaired solutions which are not stable are located at

$$\begin{aligned}
x &= -0.854446 - 0.212078\epsilon - 0.647751\epsilon^2 + O(\epsilon^3), \\
y &= 18.789145 + 9.197094\epsilon - 2.733818\epsilon^2 + O(\epsilon^3), \\
z &= 0, \quad t = 0, \\
w &= 10.540926 + 8.344899\epsilon - 16.563109\epsilon^2 + O(\epsilon^3) \quad (4.101)
\end{aligned}$$

and

$$\begin{aligned}
x &= 0.983210 - 0.011253\epsilon + 0.063259\epsilon^2 + O(\epsilon^3), \\
y &= 16.345805 + 10.658027\epsilon + 21.524495\epsilon^2 + O(\epsilon^3), \\
z &= 0, \quad t = 0,
\end{aligned}$$

$$w = 10.540926 + 8.344899\epsilon - 16.563109\epsilon^2 + O(\epsilon^3). \quad (4.102)$$

Analysing the stability matrix we find that these solutions are saddle points. For the paired solutions we have

$$\begin{aligned} x &= 0.986386 + 0.006824\epsilon + 0.023890\epsilon^2 + O(\epsilon^3) \\ y &= 3.882413 + 3.856888\epsilon + 1.139387\epsilon^2 + O(\epsilon^3) \\ z &= 0 \\ t &= -6.810006 + 3.229867\epsilon + 5.755896\epsilon^2 + O(\epsilon^3) \\ w &\in \{13.726061 + 3.729174\epsilon - 29.707955\epsilon^2 + O(\epsilon^3), 0\} \end{aligned} \quad (4.103)$$

and

$$\begin{aligned} x &= 0, \quad z = 0, \\ y &= 17.222217 + 37.874140\epsilon + 404.846200\epsilon^2 + O(\epsilon^3), \\ t &= -13.657731 - 33.103835\epsilon - 376.517213\epsilon^2 + O(\epsilon^3), \\ w &\in \{20.542650 + 42.608899\epsilon + 533.442168\epsilon^2 + O(\epsilon^3), 0\} \end{aligned} \quad (4.104)$$

which are also saddle points. The final three pairings exhibit a novel feature in that in each set the critical x and t couplings are equal

$$\begin{aligned} x &= -0.854046 - 0.211934\epsilon - 0.647273\epsilon^2 + O(\epsilon^3), \\ y &= 18.789012 + 9.196991\epsilon - 2.731101\epsilon^2 + O(\epsilon^3), \\ z &= 0, \\ t &= -0.854046 - 0.211934\epsilon - 0.647273\epsilon^2 + O(\epsilon^3), \\ w &\in \{-10.598432 + 8.327096\epsilon - 16.655991\epsilon^2 + O(\epsilon^3), 0\}, \end{aligned} \quad (4.105)$$

$$\begin{aligned} x &= 0.982680 - 0.011165\epsilon + 0.063307\epsilon^2 + O(\epsilon^3), \\ y &= 16.347740 + 10.655223\epsilon + 21.515017\epsilon^2 + O(\epsilon^3), \\ z &= 0, \\ t &= 0.982680 - 0.011165\epsilon + 0.063307\epsilon^2 + O(\epsilon^3), \\ w &\in \{10.616993 + 8.279650\epsilon - 16.867303\epsilon^2 + O(\epsilon^3), 0\} \end{aligned} \quad (4.106)$$

and

$$\begin{aligned} x &= 1.010586 - 0.0261234\epsilon + 0.022211\epsilon^2 + O(\epsilon^3), \\ y &= 6.633618 - 1.114926\epsilon + 0.960725\epsilon^2 + O(\epsilon^3) \end{aligned}$$

$$\begin{aligned}
z &= 0, \\
t &= 1.010586 - 0.026124\epsilon + 0.022211\epsilon^2 + O(\epsilon^3), \\
w &\in \{10.621358 + 8.274362\epsilon - 16.895995\epsilon^2 + O(\epsilon^3), 0\}. \quad (4.107)
\end{aligned}$$

While our focus here was on $O(1000) \times O(2)$ theory it represents a snapshot of the spectrum of potential solutions for the general symmetry group. What has emerged are both real and complex fixed point solutions in addition to the Heisenberg, chiral stable and anti-chiral unstable types which were motivated by the four dimensional theory.

Next we move on to analyse a lower value of N in order to illustrate a change in the fixed point pattern. At $N = 600$ we have one CS style fixed point solution which is a saddle point positioned at

$$\begin{aligned}
x &= -0.862204 - 0.222460\epsilon - 1.255729\epsilon^2 + O(\epsilon^3), \\
y &= 15.871131 + 5.764114\epsilon - 20.128689\epsilon^2 + O(\epsilon^3), \\
z &= 1.020205 - 0.031243\epsilon + 0.133767\epsilon^2 + O(\epsilon^3), \\
t &= -4.133094 - 2.641545\epsilon - 10.197488\epsilon^2 + O(\epsilon^3), \\
w &= 5.794456 + 1.264133\epsilon + 7.071880\epsilon^2 + O(\epsilon^3). \quad (4.108)
\end{aligned}$$

In addition there are three Heisenberg style fixed points with the one located at

$$\begin{aligned}
x &= 1.018022 - 0.037843\epsilon + 0.001985\epsilon^2 + O(\epsilon^3), \\
y &= 7.507506 - 4.490389\epsilon + 9.490485\epsilon^2 + O(\epsilon^3), \\
z &= 0, \quad t = 0, \quad w = 0 \quad (4.109)
\end{aligned}$$

being UV stable giving the following critical exponents

$$\begin{aligned}
\gamma_\phi^* &= 0.001727\epsilon - 0.003465\epsilon^2 - 0.000010\epsilon^3 + O(\epsilon^4), \\
\gamma_\sigma^* &= 1.083337\epsilon - 0.195953\epsilon^2 + 0.089727\epsilon^3 + O(\epsilon^4), \\
\gamma_T^* &= 0. \quad (4.110)
\end{aligned}$$

The other two fixed points are saddle points at

$$\begin{aligned}
x &= -0.839313 - 0.232926\epsilon - 0.736639\epsilon^2 + O(\epsilon^3), \\
y &= 14.602366 + 7.174642\epsilon - 3.193826\epsilon^2 + O(\epsilon^3), \\
z &= 0, \quad t = 0, \quad w = 0 \quad (4.111)
\end{aligned}$$

and

$$\begin{aligned}
x &= 1.007039 - 0.068389\epsilon + 0.063230\epsilon^2 + O(\epsilon^3), \\
y &= 11.302398 + 11.995559\epsilon + 13.765855\epsilon^2 + O(\epsilon^3), \\
z &= 0, \quad t = 0, \quad w = 0.
\end{aligned} \tag{4.112}$$

There is also one AU fixed point which is UV stable located at

$$\begin{aligned}
x &= 0, \quad y = 0, \quad t = 0 \\
z &= 0.996683 + 0.012238\epsilon - 0.015305\epsilon^2 + O(\epsilon^3), \\
w &= 5.033838 + 1.165363\epsilon - 2.476601\epsilon^2 + O(\epsilon^3)
\end{aligned} \tag{4.113}$$

with critical exponents

$$\begin{aligned}
\gamma_\phi^* &= 0.003311\epsilon - 0.005969\epsilon^2 - 0.001383\epsilon^3 + O(\epsilon^4), \\
\gamma_\sigma^* &= 0, \\
\gamma_T^* &= 0.993377\epsilon + 0.012333\epsilon^2 + 0.006784\epsilon^3 + O(\epsilon^4).
\end{aligned} \tag{4.114}$$

The fixed point spectra at $N = 600$ for the Heisenberg and AU cases have been illustrated in figures 4.28 and 4.29. Note that both plots include the trivial $(0, 0)$ Gaussian fixed point which appears unstable given the direction of the UV flow arrows. The Heisenberg and AU graphs illustrate the UV stable fixed points well with arrow flow direction towards this fixed point. Additional fixed points appear on both plots which are generated by symmetry relations where $g_i \leftrightarrow -g_i$. We have recorded the spectrum at $N = 600$ to contrast it with lower values of N . For $N = 519$ we have one CS style fixed point which is a saddle point located at

$$\begin{aligned}
x &= -0.860686 - 0.228611\epsilon - 1.395472\epsilon^2 + O(\epsilon^3), \\
y &= 14.937476 + 5.238428\epsilon - 21.686769\epsilon^2 + O(\epsilon^3), \\
z &= 1.023093 - 0.0347571\epsilon + 0.165366\epsilon^2 + O(\epsilon^3), \\
t &= -4.069923 - 2.780163\epsilon - 11.373918\epsilon^2 + O(\epsilon^3), \\
w &= 5.750244 + 1.435664\epsilon + 8.435080\epsilon^2 + O(\epsilon^3).
\end{aligned} \tag{4.115}$$

However we now have only one Heisenberg style fixed point which is a saddle point at

$$\begin{aligned}
x &= -0.834431 - 0.239444\epsilon - 0.765623\epsilon^2 + O(\epsilon^3), \\
y &= 13.591847 + 6.689873\epsilon - 3.246649\epsilon^2 + O(\epsilon^3),
\end{aligned}$$

$$z = 0, \quad t = 0, \quad w = 0. \quad (4.116)$$

In addition there is one UV stable AU type fixed point positioned at

$$\begin{aligned} x &= 0, & y &= 0, & t &= 0, \\ z &= 0.996169 + 0.014150\epsilon - 0.017238\epsilon^2 + O(\epsilon^3), \\ w &= 4.941667 + 1.239792\epsilon - 2.803418\epsilon^2 + O(\epsilon^3) \end{aligned} \quad (4.117)$$

giving critical exponents

$$\begin{aligned} \gamma_\phi^* &= 0.003824\epsilon - 0.006875\epsilon^2 - 0.0016281\epsilon^3 + O(\epsilon^4), \\ \gamma_\sigma^* &= 0, \\ \gamma_T^* &= 0.992352\epsilon + 0.014277\epsilon^2 + 0.008615\epsilon^3 + O(\epsilon^4). \end{aligned} \quad (4.118)$$

Therefore between $N = 600$ and $N = 519$ the behaviour of the Heisenberg style fixed point changes. This seems to indicate that a conformal window type region exists with respect to the Heisenberg structure and thus there is a new conformal window between $N = 519$ and $N = 600$. The actual location is not of major significance in the context of the LGW theory as this in effect corresponds to the original Heisenberg model with no T^{ab} field. We have illustrated the Heisenberg and AU fixed point stability structure for $N = 519$ in plots 4.30 and 4.31. The AU plot is similar to that of $N = 600$. There is one UV stable fixed point along with the trivial fixed point. However the Heisenberg plot is very different, we now have one saddle point which is mirrored in both axes due to symmetry relations. The final case we consider in detail is $N = 2$. It is of potential interest as for this value in a variety of models a supersymmetric solution emerges, [52, 170, 227].

At $N = 2$ we have three CS style fixed points, all of which are saddle points at

$$\begin{aligned} x &= -0.454392 - 1.128422\epsilon - 10.883437\epsilon^2 + O(\epsilon^3), \\ y &= 0.673205 + 1.783387\epsilon + 15.854883\epsilon^2 + O(\epsilon^3), \\ z &= 0.318954 + 0.395758\epsilon + 3.102196\epsilon^2 + O(\epsilon^3), \\ t &= 0.379850 + 0.510247\epsilon + 4.361634\epsilon^2 + O(\epsilon^3). \end{aligned} \quad (4.119)$$

The value for the coupling w has not been provided with the others as a novel feature emerged for this set. It transpired that there were three fixed points with the same x , y , z and t values but differing only in the w value. Therefore, we

note these values separately as

$$\begin{aligned}
w \in & \{0.717916 + 0.824313\epsilon + 5.193907\epsilon^2 + O(\epsilon^3), \\
& - 0.267715 - 0.020190\epsilon + 0.685452\epsilon^2 + O(\epsilon^3), \\
& - 0.450201 - 0.479646\epsilon - 3.632751\epsilon^2 + O(\epsilon^3)\} . \quad (4.120)
\end{aligned}$$

There was one Heisenberg fixed point, which is a saddle point located at

$$\begin{aligned}
x &= -0.470736 - 0.737444\epsilon - 5.708527\epsilon^2 + O(\epsilon^3) , \\
y &= 0.762184 + 0.999917\epsilon + 6.174478\epsilon^2 + O(\epsilon^3) , \\
z &= 0 , \quad t = 0 , \quad w = 0 . \quad (4.121)
\end{aligned}$$

In addition there was one AU fixed point which is UV stable at

$$\begin{aligned}
x &= 0 , \quad y = 0 , \quad t = 0 , \\
z &= 0.577350 + 1.507526\epsilon + 19.533564\epsilon^2 + O(\epsilon^3) , \\
w &= 0.800625 + 1.806817\epsilon + 27.377665\epsilon^2 + O(\epsilon^3) \quad (4.122)
\end{aligned}$$

with critical exponents

$$\begin{aligned}
\gamma_\phi^* &= \gamma_T^* = 0.333333\epsilon + 1.333333\epsilon^2 + 22.148148\epsilon^3 + O(\epsilon^4) , \\
\gamma_\sigma^* &= 0 . \quad (4.123)
\end{aligned}$$

One property of the emergent supersymmetric solutions found in earlier work [52, 170, 227] was that the critical couplings were equivalent. For this AU style solution a different feature is apparent which is that the exponents of ϕ^{ia} and T^{ab} are equal.

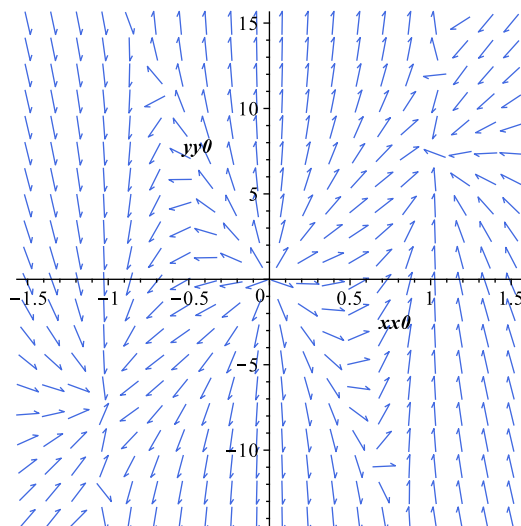


Figure 4.28: Fixed point UV stability flow of the Heisenberg fixed points, $(x, y, 0, 0, 0)$, for $O(600) \times O(2)$. Heisenberg fixed point located at $(x, y) = (1.02, 7.51)$

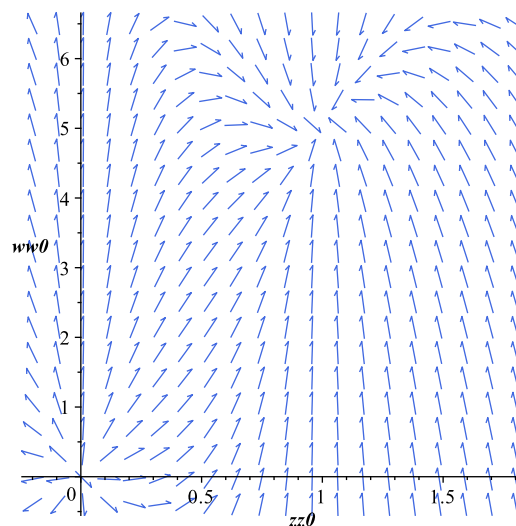


Figure 4.29: Fixed point UV stability flow of the Anti-chiral unstable fixed points, $(0, 0, z, 0, w)$, for $O(600) \times O(2)$. AU fixed point located at $(z, w) = (1.00, 5.03)$

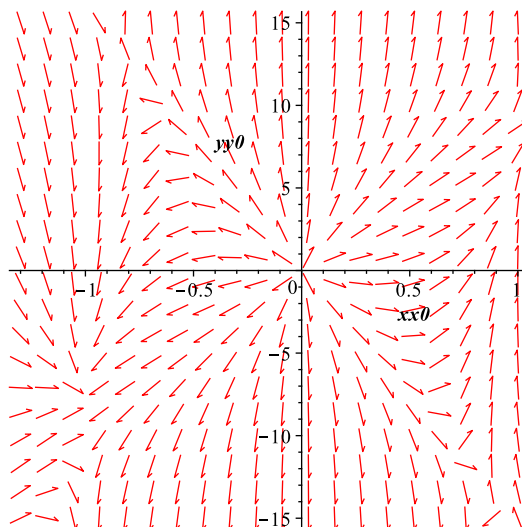


Figure 4.30: Fixed point UV stability flow of the Heisenberg fixed points, $(x, y, 0, 0, 0)$, for $O(519) \times O(2)$. Heisenberg fixed point located at $(x, y) = (-0.83, 13.59)$

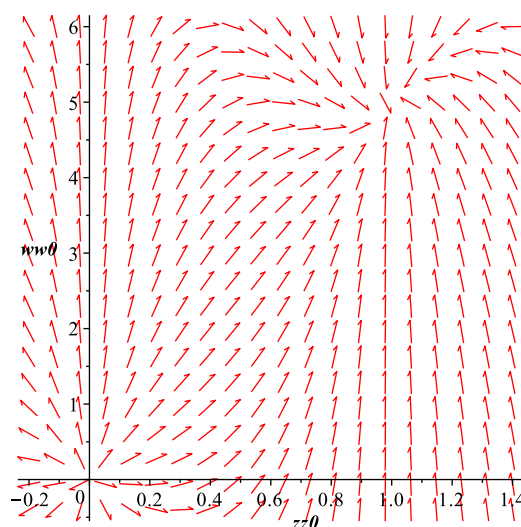


Figure 4.31: Fixed point UV stability flow of the Anti-chiral unstable fixed points, $(0, 0, z, 0, w)$, for $O(519) \times O(2)$. AU fixed point located at $(z, w) = (1.00, 4.94)$

4.10 Discussion

We have provided a comprehensive three loop analysis for the extension of the four dimensional Landau-Ginzburg-Wilson $O(N) \times O(m)$ symmetric theory to six dimensions. The universality between these two theories relies on a common

interaction which seeds the theories in four and six space-time dimensions along the thread of the Wilson-Fisher fixed point in d -dimensions. One reassuring aspect of our computation is the verification that the three loop Renormalization Group functions are consistent with the large N critical exponents of [218]. This gives confidence to the universality class as a whole as well as for the inclusion of the six dimensional extension we constructed. One consequence of the large number of coupling constants present in the six dimensional LGW theory is a richer spectrum of fixed points for specific values of N and m . Our analysis concentrated on $m = 2$ due to interest in the $O(N) \times O(2)$ model, although we do not expect the general picture of fixed points to differ conceptually for higher values of m . The primary difference will be in the boundary values which will be at different values of N for the AU conformal window. Our $m = 2$ analysis is similar to the $O(N)$ case of [52] with real and complex critical couplings present, the latter corresponding to non-unitary theories. However for real solutions we were able to isolate fixed points which had a structure in keeping with the phase plane in the four dimensional model. Their stability was studied for certain values of N . One main area of interest in this calculation, as well as in the previous $O(N)$ analysis, is whether the fixed point in five dimensions exists and if so what is its conformal window. In [59] a bootstrap study indicated that this was not an easy exercise from the lower dimensional point of view unless one was examining AU type coupling patterns. Our investigation left us with a similar conclusion. Although we were able to narrow down the leading order value of the window for CS type solutions for $m = 2$. By contrast we could solve the AU set of equations and found that a window exists above $m = 5$.

The full set of data for the Renormalization Group functions has been provided which can be mined for future studies for other values of m . As the $O(N) \times O(m)$ symmetric theory has a richer structure than the initial computation of $O(N)$ theory, this calculation again provides a good testing ground for looking into ideas on universality and conformal windows. Furthermore it opens up the gateway to model building and beyond the Standard Model (BSM) physics. Akin to the connections in both the $O(N)$ and $O(N) \times O(m)$ universality classes, one question which has been considered is what if any is the higher dimensional theory which is in the same universality class as the Banks-Zaks fixed point in QCD. It is known that QCD is in the same universality class as the non-abelian Thirring model in the large N_f expansion, [228]. QCD is perturbatively renormalizable in four space-time dimensions, while the Thirring model is perturbatively renormalizable in two dimensions. Here N_f refers to the number of massless quark flavours and not the numbers of colours N_c present in the theory. Large N_f critical exponents

to varying orders in N_f have been calculated, [229–231], and matched with exponents computed in both the Thirring model and QCD. The RG functions for the six dimensional extension to QCD were calculated in [54] to two loops. The corresponding critical exponents were also matched with known large N_f exponents, providing confidence in the universality. One important feature that was found in six dimensional QCD was the conformal window which was found to be located at $N_f = 16$ for the $SU(3)$ colour group, [54]. Extra coupling constants in the six dimensional Lagrangian produced a rich fixed point spectrum and if analysed in d -dimensions several of these may be connected to the non-trivial and non-perturbative fixed points in the companion lower dimensional model.

An interesting point to note is that six dimensional QCD was found to have strong structural similarities to the eight dimensional scalar theory with $O(N)$ symmetry, [54]. The QCD universality class has since been extended to eight-dimensions with RG functions calculated to one loop, [70]. QCD is not the only gauge theory which has gained interest from the point of view of universality classes. The six and eight dimensional extensions of Quantum Electrodynamics (QED) have also recently been studied, [54,69]. Furthermore the renormalization of the two dimensional Gross-Neveu model with $O(N)$ and $SU(N)$ symmetry has been performed to four loops, [232]. This was looked at as it is a model which is thought to have structural similarities with four dimensional QCD. Additionally the six dimensional scalar ϕ^3 theory with an F_4 symmetry to four loops has been looked at in the $\overline{\text{MS}}$ scheme, [233], with the primary aim being to complement recent bootstrap results. It also provided contrasting evidence to bootstrap claims that only non-perturbative techniques could be used for this particular model. Finally the renormalization of scalar field theories in rational space-time dimensions has been computed, [226]. These are theories with ϕ^n self interactions such as $n = 5, 7$ and 9 in their respective critical dimensions which are non-integer. This provides a non-trivial $O(N)$ symmetric extension. It is hoped that analysing fixed points of higher dimensional gauge theories and their conformal windows could give an insight into physics beyond the Standard Model. For example higher dimensional operators may continue to be relevant in four dimensions and drive the infrared dynamics. Additionally modern observations suggest there may be dualities with higher spin AdS/CFT theories which are related to six dimensional ϕ^3 theory which also has applications to quantum gravity through asymptotic safety, [56].

Higher Derivative Higher Dimensional Quantum Field Theory

5.1 Introduction

The Wilson-Fisher fixed point has provided a remarkable basis for tackling a variety of different problems in physics, [41, 44, 155]. In Chapter 3 we looked at extending the ϕ^4 universality class to ten dimensions, which is sometimes termed an ultraviolet (UV) completion. In Chapter 4 we looked at a different universality class with a more complex symmetry group. Central to these connections was the Wilson-Fisher fixed point and underlying critical Renormalization Group (RG) equation which is a core property in d -dimensions, [41, 44, 155]. The connection between theories is constructed by explicit perturbative renormalization of the respective higher dimensional $O(N)$ symmetric scalar theories and, in addition, knowledge of the critical exponents of the universal theory in arbitrary space-time dimension. The latter is possible through a perturbative expansion in the parameter $1/N$. As the $O(N)$ ϕ^4 tower of theories has been studied extensively, our aim here is to establish a new universality class and provide the corresponding perturbative and large N results to verify the underlying universality of this new tower. Importantly this new universality class will contain theories incorporating higher derivative kinetic terms.

In order to motivate the study of these higher derivative scalar theories we review the basic ϕ^4 Lagrangian endowed with $O(N)$ symmetry which is pertur-

batively renormalizable in four dimensions

$$L^{(4)} = \frac{1}{2} \partial_\mu \phi^i \partial^\mu \phi^i + \frac{g_1}{2} \sigma \phi^i \phi^i - \frac{1}{2} \sigma^2. \quad (5.1)$$

Recall that in Chapter 3 we discussed how σ was introduced as an auxiliary field in equations (3.1) and (3.2). This version of the Lagrangian is the starting point for the large N construction provided by [48–50]. Using dimensional analysis the dimension of the fields ϕ^i and σ , defined as α and β , were found in (2.58) and are restated here

$$\begin{aligned} [\phi^i] &= \alpha = \frac{d}{2} - 1 + \frac{\eta}{2}, \\ [\sigma] &= \beta = 2 - \eta - \chi. \end{aligned} \quad (5.2)$$

The canonical dimensions of the fields are determined by a dimensional analysis of the Lagrangian with the proviso that the action S is dimensionless. The space-time dimension enters via the d -dimensional measure associated with the relation between the Lagrangian and the action. The quantities η and χ correspond to critical exponents and are a measure of quantum corrections. To establish the ultraviolet completion of higher derivative $O(N)$ theories we first need to construct the relevant Lagrangians which populate the tower along a common Wilson-Fisher fixed point thread in d -dimensions. One way to proceed is to use the universal interaction as a basis for defining the canonical dimensions of the fields for a specific critical dimension, and then construct the spectator part of the Lagrangian which ensures renormalizability. This will systematically build the tower which is the UV completion of $O(N)$ ϕ^4 theory to six dimensions, [51,52], and higher, [3,53,54].

However we have chosen to begin at another point which is within the universal theory itself but at the critical point. For the established $O(N)$ tower containing the four dimensional Lagrangian (5.1) we note that the canonical dimensions of the fields were determined by dimensionally analysing the kinetic term for ϕ^i and the universal interaction. They satisfy the relation

$$2\alpha + \beta = d - \chi. \quad (5.3)$$

However the values of α and β given by equation (5.2) are not the only solutions which satisfy relation (5.3). Moreover this is not the only way to consider the dimensional analysis within the universal theory. Instead of using the kinetic term for ϕ^i and the interaction to find α and β we can write down a sequence of solutions to relation (5.3) which includes the values (5.2) as a specific case. This

general solution is

$$\begin{aligned}\alpha &= \frac{d}{2} - n + \frac{\eta}{2}, \\ \beta &= 2n - \eta - \chi\end{aligned}\tag{5.4}$$

where n is any positive integer. The value $n = 1$ gives the result (5.2) which produces the $O(N)$ ϕ^4 universality class. Viewed this way one opens up new threads of towers since the kinetic term for ϕ^i will necessarily involve higher derivatives. Although unlike the scalar field theories considered in [234–236] for example, these will be interacting theories with a conformal symmetry at a fixed point. More specifically the first few Lagrangian's representing the universal theories will be

$$L^{(8)} = \frac{1}{2}(\square\phi^i)^2 + \frac{1}{2}\sigma\phi^i\phi^i - \frac{1}{2g_1^2}\sigma^2\tag{5.5}$$

for $n = 2$, where σ as been rescaled by a power of the coupling. For $n = 3$ we find

$$L^{(12)} = \frac{1}{2}(\square\partial_\mu\phi^i)^2 + \frac{1}{2}\sigma\phi^i\phi^i - \frac{1}{2g_1^2}\sigma^2.\tag{5.6}$$

These Lagrangian's are in the formulation used for the large N expansion. Eliminating the auxiliary field σ produces

$$L^{(8)} = \frac{1}{2}(\square\phi^i)^2 + \frac{g_1^2}{8}(\phi^i\phi^i)^2,\tag{5.7}$$

$$L^{(12)} = \frac{1}{2}(\square\partial_\mu\phi^i)^2 + \frac{g_1^2}{8}(\phi^i\phi^i)^2\tag{5.8}$$

which are the higher derivative kinetic term extensions of scalar $O(N)$ ϕ^4 theory. Our notation is that the Lagrangian $L^{(D_c)}$ is perturbatively renormalizable in D_c dimensions with critical dimension $D_c = 4n$ in terms of the solution (5.4). So the critical dimension for the $n = 2$ thread is eight and for $n = 3$ it is twelve.

The focus for the remainder of the Chapter will be on the $n = 2$ thread, $n = 3$ is covered in [3]. Constructing the UV completion or tower of theories based on $L^{(8)}$ follows the method of the conventional Wilson-Fisher universality class. The key is the use of the canonical dimensions of the two basic fields and the space-time dimension the Lagrangian is to be completed in. In the large N expansion the canonical dimensions are necessarily dimension dependent as the universal theory is space-time transcendent. For the theories which are renormalizable in a fixed (even) dimension one has to use the canonical dimension for that specific dimension. So when $n = 2$, σ has dimension four and ϕ^i has dimension two, three, four, five and six in the even dimensions between eight and sixteen. One

consequence is that in each of these dimensions the $\sigma\phi^i\phi^i$ operator dimension is preserved and moreover no new $\phi^i - \sigma$ interactions can be included. Instead in order to ensure renormalizability in each dimension extra pure σ spectator interactions have to be added which can include derivative interactions similar to Chapter 3. Given this reasoning we find the following higher dimensional extensions of Lagrangian (5.7),

$$\begin{aligned}
L^{(8,10)} &= \frac{1}{2} (\square\phi^i)^2 + \frac{1}{2} \partial_\mu \sigma \partial^\mu \sigma + \frac{g_1}{2} \sigma \phi^i \phi^i, \\
L^{(8,12)} &= \frac{1}{2} (\square\phi^i)^2 + \frac{1}{2} (\square\sigma)^2 + \frac{g_1}{2} \sigma \phi^i \phi^i + \frac{g_2}{6} \sigma^3, \\
L^{(8,14)} &= \frac{1}{2} (\square\phi^i)^2 + \frac{1}{2} (\square\partial^\mu \sigma)^2 + \frac{g_1}{2} \sigma \phi^i \phi^i + \frac{g_2}{6} \sigma^2 \square\sigma, \\
L^{(8,16)} &= \frac{1}{2} (\square\phi^i)^2 + \frac{1}{2} (\square^2\sigma)^2 + \frac{g_1}{2} \sigma \phi^i \phi^i + \frac{g_2}{6} \sigma^2 \square^2\sigma \\
&\quad + \frac{g_3}{2} \sigma (\square\sigma)^2 + \frac{g_4^2}{24} \sigma^4
\end{aligned} \tag{5.9}$$

where only independent derivative interactions have been included. As a reminder, our notation of $L^{(d_1, d_2)}$ is to indicate the dimension of the base quartic theory, which is d_1 , and the particular critical dimension, d_2 , where it is renormalizable. One of the reasons why we have included a range of Lagrangians built from the base Lagrangian is to compare and contrast structural similarities. For instance the spectator Lagrangians of $L^{(4,6)}$ and $L^{(8,12)}$ are formally the same although the canonical dimension of the σ field is not the same in each case. This will generalise to the sequence $L^{(4n, 6n)}$ but in the dimensions between $4n$ and $6n$ there are no spectator interactions only a change in the σ kinetic terms.

It is worth stressing at this stage that we have merely constructed a sequence of higher dimensional renormalizable interacting Lagrangian's founded on a quartic scalar theory with a higher derivative kinetic term. We now need to make the connection with large N exponents in order to extend the Wilson-Fisher thread in this new context. In the next subsection we calculate new large N solutions for the case $n = 2$. Following that we review perturbative exponents of the Renormalization Group functions for the new Lagrangians, briefly detailing how these calculations were performed. These perturbative RG functions can then be used to compute ϵ -expansion critical exponents which can be compared with large N results. Finally we will examine the fixed point picture for these theories and compare with similar results obtained for the $O(N) \phi^4$ thread.

5.2 Critical Exponents of Higher Derivative Higher Dimensional Theories

We have introduced new sets of quartic scalar theories with critical dimension $D_c = 4n$ and $O(N)$ symmetry. We particularly focused on the tower of theories created in the $n = 2$ case which has critical dimension $D_c = 8$. It is possible to determine the large N critical exponents of the $n = 2$ theory in the same way that the $n = 1$ exponents are known [48–50]. The calculation of $n = 1$ critical exponents was reviewed in Chapter 2. The main purpose of this calculation is to provide new large N results for the critical exponents of the higher derivative tower corresponding to $n = 2$. These critical exponents will be new results that have not previously been studied. It also presents a new way of looking at the large N expansion. It turns out that the leading order exponents for the fields, η_1 and χ_1 , as well as that for η_2 can be immediately deduced from [48, 49], for any positive value of n . In the construction of the large N critical exponents, [48, 49], the $O(1/N^2)$ diagrams contributing to η_2 were computed as functions of α and β . The computation of these diagrams for $n = 1$ relied on conformal integration and more precisely, on the uniqueness condition.

Briefly the uniqueness rule states that if the sum of the exponents of the lines joining a 3-point vertex is equal to the space-time dimension then the integral over the vertex location can be performed. In the large N context for $n = 1$ this was exploited in [48, 49]. Recall that at leading order (LO) the $O(1/N^2)$ diagrams satisfied the uniqueness condition $2\alpha + \beta = d$ at leading order. Therefore LO terms of the $O(1/N^2)$ diagrams can be evaluated and were computed for $n = 1$. However, since the canonical dimension for the higher n solutions also satisfies the same uniqueness condition, $2\alpha + \beta = d$ at leading order, independent of n , then the use of uniqueness for general α and β in the derivation of the $O(1/N^2)$ exponent η_2 can be used for $n = 2$ and higher. We shall calculate the $O(1/N^2)$ Feynman diagrams in the following subsection. For clarity, the main point is summarised again here. The uniqueness condition is satisfied for the values of α and β given in (5.4) for general n at LO in $1/N$. This is why the higher derivative tower is significant and why we can build new large N results for this new tower of theories, analogous to the $n = 1$ case discussed in Chapter 2.

We therefore shall revisit the work of [48, 49] to determine η_1 , χ_1 and η_2 for $n = 2$ and hence obtain a new set of large N solutions. In Chapter 2 we explicitly detailed the derivation of the critical exponents η_1 and χ_1 for $n = 1$. The derivation for the $n = 2$ case is extremely similar, the only difference being

the values of α and β . As the same basic fields and common interaction $\sigma\phi^i\phi^i$ are present we also have the same skeleton Dyson-Schwinger equations for the fields at criticality which we shall use to determine the critical exponents. We shall therefore only review the main points here. The skeleton Dyson-Schwinger equations to NLO are given in figure 5.1 where the solid lines are ϕ^i propagators while the dotted lines illustrate σ fields.

Figure 5.1: Skeleton Dyson-Schwinger equations in the large N expansion.

The first two term in figure 5.1 of each equation are LO, the final two graphs are NLO Feynman diagrams. Note that the same counting rules used in Chapter 2 apply again here. The leading order terms were computed in equations (2.67), (2.68) and figure 2.19. Inserting these results into the leading order skeleton Dyson-Schwinger equations and equating the two equations an expression can be obtained to evaluate η_1 ,

$$p(\alpha) = \frac{2p(\beta)}{N}. \quad (5.10)$$

The left-hand side of this expression can be solved by first substituting in $\alpha = \mu - 2 + \frac{\eta}{2}$, where $d = 2\mu$, and then simplifying

$$p(\alpha) = p\left(\mu - 2 + \frac{\eta}{2}\right) = \frac{\Gamma(\mu - \frac{\eta}{2} + 2)\Gamma(\mu - 2 + \frac{\eta}{2})}{\Gamma(\frac{\eta}{2} - 2)\Gamma(2 - \frac{\eta}{2})}.$$

As only leading order terms are required all but one of the η terms can be ignored. The identity $z\Gamma(z) = \Gamma(z + 1)$ is implemented to isolate the leading order term of η ,

$$\begin{aligned} p(\alpha) &= \frac{\Gamma(\mu + 2)\Gamma(\mu - 2)(\frac{\eta}{2} - 2)(\frac{\eta}{2} - 1)(\frac{\eta}{2})}{\Gamma(\frac{\eta}{2} + 1)} \\ &= \Gamma(\mu + 2)\Gamma(\mu - 2)\left(\frac{\eta_1}{N} + O\left(\frac{1}{N^2}\right)\right). \end{aligned}$$

Calculating the right-hand side is much simpler. Substituting in $\beta = 4 - \eta - \chi$

and ignoring NLO terms in η we obtain

$$\begin{aligned} \frac{2p(\beta)}{N} &= \frac{2}{N} \frac{a(4 - \eta - \chi - \mu)}{a(4 - \eta - \chi)} \\ &= \frac{12}{N} \frac{\Gamma(2\mu - 4)}{\Gamma(4 - \mu)\Gamma(\mu - 4)}. \end{aligned}$$

Putting both sides together the result for η_1 at $n = 2$ can be found,

$$\eta_1 = \frac{12\Gamma(2\mu - 4)}{\Gamma(4 - \mu)\Gamma(\mu - 4)\Gamma(\mu + 2)\Gamma(\mu - 2)}. \quad (5.11)$$

The skeleton Dyson-Schwinger equations at leading order are

$$\begin{aligned} \frac{p(\alpha)}{A(x^2)^{2\mu-\alpha}} + \frac{AB}{(x^2)^{\alpha+\beta}} &= 0, \\ \frac{p(\beta)}{B(x^2)^{2\mu-\beta}} + \frac{NA}{2(x^2)^{2\alpha}} &= 0. \end{aligned}$$

Multiplying the first equation by A and $(x^2)^{2\mu-\alpha}$, the second equation by B and $(x^2)^{2\mu-\beta}$ and setting $z = A^2B$ we obtain

$$\begin{aligned} p(\alpha) + z + O(1/N^2) &= 0, \\ \frac{2}{N}p(\beta) + z + O(1/N^2) &= 0 \end{aligned}$$

where z is also an expansion in $1/N$. The exponent in the denominator has been simplified as $2\alpha + \beta - 2\mu = -\chi$ and χ can be ignored at leading order. As discussed in Chapter 2, since z also has an expansion in $1/N$ we must work out its leading order term before moving on to calculate χ_1 . This can be done by using the first skeleton Dyson-Schwinger equation

$$z_1 = -\eta_1\Gamma(\mu + 2)\Gamma(\mu - 2). \quad (5.12)$$

To calculate χ_1 we also only need to look at the first skeleton Dyson-Schwinger equation, however we now need to include diagrams of order $O(1/N^2)$ to incorporate the χ_1 term. In coordinate space notation the Feynman diagrams of order $O(1/N^2)$ in both skeleton Dyson-Schwinger equations are illustrated in figure 5.2. Here Σ_1 , Σ_2 , Π_1 and Π_2 are the dimensionless integrals for each respective $O(1/N^2)$ diagram.

$$\begin{aligned}
\text{Diagram 1} &= \frac{A^3 B^2 \Sigma_1}{(x^2)^{3\alpha+2\beta-2\mu}} \\
\text{Diagram 2} &= \frac{NB^3 A^5 \Sigma_2}{(x^2)^{5\alpha+3\beta-4\mu}} \\
\text{Diagram 3} &= \frac{NA^4 B \Pi_1}{(x^2)^{4\alpha+\beta-2\mu}} \\
\text{Diagram 4} &= \frac{N^2 A^6 B^2 \Pi_2}{(x^2)^{6\alpha+2\beta-4\mu}}
\end{aligned}$$

Figure 5.2: Feynman diagrams in both skeleton Dyson-Schwinger equations of order $O(1/N^2)$.

Inserting the expressions for the first two diagrams into the first skeleton Dyson-Schwinger equation and simplifying by setting $z = A^2 B$ we find

$$p(\alpha) + \frac{z}{(x^2)^{2\alpha+\beta-2\mu}} + \frac{z^2 \Sigma_1}{(x^2)^{4\alpha+2\beta-4\mu}} + \frac{N z^3 \Sigma_2}{(x^2)^{6\alpha+3\beta-6\mu}} = 0. \quad (5.13)$$

However the diagrams of order $O(1/N^2)$ are divergent, see figure 2.24, where K_1 and K_2 are the coefficients of the divergent pieces of the diagrams while Σ'_1 and Σ'_2 are finite. The two NLO diagrams in the second skeleton Dyson-Schwinger equation can also be split into their finite and divergent parts in figure 5.3.

$$\begin{aligned}
\text{Diagram 3} &= \frac{K_1}{\Delta} + \Pi'_1 \\
\text{Diagram 4} &= \frac{K_2}{\Delta} + \Pi'_2
\end{aligned}$$

Figure 5.3: The next to leading order (NLO) diagrams in the skeleton Dyson-Schwinger equation for the σ field split into finite and divergent parts.

It turns out that the coefficients of the divergent pieces of the two sets of diagrams are the same, while the finite parts differ. As the diagrams of order $O(1/N^2)$ are divergent they first need to be regularised before renormalizing the theory. This was discussed in great detail in Chapter 2 and it was concluded that after renormalization a condition is obtained which allows the computation of χ_1 ,

$$\chi_1 = -z_1 K_1 - 2z_1^2 K_2 . \quad (5.14)$$

As we have already noted, K_1 and K_2 are present in both sets of $O(1/N^2)$ diagrams so either pair can be computed to calculate χ_1 . The integration in coordinate space of the NLO Feynman diagrams will be the focus in the following subsection.

5.2.1 Calculation of NLO Diagrams

The four next-to-leading order diagrams required to compute χ_1 and η_2 can be evaluated using conformal integration. We utilize the conformal integration identities derived in Chapter 2 throughout this calculation. As only two diagrams need to be calculated to find the NLO critical exponents we compute the first set here, Π_1 and Π_2 , and simply state the results of the Σ_1 and Σ_2 diagrams for completeness. Note that the values of K_1 and K_2 were stated earlier in equation (2.83) without derivation which is provided here. As a reminder for the reader, Π_1 and Π_2 are the dimensionless values of two of the NLO diagrams, see figure 5.2. As the dimensionality of the diagrams has been included in the skeleton Dyson-Schwinger equations, we make Π_1 and Π_2 dimensionless to prevent overcounting of dimension-full terms. To begin we will evaluate the NLO Feynman diagram Π_1 which can be evaluated as an expansion in $1/N$, where X_i are some coefficients to be determined,

$$\Pi_1 \equiv X_0 + \frac{X_1}{N} + \frac{X_2}{N^2} + \dots .$$

This NLO diagram is illustrated in both momentum and coordinate space representations by figure 5.4.

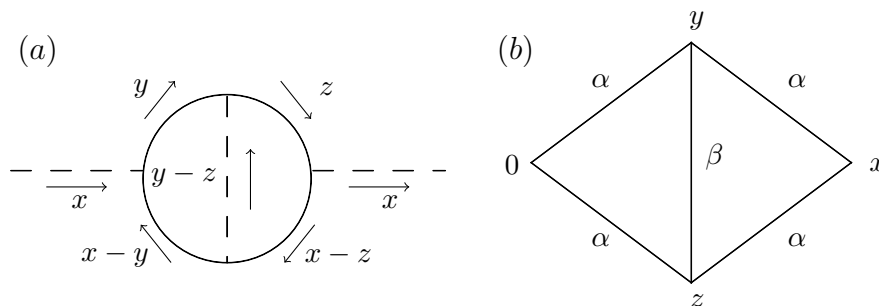


Figure 5.4: NLO Feynman diagram Π_1 in (a) momentum space and (b) coordinate space representations. In coordinate space α and β indicate the power on the propagator, while x , y and z represent the momentum flow in both representations.

To use conformal methods one has to check the sum of the exponents at each vertex in the coordinate space representation is unique. It can be seen from the uniqueness theorem that each 3-point vertex in figure 5.4 (b) is almost unique,

$$2\alpha + \beta = d - \chi \neq d .$$

However from the structure of the RG equations at criticality the χ and η exponents begin at order $O(1/N)$. Therefore at leading order in the $1/N$ expansion the vertices are completely unique. Hence at this order one can integrate at either vertex using conformal methods. It is worth contrasting the use of uniqueness here with another aspect of the conformal integration rule. This is that there is not one condition for the coordinate space vertex to be integrable. If the sum of the exponents at a vertex sum to the space-time dimension plus a positive integer then the vertex can be integrated. See [237], for example, for lectures on this construction. However the resulting expression may be cumbersome. While it is possible to consider theories based on the one step from uniqueness criterion it is not our main focus here.

It turns out that we only need to compute the leading order result for Π_1 anyway as this Feynman graph is multiplied by the term z_1^2/N in the skeleton Dyson-Schwinger equation, so the leading order result will automatically become order $O(1/N)$. Additionally the NLO Feynman diagram Π_1 will turn out to be divergent and we will have to use a new technique to cope with this. To illustrate where the divergences appear we naively first try to compute the leading order term in figure 5.4 (b). At leading order the two vertices we wish to integrate over are unique, we can therefore use the conformal integration identities given in Chapter 2, see figure 2.14. The lower 3-point vertex is integrated at first, as indicated by the boldface dot in figure 5.5, before we then integrate at the upper

vertex. This convention will be used throughout the Chapter.

$$= \nu(2, \mu - 1, \mu - 1) \nu(\mu, \mu, 0) (x^2)^{2-2\mu}$$

Figure 5.5: Coordinate space integration of NLO Feynman diagram Π_1 .

It is clear to see that we are left with divergent terms as formally

$$\nu(\mu, \mu, 0) = \frac{\Gamma(0)\Gamma(0)\Gamma(\mu)}{\Gamma(\mu)\Gamma(\mu)\Gamma(0)}$$

is ill defined due to singularities deriving from the Γ -function. Hence the diagram requires a regularisation in this critical point formulation. We use an analytic regulator of the form $\beta \rightarrow \beta - \Delta$ where the vertex anomalous dimension is shifted by an infinitesimal amount Δ , see figure 5.6. In effect we are performing a perturbative expansion in the anomalous dimension of the vertex. Consequently even at leading order the graph no longer has a unique vertex due to a non-zero Δ . We therefore use the method of subtractions, [49], to deal with the divergent pieces.

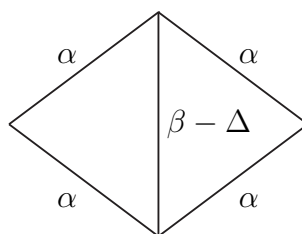


Figure 5.6: NLO Feynman diagram Π_1 with analytic regulator Δ introduced.

The method of subtractions relies on the fact that simpler graphs can be used to deal with the divergent part of the NLO diagram. We first subtract the two diagrams illustrated in figure 5.7 from the NLO diagram which gives a convergent result. These two graphs have been chosen in such a way that their singularity structure in Δ exactly matches that of figure 5.4 (b). We then add the two diagrams which allows the divergent piece of the NLO diagram to be extracted more easily. The full method of subtraction is illustrated in figure 5.9 for clarity.

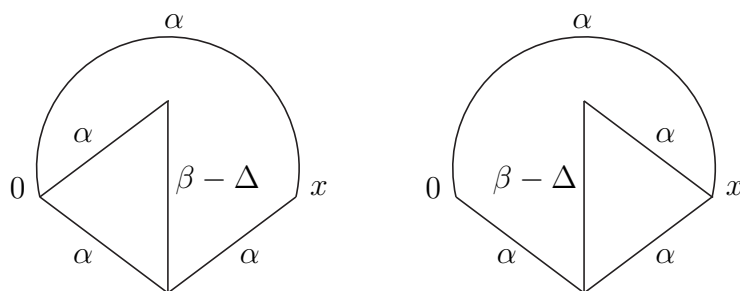


Figure 5.7: Two divergent diagrams which are first subtracted then added to figure 5.4 (b) to compute Π_1 . As both diagrams will give the same result they can both be labelled as \mathfrak{J}_f .

To begin we calculate one of the divergent diagram in figure 5.7 using simple chain integration as follows. This integration is given in figure 5.8, note that both divergent diagrams will give the same result.

$$= \nu(\alpha, \beta - \Delta, 2\mu - \alpha - \beta + \Delta)$$

$$= \nu(\alpha, \beta - \Delta, 2\mu - \alpha - \beta + \Delta) \nu(\alpha, \mu - \Delta, \mu - \alpha + \Delta) (x^2)^{\Delta - 2\alpha}$$

Figure 5.8: Coordinate space integration of the divergent Feynman diagram \mathfrak{J}_f used in the method of subtractions to calculate Π_1 .

Useful relations are listed below in equations (5.15) and (5.16) which allow the result of the chain integration to be simplified,

$$a(\alpha \pm \Delta) = a(\alpha)[1 \mp \Delta B(\alpha) + O(\Delta^2)] , \quad (5.15)$$

$$a(\mu \pm \Delta) = \mp \frac{1}{\Delta \Gamma(\mu)} [1 \mp \Delta(\psi(\mu) + \psi(1))] . \quad (5.16)$$

The result for the divergent diagrams is therefore

$$\mathfrak{J}_f = \frac{\pi^{2\mu} a^2(\alpha) a(\beta)}{\Delta \Gamma(\mu) (x^2)^{2\alpha - \Delta}} [1 + \Delta(B(\beta) - 2B(\alpha) + \psi(\mu) + \psi(1)) + O(\Delta^2)] \quad (5.17)$$

where $B(z) = \psi(\mu - z) + \psi(z)$ for z and $\mu - z$ not equal to zero or a negative integer and $\psi(z) = (d \ln \Gamma(z)) / (dz)$. It is clear to see that the singularity has been regularised.

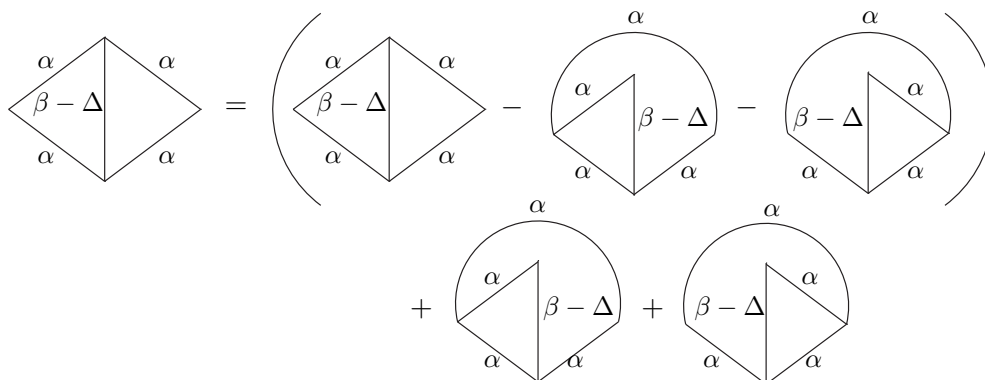


Figure 5.9: Method of subtraction to calculate the NLO diagram. The three terms in the brackets produce a convergent result, while the two Feynman graphs that have been added give a simpler way to calculate the divergences of the NLO diagram. Note that the three diagrams enclosed in the brackets are labelled \mathfrak{J}_g .

To complete the evaluation another technique is introduced to extract the finite term from a graph. This is a temporary regularisation, [49]. If one subtracts the graphs given in figure 5.7 from figure 5.6 the combination is finite with respect to Δ which is therefore not required and can be set to zero. Thus one can complete the first integration at the upper vertex of each graph. Note without a regularisation the point where one integrates in each graph has to be the same and thence the order of integration is important. Performing chain integration at each of the upper vertices of the three graphs enclosed in the brackets of figure 5.9 simplifies the diagrams. This is illustrated in figure 5.10

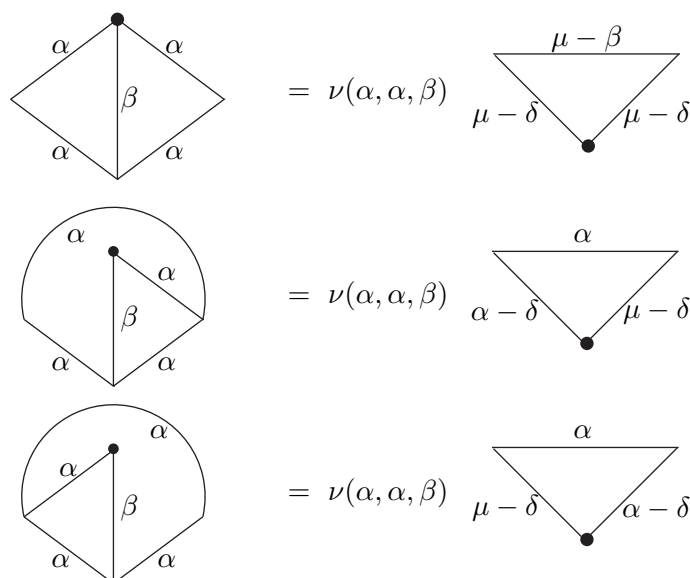


Figure 5.10: Coordinate space integration of the three diagrams enclosed in the brackets of figure 5.9, labelled \mathfrak{J}_g .

However each of the three subsequent chain integrals has a singular exponent, μ .

To circumvent this the lower two propagators of all three graphs are temporarily regularised by $\alpha \rightarrow \alpha - \delta$ and $\mu \rightarrow \mu - \delta$ where δ is arbitrary. Here δ represents the temporary analytic regulator, [49]. We can then integrate at the lower vertex of each of the three triangle graphs to produce the result for this combination of diagrams,

$$\begin{aligned} \mathfrak{I}_g &= \frac{\nu(\alpha, \alpha, \beta)}{(x^2)^{2\alpha-2\delta}} [\nu(\mu - \delta, \mu - \delta, 2\delta) - 2\nu(\alpha - \delta, \mu - \delta, \mu - \alpha + 2\delta)] \\ &= \frac{2\pi^{2\mu} a^2(\alpha) a(\beta)}{(x^2)^{2\alpha-2\delta} \Gamma(\mu)} [B(\alpha) - \psi(\mu) - \psi(1)] + O(\delta). \end{aligned} \quad (5.18)$$

This is clearly finite as $\delta \rightarrow 0$. Thus we can set $\delta = 0$ and remove the temporary regularisation. Therefore to obtain the result for the diagram given by figure 5.4 to order $O(\Delta)$ we substitute the values (5.17) and (5.18) into figure 5.9 to evaluate the final result of Π_1 , [48–50],

$$\begin{aligned} \Pi_1 &= \frac{2\nu(\alpha, \alpha, \beta)}{\Gamma(\mu)} (B(\alpha) - \psi(\mu) - \psi(1)) \\ &\quad + \frac{2\nu(\alpha, \alpha, \beta)}{\Delta \Gamma(\mu)} [1 + \Delta(B(\beta) - B(\alpha) + \psi(\mu) + \psi(1))] \\ &= \frac{2\pi^{2\mu} a^2(\alpha) a(\beta)}{\Gamma(\mu)} \left[\frac{1}{\Delta} - B(\alpha) + B(\beta) + O(\Delta) \right]. \end{aligned} \quad (5.19)$$

Note that Π_1 is the dimensionless value of the NLO diagram, therefore the term $(x^2)^{-2\alpha}$ has been excluded from the result as is it included in the skeleton Dyson-Schwinger equations.

The computation of diagram Π_2 , illustrated in figure 5.11 in both the momentum and coordinate space representations, follows a very similar derivation to that of Π_1 . The value of Π_2 will be dimensionless for the same reasons that we ensured Π_1 was dimensionless. We will again compute to order $O(1/N)$.

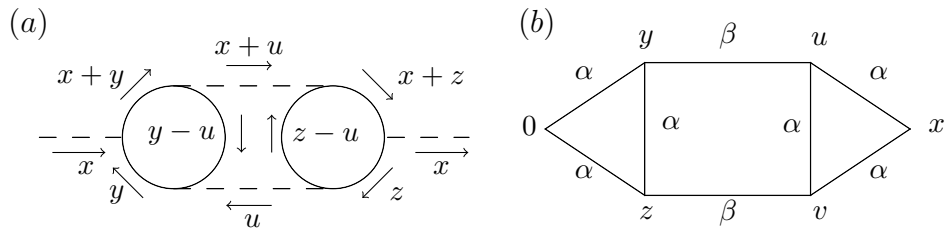


Figure 5.11: NLO Feynman diagram Π_2 in (a) momentum space and (b) coordinate space representations. In coordinate space α and β indicate the power on the propagator, while x, y, z, u and v represent momentum flow.

As in the computation of diagram Π_1 , each 3-point vertex of Π_2 will be unique

at leading order and we can therefore employ conformal methods to evaluate this diagram to leading order. If we naively try to compute Π_2 , first by integrating at the upper right vertex then at the lower right vertex the result turns out to be divergent. This is illustrated in figure 5.12.

$$\begin{aligned}
 & \text{Diagram 1} = \nu(\alpha, \alpha, \beta) \text{Diagram 2} \\
 & = \nu(\alpha, \alpha, \beta) \nu(\mu - \beta + \alpha, \beta, \mu - \alpha) \text{Diagram 3}
 \end{aligned}$$

Figure 5.12: Coordinate space integration of Π_2 .

It is clear that this diagram is divergent as it contains the divergent diagram Π_1 . Therefore a regularisation must be introduced of the same form as we used previously, that is $\beta \rightarrow \beta - \Delta$. This regularisation violates the uniqueness of the vertices, and so we must therefore use the method of subtractions, [49], to compute the divergent part of Π_2 . The two diagrams that we subtract from Π_2 are given in figure 5.13. These graphs have been chosen in such a way that their singularity structure in Δ exactly matches that of figure 5.11. Therefore when subtracting these two diagrams from 5.11 we obtain a finite result. The pole of Π_2 is recreated by the addition of these two diagrams which are simpler to evaluate, as we shall see.

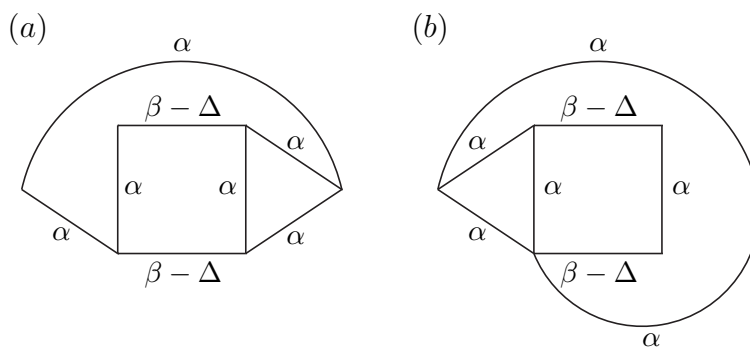


Figure 5.13: Two divergent diagrams which are first subtracted then added to figure 5.11 to compute Π_2 .

A unique complication when computing Π_2 arises at this point of the calculation. It turns out that the first diagram in our method of substitution, figure 5.13 (a), will also require a subtraction to extract the divergent part. Consequently

we need to subtract the diagram 5.14 from figure 5.13 (a). Note that we only need to substitute one diagram as the singularity structure of figure 5.14 exactly matches that of 5.13 (a).

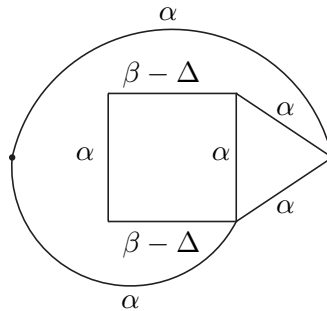


Figure 5.14: Divergent diagram \mathfrak{J}_h which is first subtracted then added to figure 5.13 (a) in the method of subtraction.

As the calculation of Π_2 is more complicated than that of Π_1 , the full method of subtraction is illustrated in figure 5.15 and we summarise how this works before continuing.

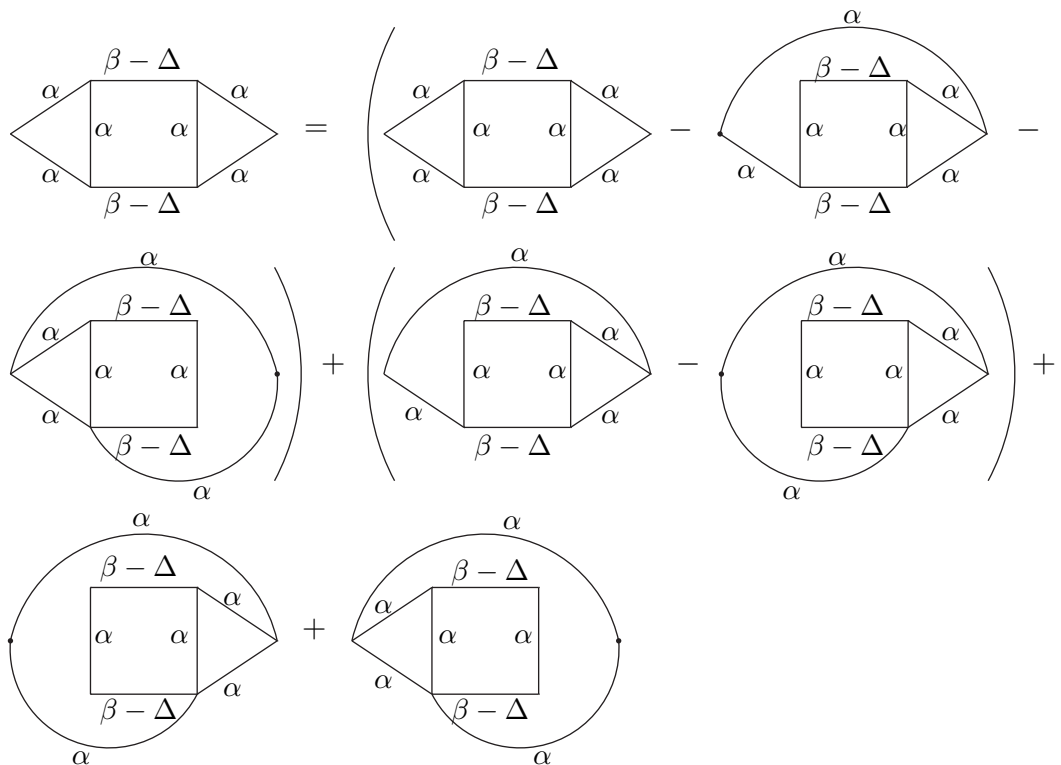


Figure 5.15: Method of subtraction to calculate the second NLO diagram Π_2 . The two combinations of diagrams in brackets are finite, while the two additional Feynman graphs have been added to produce the divergence part of the NLO diagram. The diagrams in the first set of brackets are collectively labelled as \mathfrak{J}_i , the diagrams in the second set of brackets are labelled \mathfrak{J}_j . The final two diagrams which are equal are denoted as \mathfrak{J}_h .

The two combinations of diagrams enclosed in brackets in figure 5.15 will produce finite values. The remaining two graphs outside the brackets are equivalent and produce the divergent pole term of Π_2 . Note that all diagrams illustrated so far in the computation of Π_2 are dimension-full, we will need to remove this dimension dependence when stating the final result to avoid over-counting when results are inserted into the skeleton Dyson-Schwinger equations. We begin by computing the divergent integral given in figure 5.14, which also appears in figure 5.7. We first integrate at the bottom right-hand vertex using conformal integration before integrating at the left-hand vertex of the resulting diamond graph. To avoid any ambiguity this integration process is fully illustrated in figure 5.16 with integration points noted. The next step is to integrate at the upper vertex before finally performing one last integration at the lower most vertex. The relations given in equations (5.15) and (5.16) can then be used to simplify the result.

$$\begin{aligned}
\mathfrak{J}_h &= \text{Diagram 1} = \nu(\alpha, \beta - \Delta, \alpha + \Delta) \text{Diagram 2} \\
&= \nu(\alpha, \beta - \Delta, \alpha + \Delta) \\
&\quad \times \nu(\beta - \Delta, \mu - \alpha - \Delta, \mu - \beta + \alpha + 2\Delta) \text{Diagram 3} \\
&= \nu(\alpha, \beta - \Delta, \alpha + \Delta) \\
&\quad \times \nu(\beta - \Delta, \mu - \alpha - \Delta, \mu - \beta + \alpha + 2\Delta) \\
&\quad \times \nu(\alpha, \beta - 2\Delta, \alpha + 2\Delta) \text{Diagram 4}
\end{aligned}$$

Figure 5.16: Coordinate space integration of \mathfrak{J}_h .

Performing the final integration in coordinate space \mathfrak{J}_h can then be simplified

$$\begin{aligned}
\mathfrak{J}_h &= \nu(\alpha, \beta - \Delta, \alpha + \Delta) \nu(\beta - \Delta, \mu - \alpha - \Delta, \mu + \alpha - \beta + 2\Delta) \\
&\quad \times \nu(\alpha, \beta - 2\Delta, \alpha + 2\Delta) \nu(\alpha, \mu - 2\Delta, \mu - \alpha + 2\Delta) (x^2)^{-2\alpha+2\Delta} \\
&= \times \frac{\nu^2(\alpha, \alpha, \beta) \nu(\mu + \alpha - \beta, \beta, \mu - \alpha)}{2\Delta \Gamma(\mu) (x^2)^{2\alpha-2\Delta}} \left[1 + \Delta(4B(\beta) - 4B(\alpha) \right. \\
&\quad \left. - 2B(\mu + \alpha - \beta) + 2(\psi(\mu) + \psi(1))) \right] \tag{5.20}
\end{aligned}$$

Then, for the first combination of finite diagrams, illustrated by the three dia-

grams enclosed in the first set of brackets in figure 5.15, we can set $\Delta = 0$ as this combination is finite. To compute this set of diagrams the integration is first performed at the lower right-hand vertex then at the upper right-hand vertex. This produces two $\nu(\alpha, \beta, \gamma)$ terms. Two final integrations are performed, first at the upper vertex and then at the lower vertex of the three triangle shaped graphs. Once again a temporary analytic regulator δ has been introduced to prevent propagators of the form μ which are singular. The integration process is illustrated in figure 5.17.

$$\begin{aligned}
&= \nu(\alpha, \alpha, \beta) \left(\text{Diagram 1} - \text{Diagram 2} - \text{Diagram 3} \right) \\
&= \nu(\alpha, \alpha, \beta) \times \nu(\mu - \alpha, \beta, \mu + \alpha - \beta) \left(\text{Diagram 4} - \text{Diagram 5} - \text{Diagram 6} \right) \\
&= \nu^2(\alpha, \alpha, \beta) \times \nu(\mu - \alpha, \beta, \mu + \alpha - \beta) \left(\text{Diagram 7} - \text{Diagram 8} - \text{Diagram 9} \right)
\end{aligned}$$

Figure 5.17: Coordinate space integration of \mathfrak{J}_i .

This can be reduced to a simpler form using the identities given in equations (5.15) and (5.16) to give

$$\begin{aligned}
\mathfrak{J}_i &= \frac{\nu^2(\alpha, \alpha, \beta)\nu(\mu - \alpha, \beta, \mu + \alpha - \beta)}{(x^2)^{2\alpha-2\delta}} \left[\nu(\mu - \delta, \mu - \delta, 2\delta) \right. \\
&\quad \left. - 2\nu(\mu - \delta, \alpha - \delta, \mu - \alpha + 2\delta) \right] \\
&= \frac{2\nu^2(\alpha, \alpha, \beta)\nu(\mu - \alpha, \beta, \mu + \alpha - \beta)}{(x^2)^{2\alpha-2\delta}\Gamma(\mu)} \left[B(\alpha) - \psi(\mu) - \psi(1) \right]. \quad (5.21)
\end{aligned}$$

The only remaining computation is that given by the combination of diagrams in the second set of brackets in figure 5.15 labelled now as \mathfrak{J}_j . Again we can set $\Delta = 0$ as this sequence of diagrams is finite. To begin we integrate at the upper right-hand vertex before performing a second and third conformal integration at

the respective indicated vertices illustrated in figure 5.18.

$$\begin{aligned}
\mathfrak{I}_j &= \text{Diagram 1} - \text{Diagram 2} \\
&= \nu(\alpha, \alpha, \beta) \left(\text{Diagram 3} - \text{Diagram 4} \right) \\
&= \nu^2(\alpha, \alpha, \beta) \left(\text{Diagram 5} - \text{Diagram 6} \right)
\end{aligned}$$

Figure 5.18: Coordinate space integration of \mathfrak{I}_j .

Once again a temporary regulator δ has been introduced which allows the integration with respect to the unique vertex. The temporary regulator is set to zero after the computation once it is no longer required.

$$\begin{aligned}
\mathfrak{I}_j &= \nu^2(\alpha, \alpha, \beta) \left(\nu(\beta, \alpha - \beta + \mu, \mu - \alpha) \text{Diagram 7} \right. \\
&\quad \left. - \nu(\beta, \mu - \alpha - \delta, \mu - \beta + \alpha + \delta) \text{Diagram 8} \right)
\end{aligned}$$

Performing one last conformal integration, this result can then be simplified using the identities given in equations (5.15) and (5.16),

$$\begin{aligned}
\mathfrak{I}_j &= \frac{\nu^2(\alpha, \alpha, \beta)}{(x^2)^{2\alpha-\delta}} \left[\nu(\beta, \mu + \alpha - \beta, \mu - \alpha) \nu(\mu - \alpha, \mu - \delta, \alpha + \delta) \right. \\
&\quad \left. - \nu(\beta, \mu - \alpha - \delta, \mu + \alpha - \beta + \delta) \nu(\alpha, \mu - \delta, \mu - \alpha + \delta) \right] \\
&= \frac{a^3(\alpha) a^3(\beta) a(\alpha + \mu - \beta)}{(x^2)^{2\alpha-\delta} \Gamma(\mu)} \left(B(\mu + \alpha - \beta) - B(\alpha) \right). \quad (5.22)
\end{aligned}$$

Finally the calculated components of the method of subtractions given by equa-

tions (5.20), (5.21) and (5.22) can be inserted into the full equation for Π_2 which is illustrated in figure 5.15. The final result for the NLO diagram Π_2 at leading order is given by

$$\Pi_2 = \frac{a^3(\alpha)a^3(\beta)a(\alpha + \mu - \beta)}{\Gamma(\mu)} \left[\frac{1}{\Delta} + 4B(\beta) - 3B(\alpha) - B(\mu + \alpha - \beta) + O(\Delta) \right]. \quad (5.23)$$

Note that the term $(x^2)^{2\alpha}$ has been excluded from the final result of Π_2 . This is because Π_2 is the dimensionless value of the NLO diagram. Although the results for Σ_1 and Σ_2 are not needed in the computation of χ_1 they are stated below for completeness, [49]. The full derivation of these diagrams follows the same method as for Π_1 and Π_2 ,

$$\Sigma_1 = \frac{2\mu^{2\mu}a^2(\alpha)a(\beta)}{\Gamma(\mu)} \left[\frac{1}{\Delta} + \frac{1}{2}(B(\beta) - B(\alpha)) + O(\Delta) \right], \quad (5.24)$$

$$\Sigma_2 = \frac{2\mu^{2\mu}a^3(\alpha)a^3(\beta)a(\mu + \alpha - \beta)}{\Gamma(\mu)} \left[\frac{1}{\Delta} + 2(B(\beta) - B(\alpha)) \right]. \quad (5.25)$$

Note that these are valid for arbitrary α and β .

5.2.2 Calculation of χ_1 and η_2

From the calculation of the Feynman diagrams to order $O(1/N^2)$ we have obtained the coefficients of the divergent parts of both NLO diagrams

$$\begin{aligned} K_1 &= \frac{2a^2(\alpha)a(\beta)}{\Gamma(\mu)}, \\ K_2 &= \frac{a^3(\alpha)a^3(\beta)a(\alpha + \mu - \beta)}{\Gamma(\mu)}. \end{aligned} \quad (5.26)$$

Inserting these values into equation (5.14) for χ_1 we find

$$\begin{aligned} \chi_1 &= \frac{2a^2(\alpha)a(\beta)\eta_1\Gamma(\mu + 2)\Gamma(\mu - 2)}{\Gamma(\mu)} \\ &\quad - \frac{2\eta_1^2\Gamma(\mu + 2)^2\Gamma(\mu - 2)^2a^3(\alpha)a^3(\beta)a(\alpha + \mu - \beta)}{\Gamma(\mu)}. \end{aligned}$$

Then, substituting the leading order terms of α and β for $n = 2$ into χ_1 one finds

$$\chi_1 = \left[- \frac{\mu(4\mu^3 + 26\mu^2 - 17\mu - 47)}{9(\mu - 4)(\mu - 3)} \right] \eta_1. \quad (5.27)$$

We now want to calculate the NLO critical exponent η_2 . To do this both of the skeleton Dyson-Schwinger equations up to order $O(1/N^2)$ are required. In

Chapter 2 we discovered that both the choice of counterterms and the value of χ_1 automatically cancels the pole terms with respect to Δ and the logarithms of x in the second skeleton Dyson-Schwinger equation. This is because the divergent piece of diagrams Π_i are identical to the divergences of the diagrams Σ_i . This can be verified by the direct calculation of all diagrams and is a special manifestation of the general property of renormalizability, so that the requirement of coincidence of Π_i and Σ_i poles is a method of testing the calculations, see [48]. After renormalizing and cancelling of logarithms, the skeleton Dyson-Schwinger equations take the form

$$p(\alpha) + z + z^2 \Sigma'_1 + z^3 N \Sigma'_2 = 0, \quad (5.28)$$

$$\frac{2p(\beta)}{N} + z + z^2 \Pi'_1 + z^3 N \Pi'_2 = 0 \quad (5.29)$$

where the prime denotes the finite contribution of the diagrams. We have taken the exponent χ at leading order in the denominator which removes the x terms from our equations.

If equation (5.28) is subtracted from (5.29) the lone z term can be eliminated from the computation. This removes the need to calculate the NLO coefficient z_2 and hence speeds up the computation,

$$0 = p(\alpha) - \frac{2p(\beta)}{N} + z^2 \Sigma'_1 - z^2 \Pi'_1 + z^3 N \Sigma'_2 - z^3 N \Pi'_2. \quad (5.30)$$

This equation can be solved to find η_2 . Note that η_2 is the order $O(1/N^2)$ of η . Therefore in the above expression we must compute $p(\alpha)$ to order $O(1/N^2)$ and $p(\beta)$ to order $O(1/N)$ as this term is multiplied by a factor of $1/N$. We also need diagrams Σ'_i and Π'_i to leading order in $1/N$ as they are all multiplied by $1/N^2$ which is simpler to see when noting that z is a series in $1/N$,

$$0 = p(\alpha) - \frac{2p(\beta)}{N} + \frac{z_1^2}{N^2} \Sigma'_1 - \frac{z_1^2}{N^2} \Pi'_1 + \frac{z_1^3}{N^2} \Sigma'_2 - \frac{z_1^3}{N^2} \Pi'_2. \quad (5.31)$$

As a reminder for the reader $p(\alpha) = a(\alpha - \mu)/a(\alpha)$ where $a(\alpha)$ was defined in (2.44). We begin by working out each term individually, starting with $p(\alpha)$ to order $O(1/N^2)$.

$$\begin{aligned} p(\alpha) &= p\left(\mu - 2 + \frac{\eta}{2}\right) = \frac{a\left(\frac{\eta}{2} - 2\right)}{a\left(\mu - 2 + \frac{\eta}{2}\right)} \\ &= \frac{\left(\frac{\eta}{2} - 2\right)\left(\mu - \frac{\eta}{2} + 1\right)\left(\frac{\eta}{2} - 1\right)\left(\mu - \frac{\eta}{2}\right)\left(\frac{\eta}{2}\right)\left(\mu - \frac{\eta}{2} - 1\right)a\left(\frac{\eta}{2} + 1\right)}{a(\mu - 2)\left[1 - \frac{\eta}{2N}B(\mu - 2)\right]} \end{aligned}$$

$$\begin{aligned}
&= \frac{(\frac{\eta}{2} - 2)(\mu - \frac{\eta}{2} + 1)(\frac{\eta}{2} - 1)(\mu - \frac{\eta}{2})(\frac{\eta}{2})(\mu - \frac{\eta}{2} - 1)a(1)[1 - (\eta_1/2N)B(1)]}{a(\mu - 2)[1 - (\eta_1/2N)B(\mu - 2)]} \\
&= \frac{a(1)}{a(\mu - 2)} \left(\frac{\eta}{2} - 2\right) \left(\mu - \frac{\eta}{2} + 1\right) \left(\frac{\eta}{2} - 1\right) \left(\mu - \frac{\eta}{2}\right) \left(\frac{\eta}{2}\right) \left(\mu - \frac{\eta}{2} - 1\right) \\
&\quad \times \left[1 - \frac{\eta_1}{2N}B(1)\right] \left[1 + \frac{\eta_1}{2N}B(\mu - 2)\right] \tag{5.32}
\end{aligned}$$

where we have used the identities (5.15), (5.16) and

$$a(\alpha) = \alpha(\mu - \alpha - 1)a(\alpha + 1) . \tag{5.33}$$

Expanding out to NLO in η and also noting that $B(\mu - z) = B(z)$ we find

$$\begin{aligned}
p(\alpha) &= \frac{a(1)}{a(\mu - 2)} \left(-\frac{3\eta_1^2\mu^2}{2N^2} - \frac{3\eta_1^2\mu^3}{4N^2} + \frac{\eta_1\mu^3}{N} + \frac{\eta_2\mu^3}{N^2} + \frac{3\eta_1^2\mu}{4N^2} \right. \\
&\quad - \frac{\eta_1\mu}{N} - \frac{\eta_2\mu}{N^2} + \frac{\eta_1^2}{2N^2} + \frac{\eta_1^2\mu B(1)}{2N^2} - \frac{\eta_1^2\mu^3 B(1)}{2N^2} + \frac{\eta_1^2\mu^3 B(2)}{2N^2} \\
&\quad \left. - \frac{\eta_1^2\mu B(2)}{2N^2} \right) + O\left(\frac{1}{N^3}\right) . \tag{5.34}
\end{aligned}$$

Moving on to the calculation of $p(\beta)$ to order $O(1/N)$ we use the identities given by equations (5.15), (5.16) and (5.33) to obtain

$$\begin{aligned}
p(\beta) &= \frac{a(\beta - \mu)}{a(\beta)} = \frac{a(4 - \eta - \chi - \mu)}{a(4 - \eta - \chi)} \\
&= \frac{a(4 - \mu)}{a(4)} \left[\left(1 + \left(\frac{\eta_1}{N} + \frac{\chi_1}{N}\right)B(4 - \mu) - \left(\frac{\eta_1}{N} + \frac{\chi_1}{N}\right)B(4)\right) \right] \tag{5.35}
\end{aligned}$$

for $n = 2$, where we have kept the η and χ terms in β as we want $p(\beta)$ to order $1/N$. The diagrams Π_i and Σ_i to order $O(1/N^2)$ have already been computed. The values of Σ'_i and Π'_i to leading order in α and β for $n = 2$ are

$$\Sigma'_1 = \frac{\pi^{2\mu} a^2(\mu - 2)a(4)}{\Gamma(\mu)} [B(4) - B(\mu - 2)] , \tag{5.36}$$

$$\Pi'_1 = \frac{2\pi^{2\mu} a^2(\mu - 2)a(4)}{\Gamma(\mu)} [B(4) - B(\mu - 2)] , \tag{5.37}$$

$$\Sigma'_2 = \frac{2\pi^{4\mu} a^3(\mu - 2)a^3(4)a(2\mu - 6)}{\Gamma(\mu)} [B(4) - B(\mu - 2)] \tag{5.38}$$

$$\Pi'_2 = \frac{\pi^{4\mu} a^3(\mu - 2)a^3(4)a(2\mu - 6)}{\Gamma(\mu)} [4B(4) - 3B(\mu - 2) - B(2\mu - 6)] \tag{5.39}$$

Putting all of these components into equation (5.31), incorporating only terms of

order $O(1/N^2)$ and solving for η_2 using MAPLE we find

$$\eta_2 = \left[-\frac{(2\mu^4 - 13\mu^3 - 2\mu^2 + 85\mu - 108)}{9(\mu - 3)(\mu - 4)} [B(3 - \mu) - B(\mu - 1)] + \frac{(4\mu^{10} - 72\mu^9 + 433\mu^8 - 697\mu^7 - 3085\mu^6 + 15845\mu^5 - 26504\mu^4 + 11816\mu^3 + 15436\mu^2 - 16416\mu + 2592)}{18(\mu + 1)(\mu - 1)(\mu - 2)(\mu - 3)^2(\mu - 4)^2\mu} \right] \eta_1^2 \quad (5.40)$$

where η_1 is given by equation (5.11). Compared to the same exponents for the $n = 1$ case this expression is more involved. This is because the derivation of the arguments of the Γ and ψ -functions will involve n . This is more apparent in the $n = 3$ case which is given in [3].

5.3 Perturbative Results for $n = 2$

To compare new large N results for the critical exponents with perturbative results, we need to compute the Renormalization Group functions to as high a loop order as is viable for the Lagrangians. These RG functions were calculated in [3] and we summarise the method and results here. For consistency with other work on the $O(N)$ thread of earlier Chapters the same notation and conventions as [2, 3, 53] are used. The same underlying computational technology described for the ten dimensional calculation of Chapter 3 and the LGW computation of Chapter 4 is used here. For instance in the LGW calculation an efficient algorithm was used to easily access the renormalization of 3-point vertices using an insertion on the 2-point vertex. This exploited the fact that the propagator $1/(k^2)^\alpha$ is infrared (IR) safe in $d > 2\alpha$ dimensions. This approach is applicable to every Lagrangian here containing 3-point interactions. The renormalization of all 2-point Green's functions proceeds in the same way as described in the previous calculations. For certain Lagrangians, for example $L^{(8,16)}$, the 3-point vertex functions are renormalized by considering the Green's functions at either a completely symmetric point or at a completely off-shell point. The former is appropriate to use when there is either a non-derivative 3-point interaction or a single 3-point vertex. The off-shell configuration is required when there is more than one 3-point interaction and they involve derivative couplings.

A Lagrangian with quartic and higher spectator interactions will require a more direct approach. For example, the 4-point Green's functions are calculated by evaluating the vertex function at the completely symmetric point. In terms of loop number the theories in the higher dimensions are renormalized to mostly two

loops but to three loops for a few cases above the critical dimension of the base Lagrangian. This is because there are practical limitations in the construction of the databases used to apply the Laporta and Tarasov algorithms, [192, 195, 196]. The increase in the powers on the propagators means that to build the three loop 2-point master integrals beyond twelve dimensions, which requires a significant amount of integration by parts even for non-tensor integrals, was not viable. However we take the point of view that it will be evident even with two loop Renormalization Group functions that the connection between the tower of theories will be established. We record the results for the theories along the thread for $n = 2$ based on $L^{(8)}$. We have

$$\begin{aligned}
\gamma_\phi^{(8)}(g_1) &= -\frac{[N+2]}{4320}g_1^4 + \frac{[N+2][N+8]}{9331200}g_1^6 + O(g_1^8), \\
\gamma_m^{(8)}(g_1) &= -\frac{[N+2]}{36}g_1^2 - \frac{7[N+2]}{12960}g_1^4 + O(g_1^6), \\
\beta^{(8)}(g_1) &= \frac{[N+8]}{36}g_1^4 + \frac{[41N+202]}{19440}g_1^6 + O(g_1^8)
\end{aligned} \tag{5.41}$$

for the base Lagrangian. Structurally these are similar to the four dimensional $L^{(4)}$ results from the point of view of the factors $(N+2)$ and $(N+8)$. More interestingly the β -function for $L^{(8)}$ is not asymptotically free in parallel with the four dimensional case. For the first extension to this $n = 2$ tower we find

$$\begin{aligned}
\gamma_\phi^{(8,10)}(g_1) &= \frac{g_1^2}{120} + [194N - 567]\frac{g_1^4}{864000} \\
&\quad + [-37786N^2 - 259420N + 648000\zeta_3 + 505299]\frac{g_1^6}{21772800000} \\
&\quad + O(g_1^8), \\
\gamma_\sigma^{(8,10)}(g_1) &= -\frac{Ng_1^2}{60} + \frac{167Ng_1^4}{216000} \\
&\quad + [259847N - 648000\zeta_3 + 256266]\frac{Ng_1^6}{10886400000} + O(g_1^8), \\
\beta^{(8,10)}(g_1) &= [-N + 6]\frac{g_1^3}{240} + [-197N - 297]\frac{g_1^5}{288000} \\
&\quad + [-859789N^2 + 25272000\zeta_3N - 38231814N - 38232000\zeta_3 \\
&\quad + 43101039]\frac{g_1^7}{43545600000} + O(g_1^9)
\end{aligned} \tag{5.42}$$

for $L^{(8,10)}$. Our three loop results for $L^{(8,12)}$ are

$$\begin{aligned}
\gamma_\phi^{(8,12)}(g_1, g_2) &= \frac{g_1^2}{280} + [-1587Ng_1^2 - 9334g_1^2 - 6160g_1g_2 - 1587g_2^2]\frac{g_1^2}{197568000} \\
&\quad + [-13130181N^2g_1^4 + 175046616Ng_1^4 + 8890560000\zeta_3g_1^4 \\
&\quad - 9803169176g_1^4 + 425268522Ng_1^3g_2 + 712313280g_1^3g_2
\end{aligned}$$

$$\begin{aligned}
& + 76042962Ng_1^2g_2^2 + 8890560000\zeta_3g_1^2g_2^2 - 10046446142g_1^2g_2^2 \\
& - 150402798g_1g_2^3 + 209985345g_2^4] \frac{g_1^2}{1254635827200000} \\
& + O(g_i^8) , \\
\gamma_\sigma^{(8,12)}(g_1, g_2) = & [Ng_1^2 + g_2^2] \frac{1}{560} \\
& + [-6254Ng_1^4 - 6160Ng_1^3g_2 - 1587Ng_1^2g_2^2 - 4667g_2^4] \frac{1}{197568000} \\
& + [930040938N^2g_1^6 + 8890560000\zeta_3Ng_1^6 - 9419379728Ng_1^6 \\
& + 194624640N^2g_1^5g_2 + 491748768Ng_1^5g_2 - 34230843N^2g_1^4g_2^2 \\
& + 22226400000\zeta_3Ng_1^4g_2^2 - 26093250026Ng_1^4g_2^2 \\
& + 1287984600Ng_1^3g_2^3 + 417101400Ng_1^2g_2^4 + 4445280000\zeta_3g_2^6 \\
& - 4603622893g_2^6] \frac{1}{2509271654400000} + O(g_i^8) , \\
\beta_1^{(8,12)}(g_1, g_2) = & [3Ng_1^2 + 40g_1^2 + 28g_1g_2 + 3g_2^2] \frac{g_1}{3360} \\
& + [12042Ng_1^4 - 53464g_1^4 - 133308Ng_1^3g_2 + 490392g_1^3g_2 \\
& - 14283Ng_1^2g_2^2 + 66956g_1^2g_2^2 + 57960g_1g_2^3 \\
& - 42003g_2^4] \frac{g_1}{3556224000} \\
& + [-14938245342N^2g_1^6 - 617004864000\zeta_3Ng_1^6 \\
& + 3109795833456Ng_1^6 + 2311545600000\zeta_3g_1^6 \\
& + 1737998549536g_1^6 - 2875390812N^2g_1^5g_2 \\
& + 1867017600000\zeta_3Ng_1^5g_2 - 2203538203104Ng_1^5g_2 \\
& + 547658496000\zeta_3g_1^5g_2 - 423865546832g_1^5g_2 \\
& - 308077587N^2g_1^4g_2^2 + 200037600000\zeta_3Ng_1^4g_2^2 \\
& - 178146641322Ng_1^4g_2^2 + 2261758464000\zeta_3g_1^4g_2^2 \\
& + 6401866158256g_1^4g_2^2 + 8781904656Ng_1^3g_2^3 \\
& + 497871360000\zeta_3g_1^3g_2^3 - 586662087088g_1^3g_2^3 \\
& + 3753912600Ng_1^2g_2^4 + 49787136000\zeta_3g_1^2g_2^4 \\
& + 2136750334680g_1^2g_2^4 + 373403520000\zeta_3g_1g_2^5 \\
& - 374235507660g_1g_2^5 + 40007520000\zeta_3g_2^6 \\
& - 41432606037g_2^6] \frac{g_1}{45166889779200000} + O(g_i^9) , \\
\beta_2^{(8,12)}(g_1, g_2) = & [28Ng_1^3 + 9Ng_1^2g_2 + 37g_2^3] \frac{1}{3360} \\
& + [173880Ng_1^5 + 32826Ng_1^4g_2 + 241164Ng_1^3g_2^2 \\
& - 159651Ng_1^2g_2^3 + 96073g_2^5] \frac{1}{3556224000} \\
& + [121231189296N^2g_1^7 + 1194891264000\zeta_3Ng_1^7 \\
& - 1408785519120Ng_1^7 - 4290992658N^2g_1^6g_2
\end{aligned}$$

$$\begin{aligned}
& + 1434936384000\zeta_3 N g_1^6 g_2 + 7192728107344 N g_1^6 g_2 \\
& - 90566288568 N^2 g_1^5 g_2^2 + 1344252672000\zeta_3 N g_1^5 g_2^2 \\
& - 1313378645040 N g_1^5 g_2^2 - 10178257905 N^2 g_1^4 g_2^3 \\
& + 1869684768000\zeta_3 N g_1^4 g_2^3 + 4814949206106 N g_1^4 g_2^3 \\
& + 746807040000\zeta_3 N g_1^3 g_2^4 - 890895567408 N g_1^3 g_2^4 \\
& - 34486893072 N g_1^2 g_2^5 + 941510304000\zeta_3 g_2^7 \\
& + 1196618048425 g_2^7] \frac{1}{45166889779200000} + O(g_i^9) . \quad (5.43)
\end{aligned}$$

However, for $L^{(8,14)}$ computational limitations meant we can only provide two loop results which are

$$\begin{aligned}
\gamma_\phi^{(8,14)}(g_1, g_2) &= \frac{g_1^2}{1120} + [107964 N g_1^2 - 1533897 g_1^2 + 718200 g_1 g_2 \\
&\quad - 54586 g_2^2] \frac{g_1^2}{768144384000} + O(g_i^6) , \\
\gamma_\sigma^{(8,14)}(g_1, g_2) &= [-18 N g_1^2 + 7 g_2^2] \frac{1}{136080} \\
&\quad + [13056633 N g_1^4 - 6826680 N g_1^3 g_2 + 467334 N g_1^2 g_2^2 \\
&\quad + 275849 g_2^4] \frac{1}{23332385664000} + O(g_i^6) , \\
\beta_1^{(8,14)}(g_1, g_2) &= [-18 N g_1^2 + 621 g_1^2 - 252 g_1 g_2 + 7 g_2^2] \frac{g_1}{272160} \\
&\quad + [171159480 N g_1^4 - 12056931 g_1^4 - 67296096 N g_1^3 g_2 \\
&\quad - 377785296 g_1^3 g_2 + 1869336 N g_1^2 g_2^2 - 7019838 g_1^2 g_2^2 \\
&\quad - 59274432 g_1 g_2^3 + 1103396 g_2^4] \frac{g_1}{186659085312000} \\
&\quad + O(g_i^6) , \\
\beta_2^{(8,14)}(g_1, g_2) &= [72 N g_1^3 - 6 N g_1^2 g_2 + g_2^3] \frac{1}{30240} \\
&\quad + [-7007148 N g_1^5 + 25365069 N g_1^4 g_2 + 27512136 N g_1^3 g_2^2 \\
&\quad - 639018 N g_1^2 g_2^3 + 2198333 g_2^5] \frac{1}{15554923776000} \\
&\quad + O(g_i^7) . \quad (5.44)
\end{aligned}$$

Equally for similar computational constraints we could only determine the full Renormalization Group functions for $L^{(8,16)}$ at one loop. We found

$$\begin{aligned}
\gamma_\phi^{(8,16)}(g_i) &= \frac{g_1^2}{6048} \\
&\quad + [-1468755 N g_1^2 - 55406142 g_1^2 - 4477968 g_1 g_2 - 29420424 g_1 g_3 \\
&\quad - 2792128 g_2^2 + 2456232 g_2 g_3 - 2116377 g_3^2] \frac{g_1^2}{1003811081011200} \\
&\quad + O(g_i^6) ,
\end{aligned}$$

$$\begin{aligned}
\gamma_\sigma^{(8,16)}(g_i) &= [45Ng_1^2 + 296g_2^2 - 384g_2g_3 + 159g_3^2] \frac{1}{5987520} \\
&+ [-2880219870Ng_1^4 - 1664530560Ng_1^3g_2 - 338294880Ng_1^3g_3 \\
&- 479937600Ng_1^2g_2^2 + 584739000Ng_1^2g_2g_3 - 243713475Ng_1^2g_3^2 \\
&- 1869662576g_2^4 + 691909088g_2^3g_3 - 1637070624g_2^2g_3^2 \\
&- 2769180480g_2^2g_4^2 + 4241645772g_2g_3^3 + 3466964160g_2g_3g_4^2 \\
&- 1825036161g_3^4 - 1227798000g_3^2g_4^2 \\
&- 86444820g_4^4] \frac{1}{496886485100544000} + O(g_i^6), \\
\beta_1^{(8,16)}(g_i) &= [45Ng_1^2 + 4356g_1^2 + 1584g_1g_2 + 792g_1g_3 + 296g_2^2 - 384g_2g_3 \\
&+ 159g_3^2] \frac{g_1}{11975040} + O(g_i^4), \\
\beta_2^{(8,16)}(g_i) &= [1782Ng_1^3 + 135Ng_1^2g_2 + 2516g_2^3 - 866g_2^2g_3 - 447g_2g_3^2 + 3168g_2g_4^2 \\
&- 330g_3^3 - 2376g_3g_4^2] \frac{1}{11975040} + O(g_i^5), \\
\beta_3^{(8,16)}(g_i) &= [2376Ng_1^3 + 135Ng_1^2g_3 + 176g_2^3 - 696g_2^2g_3 - 1020g_2g_3^2 \\
&+ 961g_3^3] \frac{1}{11975040} + O(g_i^5), \\
\beta_4^{(8,16)}(g_i) &= [1782Ng_1^4 + 45Ng_1^2g_4^2 + 352g_2^4 + 704g_2^3g_3 + 528g_2^2g_3^2 + 1880g_2^2g_4^2 \\
&+ 176g_2g_3^3 + 1200g_2g_3g_4^2 + 22g_3^4 + 555g_3^2g_4^2 \\
&+ 891g_4^4] \frac{1}{2993760} + O(g_i^6). \tag{5.45}
\end{aligned}$$

The two loop wave function anomalous dimensions were computed to provide a non-trivial check on the one loop coupling constant renormalization via ensuring the double pole at two loops correctly emerges consistent with the RG equation. All the Renormalization Group functions have been determined using dimensional regularisation with the renormalization constants defined with respect to the modified minimal subtraction ($\overline{\text{MS}}$) scheme. It is worth nothing that in the critical dimension of each Lagrangian we used the coupling constant dimensionless in that dimension but the standard arbitrary scale is introduced to preserve dimensionlessness of the couplings in the regularised theory.

5.4 Fixed Point Analysis

The main reason for constructing the RG functions is to verify that the critical exponents at the Wilson-Fisher fixed point are consistent with the large N critical exponents calculated in section 5.2 for the underlying theory. In order to carry out the comparison we follow the process given in [51, 52] and first find the values

of the critical coupling constants g_i^* by solving

$$\beta_i^{(d_1, d_2)}(g_j^*) = 0 \quad (5.46)$$

where g_j^* is a power series in $1/N$. Taking the $L^{(8,10)}$ theory as an example, the coupling constant is rescaled by a factor to keep the results consistent with the work of [51–53],

$$g_1 = \frac{x\sqrt{12N\epsilon}}{N}$$

where the new coupling constant x is a power series in $1/N$

$$x = x_0 + \frac{x_1}{N} + \frac{x_2}{N^2} + \frac{x_3}{N^3} + \dots$$

Each coefficient is in itself a power series in ϵ aside from the leading order $1/N$ term which only involves ϵ due to the structure of the N dependence at two and higher loops. Once these critical couplings are determined the field anomalous dimensions $\gamma_\phi^{(d_1, d_2)}(g_i)$ and $\gamma_\sigma^{(d_1, d_2)}(g_i)$ are evaluated at criticality as a series in $1/N$. Then the coefficients of each term in ϵ of each successive power of $1/N$ should be in total agreement with the critical exponents η and $\eta + \chi$ respectively. We have checked this correspondence holds for all the Renormalization Group functions in the thread $n = 2$ for the large N exponents η_1 , χ_1 and η_2 computed. For completeness the ϵ -expanded critical exponents calculated in the critical dimensions are

$$\begin{aligned} \eta_1^{(8)} &= 88\epsilon - \frac{65278}{315}\epsilon^2 - \frac{66531221}{198450}\epsilon^3 + O(\epsilon^4), \\ (\eta_1 + \chi_1)^{(8)} &= -\frac{10648}{5}\epsilon + \frac{406978}{63}\epsilon^2 + \frac{4601740271}{992250}\epsilon^3 + O(\epsilon^4), \\ \eta_1^{(8,10)} &= 936\epsilon - \frac{857938}{385}\epsilon^2 - \frac{9303326749}{2668050}\epsilon^3 + O(\epsilon^4), \\ (\eta_1 + \chi_1)^{(8,10)} &= -39104\epsilon + \frac{54864544}{495}\epsilon^2 + \frac{1224918967472}{12006225}\epsilon^3 + O(\epsilon^4), \\ \eta_1^{(8,12)} &= 10336\epsilon - \frac{1127998496}{45045}\epsilon^2 - \frac{76011160703752}{2029052025}\epsilon^3 + O(\epsilon^4), \\ (\eta_1 + \chi_1)^{(8,12)} &= -\frac{17390320}{27}\epsilon + \frac{48368473220}{27027}\epsilon^2 + \frac{19304724881269937}{10956880935}\epsilon^3 \\ &\quad + O(\epsilon^4), \\ \eta_1^{(8,14)} &= 118864\epsilon - \frac{1882358228}{6435}\epsilon^2 - \frac{852336345618763}{2029052025}\epsilon^3 + O(\epsilon^4), \\ (\eta_1 + \chi_1)^{(8,14)} &= -\frac{112683072}{11}\epsilon + \frac{4039782672}{143}\epsilon^2 + \frac{212144421361482188}{7439857425}\epsilon^3 \\ &\quad + O(\epsilon^4), \\ \eta_1^{(8,16)} &= 1415880\epsilon - \frac{42906667899}{12155}\epsilon^2 - \frac{170100399530093051}{34749394680}\epsilon^3 \end{aligned}$$

$$\begin{aligned}
& + O(\epsilon^4) , \\
(\eta_1 + \chi_1)^{(8,16)} &= - \frac{2089052280}{13} \epsilon + \frac{16109344477639}{36465} \epsilon^2 \\
& + \frac{37381478285711124137}{82973044440} \epsilon^3 + O(\epsilon^4) . \tag{5.47}
\end{aligned}$$

Such agreement should be regarded as evidence for the underlying universality of the core interaction across the dimensions in the same spirit as that of the original and well-established universality of the Wilson-Fisher fixed point of $O(N)$ ϕ^4 theory given by the $n = 1$ thread. Equally the agreement is a reassuring check that the renormalization has been correctly performed to several loop orders which relied on elevating various integrals to higher dimensions.

Having established the connection with the underlying universal theory we now analyse aspects of the non-trivial fixed point structure of each theory and in particular the location, if it exists, of the conformal window. This analysis will fall into two classes, the first class of critical points is a feature of a single coupling theory. A well established example is Quantum Chromodynamics (QCD) where the signs of the one and two loop term of the single coupling strictly four dimensional β -function are different. The subsequent non-trivial fixed point is called the Banks-Zaks fixed point, [88]. The only higher dimensional theory constructed here that possesses one coupling is given by the Lagrangian $L^{(8,10)}$. As it turns out this theory will fall into the same class as QCD. We have calculated the fixed point structure of $\beta^{(8,10)}(g_1)$ by first rescaling the coupling in the same manner as [51, 52] using the factor given in equation (5.4). This maintains consistency in the results. We then set a value for N and attempt to solve for the coupling. A selection of results are

$$\begin{aligned}
x_{N=2}^{(8,10)} &= 1.581139i + 1.707136i\epsilon + 11.843630i\epsilon^2 + O(\epsilon^3) , \\
x_{N=3}^{(8,10)} &= 2.236068i + 5.515634i\epsilon + 75.679580i\epsilon^2 + O(\epsilon^3) , \\
x_{N=4}^{(8,10)} &= 3.162278i + 21.444195i\epsilon + 697.298728i\epsilon^2 + O(\epsilon^3) , \\
x_{N=5}^{(8,10)} &= 5i + 160.25i\epsilon^2 + 21131.6928119i\epsilon^2 + O(\epsilon^3) , \\
x_{N=6}^{(8,10)} &= 0 , \\
x_{N=7}^{(8,10)} &= 5.916080 + 247.883743\epsilon + 20485.390260\epsilon^2 + O(\epsilon^3) , \\
x_{N=8}^{(8,10)} &= 4.472136 + 52.351942\epsilon + 1475.523528\epsilon^2 + O(\epsilon^3) , \\
x_{N=9}^{(8,10)} &= 3.872983 + 22.269654\epsilon + 244.424231\epsilon^2 + O(\epsilon^3) , \\
x_{N=10}^{(8,10)} &= 3.535534 + 12.523524\epsilon + 63.536945\epsilon^2 + O(\epsilon^3) .
\end{aligned}$$

It is clear to see that the boundary of the conformal window lies at the value

$N = 6$. In fact, we can see that the two loop term of $\beta^{(8,10)}(g_1)$ is always negative but the one loop term changes sign at $N = 6$. Hence it is straightforward to conclude that the conformal window is $N > 6$. When $N = 6$ the two and three loop terms are both negative which is the reason for the strict inequality. Above $N = 6$ the non-trivial critical coupling of the fixed point is real whereas it becomes pure imaginary below this value of N .

The second class of fixed point analysis concerns theories with more than one coupling constant. To access the conformal window we have to solve a set of equations, [51,52], which for two coupling theories considered are

$$\begin{aligned} \beta_1(g_i) &= \beta_2(g_i) = 0, \\ \frac{\partial\beta_1}{\partial g_1} \frac{\partial\beta_2}{\partial g_2} - \frac{\partial\beta_1}{\partial g_2} \frac{\partial\beta_2}{\partial g_1} &= 0. \end{aligned} \quad (5.48)$$

The first equation determines the critical couplings and the final equation, which is the vanishing of the Hessian, provides the condition where there is a change in the stability property of a fixed point. Moreover, as in [51,52], we can determine the window as a perturbative series in ϵ which, in principle, provides insight into other dimensions. For $L^{(8,12)}$ we find three solutions to the equation set (5.48). The critical values of N along with the fixed point values for the three solutions are

$$\begin{aligned} N_{(A)}^{(8,12)} &= 1.015123 - 0.024469\epsilon - 0.324484\epsilon^2 + O(\epsilon^3), \\ x_{(A)}^{(8,12)} &= 1.413668i - 0.113986\epsilon + 7.181859i\epsilon^2 + O(\epsilon^3), \\ y_{(A)}^{(8,12)} &= 1.290822i - 0.011116\epsilon - 5.679283i\epsilon^2 + O(\epsilon^3), \\ N_{(B)}^{(8,12)} &= -0.366698 + 0.451194\epsilon - 41.675880\epsilon^2 + O(\epsilon^3), \\ x_{(B)}^{(8,12)} &= 1.365178 - 0.688747\epsilon + 69.948018\epsilon^2 + O(\epsilon^3), \\ y_{(B)}^{(8,12)} &= -0.579975 + 0.757594\epsilon - 86.044498\epsilon^2 + O(\epsilon^3), \\ N_{(C)}^{(8,12)} &= -910.687640 + 2668.861873\epsilon - 1565.439288\epsilon^2 + O(\epsilon^3), \\ x_{(C)}^{(8,12)} &= 6.821431i + 0.214285i\epsilon + 0.194583i\epsilon^2 + O(\epsilon^3), \\ y_{(C)}^{(8,12)} &= -48.271870i + 107.514458i\epsilon^2 + O(\epsilon^3). \end{aligned}$$

Solution B has real critical couplings whereas the other two solutions are imaginary. Given the non-unitary nature of solution A and the negative corrections to the critical value of N defining the conformal window boundary, it would appear that for this theory there is no interesting structure. By contrast for the theory based on the related group $Sp(N)$, that is making the adjustment $N \rightarrow -N$ in the Renormalization Group functions, the conformal window is determined from

the negative solutions, [182]. This means that the theory would appear to have a conformal window around $N = 910$. A similar feature was observed in the eight-dimensional extension of the $O(N)$ universality class, [53]. Moving on to $L^{(8,14)}$ theory, there are three real solutions for the conformal window of $\beta_i^{(8,14)}(g_1, g_2)$ which are

$$\begin{aligned}
N_{(A)}^{(8,14)} &= 602.601144 - 33341.878584\epsilon + O(\epsilon^2) , \\
x_{(A)}^{(8,14)} &= 24.798057 + 382.085407\epsilon + O(\epsilon^2) , \\
y_{(A)}^{(8,14)} &= 794.728224 + 55417.635536\epsilon + O(\epsilon^2) , \\
N_{(B)}^{(8,14)} &= 0.627879 - 1.399181\epsilon + O(\epsilon^2) , \\
x_{(B)}^{(8,14)} &= 4.841765i - 11.017963i\epsilon + O(\epsilon^2) , \\
y_{(B)}^{(8,14)} &= 6.091652i - 35.439190i\epsilon + O(\epsilon^2) , \\
N_{(C)}^{(8,14)} &= -186.979023 + 45848.701747\epsilon + O(\epsilon^2) , \\
x_{(C)}^{(8,14)} &= 6.204761 + 433.091887\epsilon + O(\epsilon^2) , \\
y_{(C)}^{(8,14)} &= -430.028090 + 74159.460689\epsilon + O(\epsilon^2) .
\end{aligned}$$

There is a clear indication of a conformal window here with a relatively high value for N which is similar to the six-dimensional ϕ^3 theory in the $O(N)$ universality class looked at in [51–53]. The multi-coupling theory $L^{(8,16)}$ has a larger number of couplings and hence the β -functions together with a substantial Hessian means that our computer resources rather than any principle are not powerful enough to solve the system of equations in general.

5.5 Discussion

Instead of continuing research into universality classes by analysing higher dimensional extensions of other scalar or even gauge theories, we have chosen to take a different path. The ideas in this Chapter are centred on the observation that the universal theory based on the ϕ^4 interaction has an infinite number of universality classes. The core interaction $\sigma\phi^i\phi^i$ defines the linear relation between the dimensions of the separate fields. Ordinarily one regards the kinetic term as the canonical starting point for constructing a Lagrangian rather than the interaction. We instead considered the Lagrangian construction from a critical point perspective where the interaction by contrast informs the kinetic term. The variable n emerges from the general solution for the dimensions of the two fields and relates to or classifies the power of the derivatives in the kinetic term. In [48–50] specific solutions were examined at length in the $n = 1$ thread. For integers $n > 1$

higher derivative kinetic terms emerge. A higher value of n increases the critical dimension where the Lagrangian is renormalizable. It also opens up a host of new Lagrangians which can be studied within the developing d -dimensional conformal field theory formalism. Free field higher derivative kinetic terms were investigated in [234–236]. We now have an opportunity to look at interacting cases. Interacting higher derivative scalar field theories can be used as a laboratory to study connections with AdS/CFT ideas as well as being a starting point to classify and more importantly connect scalar quantum field theories. They also have links to physics via elasticity, [68].

The higher threads of n are accessible via the large N expansion developed in [48–50]. In this Chapter new large N d -dimensional solutions were computed for the critical exponents η and χ at next to leading order for $n = 2$. These large N exponents were found to be in complete agreement with the exponents calculated using traditional perturbation theory for every Lagrangian in the $n = 2$ thread. Therefore a new universality class, analogous to the existing $n = 1$ tower, was established. The next stage of research would be to compute other large N exponents for $n = 2$ such as ν as well as η at $O(1/N^3)$. Although here we have concentrated on the $n = 2$ tower of theories, results for $n = 3$ have been published in [3]. Additionally there is no reason why the analysis cannot be extended to higher values of n aside from potential computation limitations. For all Lagrangians constructed for the $n > 1$ the critical dimension will be greater than four. This opens up a new potential feature described in [3] as lower dimensional completeness. This is a speculative idea that involves constructing Lagrangians in a lower dimension than the base theory. For example six, four and two dimensional theories may be constructed using the eight dimensional Lagrangian (5.5) which will also lie in the $n = 2$ universality class.

A complicating feature which emerges in lower dimensional constructions appears to be the presence of non-localities. At the critical point this is not a major problem compared with trying to construct a viable non-local Lagrangian away from criticality. There are examples, such as that introduced by Gribov, [238], which can be renormalized after the localization process introduced by Zwanziger, [239–244]. In principle this provides a potential route to study lower dimensional complete Lagrangians. Understanding non-localities in the Lagrangian context may inform models of colour confinement in Yang-Mills theories for which the Gribov construction has already been widely studied. Further work will require going beyond the scalar theories considered. The development of higher derivative scalar quantum field theories (QFTs) has been discussed in this

Chapter in detail. Suggestions on how these ideas can be extended to fermionic models such as the $O(N)$ Gross-Neveu and non-abelian Thirring model have been indicated in [3]. The extension of general large N solutions with $n > 1$ leading to higher derivative fermionic theories is yet to be analysed in the same depth perturbatively or in the large N construction which we leave to future work.

Part II

The Banks-Zaks Fixed Point of Quantum Chromodynamics

Background

6.1 Gauge Theories

In Part I we looked at the d -dimensional Wilson-Fisher (WF) fixed point and considered only scalar quantum field theories (QFTs). Calculations involving scalar theories are much simpler than those containing gauge fields as they contain Feynman integrals with a more basic structure. While they provide a useful testing ground for ideas on universality and the stability of fixed points, scalar theories lack crucial fermionic particles which are essential if one wishes to study real world physics. In Part II we move our focus from the Wilson-Fisher fixed point to the Banks-Zaks fixed point of Quantum Chromodynamics (QCD). The Banks-Zaks fixed point is different from the Wilson-Fisher fixed point in that it is strictly four dimensional and can only be found using the β -function of QCD. The Banks-Zaks fixed point is of interest mainly due to its apparent connection with chiral symmetry breaking. We therefore use this Chapter to review the background of gauge theories to support calculations in later Chapters on the location of this fixed points and corresponding critical exponents.

A gauge theory is a type of quantum field theory (QFT) in which the Lagrangian is invariant under certain Lie groups of local transformations. Gauge theories enable the interaction of elementary particles. These interactions appear in different guises; the strong (nuclear) interaction and the electroweak interaction being the two most associated with the Standard Model. The term gauge refers to any specific mathematical formalism to regulate redundant degrees of freedom in the Lagrangian. Transformations between possible gauges form a Lie algebra of group generators and for each group generator a corresponding

gauge field arises. Moreover, physical quantities must be gauge invariant. The idea of a gauge field first appeared in 1864 in James Clerk Maxwell's theory of electromagnetism. The principle of gauge invariance dictated the form of the electromagnetic interaction. However the symmetries of the theory, both Lorentz and gauge, were not fully appreciated until the end of the 19th century. A full understanding of gauge invariance required insights of both quantum mechanics and relativity. After Einstein developed his theory of general relativity, in which a dynamical role was given to geometry, Herman Weyl conjectured that perhaps the scale of length would also be dynamical. He imagined a theory in which the scale of all dimensional quantities would vary from point to point in space and time. His motivation was to unify gravity and electromagnetism; to find a geometrical origin for electrodynamics. In 1929 Weyl showed how electrodynamics was invariant under the gauge transformation of the gauge field. However gauge invariance was still regarded as a complication and a technical difficulty that had to be carefully handled.

In 1954, Chen-Ning Yang and Robert L. Mills created what is now known as Yang-Mills gauge theory through a generalisation of Maxwell's theory for non-abelian field theories, [248]. For 20 years the idea of gauge invariance was regarded as a beautiful but ultimately useless mathematical exercise. That all changed in the 1970s when it was called upon to unify the electromagnetic and weak interactions. The main difficulty in the resulting electroweak theory was how to break gauge invariance. If unbroken the gauge bosons are necessarily massless. The fact that such particles, aside from the photon, do not exist in Nature was a major stumbling block for Yang-Mills. The solution came by insight from Peter Higgs, Robert Brout, François Englert and Tom Kibble, [8, 9, 249], in the form of the Higg's mechanism to explain how the symmetry of Yang-Mills theory may be apparently broken yet no massless vector mesons need emerge. The application of Yang-Mills to the strong interaction; the original motivation for the theory, was even trickier. Yang and Mills constructed a prototype quantum field theory of strong interactions modelled closely on Quantum Electrodynamics (QED) and its symmetries, this was named Quantum Chromodynamics. A major difficulty was that the constituents of hadrons as well as the conserved charges were all hidden by confinement. The idea that hadrons might be composed of quarks emerged in the work of Gell-Mann and Zweig in 1964, [15, 16], from the approximate flavour $SU(3)$ symmetry of the strong interaction. The Gell-Mann 'Eightfold Way' was proposed in 1961, [250], to classify baryons and mesons for the first time. The triangular 'Eightfold Way' was established in 1964. It was known as the quark model and contained three unique quarks; up, down and strange. Although this

model was mathematically sound, the problem was that no individual quark had ever been seen in Nature, a problem which still exists today. In the late 1960s an experiment by Jerome Friedman, Henry Kendall and Richard Taylor at the Stanford Linear Accelerator Centre (SLAC) produced evidence that quarks exist. All three physicists were awarded Nobel prize for their work in 1990.

The discovery that QCD was asymptotically free was a key advancement in physics, first remarked upon in 1972, [251]. A few years later QCD was found by 't Hooft and Veltman, [122], to be a renormalizable quantum field theory. Three additional and much heavier quarks were predicted but not discovered until much later. The charm quark was found in 1974 and the top quark was discovered at FermiLab, [252, 253], in 1995 with a mass of 175GeV. At present the complete quark model contains six flavours; up, down, strange, charm, bottom and top. In 1979 gluons, predicted by QCD to be carriers of the strong force which binds quarks together, were discovered via electron-positron annihilation at the Deutsches Elektronen-Synchrotron (DESY), [254]. Quantum Chromodynamics is the most realistic quantum field theory describing the strong force at both the microscopic (quarks and gluons) and macroscopic (hadronic) level. Although there has been a good agreement between theory and experiment in general, gaps in QCD as a field theory still remain. The underlying mechanism behind confinement, for example, is still unsolved. This has led to infrared (IR) QCD being a key area of interest since perturbative calculations do not suffice in this region which makes confinement difficult to probe analytically. Despite the problem that quarks are thought to be absolutely confined, QCD along with electroweak (EW) theory forms the basis for the Standard Model which is the foundation for all non-gravitational physics. In Part II we focus our perturbative calculations on QCD. The main reason being that an interesting non-trivial fixed point emerges from its β -function, the Banks-Zaks fixed point, [88]. Before attempting any perturbative calculation of the location of this fixed point we first discuss the theory of QCD in more detail. To construct the interacting QCD Lagrangian and gauge fixing terms we follow the work of [245–247].

6.2 Quantum Chromodynamics

Quantum Chromodynamics is an unbroken gauge theory which describes the interaction of quarks via their colour quantum numbers. It has a similar structure to that of QED with the main difference being that QCD is invariant under a non-abelian gauge group. The gauge bosons in QCD are gluons whereas for QED

they are photons. Nevertheless QCD can be derived in the same way as QED. We begin with a non-interacting quark Lagrangian before modifying it to be invariant under a change of gauge. The gauge transformation for QCD is the non-abelian group $SU(3)$. The special unitary Lie group $SU(N_c)$ is a group of $N_c \times N_c$ unitary matrices satisfying the conditions

$$U^\dagger U = 1 \quad \text{and} \quad \det U = 1 ,$$

where $U \in \text{Mat}_n(\mathbb{C})$ is an element of $SU(N_c)$. A complex 3×3 matrix is characterised by eighteen numbers but only eight are independent if the matrix is hermitian, traceless and has a determinant equal to one. The dimension of the $SU(3)$ gauge group is therefore equal to eight and we can form a basis of eight matrices for the group satisfying

$$\text{Tr}(\lambda^a \lambda^b) = 2\delta^{ab}$$

where λ^a are the Gell-Mann matrices, [255], given by

$$\begin{aligned} \lambda^1 &= \begin{pmatrix} 0 & 1 & 0 \\ 1 & 0 & 0 \\ 0 & 0 & 0 \end{pmatrix} & \lambda^2 &= \begin{pmatrix} 0 & -i & 0 \\ i & 0 & 0 \\ 0 & 0 & 0 \end{pmatrix} & \lambda^3 &= \begin{pmatrix} 1 & 0 & 0 \\ 0 & -1 & 0 \\ 0 & 0 & 0 \end{pmatrix} \\ \lambda^4 &= \begin{pmatrix} 0 & 0 & 1 \\ 0 & 0 & 0 \\ 1 & 0 & 0 \end{pmatrix} & \lambda^5 &= \begin{pmatrix} 0 & 0 & -i \\ 0 & 0 & 0 \\ i & 0 & 0 \end{pmatrix} & \lambda^6 &= \begin{pmatrix} 0 & 0 & 0 \\ 0 & 0 & 1 \\ 0 & 1 & 0 \end{pmatrix} \\ \lambda^7 &= \begin{pmatrix} 0 & 0 & 0 \\ 0 & 0 & -i \\ 0 & i & 0 \end{pmatrix} & \lambda^8 &= \frac{1}{\sqrt{3}} \begin{pmatrix} 1 & 0 & 0 \\ 0 & 1 & 0 \\ 0 & 0 & -2 \end{pmatrix} . \end{aligned} \quad (6.1)$$

These eight matrices play a role that is equivalent to that of the Pauli matrices of $SU(2)$. Note that the Pauli matrices are in fact contained within the matrices of (6.1). The Gell-Mann matrices are unitary and together with the 3-dimensional quark vectors on which they act form the fundamental representation. The fundamental or anti-fundamental representations are the most basic irreducible representation. By irreducible we mean that the set of matrices cannot be decomposed into block diagonal form.

Although they are the most popular to use, (6.1) are only one of several possible representations of the infinitesimal generators of $SU(3)$. The commutation

relation of the matrices is given by

$$[\lambda^a, \lambda^b] = 2if^{abc}\lambda^c \quad (6.2)$$

where the repeated index implies the sum of all eight gluon colour states, as is consistent with Einstein's summation convention. The colour group structure constants f^{abc} are anti-symmetric under exchange of any two indices for all $SU(N_c)$. The non-zero structure constants are

$$\begin{aligned} f^{123} &= 1, & f^{147} &= f^{246} = f^{257} = f^{345} = \frac{1}{2}, \\ f^{156} &= f^{367} = -\frac{1}{2}, & f^{458} &= f^{678} = \frac{\sqrt{3}}{2}. \end{aligned} \quad (6.3)$$

The generators of the gauge group in the fundamental representation can be defined by

$$t^a = \frac{1}{2}\lambda^a \quad (6.4)$$

where $a = 1, \dots, 8$ and t^a are hermitian operators which form the Lie algebra defined by the commutation relation

$$[t^a, t^b] = if^{abc}t^c. \quad (6.5)$$

The Jacobi identity can be determined using the general result for the commutator.

$$\begin{aligned} [t^a, [t^b, t^c]] + [t^b, [t^c, t^a]] + [t^c, [t^a, t^b]] &= 0 \\ if^{bce}[t^a, t^e] + if^{cae}[t^b, t^e] + if^{abe}[t^c, t^e] &= 0 \\ i^2 f^{bce} f^{aed} t^d + i^2 f^{cae} f^{bed} t^d + i^2 f^{abe} f^{ced} t^d &= 0 \\ - (f^{bce} f^{aed} + f^{cae} f^{bed} + f^{abe} f^{ced}) t^d &= 0 \\ f^{ade} f^{bce} + f^{ace} f^{dbe} + f^{abe} f^{cde} &= 0. \end{aligned}$$

In general a Lie algebra will contain n elements, r of which will commute amongst themselves and are known as the Cartan sub-algebra. For $SU(3)$ the two diagonalised generators t^3 and t^8 form the Cartan sub-algebra

$$[t^3, t^8] = 0.$$

To define the adjoint representation we first introduce the step operators which are made up of the remaining six generators. The six independent step operators

are given by

$$\begin{aligned} E_+^{12} &= i(t^1 + it^2) \quad , \quad E_-^{12} = i(t^1 - it^2) \quad , \\ E_+^{45} &= i(t^4 + it^5) \quad , \quad E_-^{45} = i(t^4 - it^5) \quad , \\ E_+^{67} &= i(t^6 + it^7) \quad , \quad E_-^{67} = i(t^6 - it^7) \quad . \end{aligned}$$

The commutation relations of these step operators with the Cartan sub-algebra can be computed as

$$\begin{aligned} [t_3, E_\pm^{12}] &= f^{123} E_\pm^{12} = E_\pm^{12} \quad , \quad [t_8, E_\pm^{12}] = f^{128} E_\pm^{12} = 0 \quad , \\ [t_3, E_\pm^{45}] &= f^{453} E_\pm^{45} = \frac{1}{2} E_\pm^{45} \quad , \quad [t_8, E_\pm^{45}] = f^{458} E_\pm^{45} = \frac{\sqrt{3}}{2} E_\pm^{45} \quad , \\ [t_3, E_\pm^{67}] &= f^{673} E_\pm^{67} = -\frac{1}{2} E_\pm^{67} \quad , \quad [t_8, E_\pm^{67}] = f^{678} E_\pm^{67} = \frac{\sqrt{3}}{2} E_\pm^{67} \quad . \end{aligned}$$

Consequently we can then define six roots of the Lie algebra,

$$\begin{aligned} \alpha_\pm^{12} &= (\pm f^{123}, \pm f^{128}) \quad , \\ \alpha_\pm^{45} &= (\pm f^{453}, \pm f^{458}) \quad , \\ \alpha_\pm^{67} &= (\pm f^{673}, \pm f^{678}) \quad . \end{aligned}$$

These roots, along with two additional roots at $\alpha_\pm^{38} = (\pm f^{383}, \pm f^{388}) = (0, 0)$ for the generators t^3 and t^8 , are plotted in figure 6.1. This is known as the ‘eight-fold way’ and displays the adjoint representation illustrating the eight gluons.

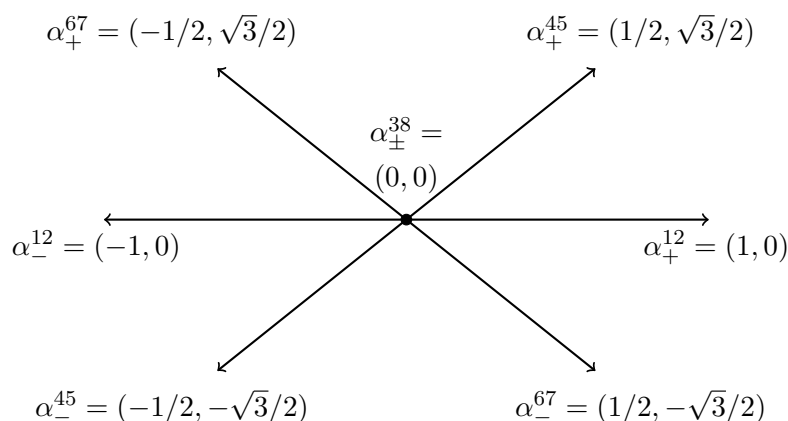


Figure 6.1: The ‘eight-fold way’ or adjoint representation of the $SU(3)$ Lie group.

The fundamental and adjoint representations are used when dealing with quarks and gluons respectively. However other representations are possible. The elementary Casimirs that commute with all generators of the group are defined for any

general lie group as

$$\begin{aligned} \text{Tr}(t^a t^b) &= T_F \delta^{ab} , \\ t^a t^b &= C_F \mathbb{I} , \\ f^{acd} f^{bed} &= C_A \delta^{ab} \end{aligned} \quad (6.6)$$

for general N_c where A and F represent the adjoint and fundamental representations respectively. The rank 2 Casimirs have dimension N_F and N_A , respectively, and hence N_F and N_A are the relative dimensions of the fundamental and adjoint representations. The Dynkin index is T_F and N_f is the number of massless quark flavours. Using these definitions of the Casimirs we are able to simplify expressions and are free to calculate in a general $SU(N_c)$ gauge group. We have again utilized the Einstein summation convention to simplify the definitions of the group Casimirs. For example, the second definition in (6.6) is used instead of $\sum_a t_{ij}^a t_{jk}^a = C_F \delta_{ik}$ where $i = 1, \dots, N_f$, to simplify the expression. For the $SU(3)$ gauge group the Casimirs take the following values

$$C_F = \frac{4}{3} \quad , \quad T_F = \frac{1}{2} \quad , \quad C_A = N_c = 3 . \quad (6.7)$$

The three dimensional quark vectors which the Gell-Mann matrices act on to form the fundamental representation are given by

$$\psi(x) = \begin{pmatrix} \psi_{\text{red}}(x) \\ \psi_{\text{blue}}(x) \\ \psi_{\text{green}}(x) \end{pmatrix} \quad , \quad \bar{\psi}(x) = \left(\bar{\psi}_{\text{red}}(x), \bar{\psi}_{\text{blue}}(x), \bar{\psi}_{\text{green}}(x) \right) . \quad (6.8)$$

Each entry represents a colour charge. There are three different quark colours for each flavour and six flavours in total; up, down, strange, charm, bottom and top. The colour charge was introduced by Greenberg as a way of solving the problem of the quark model violating the Pauli exclusion principle, [17], which says that no two electrons can occupy the same state, [256]. Since quarks have half integer spin, this also applies to them. We can at this point illustrate the fundamental and anti-fundamental representations. If we compute the Cartan sub-algebra multiplied by the first entry of the quark 3-vector then we obtain

$$t_3(1, 0, 0) = \frac{1}{2} \begin{pmatrix} 1 & 0 & 0 \\ 0 & -1 & 0 \\ 0 & 0 & 0 \end{pmatrix} (1, 0, 0) = \frac{1}{2}(1, 0, 0) = \mu_{1,1}(1, 0, 0) ,$$

$$t_8(1, 0, 0) = \frac{1}{2\sqrt{3}} \begin{pmatrix} 1 & 0 & 0 \\ 0 & 1 & 0 \\ 0 & 0 & -2 \end{pmatrix} (1, 0, 0) = \frac{1}{2\sqrt{3}}(1, 0, 0) = \mu_{1,2}(1, 0, 0).$$

Hence the first weight of the fundamental representation can be defined as

$$\mu_1 = (\mu_{1,1}, \mu_{1,2}) = \left(\frac{1}{2}, \frac{1}{2\sqrt{3}} \right).$$

Multiplying the Cartan sub-algebra by the second and third entries of the quark 3-vector we obtain the two remaining weights of the fundamental representation

$$\begin{aligned} \mu_2 &= (\mu_{2,1}, \mu_{2,2}) = \left(-\frac{1}{2}, \frac{1}{2\sqrt{3}} \right), \\ \mu_3 &= (\mu_{3,1}, \mu_{3,2}) = \left(0, -\frac{1}{\sqrt{3}} \right). \end{aligned}$$

The fundamental and anti-fundamental representations are illustrated in figures 6.2 (a) and (b), respectively. The anti-fundamental representation is found by multiplying the weights of the fundamental representation by -1 .

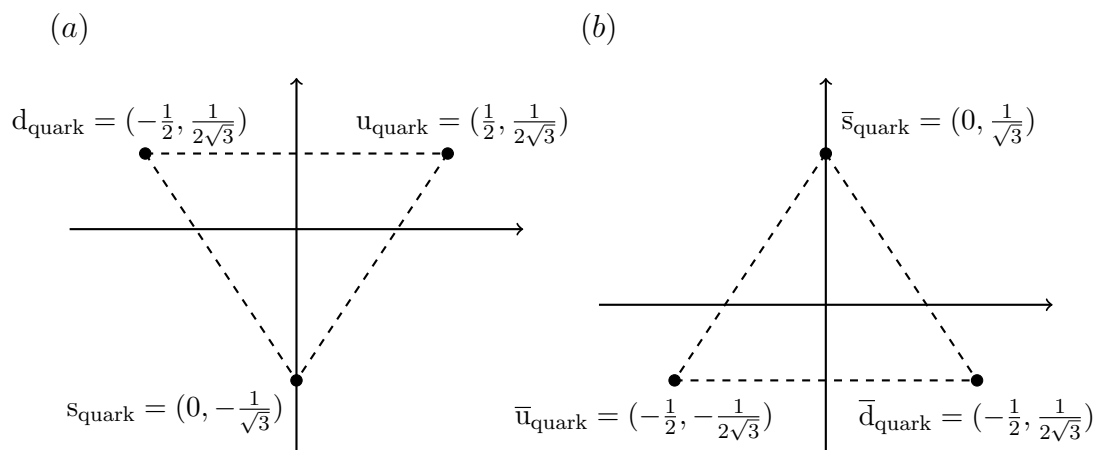


Figure 6.2: The (a) fundamental and (b) anti-fundamental representations of $SU(3)$.

In Part II we will be calculating in several representations, therefore we give explicit values for the group invariants of these representations in table 6.1. The representations included are the fundamental representation denoted by F , the adjoint representation labelled as G , the two-indexed symmetric representation denoted by $2S$ and two-indexed anti-symmetric representation given by $2A$, [97]. The notation in the table is as follows; $T(r)$ and $C_2(r)$ give the trace normalization factor and quadratic Casimir respectively. In the fundamental representation these correspond to $T(r) = T_F$ and $C_2(r) = C_F$, respectively. These group invariants enter at every loop order. Furthermore $d(r)$ gives the dimension of the

representation, in the fundamental this is denoted N_F and in the adjoint this is N_A . The fourth order tensor d_r^{abcd} is also given in table 6.1 which appears at four loops.

r	$d(r)$	$T(r)$	$C_2(r)$
F	N	$\frac{1}{2}$	$\frac{N^2-1}{2N}$
G	$N^2 - 1$	N	N
$2S$	$\frac{N(N+1)}{2}$	$\frac{N+2}{2}$	$\frac{(N-1)(N+2)}{N}$
$2A$	$\frac{N(N-1)}{2}$	$\frac{N-2}{2}$	$\frac{(N+1)(N-2)}{N}$

r	$d_r^{abcd} d_G^{abcd}$	$d_r^{abcd} d_r^{abcd}$
F	$\frac{N(N^2-1)(N^2+6)}{48}$	$\frac{(N^2-1)(N^4-6N^2+18)}{96N^2}$
G	$\frac{N^2(N^2-1)(N^2+36)}{24}$	$\frac{N^2(N^2-1)(N^2+36)}{24}$
$2S$	$\frac{N(N^2-1)(N+2)(N^2+6N+24)}{48}$	$\frac{(N^2-1)(N+2)(N^5+14N^4+72N^3-48N^2-288N+576)}{96N^2}$
$2A$	$\frac{N(N^2-1)(N-2)(N^2-6N+24)}{48}$	$\frac{(N^2-1)(N-2)(N^5-14N^4+72N^3+48N^2-288N-576)}{96N^2}$

Table 6.1: Group invariants for $SU(N)$. The explicit values for four representations r are displayed.

The non-interacting Lagrangian for QCD is given by the basic Dirac Lagrangian describing the free fermion field

$$L = i\bar{\psi}^i(x)\gamma^\mu\partial_\mu\psi^i(x) - m\bar{\psi}^i(x)\psi^i(x) , \quad (6.9)$$

here γ_μ is the Dirac matrix which satisfies the Clifford algebra

$$\{\gamma_\mu, \gamma_\nu\} = \gamma_\mu\gamma_\nu + \gamma_\nu\gamma_\mu = 2\mathbb{I}_4\eta_{\mu\nu} ,$$

and for simplicity $\not{\partial} = \gamma^\mu\partial_\mu$. Note that the metric tensor in d -dimensional Euclidean space is given by $\eta_{\mu\nu}$ and $\eta_\mu^\mu = d$. The mass of the quark is denoted by m which can be ignored in massless QCD where chiral symmetry is naturally preserved. The flavour of the quark is distinguished by the index i on $\psi^i(x)$ where $1 \leq i \leq N_f$. In Nature $N_f = 6$ according to the LHC experiment. As only colourless states are allowed in the form of hadrons we have colour singlets, usually described as ‘white’, that are invariant under rotations in colour space. The classical Lagrangian (6.9) is invariant under global $SU(3)$ transformations

$$\psi(x) \rightarrow U\psi(x) \quad , \quad \bar{\psi}(x) \rightarrow \bar{\psi}(x)U^\dagger \quad (6.10)$$

where U are the unitary 3×3 hermitian matrices of $SU(3)$. If we try to impose

this transformation locally

$$\psi(x) \rightarrow U(x)\psi(x) \quad , \quad \bar{\psi}(x) \rightarrow \bar{\psi}(x)U^\dagger(x) \quad (6.11)$$

local gauge invariance is not satisfied. This can be seen from the presence of an additional term which is the result of the derivative acting on U which depends on x and so does not commute past the partial derivative

$$i\bar{\psi}^i(x)\gamma^\mu\partial_\mu\psi^i(x) \rightarrow i\bar{\psi}^i(x)\gamma^\mu\partial_\mu\psi^i(x) + i\bar{\psi}^i(x)U^\dagger(x)\gamma^\mu(\partial_\mu U(x))\psi^i(x) .$$

The Lagrangian therefore requires a covariant derivative D_μ which replaces the partial derivative to ensure gauge invariance is restored

$$D_\mu = \partial_\mu + igA_\mu(x) . \quad (6.12)$$

The object $A_\mu(x)$ is a group valued gauge potential which acts as the gluon field. It transforms as an adjoint representation of $SU(3)$ with $a = 1, \dots, 8$ where

$$A_\mu(x) = A_\mu^a(x)t^a . \quad (6.13)$$

This introduces eight gauge gluon fields into the Lagrangian formalism. Note that the ‘+’ appearing in equation (6.12) is a convention used here, it may be different in other literature and will not alter our results or analysis in any way as only g^2 appears in physical quantities. The gauge field transforms locally as

$$A_\mu(x) \rightarrow U(x)A_\mu(x)U^\dagger(x) + \frac{i}{g}(\partial_\mu U(x))U^\dagger(x) .$$

The covariant derivative acting on the quark field transforms as

$$\begin{aligned} D_\mu\psi(x) &\rightarrow U(x)D_\mu\psi(x) \\ &= (\partial_\mu + igA_\mu(x))\psi(x) \\ &= \partial_\mu\psi(x) + igA_\mu^a(x)t^a\psi(x) \end{aligned}$$

where $A_\mu^a(x)$ is the vector potential. The covariant derivative of a group valued object X satisfies, [116],

$$D_\mu X = \partial_\mu X + ig[A_\mu, X] .$$

Therefore the covariant derivative acting on the gauge field A_μ gives

$$D_\mu A_\nu = \partial_\mu A_\nu + ig[A_\mu, A_\nu]$$

$$\begin{aligned}
(D_\mu A_\nu(x))^{at} &= (\partial_\mu A_\nu^a(x) - gf^{abc} A_\mu^b(x) A_\nu^c(x)) t^a \\
(D_\mu A_\nu(x))^a &= \partial_\mu A_\nu^a(x) - gf^{abc} A_\mu^b(x) A_\nu^c(x) .
\end{aligned}$$

The commutation relation between the covariant derivatives satisfies

$$[D_\mu, D_\nu] = ig(\partial_\mu A_\nu - \partial_\nu A_\mu + ig[A_\mu, A_\nu]) .$$

From this relation we can define the field strength tensor

$$G_{\mu\nu}^a = \partial_\mu A_\nu^a - \partial_\nu A_\mu^a - gf^{abc} A_\mu^b A_\nu^c . \quad (6.14)$$

The field strength tensor of QCD is different to that in QED in that we must add one additional term to have a gauge invariant Lagrangian. This additional term of (6.14) will give rise to asymptotic freedom due to the gluon self-interactions. Introducing a kinetic term for the field strength tensor into the Lagrangian we obtain a Lagrangian which is invariant under local $SU(3)$ gauge transformations

$$L = -\frac{1}{4}(G_{\mu\nu}^a)^2 + \bar{\psi}^{ia}(i\not{D} - m)\psi^{ib} , \quad (6.15)$$

where $\not{D} = \gamma^\mu D_\mu$. The kinetic term $(G_{\mu\nu}^a)^2$ is gauge invariant under $G_{\mu\nu} \rightarrow U(x)G_{\mu\nu}U^\dagger(x)$ and contains cubic and quartic gluon interactions. Before defining the Feynman rules which illustrate the interactions between fields we must first fix the gauge. It is not possible to do any perturbative calculations until the gauge is fixed for two important reasons. Firstly the degrees of freedom in (6.15) are incorrect. Any redundant degrees of freedom left over will give unphysical results which have no relation to Nature. The second problem is in determining the gluon propagator. To successfully construct the propagator we need to be able to invert the gluon operator associated with the quadratic terms in A_μ^a . This is not possible without first including additional terms which allow us to invert that matrix operator.

Choosing an appropriate gauge will greatly simplify perturbative calculations. We do this by introducing a gauge fixing term into Lagrangian (6.15) which will eliminate unphysical degrees of freedom in the gauge field A_μ^a . To fix the gauge Faddeev and Popov, [258], proposed a condition of the form

$$F^A[A_\mu] = 0 \quad (6.16)$$

where F^A is some function on the gauge field A_μ , [259]. The standard gauge fixing condition for an arbitrary linear covariant gauge is the Landau gauge fixing

condition

$$F^A[A_\mu] = \partial^\mu A_\mu^a = 0. \quad (6.17)$$

This is more commonly known as the Lorentz gauge and it reduces the number of independent components of A_μ from four to three, [116], as

$$\partial^0 A_0 + \partial^1 A_1 + \partial^2 A_2 + \partial^3 A_3 = 0.$$

However this gauge fixing construction is only applicable to Landau type gauges. For non-linear gauge fixing such as the Maximal Abelian gauge (MAG) the corresponding functional of (6.16) is more involved. As part of the gauge fixing program, the Faddeev Popov construction also introduces ghost terms to ensure unitarity is preserved. Unfortunately the gauge fixing procedure breaks gauge invariance and a new symmetry is needed to ensure gauge invariant independent results emerge for physical quantities. Slavnov and Taylor were the first to generalise a set of off-shell identities extending the Ward-Takahashi identities of QED, [260, 261], that must be fulfilled. A more general and easier way of gauge fixing was discovered by Becchi, Rouet, Stora and Tyutin, [262, 263], who proposed a way of using symmetry arguments, in particular global symmetries to define a set of gauge fixing terms which satisfied global gauge symmetries

$$\begin{aligned} \delta A_\mu^a &= -D_\mu c^a, \\ \delta c^a &= -\frac{g}{2} f^{abc} c^b c^c, \\ \delta \bar{c}^a &= b^a, \\ \delta b^a &= 0. \end{aligned} \quad (6.18)$$

Here δ is the BRST transform that anti-commutes with the ghost c^a and anti-ghost fields \bar{c}^a . The ghost particles are Grassmann variables. They are unphysical fields which are inserted on a purely mathematical level and do not contribute to the overall physics. As they are Grassmann variables the ghost fields anti-commute

$$c^a \bar{c}^b = -\bar{c}^b c^a.$$

The role of the ghost field is to cancel longitudinal components of the gluon propagator, leaving it fully transverse in the quantum theory, [258, 264, 265]. Without ghost fields unitarity of QCD is violated at the one loop level. The ghost fields will only appear in the internal part of Feynman diagrams in closed loops, for example, and never as an incoming or outgoing particle. This leaves the physics completely intact. Note that quarks and anti-quarks will also transform

in a BRST way

$$\begin{aligned}\delta\psi^{iI} &= igc^a(t^a)_{IJ}\psi^{iJ} , \\ \delta\bar{\psi}^{iI} &= -igc^a(t^a)_{IJ}\bar{\psi}^{iJ}\end{aligned}$$

where i is the flavour of the quark, $1 \leq i \leq N_f$ and I defines the group spinor index on a quark. Valid in the gauge fixed theory the BRST invariance, which can be applied to both linear and non-linear gauges, effectively replaces gauge invariance.

Imposing the gauge fixing of Faddeev and Popov given by equation (6.17), the full QCD Lagrangian for an arbitrary linear covariant gauge is

$$L = -\frac{1}{4}(G_{\mu\nu}^a)^2 + i\bar{\psi}^i(\not{D} - m)\psi^i - \frac{1}{2\alpha}(\partial^\mu A_\mu^a)^2 - \bar{c}^a\partial_\mu D^\mu c^a \quad (6.19)$$

where α is the arbitrary gauge parameter. Gauge invariance in the above Lagrangian has been broken since the gauge fixing terms are gauge dependent. However the BRST symmetry preserves some remnant of this lost gauge symmetry. Note that the original terms in Lagrangian (6.15) are BRST invariant since gauge invariance implies BRST invariance and the gauge fixing term in (6.19) ensures any extra terms added will not affect the original terms in (6.15). The above method of fixing the gauge is not unique and the overall result should be independent of the gauge choice. Once the gauge is fixed we can proceed to calculate with the complete Lagrangian.

6.2.1 The Banks-Zaks Fixed Point

If one were to attempt any perturbative calculation of QCD infinities would quickly emerge as we observed in the earlier part of this thesis. The Feynman diagrams of QCD in four dimensions are divergent and meaningful physics cannot be obtained without first dealing with these infinities. Helpfully, QCD is a renormalizable theory and here we shall focus on the renormalization of massless QCD. Dimensional regularisation is commonly used as the regulator to preserve gauge and Lorentz symmetry, [121, 122, 266] before the variables of the Lagrangian are rescaled via

$$\begin{aligned}A_0^\mu &= \sqrt{Z_A}A^\mu \quad , \quad g_0 = \mu^\epsilon Z_g g \quad , \quad \psi_0 = \sqrt{Z_\psi}\psi \quad , \\ c_0^a &= \sqrt{Z_c}c^a \quad , \quad \alpha_0 = \frac{Z_A}{Z_\alpha}\alpha \quad .\end{aligned}$$

The renormalization constants use the conventions of [1, 4, 102, 103] and may appear slightly different in other literature. They include the arbitrary mass scale μ introduced when dimensionally regularising the theory to keep the coupling dimensionless in d -dimensions. This naturally leads to a set of Renormalization Group (RG) functions, in particular the β -function which measures the change in the coupling over the energy scale. The one loop QCD β -function was calculated over forty years ago, [21, 22], and the two loop result followed a year later, [267, 268], along with the two loop field anomalous dimensions, [269, 270]. This β -function was then extended to three, [224], and then four loops, [271, 272]. The four loop quark mass anomalous dimension was then calculated, [273–276]. Notably the five loop result for the QCD β -function has been found recently, [277–279]. Additionally the five loop β -function and anomalous dimensions were found in [280, 281] before the five loop quark mass anomalous dimension was calculated, [282, 283]. There has also been general gauge group calculations at five loops in [284, 285] for all gauges. All these results have all been obtained using the modified minimal subtraction ($\overline{\text{MS}}$) renormalization scheme, other schemes have been looked at with the minimal momentum subtraction (mMOM) results published in [286].

We review the situation in the $\overline{\text{MS}}$ scheme here as this was the scheme in which the fixed point properties of the theory were explored initially. The three loop result of [287] is sufficient to study these properties with the β -function in four dimensions given by

$$\begin{aligned} \beta^{\overline{\text{MS}}}(a) = & - \left[\frac{11}{3}C_A - \frac{4}{3}T_F N_f \right] a^2 - \left[\frac{34}{3}C_A^2 - 4C_F T_F N_f - \frac{20}{3}C_A T_F N_f \right] a^3 \\ & + \left[2830C_A^2 T_F N_f - 2857C_A^3 + 1230C_A C_F T_F N_f - 316C_A T_F^2 N_f^2 \right. \\ & \left. - 108C_F^2 T_F N_f - 264C_F T_F^2 N_f^2 \right] \frac{a^4}{54} + O(a^5) \end{aligned} \quad (6.20)$$

where $a = g^2/(16\pi^2)$. It was observed in [88] that at two loops for a range of N_f there exists a non-trivial zero of the β -function. This is in addition to the traditional Gaussian fixed point at $g^* = 0$. The non-trivial fixed point of QCD in strictly four dimensions is known as the Banks-Zaks fixed point. It arises when the first term of the β -function is negative and the second term positive. The range of N_f values for which this non-trivial fixed point exists is known as the conformal window. The upper bound of which is determined using the one loop coefficient while the two loop term gives the lower limit. For $SU(3)$ the conformal window is estimated using perturbation theory to two loops to be $9 \leq N_f \leq 16$. The Banks-Zaks fixed point has been studied since its discovery due to its poten-

tial connection with chiral symmetry breaking. In more recent years interest in this fixed point has in the main been due to the connection with physics beyond the Standard Model such as technicolor, [288, 289]. More specifically while the early focus was on QCD itself, taking colour groups other than $SU(3)$ with quarks in non-fundamental representations as well as looking at supersymmetric QCD (SQCD) opened up the analysis to model building. This is primarily due to the need to understand where the conformal window is and the true range for which it exists.

In mass independent renormalization schemes with a single coupling the two loop term of the β -function is scheme independent, [104]. In momentum subtraction (MOM) renormalization schemes with a non-zero gauge parameter the two loop term is both α and scheme dependent. However in the Landau gauge, $\alpha = 0$, the two loop term of each MOM scheme β -function reduces to the same value as the two loop $\overline{\text{MS}}$ case. This may not be the situation in other gauges such as a non-linear gauge. As the non-trivial Banks-Zaks fixed point in massless QCD occurs for the part of the β -function which is scheme independent it should be a universal property of the theory. Computing the Banks-Zaks fixed point to higher orders will refine its location and the specific value will be scheme dependent. Note that it is possible to have more than one non-trivial fixed point with the Banks-Zaks fixed point always being located closest to the origin. For the gauge group $SU(3)$ the one loop β -function can be solved for the value of the coupling

$$g^2(\mu) = \frac{1}{\frac{(11 - \frac{2}{3}N_f)}{16\pi^2} \ln(\frac{\mu}{\Lambda_{\text{QCD}}})} . \quad (6.21)$$

The constant of integration Λ_{QCD} is similar to the Landau pole present in QED. If we denote $b = (11 - \frac{2}{3}N_f)/(16\pi^2)$, then b can be either positive or negative for a different range of quark flavours. For the entire range of the conformal window, $9 \leq N_f \leq 16$, b is positive and this ensures $\mu > \Lambda_{\text{QCD}}$. Therefore as μ increases the coupling decreases which gives the property of asymptotic freedom, [21, 22]. It implies that at high energy the quark and gluon constituents of hadrons act as quasi-free particles. Furthermore as μ decreases the value of the coupling increases. Therefore at lower energy the coupling becomes stronger. This property is known as confinement and ensures only colour singlets in the form of hadrons can propagate over macroscopic distances. Outside the range of the conformal window, that is $N_f > 16$, the value of b becomes negative. As the right-hand side of (6.21) must remain positive this produces the requirement $\mu < \Lambda_{\text{QCD}}$. In this case as μ increases the coupling also increases, much like it does in QED. Meanwhile as the energy μ decreases the coupling will also decrease

in strength. The Renormalization Group flow for QCD is illustrated in figure 6.3. The Gaussian fixed point is present in both graphs at $g^* = 0$ and is ultraviolet stable in the $b > 0$ case on but ultraviolet unstable for $b < 0$. Consequently the Banks-Zaks fixed point, $g^* \neq 0$ in figure 6.3 (b), is ultraviolet unstable and hence infrared stable. This is predicted by the properties of asymptotic freedom and confinement. The stability of the fixed points can be found by analysing the value of the first derivative of the β -function.

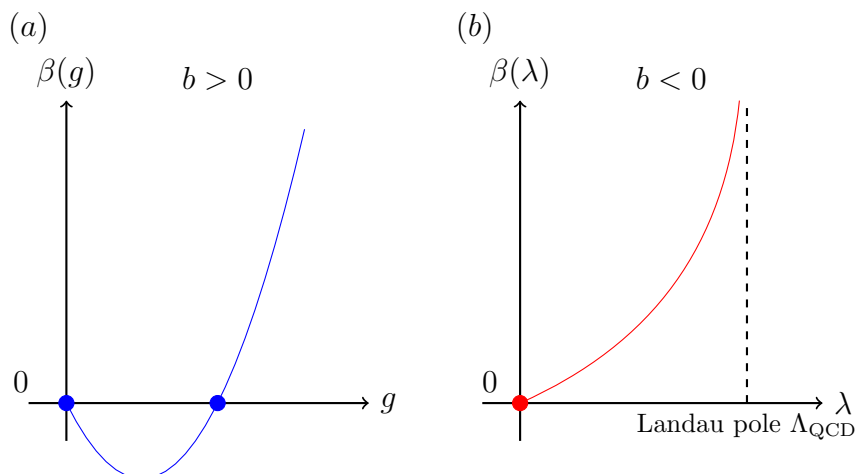


Figure 6.3: Renormalization Group flow in the ultraviolet (UV) for QCD with (a) $b > 0$ (b) $b < 0$.

6.3 Renormalization Scheme Dependence

The Banks-Zaks fixed point of QCD has been the subject of intense study in recent years with much of the interest focused on the conformal window. Pioneering this research, [88] used the two loop QCD β -function and implicitly assumed that the Banks-Zaks fixed point was accessible perturbatively. This is not necessarily true and therefore the lower end of the conformal window for QCD, that is $N_f = 9$, [267], may be beyond the range of perturbative reliability. Along with perturbative research there has been a vast array of non-perturbative work completed. Much of this is centred in the lattice community with the aim of understanding how to find non-trivial fixed points non-perturbatively. The value of $N_f = 12$ is of particular interest which is on the limit of perturbative reliability, [290–297]. There is also a desire to understand how to explore the fixed point structure for $N_f \leq 6$, if it exists, in order to tackle the relation to chiral symmetry breaking, [291, 296, 297]. Additionally non-perturbative Schwinger-Dyson methods have been used in relation to the Banks-Zaks fixed point, [298]. A key area of research is the measurement of critical exponents associated with the phase

transition corresponding to the Banks-Zaks fixed point. In particular the quark mass anomalous dimension exponent which is of interest due to the relation to the definition of a conformal theory. The full dimension of the quark mass operator must be greater than unity, which places an upper bound of two on the contribution of the anomalous dimension for this theory to be conformal, see [97]. Determining the range of the conformal window for which a theory satisfied this condition is an indication of whether conformal symmetry is present.

Critical exponents for QCD have been accurately determined on the lattice and there is good agreement between results at $N_f = 12$ for the quark mass anomalous dimension exponent with 0.235(15) found in [296] and a value of 0.235(46) found in [297]. Perturbative methods can also be used to calculate critical exponents. As critical exponents are physical quantities their values should be renormalization scheme independent. However as perturbative expansion are truncated at some order, one must calculate to a high loop order to observe this scheme independence. Additionally as the β -function is computed to a higher and higher order the location of the fixed point is refined, [299]. One immediate question which arises when looking at renormalization schemes is regarding the convergence of such schemes. Most crucially, does the value of Green's functions converge quicker in one scheme than another at the same loop order? If one knew the full series then there would be no difference in the values at the same evaluation point. However in a truncated series the numerical values of coefficients of the coupling constant differs in different schemes. Note that as Green's functions are not physical quantities there is an easier way of seeing scheme dependence. That is the computation of RG invariant critical exponents at a phase transition. Any discrepancies between the computation of critical exponents in different schemes at a high enough loop order can be seen as a potential issue with the scheme in question.

The relation between different schemes at the Banks-Zaks fixed point has been investigated in [89, 90, 93, 95–97]. In particular, a comprehensive study of scheme dependence in QCD involving several loop orders, representations and colour groups was performed in [97]. The results in alternative representations produced information relevant to several problems such as those underlying technicolor theories. One feature that emerged from [97] was that estimates for the critical exponents were more reliable when using a higher order. Values of the quark mass anomalous dimension were also provided for the specific case $N_f = 12$ which were found to be on the edge of the error ranges given in corresponding lattice results, [296, 297]. On the whole it was not completely clear whether the per-

turbative results of [97] compared favourably with lattice data. However it would not be surprising if they did not as non-perturbative properties are present within lattice regularised theories. The renormalization schemes considered in [97] were $\overline{\text{MS}}$, mMOM [301] and modified regularization invariant (RI'), [302, 303]. The $\overline{\text{MS}}$, mMOM and RI' schemes are all similar in the sense that they are defined with respect to Green's functions where there is a nullified external momenta. For example, the mMOM scheme is based on the property that in the Landau gauge the ghost-gluon vertex is finite when one ghost leg is nullified, [261]. Although it is important to note that for the 3-point nullified leg exceptional configuration potential IR issues may arise. This is not a problem at high energies, although one has to take care in any low energy analysis.

The aim in the remaining Chapters is to extend the investigation of [97] into scheme dependence of the Banks-Zaks fixed point and corresponding exponents to a different class of renormalization schemes. We look at the momentum subtraction (MOM) schemes as well as the interpolating momentum subtraction schemes (iMOM). These new schemes will be physical and renormalized at a non-exceptional point and as they are a different class to those examined in [97], will add a new layer to the analysis of scheme dependence. Before any results are presented it is important to first note that one never knows a priori which if any scheme would converge faster than another. Although the set-up of certain schemes may give a hint.

Banks-Zaks Fixed Point Analysis in Momentum Subtraction Renormalization Schemes

7.1 Introduction

The motivation for this Chapter is to analyse the renormalization scheme dependence of critical exponents associated with the Banks-Zaks fixed point of Quantum Chromodynamics (QCD), in particular the quark mass anomalous dimension exponent. Furthermore we wish to examine to what extent scheme invariance holds as a function of N_f in the conformal window. We extend the work of [97] to the kinematic momentum subtraction schemes (MOM) of Celmaster and Gonsalves, [98, 99]. The MOM schemes of [98, 99] are a different class to that of the modified minimal subtraction ($\overline{\text{MS}}$), minimal momentum subtraction (mMOM) and regularization invariant (RI') schemes so offer a more non-trivial insight into the Banks-Zaks properties. More specifically, in the $\overline{\text{MS}}$ scheme the class of numbers appearing are the rationals and the Riemann zeta function evaluated for integers $n \geq 3$. The MOM schemes additionally contain polylogarithms reflecting the kinematic information. In [98] the MOM renormalization schemes were introduced with the 3-point QCD vertices renormalized at a non-exceptional external momentum configuration. Specifically the subtraction point is defined as the point where the squares of the external momentum are all equal, [98, 99]. This is known as the symmetric subtraction point. For QCD it leads to three separate momentum subtraction schemes: MOM_q, MOM_{ggg} and MOM_h, corresponding to schemes based on the quark-gluon, triple gluon and ghost-gluon

vertices respectively. The MOM schemes are physical schemes and are therefore mass dependent. There is no doubt about infrared (IR) issues due to the non-exceptional nature of the subtraction point. In [99] it was hoped that perturbative results in MOM schemes would have faster convergence than other schemes.

The analysis here will also be performed in the $\overline{\text{MS}}$ and mMOM schemes, primarily as a check with results obtained in [97] as well as for comparison. Before perturbatively calculating the critical exponents, the Renormalization Group (RG) functions must be found. The three loop MOM β -functions have previously been calculated for an arbitrary linear covariant gauge and more specifically in the Landau gauge, [99, 307]. This was possible due to the advance in determining the two loop 3-point integrals for non-exceptional momentum configurations, [193, 197, 308, 309]. The three loop quark mass anomalous dimension has since been calculated in the MOM schemes, [1]. This required the renormalization of the quark mass operator inserted into a two loop 2-point function for the quark where a non-zero external momentum flows through the inserted operator. The Landau gauge is assumed throughout this Chapter where scheme dependence first appears at three loops. The main focus will be the scheme analysis of critical exponents, however we briefly summarise the quark mass anomalous dimension calculation first.

This Chapter is organised as follows. We begin by stating the known QCD Renormalization Group functions for the three MOM schemes. Key details of the calculation for the quark mass anomalous dimension are then summarised. The main results are presented in section 7.4 along with an analysis. The bulk of the results are given in Appendix D. All original data provided in this Chapter is published in [1]. Finally a brief conclusion of the results is provided.

7.2 Renormalization Group Functions

The β -functions for the three MOM schemes have been computed in [99, 307]. We first introduce some key notation. The β -function in the Landau gauge renormalized in the scheme \mathcal{S} is defined as

$$\beta^{\mathcal{S}}(a, 0) = \sum_{r=1}^{\infty} \beta_r^{\mathcal{S}} a^{r+1} \quad (7.1)$$

where the β -function partial sums are given by

$$\beta_n^S(a, 0) = \sum_{r=1}^n \beta_r^S a^{r+1} . \quad (7.2)$$

The second argument of the beta-function is the gauge parameter α , in the Landau gauge this is set to zero. For each renormalization scheme the Banks-Zaks fixed point a_L at the L th loop order is the first non-trivial zero of

$$\beta_L^S(a_L, 0) = 0 . \quad (7.3)$$

Furthermore, the critical exponent ω at the L th loop order is defined as

$$\omega_L = 2\beta'_L(a_L, 0) . \quad (7.4)$$

The Landau gauge quark mass anomalous dimension is perturbatively defined in a similar way to the β -function,

$$\gamma_{\bar{\psi}\psi}^S(a, 0) = \sum_{r=1}^{\infty} \gamma_r^S a^r \quad (7.5)$$

with the corresponding partial sums

$$\gamma_{\bar{\psi}\psi n}^S(a, 0) = \sum_{r=1}^n \gamma_r^S a^r . \quad (7.6)$$

We can then define the quark mass anomalous dimension exponent ρ evaluated at the L th loop order by evaluating $\gamma_{\bar{\psi}\psi}^S$ at the Banks-Zaks fixed point for each scheme

$$\rho_L = -2\gamma_{\bar{\psi}\psi L}^S(a_L, 0) . \quad (7.7)$$

The definition of ρ coincides with [97] and we can therefore make direct comparisons between the results. However our Banks-Zaks critical points will differ from [97] by a factor of 4π as we have defined the β -functions in such a way to be consistent with [307]. The expression for the MOMh scheme in the Landau gauge is recorded here as it is the more compact of the three. It is, [99, 307],

$$\begin{aligned} \beta^{\text{MOMh}}(a, 0) = & - \left[\frac{11}{3}C_A - \frac{4}{3}T_F N_f \right] a^2 \\ & - \left[\frac{34}{3}C_A^2 - 4C_F T_F N_f - \frac{20}{3}C_A T_F N_f \right] a^3 \\ & + \left[[18817920 + 103680\pi^2 - 16422912\zeta_3 \right. \\ & \left. - 155520\psi'(\frac{1}{3})] N_f T_F C_A C_F + [29167776 + 3729024\pi^2 \right. \end{aligned}$$

$$\begin{aligned}
& + 29568\pi^4 + 11562912\zeta_3 - 5593536\psi'(\tfrac{1}{3}) + 7200\pi^2\psi'(\tfrac{1}{3}) \\
& - 5400(\psi'(\tfrac{1}{3}))^2 - 11988\psi'''(\tfrac{1}{3}) - 31726080s_2(\tfrac{\pi}{6}) \\
& + 63452160s_2(\tfrac{\pi}{2}) + 52876800s_3(\tfrac{\pi}{6}) - 42301440s_3(\tfrac{\pi}{2}) \\
& + 78880\pi^3\sqrt{3} + 881280\ln(3)\pi\sqrt{3} \\
& - 73440\ln^2(3)\pi\sqrt{3} \Big] N_f T_F C_A^2 + [-4105728 - 705024\pi^2 \\
& - 3981312\zeta_3 + 1057536\psi'(\tfrac{1}{3}) + 5971968s_2(\tfrac{\pi}{6}) \\
& - 11943936s_2(\tfrac{\pi}{2}) - 9953280s_3(\tfrac{\pi}{6}) + 7962624s_3(\tfrac{\pi}{2}) \\
& - 14848\pi^3\sqrt{3} - 165888\ln(3)\pi\sqrt{3} \\
& + 13824\ln^2(3)\pi\sqrt{3} \Big] N_f^2 T_F^2 C_A + [-5723136 \\
& + 5971968\zeta_3] N_f^2 T_F^2 C_F - 559872N_f T_F C_F^2 + [-35200008 \\
& - 4741632\pi^2 - 81312\pi^4 - 1689336\zeta_3 + 7112448\psi'(\tfrac{1}{3}) \\
& - 19800\pi^2\psi'(\tfrac{1}{3}) + 14850(\psi'(\tfrac{1}{3}))^2 + 32967\psi'''(\tfrac{1}{3}) \\
& + 42083712s_2(\tfrac{\pi}{6}) - 84167424s_2(\tfrac{\pi}{2}) - 70139520s_3(\tfrac{\pi}{6}) \\
& + 56111616s_3(\tfrac{\pi}{2}) - 104632\pi^3\sqrt{3} - 1168992\ln(3)\pi\sqrt{3} \\
& + 97416\ln^2(3)\pi\sqrt{3} \Big] C_A^3 \Big] \frac{a^4}{279936} + O(a^5) \tag{7.8}
\end{aligned}$$

to three loops where $s_n(\theta)$ was defined in equation (3.24). The β -functions in the MOMq and MOMggg schemes can be found in [99, 307]. The presence of the underlying symmetric point masters in equation (7.8) are evident. Note that we are effectively quoting the full expression given in [307] but with a modification. In the three loop term of equation (5.28) in [307] an additional numerical object, Σ , was present which was a combination of harmonic polylogarithms. When [307] appeared it was not apparent that this was not an independent quantity and is known to correspond to, [101],

$$\Sigma = \frac{1}{36}\psi'''(\tfrac{1}{3}) - \frac{2\pi^4}{27} \tag{7.9}$$

in the notation of the previous Renormalization Group equations. We have substituted (7.9) in the original expression of [307] for consistency here. In comparing the β -function in (7.8) with the $\overline{\text{MS}}$ expression one can see that there is a structural question to be addressed. If when one computes the critical exponent for, say, the quark mass anomalous dimension in $\overline{\text{MS}}$ and MOMh at the Banks-Zaks fixed point then both expressions ought to be the same. This is because ultimately the critical exponent is a physical quantity and hence a Renormalization Group invariant. It is independent of the renormalization scheme in which it is determined. However, given the form of both β -functions this cannot be the case.

Indeed this is one of the motivations for examining the critical exponents at the Banks-Zaks fixed point in MOM schemes. The MOM β -functions are clearly in a different class from the point of view of the numerology when compared with the schemes analysed in [97] which were $\overline{\text{MS}}$, mMOM and RI'. The coefficients appearing in the Renormalization Group functions of these three schemes are from the set

$$\{\mathbb{Q}, \pi^2, \zeta_3, \zeta_5\}$$

to four loops. By contrast the basis for the MOM scheme coefficients to three loops is

$$\left\{ \mathbb{Q}, \pi^2, \zeta_3, \zeta_4, \psi'(\tfrac{1}{3}), \psi'''(\tfrac{1}{3}), s_2(\tfrac{\pi}{2}), s_2(\tfrac{\pi}{6}), s_3(\tfrac{\pi}{2}), s_3(\tfrac{\pi}{6}), \frac{\ln^2(3)\pi}{\sqrt{3}}, \frac{\ln(3)\pi}{\sqrt{3}}, \frac{\pi^3}{\sqrt{3}} \right\}.$$

7.3 Mass Operator Anomalous Dimension

To include several critical exponents in the analysis and to follow the work of [97], the quark mass anomalous dimension is required. In [1] this was calculated in the three MOM schemes to three loops. The calculation of the quark mass anomalous dimension uses the same technique of the mass dimension computation in Chapter 4. In that particular calculation the three mass operators were inserted into the 2-point function, $\langle \phi[\frac{1}{2}\phi^2]\phi \rangle$, before an external leg momentum was nullified and a reduction was applied with master integrals then used. For the quark mass anomalous dimension a quark mass operator can be inserted into the 2-point function for the quark, $\langle \psi[\bar{\psi}\psi]\bar{\psi} \rangle$. In Chapter 4 an added complication was the presence of three masses, all possessing the same canonical dimension and hence resulting in mass mixing. There is no such complication here as only one mass is present for the quark whose mass operator has a canonical dimension of three. Therefore rather than renormalizing the quark mass itself directly its anomalous dimension can be deduced from the renormalization of the associated quark mass operator which is $\bar{\psi}\psi$. The same approach was used in the computation of the quark mass anomalous dimension in the $\overline{\text{MS}}$ scheme to three loops, [310]. There is one important difference between the mass anomalous dimension calculation of Chapter 4 and the present computation. As the calculation in Chapter 4 was performed in the non-kinematic $\overline{\text{MS}}$ renormalization scheme, only the divergent piece of the Green's function was required for the renormalization constants. This enabled a simplification in the computation as the external leg corresponding to the mass insertion could be nullified. This gave effectively a 2-point function which could be reduced to 2-point master integrals.

However as the MOM schemes are kinematic, a finite part as well as divergent terms in the Green's function are required. Therefore for the calculation of the quark mass anomalous dimension the MOM schemes require a momentum configuration with a non-zero momentum flowing through all external legs. Known as a non-exceptional momentum configuration it possesses no potential IR problems. To determine the quark mass anomalous dimension in each of the three MOM schemes one must consider the Green's function

$$\langle \psi(p) \bar{\psi}(q) [\bar{\psi}\psi](r) \rangle \quad (7.10)$$

where

$$p + q + r = 0 \quad (7.11)$$

and p , q and r are the external momentum. We have chosen p and q to be the two independent momenta. At the symmetric point the following condition is satisfied

$$p^2 = q^2 = r^2 = -\mu^2 \quad (7.12)$$

which implies

$$pq = \frac{1}{2}\mu^2 \quad (7.13)$$

where μ is the mass scale introduced to ensure the coupling remains dimensionless in dimensional regularisation. The conventions used here for dimensional regularisation are $d = 4 - 2\epsilon$ where ϵ is the regularising parameter. As (7.10) cannot be simplified by nullifying one of the external momenta, it cannot be reduced to 2-point master integrals. Nevertheless the Laporta algorithm via REDUZE can still be used to simplify (7.10) but we will now require 3-point master integrals in the evaluation. Helpfully these master integrals have been computed explicitly, [193, 194, 308, 309]. Having described the method used to evaluate the quark mass anomalous dimension in each of the three MOM schemes we now record their explicit values for the Landau gauge. We have

$$\begin{aligned} \gamma_{\bar{\psi}\psi}^{\text{MOMq}}(a, 0) = & -3C_F a \\ & + \left[\left[2 + \frac{8}{9}\pi^2 - \frac{4}{3}\psi'(\frac{1}{3}) \right] N_f T_F C_F + \left[-\frac{13}{4} - \pi^2 \right. \right. \\ & \left. \left. + \frac{3}{2}\psi'(\frac{1}{3}) \right] C_F C_A + \left[-\frac{27}{2} - \frac{8}{9}\pi^2 + \frac{4}{3}\psi'(\frac{1}{3}) \right] C_F^2 \right] a^2 \\ & + \left[\left[41 - \frac{20}{3}\zeta_3 - \frac{16}{9}\pi^2 - \frac{8}{27}\pi^4 - 8s_2(\frac{\pi}{6}) + 16s_2(\frac{\pi}{2}) \right. \right. \\ & \left. \left. + \frac{40}{3}s_3(\frac{\pi}{6}) - \frac{32}{3}s_3(\frac{\pi}{2}) + \frac{8}{3}\psi'(\frac{1}{3}) + \frac{16}{9}\psi'(\frac{1}{3})\pi^2 - \frac{4}{3}(\psi'(\frac{1}{3}))^2 \right] \right. \end{aligned}$$

$$\begin{aligned}
& -\frac{1}{9}\psi'''(\tfrac{1}{3}) - \frac{1}{54}\ln^2(3)\sqrt{3}\pi + \frac{2}{9}\ln(3)\sqrt{3}\pi \\
& + \frac{29}{1458}\sqrt{3}\pi^3 \Big] N_f T_F C_F C_A + \left[\frac{130}{3} - \frac{32}{3}\zeta_3 + \frac{40}{9}\pi^2 \right. \\
& - \frac{64}{81}\pi^4 + 64s_2(\tfrac{\pi}{6}) - 128s_2(\tfrac{\pi}{2}) - \frac{320}{3}s_3(\tfrac{\pi}{6}) + \frac{256}{3}s_3(\tfrac{\pi}{2}) \\
& - \frac{20}{3}\psi'(\tfrac{1}{3}) + \frac{16}{9}\psi'(\tfrac{1}{3})\pi^2 - \frac{4}{3}(\psi'(\tfrac{1}{3}))^2 + \frac{2}{27}\psi'''(\tfrac{1}{3}) \\
& + \frac{4}{27}\ln^2(3)\sqrt{3}\pi - \frac{16}{9}\ln(3)\sqrt{3}\pi - \frac{116}{729}\sqrt{3}\pi^3 \Big] N_f T_F C_F^2 \\
& - 8N_f^2 T_F^2 C_F + \left[-\frac{249}{4} + \frac{2503}{48}\zeta_3 - \frac{1297}{72}\pi^2 - \frac{191}{486}\pi^4 \right. \\
& + \frac{347}{2}s_2(\tfrac{\pi}{6}) - 347s_2(\tfrac{\pi}{2}) - \frac{1735}{6}s_3(\tfrac{\pi}{6}) + \frac{694}{3}s_3(\tfrac{\pi}{2}) \\
& + \frac{1297}{48}\psi'(\tfrac{1}{3}) + \frac{175}{324}\psi'(\tfrac{1}{3})\pi^2 - \frac{175}{432}(\psi'(\tfrac{1}{3}))^2 + \frac{23}{288}\psi'''(\tfrac{1}{3}) \\
& + \frac{347}{864}\ln^2(3)\sqrt{3}\pi - \frac{347}{72}\ln(3)\sqrt{3}\pi - \frac{10063}{23328}\sqrt{3}\pi^3 \Big] C_F C_A^2 \\
& + \left[-\frac{467}{12} + \frac{106}{3}\zeta_3 + \frac{515}{9}\pi^2 + \frac{1216}{243}\pi^4 - 428s_2(\tfrac{\pi}{6}) \right. \\
& + 856s_2(\tfrac{\pi}{2}) + \frac{2140}{3}s_3(\tfrac{\pi}{6}) - \frac{1712}{3}s_3(\tfrac{\pi}{2}) - \frac{515}{6}\psi'(\tfrac{1}{3}) \\
& - \frac{1192}{81}\psi'(\tfrac{1}{3})\pi^2 + \frac{298}{27}(\psi'(\tfrac{1}{3}))^2 - \frac{1}{27}\psi'''(\tfrac{1}{3}) \\
& - \frac{107}{108}\ln^2(3)\sqrt{3}\pi + \frac{107}{9}\ln(3)\sqrt{3}\pi + \frac{3103}{2916}\sqrt{3}\pi^3 \Big] C_F^2 C_A \\
& + \left[-\frac{279}{2} + 56\zeta_3 - \frac{364}{9}\pi^2 + \frac{176}{243}\pi^4 - 48s_2(\tfrac{\pi}{6}) + 96s_2(\tfrac{\pi}{2}) \right. \\
& + 80s_3(\tfrac{\pi}{6}) - 64s_3(\tfrac{\pi}{2}) + \frac{182}{3}\psi'(\tfrac{1}{3}) + \frac{400}{81}\psi'(\tfrac{1}{3})\pi^2 \\
& - \frac{100}{27}(\psi'(\tfrac{1}{3}))^2 - \frac{8}{9}\psi'''(\tfrac{1}{3}) - \frac{1}{9}\ln^2(3)\sqrt{3}\pi + \frac{4}{3}\ln(3)\sqrt{3}\pi \\
& + \frac{29}{243}\sqrt{3}\pi^3 \Big] C_F^3 \Big] a^3 + O(a^4) \tag{7.14}
\end{aligned}$$

for the MOMq scheme and

$$\begin{aligned}
\gamma_{\bar{\psi}\psi}^{\text{MOMggg}}(a, 0) & = -3C_F a \\
& + \left[\left[\frac{2}{3} + \frac{88}{27}\pi^2 - \frac{44}{9}\psi'(\tfrac{1}{3}) \right] N_f T_F C_F + \left[-\frac{53}{6} - \frac{89}{27}\pi^2 \right. \right. \\
& \quad \left. \left. + \frac{89}{18}\psi'(\tfrac{1}{3}) \right] C_F C_A - \frac{3}{2}C_F^2 \right] a^2 \\
& + \left[\left[\frac{2369}{54} - \frac{128}{3}\zeta_3 + \frac{226}{243}\pi^2 + \frac{12688}{2187}\pi^4 - \frac{377}{243\sqrt{3}}\pi^3 \right. \right. \\
& \quad \left. \left. - \frac{52}{3\sqrt{3}}\ln(3)\pi + \frac{13}{9\sqrt{3}}\ln^2(3)\pi + 208s_2(\tfrac{\pi}{6}) - 416s_2(\tfrac{\pi}{2}) \right. \right.
\end{aligned}$$

$$\begin{aligned}
& -\frac{1040}{3}s_3\left(\frac{\pi}{6}\right) + \frac{832}{3}s_3\left(\frac{\pi}{2}\right) - \frac{113}{81}\psi'\left(\frac{1}{3}\right) - \frac{15280}{729}\psi'\left(\frac{1}{3}\right)\pi^2 \\
& + \frac{3820}{243}\left(\psi'\left(\frac{1}{3}\right)\right)^2 + \frac{4}{9}\psi'''\left(\frac{1}{3}\right)\left] N_f T_F C_F C_A + \left[18 - \frac{32}{3}\zeta_3\right. \right. \\
& + \frac{104}{27}\pi^2 - \frac{320}{243}\pi^4 - \frac{116}{243\sqrt{3}}\pi^3 - \frac{16}{3\sqrt{3}}\ln(3)\pi \\
& + \frac{4}{9\sqrt{3}}\ln^2(3)\pi + 64s_2\left(\frac{\pi}{6}\right) - 128s_2\left(\frac{\pi}{2}\right) - \frac{320}{3}s_3\left(\frac{\pi}{6}\right) \\
& + \frac{256}{3}s_3\left(\frac{\pi}{2}\right) - \frac{52}{9}\psi'\left(\frac{1}{3}\right) + \frac{272}{81}\psi'\left(\frac{1}{3}\right)\pi^2 - \frac{68}{27}\left(\psi'\left(\frac{1}{3}\right)\right)^2 \\
& + \left. \frac{2}{27}\psi'''\left(\frac{1}{3}\right)\right] N_f T_F C_F^2 + \left[-\frac{196}{27} + \frac{320}{243}\pi^2 - \frac{10240}{2187}\pi^4 \right. \\
& - \left. \frac{160}{81}\psi'\left(\frac{1}{3}\right) + \frac{10240}{729}\psi'\left(\frac{1}{3}\right)\pi^2 - \frac{2560}{243}\left(\psi'\left(\frac{1}{3}\right)\right)^2 \right] N_f^2 T_F^2 C_F \\
& + \left[-\frac{220159}{1728} + \frac{6367}{48}\zeta_3 + \frac{1643}{243}\pi^2 - \frac{9779}{17496}\pi^4 \right. \\
& + \frac{12499}{3888\sqrt{3}}\pi^3 + \frac{431}{12\sqrt{3}}\ln(3)\pi - \frac{431}{144\sqrt{3}}\ln^2(3)\pi \\
& - 431s_2\left(\frac{\pi}{6}\right) + 862s_2\left(\frac{\pi}{2}\right) + \frac{2155}{3}s_3\left(\frac{\pi}{6}\right) - \frac{1724}{3}s_3\left(\frac{\pi}{2}\right) \\
& - \frac{1643}{162}\psi'\left(\frac{1}{3}\right) + \frac{22183}{2916}\psi'\left(\frac{1}{3}\right)\pi^2 - \frac{22183}{3888}\left(\psi'\left(\frac{1}{3}\right)\right)^2 \\
& - \left. \frac{427}{576}\psi'''\left(\frac{1}{3}\right)\right] C_F C_A^2 + \left[13 + \frac{88}{3}\zeta_3 + \frac{593}{27}\pi^2 + \frac{880}{243}\pi^4 \right. \\
& + \frac{319}{243\sqrt{3}}\pi^3 + \frac{44}{3\sqrt{3}}\ln(3)\pi - \frac{11}{9\sqrt{3}}\ln^2(3)\pi - 176s_2\left(\frac{\pi}{6}\right) \\
& + 352s_2\left(\frac{\pi}{2}\right) + \frac{880}{3}s_3\left(\frac{\pi}{6}\right) - \frac{704}{3}s_3\left(\frac{\pi}{2}\right) - \frac{593}{18}\psi'\left(\frac{1}{3}\right) \\
& - \left. \frac{748}{81}\psi'\left(\frac{1}{3}\right)\pi^2 + \frac{187}{27}\left(\psi'\left(\frac{1}{3}\right)\right)^2 - \frac{11}{54}\psi'''\left(\frac{1}{3}\right)\right] C_F^2 C_A \\
& - \left. \frac{129}{2}C_F^3\right] a^3 + O(a^4), \tag{7.15}
\end{aligned}$$

$$\begin{aligned}
\gamma_{\psi\psi}^{\text{MOMh}}(a, 0) & = -3C_F a \\
& + \left[\left[2 + \frac{8}{9}\pi^2 - \frac{4}{3}\psi'\left(\frac{1}{3}\right) \right] N_f T_F C_F + \left[-\frac{55}{4} - \frac{49}{18}\pi^2 \right. \right. \\
& \left. \left. + \frac{49}{12}\psi'\left(\frac{1}{3}\right) \right] C_F C_A - \frac{3}{2}C_F^2 \right] a^2 \\
& + \left[\left[\frac{157}{2} - \frac{32}{3}\zeta_3 + \frac{313}{27}\pi^2 + \frac{104}{243}\pi^4 - \frac{29}{243\sqrt{3}}\pi^3 \right. \right. \\
& - \frac{4}{3\sqrt{3}}\ln(3)\pi + \frac{1}{9\sqrt{3}}\ln^2(3)\pi + 16s_2\left(\frac{\pi}{6}\right) - 32s_2\left(\frac{\pi}{2}\right) \\
& - \frac{80}{3}s_3\left(\frac{\pi}{6}\right) + \frac{64}{3}s_3\left(\frac{\pi}{2}\right) - \frac{313}{18}\psi'\left(\frac{1}{3}\right) - \frac{104}{81}\psi'\left(\frac{1}{3}\right)\pi^2 \\
& \left. \left. + \frac{26}{27}\left(\psi'\left(\frac{1}{3}\right)\right)^2 \right] N_f T_F C_F C_A + \left[\frac{46}{3} - \frac{32}{3}\zeta_3 - \frac{152}{27}\pi^2 \right. \right.
\end{aligned}$$

$$\begin{aligned}
& -\frac{320}{243}\pi^4 - \frac{116}{243\sqrt{3}}\pi^3 - \frac{16}{3\sqrt{3}}\ln(3)\pi + \frac{4}{9\sqrt{3}}\ln^2(3)\pi \\
& + 64s_2\left(\frac{\pi}{6}\right) - 128s_2\left(\frac{\pi}{2}\right) - \frac{320}{3}s_3\left(\frac{\pi}{6}\right) + \frac{256}{3}s_3\left(\frac{\pi}{2}\right) + \frac{76}{9}\psi'\left(\frac{1}{3}\right) \\
& + \frac{272}{81}\psi'\left(\frac{1}{3}\right)\pi^2 - \frac{68}{27}\left(\psi'\left(\frac{1}{3}\right)\right)^2 + \frac{2}{27}\psi'''\left(\frac{1}{3}\right) \left] N_f T_F C_F^2 \right. \\
& + \left[-\frac{1419}{8} + \frac{3757}{48}\zeta_3 - \frac{3383}{108}\pi^2 - \frac{469}{486}\pi^4 + \frac{1015}{3888\sqrt{3}}\pi^3 \right. \\
& + \frac{35}{12\sqrt{3}}\ln(3)\pi - \frac{35}{144\sqrt{3}}\ln^2(3)\pi - 35s_2\left(\frac{\pi}{6}\right) + 70s_2\left(\frac{\pi}{2}\right) \\
& + \frac{175}{3}s_3\left(\frac{\pi}{6}\right) - \frac{140}{3}s_3\left(\frac{\pi}{2}\right) + \frac{3383}{72}\psi'\left(\frac{1}{3}\right) + \frac{4751}{1296}\psi'\left(\frac{1}{3}\right)\pi^2 \\
& - \frac{4751}{1728}\left(\psi'\left(\frac{1}{3}\right)\right)^2 - \frac{37}{384}\psi'''\left(\frac{1}{3}\right) \left] C_F C_A^2 + \left[\frac{97}{12} + \frac{88}{3}\zeta_3 \right. \\
& + \frac{1217}{54}\pi^2 + \frac{880}{243}\pi^4 + \frac{319}{243\sqrt{3}}\pi^3 + \frac{44}{3\sqrt{3}}\ln(3)\pi \\
& - \frac{11}{9\sqrt{3}}\ln^2(3)\pi - 176s_2\left(\frac{\pi}{6}\right) + 352s_2\left(\frac{\pi}{2}\right) + \frac{880}{3}s_3\left(\frac{\pi}{6}\right) \\
& - \frac{704}{3}s_3\left(\frac{\pi}{2}\right) - \frac{1217}{36}\psi'\left(\frac{1}{3}\right) - \frac{748}{81}\psi'\left(\frac{1}{3}\right)\pi^2 + \frac{187}{27}\left(\psi'\left(\frac{1}{3}\right)\right)^2 \\
& \left. - \frac{11}{54}\psi'''\left(\frac{1}{3}\right) \right] C_F^2 C_A - 8N_f^2 T_F^2 C_F - \frac{129}{2}C_F^3 \left] a^3 \right. \\
& + O(a^4) \tag{7.16}
\end{aligned}$$

for MOMggg and MOMh respectively. Additionally as the anomalous dimensions of the quark, gluon and ghost have been computed in the $\overline{\text{MS}}$, mMOM and MOM schemes, [304, 306, 307], the analysis can be extended to include the relevant exponents. The anomalous dimensions for the quark, gluon and ghost in the Landau gauge have been listed in Appendix F.

7.4 Results

We can now use the Renormalization Group functions to analyse the Banks-Zaks fixed point and critical exponents in various renormalization schemes. The main critical exponent of interest will be the quark mass anomalous dimension exponent, due to the relation to the conformal window. We will also look at exponent ω which is related to the critical slope of the β -function and gives more insight into convergence. Our analysis will include a variety of colour groups with quarks in various representations, although the fundamental representation will form the main part of the analysis. The adjoint representation and two-index symmetric and antisymmetric representations will also be examined for comparison with the results in [97] which looked at theories that could be applied to problems beyond

the Standard Model. Another reason for looking at multiple representations is to gain as wide an analysis as possible to find where the convergence is most apparent. Note that the range of the conformal window for the Banks-Zaks fixed point depends on the particular representation. For some the conformal window will have a much smaller range of N_f values than for quarks in the fundamental representation. Explicit values of all the analysis are given in tables in Appendix D to six decimal places. We present the $\overline{\text{MS}}$ and mMOM results together to four loops. The MOMq, MOMh and MOMggg schemes are also grouped together, albeit to only three loops. For certain cases the format of the tables parallels [97] and we summarise the main results here. The order of the results in the tables is fixed point location, ω and then ρ for each choice of quark representation. Note that we have also included a brief analysis on the 't Hooft scheme of [312] in the fundamental representation for additional analysis. Briefly the Renormalization Group functions of the 't Hooft scheme are defined as that part which is renormalization scheme independent. For the β -function this is the two loop part and for the quark mass anomalous dimension it is the one loop term, [313].

We first look at the data given in tables D.1 and D.2 of Appendix D. These tables show the location of the fixed point for the $\overline{\text{MS}}$, mMOM and MOMi schemes in the fundamental representation. We make no comment on these values as the specific location of the fixed point is not physically meaningful. However we can see where the fixed point is becoming reasonably stable for certain values of N_f . One would hope the corresponding critical exponents are converging. In table D.1 for $N_c = 3$ and $N_f \geq 13$ the fixed point seems to reach a plateau for each scheme from the stability at three and four loops. As $N_f = 12$ is a value of intense interest in the lattice community and the subject of many computations, our perturbative results may therefore not be competitive when compared with these lattice calculations. A similar conclusion was reached in [97] which stated then that the convergence was best at the upper end of the conformal window for the IR fixed point. This is because we are still in the region where the coupling has a small value. For smaller N_f values perturbative results do not appear reliable. Throughout this Chapter our analysis is broadly in agreement with this point of view. For the MOMi schemes in table D.2 we only have the three loop results and are therefore not in a position to indicate whether the same range of N_f gives perturbatively reliability.

A more fitting way to look at convergence is through the analysis of the critical exponents. As the exponents are physical quantities and hence Renormalization Group invariants, their values should be the same in all schemes. Tables D.3

and D.4 give the critical exponent ω for the five different schemes in the fundamental representation using the fixed points from tables D.1 and D.2. We focus our analysis here on the conformal window for the $SU(3)$ colour group as it is related to QCD. Parallel remarks will apply for $N_c = 2$ and 4 but for different N_f values. From tables D.3 and D.4 we can see that the three loop values of ω in all five schemes are all in accord for $N_f = 16$ as expected. Although the MOMggg scheme gives a slightly lower value of ω . Similarly at $N_f = 13$ the $\overline{\text{MS}}$, mMOM and MOMi schemes at three loops all have similar ω values, again with MOMggg being slightly lower. As expected, this relative convergence is absent when $N_f = 12$. This is illustrated more clearly in the graphs of figure 7.1 for $N_f = 10$ and 14. In the left plot in figure 7.1 no clear convergence emerges, even between the $\overline{\text{MS}}$ and mMOM schemes at four loops. Note that the two loops results in both graphs are somewhat trivial, we expect exact agreement in all schemes from the two loop definition of the quark mass anomalous dimension. In the plot on the right-hand side in figure 7.1 the schemes appear to converge to a particular value, we can also see the MOMggg scheme value is noticeably below the other schemes at three loops.

In general a parallel picture emerges for tables D.5, D.6 and D.7. Note that we have included the 't Hooft scheme of [312] for additional analysis. This was not required in tables D.3 and D.4 since the two loop $\overline{\text{MS}}$ column in table D.3 corresponds to that scheme. For the ρ exponent the 't Hooft estimate lies well away from the other schemes we have looked at. This is not surprising given the way the series is defined. For $N_f = 16$ in $SU(3)$ the values of ρ are comparable in the $\overline{\text{MS}}$, mMOM and MOMi schemes. Once again MOMggg is the outlier with its value being slightly higher, this is also reflected in smaller values of N_f . For $N_f = 13$ the four loop $\overline{\text{MS}}$ and three loop MOMq results are similar, the mMOM value is slightly higher but is slowly decreasing. Finally for $N_f = 12$ the situation is the same as that for the ω exponent. No obvious value emerges which all five schemes are converging towards. However for ρ at $N_f = 12$ we can compare with lattice estimates. One analysis gives a value of $\rho = 0.235(15)$, [296], while a more recent study gives $\rho = 0.235(46)$, [297]. In both cases the lattice results are lower than the three and four loop perturbative estimates. This reinforces the observation of [97] that non-perturbative properties may be beginning to dominate the window at this point.

An interesting feature also emerges when comparing with lattice results. If the values of ρ given by the two lattice computations are correct, then the four loop $\overline{\text{MS}}$ value of ρ is the closest estimate. However for convergence, the three

loop MOM_q and MOM_h values are smaller than the corresponding three loop $\overline{\text{MS}}$ result. Hence we hope a four loop analysis of MOM_q and MOM_h may provide better estimates to compare with. This is not unsurprising since ρ gives the quark mass anomalous dimension exponent, we therefore expect MOM_q to produce the most reliable value. That the MOM_h scheme is also competitive is more surprising, however a simple explanation is that there is a similar structure of Feynman diagrams within the vertex function defining each of the MOM_q and MOM_h schemes. In each case one renormalizes the same number of graphs in the respective vertex renormalizations, [307], and the graphs are effectively the same structure topologically when examined in detail.

To further our analysis we can also look at five loop estimates. Table D.8 gives the value of the five loop quark mass anomalous dimension, [282], evaluated at the Banks-Zaks fixed point in $\overline{\text{MS}}$ for $N_c = 3$. As the five loop β -function was not available at the time of our original calculation, [1], we carried out a tentative analysis at that time using the fixed points at three and four loops. The notation is ρ_{5l} where the l -loop fixed point is given in the $\overline{\text{MS}}$ column of table D.1. It was hoped that the three and four loop fixed points would bound the actual five loop fixed point value. As $a_4 > a_3$ we have assumed without justification that there is such an alternating convergence. So if these are the bounding values the same reasoning would be that ρ_{53} and ρ_{54} bound the five loop value ρ_{55} . Note that the values of ρ_{53} and ρ_{54} from table D.8 are significantly different from lattice estimates, [296, 297]. Another way to examine the data at five loops is to take the central value of ρ_5 from [296, 297] and determine what value a_5 we should then be using, [282]. We obtain a value of $a_5 = 0.028376$ which is significantly lower than the three and four loop results. Therefore it can only be assumed that non-perturbative properties are the drive behind lattice results as we do not see such a large drop in the value of the coupling from successive loop order in $\overline{\text{MS}}$ for any N_f .

The graphs in figures 7.2 and 7.3 display this analysis more clearly. A greater convergence is seen in the right plot in figure 7.2 for $N_f = 14$ than in the left plot. Additionally we have given the lattice results in figure 7.3 with the five loop result ρ_{54} also displayed. It is clear to see from the graphs the discrepancy between perturbative and lattice results for $N_f = 12$. At the time of publication, [1], the five loop β -function was not known. However it has since been calculated in the $\overline{\text{MS}}$ scheme, [277–281]. We have therefore given ρ evaluated at the five loop fixed point, as well as the fixed point itself, in table D.9. As it turns out the value of ρ_5 for $N_f = 12$ does not sit between ρ_{53} and ρ_{54} as suspected; the value is actually slightly higher than ρ_{54} . For $N_f = 16$ the value of ρ_5 seems to indicate a continued

convergence following from the three and four loop results. Finally, to compare with lattice estimates we conclude that the value for ρ_5 at $N_f = 12$ is not only higher than the lattice results but it is also higher than the four loop result. It therefore does not seem to be converging to a result that would be competitive with lattice. Following the publication of the five loop β -function, [105] also calculated five loop results for the Banks-Zaks fixed point in $\overline{\text{MS}}$ and the corresponding quark mass anomalous dimension evaluated at this fixed point using the results of [277]. Interestingly, [105] found the conformal window to narrow at five loops with physical IR fixed points found only in the range $13 \leq N_f \leq 16$. The five loop result for the quark mass anomalous dimension was also calculated in [105] and was found to be close to the four loop value for the range $11 \leq N_f \leq 16$. Moreover the value at $N_f = 12$ was found to be in good agreement with lattice measurements.

To conclude the analysis of the fundamental representation we can look at the colour group $SU(2)$. This group was studied on the lattice in [292] for $6 \leq N_f \leq 10$. For $N_f = 10$ the lattice estimates gave a value of $\rho = 0.08$ which is in good agreement with our perturbative results. As this value of N_f is at the upper end of the $SU(2)$ conformal window, this conclusion is in keeping with what was found for $SU(3)$. The lower end of the $SU(2)$ conformal window has been a current topic of study in the lattice community. However a consensus has not yet been reached on exponent values with a value of ρ for $N_f = 6$ found to be in the region $\rho \in [0.26, 0.74]$, [294]. Only the MOMq and MOMh perturbative results at three loops fit into this band. However as perturbative reliability may be lost at lower values of N_f we must not take this as a definitive matching. Additionally the four loop corrections to MOMq and MOMh may change the situation as is the case for $\overline{\text{MS}}$.

One of the main reasons for looking at the Banks-Zaks fixed point is the possible connection it has with the phase transition associated with chiral symmetry breaking in QCD. This occurs when the quarks are in the fundamental representation. However we can also look at other representations to analyse theories beyond the Standard Model as in [97]. The fixed points and corresponding critical exponents in the adjoint representation are listed in tables E.9 to E.14. Note that these results do not give a supersymmetric version of QCD as there are not equal numbers of Bose and Fermi degrees of freedom. We have again looked at three different colour groups; $SU(2)$, $SU(3)$ and $SU(4)$, with only one non-trivial IR fixed point present at $N_f = 2$. In all schemes the two and three loop estimates of exponents ω and ρ are independent of the colour group. The N_c dependence

appears at four loops in the $\overline{\text{MS}}$ and mMOM schemes of tables E.11 and E.13. For the critical exponent ω there is a good convergence at four loops between the $\overline{\text{MS}}$ and mMOM schemes. Additionally the ρ critical exponent estimate at three loops in the MOMq schemes is competitive with four loop $\overline{\text{MS}}$ and mMOM results. This may be due to the origin of the operator being a scalar quark bilinear.

When the quarks are in a $2S$ representation this corresponds to a double index symmetric representation. The results for the $2S$ representation are given in tables D.16 to D.21. There exists only two fixed points in each of the $N_c = 3$ and $N_c = 4$ colour groups, corresponding to low values of N_f as in the adjoint representation. The critical exponents have similar properties to those found in the fundamental representation. For $N_f = 3$ in both colour groups we find convergent results when comparing the four loop $\overline{\text{MS}}$ and mMOM schemes with three loop MOMi estimates. The only potential outlier is once again the MOMggg renormalization scheme. For $N_f = 2$, the lower end of the conformal window for the $2S$ representation, no clear convergence pattern emerges for either exponent. The $2A$ representation is an antisymmetric double index partner to $2S$, the results of this representation are listed in tables E.21 to E.26. For the $SU(4)$ colour group there exists a greater number of fixed points. We do not present the $N_c = 3$ results as in the $2S$ representation the colour group Casimirs are precisely equal to their corresponding values in the fundamental representation and we have commented on these already. For the ρ critical exponent we find the same converging behaviour as that in the fundamental representation where convergence becomes apparent for values over $N_f = 12$. In the $2A$ representation this occurs above the value $N_f = 7$, with MOMggg once again excluded as an outlier. These results can also be compared with lattice estimates at $N_f = 6$, [293], obtained the result $\rho \in [0.3, 0.35]$ and only our four loop estimates are close to this.

To conclude we make general remarks on the analysis as a whole, as the analysis of different representations to give a perspective on the reliability of results may miss key features. For the critical exponent ρ as a general rule when ρ_2 is in the region of 1 or larger, higher loop estimates appear unreliable in that the values appear to be different from other schemes, not that they do not converge. Additionally for N_f close to the upper boundary of the conformal window in all schemes, ρ clearly is in line with all other schemes. More loop terms, especially for the MOMi schemes, are needed to analyse convergence further. Finally, throughout this analysis MOMggg appears to always be the outlier scheme. This is not unreasonable due to the nature of MOMggg. It is based on ensuring that the triple gluon vertex has no $O(a)$ corrections at the completely symmetric point.

Therefore for the corresponding Renormalization Group functions the content is necessarily weighted by gluonic rather than quark contributions. Hence for the quark mass anomalous dimension the quark content in the MOMggg scheme will not be dominant.

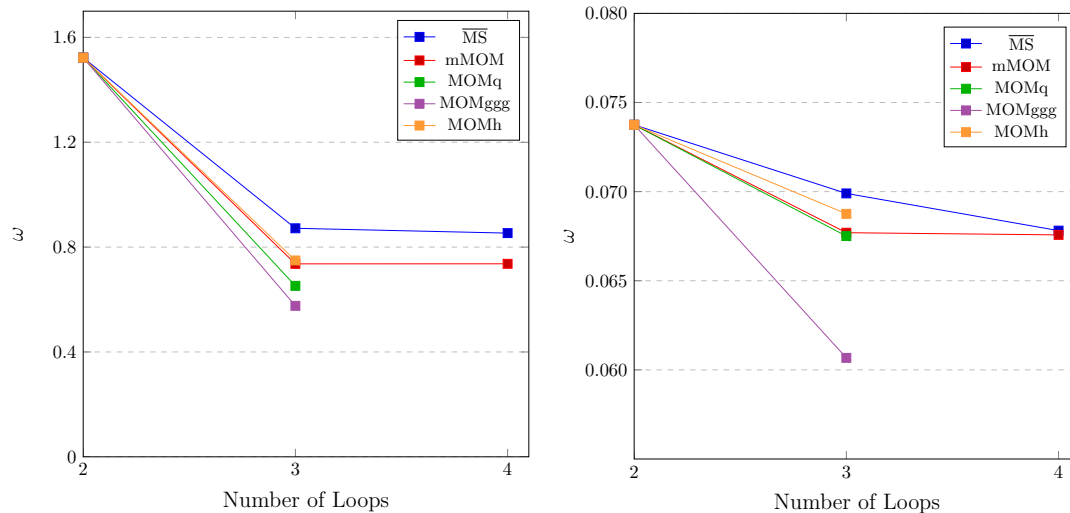


Figure 7.1: Value of the critical exponent ω in $SU(3)$ for $N_f = 10$ (left) and $N_f = 14$ (right) when the quark is in the fundamental representation.

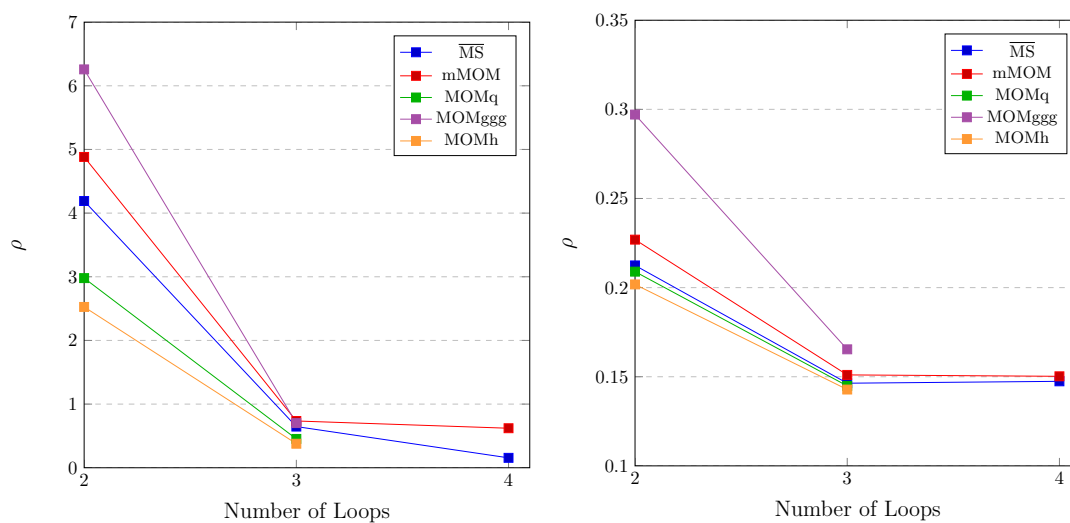


Figure 7.2: Value of the critical exponent ρ in $SU(3)$ for $N_f = 10$ (left) and $N_f = 14$ (right) when quark is in the fundamental representation.

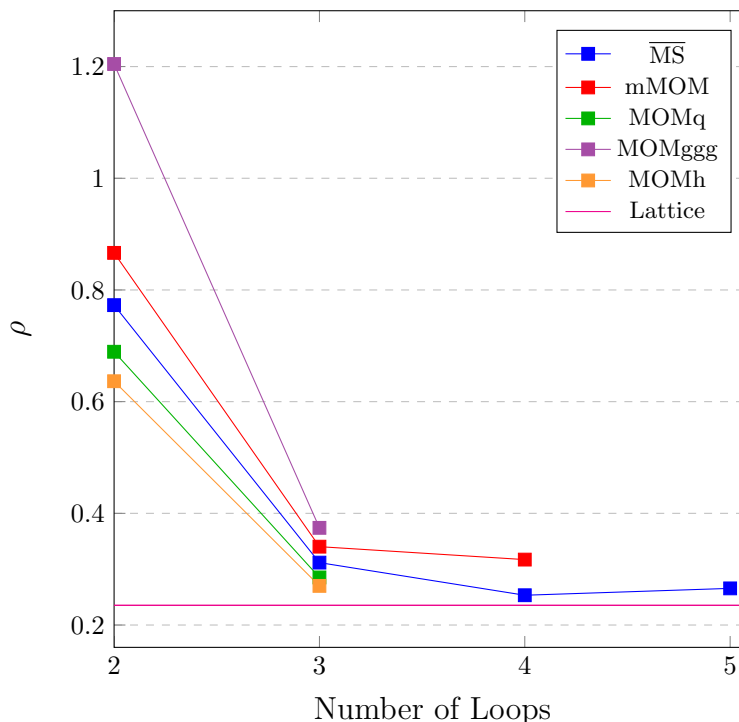


Figure 7.3: Value of the critical exponent ρ in $SU(3)$ for $N_f = 12$ when quark is in the fundamental representation. Lattice results found in [296, 297].

In addition to the critical exponents ω and ρ we can also analyse the conformal window of the quark, gluon and ghost anomalous dimensions; γ_ψ , γ_A and γ_c , evaluated at the Banks-Zaks fixed point. These Renormalization Group functions to four loop in the Landau gauge for the $\overline{\text{MS}}$ scheme are listed in Appendix F and were first published in [304, 306, 307]. The results of our analysis for the three colour groups $SU(2)$, $SU(3)$ and $SU(4)$ are given in tables D.28 to D.35. We have again studied the same range for the conformal window of the three colour groups as in the ω and ρ analysis. Additionally in tables D.34 and D.35 of Appendix D we have looked at the results for $\gamma_{AC} = (\gamma_A + \gamma_c)$ evaluated at the Banks-Zaks fixed point in all five renormalization schemes. Before moving on to discuss the results we briefly discuss the importance of the value for $\gamma_{AC} = (\gamma_A + \gamma_c)$.

Recall that the Slavnov-Taylor identities, [260, 261], are the non-abelian generalisation of a Ward-Takahashi identity. This is in turn an identity between correlation functions that follows from the global or gauged symmetries of a theory, and which remains valid after renormalization. The Ward-Takahashi identity can be thought of as a quantum version of the classical Noether's theorem. In gauge theories, such as QCD, there are relations between the renormalization constants in consequence of the Slavnov-Taylor identities, and in renormalizing QCD these identities must be satisfied. Moreover the Slavnov-Taylor identities

impose conditions on the construction of the gluon field operator, $\frac{1}{2}(A_\mu^a)^2$, so that the renormalization constants are not independent. As it turns out the mass operator of the gluon field is related to the anomalous dimensions of the gluon and ghost, [314–317]. This can be shown explicitly through the renormalization of γ_{A^2} by the insertion of the mass operator, which will match the value for $(\gamma_A + \gamma_c)$, [315, 316]. More simply it can be shown using the following Slavnov-Taylor identity, [314, 316],

$$\gamma_{A^2} = - \left(\frac{\beta(a)}{a} - \gamma_A(a) \right) \quad (7.17)$$

where $a = g^2/16\pi^2$. This relation was found to three loops in [315]. Note that $\beta(a)$ in the above relation can be replaced using a second Slavnov-Taylor identity, [316, 318],

$$2\gamma_c(a) = \frac{\beta(a)}{a} - \gamma_A(a) . \quad (7.18)$$

A purely algebraic proof of the two relations (7.17) and (7.18) is given in [314, 316] to all orders in perturbation theory in the Landau gauge. The general gauge invariant non-local gluon operator has been renormalized at one loop in an arbitrary linear covariant gauge and shown to be independent of the gauge parameter and hence equivalent to the Landau gauge value, [317]. We therefore have included the result for $(\gamma_A + \gamma_c)$ evaluated at the Banks-Zaks fixed point as it models the gluon mass anomalous dimension.

From Appendix D tables D.28 and D.31 display the two and three loop values of the anomalous dimension of the gluon, γ_A , in the $\overline{\text{MS}}$, mMOM and MOMi schemes. The four loop results are included for the $\overline{\text{MS}}$ and mMOM schemes. As with the previous analysis there seems to be a poor convergence at the lower end of the conformal window for all three colour groups, where perturbation theory is less reliable. At higher values of N_f the values seem to settle to a more stable value for all schemes. In particular the $\overline{\text{MS}}$ and mMOM results have a very good convergence at four loops. The three loop result for MOMq and MOMh is similar to the three loop results in the $\overline{\text{MS}}$ and mMOM schemes. The MOMggg value is slightly higher but not too dissimilar. Four loop results may provide more clarity. These results are plotted in figure 7.4 which successfully shows the convergence in $SU(3)$ at the upper end of the conformal window for all renormalization schemes. The values of γ_ψ evaluated at the Banks-Zaks fixed point in all five schemes are given in tables D.29 and D.32. The same conclusion can be drawn as for the γ_A tables, with the upper end of the conformal window in all three colour groups providing the best convergence. Note that at the higher values of N_f , for each

colour group, where perturbation theory is most reliable the values for γ_ψ are extremely small and in some cases negative. While the negative values can be attributed to errors margins in the calculation, the indication that $\gamma_\psi \rightarrow 0$ in the asymptotic limit is due to the fact the quark is quasi-free and the fixed point is very close to the origin. We can therefore deduce from the upper end of the conformal window of the graph that the quark appears to be a free particle. The results for the schemes $\overline{\text{MS}}$, mMOM and MOMi for $SU(3)$ are illustrated in figure 7.5.

Tables D.30 and D.33 give the results for the anomalous dimension of the ghost γ_c evaluated at the Banks-Zaks fixed point in all five schemes. All the values produced are negative which is not surprising given our conventions and the fact that we are looking at ghost particles. Once again, greater convergence is apparent at the upper end of the conformal window for all three colour groups. A higher loop order also appears to provide more convergent results. Note MOMggg at three loops appears to be a slight outlier when compared with the other four renormalization schemes. However four loop results for the MOMi schemes may resolve this issue. The results for $SU(3)$ are displayed in figure 7.6. Results for $(\gamma_A + \gamma_c)$ are listed in tables D.34 and D.35 with results to four loop in the $\overline{\text{MS}}$ and mMOM schemes, and to three loops for the MOMi schemes. In keeping with our observations for other critical exponents, there is very good convergence where perturbation theory is most reliable at the upper end of the conformal window. Note also that values in all schemes appears to be very small. The MOMq and MOMh results to three loops are similar to the three loop results in the $\overline{\text{MS}}$ and mMOM schemes. The value of $(\gamma_A + \gamma_c)$ in the MOMggg schemes is slightly different but not too dissimilar. These results for the $SU(3)$ colour group are illustrated in figure 7.7 where we observe poor convergence below $N_f \leq 13$ and fairly good convergence above this boundary.

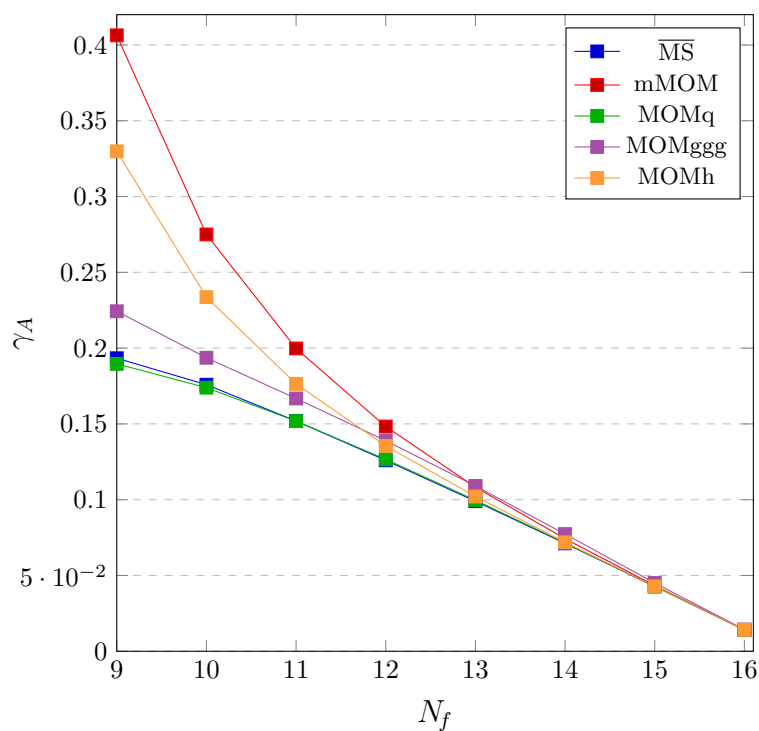


Figure 7.4: Value of the anomalous dimension of the gluon, γ_A , in $SU(3)$ to three loops when quark is in the fundamental representation.

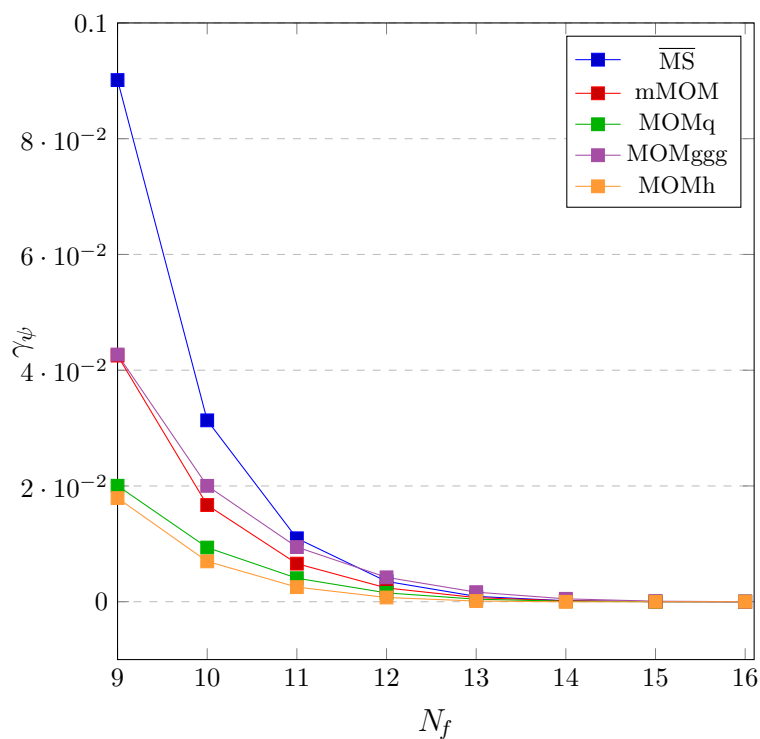


Figure 7.5: Value of the anomalous dimension of the quark, γ_ψ , in $SU(3)$ to three loops when quark is in the fundamental representation.

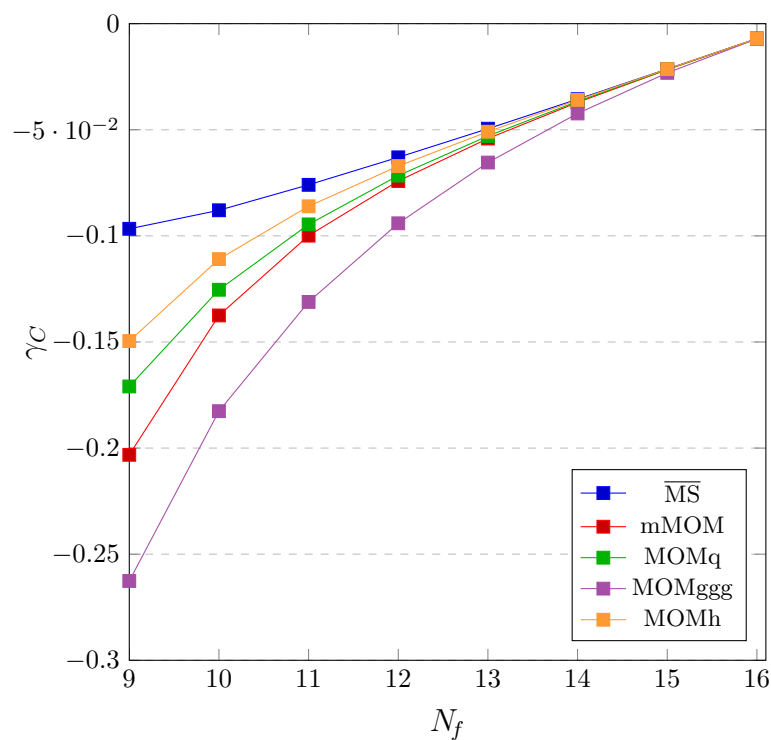


Figure 7.6: Value of the anomalous dimension of the ghost, γ_C , in $SU(3)$ to three loops when quark is in the fundamental representation.

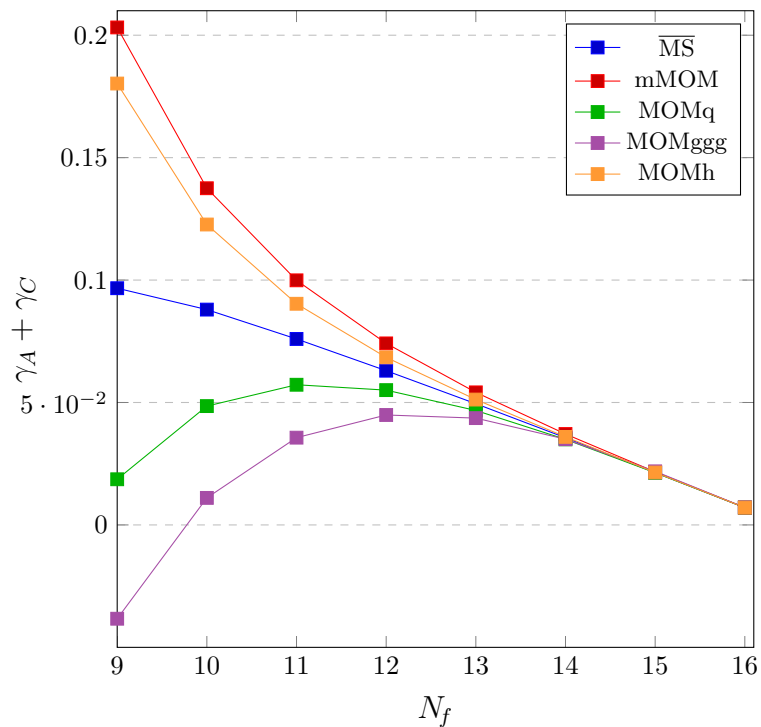


Figure 7.7: Value of $\gamma_A + \gamma_C$, in $SU(3)$ to three loops when quark is in the fundamental representation.

7.5 Discussion

It is worth making some general comments on our analysis. In [97] estimates for the quark mass anomalous dimension at the Banks-Zaks fixed point were examined in the conformal window for a variety of schemes and colour groups. We have extended this analysis by considering the MOM schemes of Celmaster and Gonsalves, [98, 99]. This adds to the discussion as the analytic structure of the MOM schemes are different from the point of view of specific numbers which appear. As critical exponents are physical quantities their values should be scheme independent. However at the Banks-Zaks fixed point renormalization scheme invariance is not exact. The Banks-Zaks fixed point is an IR stable critical point and as QCD is a high energy quantum field theory (QFT), the value of the associated exponents can only be perturbatively estimated. Until the low energy Lagrangian which drives the Banks-Zaks fixed point is found then at present a numerical evaluation of the critical exponents order by order in the loop expansion is one of the only tools available. In other words there may be a theory in the same universality class as QCD at the Banks-Zaks fixed point, with the fixed point being ultraviolet (UV) stable in the new theory, where direct computation of its anomalous dimensions in various schemes ought to be the way to see the renormalization invariance of the critical exponents. Developing a Lagrangian in higher dimensions that exists in the same universality class as QCD may be the way forward. Toy scalar theories were examined at length in Part I as a potential laboratory of these ideas and a six dimensional extension of QCD was recently considered in [54].

Nevertheless, despite differing numerical natures of the Renormalization Group functions in the MOM schemes versus those of the $\overline{\text{MS}}$, RI' and mMOM analysed in [97], scheme dependence appears to disappear for values of N_f near the upper end of the conformal window for the various representations considered. As perturbation theory is at its most reliable in the higher regions of the conformal window, this came as no great surprise. A secondary motivation for considering the MOM schemes was to provide estimates with which to compare with non-perturbative data. For $N_f = 12$ in the fundamental representation and $SU(3)$ colour group the quark mass anomalous dimension appears to converge slowly towards recent values measured on the lattice, [296, 297]. For the MOMq scheme the three loop estimate of ρ was closer than the corresponding $\overline{\text{MS}}$ value. Although this seems to indicate faster convergence in the MOMq scheme, the four loop result would be required to confirm this. The nature of the scheme however, founded on the quark-gluon vertex, indicates that this may be the case. It is

worth noting that at $N_f = 12$ non-perturbative features start to dominate, [97], which must be taken into account. A measure of that can be seen in the evaluation of the stability critical exponents ω . In tables D.3 and D.4 for $N_f = 13$ it appears ω is consistent across all schemes, except for MOMggg. The values for ρ are also consistent for this value of N_f . However for $N_f = 12$ the ω estimates have a broader range across the schemes.

Banks-Zaks Fixed Point Analysis in Interpolating Momentum Subtraction Renormalization Schemes

8.1 Introduction

We now want to re-examine the scheme dependence of Banks-Zaks critical exponents in a more general set of kinematic renormalization schemes than the original momentum subtraction (MOM) schemes. These are the interpolating momentum subtraction (iMOM) schemes which will depend on a parameter ω which tags the external momentum of one of the legs of the 3-point vertex functions of Quantum Chromodynamics (QCD). The parameter ω will be restricted to the values $0 < \omega < 4$. Note that the earlier MOM renormalization schemes correspond to $\omega = 1$. By allowing for a parameter ω we will be able to potentially quantify where and when the divergence from RG invariance of the Banks-Zaks critical exponents begins in the conformal window. The parameter ω acts as a variation on the subtraction point, its variation tracks the effect of the vertex subtraction within the graphs constituting the truncated series of the quantity of interest. In our analysis we focus on the specific values $\omega = 1/2$ and $\omega = 2$, although the Renormalization Group (RG) functions for arbitrary ω will also be stated. Analysing the exponents for these two ω values will be sufficient to band the $\omega = 1$ MOM value and gauge the tolerance on the exponents. There will be an iMOM scheme for each of the 3-point vertices of QCD; iMOMq, iMOMg and

iMOMh, parallel to the earlier MOM set. The iMOMi schemes were introduced in [101, 194] for the specific case of the quark mass operator renormalization only. The application was to assist with matching to a lattice gauge theory computation where the coupling constant was renormalized in the modified minimal subtraction ($\overline{\text{MS}}$) scheme.

The β -function in a kinematic renormalization scheme has the property of being gauge dependent, [98, 99]. In general the gauge parameter of a linear covariant gauge can be regarded as a second coupling constant. Therefore at criticality the RG function of a gauge parameter has to be zero which corresponds to the Landau gauge. Hence all MOM and iMOM data will be in that gauge. However there is a second covariant gauge that is of interest in our analysis. The maximal abelian gauge (MAG) is based on gauge fixing the gluon in the abelian subgroup of the colour group differently from other gluons. The MAG gauge was first introduced in [313, 319, 320] to study abelian monopole condensation since it is believed to be a potential mechanism for colour confinement, [321, 322]. The gauge was shown to be renormalizable in [323–327]. The three loop RG functions in the MAG gauge have been calculated in the $\overline{\text{MS}}$ renormalization scheme, [328], and in the MOM schemes, [102, 103]. In [102] it was stated that the lower bound of the conformal window seemed to drop to $N_f = 8$ for the MAG gauge. However this does not imply a lower limit ahead of a full perturbative analysis. Although the lattice study [290] does accommodate the value $N_f = 8$ in the conformal window. As the RG functions are readily available it is natural to extend our Banks-Zaks critical exponent analysis to the MAG gauge. The analysis of the second gauge will run in parallel with the Landau gauge analysis.

The aim here is to quantify how far the gauge independence of Banks-Zaks critical exponents extends into the conformal window. Additionally we will produce a comprehensive overview of scheme and gauge dependence in the new set of iMOM renormalization schemes. This Chapter is organised as follows. We begin by briefly discussing the set-up of the MAG gauge. The key points in the calculation of the Renormalization Group functions for the iMOM schemes will also be discussed. The known RG functions for the iMOM schemes in both gauges are then stated. The main results and analysis are presented in section 8.4 with the bulk of the data given in Appendix E. Finally a brief discussion follows on the results.

8.2 Maximal Abelian Gauge

Fixing the gauge in QCD is necessary to eliminate unphysical degrees of freedom in the gauge field A_μ^a . This can be done by introducing a gauge fixing term into the Lagrangian. The most common gauge fixing, which we have used thus far, is the linear Landau gauge which satisfies the gauge fixing condition

$$F^A[A_\mu] = \partial^\mu A_\mu^a = 0. \quad (8.1)$$

As well as linear gauges, obtaining multi-loop information for non-linear gauges is also important. In fact it is thought that low energy properties of Yang-Mills theories may be best described using gauges non-linear in nature. This comes from research, [313, 321, 322, 329, 330], looking into effective gluon masses and their behaviour in QCD. 't Hooft suggested some components of the gluon field may acquire dynamically generated masses due to the condensation of abelian monopoles originating from the diagonal elements of the colour group algebra. Abelian monopoles are believed to dominate the infrared (IR) dynamics, [102]. Hence confinement may be best explained using the diagonal elements of the colour group, [328], and low energy behaviour of the diagonal and off-diagonal gluons may differ. Significantly it has been speculated that the low energy behaviour of QCD may be best described using an effective abelian theory.

This is one of the main motivations for looking at non-linear gauges and the one which we shall introduce here is the MAG. The MAG splits the colour group into its diagonal and off-diagonal parts. Hence the gluon and ghost fields are also split into these two groups. Gluons corresponding to the diagonal part are named diagonal and form an abelian subgroup, while gluons not contained in this subgroup are termed off-diagonal, [102, 328]. This non-linear gauge will therefore give an insight into any strange behaviour in either sector. A recent lattice study, [331], investigated the effect of diagonal gluons on the inter-quark static potential. Within the theoretical set-up it was possible to identify the contributions made by the diagonal gluons to the potential. It was claimed that excluding these contributions forced the linearly rising potential to collapse, indicating that the abelian sector was effectively responsible for quark confinement. The data was determined on the fine lattice and the authors concluded that in studying the maximal abelian projection they had found that confinement is entirely kept in the abelian sector of QCD in the MAG. Note that studying the confinement mechanism in this way lies beyond the scope of perturbation theory. Therefore the property of the MAG we are primarily interested in is its structure and relationship with other gauges such as the Landau gauge.

The primary reason for introducing the MAG gauge is because Renormalization Group functions in the $\overline{\text{MS}}$, minimal momentum subtraction (mMOM) and iMOM schemes for this gauge have been calculated, [102,328]. Therefore we can compare results for the critical exponents in two different gauges and examine their scheme dependence without having to calculate any additional RG functions. We will however recap the essential features of this gauge fixing to better understand why it can be a useful tool and the differences compared with linear gauges. Note that the MAG will depend on gauge parameter α which is not to be confused with the same parameter in a linear covariant gauge. The basic idea of the MAG is to remove as many non-abelian degrees of freedom as possible by partially fixing the gauge, leaving the theory with a residual abelian gauge symmetry which is then gauge fixed separately. The group valued gauge field A_μ can be decomposed as

$$A_\mu = A_\mu^a t^a . \quad (8.2)$$

Recall the colour group generator are given by t^a where $1 \leq a \leq N_A$ and N_A is the dimension of the adjoint representation. The group generators can then be split into two sets, the diagonal (or photonic) and off-diagonal sectors. The diagonal sector will form an abelian subgroup. For notational purposes we use the indices i, j, k and l to denote the diagonal elements and A, B, C and D to denote off-diagonal elements. Thus A_μ can alternatively be decomposed as

$$A_\mu = A_\mu^A t^A + A_\mu^i t^i . \quad (8.3)$$

The diagonal indices range over $1 \leq i \leq N_A^d$ and the off-diagonal indices span $1 \leq A \leq N_A^o$. Clearly we have

$$N_A^d + N_A^o = N_A . \quad (8.4)$$

Additionally the field strength tensor $G_{\mu\nu}$ can be split into diagonal and off-diagonal parts

$$G_{\mu\nu} = G_{\mu\nu}^a t^a = G_{\mu\nu}^A t^A + G_{\mu\nu}^i t^i \quad (8.5)$$

with diagonal and off-diagonal parts given respectively as

$$\begin{aligned} G_{\mu\nu}^i &= \partial_\mu A_\nu^i - \partial_\nu A_\mu^i + gf^{abi} A_\mu^a A_\nu^b \\ G_{\mu\nu}^A &= D_\mu^{Ab} A_\nu^b - D_\nu^{Ab} A_\mu^b + gf^{Abc} A_\mu^b A_\nu^c \end{aligned}$$

and the covariant derivative has been redefined as

$$D_\mu^{ab} = \partial_\mu \delta^{ab} - g f^{abi} A_\mu^i .$$

Thus, taking the above into consideration, the Lagrangian in the MAG contains two field strength tensors, one for each sector,

$$L^{\text{MAG}} = -\frac{1}{4} G_{\mu\nu}^A G^{A\mu\nu} - \frac{1}{4} G_{\mu\nu}^i G^{i\mu\nu} + i\bar{\psi} \not{D} \psi + L_{\text{GF}}^{\text{MAG}} \quad (8.6)$$

where $L_{\text{GF}}^{\text{MAG}}$ is the gauge fixing term specific to the MAG. In a linear covariant gauge the corresponding gauge fixing term contains the gauge fixing condition and the consequent ghost Lagrangian. For the MAG the situation is the same but the actual Lagrangian is more complicated, [323–327, 332]. The MAG gauge fixing term can be constructed in the standard way by the BRST variation of a specific operator, see for example [332, 333]. We state the full Lagrangian including the gauge fixing term in the MAG for completeness.

$$\begin{aligned} L_{\text{GF}}^{\text{MAG}} = & -\frac{1}{2\alpha} (\partial^\mu A_\mu^A)^2 - \frac{1}{2\bar{\alpha}} (\partial^\mu A_\mu^i)^2 + \bar{c}^A \partial^\mu \partial_\mu c^A + \bar{c}^i \partial^\mu \partial_\mu c^i \\ & + g \left[f^{ABk} A_\mu^A \bar{c}^k \partial^\mu c^B - f^{ABC} A_\mu^A \bar{c}^B \partial^\mu c^C - \frac{1}{\alpha} f^{ABk} \partial^\mu A_\mu^A A_\nu^B A^{k\nu} \right. \\ & \quad - f^{ABk} \partial^\mu A_\mu^A c^B \bar{c}^k - \frac{1}{2} f^{ABC} \partial^\mu A_\mu^A \bar{c}^B c^C - 2f^{ABk} A_\mu^k \bar{c}^A \partial^\mu \bar{c}^B \\ & \quad \left. - f^{ABk} \partial^\mu A_\mu^k \bar{c}^B c^C \right] \\ & + g^2 \left[f_d^{ACBD} A_\mu^A A^{B\mu} \bar{c}^C c^D - \frac{1}{2\alpha} f_o^{AkBl} A_\mu^A A^{B\mu} A_\nu^k A^{l\nu} \right. \\ & \quad + f_o^{ADCj} A_\mu^A A^{j\mu} \bar{c}^C c^D - \frac{1}{2} f_o^{AjCD} A_\mu^A A^{j\mu} \bar{c}^C c^D \\ & \quad + f_o^{AjCl} A_\mu^A A^{j\mu} \bar{c}^C c^l + f_o^{AlCj} A_\mu^A A^{j\mu} \bar{c}^C c^l - f_o^{CjDi} A_\mu^i A^{j\mu} \bar{c}^C c^D \\ & \quad - \frac{\alpha}{4} f_d^{ABCD} \bar{c}^A \bar{c}^B c^C c^D - \frac{\alpha}{8} f_o^{ABCD} \bar{c}^A \bar{c}^B c^C c^D \\ & \quad + \frac{\alpha}{8} f_o^{ACBD} \bar{c}^A \bar{c}^B c^C c^D - \frac{\alpha}{4} f_o^{ABCl} \bar{c}^A \bar{c}^B c^C c^l + \frac{\alpha}{4} f_o^{ACBl} \bar{c}^A \bar{c}^B c^C c^l \\ & \quad \left. - \frac{\alpha}{4} f_o^{AlBC} \bar{c}^A \bar{c}^B c^C c^l + \frac{\alpha}{2} f_o^{AkBl} \bar{c}^A \bar{c}^B c^k c^l \right] . \quad (8.7) \end{aligned}$$

As noted in [328] the gauge fixing part of the MAG Lagrangian is generated automatically via a computer algebra routine from the BRST variation of the defining functional. This is to ensure that definitions and conventions are correctly implemented without errors as well as to be confident that the resulting Feynman rules are derived correctly using symbolic manipulation.

8.3 Renormalization Group Functions

Before analysing the location of the Banks-Zaks fixed point and critical exponents in the iMOM schemes we first must acquire the Renormalization Group functions. In [4] QCD was renormalized in the interpolating MOM schemes in both the Landau and MAG gauges. This renormalization follows a similar path to that of the scalar calculations with the added complication of a Lorentz tensor structure present. The computation method will be briefly discussed here before the Renormalization Group functions are stated. Note that there are common aspects of the renormalization for both the Landau and MAG gauges which can be outlined together. The renormalization will centre on the 2 and 3-point functions or the self-energy and vertex Green's functions respectively. The MINCER algorithm implemented in FORM, [334,335], is used to integrate each 2-point diagram generated by QGRAF. As only one external momentum is present the wavefunction renormalization constants can be defined at the point $p^2 = -\mu^2$, where μ is the mass scale introduced when we dimensionally regularise in $d = 4 - 2\epsilon$ dimensions. Additionally as only massless fields are present this ensures the 2-point renormalization is straightforward.

The vertex renormalization is more involved as there are two independent external momentum present. Three separate vertex functions need to be considered based on the quark-gluon, ghost-gluon and triple-gluon vertices. All 3-point graphs are generated using QGRAF. One has to be careful in specifying the point where the three Green's functions are renormalized. The momentum of the external legs are given by p , q and r , as the first two are assumed to be independent and we can set

$$r = -p - q. \quad (8.8)$$

The squared external momenta are constrained to satisfy

$$\begin{aligned} p^2 &= q^2 = -\mu^2, \\ r^2 &= -\omega\mu^2 \end{aligned} \quad (8.9)$$

in contrast to equations (7.12) and (7.13) where ω is the interpolating parameter. This leads to

$$\begin{aligned} pq &= \left[1 - \frac{\omega}{2}\right]\mu^2, \\ pr &= qr = -\omega\mu^2. \end{aligned} \quad (8.10)$$

These relations restrict the range of validity for the interpolating parameter to

$0 < \omega < 4$. The lower bound corresponds to the emergence of IR divergences, while the upper bound would produce collinear singularities. The original MOM configuration of Celmaster and Gonsalves, [98,99], corresponds to $\omega = 1$ and can be used as an internal check throughout the computation. The main difference between the renormalization of QCD and earlier scalar renormalizations is the presence of Lorentz tensor amplitudes. These can be decomposed into a set of scalar amplitudes for each vertex by the projection method discussed in [103,307]. The outcome of the projection process is to relegate the Green's functions to a sum over Lorentz scalar amplitudes for each gauge. To apply the projections the electronic representations of the 3-point graphs are individually passed through a projection algorithm once the colour, spinor, flavour and Lorentz indices have been appended. The consequence is that the amplitude for each Feynman diagram is a sum of Feynman integrals which have scalar products of the external and internal momenta.

Once all 3-point graphs for the vertices have been decomposed into a set of scalar amplitudes, the Laporta algorithm via REDUZE can be implemented. This ensures that all integrals contributing to a Feynman graph of the original Green's functions can be written as a sum over a relatively small set of master integrals. Their ϵ -expansion has to be determined by explicit evaluation. To two loops the master integrals for the iMOM renormalization have been computed in [193,197,308,309]. These results were discussed in [103] for the renormalization of the quark mass operator as a function of ω used for lattice matching. Once master integrals have been inserted the graphs for each vertex function can be summed together. As in scalar renormalization, variables such as the coupling constants and gauge parameter can be rescaled to introduce the renormalization constants. Note that the renormalization constants in the Landau gauge and MAG will differ. For example, in a linear covariant gauge in our conventions, $Z_\alpha = 1$. However this is not true in general in other gauges. In particular in the MAG the corresponding parameter of the off-diagonal gauge fixing is not unity, [323–327,332]. Note that for the iMOM schemes the subtraction prescription is that the renormalization constants for the 2- and 3-point functions are chosen so that at the subtraction point there are no $O(a)$ corrections where $a = g^2/16\pi^2$. The renormalization functions can be found by substituting the renormalization constants into the definition of the functions.

The renormalization of the quark mass operator, $\bar{\psi}\psi$, is also considered in [4]. It follows the same method as in the MOMi calculation. That is, the operator can be inserted into a 2-point function, $\langle\psi(p)[\bar{\psi}\psi](r)\bar{\psi}(q)\rangle$, before being reduced

to a set of master integrals via the Laporta algorithm. Note that once again we cannot nullify any external momenta to simplify the reduction as we require a non-exceptional momentum prescription. The renormalization constant for the quark mass operator will be the same in both the Landau gauge and MAG. For the interpolating momentum subtraction schemes the parameter ω will play the role of potentially running over a range of different possible schemes. The full list of definitions for the calculation of the RG functions via renormalization constants is

$$\begin{aligned}
\gamma_A(a, \alpha) &= \beta(a, \alpha) \frac{\partial}{\partial a} \ln Z_A + \alpha \gamma_\alpha(a, \alpha) \frac{\partial}{\partial \alpha} \ln Z_A , \\
\gamma_\alpha(a, \alpha) &= \left[\beta(a, \alpha) \frac{\partial}{\partial a} \ln Z_\alpha - \gamma_A(a, \alpha) \right] \left[1 - \alpha \frac{\partial}{\partial \alpha} \ln Z_\alpha \right]^{-1} , \\
\gamma_c(a, \alpha) &= \beta(a, \alpha) \frac{\partial}{\partial a} \ln Z_c + \alpha \gamma_\alpha(a, \alpha) \frac{\partial}{\partial \alpha} \ln Z_c , \\
\gamma_\psi(a, \alpha) &= \beta(a, \alpha) \frac{\partial}{\partial a} \ln Z_\psi + \alpha \gamma_\alpha(a, \alpha) \frac{\partial}{\partial \alpha} \ln Z_\psi , \\
\gamma_{\mathcal{O}}(a, \alpha) &= -\beta(a, \alpha) \frac{\partial}{\partial a} \ln Z_{\mathcal{O}} - \alpha \gamma_\alpha \frac{\partial}{\partial \alpha} \ln Z_{\mathcal{O}} \tag{8.11}
\end{aligned}$$

where \mathcal{O} is the quark mass operator $\mathcal{O} = \bar{\psi}\psi$. A key point in the renormalization set-up is that the renormalization constants will depend on variables such as the coupling constant defined with respect to a specific scheme. Equally we can define another set of renormalization constants which will depend on the variables in a different scheme. These two sets of renormalization constants are equally valid and are related through properties of the Renormalization Group. The three loop iMOMi Renormalization Group functions were obtained in [4] using this shortcut. We display one iMOM Renormalization Group function in analytic form. The β -function for the iMOMh scheme for colour group $SU(3)$ in the Landau gauge is given by

$$\begin{aligned}
\beta^{\text{iMOMh}}(a, 0) \Big|^{SU(3)} &= [2N_f - 33] \frac{a^2}{3} + \frac{2}{3} [19N_f - 153] a^3 \\
&+ [24192 \ln^2(\omega) \omega^4 N_f^2 - 1728 \ln^2(\omega) \omega^5 N_f^2 \\
&- 110592 \ln^2(\omega) \omega^3 N_f^2 + 165888 \ln^2(\omega) \omega^2 N_f^2 \\
&- 71928 \ln^2(\omega) \omega^5 N_f + 270864 \ln^2(\omega) \omega^4 N_f \\
&+ 787968 \ln^2(\omega) \omega^3 N_f - 2882304 \ln^2(\omega) \omega^2 N_f \\
&+ 1657260 \ln^2(\omega) \omega^5 - 11055528 \ln^2(\omega) \omega^4 \\
&+ 17107200 \ln^2(\omega) \omega^3 + 2395008 \ln^2(\omega) \omega^2 \\
&+ 2304 \ln(\omega) \Phi_{(1)\omega, \omega} \omega^5 N_f^2 - 31104 \ln(\omega) \Phi_{(1)\omega, \omega} \omega^4 N_f^2 \\
&+ 148608 \ln(\omega) \Phi_{(1)\omega, \omega} \omega^3 N_f^2 - 285696 \ln(\omega) \Phi_{(1)\omega, \omega} \omega^2 N_f^2
\end{aligned}$$

$$\begin{aligned}
&+165888 \ln(\omega) \Phi_{(1)\omega,\omega} \omega N_f^2 - 3132 \ln(\omega) \Phi_{(1)\omega,\omega} \omega^5 N_f \\
&+309096 \ln(\omega) \Phi_{(1)\omega,\omega} \omega^4 N_f - 2256336 \ln(\omega) \Phi_{(1)\omega,\omega} \omega^3 N_f \\
&+5011200 \ln(\omega) \Phi_{(1)\omega,\omega} \omega^2 N_f - 2923776 \ln(\omega) \Phi_{(1)\omega,\omega} \omega N_f \\
&-575586 \ln(\omega) \Phi_{(1)\omega,\omega} \omega^5 + 3367980 \ln(\omega) \Phi_{(1)\omega,\omega} \omega^4 \\
&-3228984 \ln(\omega) \Phi_{(1)\omega,\omega} \omega^3 - 4904064 \ln(\omega) \Phi_{(1)\omega,\omega} \omega^2 \\
&+3079296 \ln(\omega) \Phi_{(1)\omega,\omega} - 3456 \ln(\omega) \omega^5 N_f^2 \\
&+24192 \ln(\omega) \omega^4 N_f^2 - 27648 \ln(\omega) \omega^3 N_f^2 \\
&-55296 \ln(\omega) \omega^2 N_f^2 - 141696 \ln(\omega) \omega^5 N_f \\
&+1461024 \ln(\omega) \omega^4 N_f - 4886784 \ln(\omega) \omega^3 N_f \\
&+5239296 \ln(\omega) \omega^2 N_f + 505440 \ln(\omega) \omega^5 \\
&-6286896 \ln(\omega) \omega^4 + 26034048 \ln(\omega) \omega^3 \\
&-35894016 \ln(\omega) \omega^2 + 30456 \Omega_{(2)\omega,\omega} \omega^5 N_f \\
&-339552 \Omega_{(2)\omega,\omega} \omega^4 N_f + 1254528 \Omega_{(2)\omega,\omega} \omega^3 N_f \\
&-1534464 \Omega_{(2)\omega,\omega} \omega^2 N_f - 502524 \Omega_{(2)\omega,\omega} \omega^5 \\
&+5602608 \Omega_{(2)\omega,\omega} \omega^4 - 20699712 \Omega_{(2)\omega,\omega} \omega^3 \\
&+25318656 \Omega_{(2)\omega,\omega} \omega^2 - 4608 \Omega_{(2)1,\omega} \omega^5 N_f^2 \\
&+55296 \Omega_{(2)1,\omega} \omega^4 N_f^2 - 221184 \Omega_{(2)1,\omega} \omega^3 N_f^2 \\
&+294912 \Omega_{(2)1,\omega} \omega^2 N_f^2 + 102168 \Omega_{(2)1,\omega} \omega^5 N_f \\
&-1302480 \Omega_{(2)1,\omega} \omega^4 N_f + 5523552 \Omega_{(2)1,\omega} \omega^3 N_f \\
&-7824384 \Omega_{(2)1,\omega} \omega^2 N_f + 124416 \Omega_{(2)1,\omega} \omega N_f \\
&-431244 \Omega_{(2)1,\omega} \omega^5 + 6436584 \Omega_{(2)1,\omega} \omega^4 \\
&-30921264 \Omega_{(2)1,\omega} \omega^3 + 48812544 \Omega_{(2)1,\omega} \omega^2 \\
&-2052864 \Omega_{(2)1,\omega} \omega - 4374 \Phi_{(1)\omega,\omega}^2 \omega^5 N_f \\
&+34992 \Phi_{(1)\omega,\omega}^2 \omega^4 N_f - 110808 \Phi_{(1)\omega,\omega}^2 \omega^3 N_f \\
&+209952 \Phi_{(1)\omega,\omega}^2 \omega^2 N_f - 217728 \Phi_{(1)\omega,\omega}^2 \omega N_f \\
&+124416 \Phi_{(1)\omega,\omega}^2 N_f + 72171 \Phi_{(1)\omega,\omega}^2 \omega^5 \\
&-577368 \Phi_{(1)\omega,\omega}^2 \omega^4 + 1828332 \Phi_{(1)\omega,\omega}^2 \omega^3 \\
&-3464208 \Phi_{(1)\omega,\omega}^2 \omega^2 + 3592512 \Phi_{(1)\omega,\omega}^2 \omega \\
&-2052864 \Phi_{(1)\omega,\omega}^2 + 7488 \Phi_{(1)\omega,\omega} \omega^5 N_f^2 \\
&-89856 \Phi_{(1)\omega,\omega} \omega^4 N_f^2 + 376704 \Phi_{(1)\omega,\omega} \omega^3 N_f^2 \\
&-617472 \Phi_{(1)\omega,\omega} \omega^2 N_f^2 + 276480 \Phi_{(1)\omega,\omega} \omega N_f^2 \\
&-46224 \Phi_{(1)\omega,\omega} \omega^5 N_f + 618192 \Phi_{(1)\omega,\omega} \omega^4 N_f \\
&-2741472 \Phi_{(1)\omega,\omega} \omega^3 N_f + 4091904 \Phi_{(1)\omega,\omega} \omega^2 N_f
\end{aligned}$$

$$\begin{aligned}
& -235008\Phi_{(1)\omega,\omega}\omega N_f - 443880\Phi_{(1)\omega,\omega}\omega^5 \\
& + 5942808\Phi_{(1)\omega,\omega}\omega^4 - 28479600\Phi_{(1)\omega,\omega}\omega^3 \\
& + 56215296\Phi_{(1)\omega,\omega}\omega^2 - 35894016\Phi_{(1)\omega,\omega}\omega \\
& + 11664\Phi_{(2)\omega,\omega}\omega^5 N_f - 159408\Phi_{(2)\omega,\omega}\omega^4 N_f \\
& + 832032\Phi_{(2)\omega,\omega}\omega^3 N_f - 1982880\Phi_{(2)\omega,\omega}\omega^2 N_f \\
& + 1804032\Phi_{(2)\omega,\omega}\omega N_f + 124416\Phi_{(2)\omega,\omega} N_f \\
& - 192456\Phi_{(2)\omega,\omega}\omega^5 + 2630232\Phi_{(2)\omega,\omega}\omega^4 \\
& - 13728528\Phi_{(2)\omega,\omega}\omega^3 + 32717520\Phi_{(2)\omega,\omega}\omega^2 \\
& - 29766528\Phi_{(2)\omega,\omega}\omega - 2052864\Phi_{(2)\omega,\omega} \\
& - 1296\Phi_{(2)1,\omega}\omega^6 N_f + 106272\Phi_{(2)1,\omega}\omega^5 N_f \\
& - 808704\Phi_{(2)1,\omega}\omega^4 N_f + 1700352\Phi_{(2)1,\omega}\omega^3 N_f \\
& - 331776\Phi_{(2)1,\omega}\omega^2 N_f + 21384\Phi_{(2)1,\omega}\omega^6 \\
& - 1753488\Phi_{(2)1,\omega}\omega^5 + 13343616\Phi_{(2)1,\omega}\omega^4 \\
& - 28055808\Phi_{(2)1,\omega}\omega^3 + 5474304\Phi_{(2)1,\omega}\omega^2 \\
& - 6144\zeta_3\omega^5 N_f^2 - 123136\omega^5 N_f^2 + 73728\zeta_3\omega^4 N_f^2 \\
& + 1477632\omega^4 N_f^2 - 294912\zeta_3\omega^3 N_f^2 - 5910528\omega^3 N_f^2 \\
& + 393216\zeta_3\omega^2 N_f^2 + 7880704\omega^2 N_f^2 - 147456\zeta_3\omega^5 N_f \\
& + 4157856\omega^5 N_f + 1715040\zeta_3\omega^4 N_f - 49894272\omega^4 N_f \\
& - 6689088\zeta_3\omega^3 N_f + 199577088\omega^3 N_f + 8939520\zeta_3\omega^2 N_f \\
& - 266102784\omega^2 N_f - 746496\zeta_3\omega N_f + 4105728\zeta_3\omega^5 \\
& - 23466672\omega^5 - 48370608\zeta_3\omega^4 + 281600064\omega^4 \\
& + 190659744\zeta_3\omega^3 - 1126400256\omega^3 - 254555136\zeta_3\omega^2 \\
& + 1501867008\omega^2 + 12317184\zeta_3\omega] \frac{a^4}{6912\omega^2[\omega - 4]^2} \\
& + O(a^5)
\end{aligned} \tag{8.12}$$

where we have introduced the shorthand notation

$$\begin{aligned}
\Phi_{(n)1,\omega} &= \Phi_{(n)}(1, \omega) , & \Phi_{(n)\omega,\omega} &= \Phi_{(n)}\left(\frac{1}{\omega}, \frac{1}{\omega}\right) , \\
\Omega_{(n)1,\omega} &= \Omega_{(n)}(1, \omega) , & \Omega_{(n)\omega,\omega} &= \Omega_{(n)}\left(\frac{1}{\omega}, \frac{1}{\omega}\right) .
\end{aligned} \tag{8.13}$$

The analytic expressions for this β -function for an arbitrary colour group together with all other RG functions in both gauges are included in the attached data file of [4]. The decomposition of the vertex functions into the tensor basis and conversion functions are also provided in the data file. Note that for an arbitrary

colour group in the Landau gauge, the β -function has the property that one and two loop terms are in agreement with the scheme independent parts which were first computed in [21, 22, 267, 268]. For a non-zero gauge parameter α , the two loop term is in fact gauge dependent as one would expect. As α can be regarded as a second coupling constant and the β -function is only scheme dependent to two loops in a theory with one coupling. The three loop term of (8.13) is scheme dependent and also ω dependent. The results for all three β -functions for $\omega = 1/2$ and 2 are stated below. These are given in numerical form for both gauges as it is the most straightforward way to compare expressions and see effects of varying ω within the RG function. Note that the notation is iMOMi in Landau gauge while iMOMmi is the MAG gauge, [4]. For $\omega = 1/2$ we have

$$\begin{aligned}
\beta^{\text{iMOMg}}(a, 0) \Big|_{\omega=\frac{1}{2}} &= [0.666667N_f - 11.000000] a^2 + [12.666667N_f \\
&\quad - 102.000000] a^3 + [-1.958625N_f^3 + 45.770375N_f^2 \\
&\quad + 154.329226N_f - 1973.775606] a^4 + O(a^5) , \\
\beta^{\text{iMOMh}}(a, 0) \Big|_{\omega=\frac{1}{2}} &= [0.666667N_f - 11.000000] a^2 + [12.666667N_f \\
&\quad - 102.000000] a^3 + [-21.248801N_f^2 + 615.665280N_f \\
&\quad - 2861.242336] a^4 + O(a^5) , \\
\beta^{\text{iMOMq}}(a, 0) \Big|_{\omega=\frac{1}{2}} &= [0.666667N_f - 11.000000] a^2 + [12.666667N_f \\
&\quad - 102.000000] a^3 + [-21.559789N_f^2 + 599.589376N_f \\
&\quad - 2133.132445] a^4 + O(a^5) , \\
\beta^{\text{iMOMmg}}(a, 0) \Big|_{\omega=\frac{1}{2}} &= [0.666667N_f - 11.000000] a^2 + [12.666667N_f \\
&\quad - 96.417290] a^3 + [-1.958625N_f^3 + 36.668278N_f^2 \\
&\quad + 469.963542N_f - 3720.350935] a^4 + O(a^5) , \\
\beta^{\text{iMOMmh}}(a, 0) \Big|_{\omega=\frac{1}{2}} &= [0.666667N_f - 11.000000] a^2 + [12.666667N_f \\
&\quad - 108.504849] a^3 + [-24.371002N_f^2 + 689.727288N_f \\
&\quad - 3346.349782] a^4 + O(a^5) , \\
\beta^{\text{iMOMmq}}(a, 0) \Big|_{\omega=\frac{1}{2}} &= [0.666667N_f - 11.000000] a^2 + [12.666667N_f \\
&\quad - 100.990317] a^3 + [-21.514813N_f^2 + 630.898042N_f \\
&\quad - 2435.486351] a^4 + O(a^5) \tag{8.14}
\end{aligned}$$

and for $\omega = 2$ the results are

$$\begin{aligned}
\beta^{\text{iMOMg}}(a, 0) \Big|_{\omega=2} &= [0.666667N_f - 11.000000] a^2 + [12.666667N_f \\
&\quad - 102.000000] a^3 + [-3.752885N_f^3 + 99.867703N_f^2
\end{aligned}$$

$$\begin{aligned}
& -234.213856N_f - 976.833287] a^4 + O(a^5) , \\
\beta^{\text{iMOMh}}(a, 0) \Big|_{\omega=2} &= [0.666667N_f - 11.000000] a^2 + [12.666667N_f \\
& -102.000000] a^3 + [-21.654322N_f^2 + 617.879121N_f \\
& -2746.474396] a^4 + O(a^5) , \\
\beta^{\text{iMOMq}}(a, 0) \Big|_{\omega=2} &= [0.666667N_f - 11.000000] a^2 + [12.666667N_f \\
& -102.000000] a^3 + [-23.801168N_f^2 + 563.445891N_f \\
& -1355.780477] a^4 + O(a^5) , \\
\beta^{\text{iMOMmg}}(a, 0) \Big|_{\omega=2} &= [0.666667N_f - 11.000000] a^2 + [12.666667N_f \\
& -89.805313] a^3 + [-3.752885N_f^3 + 82.563084N_f^2 \\
& +297.046404N_f - 3156.729291] a^4 + O(a^5) , \\
\beta^{\text{iMOMmh}}(a, 0) \Big|_{\omega=2} &= [0.666667N_f - 11.000000] a^2 + [12.666667N_f \\
& -107.331545] a^3 + [-25.485264N_f^2 + 636.479467N_f \\
& -2354.843991] a^4 + O(a^5) , \\
\beta^{\text{iMOMmq}}(a, 0) \Big|_{\omega=2} &= [0.666667N_f - 11.000000] a^2 + [12.666667N_f \\
& -91.096267] a^3 + [-23.905680N_f^2 + 614.725445N_f \\
& -2055.563293] a^4 + O(a^5) . \tag{8.15}
\end{aligned}$$

For comparison the numerical form of the RG functions in the MOMi schemes for the MAG gauge are listed in [102, 103]. As the β -function is not a physically meaningful quantity it is more beneficial to examine the critical exponents. We will therefore also consider the quark mass anomalous dimension. Known $\overline{\text{MS}}$ and MOMi numerical results are given in [1, 273–276, 310]. The corresponding iMOMi results for the quark mass anomalous dimension for $\omega = 1/2$ and 2 in the $SU(3)$ colour group are

$$\begin{aligned}
\gamma_{\bar{\psi}\psi}^{\text{iMOMg}}(a, 0) \Big|_{\omega=\frac{1}{2}} &= -4.000000a + [-8.524052N_f + 9.467706] a^2 \\
& + [-32.491101N_f^2 + 140.861801N_f + 357.940500] a^3 \\
& + O(a^4) , \\
\gamma_{\bar{\psi}\psi}^{\text{iMOMh}}(a, 0) \Big|_{\omega=\frac{1}{2}} &= -4.000000a + [-0.607233N_f - 19.365345] a^2 \\
& + [-2.666667N_f^2 + 36.838982N_f + 341.949868] a^3 \\
& + O(a^4) , \\
\gamma_{\bar{\psi}\psi}^{\text{iMOMq}}(a, 0) \Big|_{\omega=\frac{1}{2}} &= -4.000000a + [-0.607233N_f - 33.503320] a^2 \\
& + [-2.666667N_f^2 + 30.680528N_f - 240.778923] a^3 \\
& + O(a^4) ,
\end{aligned}$$

$$\begin{aligned}
\gamma_{\bar{\psi}\psi}^{\text{iMOMmg}}(a, 0) \Big|_{\omega=\frac{1}{2}} &= -4.000000a + [-8.524052N_f - 17.879808]a^2 \\
&\quad + [-32.491101N_f^2 - 29.514002N_f + 659.067463]a^3 \\
&\quad + O(a^4), \\
\gamma_{\bar{\psi}\psi}^{\text{iMOMmh}}(a, 0) \Big|_{\omega=\frac{1}{2}} &= -4.000000a + [-0.607233N_f - 15.413838]a^2 \\
&\quad + [-2.666667N_f^2 + 20.098107N_f + 577.599012]a^3 \\
&\quad + O(a^4), \\
\gamma_{\bar{\psi}\psi}^{\text{iMOMmq}}(a, 0) \Big|_{\omega=\frac{1}{2}} &= -4.000000a + [-0.607233N_f - 41.488147]a^2 \\
&\quad + [-2.666667N_f^2 + 29.318648N_f - 337.686951]a^3 \\
&\quad + O(a^4) \tag{8.16}
\end{aligned}$$

for $\omega = \frac{1}{2}$ and

$$\begin{aligned}
\gamma_{\bar{\psi}\psi}^{\text{iMOMg}}(a, 0) \Big|_{\omega=2} &= -4.000000a + [-14.510481N_f + 61.367526]a^2 \\
&\quad + [-74.6686432N_f^2 + 492.015439N_f + 158.572781]a^3 \\
&\quad + O(a^4), \\
\gamma_{\bar{\psi}\psi}^{\text{iMOMh}}(a, 0) \Big|_{\omega=2} &= -4.000000a + [-3.551816N_f + 27.691568]a^2 \\
&\quad + [-2.666667N_f^2 - 53.424921N_f + 1239.598236]a^3 \\
&\quad + O(a^4), \\
\gamma_{\bar{\psi}\psi}^{\text{iMOMq}}(a, 0) \Big|_{\omega=2} &= -4.000000a + [-3.551816N_f + 31.128323]a^2 \\
&\quad + [-2.666667N_f^2 - 60.202636N_f + 715.222060]a^3 \\
&\quad + O(a^4), \\
\gamma_{\bar{\psi}\psi}^{\text{iMOMmg}}(a, 0) \Big|_{\omega=2} &= -4.000000a + [-14.510481N_f + 27.838788]a^2 \\
&\quad + [-74.668643N_f^2 + 138.832502N_f + 1356.765556]a^3 \\
&\quad + O(a^4), \\
\gamma_{\bar{\psi}\psi}^{\text{iMOMmh}}(a, 0) \Big|_{\omega=2} &= -4.000000a + [-3.551816N_f + 45.455562]a^2 \\
&\quad + [-2.666667N_f^2 - 50.959511N_f + 921.958650]a^3 \\
&\quad + O(a^4), \\
\gamma_{\bar{\psi}\psi}^{\text{iMOMmq}}(a, 0) \Big|_{\omega=2} &= -4.000000a + [-3.551816N_f + 24.910097]a^2 \\
&\quad + [-2.666667N_f^2 - 77.968868N_f + 999.570302]a^3 \\
&\quad + O(a^4) \tag{8.17}
\end{aligned}$$

for $\omega = 2$. Recall the scheme dependence begins at two loops here. Note that a similar pattern emerges for both the β -functions and quark mass anomalous dimensions. For the MOMi β -functions the corresponding coefficients to the N_f

independent part of each three loop term are exactly halfway between the $\omega = 1/2$ and 2 coefficients in each iMOM scheme as $|\ln(1/2)| = |\ln(2)|$. Similarly for the N_f independent two and three loop terms of the quark mass anomalous dimension we find the same general trend. More precisely, at two loops the $\omega = 1$ N_f independent coefficient lies roughly halfway between the $\omega = 1/2$ and 2 values. The effect of varying the parameter ω between $1/2$ and 2 in comparison with the symmetric point MOM schemes of [98,99] can now be quantified by analysing the critical exponents in each scheme. First we recall some internal checks that were used in this calculation. The two loop terms of all RG functions were evaluated using two different methods. A direct evaluation as well as the conversion method was performed with both of these techniques producing the same results at two loops. Additionally the 2-point three loop functions were also computed directly which matched the conversion results. The final check is the correct emergence of the $\omega \rightarrow 1$ limit.

8.4 Results

Having obtained all Renormalization Group functions for the iMOM schemes in both the Landau and MAG gauges, we can evaluate the critical exponents and perform a full analysis on the results. Note in this Chapter all analysis is performed in the fundamental representation. To a sufficiently high loop order the critical exponents should be renormalization scheme invariant. The iMOM analysis will run parallel to the MOMi schemes of Chapter 7. However the new schemes may give a greater insight into RG invariance with the choice of the two specific values of parameter ω used to quantify the variation. The notation used to define the β -function and quark mass anomalous dimensions in the Landau gauge in an arbitrary scheme \mathcal{S} was given in equations (7.1), (7.2), (7.3), (7.5) and (7.6). The same formalism applies to the MAG. The truncated critical exponents evaluated in each iMOM scheme at the Banks-Zaks fixed point are

$$\begin{aligned}\tilde{\omega}_L &= 2\beta'_L(a_L, 0), \\ \rho_L &= -2\gamma_{\bar{\psi}\psi}_L(a_L, 0).\end{aligned}\tag{8.18}$$

Here $\tilde{\omega}$ now denotes the exponent associated with the β -function as in the iMOM schemes ω signifies the interpolating parameter. Note that $\tilde{\omega}$ and ρ have the same definition as [1, 97]. However since we used the β -function conventions of [328] comparing the location of the critical coupling with [97] there will be a difference of 4π . This has been absorbed into our coupling. We solve for the Banks-Zaks

fixed points at two and three loops in each of the iMOM schemes for $\omega = 1/2$ and 2. The full set of results are listed in Appendix E and summarized here. Tables E.1 to E.5 are for the Landau gauge while the remaining tables give data corresponding to the MAG gauge. The critical couplings for the iMOMq, iMOMh and iMOMg schemes are given in table E.1 at three loops for $\omega = 1/2$ and 2. As the β -functions are scheme independent to two loops, only the three loop results are listed. Table E.2 displays the three loop $\tilde{\omega}$ exponent in all three schemes. Once again only the three loop results are given. The exponent ρ in each of the three iMOM schemes to two and three loops are given by tables E.3, E.4 and E.5. We have given the results of this exponent for $\omega = 1/2, 1$ and 2, the symmetric point values corresponding to $\omega = 1$ were computed in [1] and discussed in Chapter 7. They are included here for comparison with the new values and in order to gauge, for instance, what the range of exponent is when ω is varied. For the analysis we have concentrated on the $SU(2)$ and $SU(3)$ groups for their two loop conformal windows which are $6 \leq N_f \leq 10$ and $9 \leq N_f \leq 16$ respectively.

For the remaining tables in Appendix E the same data is given but for the MAG gauge. For example, tables E.6, E.7 and E.8 give the critical couplings for each of the iMOM schemes at two and three loops. While tables E.9, E.10 and E.11 give the corresponding critical exponent $\tilde{\omega}$ values to the fixed points. The exponent ρ is given to two and three loops for $\omega = 1/2, 1$ and 2 in tables E.12, E.13 and E.14. Note that in the MAG for several of the schemes the lower bound of the conformal window for $SU(3)$ is at $N_f = 8$ rather than 9, we have included these results. However the two loop exponents for $N_f = 8$ have been omitted as they are several orders of magnitude larger than either the subsequent N_f estimates or the three loop value. This suggests perturbative theory may not be totally reliable at $N_f = 8$. The three loop data for $N_f = 8$ has been included as it is not unreasonable when compared with $N_f = 9$.

To illustrate more clearly how the value of the exponent $\tilde{\omega}$ depends on the renormalization scheme it is evaluated in, the data for this exponent has been plotted in figures 8.1, 8.2 and 8.3. These plots are in the Landau gauge for both $SU(2)$ and $SU(3)$ to three loops. Although we have calculated discrete values of $\tilde{\omega}$ for N_f , we have chosen to present piecewise linear connections between the spot values for this and other tables similar to [97], in order to spot trends. Note that the results for exponents in the $\overline{\text{MS}}$ and mMOM schemes have been included in all figures to provide a guide point for comparing scheme results for each colour group.

One of the main themes that emerges in figures 8.1, 8.2 and 8.3 for both the $SU(2)$ and $SU(3)$ groups is that the $\overline{\text{MS}}$ values diverge away from iMOM results at about the midpoint of the conformal window as N_f decreases. This is not unexpected due to the loss of perturbative reliability at the lower end of the conformal window. This effect is most pronounced for the iMOMg scheme whereas for the the iMOMh plot there is a smaller spread for the values of ω for relatively low N_f . In general for all iMOM schemes the spread across the scheme for $\tilde{\omega}$ values is relatively small. This is perhaps surprising for low values of N_f but in keeping with our expectations for higher values where one is in the perturbative region. For the $SU(3)$ group where $N_f = 12$ the exponent $\tilde{\omega}$ appears to be in general agreement for all schemes except $\overline{\text{MS}}$. A feature of the three loop $\tilde{\omega}$ plots is a relatively small spread for the range of ω we took. However as at two loops the exponents are scheme independent we cannot say whether the momentum subtraction based schemes have any marked difference with non-kinematic schemes. Obtaining results to four loops would help with this question. As the quark mass anomalous dimension is scheme dependent at two loops we can examine features at two and three loops. For group $SU(2)$ and $SU(3)$ the values for exponent ρ are illustrated in figures 8.4-8.9 in the Landau gauge. The scheme order is the same as for figures 8.1, 8.2 and 8.3. As a general comment we note that in both $SU(2)$ and $SU(3)$ the two loop results at the lower end of the conformal window are unreliable. There is a huge difference at the lower end of the window compared with three loops. This was the same for the $\tilde{\omega}$ exponent although is more apparent for ρ . Note that even for N_f above the lower end of the conformal window there is still a large discrepancy between the two and three loop values.

A general feature for the ρ values, which is shared with $\tilde{\omega}$, is that the $\overline{\text{MS}}$ scheme and to a lesser extent the mMOM scheme have different behaviour to iMOM as N_f decreases. This discrepancy is most apparent at $N_f = 12$ for $SU(3)$ which is where perturbation theory is perhaps on the limit of credibility. There is a parallel structure when comparing each scheme for both colour groups. For the three loop plots aside from iMOMg there is a slight discrepancy between $\overline{\text{MS}}$ and mMOM scheme estimates and iMOM values. This is most pronounced for the lower N_f values in the iMOMh case. As there is a significant difference between values in all iMOM schemes at the lower end of the conformal window, no serious significance should be placed on values ρ_3 here. Acquiring four loop results will help establish to what extent scheme dependence plays a role at the lower end of the window. A feature of the three loop plots for both exponents is that the mMOM results faithfully track to $\overline{\text{MS}}$ values. This may not be surprising as both schemes are defined in a similar way. However there is one exception to this

trend. For the plot of $\tilde{\omega}$ in the iMOMh scheme given by figure 8.2, the mMOM result is virtually on top of the iMOM schemes for $\omega = 1/2, 1$ and 2 for the entire conformal window. The fact is that as the mMOM scheme preserves by definition a property of the ghost-gluon vertex then this is reflected in the agreement with the kinematic scheme behaviour. Indeed of the three schemes the iMOMh $\tilde{\omega}$ exponents have minimal spread for all N_f . Again this observation needs to be balanced by noting that the iMOMg behaviour of ρ_3 is parallel to the $\overline{\text{MS}}$ and mMOM schemes for low N_f .

Results in the MAG gauge are plotted in figures 8.10, 8.11 and 8.12. We have illustrated fewer plots in the MAG gauge as there is a strong general similarity with the results in the Landau gauge at two loops. The plots for both exponents are given in $SU(3)$ to three loops as there are similar trends in both sets of results. Note that we have excluded the data for $N_f = 8$ as this would skew the analysis. Examining only $9 \leq N_f \leq 16$ allows finer detail to be seen. The $\tilde{\omega}$ exponent three loop results are virtually the same as the Landau values. There is little difference between the $\overline{\text{MS}}$, mMOM and iMOMmi schemes in the range $13 \leq N_f \leq 16$. For the border point of $N_f = 12$ the iMOMmq and iMOMmh schemes are practically the same but backs up the earlier observation that this is probably the place where higher order corrections could remove scheme ambiguity. For the iMOMmg plot the discrepancy in the $\tilde{\omega}$ value at $N_f = 13$ is large than in the Landau gauge. This is due in part to the nature of the MAG gauge where a subset of gluon fields are isolated in the definition of the gauge itself. However with higher order corrections this discrepancy could fade.

For the ρ exponent in the MAG gauge the behaviour is different in that we have different functional behaviour for each scheme below $N_f = 16$. However the general behaviour of the three iMOMmi schemes is not dissimilar to that of the Landau gauge plots. The different behaviour lies in the nature of the quantity plotted which is the quark mass operator. This operator does not have any gluon content where the split colour group property would be significant. However, the plots may be misleading in that the difference between ρ exponent estimates between $N_f = 13$ and 15 range from 5% to 8%. Finally, what is noticeable in both gauges is that the behaviour of the schemes based on the triple gluon vertex is different from the other two schemes at the lower end of the conformal window. That this is the case in the MAG as well as the Landau gauge suggests that it is a feature of the particular vertex which has significantly more graphs at two loops and these are predominantly gluonic. It will not be until three loops that there would be a commensurate number of gluonic contributions to the quark-

and ghost-gluon vertex functions with which to compare. It may be then that the behaviour at the lower end of the window becomes similar across all three iMOMi schemes.

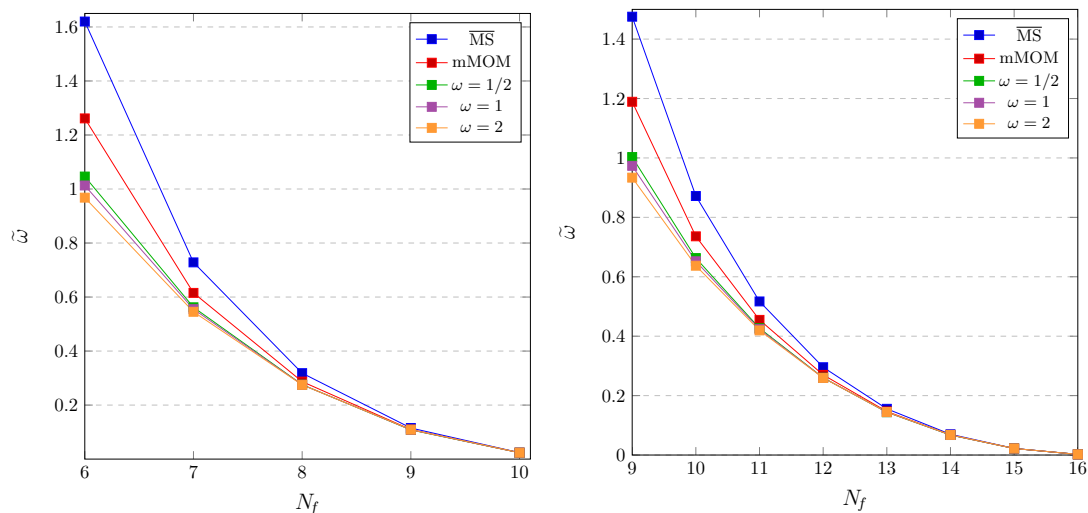


Figure 8.1: Critical exponent $\tilde{\omega}$ at three loops for $SU(2)$ (left) and $SU(3)$ (right) for the iMOMq renormalization scheme.

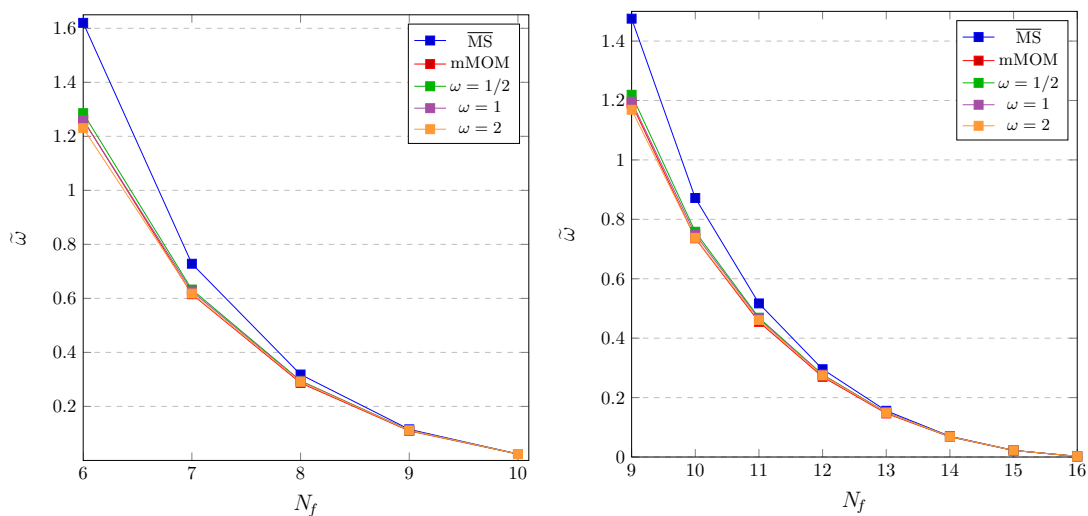


Figure 8.2: Critical exponent $\tilde{\omega}$ at three loops for $SU(2)$ (left) and $SU(3)$ (right) for the iMOMh renormalization scheme.

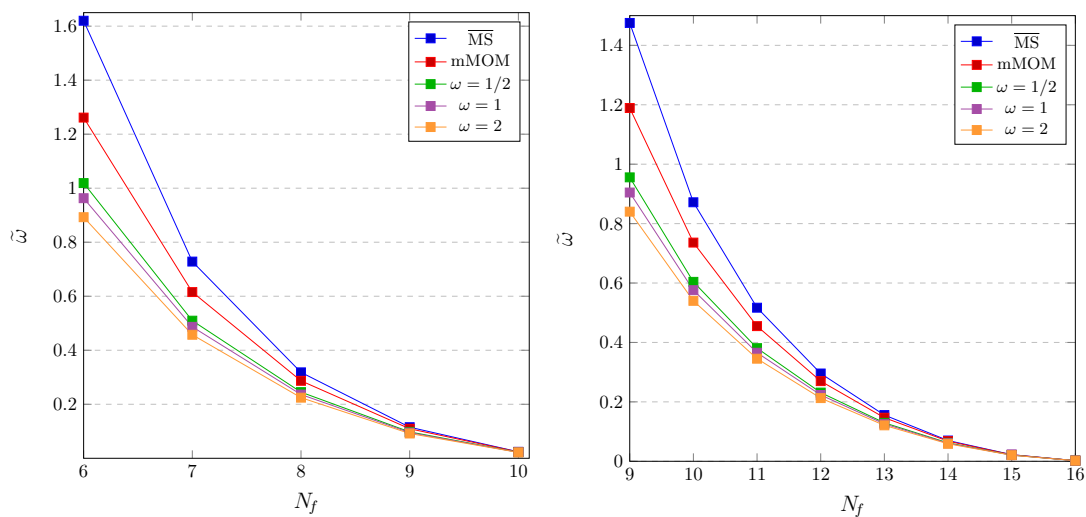


Figure 8.3: Critical exponent $\tilde{\omega}$ at three loops for $SU(2)$ (left) and $SU(3)$ (right) for the iMOMg renormalization scheme.

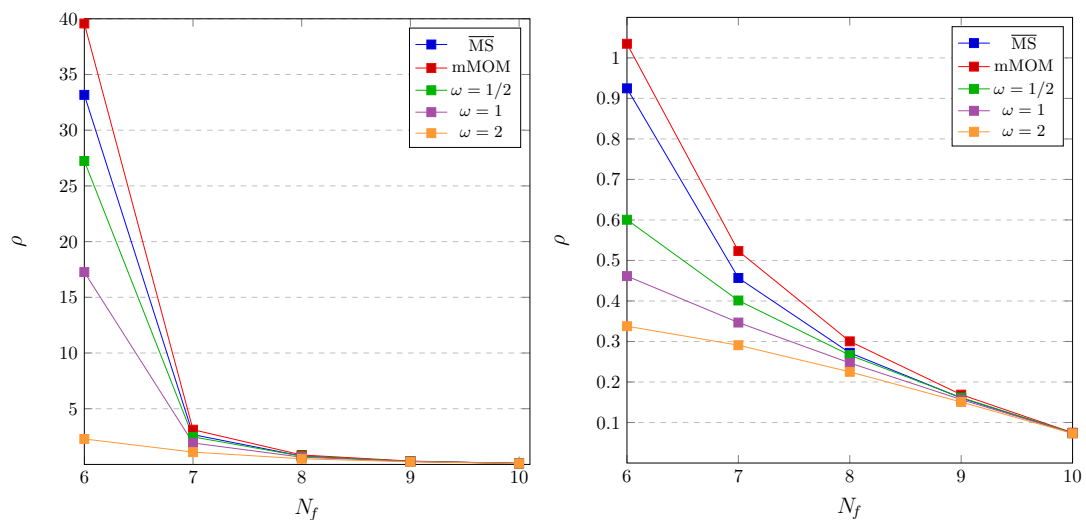


Figure 8.4: Critical exponent ρ for $SU(2)$ at two (left) and three loops (right) for the iMOMq renormalization scheme.

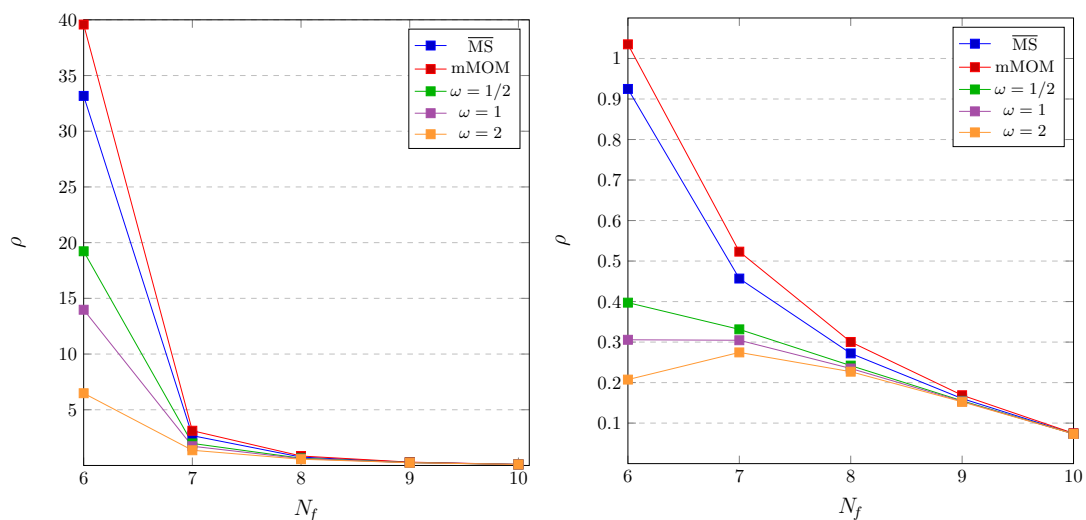


Figure 8.5: Critical exponent ρ for $SU(2)$ at two (left) and three loops (right) for the $iMOMh$ renormalization scheme.

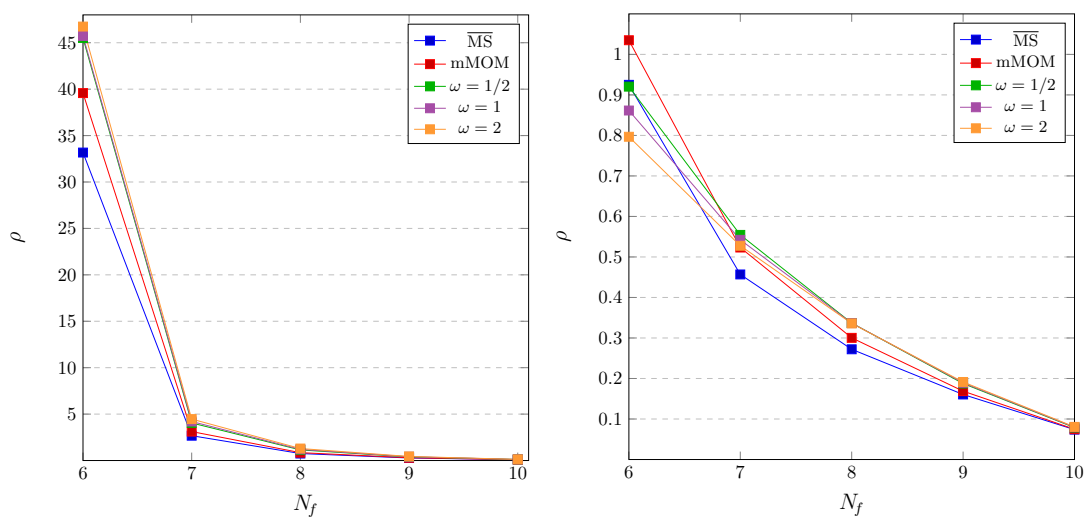


Figure 8.6: Critical exponent ρ for $SU(2)$ at two (left) and three loops (right) for the $iMOMg$ renormalization scheme.

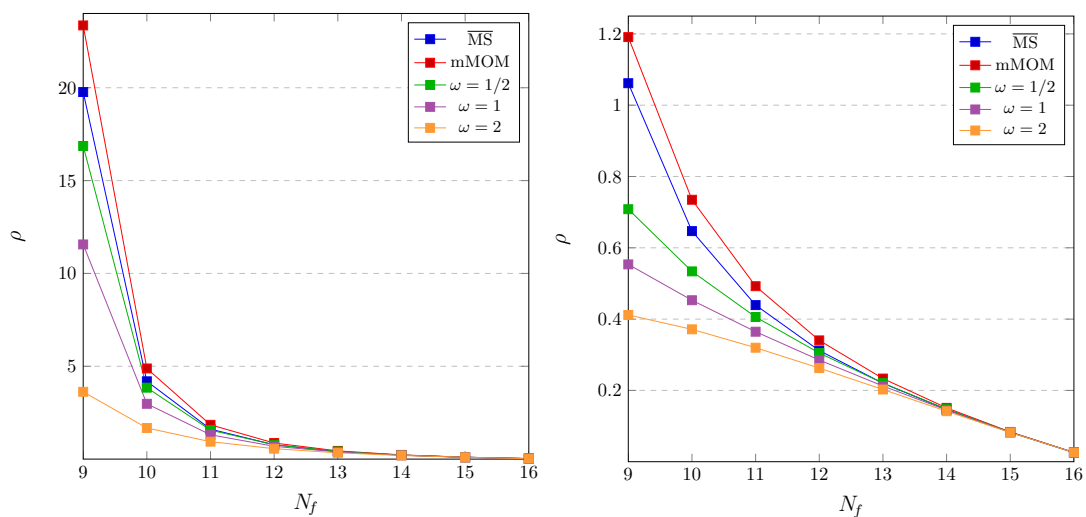


Figure 8.7: Critical exponent ρ for $SU(3)$ at two (left) and three loops (right) for the iMOMq renormalization scheme.

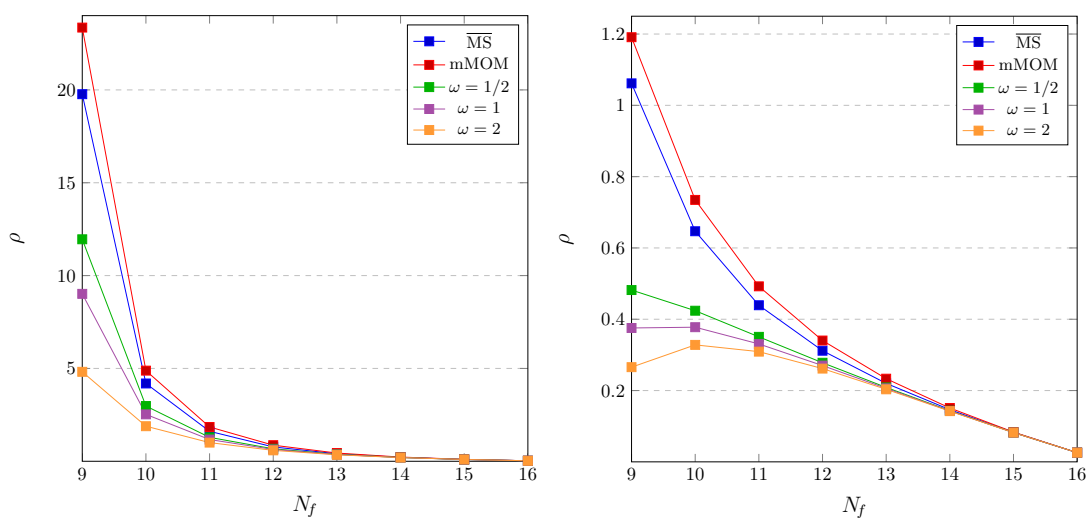


Figure 8.8: Critical exponent ρ for $SU(3)$ at two (left) and three loops (right) for the iMOMh renormalization scheme.

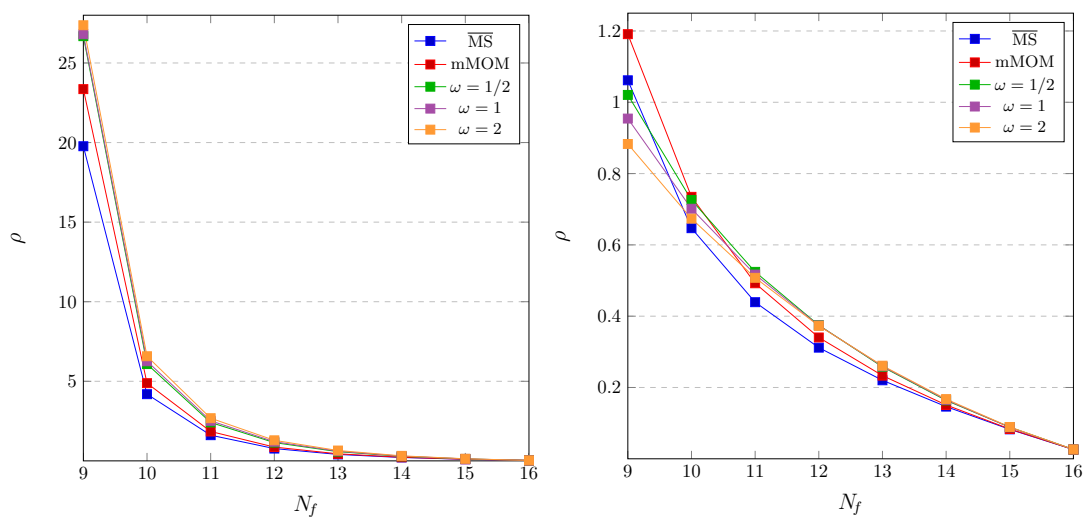


Figure 8.9: Critical exponent ρ for $SU(3)$ at two (left) and three loops (right) for the iMOMg renormalization scheme.

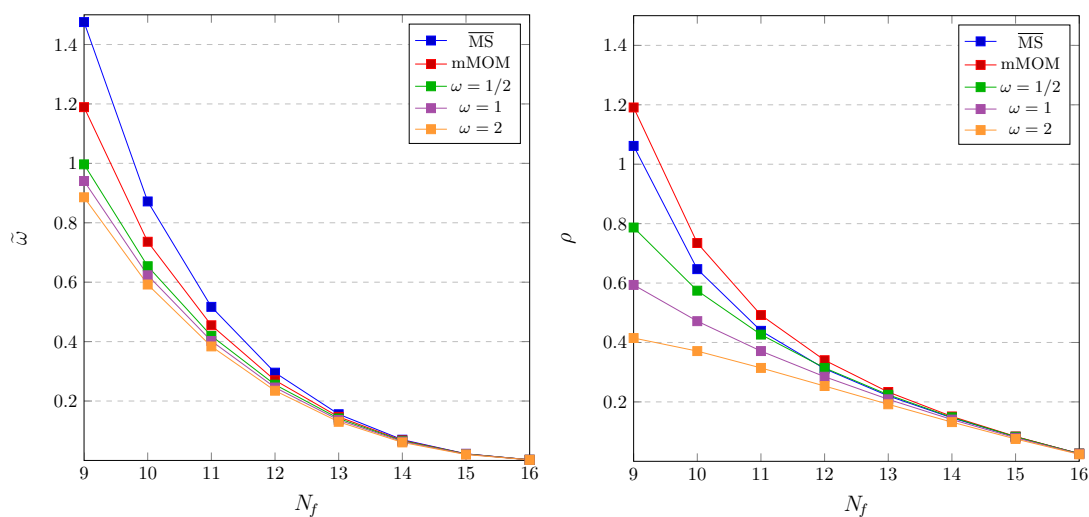


Figure 8.10: Critical exponents $\tilde{\omega}$ (left) and ρ (right) for $SU(3)$ in the MAG at three loops for the iMOMq renormalization scheme.

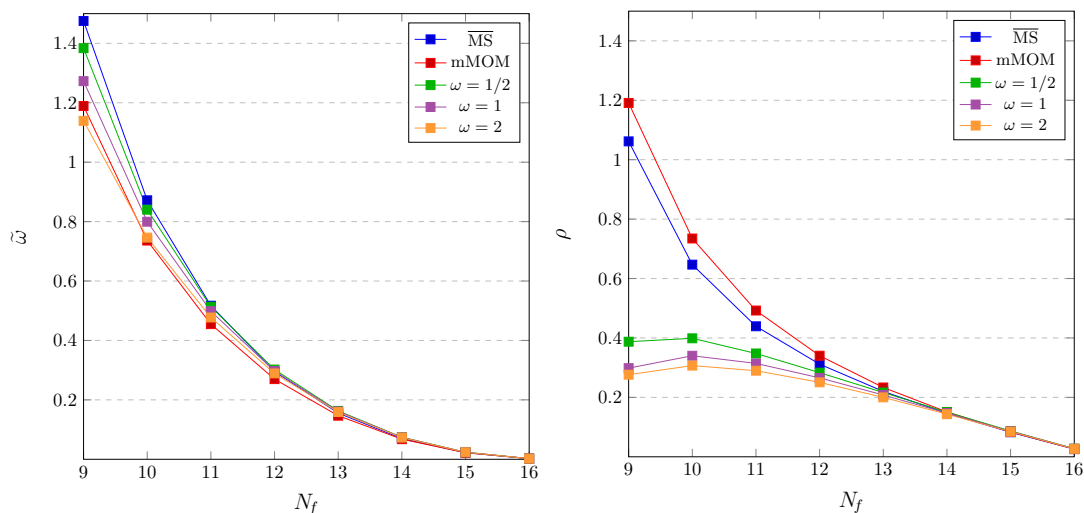


Figure 8.11: Critical exponents $\tilde{\omega}$ (left) and ρ (right) for $SU(3)$ in the MAG at three loops for the iMOMh renormalization scheme.

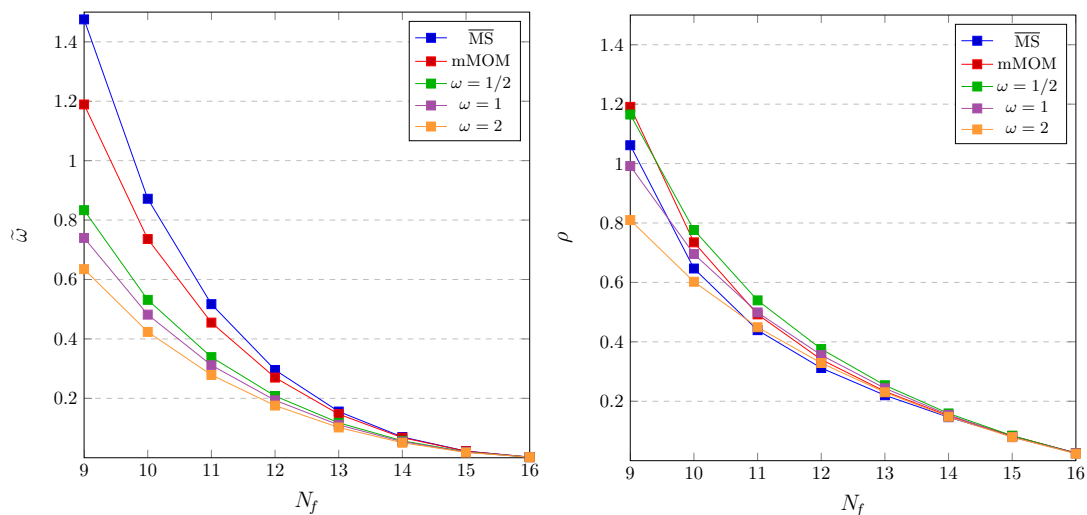


Figure 8.12: Critical exponents $\tilde{\omega}$ (left) and ρ (right) for $SU(3)$ in the MAG at three loops for the iMOMg renormalization scheme.

8.5 Discussion

We conclude with some general remarks on our analysis. We have continued the work of [97] and [1] on the Banks-Zaks analysis of critical exponents, this time extending to the iMOM schemes. The iMOM schemes are an extension of the original MOM schemes, [98,99] and depend on a parameter ω which is restricted to the values $0 < \omega < 4$. The three iMOMi schemes were considered in both the Landau gauge and MAG. The main motivation for extending the analysis to include the iMOM schemes was to provide data for exponents of interest in a truncated perturbative expansion and see how far into the conformal window

scheme independence was apparent. The conformal window is such that for values of N_f near the upper limit, perturbation theory should be a good tool for reliable information. By contrast as N_f reduces inside the window perturbation theory ceases to be a reliable guide. However, where the breakdown occurs is not immediately obvious without numerical analysis. Overall for both gauges it appears that at three loops one cannot fully rely on estimates at $N_f = 12$ and below. This should be quantified by noting that this is from raw results without re-summation to improve convergence.

There appears to be strong agreement between $\overline{\text{MS}}$ and iMOM results at the upper end of the conformal window. Numerically the data in the plots for both sets of schemes lie on top of each other. However this should be balanced by noting that the numerology of $\overline{\text{MS}}$ and iMOM schemes are different with the difference first appearing in the scheme dependent terms. Therefore this ought to motivate not only a study which includes higher loop iMOM terms but also an investigation to see if this can be established beyond numerical evidence. One possible avenue of future research would be to extend the iMOM schemes beyond the appearance of one parameter. For example, a more general set of schemes could involve two parameters related to the dimensionless variables x and y appearing in the underlying polylogarithms of the master one and two loop integrals. While we have not studied this here we expect the outcome to be the same. In other words the critical exponent values will be scheme independent.

Our MOM and iMOM analysis allows us to analyse where in the conformal window scheme dependence becomes most prominent. In the absence of a perturbative expansion to all loop orders we can only obtain a truncated approximation for the critical exponents. Following the publication of [1], a novel method was proposed in [106] to disentangle induced scheme dependence. Instead of perturbatively expanding in the coupling constant a scheme independent expansion in $\Delta_f = \widetilde{N}_f - N_f$ was used. Here \widetilde{N}_f is the number of quark flavours above which asymptotic freedom is lost. We summarise recent work done using this expansion to give an outlook of current research in this area. In [106] the anomalous dimension of the quark mass at the Banks-Zaks fixed point was calculated in $SU(2)$ and $SU(3)$ as a series expansion in Δ_f in two different schemes to three loops, $O(\Delta_f^3)$. Both schemes yielded identical results. This scheme independent expansion was then tested to three loops against exact results in supersymmetric Quantum Chromodynamics (SQCD) and found general agreement, [106]. Additionally it was observed that the scheme independent expansion also preserved supersymmetry (SUSY) which is lost in traditional perturbation theory. These

results were extended for $SU(3)$ to four loops in [107] and found good agreement with recent lattice measurements.

The scheme independent expansion has also been used to analysis asymptotically free vectorial gauge theories with non-abelian gauge groups. In [108] the critical exponent corresponding to the first derivative of the β -function was computed to four loops for a general group and general representation and to five loops for $SU(3)$. Additionally the quark mass critical exponent was calculated to four loops for $SU(2)$ and $SU(3)$ in [109] and was favourably compared with recent lattice and traditional perturbative results. In [110] these results were extended to four and five loops respectively for a general gauge group as well as for $SU(2)$, $SU(3)$ and $SU(4)$. Furthermore scheme independent expansions for the two exponents were calculated in an asymptotically free vectorial gauge theory with $SO(N_c)$ and $Sp(N_c)$ symmetry in [111]. More recently scheme independent calculations were performed in several asymptotically free chiral gauge theories, [112]. In [114] the first analytic scheme independent expansion to three loops was found for the anomalous dimensions of a variety of (gauge-invariant) baryon operators at the Banks-Zaks fixed point in asymptotically free $SU(3)$ gauge theories in the fundamental representation. Importantly the regularization invariant (RI') and several MOM schemes were used in [114] to calculate exponents in an asymptotically free gauge theory with a general gauge group. All schemes used yielded identical results for the coefficients in the scheme independent expansion.

Perspective

In Part I of this thesis the focus was on calculations involving the d -dimensional Wilson-Fisher fixed point. The central theme throughout Part I was the property of universality and how it can be used to connect theories in different space-time dimensions through this fixed point. All theories considered contained scalar fields only, with the hope of developing new ideas and techniques using scalar ‘toy’ models that may later be applied to gauge and Beyond the Standard Model (BSM) physics. The large N expansion is an invaluable aspect of universality. A comprehensive overview of this method was given in Chapter 2, predominantly as details on this technique are rarely provided in the literature. We therefore took the opportunity here to fully explain the intricacies of the method and provide steps for the computation of leading order critical exponents in the $1/N$ expansion using the non-linear σ model (NL σ M).

Chapter 3 concentrated on the universality class containing both the NL σ M and four dimensional ϕ^4 theory with $O(N)$ symmetry. We reviewed recent extensions of the universality to six and eight dimensions, [51–54], before then constructing the connected ten dimensional Lagrangian. Building the Lagrangian used dimensionality arguments for the two basic fields along with the universal interaction of the two fields, $\sigma\phi^i\phi^i$. All necessary spectator interactions containing σ fields were also included to ensure renormalizability in ten dimensions. The Renormalization Group (RG) functions for the ten dimensional theory were then computed with the β -functions and anomalous dimensions calculated to one and two loops, respectively. The subsequent ten dimensional critical exponents were also found. Many techniques were introduced which aided in this computation. The Laporta algorithm using integration by parts (IBP) and the Tarasov method were fully exploited. Additionally we introduced the vacuum bubble ex-

pansion and developed equations from the renormalization constants that allow the computation of Renormalization Group functions order by order. The two dimensional NL σ M gives the foundation for this universality and was used in Chapter 2 to derive d -dimensional critical exponents for this universality class. We compared large N results order by order with the ten dimensional critical exponents to verify the extension of the universality class to ten dimensions.

The universality of a different scalar theory was examined in Chapter 4. We constructed the six dimensional extension of the $O(N) \times O(m)$ Landau-Ginzburg-Wilson (LGW) model. The Renormalization Group functions were calculated using similar techniques to those developed in Chapter 3 and subsequent critical exponents matched to large N results. An additional motivation for the six dimensional LGW model beyond proving universality was to examine the fixed point structure and the location of the conformal window. The six dimensional LGW theory has more coupling constants than $O(N)$ theory of Chapter 3 and hence a richer fixed point structure. Our fixed point analysis was centred on $O(N) \times O(2)$ but we expect the same general picture to emerge for different values of m . We were able to isolate fixed points for various values of N which had a structure in keeping with the phase plane of the four dimensional model and analyse the stability behaviour. Real and complex fixed points were found for various values of N , with the complex values indicating a non-unitary theory. A sectioning method was applied to find an estimate for the full chiral stable (CS) conformal window which was found to be $N \geq 1106$. Computational limitations prevented a full analysis of the conformal window for all couplings, however we were able to study the anti-chiral unstable (AU) conformal window where only two of the couplings are non-zero for various values of m . We found that at leading order a conformal window exists in the six dimensional $O(N) \times O(m)$ theory for $m > 5$. We also attempted to establish whether a fixed point exists down to five dimensions and the potential conformal window. It was indicated in non-perturbative bootstrap results, [66], that a five dimensional fixed point would not be easy to find from the lower dimensional point of view unless one was examining AU type coupling patterns. We reached a similar conclusion, although it is hoped that data provided here will be useful in future for mining and comparison with non-perturbative work in five dimensions.

The scalar theories of Chapters 3 and 4 act as a laboratory for testing techniques that may be applied to non-scalar theories such as those with gauge symmetry or supersymmetry (SUSY). One interesting idea that emerges from our scalar calculations is the apparent connection of ultraviolet (UV) stable fixed

points in a higher dimension with infrared (IR) fixed points in lower dimensions. This is known as UV/IR duality, [46]. For this reason extending the universality class to a higher dimension is sometimes referred to as UV completion. The stability properties of fixed points were examined in Chapter 4, it is hoped that the same methodology can be applied to more complex theories, in particular Quantum Chromodynamics (QCD). It is known that in $2 < d < 4$ QCD lies in the same universality class as the two dimensional non-abelian Thirring model. This connection has been established through the large N_f expansion, [228–231]. The non-trivial fixed point of QCD, known as the Banks-Zaks fixed point is IR stable. QCD is a high energy quantum field theory (QFT) and in the absence of a low energy Lagrangian the value of the fixed point can only be perturbatively estimated. One possible solution however is to extend the universality class to a higher dimension and investigate whether a UV stable fixed point is present there. A six dimensional Lagrangian for QCD was constructed in [54] and the corresponding RG functions computed to two loops. It was hoped that information in four dimensions could be accessed by perturbatively calculating in six dimensions to high precision. As six dimensional QCD has extra couplings it was speculated that these additional operators could become relevant in the critical sense and be the dominant operators driving the IR behaviour in four dimensions, [54]. Moreover it was established that the quark-gluon coupling is asymptotically free in six dimensions, [54], so there is the potential to study issues of colour confinement using the six dimensional Lagrangian. It is still premature to think that links with the Banks-Zaks fixed point and higher dimensions have been established in any respect. However methods introduced in Part I could prove useful in future research.

As the RG functions of six dimensional QCD have only been calculated to two loops, one potential avenue of future work is to calculate to a higher loop order. The location of the conformal window in purely six dimensions was found to be between $N_f = 16$ and 17 similar to four dimensional QCD, [54]. It would be interesting to see what effect the three loop corrections would have on this critical N_f value. There is also the potential to look at other higher dimensional gauge theories. In recent years an eight dimensional extension of QCD was examined, [70], as well as QED in six and eight dimensions, [54, 69]. In Part I we speculated that a universality class can be looked at from an alternative point of view. Instead of having a tower of separate theories in different dimensions, connected via the Wilson-Fisher fixed point, we could instead have one single d -dimensional universal theory. All potential interactions between the fields in the theory exist in d -dimensions, with only certain couplings becoming relevant

in a fixed dimension. We could therefore write a Lagrangian in a fixed dimension that would only contain relevant interactions. The universal interaction of the theory will continue to be relevant in d -dimensions and therefore will appear in every fixed dimension Lagrangian of the universality class and drive the dynamics. Recall in Chapter 3 this universal interaction was $\sigma\phi^i\phi^i$. In future work it may therefore be possible to construct a d -dimensional theory with gauge symmetry $SU(3) \times SU(2) \times U(1)$, from which the Standard Model emerges in four dimensions. If one could find a non-trivial fixed point of the Standard Model it may then possibly be part of some d -dimensional universal theory.

In Chapter 5 we constructed a new set of universality classes with a ϕ^4 interaction. However instead of constructing a Lagrangian using the dimensionality of the fields based on the kinetic terms, we instead started from a critical point perspective where the interaction term informs the kinetic term. This produced an infinite number of higher derivative universality classes. While free field higher derivative kinetic terms have been investigated in [234–236], for instance, we now had the opportunity to study interacting cases. We focused our attention on the $n = 2$ tower where n relates or classifies powers of the derivatives in the matter field kinetic term. As well as opening up higher derivative kinetic term Lagrangians, setting $n = 2$ also increased the critical dimension in which the Lagrangian is renormalizable. We studied the UV completion of the $n = 2$ universality class, calculating RG functions for each theory in the tower to as high an order as was computationally viable. Moreover we proved that the higher threads of n are accessible via the large N expansion developed in [48–50]. In Chapter 5 we calculated the exponents η_1 , η_2 and χ_1 for $n = 2$. We hope in future work to find the exponents to a higher order to provide further analysis. Additionally we hope to apply these ideas to higher derivative fermionic theories which have yet to be analysed in the same depth perturbatively or in the large N construction.

Techniques presented in Part I for obtaining UV stable fixed points could in future also be applied to ideas beyond the Standard Model, such as asymptotic safety in quantum gravity. As quantum gravity is non-renormalizable in four dimensions, it is not a predictive QFT. Similarly the NL σ M is non-renormalizable in two dimensions, it is however renormalizable through the large N expansion and connected to ϕ^4 theory through the Wilson-Fisher fixed point. One hope is that a similar situation will occur in the theory of gravity with a higher dimensional quantum gravity Lagrangian containing a UV stable fixed point. It is at this fixed point that UV properties of gravity may be studied. As gravity has not yet been tested at very high energies there is ample space for ‘new’ physics to

emerge such as dark matter, dark energy and modifications of general relativity. One advantage of exploring asymptotic safety is that it can be tested in the physical world via cosmology. For example, [336] speculated that although a classical black hole has a temperature that diverges, if we were to look at a black hole with asymptotic safety there should be a maximum temperature. As the majority of research into asymptotic safety has been non-perturbative using methods such as functional Renormalization Group (FRG) used, [78–84], perturbative techniques introduced in Part I may be used for comparison. Another potential avenue for future research is to consider emergent symmetries. A fundamental symmetry is one which exists for the whole spectrum of energy. In contrast an emergent symmetry only manifests in specific sectors such as at fixed points, [337]. Emergent symmetries can be used to explore deep questions concerning the microscopic structure of the space-time and its constituents. In Chapter 4 an emergent symmetry appeared at $N = 2$ for the AU styled fixed point with the anomalous dimensions of the σ and T^{ab} fields found to be equal at that fixed point.

In Part II of this thesis we focused on the computation of another type of fixed point, the Banks-Zaks fixed point of QCD in four dimensions. This fixed point is IR stable and although QCD is a high energy QFT, if the coupling is small its value can be perturbatively estimated. Similarly critical exponents corresponding to this fixed point can also be perturbatively evaluated. As critical exponents are physical their value should be independent of the renormalization scheme used. However as perturbation theory must be truncated at some order this does not happen in practice. We extended the work of [97] by calculating the value of the Banks-Zaks fixed point and critical exponents in a variety of schemes, in particular we computed exponent associated with the quark mass anomalous dimension. The main motivation was to understand where in the conformal window scheme dependence becomes most apparent. We analysed the conformal window for a variety of colour groups and representations to understand where the true value of the conformal window lies in perturbation theory. Additionally the results for different representations, such as the two-indexed symmetric and anti-symmetric representations, may be used for problems in BSM physics such as technicolor. In Chapter 7 we calculated in the modified minimal subtraction ($\overline{\text{MS}}$), minimal momentum subtraction (mMOM) and momentum subtraction (MOM). Chapter 8 used the interpolating momentum subtraction (iMOM) schemes which depended on some interpolating parameter. All critical exponents were computed in the Landau gauge for all schemes, additionally the maximal abelian gauge (MAG) was used for the iMOM schemes as the RG functions were already available, [102,328]. Along with analysing the conformal window the main motivation

was to find which, if any, scheme had the best convergence at a particular loop order.

Overall scheme dependence seemed to disappear for values of N_f near the upper end of the conformal window for various groups and representations. This was not a surprising result as this is where perturbation theory is most reliable. We were also able to compare our result with non-perturbative methods, in particular with recent lattice estimates. In Chapter 7 we found that in the fundamental representation for $SU(3)$ at $N_f = 12$ the value for the quark mass anomalous dimension appeared to be converging slowly towards recent lattice values measured, [296,297]. Significantly, the MOMq scheme seemed to converge better to the lattice value at three loops than the $\overline{\text{MS}}$ value at four loops. Therefore a possible avenue for future research would be to extend the calculation in the MOM and iMOM schemes to four loops. However it is worth acknowledging that $N_f = 12$ is at the boundary of where perturbation theory loses reliability. Another logical extension of our work in Part II is to examine if scheme independence can be established beyond numerical evidence. In fact this has been achieved recently since publication of our results, [1,4], using a scheme independent perturbative expansion. The expansion parameter involves only the number of quark flavours and the point at which asymptotic freedom is lost. Critical exponents have been consistently calculated in a scheme independent way using this expansion in a variety of schemes including QCD with $SU(2)$, $SU(3)$ and general $SU(N_c)$, [106,107,114]. Additionally this scheme independent expansion was used for general asymptotically free vectorial gauge theories, [108–111] and chiral theories, [112]. Values for the critical exponents found using this expansion were favourably compared with lattice estimated and were matched against known supersymmetric QCD (SQCD) results.

Master Integrals for Scalar Calculations

We state here the explicit values of the master integrals used in both the ten dimensional $O(N)$ calculation of Chapter 3 and the six dimensional $O(N) \times O(m)$ Landau-Ginzburg-Wilson calculation of Chapter 4. We begin by looking at the 2-point master integrals used in both calculations. The 2-point master integrals in ten dimensions are required to two loops, while three loop results are needed in six dimensions. To begin we state the one loop 2-point master integrals in four, six, eight and ten dimensions. As a reminder the notation here is $\mathcal{I}_{ij}(\alpha_1, \dots, \alpha_n)$ where i signifies the number of external propagators and j denotes the loop order. The values $\alpha_1, \dots, \alpha_n$ give the power on each propagator of the Feynman integral. The dimension the integral has been computed in is given in the superscript. All integrals are assumed to be at the completely symmetric point unless otherwise stated. All of the one loop master integrals are calculated by hand as they are straightforward to construct directly by expanding products of Γ -functions. We have

$$\begin{aligned}
 \mathcal{I}_{21}^{(d=4)}(1, 1) &= \left[\frac{1}{\epsilon} + 2 + \left(-\frac{\pi^2}{12} + 4 \right) \epsilon + \left(-\frac{7}{3} \zeta_3 - \frac{\pi^2}{6} + 8 \right) \epsilon^2 \right. \\
 &\quad \left. + \left(-\frac{14}{3} \zeta_3 + 16 - \frac{\pi^2}{3} - \frac{47\pi^4}{1440} \right) \epsilon^3 + O(\epsilon^4) \right] \frac{1}{(4\pi)^2}, \\
 \mathcal{I}_{21}^{(d=6)}(1, 1) &= \left[-\frac{1}{6\epsilon} - \frac{4}{9} + \left(\frac{\pi^2}{72} - \frac{26}{27} \right) \epsilon + \left(-\frac{160}{81} + \frac{7}{18} \zeta_3 + \frac{\pi^2}{27} \right) \epsilon^2 \right. \\
 &\quad \left. + \left(\frac{28}{27} \zeta_3 + \frac{13\pi^2}{162} + \frac{47\pi^4}{8640} - \frac{968}{243} \right) \epsilon^3 + O(\epsilon^4) \right] \frac{(-\mu^2)}{(4\pi)^3}, \\
 \mathcal{I}_{21}^{(d=8)}(1, 1) &= \left[\frac{1}{60\epsilon} + \frac{23}{450} + \left(-\frac{\pi^2}{720} + \frac{394}{3375} \right) \epsilon \right.
 \end{aligned}$$

$$\begin{aligned}
 & + \left(\frac{12364}{50625} - \frac{23\pi^2}{5400} - \frac{7}{180}\zeta_3 \right) \epsilon^2 \\
 & + \left(-\frac{161}{1350}\zeta_3 + \frac{376684}{759375} - \frac{197\pi^2}{20250} - \frac{47\pi^4}{86400} \right) \epsilon^3 \\
 & + O(\epsilon^4) \left] \frac{(-\mu^2)^2}{(4\pi)^4} , \\
 \mathcal{I}_{21}^{(d=10)}(1, 1) = & \left[-\frac{1}{840\epsilon} - \frac{44}{11025} + \left(\frac{\pi^2}{10080} - \frac{10973}{1157625} \right) \epsilon \right. \\
 & + \left(-\frac{2449616}{121550625} + \frac{11\pi^2}{33075} + \frac{\zeta_3}{360} \right) \epsilon^2 \\
 & + \left(\frac{44}{4725}\zeta_3 - \frac{525697622}{12762815625} + \frac{10973\pi^2}{13891500} + \frac{47\pi^4}{1209600} \right) \epsilon^3 \\
 & \left. + O(\epsilon^4) \right] \frac{(-\mu^2)^3}{(4\pi)^3} . \tag{A.0.1}
 \end{aligned}$$

All integrals have been computed at the completely symmetric point so that $p^2 = -\mu^2$ where μ is the parameter introduced during dimensional regularisation. The 2-point master integrals at two loops are given below in four, six, eight and ten dimensions. Once again these can be easily computed by hand. There are two different master integrals at two loops, both illustrated in figure . The notation $(\mathcal{I}_{21}(1, 1))^2$ and $\mathcal{I}_{22}(1, 1, 0, 0, 1)$ is used. For the first master integral we have

$$\begin{aligned}
 (\mathcal{I}_{21}^{(d=4)}(1, 1))^2 & = \left[\frac{1}{\epsilon^2} + \frac{4}{\epsilon} - \frac{\pi^2}{6} + 12 + \left(-\frac{14}{3}\zeta_3 - \frac{2\pi^2}{3} + 32 \right) \epsilon \right. \\
 & \left. + \left(-\frac{56}{3}\zeta_3 + 80 - 2\pi^2 - \frac{7\pi^4}{120} \right) \epsilon^2 + O(\epsilon^3) \right] \frac{1}{(4\pi)^4} , \\
 (\mathcal{I}_{21}^{(d=6)}(1, 1))^2 & = \left[\frac{1}{36\epsilon^2} + \frac{4}{27\epsilon} - \frac{\pi^2}{216} + \frac{14}{27} + \left(\frac{368}{243} - \frac{7}{54}\zeta_3 - \frac{2\pi^2}{81} \right) \epsilon \right. \\
 & \left. + \left(-\frac{56}{81}\zeta_3 - \frac{7\pi^2}{81} - \frac{7\pi^4}{4320} + \frac{2924}{729} \right) \epsilon^2 + O(\epsilon^3) \right] \frac{(-\mu^2)^2}{(4\pi)^6} , \\
 (\mathcal{I}_{21}^{(d=8)}(1, 1))^2 & = \left[\frac{1}{3600\epsilon^2} + \frac{23}{13500\epsilon} - \frac{\pi^2}{21600} + \frac{439}{67500} \right. \\
 & + \left(\frac{15244}{759375} - \frac{7}{5400}\zeta_3 - \frac{23\pi^2}{81000} \right) \epsilon \\
 & + \left(-\frac{322}{40500}\zeta_3 + \frac{25118}{455625} - \frac{439\pi^2}{405000} - \frac{7\pi^4}{432000} \right) \epsilon^2 \\
 & \left. + O(\epsilon^3) \right] \frac{(-\mu^2)^4}{(4\pi)^8} , \\
 (\mathcal{I}_{21}^{(d=10)}(1, 1))^2 & = \left[\frac{1}{705600\epsilon^2} + \frac{11}{1157625\epsilon} - \frac{\pi^2}{4233600} + \frac{6239}{162067500} \right. \\
 & \left. + \left(\frac{1578028}{12762815625} - \frac{1}{151200}\zeta_3 - \frac{11\pi^2}{6945750} \right) \epsilon \right.
 \end{aligned}$$

$$\begin{aligned}
 & + \left(-\frac{22}{496125}\zeta_3 + \frac{186958937}{536038256250} - \frac{6239\pi^2}{972405000} \right. \\
 & \quad \left. - \frac{\pi^4}{12096000} \right) \epsilon^2 + O(\epsilon^3) \Big] \frac{(-\mu^2)^6}{(4\pi)^{10}} \quad (\text{A.0.2})
 \end{aligned}$$

and for the second master integral we find

$$\begin{aligned}
 \mathcal{I}_{22}^{(d=4)}(1, 1, 0, 0, 1) &= \left[-\frac{1}{4\epsilon} - \frac{13}{8} + \left(\frac{\pi^2}{24} - \frac{115}{16} \right) \epsilon \right. \\
 & \quad \left. + \left(-\frac{865}{32} + \frac{8}{3}\zeta_3 + \frac{13\pi^2}{48} \right) \epsilon^2 + O(\epsilon^3) \right] - \mu^2 \pi^4, \\
 \mathcal{I}_{22}^{(d=6)}(1, 1, 0, 0, 1) &= \left[-\frac{1}{1440\epsilon} + \frac{451}{86400} + \left(\frac{\pi^2}{8640} - \frac{129811}{5184000} \right) \epsilon \right. \\
 & \quad \left. + \left(-\frac{30725071}{311040000} + \frac{\zeta_3}{135} + \frac{451\pi^2}{518400} \right) \epsilon^2 \right. \\
 & \quad \left. + O(\epsilon^3) \right] (-\mu^2)^3 \pi^6, \\
 \mathcal{I}_{22}^{(d=8)}(1, 1, 0, 0, 1) &= \left[-\frac{1}{1209600\epsilon} - \frac{1381}{203212800} \right. \\
 & \quad \left. + \left(\frac{\pi^2}{7257600} - \frac{29431831}{853493760000} \right) \epsilon \right. \\
 & \quad \left. + \left(-\frac{20213631169}{143386951680000} + \frac{\zeta_3}{113400} + \frac{1381\pi^2}{1219276800} \right) \epsilon^2 \right. \\
 & \quad \left. + O(\epsilon^3) \right] (-\mu^2)^5 \pi^8, \\
 \mathcal{I}_{22}^{(d=10)}(1, 1, 0, 0, 1) &= \left[-\frac{1}{1862784000\epsilon} - \frac{80807}{17212124160000} \right. \\
 & \quad \left. + \left(\frac{\pi^2}{11176704000} - \frac{789462991}{31808005447680000} \right) \epsilon \right. \\
 & \quad \left. + \left(-\frac{30637637417407}{293905970336563200000} + \frac{\zeta_3}{174636000} \right. \right. \\
 & \quad \left. \left. + \frac{80807\pi^2}{103272744960000} \right) \epsilon^2 + O(\epsilon^3) \right] (-\mu^2)^7 \pi^{10}. \quad (\text{A.0.3})
 \end{aligned}$$

Finally the 2-point master integrals to three loops are stated in four and six dimensions. We calculate only to six dimensions here as the three loops results are required for the $O(N) \times O(m)$ Landau-Ginzburg-Wilson calculation of Chapter 4 only. There are six three loop 2-point master integrals, the non-planar master integral is illustrated in figure and the other five are depicted in figure 4.18. The notation used here is $\mathcal{I}_{23l}(\alpha, \beta, \gamma, \rho, \delta, \theta, \lambda, \tau)$ for the five planar master integrals and $\mathcal{I}_{23n}(\alpha, \beta, \gamma, \rho, \delta, \theta, \lambda, \tau)$ for the non-planar master integral. Four of these master integrals can be computed by hand, we state these results in four and six

dimensions first. We have

$$\begin{aligned}
 \mathcal{I}_{23l}^{(d=4)}(0, 1, 1, 0, 0, 0, 1, 1) &= \left[\frac{1}{36\epsilon} + \frac{71}{216} + \left(-\frac{\pi^2}{144} + \frac{3115}{1296} \right) \epsilon \right. \\
 &\quad \left. + \left(\frac{109403}{7776} - \frac{29}{36} \zeta_3 - \frac{71\pi^2}{864} \right) \epsilon^2 + O(\epsilon^3) \right] (-\mu^2)^2, \\
 \mathcal{I}_{23l}^{(d=6)}(0, 1, 1, 0, 0, 0, 1, 1) &= \left[-\frac{1}{1814400\epsilon} - \frac{617}{84672000} \right. \\
 &\quad \left. + \left(\frac{\pi^2}{7257600} - \frac{18360367}{320060160000} \right) \epsilon \right. \\
 &\quad \left. + \left(-\frac{3163717187}{8961684480000} + \frac{29}{1814400} \zeta_3 \right. \right. \\
 &\quad \left. \left. + \frac{617\pi^2}{338688000} \right) \epsilon^2 + O(\epsilon^3) \right] (-\mu^2)^5, \\
 \mathcal{I}_{23l}^{(d=4)}(0, 1, 1, 1, 1, 0, 1, 0) &= \left[-\frac{1}{4\epsilon^2} - \frac{17}{8\epsilon} - \frac{183}{16} + \frac{\pi^2}{16} \right. \\
 &\quad \left. + \left(-\frac{1597}{32} + \frac{17\pi^2}{32} + \frac{13}{4} \zeta_3 \right) \epsilon \right. \\
 &\quad \left. + \left(-\frac{12359}{64} + \frac{221}{8} \zeta_3 + \frac{183\pi^2}{64} + \frac{17\pi^4}{384} \right) \epsilon^2 \right. \\
 &\quad \left. + O(\epsilon^3) \right] \frac{1}{(-\mu^2)^2}, \\
 \mathcal{I}_{23l}^{(d=6)}(0, 1, 1, 1, 1, 0, 1, 0) &= \left[\frac{1}{8640\epsilon^2} + \frac{611}{518400\epsilon} + \frac{74257}{10368000} - \frac{\pi^2}{34560} \right. \\
 &\quad \left. + \left(\frac{63435631}{1866240000} - \frac{611\pi^2}{2073600} - \frac{13}{8640} \zeta_3 \right) \epsilon \right. \\
 &\quad \left. + \left(\frac{15631687091}{111974400000} - \frac{7943}{518400} \zeta_3 - \frac{74257\pi^2}{41472000} \right. \right. \\
 &\quad \left. \left. - \frac{17\pi^4}{829440} \right) \epsilon^2 + O(\epsilon^3) \right] \frac{1}{(-\mu^2)^5}, \\
 \mathcal{I}_{23l}^{(d=4)}(0, 1, 0, 1, 1, 0, 1, 1) &= \left[-\frac{1}{576\epsilon} - \frac{71}{2304} + \left(\frac{\pi^2}{1728} - \frac{26815}{82944} \right) \epsilon \right. \\
 &\quad \left. + \left(\frac{23\zeta_3}{216} + \frac{71\pi^2}{6912} - \frac{872675}{331776} \right) \epsilon^2 + O(\epsilon^3) \right] (-\mu^2)^5, \\
 \mathcal{I}_{23l}^{(d=6)}(0, 1, 0, 1, 1, 0, 1, 1) &= \left[\frac{1}{19440\epsilon^2} + \frac{167}{291600\epsilon} - \frac{\pi^2}{77760} + \frac{8477}{2187000} \right. \\
 &\quad \left. + \left(-\frac{167\pi^2}{1166400} - \frac{23}{19440} \zeta_3 + \frac{114329}{5467500} \right) \epsilon \right. \\
 &\quad \left. + \left(\frac{1363033}{13668750} - \frac{8477\pi^2}{8748000} - \frac{11\pi^4}{622080} \right. \right. \\
 &\quad \left. \left. - \frac{3841}{291600} \zeta_3 \right) \epsilon^2 + O(\epsilon^3) \right] (-\mu^2)^4,
 \end{aligned}$$

$$\begin{aligned}
 \mathcal{I}_{23l}^{(d=4)}(1, 1, 1, 1, 1, 1, 0, 0) &= \left[\frac{1}{\epsilon^3} + \frac{6}{\epsilon^2} + \left(-\frac{\pi^2}{4} + 24 \right) \frac{1}{\epsilon} + 80 - \frac{3\pi^2}{2} - 7\zeta_3 \right. \\
 &+ \left(-42\zeta_3 - \frac{37\pi^4}{480} - 6\pi^2 + 240 \right) \epsilon \\
 &+ \left(\frac{7\pi^2}{4}\zeta_3 - 168\zeta_3 + 672 - \frac{93}{5}\zeta_5 - \frac{37\pi^4}{80} \right. \\
 &\quad \left. \left. - 20\pi^2 \right) \epsilon^2 + O(\epsilon^3) \right], \\
 \mathcal{I}_{23l}^{(d=6)}(1, 1, 1, 1, 1, 1, 0, 0) &= \left[-\frac{1}{216\epsilon^3} - \frac{1}{27\epsilon^2} + \left(\frac{\pi^2}{864} - \frac{29}{162} \right) \frac{1}{\epsilon} \right. \\
 &+ \frac{\pi^2}{108} + \frac{7}{216}\zeta_3 - \frac{496}{729} \\
 &+ \left(\frac{7}{27}\zeta_3 - \frac{1636}{729} + \frac{37\pi^4}{103680} + \frac{29\pi^2}{648} \right) \epsilon \\
 &+ \left(-\frac{7\pi^2}{864}\zeta_3 + \frac{203}{162}\zeta_3 + \frac{31}{360}\zeta_5 + \frac{37\pi^4}{12960} + \frac{124\pi^2}{729} \right. \\
 &\quad \left. \left. - \frac{14752}{2187} \right) \epsilon^2 + O(\epsilon^3) \right] (-\mu^2)^3. \quad (\text{A.0.4})
 \end{aligned}$$

The final two three loop 2-point master integrals cannot be computed by hand. Instead we take known four dimensional results found in [223] and lift to six dimensions using the Tarasov method. We find

$$\begin{aligned}
 \mathcal{I}_{23l}^{(d=6)}(1, 1, 1, 1, 0, 0, 1, 1) &= \left[\frac{1}{1296\epsilon^3} + \frac{103}{15552\epsilon^2} + \left(-\frac{\pi^2}{5184} + \frac{30161}{933120} \right) \frac{1}{\epsilon} \right. \\
 &+ \frac{7\zeta_3}{1296} - \frac{103\pi^2}{62208} + \frac{6057823}{55987200} \\
 &+ \left(\frac{680542229}{3359232000} - \frac{30161\pi^2}{3732480} + \frac{721\zeta_3}{15552} + \frac{25\zeta_4}{2304} \right) \epsilon \\
 &+ \left(-\frac{94706404133}{201553920000} - \frac{7\pi^2\zeta_3}{5184} - \frac{6057823\pi^2}{223948800} \right. \\
 &\quad \left. + \frac{296591\zeta_3}{933120} + \frac{2575\zeta_4}{27648} + \frac{599\zeta_5}{2160} \right) \epsilon^2 \\
 &\quad \left. + O(\epsilon^3) \right] (-\mu^2)^3, \\
 \mathcal{I}_{23n}^{(d=6)}(1, 1, 1, 1, 1, 1, 1, 1) &= \left[-\frac{1}{36\epsilon^2} + \left(-\frac{23}{72} + \frac{\zeta_3}{18} \right) \frac{1}{\epsilon} \right. \\
 &- \frac{2683}{1296} + \frac{\zeta_4}{12} + \frac{\zeta_3}{2} + \frac{\pi^2}{144} \\
 &+ \left(-\frac{2803}{288} - \frac{4\zeta_5}{9} + \frac{3\zeta_4}{4} + \frac{875\zeta_3}{324} + \frac{23\pi^2}{288} \right. \\
 &\quad \left. \left. - \frac{\pi^2\zeta_3}{72} \right) \epsilon \right]
 \end{aligned}$$

$$\begin{aligned}
 & + \left(-\frac{1652863}{46656} - \frac{47\zeta_3}{32} - \frac{101\zeta_5}{9} + \frac{6829\zeta_4}{1728} \right. \\
 & \quad \left. + \frac{7163\zeta_3}{648} + \frac{7\zeta_3^2}{18} + \frac{2683\pi^2}{5184} - \frac{\pi^2\zeta_3}{8} \right) \epsilon^2 \\
 & + O(\epsilon^3) \Big] (-\mu^2). \tag{A.0.5}
 \end{aligned}$$

There is only one master integral for the 3-point Green's function which is required in the ten dimensional $O(N)$ scalar calculation. We therefore only need the 3-point function to one loop order. We do however require both the master integrals in the completely symmetric momentum configuration and off-shell configuration. The symmetric results will be stated first. The four dimensional master integral was calculated in [194] and is stated below using the notation of [194]. We have

$$\begin{aligned}
 \mathcal{I}_{31}^{(d=4)}(1, 1, 1) &= \frac{1}{\mu^2} \left[\left(\frac{2}{3}\pi \right)^2 - \frac{2}{3}\Psi' \left(\frac{1}{3} \right) \right. \\
 & \quad \left. + \left(12s_3 \left(\frac{\pi}{6} \right) - \frac{35}{108} \frac{\pi^3}{\sqrt{3}} - \frac{\log^2(3)\pi}{4\sqrt{3}} \right) \epsilon + O(\epsilon^2) \right] \tag{A.0.6}
 \end{aligned}$$

where $s_n(z)$ was defined in equation (3.24). The Tarasov method is used to find the 3-point one loop master integral in dimensions six to ten which are

$$\begin{aligned}
 \mathcal{I}_{31}^{(d=6)}(1, 1, 1) &= \left[\frac{1}{2\epsilon} + \frac{3}{2} + \frac{4\pi^2}{27} - \frac{2}{9}\Psi' \left(\frac{1}{3} \right) \right. \\
 & \quad + \left(\frac{7}{2} + \frac{23\pi^2}{216} + 4s_3 \left(\frac{\pi}{6} \right) - \frac{2}{9}\Psi' \left(\frac{1}{3} \right) - \frac{35}{972}\sqrt{3}\pi^3 \right. \\
 & \quad \left. \left. - \frac{1}{36}\sqrt{3}\ln(3)^2\pi \right) \epsilon \right. \\
 & \quad + \left(\frac{15}{2} + \frac{1}{2}s_3 \left(\frac{1}{2} \right) - \frac{7}{6}\zeta_3 + \frac{5\pi^2}{216} + 4s_3 \left(\frac{\pi}{6} \right) - \frac{2}{9}\Psi' \left(\frac{1}{3} \right) \right. \\
 & \quad \left. \left. - \frac{35}{972}\sqrt{3}\pi^3 - \frac{1}{36}\sqrt{3}\ln(3)^2\pi \right) \epsilon^2 + O(\epsilon^3) \right], \\
 \mathcal{I}_{31}^{(d=8)}(1, 1, 1) &= \left[\frac{1}{8\epsilon} + \frac{61}{144} + \frac{2\pi^2}{81} - \frac{1}{27}\Psi' \left(\frac{1}{3} \right) \right. \\
 & \quad + \left(\frac{895}{864} + \frac{23\pi^2}{864} + \frac{2}{3}s_3 \left(\frac{\pi}{6} \right) - \frac{1}{18}\Psi' \left(\frac{1}{3} \right) - \frac{32}{5832}\sqrt{3}\pi^3 \right. \\
 & \quad \left. \left. - \frac{1}{216}\sqrt{3}\ln(3)^2\pi \right) \epsilon + O(\epsilon^2) \right] \mu^2, \\
 \mathcal{I}_{31}^{(d=10)}(1, 1, 1) &= \left[-\frac{1}{56\epsilon} - \frac{2995}{42336} - \frac{\pi^2}{243} + \frac{1}{162}\Psi' \left(\frac{1}{3} \right) \right. \\
 & \quad \left. + \left(-\frac{267\pi^2}{54432} - \frac{1}{9}s_3 \left(\frac{\pi}{6} \right) + \frac{1}{81}\Psi' \left(\frac{1}{3} \right) + \frac{35}{34992}\sqrt{3}\pi^3 \right) \right.
 \end{aligned}$$

$$\begin{aligned}
 & + \frac{1}{1296} \sqrt{3} \ln(3)^2 \pi - \frac{1883120973}{100000000000} \epsilon \\
 & + O(\epsilon^2) \Big] \mu^4 . \tag{A.0.7}
 \end{aligned}$$

The 3-point one loop master integral in the off-shell configuration was illustrated in figure 3.20 and has three independent external momenta and $p + q + r = 0$. The four dimensional result was given in [197] and we state it here for completeness. The notation for the 3-point master integral at one loop in an off-shell configuration is $\mathcal{I}_{31}^o(1, 1, 1)$. We have

$$\mathcal{I}_{31}^{o(d=4)} = \frac{i\pi^2}{p_3^2} \phi_1(x, y) \tag{A.0.8}$$

where the function $\phi_1(x, y)$ can be written in terms of dilogarithms

$$\begin{aligned}
 \phi_1(x, y) = \frac{1}{\lambda} \Big[& 2\text{Li}_2(-\rho x) + 2\text{Li}_2(-\rho y) + \ln\left(\frac{y}{x}\right) \ln\left(\frac{(1+\rho y)}{(1+\rho x)}\right) \\
 & + \ln(\rho x) \ln(\rho y) + \frac{\pi^2}{3} \Big] \tag{A.0.9}
 \end{aligned}$$

and

$$\lambda(x, y) = \sqrt{(1-x-y)^2 - 4xy} \quad , \quad \rho(x, y) = 2(1-x-y+\lambda)^{-1}$$

with

$$x = \frac{p^2}{r^2} \quad , \quad y = \frac{q^2}{r^2} . \tag{A.0.10}$$

The Tarasov method is used to compute this 3-point master integral in higher dimensions. We state only the leading order terms here as we only require the divergent pieces from the Green's function,

$$\begin{aligned}
 \mathcal{I}_{31}^{o(d=6)}(1, 1, 1) &= \frac{1}{2\epsilon} + O(\epsilon) , \\
 \mathcal{I}_{31}^{o(d=8)}(1, 1, 1) &= \frac{(y+1+x)\mu^2}{24\epsilon} + O(\epsilon) , \\
 \mathcal{I}_{31}^{o(d=10)}(1, 1, 1) &= \frac{((y+1+x)x + y^2 + y + 1)\mu^4}{360\epsilon} \\
 & + \frac{(51x^2 - 25y - 51(y+1)x)x^2 + 51(y^2 + y + 1)(y-1)^2}{5400((y-1)^2 + x^2 - 2(y+1)x)} \\
 & - \frac{(51y^2 - 26y + 51)(y+1)x - 15(y-1-x) \ln(\mu^2 y) y^3}{5400((y-1)^2 + x^2 - 2(y+1)x)} \\
 & + \frac{15(y+1-x) \ln(\mu^2 x) x^3 + 15(y-1+x) \ln(\mu^2) \mu^4}{5400((y-1)^2 + x^2 - 2(y+1)x)} \\
 & + O(\epsilon) . \tag{A.0.11}
 \end{aligned}$$

Finally, the one loop 4-point master integral is known in four dimensions and

we use the Tarasov method to lift this result to higher dimensions. The four dimensional one loop 4-point master integral is, [199, 200],

$$\mathcal{I}_{41}^{(d=4)}(1, 1, 1, 1) = \frac{i\pi^2}{st} \phi_1(x, y) \quad (\text{A.0.12})$$

where for the 4-point function

$$x = \frac{p^2 r^2}{(p+q)^2 (q+r)^2} \quad , \quad y = \frac{q^2 (-p-q-r)^2}{(p+q)^2 (q+r)^2} . \quad (\text{A.0.13})$$

Note p , q and r are the three independent incoming momenta of the 4-point one loop diagram. This diagram is illustrated in figure 3.23. Using the Tarasov method this master integral can be lifted up to six, eight and ten dimensions. We have

$$\begin{aligned} \mathcal{I}_{41}^{(d=6)}(1, 1, 1, 1) &= \frac{-3}{32\mu^2} \left[8\phi_1\left(\frac{3}{4}, \frac{3}{4}\right) - 5\phi_1\left(\frac{9}{16}, \frac{9}{16}\right) \right] + O(\epsilon) , \\ \mathcal{I}_{41}^{(d=8)}(1, 1, 1, 1) &= \frac{1}{6\epsilon} + \left[\frac{5}{18} \left(\frac{11}{5} + \frac{15}{32} \phi_1\left(\frac{9}{16}, \frac{9}{16}\right) - \frac{87}{80} \phi_1\left(\frac{3}{4}, \frac{3}{4}\right) \right. \right. \\ &\quad \left. \left. - \frac{3}{5} \ln(-\mu^2) - \frac{3}{10} \ln(2) + \frac{3}{20} \ln(3) \right] + O(\epsilon) , \\ \mathcal{I}_{41}^{(d=10)}(1, 1, 1, 1) &= \frac{1}{18\epsilon} \mu^2 + \left[-4209\phi_1\left(\frac{3}{4}, \frac{3}{4}\right) - 1500\phi_1\left(\frac{9}{16}, \frac{9}{16}\right) \right. \\ &\quad \left. - 15088 + 1992 \ln(2) - 996 \ln(3) \right. \\ &\quad \left. + 3840 \ln(-\mu^2) \right] \left(\frac{\mu^2}{69120} \right) + O(\epsilon) . \end{aligned} \quad (\text{A.0.14})$$

The finite piece can also be written in terms of the Clausen function $\text{Cl}_2(\theta)$ via [338],

$$\begin{aligned} \phi_1\left(\frac{3}{4}, \frac{3}{4}\right) &= \sqrt{2} \left[2\text{Cl}_2\left(2 \cos^{-1}\left(\frac{1}{\sqrt{3}}\right)\right) + \text{Cl}_2\left(2 \cos^{-1}\left(\frac{1}{3}\right)\right) \right] , \\ \phi_1\left(\frac{9}{16}, \frac{9}{16}\right) &= \frac{4}{\sqrt{5}} \left[2\text{Cl}_2\left(2 \cos^{-1}\left(\frac{2}{3}\right)\right) + \text{Cl}_2\left(2 \cos^{-1}\left(\frac{1}{9}\right)\right) \right] . \end{aligned}$$

Feynman Diagrams for $O(N) \times O(m)$ Landau-Ginzburg-Wilson Theory in Six Dimensions

For completeness and to illustrate the types of interactions present at a higher loop order, we present all 2-point Feynman diagrams in the six dimensional Landau-Ginzburg-Wilson theory to two loops. All diagrams have been generated using QGRAF, [184], and presented using JAXODRAW, [188, 189]. To begin the ϕ^{ia} 2-point functions are displayed in figure B.1. There are 23 such diagrams at two loops.

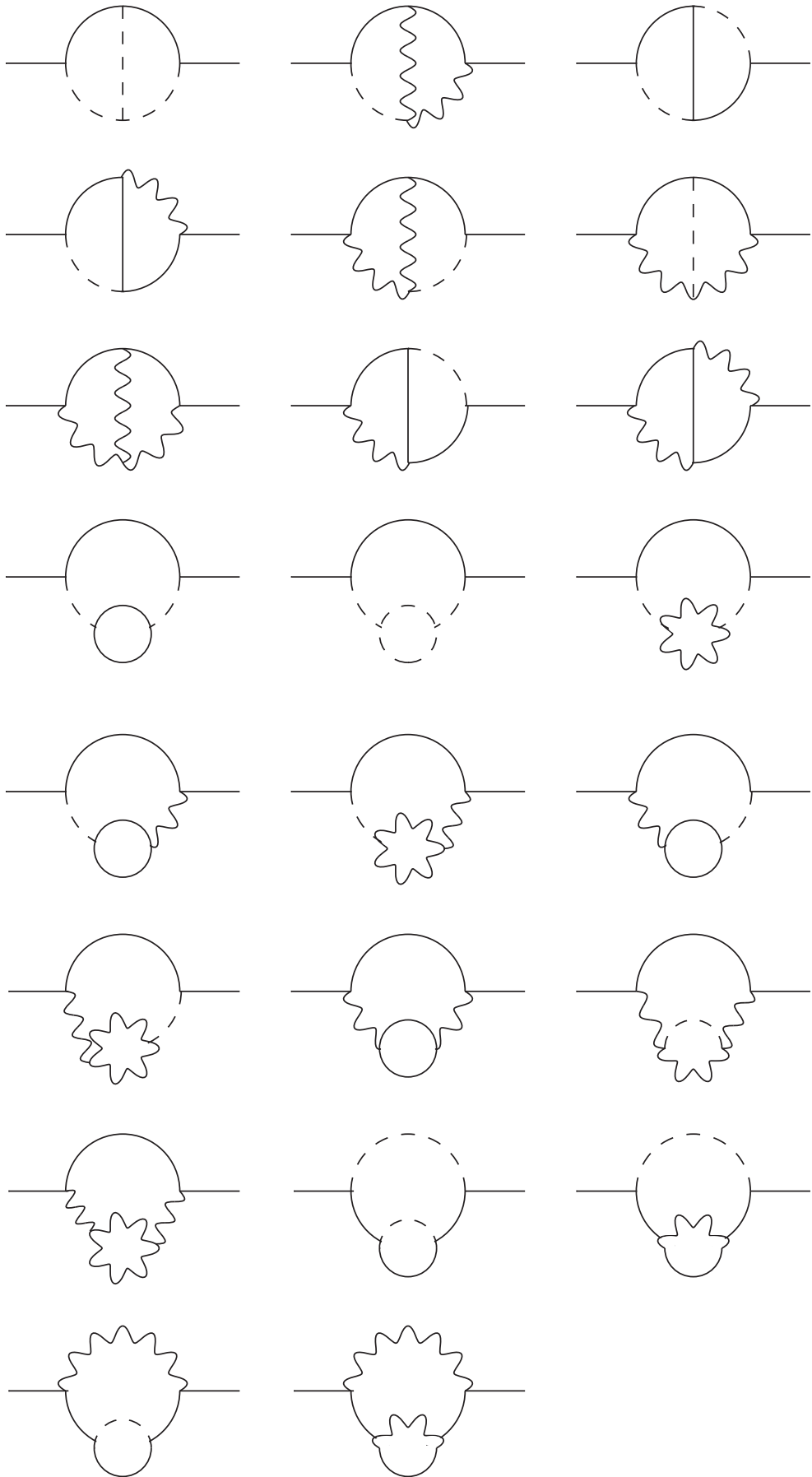


Figure B.1: All Feynman diagrams for the ϕ^{ia} 2-point function at two loops.

Next the 2-point diagrams for the σ 2-point function are illustrated in figure B.2. There are 19 graphs of this type to two loops.

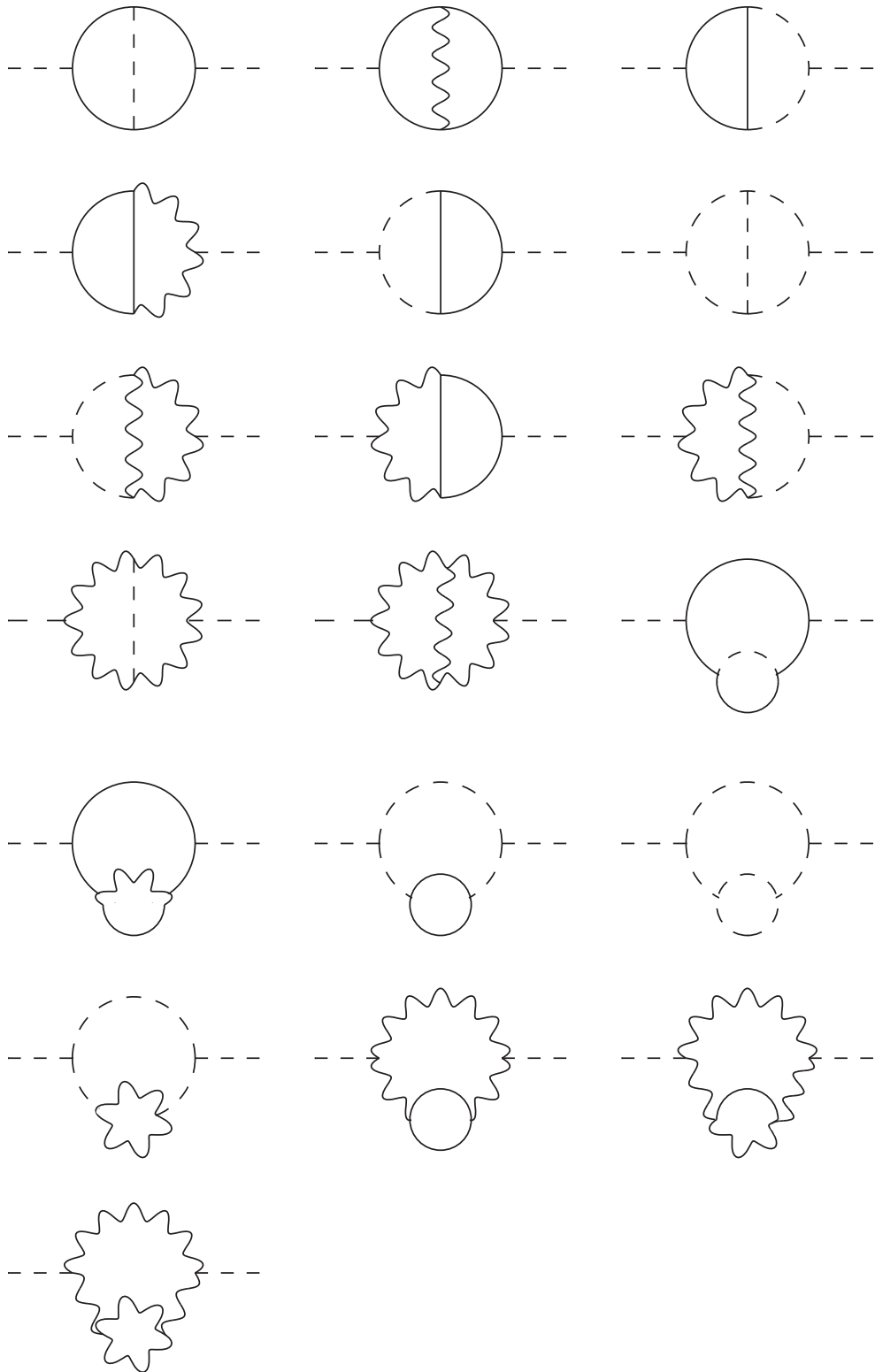
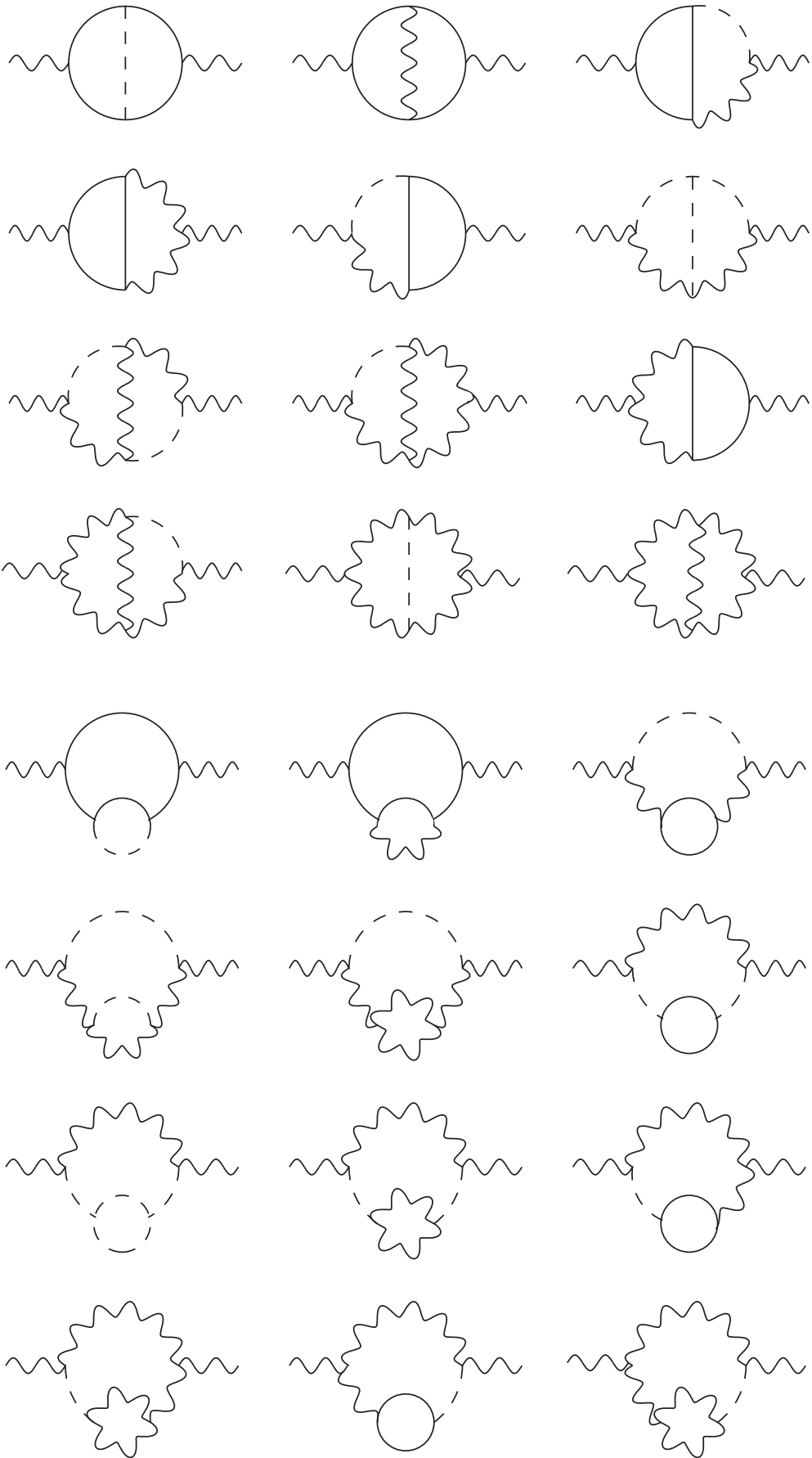


Figure B.2: All Feynman diagrams for the σ 2-point function at two loops.

Finally the T^{ab} 2-point function is depicted in figure B.3 at two loops. There are 27 such graphs.



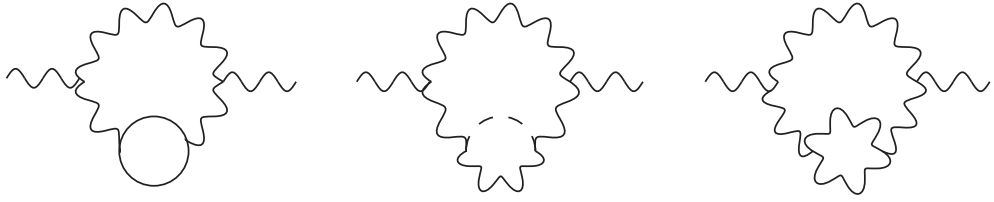


Figure B.3: All Feynman diagrams for the T^{ab} 2-point function at two loops.

Altogether there are 69 2-point Feynman diagrams at two loops for the fields ϕ^{ia} , σ and T^{ab} .

Reduction Relations for the 2-point Function in Landau-Ginzburg-Wilson Theory at Three Loops

Using the REDUZE package two databases can be constructed to reduce the 2-point Green's function of the six dimensional Landau-Ginzburg-Wilson theory at three loops. Two databases are needed at three loops as the 2-point function has three auxiliary topologies at three loops, illustrated in figure A. Two of the topologies will reduce down to the other plus the remaining third topology, known as the 'non-planar' auxiliary topology. Therefore one database is required for integration by parts (IBP) relations for the 'ladder', or alternatively the 'benz' topology, while the second database is required for relations involving the 'non-planar' topology. These databases contain relations developed using IBP which relate diagrams to six master integrals computable by hand or using the Tarasov relation. Five of these master integrals come from reducing the 'ladder' topology. The sixth master integral is the non-planar diagram. Note that the notation $\mathcal{I}_{23l}(\alpha, \beta, \gamma, \rho, \delta, \theta, \lambda, \tau)$ signifies the labelling of the 'Ladder' auxiliary topology which is given in figure 4.17, while $\mathcal{I}_{23n}(\alpha, \beta, \gamma, \rho, \delta, \theta, \lambda, \tau)$ signifies the 'non-planar' diagram. A relation between a higher power integral and its corresponding master integrals is displayed here to illustrate the kind of form these relations take. It is,

$$\mathcal{I}_{23l}(1, 2, 1, 1, 1, 1, 1, 1) =$$

$$\begin{aligned}
 & + \frac{3(-420 + 356d - 99d^2 + 9d^3)}{4(d-5)(d-4)(p^2)^3} \mathcal{I}_{23l}(1, 1, 1, 1, 0, 0, 1, 1) \\
 & + \frac{16(-27 + 15d - 2d^2)}{3(d-5)(d-4)(p^2)^3} \mathcal{I}_{23l}(0, 1, 0, 1, 2, 0, 1, 1) \\
 & + \frac{16(-99 + 49d - 6d^2)}{3(d-5)(d-4)(p^2)^3} \mathcal{I}_{23l}(0, 1, 0, 1, 1, 0, 1, 2) \\
 & - \frac{16(-99 + 15d - 2d^2)}{3(d-5)(d-4)(d-6)(p^2)^3} \mathcal{I}_{23l}(1, 0, 0, 2, 1, 1, 0, 1) \\
 & - \frac{16(-99 + 49d - 6d^2)}{3(d-5)(d-4)(d-6)(p^2)^3} \mathcal{I}_{23l}(1, 0, 0, 1, 1, 1, 0, 2) \\
 & + \frac{3(-340 + 222d - 46d^2 + 3d^3)}{(d-5)(d-4)(d-6)(p^2)^3} \mathcal{I}_{23l}(1, 1, 0, 1, 1, 0, 0, 2) \\
 & - \frac{8(-378 + 291d - 73d^2 + 6d^3)}{3(d-5)(d-4)(d-6)(p^2)^3} \mathcal{I}_{23l}(0, 2, 1, 0, 1, 1, 1, 0) \\
 & + \frac{8(-1386 + 983d - 231d^2 + 18d^3)}{3(d-5)(d-4)(6p^2 - p^2d)(p^2)^3} \mathcal{I}_{23l}(0, 1, 1, 0, 1, 1, 2, 0) \\
 & - \frac{3(-140 + 72d - 9d^2)}{(d-4)(d-6)(p^2)^3} \mathcal{I}_{23l}(0, 1, 1, 1, 1, 0, 2, 0) \\
 & - \frac{\left(\begin{array}{l} -46200 + 48716d + 9d^5 - 312d^4 \\ -19538d^2 + 3665d^3 \end{array} \right)}{2(d-5)^2(d-4)^2(d-3)(3d-10)(p^2)^3} \mathcal{I}_{23l}(1, 0, 0, 1, 0, 0, 1, 3) \\
 & - \frac{\left(\begin{array}{l} -4090080 + 493100d + 297d^5 - 6456d^4 \\ -235154d^2 + 55433d^3 \end{array} \right)}{2(d-5)^2(d-4)^2(d-3)(3d-10)(p^2)^3} \mathcal{I}_{23l}(0, 1, 1, 0, 0, 0, 1, 3) \\
 & + \frac{12(-4158 + 3876d - 12d^4 - 1349d^2 + 208d^3)}{(d-5)^2(d-4)^2(d-3)(p^2)^3} \mathcal{I}_{23l}(0, 1, 0, 0, 1, 1, 0, 3) \\
 & + \frac{12(-882 - 637d - 152d^2 + 12d^3)}{(d-5)^2(d-4)^2(d-3)(p^2)^3} \mathcal{I}_{23l}(0, 0, 0, 1, 1, 1, 3, 0) . \quad (\text{C.0.1})
 \end{aligned}$$

The master integrals contained in this reduction are illustrated in figure C.1.

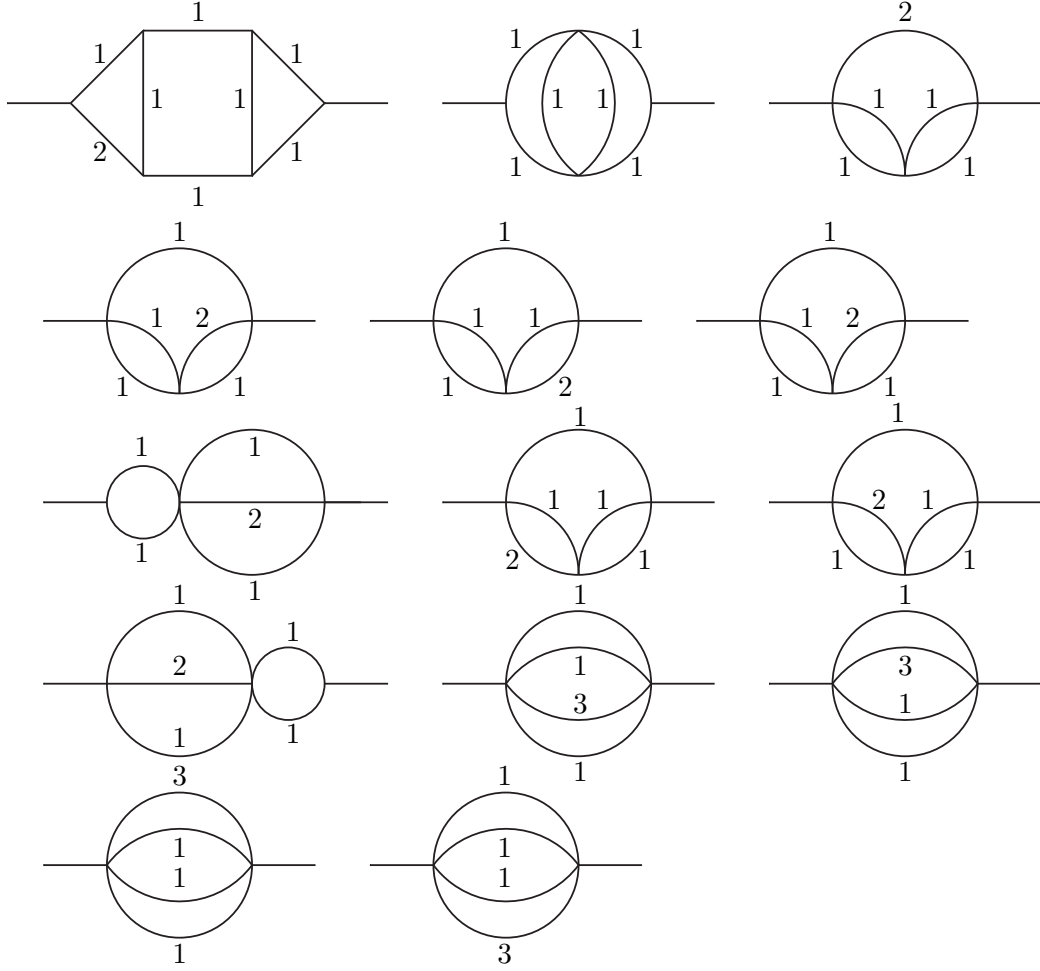


Figure C.1: Feynman diagrams containing in the IBP relation of equation (C.0.1).

Beginning with the top row and working our way down the labelled for the Feynman diagrams in figure C.1 is from left to right:

$$\text{First row: } \mathcal{I}_{23l}(1, 1, 1, 1, 1, 1, 1, 2) , \quad \mathcal{I}_{23l}(1, 1, 1, 1, 0, 0, 1, 1) ,$$

$$\mathcal{I}_{23l}(0, 1, 0, 1, 2, 0, 1, 1) ,$$

$$\text{Second row: } \mathcal{I}_{23l}(0, 1, 0, 1, 1, 0, 1, 2) , \quad \mathcal{I}_{23l}(1, 0, 0, 2, 1, 1, 0, 1) ,$$

$$\mathcal{I}_{23l}(1, 0, 0, 1, 1, 1, 0, 2) ,$$

$$\text{Third row: } \mathcal{I}_{23l}(1, 1, 0, 1, 1, 0, 0, 2) , \quad \mathcal{I}_{23l}(0, 2, 1, 0, 1, 1, 1, 0) ,$$

$$\mathcal{I}_{23l}(0, 1, 1, 0, 1, 1, 2, 0) ,$$

$$\text{Fourth row: } \mathcal{I}_{23l}(0, 1, 1, 1, 1, 0, 2, 0) , \quad \mathcal{I}_{23l}(1, 0, 0, 1, 0, 0, 1, 3) ,$$

$$\mathcal{I}_{23l}(0, 1, 1, 0, 0, 0, 1, 3) ,$$

$$\text{Final row: } \mathcal{I}_{23l}(0, 1, 0, 0, 1, 1, 0, 3) , \quad \mathcal{I}_{23l}(0, 0, 0, 1, 1, 1, 3, 0) .$$

Banks-Zaks Fixed Points and Critical Exponents for $\overline{\text{MS}}$, mMOM and MOMi Renormalization Schemes

Tables containing the results of the Banks-Zaks analysis in the $\overline{\text{MS}}$, mMOM and MOMi renormalization schemes are presented below. The first few tables contain values for the Banks-Zaks fixed point while results for the corresponding critical exponents are contained in the following tables. A variety of colour groups and representations are presented. We calculate to two, three and four loops which are labelled in the subsequent tables. Note that all results presented in Appendix D are in the Landau gauge.

F		$\overline{\text{MS}}$			mMOM		
N_c	N_f	a_2	a_3	a_4	a_2	a_3	a_4
2	6	0.909091	0.130937	0.190588	0.909091	0.100122	0.088677
2	7	0.225352	0.083898	0.096318	0.225352	0.067933	0.062904
2	8	0.100000	0.054773	0.060487	0.100000	0.046821	0.045404
2	9	0.047337	0.033280	0.035339	0.047337	0.030031	0.029984
2	10	0.018349	0.015622	0.015944	0.018349	0.014878	0.014954
3	9	0.416667	0.081803	0.085291	0.416667	0.064438	0.054935
3	10	0.175676	0.060824	0.064860	0.175676	0.049421	0.044230
3	11	0.098214	0.046039	0.049832	0.098214	0.038603	0.036070
3	12	0.060000	0.034607	0.037434	0.060000	0.029962	0.028981
3	13	0.037234	0.025191	0.026853	0.037234	0.022535	0.022329
3	14	0.022124	0.017070	0.017793	0.022124	0.015786	0.015838
3	15	0.011364	0.009818	0.010001	0.011364	0.009383	0.009431
3	16	0.003311	0.003162	0.003170	0.003311	0.003118	0.003121
4	12	0.281690	0.060040	0.060411	0.281690	0.047748	0.040336
4	13	0.147239	0.048027	0.049944	0.147239	0.039016	0.034347
4	14	0.092219	0.038926	0.041445	0.092219	0.032328	0.029529
4	15	0.062291	0.031616	0.034072	0.062291	0.026858	0.025323
4	16	0.043478	0.025488	0.027490	0.043478	0.022159	0.021442
4	17	0.030558	0.020179	0.021580	0.030558	0.017964	0.017724
4	18	0.021136	0.015460	0.016291	0.021136	0.014097	0.014086
4	19	0.013962	0.011175	0.011573	0.013962	0.010440	0.010493
4	20	0.008316	0.007218	0.007350	0.008316	0.006907	0.006943
4	21	0.003758	0.003511	0.003530	0.003758	0.003438	0.003446

Table D.1: Location of the Banks-Zaks fixed points for $\overline{\text{MS}}$ and mMOM renormalization schemes at two, three and four loops.

F		MOMq		MOMggg		MOMh	
N_c	N_f	a_2	a_3	a_2	a_3	a_2	a_3
2	6	0.909091	0.079453	0.909091	0.075345	0.909091	0.100010
2	7	0.225352	0.060047	0.225352	0.051522	0.225352	0.069384
2	8	0.100000	0.044163	0.100000	0.035988	0.100000	0.048379
2	9	0.047337	0.029574	0.047337	0.023848	0.047337	0.031152
2	10	0.018349	0.014999	0.018349	0.012674	0.018349	0.015317
3	9	0.416667	0.051906	0.416667	0.047997	0.416667	0.064858
3	10	0.175676	0.042853	0.175676	0.037161	0.175676	0.050466
3	11	0.098214	0.035202	0.098214	0.029277	0.098214	0.039778
3	12	0.060000	0.028357	0.060000	0.023018	0.060000	0.031047
3	13	0.037234	0.021938	0.037234	0.017681	0.037234	0.023405
3	14	0.022124	0.015687	0.022124	0.012809	0.022124	0.016367
3	15	0.011364	0.009437	0.011364	0.008032	0.011364	0.009655
3	16	0.003311	0.003136	0.003311	0.002914	0.003311	0.003156
4	12	0.281690	0.038650	0.281690	0.035451	0.281690	0.048181
4	13	0.147239	0.033425	0.147239	0.029214	0.147239	0.039802
4	14	0.092219	0.028879	0.092219	0.024372	0.092219	0.033229
4	15	0.062291	0.024786	0.062291	0.020409	0.062291	0.027756
4	16	0.043478	0.020992	0.043478	0.017023	0.043478	0.022982
4	17	0.030558	0.017383	0.030558	0.014013	0.030558	0.018663
4	18	0.021136	0.013876	0.021136	0.011238	0.021136	0.014641
4	19	0.013962	0.010408	0.013962	0.008578	0.013962	0.010810
4	20	0.008316	0.006940	0.008316	0.005922	0.008316	0.007105
4	21	0.003758	0.003461	0.003758	0.003134	0.003758	0.003498

Table D.2: Location of the Banks-Zaks fixed points for MOMq, MOMggg and MOMh renormalization schemes at two and three loops.

F		$\overline{\text{MS}}$			mMOM		
N_c	N_f	ω_2	ω_3	ω_4	ω_2	ω_3	ω_4
2	6	6.060606	1.620106	0.974775	6.060606	1.261453	1.245537
2	7	1.201878	0.728326	0.676986	1.201878	0.615403	0.618233
2	8	0.400000	0.318182	0.299703	0.400000	0.286878	0.289100
2	9	0.126233	0.115100	0.110454	0.126233	0.109360	0.109439
2	10	0.024465	0.023925	0.023541	0.024465	0.023590	0.023507
3	9	4.166667	1.475455	1.464386	4.166667	1.189101	1.165667
3	10	1.522523	0.871775	0.853407	1.522533	0.736141	0.736306
3	11	0.720238	0.516977	0.498035	0.720238	0.454913	0.459085
3	12	0.360000	0.295517	0.282328	0.360000	0.269774	0.272234
3	13	0.173759	0.155581	0.149130	0.173759	0.146681	0.147243
3	14	0.073746	0.069899	0.067812	0.073746	0.067695	0.067572
3	15	0.022727	0.022307	0.021975	0.022727	0.022037	0.021957
3	16	0.002208	0.002203	0.002198	0.002208	0.002200	0.002198
4	12	3.755869	1.430447	1.429308	3.755897	1.165365	1.140669
4	13	1.766871	0.964661	0.954675	1.766861	0.812318	0.809419
4	14	0.983670	0.655163	0.639277	0.983670	0.568776	0.572539
4	15	0.581387	0.440398	0.424261	0.581387	0.393264	0.397364
4	16	0.347826	0.288274	0.275809	0.347826	0.264197	0.266663
4	17	0.203718	0.180219	0.172523	0.203718	0.169115	0.170002
4	18	0.112726	0.104596	0.100807	0.112726	0.100224	0.100263
4	19	0.055846	0.053622	0.052223	0.055846	0.052293	0.052131
4	20	0.022176	0.021789	0.021468	0.022176	0.021539	0.021457
4	21	0.005010	0.004989	0.004965	0.005010	0.004974	0.004964

Table D.3: Critical exponent ω for the Banks-Zaks fixed point for $\overline{\text{MS}}$ and mMOM renormalization schemes at two, three and four loops.

F		MOMq		MOMggg		MOMh	
N_c	N_f	ω_2	ω_3	ω_2	ω_3	ω_2	ω_3
2	6	6.060606	1.013077	6.060606	0.962970	6.060606	1.260113
2	7	1.201878	0.555171	1.201878	0.486742	1.201878	0.626165
2	8	0.400000	0.275290	0.400000	0.236097	0.400000	0.293412
2	9	0.126233	0.108457	0.126233	0.095150	0.126233	0.111475
2	10	0.024465	0.023649	0.024465	0.022125	0.024465	0.023797
3	9	4.166667	0.973459	4.166667	0.904648	4.166667	1.196201
3	10	1.522523	0.652189	1.522533	0.575996	1.522533	0.749100
3	11	0.720238	0.423769	0.720238	0.365393	0.720238	0.465266
3	12	0.360000	0.259872	0.360000	0.223235	0.360000	0.276171
3	13	0.173759	0.144437	0.173759	0.125839	0.173759	0.149791
3	14	0.073746	0.067504	0.073746	0.060674	0.073746	0.068753
3	15	0.022727	0.022074	0.022727	0.020774	0.022727	0.022213
3	16	0.002208	0.002201	0.002208	0.002176	0.002208	0.002203
4	12	3.755869	0.959967	3.755869	0.885870	3.755869	1.174951
4	13	1.766871	0.711138	1.766871	0.631571	1.766871	0.826128
4	14	0.983670	0.519614	0.983670	0.451225	0.983670	0.581177
4	15	0.581387	0.370624	0.581387	0.318564	0.581387	0.402677
4	16	0.347826	0.254787	0.347826	0.219046	0.347826	0.270526
4	17	0.203718	0.165850	0.203718	0.144003	0.203718	0.172852
4	18	0.112726	0.099425	0.112726	0.088003	0.112726	0.102081
4	19	0.055846	0.052229	0.055846	0.047543	0.055846	0.053001
4	20	0.022176	0.021569	0.022176	0.020338	0.022176	0.021706
4	21	0.005010	0.004979	0.005010	0.004872	0.005010	0.004986

Table D.4: Critical exponent ω for the Banks-Zaks fixed point for MOMq, MOMggg and MOMh renormalization schemes at two and three loops.

F		$\overline{\text{MS}}$			mMOM		
N_c	N_f	ρ_2	ρ_3	ρ_4	ρ_2	ρ_3	ρ_4
2	6	33.171488	0.924853	- 4.019013	39.576446	1.034933	0.893430
2	7	2.674073	0.456824	0.032536	3.118429	0.523238	0.455155
2	8	0.751875	0.272074	0.203618	0.849375	0.300337	0.279549
2	9	0.275060	0.160546	0.157402	0.299149	0.168800	0.165956
2	10	0.091049	0.073829	0.074794	0.095005	0.074836	0.075064
3	9	19.768519	1.061659	- 0.143490	23.356481	1.191042	0.979184
3	10	4.189838	0.646806	0.155885	4.882518	0.734781	0.620806
3	11	1.613131	0.439241	0.249686	1.846779	0.492300	0.436592
3	12	0.772800	0.311751	0.253328	0.866400	0.340313	0.317156
3	13	0.404469	0.220154	0.209757	0.442979	0.233293	0.226367
3	14	0.212450	0.146369	0.147421	0.226917	0.151029	0.150241
3	15	0.099690	0.082573	0.083600	0.103736	0.083547	0.083816
3	16	0.027187	0.025833	0.025895	0.027550	0.025868	0.025896
4	12	17.296915	1.107600	0.058357	20.371702	1.243981	1.009616
4	13	5.380895	0.755292	0.192015	6.275170	0.855872	0.712621
4	14	2.445332	0.552297	0.258813	2.817397	0.622351	0.537602
4	15	1.318886	0.420081	0.280672	1.498346	0.466289	0.419073
4	16	0.778444	0.324942	0.268806	0.870599	0.353508	0.329838
4	17	0.480849	0.250606	0.234022	0.528704	0.266804	0.256937
4	18	0.300568	0.188596	0.186947	0.324580	0.196704	0.193870
4	19	0.183246	0.134334	0.136002	0.194211	0.137668	0.137526
4	20	0.102410	0.085397	0.086461	0.106473	0.086356	0.086657
4	21	0.043993	0.040685	0.040877	0.044858	0.040801	0.040884

Table D.5: Quark mass critical exponent at the Banks-Zaks fixed point for $\overline{\text{MS}}$ and mMOM renormalization schemes at two, three and four loops.

F		't Hooft
N_c	N_f	ρ
2	6	4.090909
2	7	1.014085
2	8	0.450000
2	9	0.213018
2	10	0.082569
3	9	3.333333
3	10	1.405405
3	11	0.785714
3	12	0.480000
3	13	0.297872
3	14	0.176991
3	15	0.090909
3	16	0.026490
4	12	3.169014
4	13	1.656442
4	14	1.037464
4	15	0.700779
4	16	0.489130
4	17	0.343774
4	18	0.237781
4	19	0.157068
4	20	0.093555
4	21	0.042273

Table D.6: Quark mass critical exponent at the Banks-Zaks fixed point for the 't Hooft scheme.

F		MOMq		MOMggg		MOMh	
N_c	N_f	ρ_2	ρ_3	ρ_2	ρ_3	ρ_2	ρ_3
2	6	17.262397	0.461381	45.730994	0.861480	13.977991	0.305679
2	7	1.925820	0.346755	4.202074	0.542352	1.724000	0.304515
2	8	0.649692	0.247039	1.201675	0.336642	0.609951	0.234852
2	9	0.262282	0.156674	0.409221	0.189326	0.253377	0.153796
2	10	0.090649	0.073686	0.116219	0.079602	0.089311	0.073373
3	9	11.561746	0.553462	26.804208	0.954324	9.016606	0.375534
3	10	2.978729	0.452897	6.257561	0.701362	2.526293	0.377682
3	11	1.312033	0.364656	2.514774	0.516777	1.170622	0.330763
3	12	0.689329	0.285218	1.204608	0.374024	0.636553	0.270097
3	13	0.383454	0.212345	0.607462	0.259356	0.363130	0.206167
3	14	0.208960	0.144860	0.297076	0.165375	0.201785	0.142818
3	15	0.099806	0.082504	0.125435	0.088262	0.097913	0.082094
3	16	0.027285	0.025840	0.029663	0.026154	0.027124	0.025826
4	12	10.475472	0.586353	23.326276	0.984386	8.082819	0.401265
4	13	3.761930	0.503058	7.835301	0.780943	3.108222	0.406260
4	14	1.906259	0.428513	3.724747	0.622031	1.649824	0.375454
4	15	1.116733	0.360679	2.047092	0.493265	0.999731	0.331200
4	16	0.701301	0.298087	1.203586	0.386035	0.644300	0.281973
4	17	0.453285	0.239729	0.725617	0.294985	0.425128	0.231347
4	18	0.292424	0.184975	0.434301	0.216727	0.278953	0.181016
4	19	0.181893	0.133522	0.248856	0.149155	0.176016	0.131953
4	20	0.102711	0.085353	0.128262	0.091032	0.100626	0.084913
4	21	0.044214	0.040704	0.049797	0.041635	0.043788	0.040652

Table D.7: Quark mass critical exponent at the Banks-Zaks fixed point for MOMq, MOMggg and MOMh renormalization schemes at two and three loops.

F		$\overline{\text{MS}}$	
N_c	N_f	ρ_{53}	ρ_{54}
3	9	- 0.370415	- 0.596381
3	10	0.198718	0.105449
3	11	0.289590	0.266959
3	12	0.262582	0.268132
3	13	0.205572	0.215243
3	14	0.143001	0.148548
3	15	0.082153	0.083692
3	16	0.025828	0.025895

Table D.8: Estimates of quark mass critical exponent at the Banks-Zaks fixed point for the $\overline{\text{MS}}$ renormalization scheme at five loops using the three and four loop critical coupling.

F		$\overline{\text{MS}}$	
N_c	N_f	a_5	ρ_5
3	9	0.068656	0.180468
3	10	0.056886	0.264038
3	11	0.048471	0.276783
3	12	0.042030	0.265626
3	13	0.032315	0.238701
3	14	0.018526	0.154060
3	15	0.010078	0.084340
3	16	0.003171	0.025903

Table D.9: Location of Banks-Zaks critical coupling and quark mass critical exponent for $\overline{\text{MS}}$ at five loops.

G		$\overline{\text{MS}}$			mMOM		
N_c	N_f	a_2	a_3	a_4	a_2	a_3	a_4
2	2	0.050000	0.036525	0.035814	0.050000	0.033778	0.031703
3	2	0.033333	0.024350	0.024537	0.033333	0.022519	0.021491
4	2	0.025000	0.018263	0.018596	0.025000	0.016889	0.016217

Table D.10: Location of the Banks-Zaks fixed points for $\overline{\text{MS}}$ and mMOM renormalization schemes at two, three and four loops for the quarks in the adjoint representation.

G		MOMq		MOMggg		MOMh	
N_c	N_f	a_2	a_3	a_2	a_3	a_2	a_3
2	2	0.050000	0.032037	0.050000	0.026198	0.050000	0.035416
3	2	0.033333	0.021358	0.033333	0.017465	0.033333	0.023611
4	2	0.025000	0.016019	0.025000	0.013099	0.025000	0.017708

Table D.11: Location of the Banks-Zaks fixed points for MOMq, MOMggg and MOMh renormalization schemes at two and three loops for the quarks in the adjoint representation.

G		$\overline{\text{MS}}$			mMOM		
N_c	N_f	ω_2	ω_3	ω_4	ω_2	ω_3	ω_4
2	2	0.200000	0.185475	0.187427	0.200000	0.178949	0.183383
3	2	0.200000	0.185475	0.184637	0.200000	0.178949	0.182466
4	2	0.200000	0.185475	0.183419	0.200000	0.178949	0.182086

Table D.12: Critical exponent ω for the Banks-Zaks fixed point for $\overline{\text{MS}}$ and mMOM renormalization schemes at two, three and four loops for the quarks in the adjoint representation.

G		MOMq		MOMggg		MOMh	
N_c	N_f	ω_2	ω_3	ω_2	ω_3	ω_2	ω_3
2	2	0.200000	0.174187	0.200000	0.154678	0.200000	0.182985
3	2	0.200000	0.174187	0.200000	0.154678	0.200000	0.182985
4	2	0.200000	0.174187	0.200000	0.154678	0.200000	0.182985

Table D.13: Critical exponent ω for the Banks-Zaks fixed point for MOMq, MOMggg and MOMh renormalization schemes at two and three loops for the quarks in the adjoint representation.

G		$\overline{\text{MS}}$			mMOM		
N_c	N_f	ρ_2	ρ_3	ρ_4	ρ_2	ρ_3	ρ_4
2	2	0.820000	0.543233	0.499621	0.885000	0.569034	0.520679
3	2	0.820000	0.543233	0.522652	0.885000	0.569034	0.537795
4	2	0.820000	0.543233	0.531736	0.885000	0.569034	0.544255

Table D.14: Quark mass critical exponent at the Banks-Zaks fixed point for $\overline{\text{MS}}$ and mMOM renormalization schemes at two, three and four loops for the quarks in the adjoint representation.

G		MOMq		MOMggg		MOMh	
N_c	N_f	ρ_2	ρ_3	ρ_2	ρ_3	ρ_2	ρ_3
2	2	0.843280	0.523076	1.119867	0.563241	0.725384	0.493780
3	2	0.843279	0.523076	1.119867	0.563241	0.725384	0.493780
4	2	0.843280	0.523076	1.119867	0.563241	0.725384	0.493780

Table D.15: Quark mass critical exponent at the Banks-Zaks fixed point for MOMq, MOMggg and MOMh renormalization schemes at two and three loops for the quarks in the adjoint representation.

$2S$		$\overline{\text{MS}}$			mMOM		
N_c	N_f	a_2	a_3	a_4	a_2	a_3	a_4
3	2	0.067010	0.039795	0.037400	0.067010	0.036641	0.031345
3	3	0.006757	0.006290	0.006324	0.006757	0.006133	0.006137
4	2	0.076923	0.038610	0.034993	0.076923	0.035879	0.028481
4	3	0.012085	0.010266	0.010429	0.012085	0.009773	0.009706

Table D.16: Location of the Banks-Zaks fixed point for $\overline{\text{MS}}$ and mMOM renormalization schemes at two, three and four loops for quarks in the $2S$ representation.

$2S$		MOMq		MOMggg		MOMh	
N_c	N_f	a_2	a_3	a_2	a_3	a_2	a_3
3	2	0.067010	0.033185	0.067010	0.026936	0.067010	0.038706
3	3	0.006757	0.006043	0.006757	0.005449	0.006757	0.006272
4	2	0.076923	0.031380	0.076923	0.025513	0.076923	0.037977
4	3	0.012085	0.009452	0.012085	0.008038	0.012085	0.010154

Table D.17: Location of the Banks-Zaks fixed point for MOMq, MOMggg and MOMh renormalization schemes at two and three loops for quarks in the $2S$ representation.

$2S$		$\overline{\text{MS}}$			mMOM		
N_c	N_f	ω_2	ω_3	ω_4	ω_2	ω_3	ω_4
3	2	0.580756	0.484962	0.494313	0.580756	0.461475	0.470733
3	3	0.013514	0.013449	0.013385	0.013514	0.013398	0.013391
4	2	1.025641	0.771209	0.784341	1.025641	0.733643	0.730358
4	3	0.064451	0.062991	0.062225	0.064451	0.062094	0.062379

Table D.18: Critical exponent ω for the Banks-Zaks fixed point for $\overline{\text{MS}}$ and mMOM renormalization schemes at two, three and four loops for quarks in the $2S$ representation.

2S		MOMq		MOMggg		MOMh	
N_c	N_f	ω_2	ω_3	ω_2	ω_3	ω_2	ω_3
3	2	0.580756	0.432782	0.580756	0.373054	0.580756	0.477139
3	3	0.013514	0.013363	0.013514	0.013007	0.013514	0.013444
4	2	1.025641	0.666122	1.025641	0.567521	1.025641	0.762733
4	3	0.064451	0.061393	0.064451	0.057224	0.064451	0.062807

Table D.19: Critical exponent ω for the Banks-Zaks fixed point for the MOMq, MOMggg and MOMh renormalization schemes at two and three loops for quarks in the 2S representation.

2S		$\overline{\text{MS}}$			mMOM		
N_c	N_f	ρ_2	ρ_3	ρ_4	ρ_2	ρ_3	ρ_4
3	2	2.442844	1.284021	1.122151	2.694805	1.422422	1.210883
3	3	0.143809	0.132625	0.133158	0.147386	0.133175	0.133159
4	2	4.815089	2.077658	1.787181	5.365385	2.436574	1.949337
4	3	0.380719	0.313071	0.314964	0.399558	0.318680	0.315594

Table D.20: Quark mass critical exponent at the Banks-Zaks fixed point for the $\overline{\text{MS}}$ and mMOM renormalization schemes at two, three and four loops for quarks in the 2S representation.

2S		MOMq		MOMggg		MOMh	
N_c	N_f	ρ_2	ρ_3	ρ_2	ρ_3	ρ_2	ρ_3
3	2	2.440100	1.088873	3.194973	1.123601	1.837734	0.959833
3	3	0.148363	0.133049	0.166564	0.135940	0.142239	0.132247
4	2	4.616444	1.554419	5.894166	1.548531	3.166038	1.294776
4	3	0.399558	0.313149	0.485641	0.326803	0.363762	0.305782

Table D.21: Quark mass critical exponent at the Banks-Zaks fixed point for the MOMq, MOMggg and MOMh renormalization schemes at two and three loops for quarks in the 2S representation.

2A		$\overline{\text{MS}}$			mMOM		
N_c	N_f	a_2	a_3	a_4	a_2	a_3	a_4
4	6	0.172414	0.052865	0.061243	0.172414	0.044308	0.038398
4	7	0.070796	0.034771	0.039931	0.070796	0.029895	0.028047
4	8	0.035714	0.022840	0.025409	0.035714	0.020324	0.020083
4	9	0.017937	0.013814	0.014662	0.017937	0.012777	0.012908
4	10	0.007194	0.006401	0.006518	0.007194	0.006164	0.006212

Table D.22: Location of the Banks-Zaks fixed points for $\overline{\text{MS}}$ and mMOM renormalization schemes at two, three and four loops for quarks in the 2A representation.

2A		MOMq		MOMggg		MOMh	
N_c	N_f	a_2	a_3	a_2	a_3	a_2	a_3
4	6	0.172414	0.036860	0.172414	0.032342	0.172414	0.045374
4	7	0.070796	0.027053	0.070796	0.022389	0.070796	0.031004
4	8	0.035714	0.019325	0.035714	0.015630	0.035714	0.021179
4	9	0.017937	0.012543	0.017937	0.010258	0.017937	0.013285
4	10	0.007194	0.006161	0.007194	0.005338	0.007194	0.006332

Table D.23: Location of the Banks-Zaks fixed points for MOMq, MOMggg and MOMh renormalization schemes at two and three loops for quarks in the 2A representation.

2A		$\overline{\text{MS}}$			mMOM		
N_c	N_f	ω_2	ω_3	ω_4	ω_2	ω_3	ω_4
4	6	2.298851	1.193609	1.109724	2.298851	1.029719	1.022181
4	7	0.755162	0.559626	0.511494	0.755162	0.503114	0.508341
4	8	0.285714	0.248588	0.229893	0.285714	0.232661	0.233704
4	9	0.095665	0.090611	0.086504	0.095665	0.087749	0.087236
4	10	0.019185	0.018951	0.018660	0.019185	0.018791	0.018680

Table D.24: Critical exponent ω for the Banks-Zaks fixed points for $\overline{\text{MS}}$ and mMOM renormalization schemes at two, three and four loops for quarks in the 2A representation.

2A		MOMq		MOMggg		MOMh	
N_c	N_f	ω_2	ω_3	ω_2	ω_3	ω_2	ω_3
4	6	2.298851	0.877863	2.298851	0.781571	2.298851	1.050754
4	7	0.755162	0.466867	0.755162	0.402103	0.755162	0.516585
4	8	0.285714	0.225543	0.285714	0.195358	0.285714	0.238387
4	9	0.095665	0.087014	0.095665	0.078133	0.095665	0.089231
4	10	0.019185	0.018789	0.019185	0.017908	0.019185	0.018909

Table D.25: Critical exponent ω for the Banks-Zaks fixed points for MOMq, MOMggg and MOMh renormalization schemes at two and three loops for quarks in the 2A representation.

2A		$\overline{\text{MS}}$			mMOM		
N_c	N_f	ρ_2	ρ_3	ρ_4	ρ_2	ρ_3	ρ_4
4	6	9.782501	1.381815	0.292995	11.318371	1.566192	1.377240
4	7	2.191767	0.695302	0.435137	2.484143	0.769888	0.703235
4	8	0.801977	0.401949	0.368304	0.884885	0.429906	0.414671
4	9	0.330860	0.228000	0.231646	0.353918	0.235533	0.235585
4	10	0.116993	0.101120	0.102557	0.121047	0.101969	0.102620

Table D.26: Quark mass critical exponent at the Banks-Zaks fixed points for $\overline{\text{MS}}$ and mMOM renormalization schemes at two, three and four loops for quarks in the 2A representation.

2A		MOMq		MOMggg		MOMh	
N_c	N_f	ρ_2	ρ_3	ρ_2	ρ_3	ρ_2	ρ_3
4	6	7.054427	0.805527	12.794194	1.154631	5.180018	0.582067
4	7	1.882686	0.560447	3.197151	0.730752	1.566644	0.491650
4	8	0.761721	0.375009	1.184460	0.452628	0.681294	0.353174
4	9	0.330392	0.225207	0.459282	0.253314	0.310104	0.219754
4	10	0.118476	0.101235	0.142790	0.106250	0.115212	0.100632

Table D.27: Quark mass critical exponent at the Banks-Zaks fixed points for MOMq, MOMggg and MOMh renormalization schemes at two and three loops for quarks in the 2A representation.

F		$\overline{\text{MS}}$			mMOM		
N_c	N_f	γ_{A2}	γ_{A3}	γ_{A4}	γ_{A2}	γ_{A3}	γ_{A4}
2	6	7.548209	0.161858	-1.141471	11.818182	0.428280	0.323136
2	7	0.887655	0.159141	0.077254	1.183892	0.244022	0.205665
2	8	0.325000	0.127791	0.121549	0.390000	0.155189	0.144550
2	9	0.143879	0.088522	0.091514	0.159938	0.095361	0.094193
2	10	0.054765	0.045143	0.045986	0.057403	0.045893	0.046085
3	9	4.153646	0.193341	-0.017807	6.171875	0.406353	0.292463
3	10	1.118449	0.175883	0.096514	1.508081	0.275001	0.218958
3	11	0.520338	0.151892	0.125835	0.651766	0.199789	0.173654
3	12	0.290250	0.125974	0.121873	0.342900	0.148283	0.137930
3	13	0.171886	0.099007	0.101310	0.193548	0.108285	0.105460
3	14	0.099863	0.071194	0.073373	0.108001	0.074248	0.074090
3	15	0.050894	0.042753	0.043478	0.053170	0.043354	0.043538
3	16	0.014853	0.014138	0.014174	0.015057	0.014158	0.014174
4	12	3.541625	0.201447	0.036834	5.181512	0.399171	0.284083
4	13	1.317024	0.184656	0.098283	1.793970	0.295580	0.228526
4	14	0.695053	0.165357	0.123254	0.893488	0.229594	0.191094
4	15	0.425485	0.145404	0.128680	0.521197	0.182533	0.161674
4	16	0.279773	0.125194	0.121597	0.328922	0.145999	0.135909
4	17	0.189571	0.104756	0.106440	0.215094	0.115697	0.111740
4	18	0.128305	0.084056	0.086672	0.141112	0.089218	0.088260
4	19	0.083770	0.063101	0.064866	0.089617	0.065123	0.065220
4	20	0.049666	0.041969	0.042670	0.051832	0.042527	0.042719
4	21	0.022452	0.020839	0.020948	0.022913	0.020904	0.020950

Table D.28: Value of the γ_A anomalous dimension evaluated at the Banks-Zaks fixed point for $\overline{\text{MS}}$ and mMOM renormalization schemes at two, three and four loops.

F		$\overline{\text{MS}}$			mMOM		
N_c	N_f	$\gamma_{\psi 2}$	$\gamma_{\psi 3}$	$\gamma_{\psi 4}$	$\gamma_{\psi 2}$	$\gamma_{\psi 3}$	$\gamma_{\psi 4}$
2	6	3.331612	0.097917	-0.390702	3.331612	0.042897	-0.014429
2	7	0.166634	0.020246	-0.030731	0.166634	0.011029	-0.005206
2	8	0.025312	0.004037	-0.005989	0.025313	0.002703	-0.001740
2	9	0.003991	0.000586	-0.000738	0.003991	0.000487	-0.000329
2	10	0.000347	0.000050	-0.000005	0.000347	0.000051	0.000004
3	9	1.793981	0.090126	-0.048726	1.793981	0.042526	-0.010391
3	10	0.277757	0.031336	-0.026915	0.277757	0.016702	-0.006569
3	11	0.073953	0.010955	-0.012892	0.073953	0.006576	-0.003834
3	12	0.022800	0.003509	-0.005073	0.022800	0.002376	-0.001939
3	13	0.006932	0.000920	-0.001559	0.006932	0.000708	-0.000786
3	14	0.001795	0.000163	-0.000337	0.001795	0.000146	-0.000220
3	15	0.000301	0.000015	-0.000034	0.000301	0.000017	-0.000027
3	16	0.000011	0.000002	-0.000001	0.000011	0.000002	0.000001
4	12	1.515696	0.087156	0.032770	1.515696	0.042094	-0.009169
4	13	0.373462	0.039322	-0.025492	0.373462	0.020680	-0.007017
4	14	0.695053	0.017958	-0.016739	0.130555	0.010274	-0.005009
4	15	0.052292	0.007972	-0.009604	0.052292	0.004961	-0.003310
4	16	0.021931	0.003297	-0.004823	0.021931	0.002235	-0.001992
4	17	0.009082	0.001200	-0.002101	0.009082	0.000889	-0.001062
4	18	0.003508	0.000348	-0.000775	0.003508	0.000284	-0.000479
4	19	0.001165	0.000063	-0.000228	0.001165	0.000059	-0.000169
4	20	0.000284	0.000002	-0.000044	0.000284	0.000004	-0.000038
4	21	0.000031	0.000000	-0.000002	0.000031	0.000000	-0.000002

Table D.29: Value of the γ_{ψ} anomalous dimension evaluated at the Banks-Zaks fixed point for $\overline{\text{MS}}$ and mMOM renormalization schemes at two, three and four loops.

F		$\overline{\text{MS}}$			mMOM		
N_c	N_f	$-\gamma_{C2}$	$-\gamma_{C3}$	$-\gamma_{C4}$	$-\gamma_{C2}$	$-\gamma_{C3}$	$-\gamma_{C4}$
2	6	3.774105	0.080929	-0.570736	5.909091	0.214140	0.161568
2	7	0.443827	0.079570	0.038627	0.591946	0.122011	0.102833
2	8	0.162500	0.063896	0.060774	0.195000	0.077595	0.072275
2	9	0.071940	0.044261	0.045757	0.079969	0.047680	0.047097
2	10	0.027383	0.022572	0.022993	0.028701	0.022946	0.023043
3	9	2.076823	0.096670	-0.008903	3.085938	0.203177	-0.146232
3	10	0.559224	0.087941	0.048257	0.754040	0.137501	0.109479
3	11	0.260169	0.075946	0.062918	0.325883	0.099894	0.086827
3	12	0.145125	0.062987	0.060936	0.171450	0.074142	0.068965
3	13	0.085943	0.049504	0.050655	0.096774	0.054143	0.052730
3	14	0.049932	0.035597	0.036686	0.054000	0.037124	0.037045
3	15	0.025447	0.021377	0.021739	0.026585	0.021677	0.021769
3	16	0.007426	0.007069	0.007087	0.007528	0.007079	0.007087
4	12	1.770813	0.100724	0.018417	2.590756	0.199586	0.142041
4	13	0.658512	0.092328	0.049142	0.896985	0.147790	0.114263
4	14	0.347527	0.082678	0.061627	0.446744	0.114797	0.095547
4	15	0.212742	0.072702	0.064340	0.260599	0.091266	0.080837
4	16	0.139887	0.062597	0.060798	0.164461	0.072999	0.067954
4	17	0.094786	0.052378	0.053220	0.107547	0.057848	0.055870
4	18	0.064153	0.042028	0.043336	0.070556	0.044609	0.044130
4	19	0.041885	0.031550	0.032433	0.044809	0.032562	0.032610
4	20	0.024833	0.020985	0.021335	0.025916	0.021264	0.021359
4	21	0.011226	0.010420	0.010474	0.011456	0.010452	0.010475

Table D.30: Value of the γ_C anomalous dimension evaluated at the Banks-Zaks fixed point for $\overline{\text{MS}}$ and mMOM renormalization schemes at two, three and four loops.

F		MOMq		MOMggg		MOMh	
N_c	N_f	γ_{A2}	γ_{A3}	γ_{A2}	γ_{A3}	γ_{A2}	γ_{A3}
2	6	12.394900	0.186489	10.286115	0.237565	12.638190	0.345390
2	7	1.14845	0.164475	1.317065	0.189268	1.133504	0.210168
2	8	0.369065	0.129721	0.491728	0.146375	0.360234	0.141038
2	9	0.152120	0.089190	0.206542	0.098860	0.148822	0.090802
2	10	0.055758	0.045253	0.069017	0.047961	0.055064	0.045254
3	9	6.400386	0.189612	5.447734	0.224312	6.559457	0.329837
3	10	1.494540	0.173917	1.562849	0.193650	1.485115	0.233644
3	11	0.630605	0.151840	0.755891	0.166770	0.615875	0.176389
3	12	0.328685	0.126653	0.425300	0.138971	0.318789	0.135538
3	13	0.185640	0.099677	0.246309	0.109064	0.180136	0.102106
3	14	0.104350	0.071577	0.135558	0.077336	0.101809	0.071889
3	15	0.051980	0.042870	0.063193	0.045066	0.051152	0.042821
3	16	0.014937	0.014144	0.016175	0.014301	0.014853	0.014138
4	12	5.354649	0.190709	4.593120	0.220072	5.496436	0.324713
4	13	1.793970	0.178866	1.793970	0.197233	1.793970	0.249036
4	14	0.874932	0.163007	0.982694	0.177188	0.859736	0.199375
4	15	0.504264	0.144956	0.614529	0.157308	0.490397	0.162942
4	16	0.316548	0.125591	0.405843	0.136555	0.306415	0.133706
4	17	0.206944	0.105371	0.271497	0.114616	0.200270	0.108473
4	18	0.136238	0.084573	0.178276	0.091587	0.132247	0.085421
4	19	0.087065	0.063408	0.110874	0.067868	0.084976	0.063472
4	20	0.050776	0.042089	0.061375	0.044133	0.049911	0.042025
4	21	0.022666	0.020858	0.025313	0.021271	0.022465	0.020840

Table D.31: Value of the γ_A anomalous dimension evaluated at the Banks-Zaks fixed point for MOMq, MOMggg and MOMh renormalization schemes at two and three loops.

F		MOMq		MOMggg		MOMh	
N_c	N_f	$\gamma_{\psi 2}$	$\gamma_{\psi 3}$	$\gamma_{\psi 2}$	$\gamma_{\psi 3}$	$\gamma_{\psi 2}$	$\gamma_{\psi 3}$
2	6	3.33161	0.018225	3.331612	0.043123	3.331612	0.018792
2	7	0.166634	0.006015	0.166634	0.013976	0.166634	0.004888
2	8	0.025313	0.001636	0.025313	0.004386	0.025313	0.001079
2	9	0.003991	0.000296	0.003991	0.001055	0.003991	0.000159
2	10	0.000347	0.000035	0.000347	0.000118	0.000347	0.000026
3	9	1.793981	0.020033	1.793981	0.042710	1.793981	0.017904
3	10	0.277757	0.009356	0.277757	0.020019	0.277757	0.006970
3	11	0.073953	0.004063	0.073953	0.009440	0.073953	0.002517
3	12	0.022800	0.001526	0.022800	0.004212	0.022800	0.000730
3	13	0.006932	0.000439	0.006932	0.001649	0.006932	0.000115
3	14	0.001795	0.000074	0.001795	0.000497	0.001795	-0.000017
3	15	0.000301	0.000005	0.000301	0.000086	0.000301	-0.000007
3	16	0.000011	0.000002	0.000011	0.000003	0.000011	0.000001
4	12	1.515696	0.020544	1.515696	0.042342	1.515696	0.017410
4	13	0.373462	0.011550	0.373462	0.023910	0.373462	0.008473
4	14	0.130555	0.006270	0.130555	0.013640	0.130555	0.003978
4	15	0.052292	0.003194	0.052292	0.007658	0.052292	0.001697
4	16	0.021931	0.001467	0.021931	0.004121	0.021931	0.000589
4	17	0.009082	0.000566	0.009082	0.002055	0.009082	0.000112
4	18	0.003508	0.000157	0.003508	0.000901	0.003508	-0.000040
4	19	0.001165	0.000016	0.001165	0.000317	0.001165	-0.000049
4	20	0.000284	-0.000006	0.000284	0.000073	0.000284	-0.000020
4	21	0.000031	-0.000001	0.000031	0.000006	0.000031	-0.000001

Table D.32: Value of the γ_{ψ} anomalous dimension evaluated at the Banks-Zaks fixed point for MOMq, MOMggg and MOMh renormalization schemes at two and three loops.

F		MOMq		MOMggg		MOMh	
N_c	N_f	$-\gamma_{C2}$	$-\gamma_{C3}$	$-\gamma_{C2}$	$-\gamma_{C3}$	$-\gamma_{C2}$	$-\gamma_{C3}$
2	6	3.313858	0.173942	12.803390	0.284140	2.219056	0.154933
2	7	0.432474	0.111550	1.191225	0.165443	0.365200	0.100800
2	8	0.163598	0.074092	0.347592	0.100421	0.150351	0.069676
2	9	0.072933	0.046554	0.121912	0.056866	0.069964	0.045318
2	10	0.027644	0.022763	0.036167	0.024733	0.027198	0.022628
3	9	2.057640	0.170966	6.344571	0.262619	1.341819	0.149574
3	10	0.571245	0.125391	1.493417	0.182608	0.443998	0.110954
3	11	0.268749	0.094592	0.607020	0.131130	0.228978	0.086067
3	12	0.150127	0.071601	0.295049	0.094074	0.135284	0.067109
3	13	0.088562	0.052935	0.151565	0.065442	0.082846	0.050907
3	14	0.051101	0.036630	0.075884	0.042319	0.049083	0.035931
3	15	0.025820	0.021550	0.033028	0.023188	0.025288	0.021412
3	16	0.007464	0.007073	0.008132	0.007163	0.007418	0.007069
4	12	1.811636	0.169926	5.238517	0.255811	1.173595	0.147783
4	13	0.684118	0.133971	1.770351	0.194294	0.509796	0.117458
4	14	0.363241	0.107717	0.848171	0.150966	0.294858	0.096331
4	15	0.222499	0.087373	0.470595	0.118161	0.191299	0.079967
4	16	0.145900	0.070766	0.279843	0.092031	0.130700	0.000039
4	17	0.098379	0.056564	0.171001	0.070450	0.090870	0.054037
4	18	0.066170	0.043910	0.104003	0.052164	0.062577	0.042665
4	19	0.042895	0.032234	0.060751	0.036405	0.041327	0.031734
4	20	0.025237	0.021153	0.032051	0.022692	0.024681	0.021015
4	21	0.011318	0.010436	0.012807	0.010689	0.011204	0.010421

Table D.33: Value of the γ_C anomalous dimension evaluated at the Banks-Zaks fixed point for MOMq, MOMggg and MOMh renormalization schemes at two and three loops.

F		$\overline{\text{MS}}$			mMOM		
N_c	N_f	$(\gamma_{AC})_2$	$(\gamma_{AC})_3$	$(\gamma_{AC})_4$	$(\gamma_{AC})_2$	$(\gamma_{AC})_3$	$(\gamma_{AC})_4$
2	6	3.774104	0.080929	-0.570735	5.909091	0.214140	0.161568
2	7	0.443828	0.079571	0.038627	0.591946	0.122011	0.102832
2	8	0.162500	0.063895	0.060775	0.195000	0.077594	0.072275
2	9	0.071939	0.044261	0.045757	0.079969	0.047681	0.047096
2	10	0.027382	0.022571	0.022993	0.028702	0.022947	0.023042
3	9	2.076823	0.096671	-0.008904	3.085937	0.203176	0.146231
3	10	0.559225	0.087942	0.048257	0.754041	0.137500	0.109479
3	11	0.260169	0.075946	0.062917	0.325883	0.099895	0.086827
3	12	0.145125	0.062987	0.060937	0.171450	0.074141	0.068965
3	13	0.085943	0.049503	0.050655	0.096774	0.054142	0.052730
3	14	0.049931	0.035597	0.036687	0.054001	0.037124	0.037045
3	15	0.025447	0.021376	0.021739	0.026585	0.021677	0.021769
3	16	0.007427	0.007069	0.007087	0.007529	0.007079	0.007087
4	12	1.770812	0.100723	0.018417	2.590756	0.199585	0.142042
4	13	0.658512	0.092328	0.049141	0.896985	0.147790	0.114263
4	14	0.347526	0.082679	0.061627	0.446744	0.114797	0.095547
4	15	0.212743	0.072702	0.064340	0.260598	0.091267	0.080837
4	16	0.139886	0.062597	0.060799	0.164461	0.073000	0.067955
4	17	0.094785	0.052378	0.053220	0.107547	0.057849	0.055870
4	18	0.064152	0.042028	0.043336	0.070556	0.044609	0.044130
4	19	0.041885	0.031551	0.032433	0.044808	0.032561	0.032610
4	20	0.024833	0.020984	0.021335	0.025916	0.021263	0.021360
4	21	0.011226	0.010419	0.010474	0.011457	0.010452	0.010475

Table D.34: Value of $\gamma_{AC} = \gamma_A + \gamma_C$ evaluated at the Banks-Zaks fixed point for $\overline{\text{MS}}$ and mMOM renormalization schemes at two, three and four loops.

F		MOM _q		MOM _{ggg}		MOM _h	
N_c	N_f	$(\gamma_{AC})_2$	$(\gamma_{AC})_3$	$(\gamma_{AC})_2$	$(\gamma_{AC})_3$	$(\gamma_{AC})_2$	$(\gamma_{AC})_3$
2	6	9.081042	0.012547	-2.517275	-0.046575	10.419134	0.190457
2	7	0.715976	0.052925	0.125840	0.023825	0.768304	0.109368
2	8	0.205467	0.055629	0.144136	-0.000010	0.209883	0.071362
2	9	0.079187	0.042636	0.084630	0.041994	0.078858	0.045484
2	10	0.028114	0.022490	0.032850	0.023228	0.027866	0.022626
3	9	4.342746	0.018646	-0.896837	-0.038307	5.217638	0.180263
3	10	0.923295	0.048526	0.069432	0.011042	1.041117	0.122690
3	11	0.361856	0.057248	0.148871	0.035640	0.386897	0.090322
3	12	0.178558	0.055052	0.130251	0.044897	0.183505	0.068429
3	13	0.097078	0.046742	0.094744	0.043622	0.097290	0.051199
3	14	0.053249	0.034947	0.059674	0.035017	0.052726	0.035958
3	15	0.026160	0.021320	0.030165	0.021878	0.025864	0.021409
3	16	0.007473	0.007071	0.008043	0.007138	0.007435	0.007069
4	12	3.543013	0.020783	-0.645397	-0.035739	4.322841	0.176930
4	13	1.109852	0.044895	0.023619	0.002939	1.284174	0.131578
4	14	0.511691	0.055290	0.134523	0.026222	0.564878	0.103044
4	15	0.281765	0.057583	0.143934	0.039147	0.299098	0.082975
4	16	0.170648	0.054825	0.126000	0.044524	0.175715	0.133667
4	17	0.108565	0.048807	0.100496	0.044166	0.109400	0.054436
4	18	0.070068	0.040663	0.074273	0.039423	0.069670	0.042756
4	19	0.044170	0.031174	0.050123	0.031463	0.043649	0.031738
4	20	0.025539	0.020936	0.029324	0.021441	0.025230	0.021010
4	21	0.011348	0.010422	0.012506	0.010582	0.011261	0.010419

Table D.35: Value of $\gamma_{AC} = \gamma_A + \gamma_C$ evaluated at the Banks-Zaks fixed point for MOM_q, MOM_{ggg} and MOM_h renormalization schemes at two and three loops.

Banks-Zaks Fixed Points and Critical Exponents for iMOMi Renormalization Schemes

Tables containing the results of the Banks-Zaks analysis in the iMOMi renormalization schemes are presented below. The first table contains values for the Banks-Zaks critical point while results for the corresponding critical exponents are contained in the subsequent tables. A variety of colour groups and representations are presented, along with results in both the Landau gauge and MAG. Note a slight change in the notation in Appendix E. In the previous Appendix ω denoted the critical exponent associated with the first derivative of the β -function. Now however as we have an interpolating parameter labelled ω which takes the values $\omega = 1/2$ and $\omega = 2$ in this analysis, the exponent is relabelled $\tilde{\omega}$. Therefore, $\tilde{\omega} = 2\beta'_L(a_L^*)$ where a_L^* is the Banks-Zaks fixed point at L loop order.

F		$\omega = 1/2$			$\omega = 2$		
N_c	N_f	iMOMq	iMOMh	iMOMg	iMOMq	iMOMh	iMOMg
2	6	0.082180	0.102178	0.079931	0.075759	0.097485	0.069611
2	7	0.060932	0.070282	0.054313	0.058801	0.068282	0.047987
2	8	0.044235	0.048765	0.037734	0.044086	0.047873	0.033758
2	9	0.029369	0.031291	0.024820	0.029912	0.030949	0.022590
2	10	0.014858	0.015344	0.013027	0.015226	0.015270	0.012204
3	9	0.053594	0.066233	0.050891	0.049640	0.063241	0.044376
3	10	0.043677	0.051213	0.039222	0.041718	0.049554	0.034557
3	11	0.035531	0.040203	0.030790	0.034749	0.039239	0.027353
3	12	0.028408	0.031285	0.024117	0.028304	0.030730	0.021614
3	13	0.021854	0.023529	0.018438	0.022984	0.023223	0.016704
3	14	0.015572	0.016421	0.013274	0.015876	0.016283	0.012202
3	15	0.009362	0.009671	0.008248	0.009557	0.009627	0.007743
3	16	0.003123	0.003158	0.002949	0.003156	0.003154	0.002865

Table E.1: Three loop critical couplings for the three renormalization schemes iMOMq, iMOMh and iMOMg for $\omega = 1/2$ and $\omega = 2$.

F		$\omega = 1/2$			$\omega = 2$		
N_c	N_f	iMOMq	iMOMh	iMOMg	iMOMq	iMOMh	iMOMg
2	6	1.046201	1.285814	1.018897	0.968029	1.230113	0.892618
2	7	0.562075	0.632772	0.509522	0.545385	0.618001	0.457363
2	8	0.275610	0.295000	0.244918	0.274943	0.291309	0.224482
2	9	0.108045	0.1111728	0.097670	0.109128	0.111102	0.091733
2	10	0.023580	0.023809	0.022407	0.023756	0.023776	0.021721
3	9	1.002950	1.219382	0.955671	0.933669	1.168830	0.840254
3	10	0.662954	0.758306	0.603957	0.637256	0.737797	0.540073
3	11	0.426862	0.468961	0.380803	0.419495	0.460538	0.345318
3	12	0.260195	0.277545	0.231243	0.259538	0.274324	0.212649
3	13	0.144113	0.150218	0.129481	0.144993	0.149178	0.120933
3	14	0.067279	0.068846	0.061947	0.067865	0.068606	0.058914
3	15	0.022022	0.022223	0.021019	0.022153	0.022196	0.020420
3	16	0.002200	0.002203	0.002181	0.002203	0.002202	0.002167

Table E.2: Three loop exponent $\tilde{\omega}$ for the three renormalization schemes iMOMq, iMOMh and iMOMg for $\omega = 1/2$ and $\omega = 2$.

F		Two loops			Three loops		
N_c	N_f	$\omega = 1/2$	$\omega = 1$	$\omega = 2$	$\omega = 1/2$	$\omega = 1$	$\omega = 2$
2	6	27.239861	17.262397	2.285966	0.600572	0.461381	0.337700
2	7	2.471236	1.925820	1.106095	0.401204	0.346755	0.290809
2	8	0.743765	0.649692	0.508076	0.266242	0.247039	0.225155
2	9	0.280376	0.262282	0.234985	0.161626	0.156674	0.150586
2	10	0.092919	0.090649	0.087215	0.074218	0.073686	0.073000
3	9	16.864034	11.561746	3.624314	0.708237	0.553462	0.411676
3	10	3.848168	2.978729	1.676364	0.533844	0.452897	0.371313
3	11	1.560926	1.312033	0.938925	0.405984	0.364656	0.319805
3	12	0.773689	0.689329	0.562753	0.304867	0.285218	0.262590
3	13	0.412657	0.383454	0.339589	0.220487	0.212345	0.202509
3	14	0.218111	0.208960	0.195196	0.147470	0.144860	0.141586
3	15	0.101914	0.099806	0.096629	0.082990	0.082504	0.081877
3	16	0.027438	0.027285	0.027054	0.025855	0.025840	0.025821

Table E.3: Exponent ρ for the iMOMq renormalization scheme for $\omega = 1/2, 1$ and 2 at two and three loops.

F		Two loops			Three loops		
N_c	N_f	$\omega = 1/2$	$\omega = 1$	$\omega = 2$	$\omega = 1/2$	$\omega = 1$	$\omega = 2$
2	6	19.223415	13.977991	6.482302	0.397351	0.305679	0.207404
2	7	1.978641	1.724000	1.363952	0.331401	0.304515	0.274502
2	8	0.646766	0.609951	0.558852	0.241931	0.234852	0.226952
2	9	0.258640	0.253377	0.246363	0.155029	0.153796	0.152490
2	10	0.089653	0.089311	0.088924	0.073435	0.073373	0.073325
3	9	11.955015	9.016606	4.817632	0.481863	0.375534	0.265557
3	10	2.975518	2.526293	1.888493	0.423952	0.377682	0.328109
3	11	1.288175	1.170622	1.005228	0.350646	0.330763	0.309163
3	12	0.671895	0.636553	0.587498	0.277955	0.270097	0.261584
3	13	0.373456	0.363130	0.349118	0.208770	0.206167	0.203416
3	14	0.204271	0.201785	0.198561	0.143428	0.142818	0.142216
3	15	0.098263	0.097913	0.097517	0.082160	0.082094	0.082043
3	16	0.027128	0.027124	0.027129	0.025826	0.025826	0.025827

Table E.4: Exponent ρ for the iMOMh renormalization scheme for $\omega = 1/2, 1$ and 2 at two and three loops.

F		Two loops			Three loops		
N_c	N_f	$\omega = 1/2$	$\omega = 1$	$\omega = 2$	$\omega = 1/2$	$\omega = 1$	$\omega = 2$
2	6	45.515760	45.730994	46.741820	0.920418	0.861479	0.796716
2	7	4.046556	4.202074	4.463909	0.554462	0.542352	0.527694
2	8	1.143032	1.201675	1.292562	0.336918	0.336642	0.335932
2	9	0.389802	0.409221	0.438400	0.187578	0.189326	0.191453
2	10	0.112358	0.116219	0.121927	0.078876	0.079602	0.080609
3	9	26.683597	26.804168	27.370418	1.020688	0.954324	0.883068
3	10	6.082398	6.257561	6.573996	0.725820	0.701362	0.673553
3	11	2.411977	2.514774	2.681119	0.524318	0.516777	0.507645
3	12	1.148311	1.204608	1.291859	0.374713	0.374024	0.372958
3	13	0.578876	0.607462	0.650756	0.257811	0.259356	0.261181
3	14	0.284546	0.297076	0.315784	0.163806	0.165375	0.167404
3	15	0.121486	0.125435	0.131273	0.088730	0.088262	0.089284
3	16	0.029273	0.029663	0.030236	0.026094	0.026154	0.026247

Table E.5: Exponent ρ for the iMOMg renormalization scheme for $\omega = 1/2, 1$ and 2 at two and three loops.

F		Two loops			Three loops		
N_c	N_f	$\omega = 1/2$	$\omega = 1$	$\omega = 2$	$\omega = 1/2$	$\omega = 1$	$\omega = 2$
2	6	0.799071	0.537774	0.365556	0.085019	0.080231	0.081241
2	7	0.216131	0.185636	0.154275	0.061121	0.059714	0.059190
2	8	0.097538	0.088764	0.078600	0.043575	0.042749	0.042380
2	9	0.046504	0.043433	0.039661	0.028639	0.028092	0.027695
2	10	0.018097	0.017153	0.015955	0.014474	0.014104	0.013695
3	8	16.520099	1.288823	0.553544	0.067606	0.064207	0.061489
3	9	0.384329	0.293024	0.218305	0.053563	0.051567	0.050019
3	10	0.168767	0.145756	0.121824	0.043260	0.042012	0.041088
3	11	0.095628	0.086485	0.076013	0.034976	0.034165	0.033589
3	12	0.058812	0.054483	0.049258	0.027846	0.027301	0.026914
3	13	0.036644	0.034450	0.031716	0.021368	0.020986	0.020687
3	14	0.021831	0.020731	0.019327	0.015219	0.014936	0.014671
3	15	0.011235	0.010745	0.010111	0.009169	0.008966	0.008733
3	16	0.003278	0.003153	0.002988	0.003078	0.002985	0.002865

Table E.6: Critical coupling for the MAG in the iMOMmq renormalization scheme for $\omega = 1/2, 1$ and 2 at two and three loops.

F		Two loops			Three loops		
N_c	N_f	$\omega = 1/2$	$\omega = 1$	$\omega = 2$	$\omega = 1/2$	$\omega = 1$	$\omega = 2$
2	7	0.352911	0.348066	0.342161	0.078831	0.073482	0.066826
2	8	0.127203	0.126358	0.125311	0.053505	0.051563	0.048882
2	9	0.055812	0.055568	0.055263	0.034175	0.033613	0.032775
2	10	0.020797	0.020729	0.020644	0.016844	0.016771	0.016655
3	9	0.909893	0.833333	0.749799	0.072040	0.066273	0.059306
3	10	0.238596	0.232143	0.224117	0.054752	0.051951	0.048238
3	11	0.118938	0.117021	0.114577	0.042665	0.041258	0.039270
3	12	0.068973	0.068182	0.067161	0.033125	0.032451	0.031448
3	13	0.041547	0.041176	0.040696	0.024931	0.024651	0.024211
3	14	0.024215	0.024038	0.023809	0.017440	0.017353	0.017207
3	15	0.012271	0.012195	0.012097	0.010298	0.010279	0.010245
3	16	0.003540	0.003521	0.003496	0.003366	0.003356	0.003343

Table E.7: Critical coupling for the MAG in the iMOMmh renormalization scheme for $\omega = 1/2, 1$ and 2 at two and three loops.

F		Two loops			Three loops		
N_c	N_f	$\omega = 1/2$	$\omega = 1$	$\omega = 2$	$\omega = 1/2$	$\omega = 1$	$\omega = 2$
2	6	0.456502	0.368962	0.293214	0.068321	0.058604	0.048399
2	7	0.172393	0.155029	0.136508	0.046244	0.041077	0.035270
2	8	0.084619	0.078840	0.072198	0.032787	0.029333	0.025796
2	9	0.041926	0.039760	0.037173	0.021571	0.019852	0.017805
2	10	0.016680	0.015987	0.015140	0.011542	0.010807	0.009909
3	8	1.152688	0.733566	0.491556	0.062251	0.053790	0.044666
3	9	0.284370	0.245200	0.206657	0.045268	0.040311	0.034640
3	10	0.143254	0.131082	0.117558	0.034919	0.031600	0.027699
3	11	0.085438	0.080190	0.074032	0.027530	0.025184	0.022383
3	12	0.053974	0.051377	0.048236	0.021688	0.020014	0.017991
3	13	0.034188	0.032837	0.031169	0.016696	0.015532	0.014111
3	14	0.020597	0.019906	0.019041	0.012119	0.011373	0.010500
3	15	0.010686	0.010374	0.009981	0.007610	0.007219	0.006726
3	16	0.003137	0.003056	0.002953	0.002766	0.002665	0.002534

Table E.8: Critical coupling for the MAG in the iMOMmg renormalization scheme for $\omega = 1/2, 1$ and 2 at two and three loops.

F		Two loops			Three loops		
N_c	N_f	$\omega = 1/2$	$\omega = 1$	$\omega = 2$	$\omega = 1/2$	$\omega = 1$	$\omega = 2$
2	6	5.327143	3.585161	2.437039	1.073281	1.013502	0.962845
2	7	1.152701	0.990057	0.822798	0.559772	0.534507	0.510243
2	8	0.390152	0.355055	0.314319	0.270730	0.259641	0.247612
2	9	0.124010	0.115822	0.105762	0.105709	0.101371	0.096136
2	10	0.024130	0.022871	0.021273	0.023162	0.022148	0.020846
3	8				1.529262	1.419098	1.316340
3	9	3.843291	2.930241	2.183050	0.996607	0.940596	0.885769
3	10	1.462652	1.263216	1.055809	0.653734	0.623259	0.592086
3	11	0.701272	0.634220	0.557432	0.419166	0.402108	0.383796
3	12	0.352874	0.326896	0.295548	0.255045	0.245527	0.234734
3	13	0.171004	0.160769	0.148006	0.141288	0.136210	0.130111
3	14	0.072771	0.068102	0.064422	0.066093	0.063703	0.060684
3	15	0.022469	0.021491	0.020222	0.021710	0.020901	0.019846
3	16	0.002186	0.002102	0.001992	0.002177	0.002096	0.001988

Table E.9: Critical exponent $\tilde{\omega}$ for the MAG in the iMOMmq renormalization scheme for $\omega = 1/2, 1$ and 2 at two and three loops.

F		Two loops			Three loops		
N_c	N_f	$\omega = 1/2$	$\omega = 1$	$\omega = 2$	$\omega = 1/2$	$\omega = 1$	$\omega = 2$
2	7	1.882193	1.856353	1.824856	0.746948	0.701073	0.643199
2	8	0.508813	0.505432	0.501244	0.338018	0.328334	0.314785
2	9	0.148833	0.148181	0.147369	0.126465	0.125049	0.122966
2	10	0.027729	0.027638	0.027525	0.026727	0.026631	0.026498
3	9	9.098932	8.333333	7.497988	1.383771	1.272760	1.139203
3	10	2.067830	2.011905	1.942349	0.840139	0.799725	0.746148
3	11	0.872209	0.858156	0.840231	0.513518	0.498442	0.477261
3	12	0.413839	0.409091	0.402969	0.302051	0.296744	0.289024
3	13	0.193884	0.192157	0.189917	0.162873	0.161206	0.158755
3	14	0.080716	0.080128	0.079363	0.074398	0.073931	0.073261
3	15	0.024541	0.024390	0.024193	0.023907	0.023788	0.023626
3	16	0.002360	0.022347	0.002331	0.002354	0.002342	0.002326

Table E.10: Critical exponent $\tilde{\omega}$ for the MAG in the iMOMmh renormalization scheme for $\omega = 1/2, 1$ and 2 at two and three loops.

F		Two loops			Three loops		
N_c	N_f	$\omega = 1/2$	$\omega = 1$	$\omega = 2$	$\omega = 1/2$	$\omega = 1$	$\omega = 2$
2	6	3.043344	2.459744	1.954763	0.842774	0.719335	0.592056
2	7	0.919427	0.826824	0.728041	0.427109	0.380106	0.327615
2	8	0.338478	0.315362	0.288792	0.209472	0.191012	0.169503
2	9	0.111803	0.106027	0.099128	0.085449	0.079444	0.072219
2	10	0.022240	0.021316	0.020186	0.020130	0.019078	0.017776
3	8				3.123205	2.479437	1.868995
3	9	2.843703	2.452003	2.066569	0.833292	0.739952	0.634737
3	10	1.241532	1.136045	1.018833	0.531501	0.481717	0.423555
3	11	0.626546	0.588059	0.542903	0.338716	0.311363	0.278660
3	12	0.323842	0.308264	0.289414	0.207970	0.193387	0.175627
3	13	0.159546	0.153239	0.145454	0.117778	0.110682	0.101890
3	14	0.068658	0.066355	0.063472	0.057024	0.054161	0.050550
3	15	0.021371	0.020749	0.019961	0.019601	0.018829	0.017838
3	16	0.002092	0.002038	0.001969	0.002062	0.002004	0.001929

Table E.11: Critical exponent $\tilde{\omega}$ for the MAG in the iMOMmg renormalization scheme for $\omega = 1/2, 1$ and 2 at two and three loops.

F		Two loops			Three loops		
N_c	N_f	$\omega = 1/2$	$\omega = 1$	$\omega = 2$	$\omega = 1/2$	$\omega = 1$	$\omega = 2$
2	6	27.151323	9.421916	2.329600	0.727579	0.529330	0.340358
2	7	2.727786	1.739164	0.911281	0.448441	0.372273	0.295462
2	8	0.802887	0.621964	0.434591	0.282612	0.252537	0.221015
2	9	0.293480	0.252532	0.205388	0.165442	0.154232	0.141942
2	10	0.094414	0.086687	0.077168	0.074136	0.070596	0.066387
3	8				1.133708	0.749544	0.423023
3	9	16.945454	7.666846	2.419001	0.786991	0.593762	0.414971
3	10	4.059420	2.559142	1.289464	0.574469	0.471709	0.371009
3	11	1.645984	1.209145	0.771741	0.426561	0.371078	0.314365
3	12	0.807914	0.651783	0.480014	0.314378	0.284772	0.253448
3	13	0.425766	0.366189	0.296502	0.223991	0.208688	0.191928
3	14	0.222301	0.200185	0.173150	0.148067	0.140545	0.131936
3	15	0.102650	0.095603	0.086687	0.082627	0.079281	0.075218
3	16	0.027328	0.026087	0.024471	0.025626	0.024694	0.023492

Table E.12: Critical exponent ρ for the MAG in the iMOMmq renormalization scheme for $\omega = 1/2, 1$ and 2 at two and three loops.

F		Two loops			Three loops		
N_c	N_f	$\omega = 1/2$	$\omega = 1$	$\omega = 2$	$\omega = 1/2$	$\omega = 1$	$\omega = 2$
2	7	3.747300	2.473367	0.815222	0.319711	0.282781	0.262300
2	8	0.863985	0.720339	0.529470	0.252724	0.234933	0.220454
2	9	0.309416	0.285623	0.254192	0.166848	0.160562	0.154358
2	10	0.101970	0.099095	0.095369	0.080456	0.079152	0.077654
3	9	41.850719	15.814616	- 9.168835	0.387396	0.298384	0.276381
3	10	4.355094	2.760172	0.794656	0.398791	0.340127	0.306951
3	11	1.576575	1.214713	0.748957	0.347815	0.314402	0.289775
3	12	0.767773	0.656673	0.511728	0.283215	0.265652	0.250555
3	13	0.412837	0.376052	0.327950	0.216388	0.208016	0.199960
3	14	0.221764	0.210274	0.195312	0.150500	0.147053	0.143388
3	15	0.105550	0.102718	0.099061	0.086974	0.085862	0.084554
3	15	0.028950	0.028643	0.028250	0.027477	0.027288	0.027045

Table E.13: Critical exponent ρ for the MAG in the iMOMmh renormalization scheme for $\omega = 1/2, 1$ and 2 at two and three loops.

F		Two loops			Three loops		
N_c	N_f	$\omega = 1/2$	$\omega = 1$	$\omega = 2$	$\omega = 1/2$	$\omega = 1$	$\omega = 2$
2	6	18.889955	13.115654	9.026188	1.137715	0.904094	0.686813
2	7	3.461711	3.017882	2.588851	0.596908	0.522030	0.439606
2	8	1.096596	1.031878	0.962335	0.338991	0.311343	0.277765
2	9	0.381247	0.370717	0.358819	0.181255	0.171390	0.158654
2	10	0.108207	0.106115	0.103640	0.074094	0.071156	0.067335
3	8				2.311115	1.831479	1.380792
3	9	17.574292	13.681752	10.430036	1.165083	0.991664	0.809849
3	10	5.378418	4.779519	4.181646	0.776540	0.695456	0.602230
3	11	2.313440	2.179419	2.036729	0.539557	0.498978	0.449066
3	12	1.131927	1.100464	1.066610	0.375802	0.355280	0.328634
3	13	0.574349	0.568081	0.561776	0.253855	0.243752	0.230073
3	14	0.281210	0.280212	0.279458	0.159044	0.154304	0.147767
3	15	0.118769	0.095603	0.086687	0.084019	0.079281	0.079108
3	16	0.028135	0.026087	0.027193	0.024828	0.024694	0.023407

Table E.14: Critical exponent ρ for the MAG in the iMOMmg renormalization scheme for $\omega = 1/2, 1$ and 2 at two and three loops.

Renormalization Group Functions γ_A , γ_ψ and γ_c of QCD in $\overline{\text{MS}}$ Scheme

The anomalous dimensions of the quark, ghost and gluon; γ_ψ , γ_c and γ_A , in the $\overline{\text{MS}}$, mMOM to four loops and MOMi schemes to three loops have been calculated for an arbitrary colour group and gauge in [304,306,307]. Additionally the three loop Feynman gauge results for these anomalous dimensions were computed in [225]. We state the $\overline{\text{MS}}$ result here in the Landau gauge for completeness. Note that $a^2 = g^2/(16\pi^2)$. We have

$$\begin{aligned}
\gamma_A^{\overline{\text{MS}}} &= \frac{1}{6} \left(-13N_c + 4N_f \right) a + \frac{1}{8N_c} \left(-59N_c^3 + 28N_c^2 N_f - 8N_f \right) a^2 \\
&+ \frac{1}{288N_c^2} \left(-\frac{4885133391}{500000} N_c^5 + \frac{1549355709}{250000} N_c^4 N_f - 784N_c^3 N_f^2 \right. \\
&\quad \left. - \frac{244144291}{125000} N_c^2 N_f + 176N_c N_f^2 - 72N_f \right) a^3 \\
&+ \frac{1}{62208N_c^3} \left(178848N_f - \frac{10476853}{8} N_c N_f^2 + \frac{13509196}{125} N_c^2 N_f \right. \\
&\quad + \frac{923699533}{500} N_c^3 N_f^2 - \frac{44730081}{250} 178920.324 N_c^4 N_f \\
&\quad + \frac{58968}{5} N_c^6 N_f \pi^4 - \frac{10368}{5} N_c^5 N_f^2 \pi^4 + \frac{114048}{5} N_c^4 N_f \pi^4 \\
&\quad - \frac{20736}{5} N_c^3 N_f^2 \pi^4 - \frac{10692}{5} N_c^7 \pi^4 + 19712 N_c^2 N_f^3 \\
&\quad + \frac{131693851}{100000} N_c^4 N_f^3 - \frac{89282723}{40} N_c^5 N_f^2 + \frac{47168091}{5} N_c^6 N_f \\
&\quad \left. - \frac{309994413}{25} N_c^7 - \frac{2421544053}{100} N_c^5 \right) a^4, \quad (\text{F.0.1})
\end{aligned}$$

$$\begin{aligned}
\gamma_\psi^{\overline{\text{MS}}} = & -16 \left(N_f \left[-\frac{1}{32N_c} + \frac{1}{32}N_c \right] + \frac{19}{128} + \frac{3}{128N_c^2} - \frac{11}{64}N_c^2 \right) a^2 \\
& -64 \left(N_f \left[-\frac{65}{576} - \frac{3}{512N_c^2} + \frac{547}{4608}N_c^2 \right] \right. \\
& \quad \left. + N_f^2 \left(\frac{5}{1152N_c} - \frac{5}{1152}N_c \right) + \frac{3}{1024N_c^3} + \frac{74513}{1000000N_c} \right. \\
& \quad \left. + \frac{128939}{500000}N_c - \frac{8383}{25000}N_c^3 \right) a^3 \\
& -256 \left(N_f \left[\frac{171409}{500000}N_c^3 - \frac{25719}{100000}N_c - \frac{166781}{1000000N_c} + \frac{7}{122880}N_c^3\pi^4 \right. \right. \\
& \quad \left. \left. + \frac{81153}{1000000N_c^3} + \frac{3}{40960}N_c\pi^4 - \frac{\pi^4}{7680N_c} \right] \right. \\
& \quad \left. + N_f^2 \left[\frac{32389}{1000000} + \frac{229}{200000N_c^2} - \frac{16767}{500000}N_c^2 \right] \right. \\
& \quad \left. + N_f^3 \left[\frac{35}{41472N_c} - \frac{35}{41472N_c} \right] \right. \\
& \quad \left. + \frac{10369}{125000} + \frac{11}{15360}\pi^4 + \frac{447887}{1000000}N_c^2 + \frac{15289}{500000N_c^2} \right. \\
& \quad \left. - \frac{548127}{1000000}N_c^4 - \frac{77}{245760}N_c^4\pi^4 - \frac{33}{81920}N_c^2\pi^4 - \frac{1329}{100000N_c^4} \right) a^4 \\
& \hspace{15em} (\text{F.0.2})
\end{aligned}$$

and

$$\begin{aligned}
\gamma_C^{\overline{\text{MS}}} = & -\frac{3}{4}N_c a + \frac{1}{48}N_c \left(-95N_c + 20N_f \right) a^2 \\
& + \frac{1}{1728} \left(-\frac{328023993}{20000}N_c^3 + \frac{8751731493}{1000000}N_c^2N_f + 560N_cN_f^2 \right. \\
& \quad \left. + \frac{274292597}{200000}N_f \right) a^3 \\
& + \frac{1}{124416} \left(\frac{3134485073}{500}N_c^4N_f - \frac{6812797791}{10000}N_c^3N_f^2 + \frac{10692}{5}N_c^5\pi^4 \right. \\
& \quad - \frac{3407677791}{5000}N_cN_f^2 + \frac{2857386613}{1000}N_c^2N_f - \frac{58968}{5}N_c^4N_f\pi^4 \\
& \quad + \frac{10368}{5}N_c^3N_f^2\pi^4 + \frac{20055527}{100}N_f - \frac{114048}{5}N_c^2N_f\pi^4 \\
& \quad + \frac{20736}{5}N_cN_f^2\pi^4 - \frac{31920478}{25}N_c^3 - \frac{180658666}{25}N_c^5 \\
& \quad \left. - \frac{3459693851}{100000}N_c^2N_f^3 \right) \frac{a^4}{N_c} . \\
& \hspace{15em} (\text{F.0.3})
\end{aligned}$$

Bibliography

- [1] J.A. Gracey and R.M. Simms, *Banks-Zaks Fixed Point Analysis in Momentum Subtraction Schemes*, Phys. Rev. **D91** (2015) no.8, 085037.
- [2] J.A. Gracey and R.M. Simms, *Six dimensional Landau-Ginzburg-Wilson theory*, Phys. Rev. **D95** (2017) no.2, 025029.
- [3] J.A. Gracey and R.M. Simms, *Higher Dimensional Higher Derivative ϕ^4 Theory*, Phys. Rev. **D96** (2017) no.2, 025022.
- [4] J.A. Gracey and R.M. Simms, *Renormalization of QCD in the Interpolating Momentum Subtraction Scheme at Three Loops*, Phys. Rev. **D97** (2018) no.8, 085016.
- [5] S.L. Glashow, *Partial Symmetries of Weak Interactions*, Nucl. Phys. **22** (1961) 579-588.
- [6] S. Weinberg, *A Model of Leptons*, Phys. Rev. Lett. **19** (1967) 1264-1266.
- [7] A. Salam, *Weak and Electromagnetic Interactions*, Proceedings of the 8th Nobel Symposium Lerum, Sweden (1968).
- [8] F. Englert and R. Brout, *Broken Symmetry and the Mass of Gauge Vector Mesons*, Phys. Rev. Lett. **13** (1964) 321-323.
- [9] P. W. Higgs, *Broken Symmetries and the Masses of Gauge Bosons*, Phys. Rev. Lett. **13** (1964) 508-509.
- [10] P. W. Higgs, *Broken Symmetries, Massless Particles and Gauge Fields*, Phys. Lett. **12** (1964) 132-133.
- [11] G.S. Guralnik, C.R. Hagen and T.W.B. Kibble, *Global Conservation Laws and Massless Particles*, Phys. Rev. Lett. **13** (1964) 585-587.
- [12] F.J. Hasert et al., *Search for Elastic ν_μ Electron Scattering*, Phys. Lett. **B46** (1973) 121-124.

- [13] F.J. Hasert et al., *Observation of Neutrino Like Interactions Without Muon or Electron in the Gargamelle Neutrino Experiment*, Phys. Lett. **B46** (1973) 138-140.
- [14] F.J. Hasert et al., *Observation of Neutrino Like Interactions without Muon or Electron in the Gargamelle Neutrino Experiment*, Nucl. Phys. **B73** (1974) 1-22.
- [15] M. Gell-Mann, *A Schematic Model of Baryons and Mesons*, Phys. Lett. **8** (1964) 214-215.
- [16] G. Zweig, *An SU(3) Model for Strong Interaction Symmetry and its Breaking*, CERN-TH-412 (1964).
- [17] O.W. Greenberg, *Spin and Unitary Spin Independence in a Paraquark Model of Baryons and Mesons*, Phys. Rev. Lett. **13** (1964) 598-602.
- [18] M.Y. Han and Y. Nambu, *Three Triplet Model with Double SU(3) Symmetry*, Phys. Rev. **B139** (1965) 1006-1010.
- [19] J.J. Aubert et al., *Experimental Observation of a Heavy Particle J*, Phys. Rev. Lett. **33** (1974) 1404-1406.
- [20] J.E. Augustin et al., *Discovery of a Narrow Resonance in e^+e^- Annihilation*, Phys. Rev. Lett. **33** (1974) 1406-1408.
- [21] D.J. Gross and F. Wilczek, *Ultraviolet Behavior of Nonabelian Gauge Theories*, Phys. Rev. Lett. **30** (1973) 1343-1346.
- [22] H.D. Politzer, *Reliable Perturbative Results for Strong Interactions?*, Phys. Rev. Lett. **30** (1973) 1346-1349.
- [23] T.Y. Cao, *Conceptual Developments of 20th Century Field Theories*, Cambridge University Press, Cambridge (1998).
- [24] S. Weinberg, *The Quantum Theory of Fields. Volume 1: Foundations*, Cambridge University Press, Cambridge (1995).
- [25] P.A.M. Dirac, *Quantum Theory of Emission and Absorption of Radiation*, Proc. Roy. Soc. Lond. **A114** (1927) 243-265.
- [26] W. Heisenberg and W. Pauli, *On Quantum Field Theory*, Z. Phys. **56** (1929) 1-61.
- [27] W. Heisenberg and W. Pauli, *On Quantum Field Theory. 2.*, Z. Phys. **59** (1930) 168-190.

- [28] H.A. Bethe, *The Electromagnetic shift of energy levels*, Phys. Rev. **72** (1947) 339-341.
- [29] J.S. Schwinger, *On Quantum Electrodynamics and the Magnetic Moment of the Electron*, Phys. Rev. **73** (1948) 416-417.
- [30] J.S. Schwinger, *Quantum Electrodynamics. I A Covariant Formulation*, Phys. Rev. **74** (1948) 1439.
- [31] J.S. Schwinger, *Quantum Electrodynamics. 2. Vacuum Polarization and Self Energy*, Phys. Rev. **75** (1948) 651.
- [32] J.S. Schwinger, *Quantum electrodynamics. III: The Electromagnetic Properties of the Electron: Radiative Corrections to Scattering*, Phys. Rev. **76** (1949) 790-817.
- [33] R.P. Feynman, *Space-time Approach to Nonrelativistic Quantum Mechanics*, Rev. Mod. Phys. **20** (1948) 367-387.
- [34] R.P. Feynman, *A Relativistic Cutoff for Classical Electrodynamics*, Phys. Rev. **74** (1948) 939-946.
- [35] R.P. Feynman, *Relativistic Cutoff for Quantum Electrodynamics*, Phys. Rev. **74** (1948) 1430-1438.
- [36] S. Tomonaga, *On a Relativistically Invariant Formulation of the Quantum Theory of Wave Fields*, Prog. Theor. Phys. **1** (1946) 27-42.
- [37] F.J. Dyson, *The Radiation Theories of Tomonaga, Schwinger, and Feynman*, Phys. Rev. **75** (1949) 486-502.
- [38] C.G. Callan, Jr., *Broken Scale Invariance in Scalar Field Theory*, Phys. Rev. **D2** (1970) 1541-1547.
- [39] K. Symanzik, *Small Distance Behavior in Field Theory and Power Counting*, Commun. Math. Phys. **18** (1970) 227-246.
- [40] L.P. Kadanoff, *Scaling Laws for Ising Models near T_c* , Physique Fizika **2** (1966) 263-272.
- [41] M.E. Fisher and K.G Wilson, *Critical Exponents in 3.99 Dimensions*, Phys. Rev. Lett. **28** (1972) 240-243.
- [42] K.G Wilson, *The Renormalization Group: Critical Phenomena and the Kondo Problem*, Rev. Mod. Phys. **47** (1975) 773.

- [43] K. G. Wilson, *Renormalization Group and Critical Phenomena. 1. Renormalization Group and the Kadanoff Scaling Picture*, Phys. Rev. **B4** (1971) 3174-3183.
- [44] K. G. Wilson, *Renormalization Group and Critical Phenomena. 2. Phase Space Cell Analysis of Critical Behaviour*, Phys. Rev. **B4** (1971) 3184-3205.
- [45] R. Shankar, *Renormalization Group Approach to Interacting Fermions*, Rev. Mod. Phys. **66** (1994) 129-192.
- [46] A.J. McKane, D.J. Wallace and R.K.P Zia, *Models for Strong Interactions in Six Epsilon Dimensions*, Phys. Lett. **B65** (1976) 171-173.
- [47] A.N. Vasil'ev and M.Yu. Nalimov, *Analog of Dimensional Regularization for Calculation of the Renormalization-Group Functions in the $1/n$ Expansion for Arbitrary Dimension of Space*, Theor. Math. Phys. **55** (1983) 423-431.
- [48] A.N. Vasil'ev, Y.M. Pismak and J.R. Honkonen, *Simple Method of Calculating the Critical Indices in the $1/N$ Expansion*, Theor. Math. Phys. **46** (1981) 104-113.
- [49] A.N. Vasil'ev, Y.M. Pismak and J.R. Honkonen, *$1/N$ expansion: Calculation of the Exponents η and ν in the order $1/N^2$ for arbitrary number of dimensions*, Theor. Math. Phys. **47** (1981) 465-475.
- [50] A.N. Vasil'ev, Y.M. Pismak and J.R. Honkonen, *$1/N$ Expansion: Calculation Of The Exponent η In The Order $1/N^3$ By The Conformal Bootstrap Method*, Theor. Math. Phys. **50** (1982) 127-134.
- [51] L. Fei, S. Giombi and I.R. Klebanov, *Critical $O(N)$ Models in $6 - \epsilon$ Dimensions*, Phys. Rev. **D90** (2014) no.2, 025018.
- [52] L. Fei, S. Giombi, I.R. Klebanov and G. Tarnopolsky, *Three Loop Analysis of the Critical $O(N)$ Models in $6 - \epsilon$ Dimensions*, Phys. Rev. **D91** (2015) no.4, 045011.
- [53] J.A. Gracey, *Four loop Renormalization of ϕ^3 Theory in Six Dimensions*, Phys. Rev. **D92** (2015) no.2, 025012.
- [54] J.A. Gracey, *Six Dimensional QCD at Two Loops*, Phys. Rev. **D93** (2016) no.2, 025025.
- [55] S. Giombi, I.R. Klebanov, Z.M. Tan and E. Normale, *The ABC of Higher-Spin AdS/CFT*, Universe **4** (2018) no.1, 18.

- [56] I.R. Klebanov and A.M. Polyakov, *AdS dual of the Critical $O(N)$ Vector Model*, Phys. Lett. **B550** (2002) 213-219.
- [57] Z. Li and N. Su, *Bootstrapping Mixed Correlators in the Five Dimensional Critical $O(N)$ Models*, JHEP **1704** (2017) 098.
- [58] J.B. Bae and S.J. Rey, *Conformal Bootstrap Approach to $O(N)$ Fixed Points in Five Dimensions*, hep-th/1412.6549.
- [59] Y. Nakayama and T. Ohtsuki, *Five Dimensional $O(N)$ -symmetric CFTs from Conformal Bootstrap*, Phys. Lett. **B734** (2014) 193-197.
- [60] Y. Pang, J. Rong and N. Su, *ϕ^3 Theory with F_4 Flavor Symmetry in $6 - 2\epsilon$ Dimensions: 3-loop Renormalization and Conformal Bootstrap*, JHEP **1612** (2016) 057.
- [61] F. Kos, D. Poland and D. Simmons-Duffin, *Bootstrapping the $O(N)$ Vector Models*, JHEP **1406** (2014) 091.
- [62] S.M. Chester, S.S. Pufu and R. Yacoby, *Bootstrapping $O(N)$ Vector Models in $4 < d < 6$* , Phys. Rev. **D91** (2015) no.8, 086014.
- [63] K. Kamikado and T. Kanazawa, *Nonperturbative RG analysis of Five-Dimensional $O(N)$ Models with Cubic Interactions*, hep-th/1604.04830.
- [64] N. Strodthoff, *Self-Consistent Spectral Functions in the $O(N)$ Model from the Functional Renormalization Group*, Phys. Rev. **D95** (2017) no.7, 076002.
- [65] A. Eichhorn, L. Janssen and M.M. Scherer, *Critical $O(N)$ Models Above Four Dimensions: Small- N Solutions and Stability*, Phys. Rev. **D93** (2016) no.12, 125021.
- [66] Y. Nakayama and T. Ohtsuki, *Approaching the Conformal Window of $O(n) \times O(m)$ Symmetric Landau-Ginzburg models using the Conformal Bootstrap*, Phys. Rev. **D89** (2014) no.12, 126009.
- [67] Y. Nakayama and T. Ohtsuki, *Bootstrapping Phase Transitions in QCD and Frustrated Spin Systems*, Phys. Rev. **D91** (2015) no.2, 021901.
- [68] M. Safari and G.P. Vacca, *Uncovering Novel Phase Structures in \square^k Scalar Theories with the Renormalization Group*, Eur. Phys. J. **C78** (2018) no.3, 251.

- [69] S. Giombi, I.R. Klebanov and G. Tarnopolsky, *Conformal QED_d, F–Theorem and the ϵ Expansion*, J. Phys. **A49** (2016) no.13, 135403.
- [70] J.A. Gracey, *Eight Dimensional QCD at One Loop*, Phys. Rev. **D97** (2018) no.2, 025009.
- [71] S. Weinberg, *Ultraviolet Divergences in Quantum Theories of Gravitation, General Relativity: An Einstein centenary survey*, Cambridge University Press, Cambridge (1979) 790-831.
- [72] I.F. Herbut and L. Janssen, *Critical $O(2)$ and $O(3)$ ϕ^4 Theories near Six Dimensions*, Phys. Rev. **D93** (2016) no.8, 085005.
- [73] D.F. Litim, E. Marchais and P. Mati, *Fixed Points and the Spontaneous Breaking of Scale Invariance*, Phys. Rev. **D95** (2017) no.12, 125006.
- [74] D.F. Litim and F. Sannino, *Asymptotic Safety Guaranteed*, JHEP **1412** (2014) 178.
- [75] D.F. Litim, M. Mojaza and F. Sannino, *Vacuum Stability of Asymptotically Safe Gauge-Yukawa Theories*, JHEP **1601** (2016) 081.
- [76] A.D. Bond, D.F. Litim, *Theorems for Asymptotic Safety of Gauge Theories*, Eur. Phys. J. **C77** (2017) no.6, 429, Erratum: Eur. Phys. J. **C77** (2017) no.8, 525.
- [77] A.D. Bond and D.F. Litim, *More Asymptotic Safety Guaranteed*, Phys. Rev. **D97** (2018) no.8, 085008.
- [78] A. Eichhorn, *Status of the Asymptotic Safety Paradigm for Quantum Gravity and Matter*, gr-gc/1709.03696.
- [79] A. Eichhorn, *Nonminimal Hints for Asymptotic Safety*, Phys. Rev. **D97** (2018) no.2, 026002.
- [80] A. Eichhorn, *Quantum-Gravity Predictions for the Fine-Structure Constant*, Phys. Lett. **B782** (2018) 198-201.
- [81] A. Eichhorn, *Top Mass from Asymptotic Safety*, Phys. Lett. **B777** (2018) 217-221.
- [82] A. Eichhorn, *Mass Difference for Charged Quarks from Quantum Gravity*, hep-th/1803.04027.
- [83] A. Eichhorn, *Upper Bound on the Abelian Gauge Coupling from Asymptotic Safety*, JHEP **1801** (2018) 030.

- [84] R. Mann, J. Meffe, F. Sannino, T. Steele, Z.W. Wang and C. Zhang, *Asymptotically Safe Standard Model via Vector like Fermions*, Phys. Rev. Lett. **119** (2017) no.26, 261802.
- [85] A. Eichhorn, *Asymptotic Safety in the Dark*, hep-ph/1802.08589.
- [86] A.D. Bond and D.F. Litim, *Asymptotic Safety Guaranteed in Supersymmetry*, Phys. Rev. Lett. **119** (2017) no.21, 211601.
- [87] B.H. Wellegehausen, D. Körner and A. Wipf, *Asymptotic Safety on the Lattice: The Nonlinear $O(N)$ Sigma Model*, Annals Phys. **349** (2014) 374-394.
- [88] T. Banks and A. Zaks, *On the Phase Structure of Vector-Like Gauge Theories with Massless Fermions*, Nucl. Phys. **B196** (1982) 189-204.
- [89] T.A. Ryttov and R. Shrock, *Scheme Transformations in the Vicinity of an Infrared Fixed Point*, Phys. Rev. **D86** (2012) 065032.
- [90] T.A. Ryttov and R. Shrock, *An Analysis of Scheme Transformations in the Vicinity of an Infrared Fixed Point*, Phys. Rev. **D86** (2012) 085005.
- [91] R. Shrock, *Study of Scheme Transformations to Remove Higher-Loop Terms in the β -function of a Gauge Theory*, Phys. Rev. **D88** (2013) 036003.
- [92] T.A. Ryttov, *Higher Loop Corrections to the Infrared Evolution of Fermionic Gauge Theories in the $R\bar{I}$ Scheme*, Phys. Rev. **D89** (2014) no.1, 016013.
- [93] R. Shrock, *Study of Possible Ultraviolet Zero of the β -function in Gauge Theories with Many Fermions*, Phys. Rev. **D89** (2014) no.4, 045019.
- [94] T.A. Ryttov, *Infrared Fixed Points in the Minimal Momentum Subtraction Scheme*, Phys. Rev. **D89** (2014) no.5, 056001.
- [95] G. Choi and R. Shrock, *New Scheme Transformations and Application to Study Scheme Dependence of an Infrared Zero of the β -function in Gauge Theories*, Phys. Rev. **D90** (2014) no.12, 125029.
- [96] R. Shrock, *Generalized Scheme Transformations for the Elimination of Higher-Loop Terms in the β -function of a Gauge Theory*, Phys. Rev. **D90** (2014) 045011.
- [97] T.A. Ryttov, *Conformal Behavior at Four Loops and Scheme (In)Dependence*, Phys. Rev. **D90** (2014) no.5, 056007, Erratum: Phys. Rev. **D91** (2015) no.3, 039906.

- [98] W. Celmaster and R.J. Gonsalves, *QCD Perturbation Expansions in a Coupling Constant Renormalized by Momentum Space Subtraction*, Phys. Rev. Lett. **42** (1979) 1435.
- [99] W. Celmaster and R.J. Gonsalves, *The Renormalization Prescription Dependence of the QCD Coupling Constant*, Phys. Rev. **D20** (1979) 1420.
- [100] C. Sturm, Y. Aoki, N.H. Christ, T. Izubuchi, C.T.C. Sachrajda and A. Soni, *Renormalization of Quark Bilinear Operators in a Momentum-Subtraction Scheme with a Non-exceptional Subtraction Point*, Phys. Rev. **D80** (2009) 014501.
- [101] M. Gorbahn and S. Jäger, *Precise \overline{MS} Light-quark Masses from Lattice QCD in the RI/SMOM Scheme*, Phys. Rev. **D82** (2010) 114001.
- [102] J.M. Bell and J.A. Gracey, *Momentum Subtraction Scheme Renormalization Group Functions in the Maximal Abelian Gauge*, Phys. Rev. **D88** (2013) no.8, 085027.
- [103] J.M. Bell and J.A. Gracey, *Maximal Abelian and Curci-Ferrari Gauges in Momentum Subtraction at Three Loops*, Phys. Rev. **D92** (2015) 125001.
- [104] G. 't Hooft, *Dimensional regularization and the Renormalization Group*, Nucl. Phys. **B61** (1973) 455-468.
- [105] T.A. Ryttov and R. Shrock, *Infrared Zero of β and Value of γ_m for an $SU(3)$ Gauge Theory at the Five-Loop Level*, Phys. Rev. **D94** (2016) no.10, 105015.
- [106] T.A. Ryttov, *Consistent Perturbative Fixed Point Calculations in QCD and Supersymmetric QCD*, Phys. Rev. Lett. **117** (2016) no.7, 071601.
- [107] T.A. Ryttov and R. Shrock, *Scheme-Independent Calculation of $\gamma_{\bar{\psi}\psi,IR}$ for an $SU(3)$ gauge theory*, Phys. Rev. **D94** (2016) no.10, 105014.
- [108] T.A. Ryttov and R. Shrock, *Scheme-Independent Series Expansions at an Infrared Zero of the β -function in Asymptotically Free Gauge Theories*, Phys. Rev. **D94** (2016) no.12, 125005.
- [109] T.A. Ryttov, *Higher-Order Scheme-Independent Calculations of Physical Quantities in the Conformal Phase of a Gauge Theory*, Phys.Rev. **D95** (2017) no.8, 085012.

- [110] T.A. Rytto and R. Shrock, *Higher-Order Scheme-Independent Series Expansions of $\gamma_{\bar{\psi}\psi,IR}$ and β'_{IR} in Conformal Field Theories*, Phys. Rev. **D95** (2017) no.10, 105004.
- [111] T.A. Rytto and R. Shrock, *Infrared Fixed Point Physics in $SO(N_c)$ and $Sp(N_c)$ Gauge Theories*, Phys. Rev. **D96** (2017) no.10, 105015.
- [112] T.A. Rytto and R. Shrock, *β'_{IR} at an Infrared Fixed Point in Chiral Gauge Theories*, Phys. Rev. **D97** (2018) no.1, 016020.
- [113] T.A. Rytto and R. Shrock, *Duality in a Supersymmetric Gauge Theory From a Perturbative Viewpoint*, Phys. Rev. **D97** (2018) no.6, 065020.
- [114] J.A. Gracey, T.A. Rytto and R. Shrock, *Scheme-Independent Calculations of Anomalous Dimensions of Baryon Operators in Conformal Field Theories*, Phys. Rev. **D97** (2018) no.11, 116018.
- [115] M.E. Peskin and D.V. Schröder, *An Introduction to Quantum Field Theory*, Westview Press, Reading (1995).
- [116] L.H. Ryder, *Quantum Field Theory*, Cambridge University Press, 2nd edition, Cambridge (1996).
- [117] T.J. Hollowood, *6 Lectures on QFT, RG and SUSY*, hep-th/0909.0859.
- [118] J. Cardy, *Scaling and Renormalization in Statistical Physics*, Cambridge University Press, Cambridge (1996).
- [119] I. Herbut, *A Modern Approach to Critical Phenomena*, Cambridge University Press, Cambridge (2007).
- [120] J.A. Gracey, *Renormalization*, Post-Graduate Lectures presented at the University of Liverpool, Liverpool (2015).
- [121] C.G. Bollini and J.J. Giambiagi, *Dimensional Renormalization: The Number of Dimensions as a Regularizing Parameter*, Nuovo Cim. **B12** (1972) 20-26.
- [122] G. 't Hooft and M.J.G. Veltman, *Regularization and Renormalization of Gauge Fields*, Nucl. Phys. **B44** (1972) 189-213.
- [123] L. Brink, J.H. Schwarz and J. Scherk, *Supersymmetric Yang-Mills Theories*, Nucl. Phys. **B121** (1977) 77-92.
- [124] W. Siegel, *Supersymmetric Dimensional Regularization via Dimensional Reduction*, Phys. Lett. **84B** (1979) 193-196.

- [125] D.M. Capper, D.R.T. Jones and P. van Nieuwenhuizen, *Regularization by Dimensional Reduction of Supersymmetric and Nonsupersymmetric Gauge Theories*, Nucl. Phys. **B167** (1980) 479-499.
- [126] W.A. Bardeen, A.J. Buras, D.W. Duke and T. Muta, *Deep Inelastic Scattering Beyond the Leading Order in Asymptotically Free Gauge Theories*, Phys. Rev. **D18** (1978) 3998.
- [127] S. Weinberg, *High-Energy Behaviour in Quantum Field Theory*, Phys. Rev. **118** (1960) 838-849.
- [128] J.A. Gracey, *Conformal Methods for Massless Feynman Integrals and Large N_f Methods*, Computer Algebra in Quantum Field Theory, Springer, Vienna (2013).
- [129] M. D’Eramo, G. Parisi and L. Peliti, *Theoretical Predictions For Critical Exponents At The Lambda Point Of Bose Liquids*, Lett. Nuovo Cim. **2** (1971) no.17, 878-880.
- [130] D.I. Kazakov, *The Method Of Uniqueness, A New Powerful Technique For Multiloop Calculations*, Phys. Lett. **B133** (1983) 406-410.
- [131] D.I. Kazakov, *Multiloop Calculations: Method of Uniqueness and Functional Equations*, Theor. Math. Phys. **62** (1985) 84-89.
- [132] D.I. Kazakov, *Calculation Of Feynman Integrals By The Method Of ‘uniqueness’*, Theor. Math. Phys. **58** (1984) 223-230.
- [133] J.A. Gracey, *On the Evaluation of Massless Feynman Diagrams by the Method of Uniqueness*, Phys. Lett. **B277** (1992) 469-473.
- [134] N.I Ussyukina, *Calculation of Multiloop Diagrams in Arbitrary Order*, Phys. Lett. **B267** (1991) 382-388.
- [135] D.J. Gross and A. Neveu, *Dynamical Symmetry Breaking in Asymptotically Free Field Theories*, Phys. Rev. **D10** (1974) 3235.
- [136] J.A. Gracey, *Calculation of Exponent η to $O(1/N^2)$ in the $O(N)$ Gross-Neveu model*, Int. J. Mod. Phys. **A6** (1991) 395-408, Erratum: Int. J. Mod. Phys. **A6** (1991) 2755.
- [137] J.A. Gracey, *Anomalous Mass Dimension at $O(1/N^2)$ in the $O(N)$ Gross-Neveu Model*, Phys. Lett. **B297** (1992) 293-297.

- [138] S.E. Dérickachov, N.A. Kivel, A.S. Stepanenko and A.N. Vasil'ev, *On Calculation in $1/n$ Expansions of Critical Exponents in the Gross-Neveu Model with the Conformal Technique*, hep-th/9302034.
- [139] S.E. Dérickachov, N.A. Kivel, A.S. Stepanenko and A.N. Vasil'ev, *The $1/n$ Expansion in the Gross-Neveu Model: Conformal Bootstrap Calculation of the Index η in Order $1/n^3$* , Theor. Math. Phys. **94** (1993) 127-136.
- [140] A.S. Stepanenko and A.N. Vasil'ev, *The $1/n$ Expansion in the Gross-Neveu Model: Conformal bootstrap Calculation of the Exponent $1/\nu$ to the Order $1/n^2$* , Theor. Math. Phys. **97** (1993) 1349-1354.
- [141] J.A. Gracey, *Computation of $\beta'(g_c)$ at $O(1/N^2)$ in the $O(N)$ Gross-Neveu Model in Arbitrary Dimensions*, Int. J. Mod. Phys. **A9** (1994) 567-590.
- [142] J.A. Gracey, *Computation of Critical Exponent η at $O(1/N^3)$ in the Four Fermi Model in Arbitrary Dimensions*, Int. J. Mod. Phys. **A9** (1994) 727-744.
- [143] C. Rim and W.I. Weisberger, *Ultraviolet Divergences in $1/N$ Expansions of Asymptotically Free Theories*, Phys. Rev. **D30** (1984) 1763.
- [144] C. Rim and W.I. Weisberger, *Quadratic Divergences In Dimensional Renormalization of $1/n$ Expansions*, Phys. Rev. **D32** (1985) 3244.
- [145] N.N. Bogolyubov and D.V. Shirkov, *Introduction To The Theory of Quantized Fields*, Intersci. Monogr. Phys. Astron. **3** (1959) 1-720.
- [146] J. Polchinski, *Scale and Conformal Invariance in Quantum Field Theory*, Nucl. Phys. **B303** (1988) 226-236.
- [147] A.B. Zomolodchikov, *Irreversibility of the Flux of the Renormalization Group in a 2D Field Theory*, JETP Lett. **43** (1986) 730-732.
- [148] D. Dorigoni and V.S. Rychkov, *Scale Invariance + Unitarity \Rightarrow Conformal Invariance?*, hep-th/0910.1087.
- [149] M.A. Luty, J. Polchinski and R. Rattazzi, *The a -theorem and the Asymptotics of 4D Quantum Field Theory*, JHEP **1301** (2013) 152.
- [150] J.F. Fortin, B. Grinstein and A. Stergiou, *Limit Cycles and Conformal Invariance*, JHEP **1301** (2013) 184.
- [151] A. Dymarsky, Z. Komargodski, A. Schwimmer and S. Theisen, *On Scale and Conformal Invariance in Four Dimensions*, JHEP **1510** (2015) 171.

- [152] H. Elvang, D.Z. Freedman, L.Y. Hung, M. Kiermaier, R.C. Myers and S. Theisen, *On Renormalization Group Flows and the a -theorem in 6d*, JHEP **1210** (2012) 011.
- [153] C. Cordova, T.T. Dumitrescu and K. Intriligator, *Anomalies, Renormalization Group Flows, and the a -theorem in Six-Dimensional (1,0) theories*, JHEP **1610** (2016) 080.
- [154] B. Grinstein, A. Stergiou and D. Stone, *Consequences of Weyl Consistency Conditions*, JHEP **1311** (2013) 195.
- [155] K.G. Wilson, *Feynman Graph Expansion for Critical Exponents*, Phys. Rev. Lett. **28** (1972) 548-551.
- [156] J.A. Gracey, *β -functions in Higher Dimensional Field Theories*, 13th DESY Workshop on Elementary Particle Physics: Loops and Legs in Quantum Field Theory, Leipzig (2016) 063.
- [157] E. Brezin, J.C. Le Guillou, J. Zinn-Justin and B.G. Nickel, *Higher Order Contributions to Critical Exponents*, Physics Letters **A44** (1973) 227228.
- [158] D.I. Kazakov, O.V. Tarasov and A.A. Vladimirov, *Calculation of Critical Exponents by Quantum Field Theory Methods*, Sov. Phys. JETP **50** (1979) 521.
- [159] F.M. Dittes, Y.A. Kubyshin and O.V. Tarasov, *Four Loop Approximation in the ϕ^4 Model*, Theor. Math. Phys. **37** (1979) 879.
- [160] S.G. Gorishnii, S.A. Larin, F.V. Tkachov and K.G. Chetyrkin, *Five Loop Renormalization Group Calculations in the $g\phi^4$ in Four-Dimensions Theory*, Phys. Lett. **B132** (1983) 351.
- [161] H. Kleinert, J. Neu, V. Schulte-Frohlinde, K.G. Chetyrkin and S.A. Larin, *Five Loop Renormalization Group Functions of $O(n)$ Symmetric ϕ^4 Theory and Epsilon Expansions of Critical Exponents up to ϵ^5* , Phys. Lett. **B272** (1991) 39-44, Erratum: Phys. Lett. **B319** (1993) 545.
- [162] D.V. Batkovich, K.G. Chetyrkin and M.V. Kompaniets, *Six loop Analytical Calculation of the Field Anomalous Dimension and the Critical exponent η in $O(n)$ -symmetric ϕ^4 Model*, Nucl. Phys. **B906** (2016) 147-167.
- [163] M.V. Kompaniets and E. Panzer, *Renormalization Group Functions of ϕ^4 Theory in the \overline{MS} -scheme to Six Loops*, 13th DESY Workshop on Elementary Particle Physics: Loops and Legs in Quantum Field Theory, Leipzig (2016) 038.

- [164] M.V. Kompaniets and E. Panzer, *Minimally Subtracted Six Loop Renormalization of $O(n)$ -symmetric ϕ^4 Theory and Critical Exponents*, Phys. Rev. **D96** (2017) no.3, 036016.
- [165] O. Schnetz, *Numbers and Functions in Quantum Field Theory*, hep-th/1606.08598.
- [166] J.B Kogut and K.G. Wilson, *The Renormalization Group and the Epsilon Expansion*, Phys. Rept. **12** (1974) 75-200.
- [167] D.J. Broadhurst, J.A. Gracey and D. Kreimer, *Beyond the Triangle and Uniqueness Relations: Nonzeta counterterms at Large N from Positive Knots*, Z. Phys. **C75** (1997) 559-574.
- [168] K. Yonekura, *Perturbative c -theorem in d -dimensions*, JHEP **1304** (2013) 011.
- [169] B. Grinstein, D. Stone, A. Stergiou and M. Zhong, *Challenges to the a Theorem in Six Dimensions*, Phys. Rev. Lett. **113** (2014) no.23, 231602.
- [170] M.E. Fisher, *Yang-Lee Edge Singularity and ϕ^3 Field Theory*, Phys. Rev. Lett. **40** (1978) 1610-1613.
- [171] O.F. de Alcantara Bonfim, J.E. Kirkham and A.J. McKane, *Critical Exponents to Order ϵ^3 for ϕ^3 Models of Critical Phenomena in Six ϵ -dimensions*, J. Phys. **A13** (1980) L247-L251, Erratum: J. Phys. **A13** (1980) 3785.
- [172] O.F. de Alcantara Bonfim, J.E. Kirkham and A.J. McKane, *Critical Exponents for the Percolation Problem and the Yang-Lee Edge Singularity*, J. Phys. **A14** (1981) 2391-2413.
- [173] M.C. Barboda, M.A. Gusmao and W.K. Theumann, *Renormalization and Phase Transitions in Potts ϕ^3 Field Theory With Quadratic and Trilinear Symmetry Breaking*, Phys. Rev. **B34** (1986) 3165-3176.
- [174] E. Ma, *Asymptotic Freedom and a Quark Model in Six-Dimensions*, Prog. Theor.Phys. **54** (1975) 1828-1832.
- [175] D.B. Kaplan, J.W. Lee, D.T. Son and M.A. Stephanov, *Conformality Lost*, Phys. Rev. **D80** (2009) 125005.
- [176] P. Butera and M. Pernici, *Yang-Lee Edge Singularities from Extended Activity Expansions of the Dimer Density for Bipartite Lattices of Dimensionality $2 \leq d \leq 7$* , Phys. Rev. **E86** (2012) 011104.

- [177] F. Gliozzi and A. Rago, *Critical Exponents of the 3d Ising and Related Models from Conformal Bootstrap*, JHEP **1410** (2014) 042.
- [178] S. El-Showk, D. Poland, S. Rychkov, D. Simmons-Duffin and A. Vichi, *Conformal Field Theories in Fractional Dimensions*, Phys. Rev. Lett. **112** (2014) 141601.
- [179] M. Moshe and J. Zinn-Justin, *Quantum field theory in the large N Limit: A Review*, Phys. Rept. **385** (2003) 69-228.
- [180] B.I. Halperin, T.C. Lubensky and S.K. Ma, *First Order Phase Transitions in Superconductors and Smectic A Liquid Crystals*, Phys. Rev. Lett. **32** (1974) 292-295.
- [181] R. Percacci and G. P. Vacca, *Are there Scaling Solutions in the $O(N)$ -models for Large N in $d > 4$?*, Phys. Rev. **D90** (2014) 107702.
- [182] L. Fei, S. Giombi, I.R. Klebanov and G. Tarnopolsky, *Critical $Sp(N)$ Models in $6 - \epsilon$ Dimensions and Higher Spin dS/CFT* , JHEP **1509** (2015) 076.
- [183] A. Stergiou, *Symplectic Critical Models in $6 + \epsilon$ Dimensions*, Phys. Lett. **B751** (2015) 184-187.
- [184] P. Nogueira, *Automatic Feynman Graph Generation*, J. Comput. Phys. **105** (1993) 279-289.
- [185] J.A.M. Vermaseren, *New Features of FORM*, math-ph/0010025v2.
- [186] M. Tentyukov and J.A.M. Vermaseren, *The Multithreaded Version of FORM*, Comput. Phys. Commun. **181** (2010) 1419-1427.
- [187] C. Studerus, *REDUZE - Feynman Integral Reduction in C++*, Comput. Phys. Commun. **181** (2010) 1293-1300.
- [188] D. Binosi and L. Theussl, *JaxoDraw: A Graphical User Interface for Drawing Feynman diagrams*, Comput. Phys. Commun. **161** (2004) 76-86.
- [189] D. Binosi, J. Collins, C. Kaufhold and L. Theussl, *JaxoDraw: A Graphical User Interface for Drawing Feynman Diagrams. Version 2.0 Release Notes*, Comput. Phys. Commun. **180** (2009) 1709-1715.
- [190] A. von Manteuffel and C. Studerus, *REDUZE 2 - Distributed Feynman Integral Reduction*, hep-ph/1201.4330.

- [191] C. Bauer, A. Frink and R. Kreckel, *Introduction to the GINAC Framework for Symbolic Computation within the C++ Programming Language*, J. Symb. Comput. **33** 1-12 (2000).
- [192] S. Laporta, *High-precision Calculation of Multi-loop Feynman Integrals by Difference Equations*, Int. J. Mod. Phys. **A15** (2000) 5087-5159.
- [193] A.I. Davydychev, *Recursive Algorithm of Evaluating Vertex-Type Feynman Integrals*, J. Phys. **A25** (1992) 5587-5596.
- [194] L.G. Almeida and C. Sturm, *Two-loop Matching Factors for Light Quark Masses and Three-loop Mass Anomalous Dimensions in the Regularization Invariant Symmetric Momentum-subtraction Schemes*, Phys. Rev. **D82** (2010) 054017.
- [195] O.V. Tarasov, *Connection Between Feynman Integrals Having Different Values of the Space-time Dimension*, Phys. Rev. **D54** (1996) 6479-6490.
- [196] O.V. Tarasov, *Generalized Recurrence Relations for Two Loop Propagator Integrals with Arbitrary Masses*, Nucl. Phys. **B502** (1997) 455-482.
- [197] N.I. Ussyukina and A.I. Davydychev, *New Results for Two Loop Off-shell Three Point Diagrams*, Phys. Lett. **B332** (1994) 159-167.
- [198] J. Ablinger, J. Blümlein and C. Schneider, *Harmonic Sums and Polylogarithms Generated by Cyclotomic Polynomials*, J. Math. Phys. **52** (2011) 102301.
- [199] N.I. Ussyukina and A.I. Davydychev, *An Approach to the Evaluation of Three- and Four-point Ladder Diagrams*, Phys. Lett. **B298** (1993) 363-370.
- [200] N.I. Ussyukina and A.I. Davydychev, *Exact Results for Three- and Four-point Ladder Diagrams with an Arbitrary Number of Rungs*, Phys. Lett. **B305** (1993) 136-143.
- [201] K. Chetyrkin, M. Misiak and M. Münz, *β -functions and Anomalous Dimensions up to Three Loops*, Nucl. Phys. **B518** (1998) 473-494.
- [202] M. Misiak and M. Münz, *Two-loop Mixing of Dimension-five Flavour-changing Operators*, Phys. Lett. **B344** (1995) 308-318.
- [203] C. Ford, I. Jack and D.R.T. Jones, *The Standard Model Effective Potential at Two Loops*, Nucl. Phys. **B387** (1992) 373-390.

- [204] G. Mack and A. Salam, *Finite Component Field Representations of the Conformal Group*, Annals Phys. **53** (1969) 174-202.
- [205] S. Ferrara, A.F. Grillo and R. Gatto, *Manifestly Conformal Covariant Operator-product Expansion*, Lett. Nuovo Cim. **2S2** (1971) 1363-1369 and Lett. Nuovo Cim. **2** (1971) 1363-1369.
- [206] S. Ferrara, A.F. Grillo, G. Parisi and R. Gatto, *Covariant Expansion of the Conformal Four-point Function*, Nucl. Phys. **B49** (1972) 77-98, Erratum: Nucl. Phys. **B53** (1973) 643-643.
- [207] S. Ferrara, A.F. Grillo, and R. Gatto, *Tensor Representations of Conformal Algebra and Conformally Covariant Operator Product Expansion*, Annals Phys. **76** (1973) 161-188.
- [208] S. Ferrara, A.F. Grillo, R. Gatto and G. Parisi, *Analyticity Properties and Asymptotic Expansions of Conformal Covariant Green's Functions*, Nuovo Cim. **A19** (1974) 667-695.
- [209] S. Ferrara, R. Gatto and A.F. Grillo, *Positivity Restrictions on Anomalous Dimensions*, Phys. Rev. **D9** (1974) 3564-3565.
- [210] A.M. Polyakov, *Nonhamiltonian Approach to Conformal Quantum Field Theory*, Zh. Eksp. Teor. Fiz. **66** (1974) 23-42 and Sov. Phys. JETP **39** (1974) 9-18.
- [211] F.A. Dolan and H. Osborn, *Conformal Four Point Functions and the Operator Product Expansion*, Nucl. Phys. **B599** (2001) 459-496.
- [212] R. Rattazzi, V.S. Rychkov, E. Tonni and A. Vichi, *Bounding Scalar Operator Dimensions in 4D CFT*, JHEP **0812** (2008) 031.
- [213] S. El-Showk, M.F. Paulos, D. Poland, S. Rychkov, D. Simmons-Duffin and A. Vichi, *Solving the 3D Ising Model with the Conformal Bootstrap*, Phys. Rev. **D86** (2012) 025022.
- [214] A.B. Zamolodchikov, *Irreversibility of the Flux of the Renormalization Group in a 2D Field Theory*, JETP Lett. **43** (1986) 730-732 and Pisma Zh. Eksp. Teor. Fiz. **43** (1986) 565-567.
- [215] A. Pelissetto and E. Vicari, *Randomly Dilute Spin Models: A Six Loop Field Theoretic Study*, Phys. Rev. **B62** (2000) 6393-6409.
- [216] P. Calabrese, A. Pelissetto and E. Vicari, *Randomly Dilute Spin Models with Cubic Symmetry*, Phys. Rev. **B67** (2003) 024418.

- [217] A.J. McKane, *An $SU(3) \times SU(3)$ Field Theory of Strong Interactions in Six Epsilon Dimensions*, J. Phys. **G3** (1977) 1165-1177.
- [218] A. Pelissetto, P. Rossi and E. Vicari, *Large n Critical Behavior of $O(n) \times O(m)$ Spin Models*, Nucl. Phys. **B607** (2001) 605-634.
- [219] H. Kawamura, *Renormalization Group Analysis of Chiral Transitions*, Phys. Rev. **B38** (1988) 4916-4928, Erratum: Phys. Rev. **B42** (1990) 2610-2610.
- [220] J.A. Gracey, *Critical Exponent ω at $O(1/N)$ in $O(N) \times O(m)$ Spin Models*, Nucl. Phys. **B644** (2002) 433-450.
- [221] K.G. Chetyrkin and F.V. Tkachov, *Integration by Parts: The Algorithm to Calculate β -functions in 4 Loops*, Nucl. Phys. **B192** (1981) 159-204.
- [222] F.V. Tkachov, *A Theorem on Analytical Calculability of Four Loop Renormalization Group Functions*, Phys. Lett. **B100** (1981) 65-68.
- [223] P.A. Baikov and K.G. Chetyrkin, *Four Loop Massless Propagators: An Algebraic Evaluation of All Master Integrals*, Nucl. Phys. **B837** (2010) 186-220.
- [224] O.V. Tarasov, A.A. Vladimirov and A.Yu. Zharkov, *The Gell-Mann-Low Function of QCD in the Three Loop Approximation*, Phys. Lett. **B93** (1980) 429-432.
- [225] S.A. Larin and J.A.M. Vermaseren, *The Three loop QCD β -function and anomalous dimensions*, Phys. Lett. **B303** (1993) 334-336.
- [226] J.A. Gracey, *Renormalization of Scalar Field Theories in Rational Space-time Dimensions*, hep-th/1703.09685.
- [227] L. Fei, S. Giombi, I.R. Klebanov and G. Tarnopolsky, *Yukawa CFTs and Emergent Supersymmetry*, PTEP **2016** (2016) no.12, 12C105, hep-th/1607.05316.
- [228] A. Hasenfratz and P. Hasenfratz, *The Equivalence of the $SU(N)$ Yang-Mills theory with a Purely Fermionic Model*, Phys. Lett. **B297** (1992) 166-170.
- [229] J.A. Gracey, *Quark, Gluon and Ghost Anomalous Dimensions at $O(1/N_f)$ in Quantum Chromodynamics*, Phys. Lett. **B318** (1993) 177-183.
- [230] J.A. Gracey, *The QCD β -function at $O(1/N_f)$* , Phys. Lett. **B373** (1996) 178-184.

- [231] M. Ciuchini, S.E. Derkachov, J.A. Gracey and A.N. Manashov, *Computation of Quark Mass Anomalous Dimension at $O(1/N_f^2)$ in Quantum Chromodynamics*, Nucl. Phys. **B579** (2000) 56-100.
- [232] J.A. Gracey, T. Luthe and Y. Schröder, *Four loop Renormalization of the Gross-Neveu Model*, Phys. Rev. **D94** (2016) no.12, 125028.
- [233] J.A. Gracey, *F_4 Symmetric ϕ^3 Theory at Four Loops*, Phys. Rev. **D95** (2017) no.6, 065030.
- [234] C. Brust and K. Hinterbichler, *Free \square^k Scalar Conformal Field Theory*, JHEP **1702** (2017) 066.
- [235] C. Brust and K. Hinterbichler, *Partially Massless Higher-Spin Theory*, JHEP **1702** (2017) 086.
- [236] C. Brust and K. Hinterbichler, *Partially Massless Higher-Spin Theory II: One-Loop Effective Actions*, JHEP **1701** (2017) 126.
- [237] D.I. Kazakov, *Analytical Methods For Multiloop Calculations: Two Lectures On The Method Of Uniqueness*, JINR-E2-84-410 (1984).
- [238] V.N. Gribov, *Quantization of Nonabelian Gauge Theories*, Nucl. Phys. **B139** (1978) 1-19.
- [239] D. Zwanziger, *Nonperturbative Modification of the Faddeev-Popov Formula and Banishment of the Naive Vacuum*, Nucl. Phys. **B209** (1982) 336-348.
- [240] D. Zwanziger, *Action From the Gribov Horizon*, Nucl. Phys. **B321** (1989) 591-604.
- [241] D. Zwanziger, *Local and Renormalizable Action From the Gribov Horizon*, Nucl. Phys. **B323** (1989) 513-544.
- [242] D. Zwanziger, *Vanishing of Zero Momentum Lattice Gluon Propagator and Color Confinement*, Nucl. Phys. **B364** (1991) 127-161.
- [243] D. Zwanziger, *Critical Limit of Lattice Gauge Theory*, Nucl. Phys. **B378** (1992) 525-590.
- [244] D. Zwanziger, *Renormalizability of the Critical Limit of Lattice Gauge Theory by BRS Invariance*, Nucl. Phys. **B399** (1993) 477-513.
- [245] M. Botje, *Particle Physics II: Quantum Chromodynamics*, Lectures presented at NIKHEF, Science Park, Amsterdam (2013).

- [246] M.H. Seymour, *Quantum chromodynamics*, Lectures presented at European School of High-Energy Physics, Barcelona (2004).
- [247] J. M. Bell, *The Structure of Quantum Chromodynamics at the Symmetric point*, Ph.D. Thesis, University of Liverpool (2015).
- [248] D.J. Gross, *Gauge Theory-Past, Present, and Future?*, Chinese Journal of Phys. Vol. **30** (1992) 7.
- [249] T.W.B. Kibble, *Symmetry breaking in non-Abelian Gauge Theories*, Phys. Rev. **155** (1967) 1554-1561.
- [250] M. Gell-Mann, *The Eightfold Way*, Benjamin, New York (1964).
- [251] G. 't Hooft, *Quarks and Gauge Fields*, Proceedings of the Recent Progress In Lagrangian Field Theory and Applications Conference, Marseille (1975).
- [252] F. Abe et al., *Observation of Top Quark Production in $\bar{p}p$ Collisions*, Phys. Rev. Lett. **74** (1995) 2626-2631.
- [253] S. Abachi et al., *Observation of the Top Quark*, Phys. Rev. Lett. **74** (1995) 2632-2637.
- [254] D.P. Barber et al., *Discovery of Three Jet Events and a Test of Quantum Chromodynamics at PETRA Energies*, Phys. Rev. Lett. **43** (1979) 830-833.
- [255] A.J. MacFarlane, A. Sudbery, P.H. Weisz, *On Gell-Mann's Lambda-matrices, d- and f-tensors, Octets, and Parametrizations of SU(3)*, Commun. Math. Phys. **11** (1968) 77-90.
- [256] D. Griffiths, *Introduction to Elementary Particles*, Wiley, Weinherim (2008).
- [257] J.A. Gracey, *Classification and One Loop Renormalization of Dimension-six and Dimension-eight Operators in Quantum Gluodynamics*, Nucl. Phys. **B634** (2002) 192-208, Erratum: Nucl. Phys. **B696** (2004) 295-297.
- [258] L.D. Faddeev and V.N. Popov, *Feynman Diagrams for the Yang-Mills Field*, Phys. Lett. **B25** (1967) 29-30.
- [259] R. Parthasarathy, *Quantization In A Nonlinear Gauge And Feynman Rules*, J. Phys. **A21** (1988) 4593-4607.
- [260] A.A. Slavnov, *Ward Identities in Gauge Theories*, Theor. Math. Phys. **10** (1972) 99-107 and Teor. Mat. Fiz. **10** (1972) 153-161.

- [261] J.C. Taylor, *Ward Identities and Charge Renormalization of the Yang-Mills Field*, Nucl. Phys. **B33** (1971) 436-444.
- [262] C. Becchi, A. Rouet and R. Stora, *The Abelian Higgs-Kibble Model. Unitarity of the S Operator*, Phys. Lett. **B52** (1974) 344-346.
- [263] C. Becchi, A. Rouet and R. Stora, *Renormalization of the Abelian Higgs-Kibble Model*, Commun. Math. Phys. **42** (1975) 127-162.
- [264] B.S. DeWitt, *Theory of Radiative Corrections for Non-abelian Gauge Fields*, Phys. Rev. Lett. **12** (1964) 742-746.
- [265] R.P. Feynman, *Quantum Theory of Gravitation*, Acta Phys. Polon. **24** (1963) 697-722.
- [266] C.G. Bollini and J.J. Giambiagi, *Lowest Order Divergent Graphs in ν -dimensional Space*, Phys. Lett. **B40** (1972) 566-568.
- [267] W.E. Caswell, *Asymptotic Behavior of Nonabelian Gauge Theories to Two Loop Order*, Phys. Rev. Lett. **33** (1974) 244.
- [268] D.R.T. Jones, *Two Loop Diagrams in Yang-Mills Theory*, Nucl. Phys. **B75** (1974) 531-538.
- [269] O.V. Tarasov and A.A. Vladimirov, *Two Loop Renormalization of the Yang-Mills Theory in an Arbitrary Gauge*, Sov. J. Nucl. Phys. **25** (1977) 585-592.
- [270] E. Egorian and O.V. Tarasov, *Two Loop Renormalization of the (QCD) in an Arbitrary Gauge*, Teor. Mat. Fiz. **41** (1979) 26-32.
- [271] T. van Ritbergen, J.A.M. Vermaseren and S.A. Larin, *The Four loop β -function in Quantum Chromodynamics*, Phys. Lett. **B400** (1997) 379-384.
- [272] M. Czakon, *The Four-loop QCD β -function and Anomalous Dimensions*, Nucl. Phys. **B710** (2005) 485-498.
- [273] O. Nachtmann and W. Wetzel, *The β -function for Effective Quark Masses to Two Loops in (QCD)*, Nucl. Phys. **B187** (1981) 333-342.
- [274] R. Tarrach, *The Pole Mass in Perturbative QCD*, Nucl. Phys. **B183** (1981) 384-396.
- [275] K.G. Chetyrkin, *Quark Mass Anomalous Dimension to $O(\alpha_s^4)$* , Phys. Lett. **B404** (1997) 161-165.

- [276] J.A.M. Vermaseren, S.A. Larin and T. van Ritbergen, *The Four Loop Quark Mass Anomalous Dimension and the Invariant Quark Mass*, Phys. Lett. **B405** (1997) 327-333.
- [277] P.A. Baikov, K.G. Chetyrkin and J.H. Kühn, *Five-Loop Running of the QCD coupling constant*, Phys. Rev. Lett. **118** (2017) no.8, 082002.
- [278] F. Herzog, B. Ruijl, T. Ueda, J.A.M. Vermaseren and A. Vogt, *The five-loop β -function of Yang-Mills Theory with Fermions*, JHEP **1702** (2017) 090.
- [279] T. Luthe, A. Maier, P. Marquard and Y. Schröder, *Towards the five-loop β -function for a General Gauge Group*, JHEP **1607** (2016) 127.
- [280] T. Luthe, A. Maier, P. Marquard and Y. Schröder, *The Five-loop β -function for a General Gauge Group and Anomalous Dimensions Beyond Feynman Gauge*, JHEP **1710** (2017) 166.
- [281] K.G. Chetyrkin, G. Falcioni, F. Herzog and J.A.M. Vermaseren, *Five-loop Renormalisation of QCD in Covariant Gauges*, JHEP **1710** (2017) 179, Addendum: JHEP **1712** (2017) 006.
- [282] P.A. Baikov, K.G. Chetyrkin and J.H. Kühn, *Quark Mass and Field Anomalous Dimensions to $O(\alpha_s^5)$* , JHEP **1410** (2014) 076.
- [283] P.A. Baikov, K.G. Chetyrkin and J.H. Kühn, *Five-loop Fermion Anomalous Dimension for a General Gauge Group from Four-loop Massless Propagators*, JHEP **1704** (2017) 119.
- [284] T. Luthe, A. Maier, P. Marquard and Y. Schröder, *Five-loop Quark Mass and Field Anomalous Dimensions for a General Gauge Group*, JHEP **1701** (2017) 081.
- [285] T. Luthe, A. Maier, P. Marquard and Y. Schröder, *Complete Renormalization of QCD at Five Loops*, JHEP **1703** (2017) 020.
- [286] B. Ruijl, T. Ueda, J.A.M. Vermaseren and A. Vogt, *Four-loop QCD Propagators and Vertices with One Vanishing External Momentum*, JHEP **1706** (2017) 040.
- [287] O.V. Tarasov, A.A. Vladimirov and A.Y. Zharkov, *The Gell-Mann-Low Function of QCD in the Three Loop Approximation*, Phys. Lett. **B93** (1980) 429-432.
- [288] E. Farhi and L. Susskind, *Technicolor*, Phys. Rept. **74** (1981) 277.

- [289] K. Yamawaki, M. Bando and K.I. Matumoto, *Scale Invariant Technicolor Model and a Technidilaton*, Phys. Rev. Lett. **56** (1986) 1335-1338.
- [290] T. Appelquist, G.T. Fleming and E.T. Neil, *Lattice Study of Conformal Behavior in $SU(3)$ Yang-Mills Theories*, Phys. Rev. **D79** (2009) 076010.
- [291] Z. Fodor, K. Holland, J. Kuti, D. Nogradi and C. Schröeder, *Twelve Massless Flavors and Three Colors Below the Conformal Window*, Phys. Lett. **B703** (2011) 348-358.
- [292] T. Karavirta, J. Rantaharju, K. Rummukainen and K. Tuominen, *Determining the Conformal Window: $SU(2)$ Gauge Theory with $N_f = 4, 6$ and 10 Fermion Flavours*, JHEP **1205** (2012) 003.
- [293] T. DeGrand, Y. Shamir and B. Svetitsky, *Near the Sill of the Conformal Window: Gauge Theories with Fermions in Two-index Representations*, Phys. Rev. **D88** (2013) no.5, 054505.
- [294] M. Hayakawa, K.I. Ishikawa, S. Takeda and N. Yamada, *Running Coupling Constant and Mass Anomalous Dimension of Six-flavor $SU(2)$ Gauge Theory*, Phys. Rev. **D88** (2013) no.9, 094504.
- [295] M. Hayakawa, K.I. Ishikawa, S. Takeda, M. Tomii and N. Yamada, *Lattice Study on Quantum-Mechanical Dynamics of Two-color QCD with Six Light Flavors*, Phys. Rev. **D88** (2013) no.9, 094506.
- [296] A. Cheng, A. Hasenfratz, Y. Liu, G. Petropoulos and D. Schaich, *Finite Size Scaling of Conformal Theories in the Presence of a Near-marginal Operator*, Phys. Rev. **D90** (2014) no.1, 014509.
- [297] M.P. Lombardo, K. Miura, T.J. N. da Silva and E. Pallante, *On the Particle Spectrum and the Conformal Window*, JHEP **1412** (2014) 183.
- [298] M. Hopfer, C.S. Fischer and R. Alkofer, *Running Coupling in the Conformal Window of Large- N_f QCD*, JHEP **1411** (2014) 035.
- [299] S.A. Caveny and P.M. Stevenson, *The Banks-Zaks Expansion and ‘Freezing’ in Perturbative QCD*, hep-th/9705319.
- [300] M. Bohm, H. Spiesberger and W. Hollik, *On the One Loop Renormalization of the Electroweak Standard Model and Its Application to Leptonic Processes*, Fortsch. Phys. **34** (1986) 687-751.

- [301] S. Edwards and L. von Smekal, *SU(2) Lattice Gauge Theory in 2 + 1 Dimensions: Critical Couplings from Twisted Boundary Conditions and Universality*, Phys. Lett. **B681** (2009) 484-490.
- [302] G. Martinelli, C. Pittori, C.T. Sachrajda, M. Testa and A. Vladikas, *A General Method for Nonperturbative Renormalization of Lattice Operators*, Nucl. Phys. **B445** (1995) 81-108.
- [303] E. Franco and V. Lubicz, *Quark Mass Renormalization in the \overline{MS} and RI' Schemes up to the NNLO Order*, Nucl. Phys. **B531** (1998) 641-651.
- [304] K.G. Chetyrkin and A. Rétey, *Renormalization and Running of Quark Mass and Field in the Regularization Invariant and \overline{MS} Schemes at Three Loops and Four Loops*, Nucl. Phys. **B583** (2000) 3-34.
- [305] J.A. Gracey, *Three Loop Anomalous Dimension of Nonsinglet Quark Currents in the RI' Scheme*, Nucl. Phys. **B662** (2003) 247-278.
- [306] J.A. Gracey, *Renormalization Group Functions of QCD in the Minimal MOM Scheme*, J. Phys. **A46** (2013) 225403.
- [307] J.A. Gracey, *Two loop QCD Vertices at the Symmetric Point*, Phys. Rev. **D84** (2011) 085011.
- [308] N.I. Usyukina and A.I. Davydychev, *Some Exact Results for Two Loop Diagrams with Three and Four External Lines*, Phys. Atom. Nucl. **56** (1993) 1553-1557 and Yad. Fiz. **56N11** (1993) 172-179.
- [309] T.G. Birthwright, E.W.N. Glover and P. Marquard, *Master Integrals for Massless Two-loop Vertex Diagrams with Three Offshell Legs*, JHEP **0409** (2004) 042.
- [310] O.V. Tarasov, *Anomalous Dimensions Of Quark Masses In Three Loop Approximation*, (In Russian) JINR-P2-82-900.
- [311] S.A. Larin, *The Renormalization of the Axial Anomaly in Dimensional Regularization*, Phys. Lett. **B303** (1993) 113-118.
- [312] G. 't Hooft, *Can We Make Sense Out of Quantum Chromodynamics?*, Subnucl. Ser. **15** (1979) 943.
- [313] G. 't Hooft, *Topology of the Gauge Condition and New Confinement Phases in Nonabelian Gauge Theories*, Nucl. Phys. **B190** (1981) 455-478.

- [314] R.M. Doria, F.A.B. Rabelo de Carvalho and S.P. Sorella, *A Note on the Landau gauge in Yang-Mills Theory*, Braz. J. Phys. **20** (1992) 316-321.
- [315] J.A. Gracey, *Three loop \overline{MS} Renormalization of the Curci-Ferrari Model and the Dimension Two BRST Invariant Composite Operator in QCD*, Phys. Lett. **B552** (2003) 101-110.
- [316] D. Dudal, H. Verschelde and S.P. Sorella, *The Anomalous Dimension of the Composite Operator A^2 in the Landau Gauge*, Phys. Lett. **B555** (2003) 126-131.
- [317] J.A. Gracey, *One Loop Renormalization of the Non-local Gauge Invariant Operator $\min_{\{U\}} \int d^4x (A_\mu^{aU})^2$ in QCD*, Phys. Lett. **B651** (2007) 253-256.
- [318] A. Blasi, O. Piguet and S.P. Sorella, *Landau Gauge and Finiteness*, Nucl. Phys. **B356** (1991) 154-162.
- [319] A.S. Kronfeld, G. Schierholz and U.J. Wiese, *Topology and Dynamics of the Confinement Mechanism*, Nucl. Phys. **B293** (1987) 461-478.
- [320] A.S. Kronfeld, M.L. Laursen, G. Schierholz and U.J. Wiese, *Monopole Condensation and Color Confinement*, Phys. Lett. **B198** (1987) 516-520.
- [321] Y. Nambu, *Strings, Monopoles and Gauge Fields*, Phys. Rev. **D10** (1974) 4262-4268.
- [322] Z.F. Ezawa and A. Iwazaki, *Abelian Dominance and Quark Confinement in Yang-Mills Theories*, Phys. Rev. **D25** (1982) 2681-2689.
- [323] H. Min, T. Lee and P.Y. Pac, *Renormalization of (Yang-Mills) Theory in the Abelian Gauge*, Phys. Rev. **D32** (1985) 440-449.
- [324] A.R. Fazio, V.E.R. Lemes, M.S. Sarandy and S.P. Sorella, *The Diagonal Ghost Equation Ward Identity for Yang-Mills Theories in the Maximal Abelian Gauge*, Phys. Rev. **D64** (2001) 085003.
- [325] K.I. Kondo, T. Shinohara, *Renormalizable Abelian Projected Effective Gauge Theory Derived from Quantum Chromodynamics*, Prog. Theor. Phys. **105** (2001) 649-665.
- [326] T. Shinohara, *Renormalizable Abelian Projected Effective Gauge Theory Derived from Quantum Chromodynamics. 2.*, Mod. Phys. Lett. **A18** (2003) 1398-1412.

- [327] T. Shinohara, T. Imai and K.I. Kondo, *The Most General and Renormalizable Maximal Abelian Gauge*, Int. J. Mod. Phys. **A18** (2003) 5733-5756.
- [328] J.A. Gracey, *Three Loop \overline{MS} Renormalization of QCD in the Maximal Abelian Gauge*, JHEP **0504** (2005) 012.
- [329] S. Mandelstam, *Vortices and Quark Confinement in Nonabelian Gauge Theories*, Phys. Rept. **23** (1976) 245-249.
- [330] G. 't Hooft, *Gauge Fields with Unified Weak, Electromagnetic, and Strong Interactions*, Proceedings of High-Energy Particle Physics Divisional Conference of EPS, Palermo (1975).
- [331] N. Sakumichi and H. Suganuma, *Perfect Abelian Dominance of Quark Confinement in $SU(3)$ QCD*, Phys. Rev. **D90** (2014) no.11, 111501.
- [332] D. Dudal, J.A. Gracey, V.E.R. Lemes, M.S. Sarandy, R.F. Sobreiro, S.P. Sorella and H. Verschelde, *An Analytic Study of the Off-diagonal Mass Generation for Yang-Mills Theories in the Maximal Abelian Gauge*, Phys. Rev. **D70** (2004) 114038.
- [333] K.I. Kondo and T. Shinohara, *Abelian Dominance in Low-energy Gluodynamics due to Dynamical Mass Generation*, Phys. Lett. **B491** (2000) 263-274.
- [334] S.G. Gorishnii, S.A. Larin, L.R. Surguladze and F.V. Tkachov, *Mincer: Program for Multiloop Calculations in Quantum Field Theory for the Schoonschip System*, Comput. Phys. Commun. **55** (1989) 381-408.
- [335] S.A. Larin, F.V. Tkachov and J.A.M. Vermaseren, *The FORM version of MINCER*, NIKHEF-H-91-18 (1991).
- [336] D. F. Litim and K. Nikolakopoulos, *Quantum Gravity Effects in Myers-Perry Space-times*, JHEP **1404** (2014) 021.
- [337] P. R. S. Gomes, *Aspects of Emergent Symmetries*, Int. J. Mod. Phys. **A31** (2016) no.10, 1630009.
- [338] A.I. Davydychev and J.B. Tausk, *A Magic Connection Between Massive and Massless Diagrams*, Phys. Rev. **D53** (1996) 7381-7384.